

Spring 1991

Use of the 9-arm self-boring pressure meter to measure horizontal in situ stress, stress anisotropy, and stress-strain behavior in soft clay

R Craig Findlay

University of New Hampshire, Durham

Follow this and additional works at: <https://scholars.unh.edu/dissertation>

Recommended Citation

Findlay, R Craig, "Use of the 9-arm self-boring pressure meter to measure horizontal in situ stress, stress anisotropy, and stress-strain behavior in soft clay" (1991). *Doctoral Dissertations*. 1643.

<https://scholars.unh.edu/dissertation/1643>

This Dissertation is brought to you for free and open access by the Student Scholarship at University of New Hampshire Scholars' Repository. It has been accepted for inclusion in Doctoral Dissertations by an authorized administrator of University of New Hampshire Scholars' Repository. For more information, please contact nicole.hentz@unh.edu.

INFORMATION TO USERS

This manuscript has been reproduced from the microfilm master. UMI films the text directly from the original or copy submitted. Thus, some thesis and dissertation copies are in typewriter face, while others may be from any type of computer printer.

The quality of this reproduction is dependent upon the quality of the copy submitted. Broken or indistinct print, colored or poor quality illustrations and photographs, print bleedthrough, substandard margins, and improper alignment can adversely affect reproduction.

In the unlikely event that the author did not send UMI a complete manuscript and there are missing pages, these will be noted. Also, if unauthorized copyright material had to be removed, a note will indicate the deletion.

Oversize materials (e.g., maps, drawings, charts) are reproduced by sectioning the original, beginning at the upper left-hand corner and continuing from left to right in equal sections with small overlaps. Each original is also photographed in one exposure and is included in reduced form at the back of the book.

Photographs included in the original manuscript have been reproduced xerographically in this copy. Higher quality 6" x 9" black and white photographic prints are available for any photographs or illustrations appearing in this copy for an additional charge. Contact UMI directly to order.

U·M·I

University Microfilms International
A Bell & Howell Information Company
300 North Zeeb Road, Ann Arbor, MI 48106-1346 USA
313 761-4700 800 521 0600

Order Number 9131285

**Use of the 9-arm self-boring pressuremeter to measure
horizontal *in situ* stress, stress anisotropy, and stress-strain
behavior in soft clay**

Findlay, R. Craig, Ph.D.

University of New Hampshire, 1991

U·M·I

300 N. Zeeb Rd.
Ann Arbor, MI 48106

USE OF THE 9-ARM SELF-BORING PRESSUREMETER TO MEASURE
HORIZONTAL IN SITU STRESS, STRESS ANISOTROPY,
AND STRESS-STRAIN BEHAVIOR IN SOFT CLAY

BY

R. CRAIG FINDLAY
BSCE - University of New Hampshire, 1976
MSCE - University of New Hampshire, 1981

DISSERTATION

Submitted to the University of New Hampshire
in Partial Fulfillment of
the Requirements of the Degree of

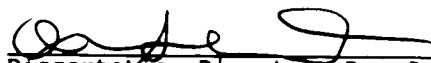
Doctor of Philosophy

in

Engineering

May, 1991

This dissertation has been examined and approved.



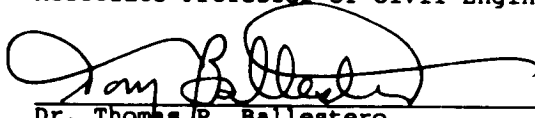
Dissertation Director, Dr. Jean Benoit,
Associate Professor of Civil Engineering



Dr. Pedro A. DeAlba,
Associate Professor of Civil Engineering



Dr. David L. Gress,
Associate Professor of Civil Engineering



Dr. Thomas P. Ballester,
Associate Professor of Civil Engineering



Dr. Francis Hall,
Professor of Hydrogeology

1/25/91
Date

DEDICATION

This dissertation is dedicated to my parents, Ronald Robert Findlay and Eleanor Mae Findlay. Without their patient example and boundless loving support I never would have achieved the level of discipline and perseverance necessary to complete the work summarized herein.

ACKNOWLEDGEMENTS

My gratitude must first be expressed to my wife Elaine and my step children Jessica and Jenna for their patience, support and understanding of near-abandonment they endured while I perused the work summarized herein. I promise I will make it up to you.

I would like to thank my advisor, Dr. Jean Benoit, for presenting me with this opportunity and providing the necessary support and guidance along the way. I wish to thank Dr. Pedro DeAlba for getting me started on my master's degree; his flexibility in providing his time for several independent study courses provided the means for a working person to obtain an advanced degree. I wish to thank the other members of my committee, Dr. Tom Ballestero, Dr. David Gress and Dr. Francis Hall, for their time and knowledge provided in this endeavor.

I would like to thank Mr. Robert M. Leary, the person I credit for introducing me to Geotechnical Engineering during my undergraduate work and employment with the Geotechnical Section of the New Hampshire Department of Public Works and Highways. Also, thanks are due to ABB-Environmental Services, Inc. (formerly E.C. Jordan Co. and Jordan Gorrill Associates), my employer for the last 10 years, for their patience with my pursuit of this research.

Last, and certainly not least, I would like to thank the other graduate students who helped along the way: Mike Atwood, Louis Nejame, and Adam Jones. Also, I would like to thank all the various work study students and others who helped with field and laboratory work throughout the research.

This research would not have been possible without the financial support of the National Science Foundation (Grant No. MSS-8619935) and the Bedford Institute of Oceanography (Ms. Kate Moran, Contract No. 23420-6-M693/01-SC).

TABLE OF CONTENTS

DEDICATION.....	iii
ACKNOWLEDGEMENTS.....	iv
LIST OF TABLES.....	ix
LIST OF FIGURES.....	x
LIST OF SYMBOLS.....	xiv
CONVERSION FACTORS.....	xvi
ABSTRACT.....	xvii

CHAPTER	PAGE
I. INTRODUCTION.....	1
II. SELF-BORING PRESSUREMETER AND RELATED TECHNOLOGY.....	5
2.1 History of the Pressuremeter.....	5
2.2 In Situ Horizontal Stress.....	13
2.2.1 Estimation and Measurement Technology.....	13
2.2.2 SBPM In Situ Stress Measurement.....	17
2.2.3 Determination of the Direction and Magnitude of Major Principal Stress.....	18
2.3 Mechanics of Pressuremeter Expansion.....	22
2.4 Determination of Undrained Shear Strength.....	25
2.4.1 Gibson and Anderson Method.....	25
2.4.2 Baguelin et al.-Ladanyi-Palmer Method.....	27
2.4.3 Denby and Clough Method.....	30
2.4.4 Ménard Method.....	33
2.4.5 Discussion of Shear Strength Methods.....	35
2.5 Soil Moduli.....	39
2.6 Horizontal Coefficient of Consolidation.....	42
III. SBPM EQUIPMENT AND TESTING METHODS.....	47
3.1 SBPM Description.....	47
3.2 Calibration of SBPM.....	47
3.3 Drilling.....	48
3.4 Expansion.....	53
IV. FIELD TEST SITES.....	57

4.1	Introduction.....	57
4.2	Pease Air Force Base.....	57
4.2.1	Geology of Pease AFB Area.....	57
4.2.2	Site Description.....	60
4.2.3	Engineering Properties from Previous Research.....	62
4.2.4	Field Testing and Sampling.....	64
4.2.4.1	Undisturbed Sampling.....	65
4.2.4.2	Field Vane.....	67
4.2.4.3	Self-Boring Pressuremeter Testing.....	70
4.2.4.4	Flat Dilatometer Testing.....	72
4.2.4.5	Pneumatic Piezometers.....	76
4.2.5	Laboratory Testing.....	78
4.2.5.1	Index Properties.....	78
4.2.5.2	One-Dimensional Consolidation Testing.....	80
4.2.5.3	CU Triaxial Testing.....	87
4.3	Hamilton Air Force Base.....	92
4.3.1	Geology.....	92
4.3.2	Site Description.....	94
4.3.3	Engineering Properties from Previous Research.....	97
4.3.4	Field Investigation for Present Research.....	100
V.	FINITE ELEMENT ANALYSIS.....	103
5.1	Introduction.....	103
5.2	SOILSTRUCT.....	106
5.2.1	Description of the Program.....	106
5.2.2	Derivation of Input Parameters.....	106
5.2.3	FEM Mesh and Construction Sequence.....	116
5.2.4	SOILSTRUCT Results.....	119
5.3	JFEST.....	121
5.3.1	Description of the Program.....	121
5.3.2	Derivation of Input Parameters.....	123
5.3.3	FEM Mesh and Construction Sequence.....	126
5.3.4	JFEST Results.....	130
5.4	Comparison of SOILSTRUCT and JFEST Results.....	130
VI.	TEST RESULTS: MEASUREMENT OF IN SITU STRESS.....	136
6.1	Introduction.....	136
6.2	Assessment of Horizontal Stress Results.....	136
6.2.1	Assessment of Test Results Affected by Disturbance.....	136
6.2.2	Correction for Excess Pore Pressures Due to Insertion.....	147
6.3	In Situ Horizontal Stress.....	148
6.3.1	In Situ Horizontal Stress at Pease AFB.....	149
6.3.1.1	Pease K_0 Area.....	149
6.3.1.2	Pease Embankment Toe Area.....	157
6.3.2	In Situ Horizontal Stress at Hamilton AFB.....	166
6.4	Stress Anisotropy in the Horizontal Plane.....	176
6.4.1	Pease AFB Embankment Toe Area.....	178

6.4.2 Pease AFB K_0 Area.....	184
6.4.3 Hamilton AFB Site.....	189
6.5 Summary.....	191
VII. TEST RESULTS: MEASUREMENT OF IN SITU STRESS-STRAIN BEHAVIOR.....	195
7.1 Introduction.....	195
7.2 SBPM Stress Paths.....	195
7.3 Undrained Shear Strength.....	200
7.3.1 Shear Strength at Pease AFB K_0 Site.....	202
7.3.1.1 Comparison of Methods.....	202
7.3.1.2 Effect of Failure Strain and Disturbance.....	207
7.3.1.3 Results of Push-In Tests.....	210
7.3.1.4 Effect of Inflation/Radial Strain Rate.....	213
7.3.1.5 Ménard Method.....	213
7.3.2 Shear Strength at Pease AFB Embankment Toe Site.....	215
7.3.2.1 Trend of s_u with Distance from Embankment.....	215
7.3.2.2 Ménard Method.....	219
7.3.2.3 Shear Strength from Shower Head Insertion.....	219
7.3.3 Shear Strength at Hamilton AFB.....	219
7.3.3.1 Comparison of Methods.....	219
7.3.3.2 Push-In and Re-Expansion Tests.....	224
7.3.3.3 Ménard Method.....	225
7.4 Shear Modulus.....	225
7.4.1 Shear Modulus at Pease AFB K_0 Area.....	225
7.4.2 Shear Modulus at Pease AFB Embankment Toe Site.....	235
7.4.3 Shear Modulus at Hamilton AFB.....	235
7.5 R_f by Denby and Clough Method.....	240
7.6 Skempton "A" Parameter at Failure.....	242
7.7 Consolidation Parameters.....	243
7.8 Summary.....	250
VIII. FINDINGS SPECIFIC TO THE 9-ARM SBPM.....	254
8.1 Introduction.....	254
8.2 Trend of Soil Strength and Stiffness with Depth..	254
8.3 Horizontal Stress from Upper/Lower Arms.....	258
8.4 Undrained Shear Strength from Upper/Lower Arms...	261
8.5 Unload/Reload Modulus from Upper/Lower Arms.....	266
8.6 Plane Strain and Axisymmetric Assumptions.....	269

8.7 Summary	275
IX. SUMMARY, CONCLUSIONS AND RECOMMENDATIONS.....	277
9.1 Summary of Research Activities.....	277
9.2 Summary of Research Findings.....	277
9.3 Conclusions With Regard to SBPM Use.....	281
9.4 Recommendations for Future Research.....	275
REFERENCES.....	285
APPENDIX A - FACTORS INFLUENCING SBPM MEASUREMENTS.....	292
A.1 Introduction.....	293
A.2 Factors Influencing Pore Pressure Measurements...	293
A.2.1 Instrumentation of the SBPM.....	293
A.2.2 Conventional Computation of SBPM Pore Pressures.....	293
A.2.3 Measurement Errors.....	295
A.2.3.1 Influence of Atmospheric Pressure.....	295
A.2.3.2 Influence of Temperature.....	299
A.2.3.3 Influence of System Resistance.....	303
A.2.3.4 Influence of Internal Humidity.....	303
A.2.3.5 Discussion.....	307
A.2.4 Determination of Excess Pore Pressures Due to Deployment.....	307
A.2.4.1 Description of the Method.....	307
A.2.4.2 Example Problem.....	308
A.2.4.3 Excess Pore Pressures for Research Test Results.....	310
A.3 Influence of Membrane Stiffness on Measurements.....	314
A.3.1 Introduction.....	314
A.3.2 Stiffness at Lift-Off.....	314
A.3.3 Membrane Stiffness After Lift-Off.....	324
A.3.4 Method for Correcting Membrane Stiffness...	326
A.3.4.1 Lift-Off Stiffness Correction.....	326
A.3.4.2 Post Lift-Off Stiffness Correction....	329
A.4 Drilling Rig Influence on SBPM Measurements.....	329
A.4.1 Introduction.....	329
A.4.2 Effect of SBPM Inclination.....	329
A.4.3 Effect of Drill Rig Weight.....	334
APPENDIX B - TABULATIONS OF SBPM CURVE RATING BY C_d METHOD.....	336
APPENDIX C - PLOTS OF PRESSUREMETER TESTS AND HOLDING TESTS....	343
APPENDIX D - PROFILES OF SBPM HORIZONTAL STRESS AND DILATOMETER I_d VALUES.....	412
APPENDIX E - USERS GUIDE TO PROGRAM SOSAP.....	423

LIST OF TABLES

SECTION	DESCRIPTION	PAGE
3-1	SBPM Cutting Insertion and Testing Parameters at Pease AFB (adapted from Atwood, 1990).....	50
3-2	SBPM Jetting Insertion and Testing Parameters at Pease AFB (adapted from Atwood, 1990).....	51
3-1	SBPM Jetting Insertion and Testing Parameters at Hamilton AFB (adapted from Atwood, 1990).....	52
4-1	Summary of Index Properties.....	63
4-2	Summary of Dilatometer c_v Values (after Nejame, 1991).....	75
4-3	Summary of Compressibility Data.....	82
4-4	Summary of Stress History Data.....	83
4-5	Summary of Triaxial Tests.....	89
4-6	Summary of Soil Properties (after Bonaparte and Mitchell, 1979).....	99
5-1	Summary of Hyperbolic Parameters.....	115
5-2	Hyperbolic Parameters of Fill Materials (after Boscardin, et al., 1990).....	117
5-3	Summary of Cam-Clay Properties for JFEST Input.....	127
6-1	Disturbance Ratio for K_0 Undisturbed Tests.....	141
6-2	Disturbance Ratio for Non- K_0 Undisturbed Tests.....	142
6-3	Disturbance Ratio for Push-In Tests.....	143
6-4	Disturbance Ratio for Re-Expansion Tests.....	144
6-5	Summary of Horizontal Stresses Measured at Pease K_0 Area.....	152
6-6	Summary of Horizontal Stresses Measured at Pease AFB Embankment Toe Area.....	161
6-7	Summary of Horizontal Stresses Measured at Hamilton AFB.....	174
7-1	Summary of Computed SBPM A_v Values.....	244
7-2	Summary of SBPM C_c Measurements.....	246
8-1	Summary of Maximum Test Strains for PMC4.....	255
8-2	Summary of Undrained Shear Strength from All 9 Arms in Boring PMC4.....	263
8-3	Summary of G_w from All 9 Arms in Boring PMC4.....	267
A-1	Excess Pore Pressure Variables.....	296
A-2	Summary of Computed Excess Pore Pressures.....	305
A-3	Summary of Mock Pressuremeter Results.....	315
A-4	Summary of Membrane Stiffness Experiment.....	323

LIST OF FIGURES

SECTION	DESCRIPTION	PAGE
2-1	Sketch of Ménard or Pre-Bored Pressuremeter.....	6
2-2	Typical Pressuremeter Curves From Different Pressuremeters (adapted from Lacasse, 1986).....	8
2-3	Sketch of SBPM (adapted from Wroth & Hughes, 1974)...	9
2-4	Jetting Deployment Setup (adapted from Benoit, 1987).....	11
2-5	K_0 from OCR and Plasticity Index (after Brooker and Ireland, 1965).....	15
2-6	Interpretation of Horizontal Stress in Self-Boring Pressuremeter Test (after Lacasse and Lunne, 1982).....	19
2-7	Mohr's Circle Representation of Stresses Around Probe as Measured by Three Strain Feeler Arms.....	20
2-8	Stress and Displacement Components of a Soil Element at Radial Distance r (after Fung, 1977).....	23
2-9	The Gibson and Anderson (1961) Undrained Shear Strength Method.....	28
2-10	The Sub-Tangent Undrained Shear Strength Method....	31
2-11	Determination of Φ' from p' - q Data.....	32
2-12	The Denby-Clough Undrained Shear Strength Method....	34
2-13	Modes of Undrained Deformation from Various Field and Laboratory Tests (after Wood and Wroth, 1977)...	36
2-14	Moduli Obtained from Pressuremeter and Triaxial Tests (adapted from Benoit, 1983).....	40
2-15	Determination of t_{50} from Holding Test (after Clarke, Carter and Wroth, 1979).....	43
2-16	Pore Pressures Adjacent to SBPM During Holding Test and Determination of T_{50}	45
3-1	Pressure Control Panel.....	54
4-1	Location of Field Test Sites.....	58
4-2	Site Location Map - Pease Air Force Base.....	59
4-3	Pease Air Force Base Test Site.....	61
4-4	Pease Air Force Base K_0 Area.....	66
4-5	Profile at Pease AFB K_0 Area.....	68
4-6	Profile at Pease AFB Embankment Toe Area.....	69
4-7	Profile of Field Shear Vane Data.....	71
4-8	Profile of I_p and Horizontal Stress, PMC3.....	74
4-9	Summary of Hydrostatic Pressure Measurements at Pease AFB K_0 Area.....	77
4-10	OCR Versus Normalized Shear Strength.....	84
4-11	Vertical Coefficient of Consolidation.....	85
4-12	Horizontal Coefficient of Consolidation.....	86
4-13	CU Triaxial Stress Paths - Normally Consolidated....	90
4-14	CU Triaxial Stress Paths - Overconsolidated.....	91
4-15	Site Location Map - Hamilton Air Force Base.....	93
4-16	Log of USGS Boring at Hamilton AFB (after Denby, 1978).....	95
4-17	Schematic Plan of Hamilton AFB Test Site (after Denby, 1978).....	96
4-18	Hamilton AFB Test Site Soil Property Profile (after Clough and Denby, 1980).....	98
4-19	SBPM Shear Strength Profile from Previous Research (after Benoit, 1983).....	101
5-1	Stage Construction Sequence of I-95 Highway Embankment.....	104

5-2	Axial Strain at 70 and 95 Percent Shear Strength....	109
5-3	Determination of Failure Ratio, R_f	110
5-4	Determination of Normalized Tangent Modulus, E_t	112
5-5	Incremental Coefficient of Lateral Earth Pressure During Unloading.....	114
5-6	SOILSTRUCT Finite Element Mesh.....	118
5-7	SOILSTRUCT Horizontal Stresses Due to Embankment Load.....	120
5-8	SOILSTRUCT Percent Horizontal Stress Increase Due to Embankment Load.....	122
5-9	Cam-Clay Model.....	124
5-10	Definition of Cam-Clay Parameters.....	125
5-11	Determination of Critical State Void Ratio.....	128
5-12	JFEST Finite Element Mesh.....	129
5-13	JFEST Horizontal Stresses Due to Embankment Load....	131
5-14	JFEST Percent Horizontal Stress Increase Due to Embankment Load.....	132
5-15	Comparison of SOILSTRUCT and JFEST Computed Horizontal Stress Increase Due to Embankment Load Versus Distance from Embankment Toe.....	134
6-1	Typical SBPM Pressuremeter Curves.....	137
6-2	Effects of Disturbance on Measured Horizontal Stress.....	139
6-3	Minimum and Maximum Total Horizontal Stress Profiles at Pease K_0 Area.....	150
6-4	Pease AFB K_0 Area SBPM Total Horizontal Stress Profile.....	156
6-5	I_p and Horizontal Stress Profile, PMC3.....	158
6-6	Pease AFB SBPM Profile of K_0	159
6-7	Minimum and Maximum Measured Total Horizontal Stress at PMJ6 Compared to K_0 Area.....	162
6-8	Minimum and Maximum Measured Total Horizontal Stress at PMJ7/PMJ8 Compared to K_0 Area.....	164
6-9	Comparison of PMJ6 Measured Horizontal Stress to FEM Predictions.....	165
6-10	Comparison of PMJ7/PMJ8 Measured Horizontal Stress to FEM Predictions.....	167
6-11	Stress Decrease with Distance from Toe of Highway Embankment.....	168
6-12	Percent Increase in Total Horizontal Stress at Toe Due to Embankment Construction.....	169
6-13	Total Horizontal Stress at Hamilton AFB from Previous Research.....	171
6-14	K_0 at Hamilton AFB.....	172
6-15	SBPM Total Horizontal Stress at Hamilton AFB.....	175
6-16	Horizontal Stress from All Arms Compared to Benoit (1983).....	177
6-17	Horizontal Stress Results from All Middle Arms at Highway Embankment Toe.....	180
6-18	Principal Stresses at Highway Embankment Toe.....	181
6-19	Direction of Major Principal Stress for All Arm Tiers at Highway Embankment Toe.....	182
6-20	Plan View of SBPM Principal Stress Orientation at Pease AFB Test Sites.....	183
6-21	Profile of Minimum and Maximum Principal Stresses at Pease K_0 Area.....	185
6-22	Minimum and Maximum Principal Stresses from All Tests at Pease K_0 Area Stress at Pease K_0 Area.....	187
6-23	Profile of Direction of Maximum Principal Stress at Pease K_0 Area.....	188
6-24	Major and Minor Principal Stress at Hamilton AFB....	190
6-25	Strike of Major Principal Stress at Hamilton AFB....	192

7-1	Typical Total Stress Paths.....	196
7-2	Typical Effective Stress Paths.....	198
7-3	Typical Gibson and Anderson (1961) Shear Strength Determination Plot.....	201
7-4	Undrained Shear Strength Profile at Pease K_v Area.....	203
7-5	Comparison of Gibson and Anderson 5 to 10 and 2 to 5 Percent Volumetric Strain Results at K_v Area.....	205
7-6	Comparison of Shear Strength Uncorrected and Corrected by Yeung and Carter Method at K_v Area.....	206
7-7	Triaxial Failure Strain Versus OCR for Pease AFB Silty Clay.....	208
7-8	Effect of Insertion Disturbance on Pressuremeter Curve.....	211
7-9	Push-In Shear Strength at Pease AFB.....	212
7-10	Effect of Strain Rate on Measured Undrained Shear Strength.....	214
7-11	Comparison of SBPM Shear Strength Profiles at Pease Embankment Toe and K_v Area.....	216
7-12	Comparison of SBPM Shear Strength Profiles at PMJ6 and PMJ7/PMJ8.....	218
7-13	Shear Strength at Hamilton AFB.....	221
7-14	Sub-Tangent and Denby and Clough Method SBPM Shear Strength at Hamilton AFB.....	223
7-15	Unload/Reload Modulus Profile at Pease K_v Area.....	226
7-16	Unload/Reload Modulus Versus Radial Strain at Pease K_v Area.....	228
7-17	Effect of Strain at Which G_w Occurs Within a Particular Test.....	230
7-18	G_w from all Borings at Pease K_v Area.....	232
7-19	Profile of G_i and G_w at Pease K_v Area.....	234
7-20	G_w at Pease Embankment Toe Area.....	236
7-21	Profile of G_i and G_w at Pease Embankment Toe Area...	237
7-22	Shear Modulus at Hamilton AFB.....	238
7-23	R_f Profiles at Current Research Test Sites.....	241
7-24	Results of Holding Test PMC3.2H.....	247
7-25	Profile of Horizontal Coefficient of Consolidation..	249
8-1	Use of Trend of Maximum Test Strain to Predict Trend of Shear Strength Versus Depth.....	257
8-2	Typical Plot of Field Test TP Versus PPB (Test PMC4.2).....	260
8-3	Profile of Shear Strength from All 9 Arms.....	264
8-4	Ratio of s_u from Upper/Lower Arms to s_u from Middle Arms Versus Depth.....	265
8-5	Profile of G_w Versus Depth for All 9 Arms in Boring PMC4.....	270
8-6	G_w Versus Strain for All 9 Arms in Boring PMC4.....	270
8-7	Non-Radial and Axial Components of Strain During SBPM Expansion.....	273
A-1	Schematic of an Effective Stress Cell (after Benoit, 1983).....	294
A-2	TP, PPA and PPB Versus Barometric Pressure.....	300
A-3	Time for Temperature Adjustment of SBPM to Warm Bath.....	301
A-4	TP, PPA and PPB Versus Probe Temperature.....	302
A-5	TP Versus PPB at Atmospheric Pressure.....	304
A-6	Air Expansion, PPB Versus TP.....	309
A-7	Pore Pressures Versus Insertion Rate.....	311
A-8	Schematic of Mock Pressuremeter.....	313
A-9	Excess Pore Pressure Versus Insertion Rate.....	316

A-10	Components of Stiffness Correction.....	317
A-11	Schematic of Pressuremeter Chamber (after Mayu, 1987).....	318
A-12	Stiffness Effects of Confinement, No Chinese Lantern.....	320
A-13	Stiffness Effects of Confinement, With Chinese Lantern.....	321
A-14	Forced First Lift-Off.....	322
A-15	Pressuremeter Curves for Typical Air Expansions.....	325
A-16	Effects of Confinement Pressure.....	327
A-17	Effects of Interface Friction.....	328
A-18	Effect on δ_v' of SBPM Inclination.....	330
A-19	Determination of δ_v' from Mohr's Circle.....	332
A-20	The Effect of SBPM Inclination on Measured Lateral Stress.....	333
A-21	Schematic Plan of Borehole and Drill Rig Skids.....	335
E-1	Configuration of SBPM.CAL File.....	426
E-2	Structure of Reduced Data Output File.....	430

LIST OF SYMBOLS

SYMBOL	DESCRIPTION
γ	Unit weight (weight per cubic length)
ϵ_c	Cavity strain (unitless)
ϵ_θ	Tangential strain (unitless)
ϵ_r	Radial strain (unitless)
ϵ_z	Vertical strain (unitless)
κ	Unload/reload slope for Cam Clay model (unitless)
λ	Virgin compression slope for Cam Clay model (unitless)
μ	Poisson's Ratio (unitless)
σ_1	Major principal stress (units of pressure)
σ_2	Intermediate principal stress (units of pressure)
σ_3	Minor principal stress (units of pressure)
σ_{min}	Minimum Stress (units of pressure)
σ_{max}	Maximum Stress (units of pressure)
σ_θ	Tangential stress (units of pressure)
σ_{ppa}	Pressure measured by the PPA transducer (units of pressure)
σ_{ppb}	Pressure measured by the PPB transducer (units of pressure)
σ_{ppbc}	Computed test zero for PPB transducer (volts)
σ_{ppbd}	PPB transducer reading prior to starting test (volts)
σ_{ppbd0}	PPB transducer reading prior to start of surface calibration expansion (volts)
σ_r	Radial stress (units of pressure)
σ_{tp}	Pressure measured by the TP transducer (units of pressure)
σ_{tp0}	TP transducer reading prior to starting test (volts)
σ_{tpd0}	TP transducer reading prior to start of surface calibration expansion (volts)
σ_z	Vertical stress (units of pressure)
τ	Shear stress (units of pressure)
Φ'	Drained Friction Angle (degrees)
A_f	Skempton A parameter at failure (unitless)
c	Cohesion (units of pressure)
c'	Effective cohesion (units of pressure)
C_b	Horizontal coefficient of consolidation (units of length per time)
c/p	Normalized shear strength (unitless)
C_u	Undrained shear strength (units of pressure)
C_v	Vertical coefficient of consolidation (units of length per time)
C_c	Compression index (unitless)
C_d	Disturbance ratio (unitless)
C_r	Recompression index (unitless)
e	Void ratio (unitless)
e_0	Initial void ratio (unitless)
e_{sc}	Critical state void ratio for Cam Clay model (unitless)
E	Youngs Modulus (units of pressure)
E_i	Initial tangent modulus (units of pressure)
E_t	Tangent modulus (units of pressure)
E_{ur}	Unload/reload modulus (units of pressure)
G	Shear modulus (units of pressure)
G_i	Initial shear modulus (units of pressure)

G_w	Unload/reload shear modulus (units of pressure)
I_d	Dilatometer soil identification parameter (unitless)
k	Coefficient of hydraulic conductivity (units of length per time)
k_h	Horizontal coefficient of hydraulic conductivity (units of length per time)
k_v	Vertical coefficient of hydraulic conductivity (units of length per time)
K	Modulus parameter for Duncan and Chang model (unitless)
K_o	At-rest ratio of horizontal to vertical effective stress (unitless)
K_o^Δ	Lateral stress change ratio for Duncan and Chang model determination of E_w (unitless)
K_w	Unload/reload modulus parameter for Duncan and Chang model (unitless)
LL	Liquid limit (percent)
M	Slope of critical state line for Cam Clay model (unitless)
M	Slope of PPB output voltage versus TP output voltage from surface calibration (unitless)
n	Modulus parameter for Duncan and Chang model (unitless)
N	Ménard correction factor (unitless)
OCR	Overconsolidation Ratio (unitless)
P_a	Atmospheric pressure (units of pressure)
ΔP	Change in pressure (units of pressure)
PI	Plasticity index (percent)
P_L	Limit pressure (units of pressure)
PL	Plastic limit (percent)
P_o	Horizontal stress (units of pressure)
P_o'	Effective horizontal stress (units of pressure)
P_p'	Maximum past pressure (units of pressure)
r	Pressuremeter radius (units of length)
r_1	Highest lift-off pressure (units of pressure)
r_2	Intermediate lift-off pressure (units of pressure)
r_3	Lowest lift-off pressure (units of pressure)
r_m	Maximum radius of holding test (units of length)
r_o	Radius of pressuremeter (units of length)
r_p	Radius to outer limit of plastic zone (units of length)
r_u	Expanded pressuremeter radius (units of length)
R_f	Failure ratio (unitless)
s_u	Undrained shear strength (units of pressure)
s_{um}	Gibson and Anderson s_u (units of pressure)
t_{50}	Time for 50 percent consolidation (units of time)
T_{50}	Time factor for 50 percent consolidation (unitless)
u	pore pressure (units of pressure)
Δu	Excess pore pressure (units of pressure)
Δu_{max}	Maximum excess pore pressure (units of pressure)
u_θ	Tangential displacement (units of length)
u_o	Initial pore pressure (units of pressure)
u_r	Radial displacement (units of length)
V	Current volume (units of volume)
ΔV	Change in volume (units of volume)
V_o	Initial volume (units of volume)
Z	Vertical distance from edge of cutting shoe to center of jetting orifice (inch)

CONVERSION FACTORS

To convert from:	To:	Multiply by:
in	cm	2.540000
in	m	0.025400
ft	m	0.304800
gallon (U.S. liquid)	m ³	3.785412 x 10 ⁻³
gram	dyne	980.665000
kg (force of mass)	N	9.806650
lb (mass)	kg (mass)	0.453592
lb/ft	kg/m	1.488164
kg (force of mass)	N	9.806650
kg/m	N/m ² (pascal)	9.806650
kg/cm ²	kN/m ² (kPa)	98.066500
lb/in ² (psi)	kN/m ²	6.894757
lb/ft ² (psf)	kN/m ²	0.047880
ft·lb	N·m	1.355818
lb/ft ³ (pcf)	kg/m ³	16.018460
g/cm ³	lb/ft ³	62.427900
g/cm ³	kN/m ³	9.806650
cm ² /sec	ft ² /day	2834.64
cm ² /sec	ft ² /year	3.39447 x 10 ⁴

ABSTRACT

USE OF THE 9-ARM SELF-BORING PRESSUREMETER TO MEASURE
HORIZONTAL IN SITU STRESS, STRESS ANISOTROPY,
AND STRESS-STRAIN BEHAVIOR IN SOFT CLAY

by

R. Craig Findlay
University of New Hampshire, May, 1991

Self-boring pressuremeter (SBPM) tests were conducted at Interstate I-95 in Portsmouth, New Hampshire and Hamilton Air Force Base in Novato, California, in clays of low and high plasticity, respectively. Both sites were subjects of significant previous research.

Field testing, conducted at and away from the toe of an existing highway embankment, indicated that the SBPM is capable of measuring horizontal stress changes and stress anisotropy when stress differences are more significant than the measurement error of the test equipment and error due to insertion disturbance effects. Finite element modeling was used to assess the embankment stress effects as a basis for comparison to the SBPM measured horizontal stresses. The SBPM was used to evaluate shear strength, shear modulus, the horizontal coefficient of consolidation, and other stress-strain parameters in both K_0 and non- K_0 stress conditions. SBPM shear strength was found to be significantly greater than field vane results at Pease AFB, however, SBPM and vane results were similar at Hamilton AFB. These results seem to indicate that clays which mobilize peak strength at high strain are better suited to SBPM shear strength measurement than clays that peak at low strain.

A 9-arm Cambridge SBPM was used for the field testing which allowed improved definition of cavity deformation compared to conventional 3-arm versions. The 9-strain arms of the probe were found to be useful in predicting the trend of shear strength with depth. The results from the extra arms also suggest that the effect of deviation from plane strain

conditions due to the limited length of the probe may not affect shear strength results to the extent previously reported.

Laboratory testing was conducted to assess mechanical characteristics and environmental effects on the SBPM. Findings from these tests facilitated development of a method of assessing excess pore pressures due to SBPM deployment and improvements to conventional membrane stiffness correction necessary for accurate horizontal stress determination.

CHAPTER I

INTRODUCTION

The science of Geotechnology has advanced rapidly with respect to the available methods of analysis. At the present time, several different constitutive models of varying complexity exist for assessment of the influence of stress changes on the strain and stress behavior of soil. In each of these models, the initial stress condition is the starting point of analysis. In contrast to the advanced state of constitutive modeling and its application in numerical analysis, determination of the initial stress condition remains one of the most difficult measurements to be made in geotechnical practice. The difficulty in measurement is a consequence of disturbance which inevitably results from sampling and laboratory testing or, alternatively, from installation of a measurement device into the soil. Even the small amount of disturbance due to displacement of soil around very thin stress measuring devices such as the Glötzl stress cell has been found to result in significant errors in field stress measurements. To address the soil disturbance problem, the self-boring pressuremeter (SBPM) was developed with much fanfare in the early 1970's by two separate research teams. The SBPM is a long cylindrical device which is tunneled into the ground to the depth at which a measurement is desired, ideally without displacement or disturbance of the surrounding soil. Once in place, measurements of in situ stress and stress-strain behavior of the surrounding soil can be made by expanding a rubber-like membrane which covers the probe. This expansion is caused by increasing the internal pressure within the probe. The internal pressure and resulting radial deformation (shear) of the soil are monitored during the test. The resulting pressure-displacement data can then be theoretically analyzed to quantify in situ stress and stress-strain behavior.

However, the results of the SBPM have been somewhat mixed. Although the principle of installation by tunneling is theoretically good, the results are markedly affected by the method by which this installation is performed. As more is understood about the SBPM, and uniform testing procedures develop, it is expected that results will become more dependable. It is hoped that the findings of this research will contribute to that evolution. The objectives of the research presented in this dissertation were as follows:

- 1) Evaluate the use of the SBPM to measure lateral stresses in both K_0 and non- K_0 environments.
- 2) Evaluate the ability of the SBPM to measure consolidation characteristics of soft soil.
- 3) Evaluate the influence of disturbance on stress-strain behavior.
- 4) Use the data from the 9-strain measuring arms to assess the plane strain assumption for cavity expansion. Also assess the use of the additional data provided by the 9-arm device over the conventional 3-arm device.

The research summarized in this dissertation involved using the SBPM at two separate soft clay test sites. The test sites are located at Pease Air Force Base in Portsmouth, New Hampshire, and Hamilton Air Force Base in Novato, California. The primary test site was at Pease AFB. This site was chosen because significant, well-documented geotechnical engineering and performance monitoring had previously been conducted near the test area for design and construction of the Interstate I-95 Portsmouth Traffic Circle Interchange. In addition, the proximity of the site to the University of New Hampshire campus was a major logistical benefit. A significant laboratory test program was carried out as part of this research on undisturbed samples from the Pease AFB test site. Testing included 29 one-dimensional consolidation and 12 triaxial compression tests as well as numerous standard index tests. Also, as a basis for determining the influence of the Interstate

I-95 highway embankment on SBPM measurements of lateral stress, finite element modeling (FEM) using two codes was undertaken.

An opportunity for two days of field testing at Hamilton AFB materialized toward the end of the research field effort. Hamilton AFB had the benefit of significant, well-documented, previous field and laboratory testing research by both Stanford and U.C. Berkeley, including two previous SBPM programs, one of which was conducted by the writer's advisor.

The research presented in this dissertation differs from previous work in a number of ways. First, SBPM testing was performed with a 9-arm pressuremeter rather than the conventional 3-arm model. The extra arms allow better assessment of the shape of the expanding soil cavity which, in analysis, is assumed to develop radially and uniformly around and along the probe body.

The field testing at Pease Air Force Base was conducted in both K_0 and non- K_0 stress conditions. A K_0 stress condition exists when in situ stresses in a soil mass result from natural soil deposition under gravity forces with a level ground surface, while a non- K_0 stress condition results when a sloped ground surface exists or when the natural stress condition has been altered (e.g., at the toe of a soil embankment as is the case at Pease Air Force Base). Testing in soil under these two stress conditions allowed assessment of whether the SBPM is applicable for accurate measurement of the direction of the major principal stress in the horizontal plane. Further, use of the probe in both K_0 and non- K_0 situations allowed assessment of the effect of stress anisotropy on measurement of stress-strain behavior.

Use of the SBPM for measurement of stress anisotropy required reassessment of the conventional methods of calibration in an effort to increase measurement accuracy. As a result of this reassessment, new approaches to correcting for lift-off and expansion stiffness of the membrane are proposed and used. Finally, an assessment of excess pore pressure due to installation of the SBPM to test depth was made and a

method for correction for such pore pressure was developed and used.

This dissertation has been formatted into 9 chapters and 5 appendices. The history of the development of the SBPM and related technology is presented in Chapter II. Chapter III discusses the operation of the 9-arm SBPM used for the field testing program. The field test sites are described in Chapter IV, including a discussion of geologic history and the results of current and previous laboratory testing programs. Field testing, both previous and current is also described. Finite element analysis of the highway embankment adjacent to the Pease AFB site is described in Chapter V. The results of stress and stress-strain measurements using the SBPM are presented in Chapters VI and VII, respectively, and the findings with regard to these issues specific to the use of the 9-arm version of the SBPM are presented in Chapter VIII. Conclusions of the research and recommendations for future investigation are summarized in Chapter IX. The Appendices of this dissertation include a detailed discussion pertaining to the calibration and test effect findings of the research (Appendix A). Appendices B and C present tabulations and plots of the SBPM results. Appendix D presents profiles of each of the Pease AFB SBPM borings along with profiles of dilatometer I_d values. I_d values are an index determined by the flat dilatometer, and can be used to estimate soil stratigraphy. These profiles were developed to observe soil layering at the Pease Site which was reflected in some of the SBPM results. Finally, Appendix E presents a user's manual for the PC-compatible program SOSAP used to reduce the SBPM data.

CHAPTER II

SELF-BORING PRESSUREMETER AND RELATED TECHNOLOGY

2.1 History of the Pressuremeter

The pressuremeter is an in situ testing device which has evolved over the past sixty or so years into a highly sophisticated soil testing tool used to measure the in place stress-strain behavior of soil. Initial development of the pressuremeter is generally credited to Ménard (1956), although a crude version is reported to have been experimented with by Kögler in 1933. However, even before Kögler, Ktatorov (1930) described how radial expansion of a cast-in-place concrete pile in soil could be quantified to extrapolate soil compactness.

The pressuremeter is cylindrical shaped, one end of which concentrically attaches to drill rods. It is either inserted into a pre-existing borehole, or alternatively is itself drilled or pushed into the ground to the desired test depth. A pressuremeter test is conducted by expanding (with gas or fluid pressure) the elastic membrane which covers the probe. The membrane expands outward into the side of the borehole, deforming the soil laterally in shear. Expansion can be strain or stress controlled, and when stress controlled, pressure can be applied either incrementally or continuously. Depending on the sophistication of the test device, measurements of volume change or lateral strain (with strain measuring arms) are made so that the progress of membrane expansion versus pressure increase can be monitored.

Early in its development, the pressuremeter was exclusively inserted into a pre-drilled borehole. The first modern pressuremeter, developed by Ménard (1956), is schematically pictured in Figure 2-1. Ménard developed this version of the pressuremeter at the University of Illinois under the guidance of Dr. Ralph Peck, and since then it has been marketed and used in France and throughout the world. Originally, the

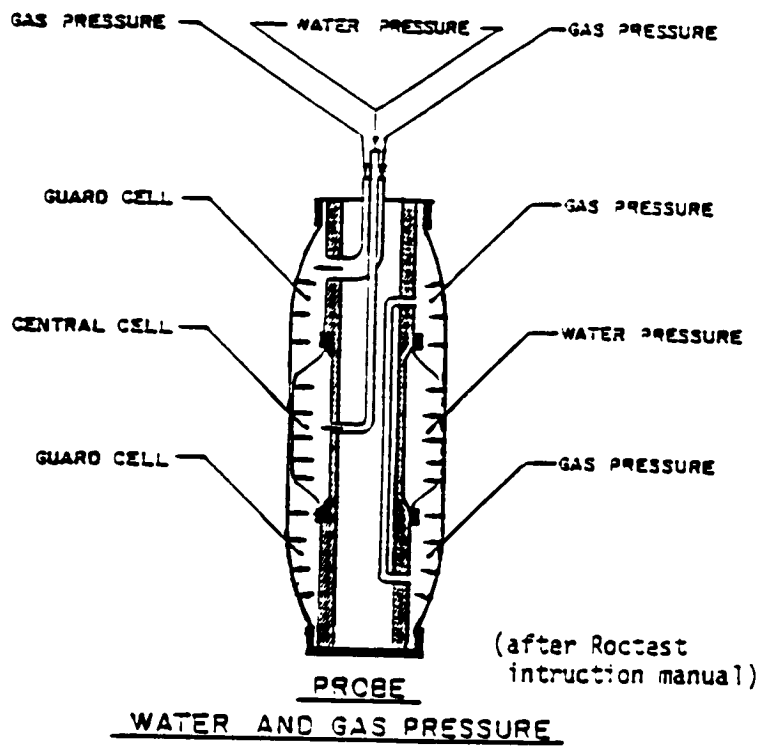
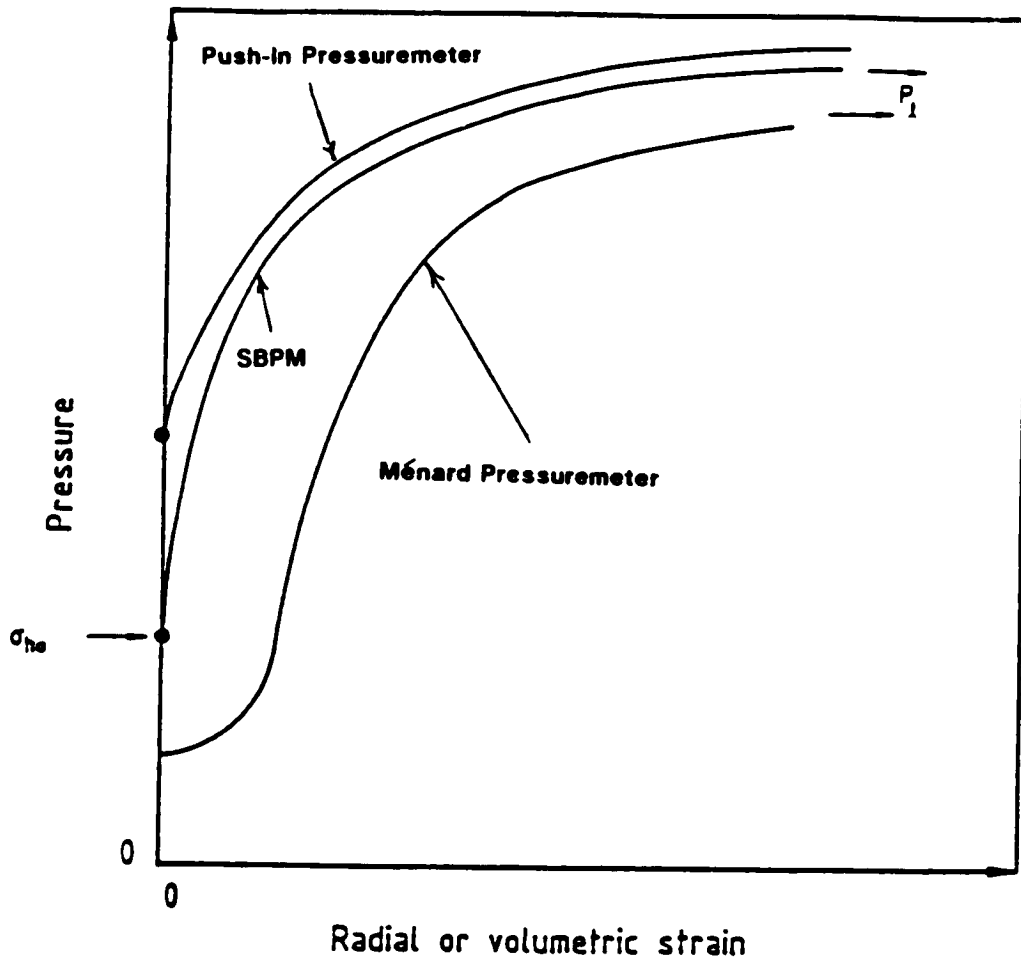


Figure 2-1 Sketch of Ménard or Pre-Bored Pressuremeter

Ménard pressuremeter was a mono-cell device. Because this device was relatively short, the top and bottom of the membrane which are rigidly attached to the body of the probe caused end stiffness which adversely affected the test results. To address the end effect problem, Ménard developed a tri-cell pressuremeter, consisting of a measuring cell and two guard cells as shown on Figure 2-1. The guard cells are above and below the measuring cell. The guard cells permit the measuring cell to deform only outward, rather than up or downward, in an effort to maintain plane strain conditions. Even with this improvement, some inherent problems exist with the Ménard pressuremeter, since the probe is inserted into a pre-drilled borehole. The problems of pre-drilling a borehole are that drilling introduces soil disturbance; removing the soil from the borehole causes stress relief, and the drilling process can affect soil moisture content (and thus void ratio and strength). Consequently, interpretation of the results of the Ménard pressuremeter is empirical. A typical plot of expansion pressure versus volumetric or radial strain (called a pressuremeter curve) from a Ménard pressuremeter is included on Figure 2-2. Stress relief due to pre-drilling of the borehole is evidenced by the initially flat portion of the pressuremeter curve, indicating little resistance to outward deformation of the pressuremeter membrane.

Because of the problems associated with pre-drilling of a borehole, a new type of probe, called the Self-Boring Pressuremeter (SBPM) was developed. The SBPM was simultaneously developed in France by Baguelin, Jézéquel, and Lémée (1972) and in England by Wroth and Hughes (Hughes, 1973). The French version is called the Pressiomètre Autoforeur (PAF for soft soils and PAFSOR for stiff soils) and the English version as shown in Figure 2-3 was originally called the Camkometer (Cambridge K_c Meter), although it is now simply called SBPM (currently, a Camkometer is a pressuremeter-like device that expands rigid plates into the soil rather than a flexible membrane). The idea behind the self-boring pressuremeter is that if the probe could be inserted into the soil with minimal



σ_{ho} = In situ horizontal stress
 P_l = Limit pressure

Figure 2-2 Typical Pressuremeter Curves From Different Pressuremeters (adapted from Lacasse, 1986)

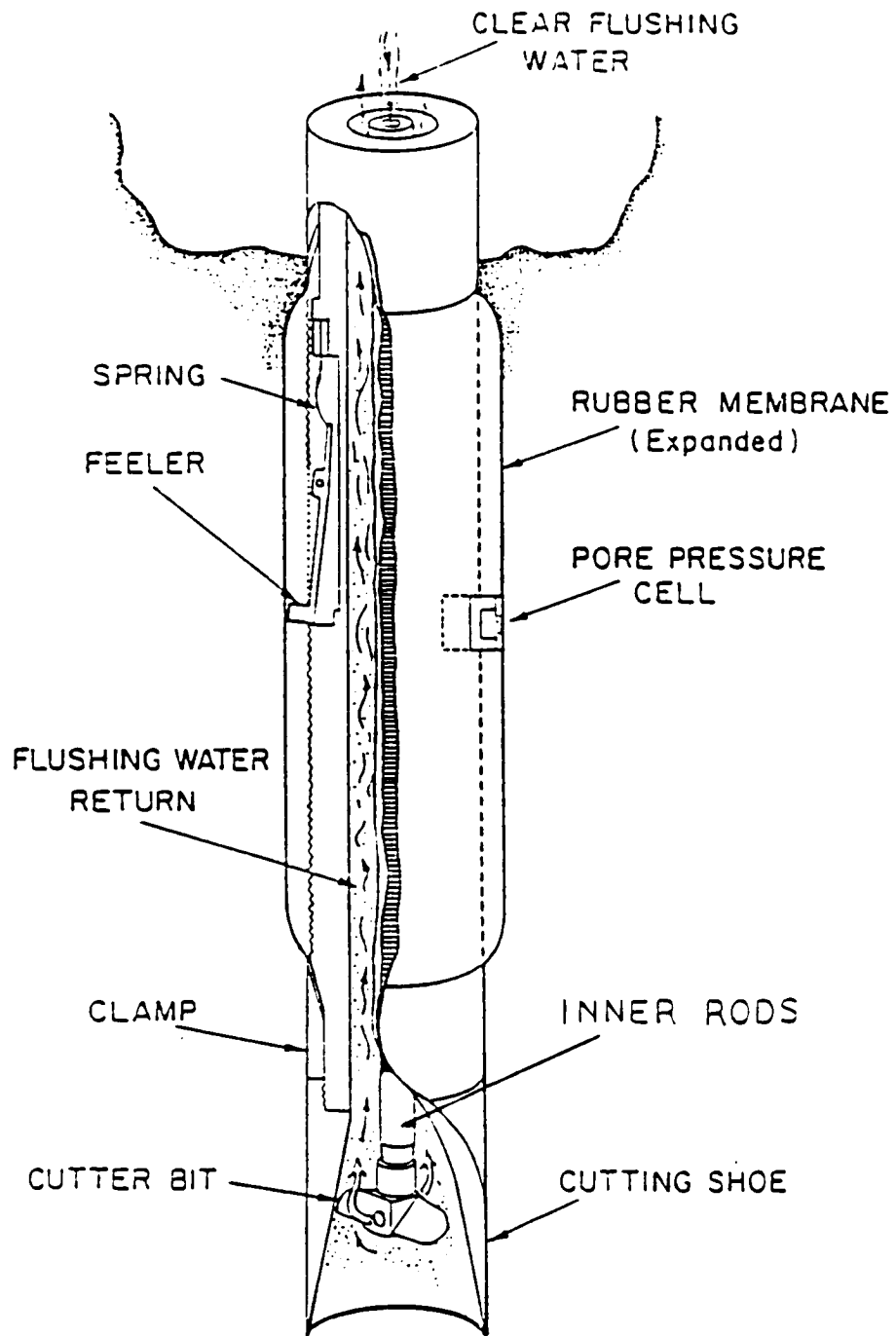


Figure 2-3 Sketch of SBPM (adapted from Wroth and Hughes, 1974)

disturbance and soil displacement, and without allowing the stress relief of pre-drilling, much higher quality test data could be obtained allowing theoretical interpretation of the test results. A typical pressuremeter curve from an SBPM test is included on Figure 2-2. It is seen that the initial portion of the curve is significantly steeper than that from a Ménard test, and that radial strain begins when the expansion pressure (correcting for membrane stiffness) is equal to the in situ horizontal stress.

The English SBPM is cylindrical shaped, about 3-inches in diameter and approximately 4-feet long. A 24-inch length of the probe is covered by a thin (1/8-inch or less) seamless elastic membrane, typically made of a rubber-like material called adiprene. The top of the probe is connected to a drill string, and the bottom of the probe is fitted with a sharp cutting shoe.

Conventionally, the SBPM has been advanced to test depth using the cutting procedure. Insertion using the cutting procedure is done by a combination of downward pressure on the drill string and cutting action of a rotating chopping bit located just inside the cutting shoe as indicated on Figure 2-3. The chopping bit is rotated via a string of hollow rods (called "inner" rods) inside the drill casing as indicated on the figure. These inner rods are rotated at the surface by means of a pneumatic drive while water is simultaneously pumped down the hollow of the inner rods to flush away the cuttings at the chopping bit. The downward pressure exerted on the casing causes the SBPM to move downward, pushing the cutting shoe into the soil. The soil entering the shoe is cut by the rotating cutting blades and washed to the surface through the annulus between the casing and the inner rods. Previous research (Benoit, 1983) has indicated that the rate of advancement of the SBPM into the ground and set-back of the chopping bit affect the degree of disturbance that occurs during insertion and must be optimized. This is generally a trial and error procedure.

As an alternative to the cutting, a method employed by Hughes,

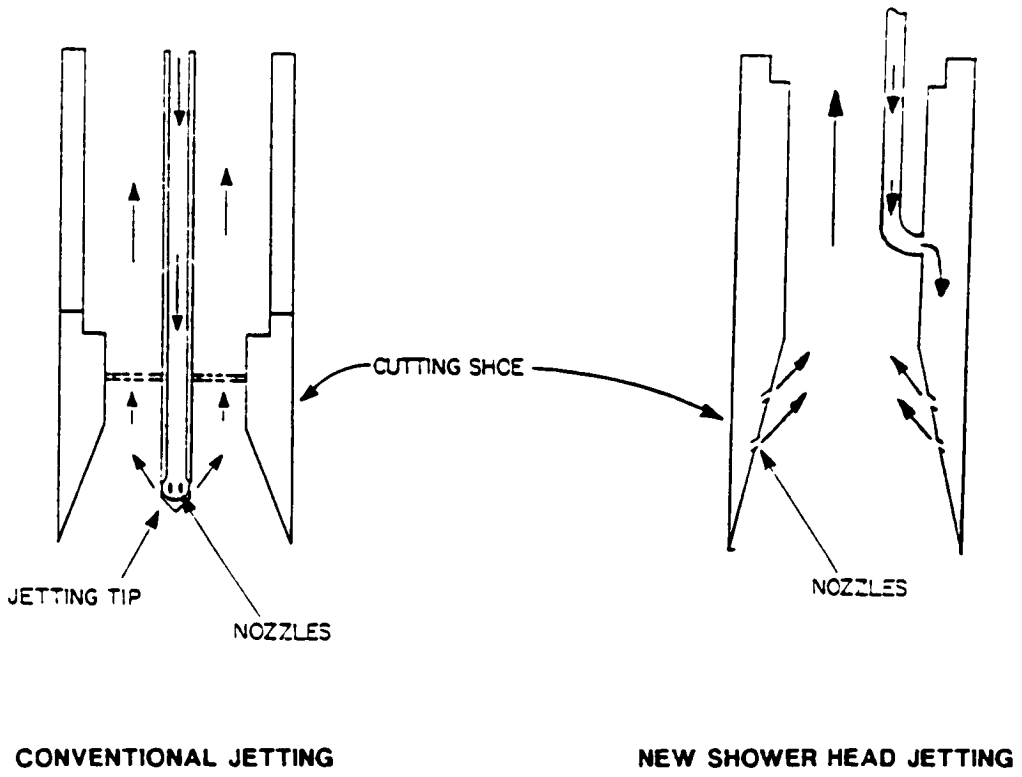


Figure 2-4 Jetting Deployment Setup (adapted from Benoit, 1987)

Jefferies, and Morris (1984) involves using jets of high velocity water (rather than a chopping bit) to break up the soil within the shoe. This type of insertion technology was previously used in the mid 1970's by British and French research groups (Baguelin, et al., 1978, and Powell, 1990). Insertion using the jetting method is done by pumping water down the drill rod and into a central tube which runs through the probe to the jetting tip as indicated in the first frame of Figure 2-4. The holes in the jetting tip constrict the water flow which greatly increases the flow velocity. The holes in the tip are pointed to cause the resulting jets of water to be directed upward into the probe, to mitigate soil disturbance below or outside of the cutting shoe. The water is pumped at a flow sufficient to cause the resulting jet to cut and remove the soil that enters the cutting shoe as a result of downward pressure applied to the drill rods to advance the probe. The cut soil fragments (actually a slurry) flow upward through the probe, up the borehole and to the ground surface. Similar to the set-back of the chopping bit, rate of probe advance and the set-back of the tip have been reported to be key parameters in undisturbed insertion (Atwood, 1990). Atwood further reported that the velocity of the water jets is also critical.

A second jetting method was recently developed and designed by Dr. Jean Benoit. Rather than water streams emitted from center jetting rod as in conventional jetting, the water streams are radial inward and upward, from the sidewall of the cutting shoe as indicated in the second frame of Figure 2-4. This method is similar to that previously reported by Baguelin, et al. (1978). All other aspects of this new jetting technique are the same as the conventional jetting method. The advantage of the new method is that without the central jetting rod, larger stones could be encountered without resulting in a blockage of water flow or cutting efficiency.

In addition to cutting and jetting insertions, the pressuremeter can also be advanced to test depth by pushing (push-in insertion), without tunneling into the soil. This method causes displacement of soil

around the outside of the probe. A typical pressuremeter curve from a push-in test is included on Figure 2-2. As can be seen, radial strain of the pressuremeter membrane begins at an expansion pressure somewhat greater than an SBPM test, and thus greater than the in situ horizontal stress.

Whether advanced by cutting, jetting, or push-in techniques, once the probe is at test depth, the drilling is stopped and the excess pore pressures developed around the probe due to insertion allowed to dissipate to some extent. In previous research, dissipation periods of over 75 minutes (Benoit, 1983) to over 3 hours (Denby, 1978) have been observed prior to initiating an expansion test.

The results of the SBPM test can be used to measure and/or evaluate: lateral horizontal stress, soil moduli, shear strength parameters and in some cases, the horizontal coefficient of consolidation. Methods of interpretation of test results have been devised by several different researchers; many of these procedures are summarized by Lacasse (1986), and Mair and Woods (1987). Later sections in this chapter review these methods as they apply to soft clays.

2.2 In Situ Horizontal Stress

2.2.1 Estimation and Measurement Technology

Determination of in situ horizontal stress, or the stress acting along the horizontal plane in a soil mass, is one of the more significant measurements that can be made with the SBPM. Many researchers (Clough, Briaud, and Hughes, 1990; Lacasse, D'orazio and Bandis, 1990) believe that the SBPM is the only tool which can measure this parameter with a high degree of accuracy.

Because of difficulties in measurement of in situ horizontal stress, empirical methods are often employed to provide estimates. In general, these methods are used to derive the ratio of horizontal to vertical effective stress. Effective horizontal stress is then estimated by computing the effective vertical stress using a profile of the unit weight of the overburden soil and multiplying by the ratio.

The ratio of horizontal to vertical effective stress can be estimated by several methods. Jaky (1944) presented the following well-known empirical formula:

$$K_0 = 1.0 - \sin \phi' \quad (\text{Eq 2-1})$$

where: ϕ' = drained friction angle

This formula is used to estimate K_0 of normally consolidated soils. Brooker and Ireland (1965) noted by statistical analysis of data from numerous sites that K_0 seems to increase with plasticity index (PI). This data was used to derive the family of curves shown on Figure 2-5, which can be used to estimate K_0 . Other researchers, including Massarsch (1979), Schmidt (1966) and Mayne and Kulhawy (1982) have posed other relationships which appear to work well.

As a basis for assessment of the adequacy of the empirical methods and the inherent desire of engineering practice to measure rather than empirically estimate, methods of field measurement of in situ horizontal stress have been developed in the past 20 years. Wroth (1975) has indicated that there are basically three proven techniques for measurement of in situ horizontal stress. These include total pressure cells, hydraulic fracture tests, and pressuremeter tests.

The use of total pressure cells to measure in situ stress requires installation by direct pushing of the instrument into the soil. This installation results in displacement of soil and as a result, in situ stresses are changed from the undisturbed stress condition. The best form of push-in pressure cell consists of a thin blade on which a stress transducer is flush mounted. Such push-in cells include the Glötzl pressure cell (Wroth, 1975). This type of cell is superior because it is relatively thin and spade-shaped, which limits soil displacement during insertion. However, because some displacement does occur, it is likely that measured stresses would be somewhat higher than actual in situ stresses. Tedd and Charles (1983) have developed an empirical

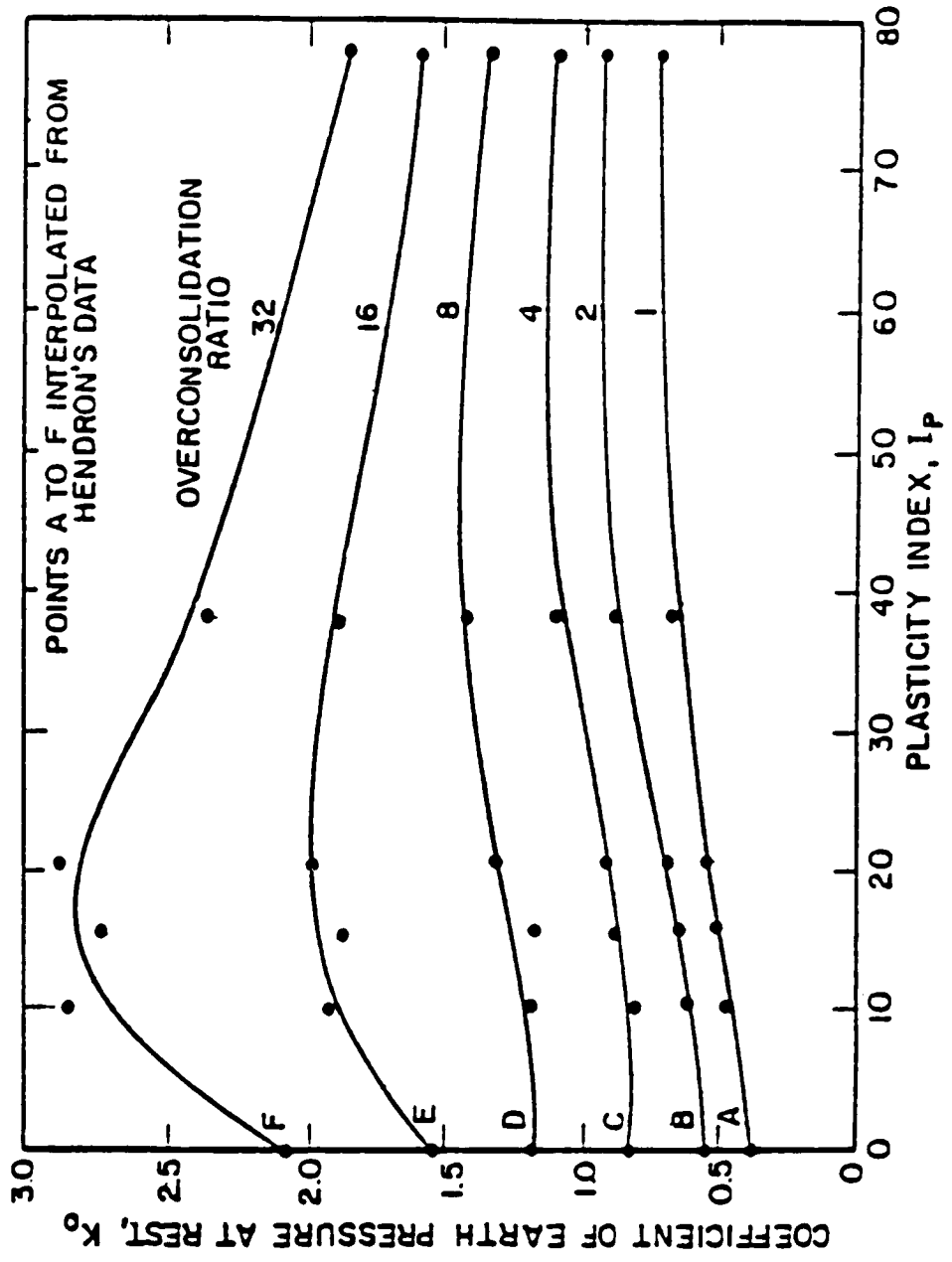


Figure 2-5 K_0 from OCR and Plasticity Index (after Brooker and Ireland, 1965)

correction of horizontal stress determined by Glötzl type total pressure cells for insertion disturbance based on soil shear strength. This correction is in the form of an over reading and becomes more significant as the soil stiffness increases.

Hydraulic fracture by injection of pressurized water through a piezometer tip has also been used to measure in situ horizontal stress. However, because of disturbance due to installation of the piezometer tip, soil layering and the potential for leakage of the piezometer-ground seal, the horizontal stress indicated by the hydraulic fracture method is typically erratic and unrepeatable. Direct comparisons made by Massarsch (1975) have indicated that the Glötzl cell measurements of in situ lateral stress are more consistent and representative than those measured by hydraulic fracture. Tavenas (1975) has indicated similar findings.

The pressuremeter is another method for measuring lateral stress in the soil. Baguelin, et al. (1974) conducted a series of tests to compare lateral stresses measured by the SBPM with those of a self-boring total pressure cell (SBPC) and the hydraulic fracture test. Generally, good agreement between the SBPM and the SBPC were observed, and the values were generally less than those determined by hydraulic fracture. While the SBPC may sometimes give good results, the SBPM results can generally be considered more reliable. This is because the SBPC provides only a lateral stress reading with no way to assess if soil disturbance has occurred during insertion. The SBPM provides a lateral stress reading at membrane lift-off and a load-deformation curve. Visual examination of the load-deformation curve provides a method of assessing the quality of the stress reading in that the shape of the curve is directly affected by disturbance. However, even with the SBPM, Clough, Briaud and Hughes (1990) indicate that problems with probe deployment and calibration can easily lead to inaccurate results.

Since development of the SBPM, attempts to measure in situ lateral stress have been made with the flat dilatometer (Marchetti, 1980), the

K_0 stepped blade (Handy, et al., 1982) and other exotic devices, with limited success. On its own, the use of the dilatometer does not appear very promising for lateral stress determination, and can only be considered empirical because of induced disturbance during insertion. The K_0 stepped blade shows some promise in normally consolidated soils, but gives results that are too large for overconsolidated soils (Lutenegger and Timian, 1986). The stepped blade also has the added disadvantage of being easily damaged during insertion. Most recently, it has been observed that trends of the dilatometer P_0 readings (the pressure at which the membrane lifts away from the dilatometer blade) seem to follow similar trends to SBPM determined lateral stress with depth. As a result, calibration of P_0 by an SBPM test shows promise for use of the dilatometer for empirical profiling of lateral stresses (Clarke and Wroth, 1988; and Benoit, et al., 1990).

2.2.2 SBPM In Situ Horizontal Stress Measurement

During development and research with the SBPM, several methods have evolved to interpret SBPM data to obtain the in situ horizontal stress. Using the SBPM, horizontal stress is equivalent to the pressure (corrected for membrane stiffness) required to just lift the membrane away from the body of the probe, assuming the probe has been drilled to the test depth without causing significant disturbance to the surrounding soil. Lacasse and Lunne (1982) and Benoit (1983) have indicated that the single best method for in situ interpretation of horizontal stress is by inspection. Inspection is best accomplished by enlarging a plot of the lift-off portion of the pressuremeter curve so that all of the recorded data points are individually distinguishable. Inspection of these enlarged curves coupled with inspection of a "hard copy" printout of the raw data allows screening of the data for "noise", thus improving determination of lift-off over examination of a full pressuremeter expansion curve whose scale is too small to adequately distinguish individual data points. A summary of methods to determine in situ horizontal stress is presented on Figure 2-6.

Besides inspection, other methods include examination of slope change in expansion versus effective pressure, strain versus time, and pressure versus log of strain. Also on the figure are methods which involve constructions or curve fitting of the pressuremeter curve. More recently, Jefferies (1989) devised a computer code which curve fits the complete pressuremeter curve and theoretically determines several pressuremeter parameters, including in situ horizontal stress, based on an extension of the equations derived by Gibson and Anderson (1961). While these other methods generally seem to provide reasonable values of lateral stress, they are more cumbersome in application than inspection. As a result, inspection remains the method of choice in determination of lateral stress.

2.2.3 Determination of the Direction and Magnitude of Major Principal Horizontal Stress

Dalton and Hawkins (1982) have noted at several sites that lift-off usually occurs at different pressures for each of the three strain measuring arms, suggesting that a field of varying stress may exist in the horizontal plane. In response to this observation, Dalton and Hawkins (1982) derived a method for determining the magnitude and direction of the principal stress within the horizontal plane from SBPM data. The method is applicable to the Cambridge Insitu version of SBPM which measures membrane displacement using three strain measuring arms mounted at 120° circumferentially around the probe midpoint. The method is derived from Mohr's circle, using the order of liftoff, and corresponding expansion pressures. A summary of equations for the method is as follows, based on the Mohr's circle representation illustrated on Figure 2-7:

$$\sigma_{\min} = 1/3(r_1 + r_2 + r_3) - 2/3(r_1^2 + r_2^2 + r_3^2 - r_1 r_2 - r_2 r_3 - r_3 r_1)^{1/2} \quad (\text{Eq 2-2})$$

$$\sigma_{\max} = 1/3(r_1 + r_2 + r_3) + 2/3(r_1^2 + r_2^2 + r_3^2 - r_1 r_2 - r_2 r_3 - r_3 r_1)^{1/2} \quad (\text{Eq 2-3})$$

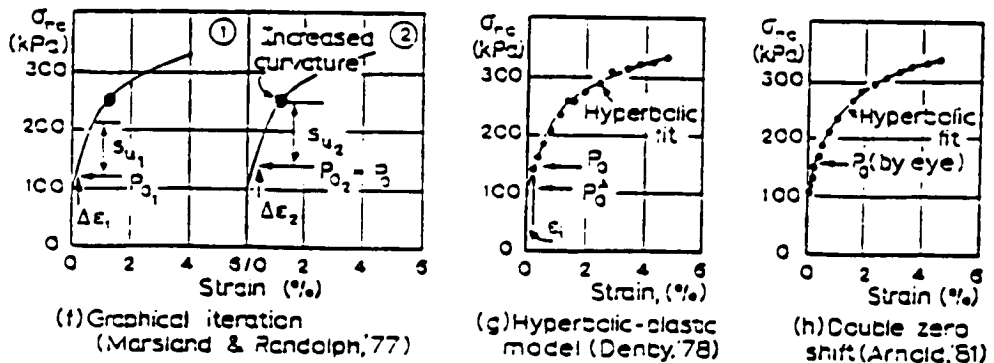
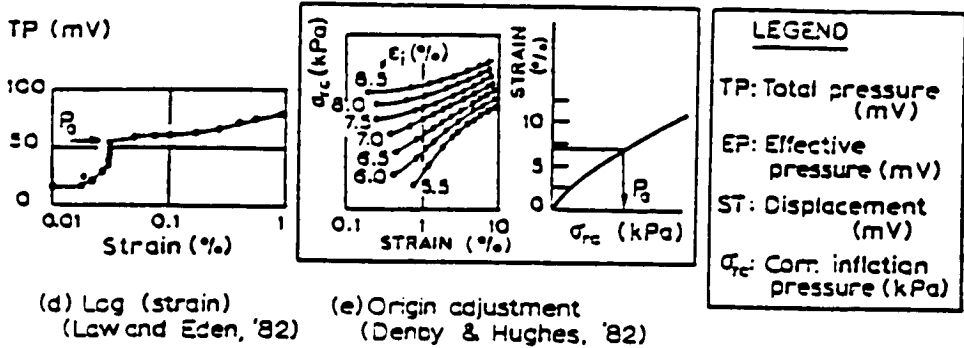
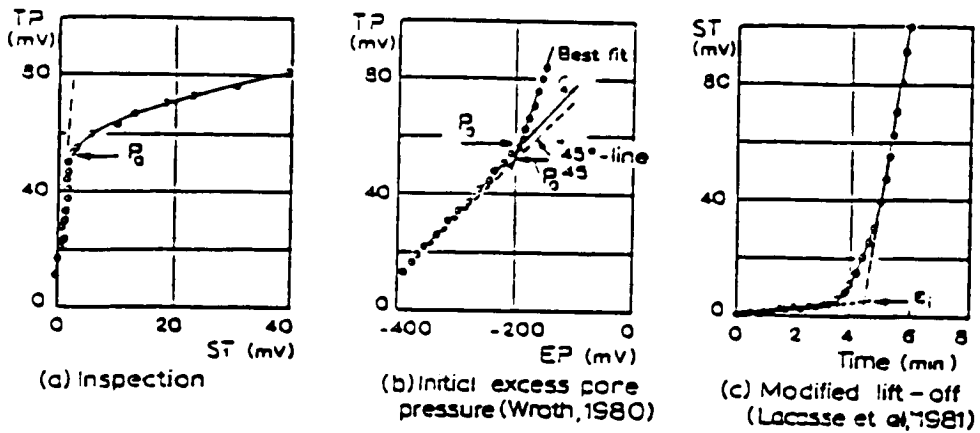


Figure 2-6 Interpretation of Horizontal Stress in Self-Boring Pressuremeter Test (after Lacasse and Lunne, 1982)

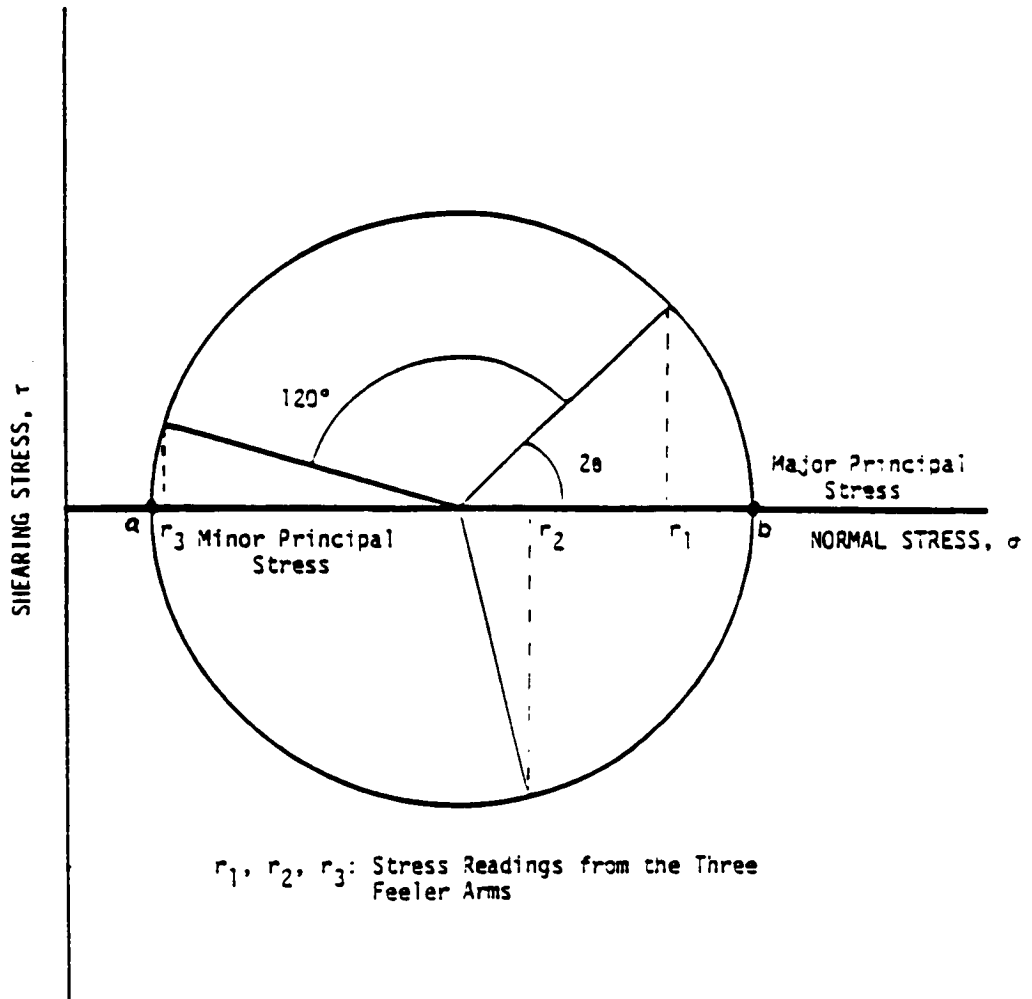


Figure 2-7 Mohr's Circle Representation of Stresses Around Probe as Measured by Three Strain Feeler Arms (after Benoit, 1983)

$$\sin 2\theta = \frac{1/((3(r_2-r_3))^4)}{2/3(r_1^2+r_2^2+r_3^2-r_1r_2-r_2r_3-r_3r_1)^4} \quad (\text{Eq 2-4})$$

where: σ_{\min} = minor principal horizontal stress
 σ_{\max} = major principal horizontal stress
 r_1 = pressure at 3rd liftoff (highest pressure)
 r_2 = pressure at 2nd liftoff (intermediate pressure)
 r_3 = pressure at 1st liftoff (lowest pressure)

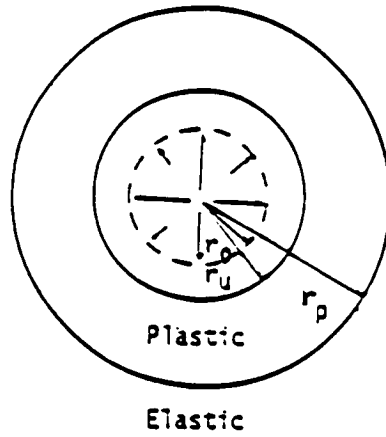
To test the method, Dalton and Hawkins (1982) conducted three SBPM borings in a gently sloping grass meadow located in Little Eversden, Chambridgeshire, England. After reducing the data using their principal stress method and comparing the resulting direction of the principal stresses, consistency in the direction of the major principal stress between each test made in a particular borehole was observed. However, after comparing the results of all three borings, little consistency in the direction of the major principal stress between borings was observed. Mechanical reasons for inconsistency were reportedly not suspected, and the inconsistency was not thought to be a result of disturbance because the pressuremeter curves resulting from the tests seemed to be of high quality.

The Dalton and Hawkins method has also been used at Hamilton AFB as described by Benoit (1983). Two borings were compared, and consistency of the direction of the major principal stress was observed between tests within a boring. But again, as was found by Dalton and Hawkins (1982), the indicated direction of the major principal stress between borings tended to be less consistent. Because of the unanswered question as to why adjacent boreholes do not generally agree with respect to the direction of the major principal stress, a question lingers as to whether the differing measured horizontal stress was a result of stress anisotropy or not. Benoit (1983) indicated that further controlled investigations would be necessary to assess the validity of the principal stress technique.

2.3 Mechanics of Pressuremeter Expansion

Expansion of the pressuremeter membrane is modeled as expansion of an infinitely long cylindrical cavity, thus, soil deformation is assumed to occur with axial symmetry. This implies that radial (σ_r), circumferential (σ_θ), and vertical (σ_z) stresses on a soil element are principal stresses. Plane strain conditions are assumed to exist at all stages of loading, so σ_z is a direct function of σ_r and σ_θ and ϵ_z equals 0. The orientations of σ_r and σ_θ are indicated on Figure 2-8.

With the self-boring pressuremeter, insertion is considered to ideally occur without disturbance to the surrounding soil. During a test, as pressure is increased within the SBPM, no outward strain of the membrane occurs until the internal pressure within the pressuremeter (assumed corrected for membrane stiffness) equals the total horizontal stress in the ground (P_0). Discussion of stress conditions at probe pressures greater than P_0 requires definition of the mode of strength behavior. For pressuremeter expansion in clays, it is generally assumed that the soil remains undrained during expansion (shear) and that soil deformation is elasto-plastic. As such, strength is governed by the undrained shear strength (S_u), which defines the point of yield. As pressure within the pressuremeter is increased above P_0 , radial deformation is assumed to be elastic as long as expansion pressure is less than $P_0 + S_u$. When expansion pressure exceeds $P_0 + S_u$, a zone of soil adjacent to the pressuremeter experiences plastic strain. If r_e is the expanded radius of the pressuremeter and r_p is the radius extending to the outer limit of the plastic zone (see Figure 2-8), then the soil within this concentric zone or annulus defined by these two radii is considered to be in a plastic strain state. Beyond r_p , the soil is in an elastic strain state since insufficient deformation has occurred to mobilize plastic strain. Since σ_r and σ_θ are principal stresses, it follows that ϵ_r and ϵ_θ are principal strains. Fung (1977) defines plastic strains within the plastic zone as:



Elastic and Plastic States of Soil Surrounding an Expanding Cavity

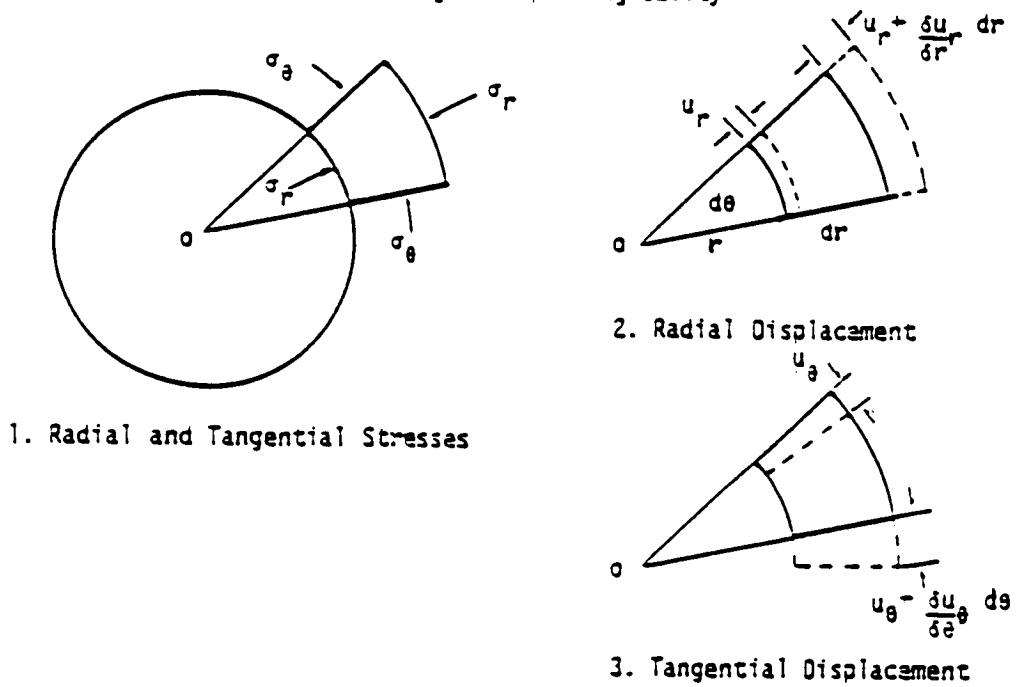


Figure 2-8 Stress and Displacement Components of a Soil Element at Radial Distance r (after Fung, 1977)

$$\epsilon_r = \frac{\delta u_r}{\delta r} \quad \text{and} \quad \epsilon_\theta = \frac{u_r}{r} + \frac{1}{r} \frac{\delta u_\theta}{\delta \theta} \quad (\text{Eq 2-5a, b})$$

where: u_r and u_θ are radial and tangential displacements

For the elastic zone beyond r_p , strains are elastic. From Hooke's Law (assuming small deformations):

$$\epsilon_\theta = (1/E) [\sigma_\theta - \mu(\sigma_r + \sigma_z)] \quad (\text{Eq 2-6})$$

$$\epsilon_r = (1/E) [\sigma_r - \mu(\sigma_\theta + \sigma_z)] \quad (\text{Eq 2-7})$$

$$\epsilon_z = (1/E) [\sigma_z - \mu(\sigma_\theta + \sigma_r)] \quad (\text{Eq 2-8})$$

where: E = Young's Modulus
 μ = Poisson's Ratio

Since $\epsilon_z = 0$, (assuming plane strain conditions) solving Equation 2-8 yields:

$$\sigma_z = \mu(\sigma_\theta + \sigma_r) \quad (\text{Eq 2-9})$$

Inserting this expression into the equations for ϵ_r and ϵ_θ will result in:

$$\epsilon_\theta = (1/E) [(1 - \mu^2)\sigma_\theta - \mu(1 + \mu)\sigma_r] \quad (\text{Eq 2-10})$$

$$\epsilon_r = (1/E) [(1 - \mu^2)\sigma_r - \mu(1 + \mu)\sigma_\theta] \quad (\text{Eq 2-11})$$

The above equations, for both the plastic and elastic zones define the stress-strain behavior of pressuremeter expansion assuming elasto-plastic behavior.

An equation of equilibrium is required to relate radial and tangential stresses (e.g., Vesic, 1972):

$$\frac{\delta \sigma_r}{\delta r} + \frac{\sigma_r - \sigma_\theta}{r} = 0 \quad (\text{Eq 2-12})$$

This differential equation can be solved by assuming appropriate boundary conditions to determine the tangential stress conditions, given the radial stress.

2.4 Determination of Undrained Shear Strength

Several methods have been derived for determination of undrained shear strength from SBPM data. The more significant methods are discussed in this section. Determination of undrained shear strengths falls into two general classes, namely, those that make an assumption as to the shape of the stress-strain curve, and those that do not. The methods which assume a shape for the stress-strain curve include Ménard (1956), Gibson and Anderson (1961), Prévost and Høeg (1975), Denby and Clough (1980), Arnold (1981), and Stordal (1985). Only the method simultaneously derived by Baguelin et al. (1972), Palmer (1972), and Ladanyi (1972) does not assume a shape of the stress-strain curve. This method is referred to as the "sub-tangent method".

The methods of undrained shear strength analysis discussed in the following subsections are used for determination of shear strength characteristics of soils that can be assumed to shear in an undrained state. This includes primarily fine grained silt or clay soils. The methods reviewed here include Ménard (1956), Gibson and Anderson (1961), Denby and Clough (1980), and the method simultaneously derived by Baguelin et al. (1972), Palmer (1972), and Ladanyi (1972). After describing the methods, a section is presented which discusses previous experience with the methods and factors affecting SBPM shear strength measurement.

2.4.1 Gibson and Anderson Method

The Gibson and Anderson (1961) derived an exact solution for the relationship between cavity pressure and volumetric strain which can be used to compute the undrained shear strength of the soil adjacent to an expanding pressuremeter. The method assumes that the stress-strain response of the tested soil is elastic prior to yield and perfectly plastic after yield. Also, it is assumed that the pressuremeter is expanded at a fast enough rate such that undrained conditions exist.

Soil cavity expansion is considered to be a shearing process. At small strains, it is assumed the stress-strain response is elastic, and

the change in volumetric strain ($\Delta V/V_0$) can be shown to be approximately equal to the change in expansion pressure (Δp) divided by the shear modulus (G):

$$\Delta V/V_0 = \Delta P/G \quad (\text{Eq 2-13})$$

When the expansion pressure, P , equals the in situ horizontal stress, P_0 , the membrane begins to move outward, deforming the soil wall. It is assumed that this deformation is initially elastic. However, since elastic-plastic behavior is assumed, plastic yield occurs when the expansion pressure is equal to the initial in situ horizontal stress plus the undrained shear strength:

$$P_{y,u} = P_0 + s_u \quad (\text{Eq 2-14})$$

At this pressure, the difference between the radial stress and the tangential stress is equal to twice the shear strength, and annulus of plastic soil begins to form, starting at the cavity wall and then expanding outward. As pressure increases above yield, the annulus becomes thicker.

The equation of equilibrium relating the change in stresses due to cavity expansion:

$$\frac{\delta \sigma_r}{\delta r} + \frac{\sigma_r - \sigma_\theta}{r} = 0 \quad (\text{Eq 2-15})$$

can be solved at yield for the conditions:

$$\frac{\Delta v}{v} \approx \frac{\Delta v}{v_0} = \frac{s_u}{G} \quad (\text{assuming small strains}) \quad (\text{Eq 2-16})$$

$$\text{and: } \sigma_r - \sigma_\theta = 2s_u \quad (\text{at yield}) \quad (\text{Eq 2-17})$$

where:

v_0 = initial volume
 Δv = change from initial volume
 v = current volume ($\Delta v + v_0$)

The solution is of the form:

$$P = P_o + s_u [1 + \ln(G/s_u)] + s_u [\ln(\Delta v/v)] \quad (\text{Eq 2-18})$$

A "limit" pressure, P_L , can be defined as the expansion pressure that causes $(\Delta v/v)$ to equal 1. Inserting $(\Delta v/v) = 1$ into Equation 2-18 and solving for P (now P_L) yields:

$$P_L = P_o + s_u [1 + \ln(G/s_u)] \quad (\text{Eq 2-19})$$

Since in the plastic range, $P_o + s_u \leq P \leq P_L$,

$$P = P_L + s_u [\ln(G/s_u)] \quad (\text{Eq 2-20})$$

Substituting Equation 2-16 yields:

$$P = P_L + s_u [\ln(\Delta v/v)] \quad (\text{Eq 2-21})$$

Using the Cambridge Insitu SBPM, radial strain has to be converted to volumetric strain for input into the above equation by the following:

$$\Delta v/v = 1 - (1 + \epsilon_r)^2 \quad (\text{Eq 2-22})$$

Shear strength is determined using the Gibson and Anderson method by plotting expansion pressure (P) corrected for membrane stiffness versus the natural logarithm of volumetric strain $[\ln(\Delta v/v)]$ as indicated on Figure 2-9. During plastic yield, the slope of the resulting line is equal to the undrained shear strength.

2.4.2 Baguelin, et al.-Ladanyi-Palmer Method

In the early 1970's, Baguelin et al. (1972), Ladanyi (1972), and Palmer (1972) simultaneously developed a method for determination of undrained shear strength (S_u) which makes no assumption of the shape of the stress-strain curve. The method is sometimes referred to as the

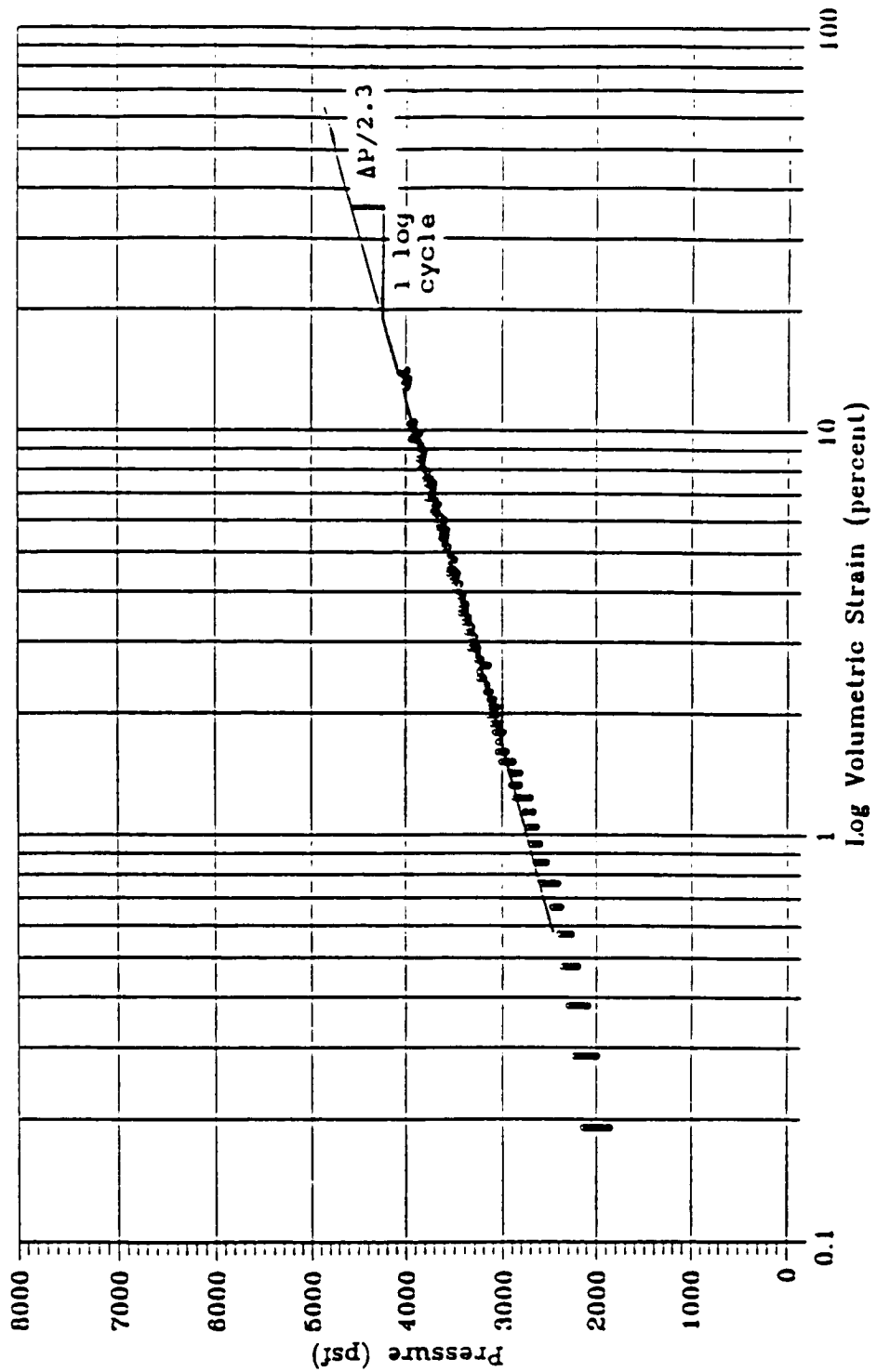


Figure 2-9 The Gibson and Anderson (1961) Undrained Shear Strength Method

"sub-tangent" method. While the method makes no assumption as to the shape of the stress-strain curve, it does assume that the stress-strain relationship is unique, but at different stages of strain at various distances from the pressuremeter membrane. Briefly, the method is derived from the equilibrium equation, which relates radial and tangential stresses:

$$\frac{\sigma_r - \sigma_\theta}{r} = \frac{\delta \sigma_r}{\delta r} \quad (\text{Eq 2-23})$$

and

$$\sigma_r - \sigma_\theta = r \frac{\delta \sigma_r}{\delta r} \quad (\text{Eq 2-24})$$

It can be shown that the principal stress difference is a function of the principal strains, $f(\epsilon_\theta)$, and thus Equation 2-24 can be written:

$$-f(\epsilon_\theta) = r \frac{\delta \sigma_r}{\delta r} \quad (\text{Eq 2-25})$$

by integrating Equation 2-25 from the borehole wall outward indefinitely, after substituting Equation 2-5b for ϵ_θ (neglecting the tangential strain term):

$$\sigma_r - \sigma_\theta = \epsilon_r (1 + \epsilon_r) (2 + \epsilon_r) (\delta \sigma_r / \delta \epsilon_r) \quad (\text{Eq 2-26})$$

Assuming small strains:

$$(\sigma_r - \sigma_\theta) / 2 = \epsilon_r (\delta \sigma_r / \delta \epsilon_r) \quad (\text{Eq 2-27})$$

Thus, the slope of the pressuremeter curve, $(\delta \sigma_r / \delta \epsilon_r)$, multiplied by the radial strain, ϵ_r , will yield values of shear stress, $(\sigma_r - \sigma_\theta) / 2$, unique to ϵ_r . By plotting $(\sigma_r - \sigma_\theta) / 2$ versus ϵ_r over the range of the expansion part of the test, the maximum value represents the peak undrained strength of the test. Alternatively, the σ_r versus ϵ_r pressuremeter curve can be mathematically fitted, allowing integration of the equation of the curve to find continuous values of shear resistance. The resulting stress-strain curve from the method is illustrated on Figure 2-10.

The drained angle of internal friction can be determined from data derived by the sub-tangent method. The tangential stress (σ_θ) at various radial strains can be determined from the $(\sigma_r - \sigma_\theta)/2$ data yielded from the sub-tangent method. From this, and knowing the measured pore pressure during the test, p' and q are determined as follows:

$$p' = (\sigma_r + \sigma_\theta - 2u)/2 \quad (\text{Eq 2-28})$$

$$q = (\sigma_r - \sigma_\theta)/2 \quad (\text{Eq 2-29})$$

By plotting the resulting p' - q stress path diagram, the effective angle of internal friction, ϕ' , can be found as indicated on Figure 2-11 by drawing a line through the origin, tangent to the maximum obliquity of the stress path.

2.4.3 Denby and Clough Method

Denby and Clough (1980) developed a method for determining undrained shear strength by assuming the stress-strain curve can be described by a modified hyperbolic shape. If a curve fitting/integration method is used to determine shear strength by the sub-tangent method (described in Section 2.4.2), then Denby and Clough can easily be implemented. The method consists of fitting two modified hyperbolic model equations for the slopes of the pressuremeter curve in the elastic and plastic ranges of the pressuremeter curve. In the elastic range, Denby (1978) indicates:

$$\frac{d\epsilon_r}{d\sigma_r} = \frac{1}{2G_i} + \frac{R_f}{S_u} \epsilon_r \quad (\text{Eq 2-30})$$

where: R_f = failure ratio
 G_i = initial shear modulus

The failure ratio, R_f , is a parameter used in the hyperbolic stress-strain model devised by Duncan and Chang (1970). The Duncan and Chang hyperbolic model is implemented by fitting a hyperbolic curve to the pre-

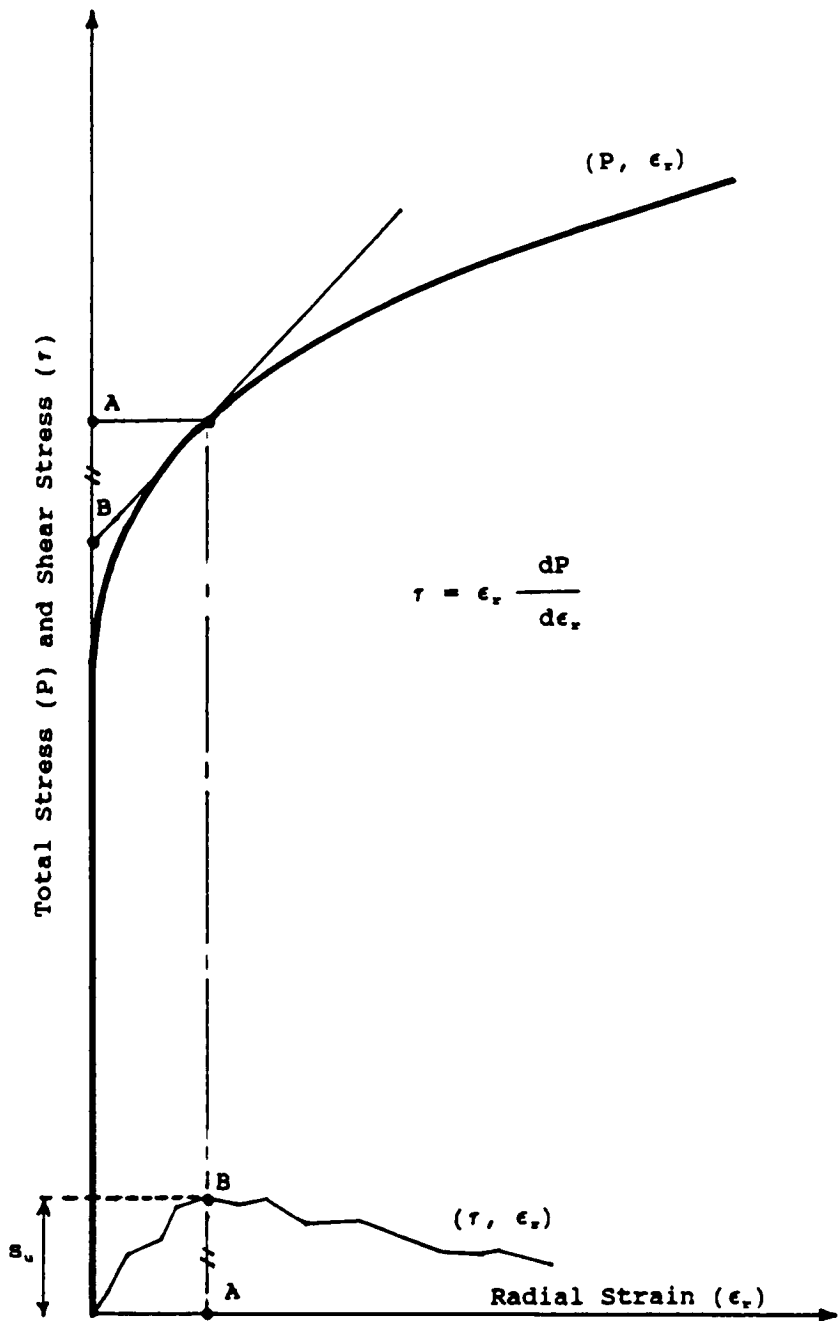


Figure 2-10 The Sub-Tangent Method (after Lacasse, 1986)

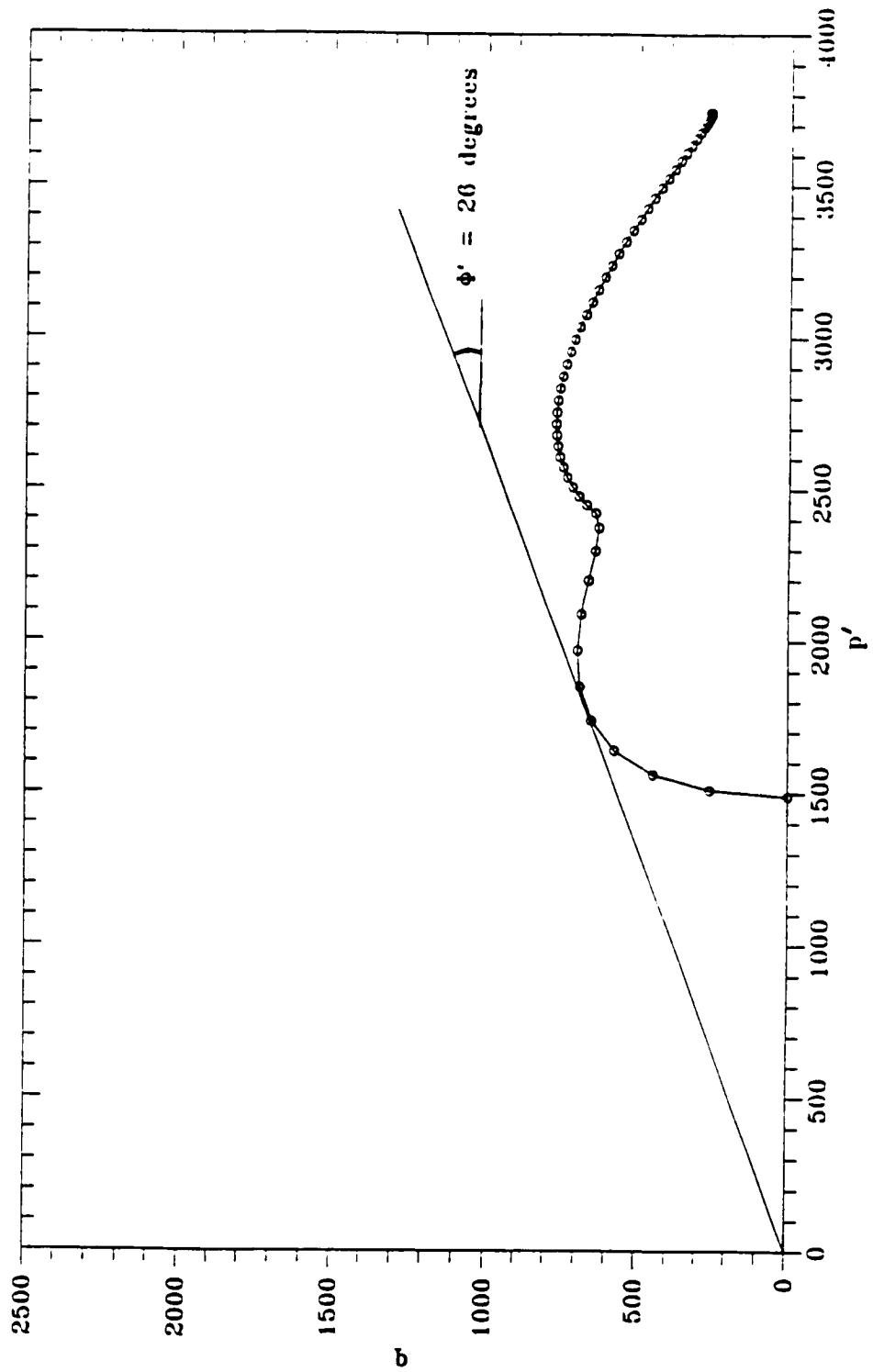


Figure 2-11 Determination of ϕ' from p' - q Data

failure portion of the stress-strain curve from triaxial shear test results. While the hyperbolic curve provides a reasonable model of the pre-failure stress-strain condition, it does not, in general, adequately model the post-failure condition. The problem here is that the hyperbolic curve continues to increase, after failure, to an asymptotic value of shear stress higher than the actual ultimate stress generally defined by triaxial shear tests, particularly if strain softening occurs. To provide a more realistic failure model, Duncan and Chang devised the R_f value. R_f is a factor applied after failure to the ultimate principal stress difference predicted by the hyperbolic curve to obtain a stress difference which is similar to that determined by triaxial tests.

From Equation 2-30, and as shown on Figure 2-12, the intercept of a $(d\epsilon_i/d\sigma_s)$ curve versus ϵ_i is $1/(2G_s)$. Thus, the slope of the elastic portion of the curve would be R_f/S_u . For the plastic range, Denby gives:

$$d\epsilon_i/d\sigma_s = \epsilon_i/S_u \quad (\text{Eq 2-31})$$

Thus, the slope of $(d\epsilon_i/d\sigma_s)$ versus ϵ_i curve would be the inverse of the undrained shear strength.

2.4.4 Ménard Method

This is an empirical method which developed out of use of the Ménard pressuremeter. Knowing the in situ horizontal stress, P_o , and determining the limit pressure (P_L), which is the pressure at which $(\Delta v/v) = 1$, and assuming an N value (site-specific, from correlations with field vane or laboratory tests), s_u can be estimated by:

$$s_u = (P_L - P_o)/N \quad (\text{Eq 2-32})$$

where: N usually varies between 4 and 6

When SBPM data are used, Hughes (1982) has suggested that the expansion pressure at 10 percent radial strain can be used in lieu of P_L while

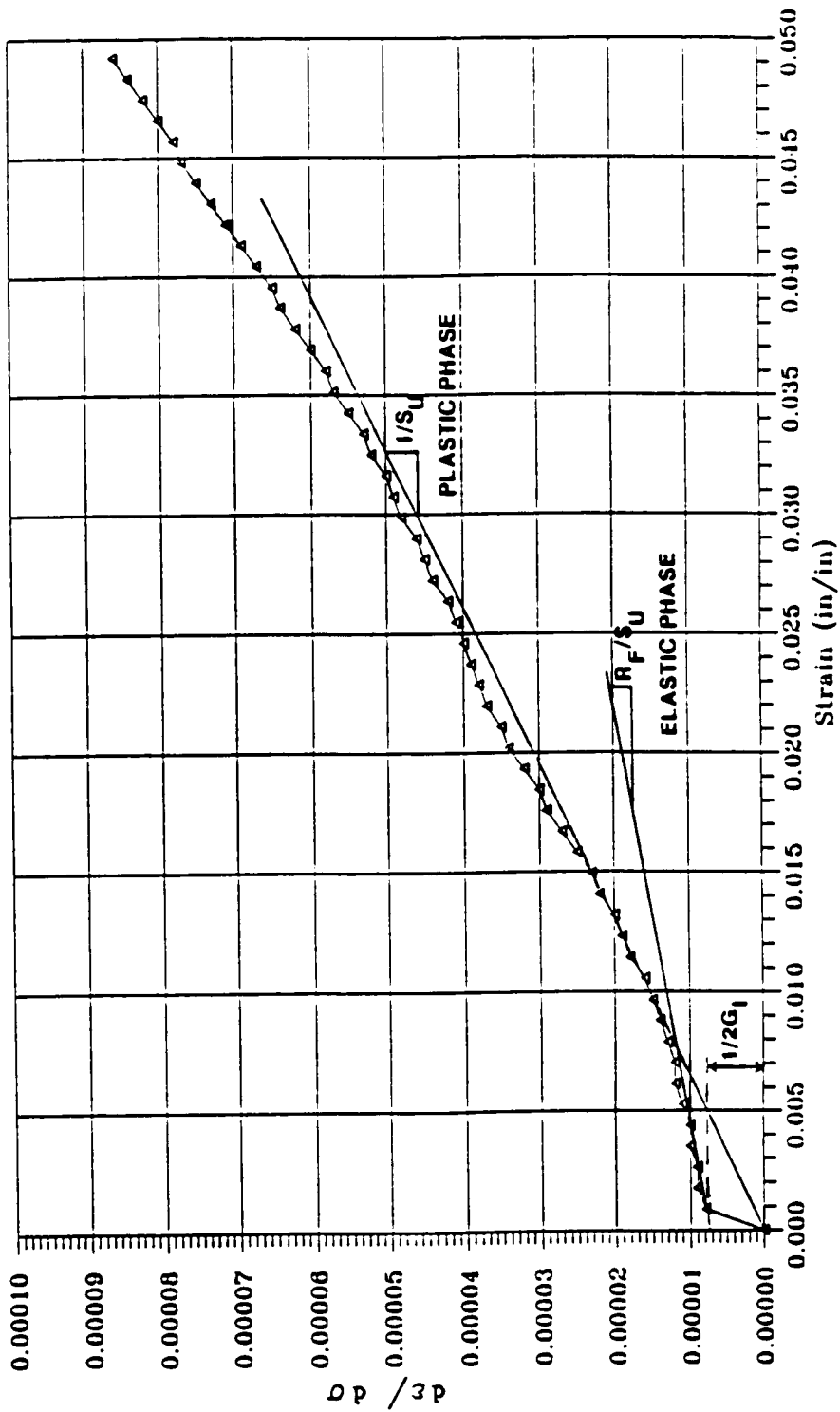


Figure 2-12 The Denby and Clough Undrained Shear Strength Method

modifying the N factor.

2.4.5 Discussion of Shear Strength Methods

With respect to the Gibson and Anderson, sub-tangent, Denby and Clough, and Ménard shear strength methods, the Ménard method is probably the easiest to apply, followed by the Gibson and Anderson method. The Denby and Clough and sub-tangent methods require somewhat more manipulation than Ménard and Gibson and Anderson. With the exception of the Ménard method, Denby (1978) found that the other three methods yielded similar results. Similar findings have been reported by Ghionna, et al. (1981) and Lacasse, et al. (1981), both referenced by Lacasse (1986). Based on the observed similarity of results, Wroth (1982) has indicated that the increased sophistication of the "sub-tangent method" is not warranted over the relatively simpler Gibson and Anderson method.

Many researchers have observed that SBPM data yields values of shear strength that are significantly higher than those measured by laboratory triaxial, direct simple shear or field vane methods (Mair and Woods, 1987, Lacasse, 1986, Yeung and Carter, 1990, and others). Some of this overestimation may be due to the fact that the SBPM test is less disturbed than laboratory or other field tests to which SBPM test results are compared. More importantly, it has been noted (Mair and Woods, 1987) that the mode of shear imposed by the pressuremeter test is quite different than that imposed by other in situ and laboratory testing techniques. The modes of undrained deformation for several different tests are illustrated on Figure 2-13. Each of these shear modes results in different shear strength values for a given clay (Wood and Wroth, 1977). Thus, shear strength is not a unique parameter of a soil, and is dependent on the mode of constant volume deformation, e.g., stress path dependent. Based on their work, Mair and Wood (1987) have indicated that deformation during a pressuremeter test is most similar to that which occurs during plane strain active compression or extension on a horizontal sample. Typically, the plane strain active compressive strength is greater than strength determined by other modes of shear

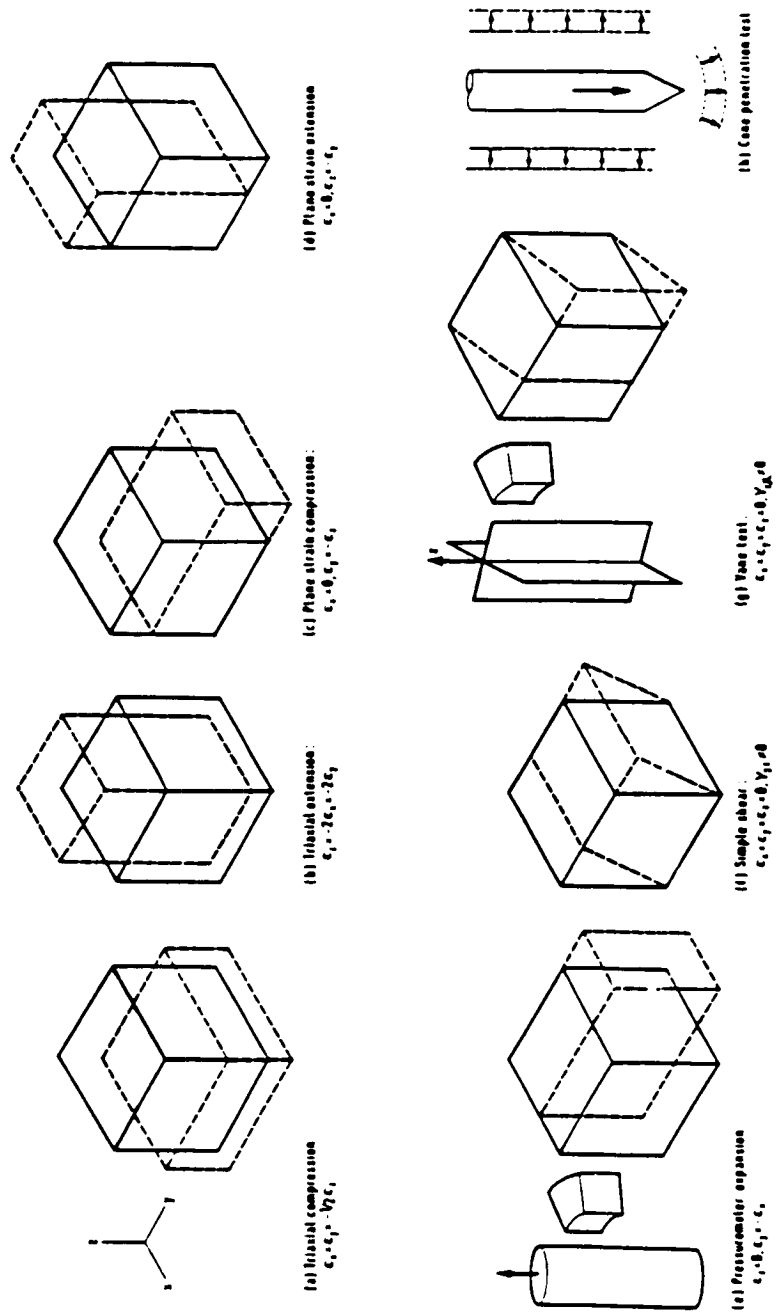


Figure 2-13 Modes of Undrained Deformation from Various Field and Laboratory Tests (after Wood and Wroth, 1977)

(Ladd and Foott, 1977). This is at least part of the explanation for the higher strength measured by the SBPM over other test methods.

However, on many sites, the observed error is generally larger than can be attributed to differences in mode of shear between SBPM and other test methods. Lacasse (1986) indicates that the reasons for the overestimation are likely due to disturbance during installation, probe length (non-plane strain conditions), partial drainage during assumed undrained shear, strain rate, inadequacy of data interpretation techniques, and experimental error. Lacasse, et al. go on to say that the pressuremeter should not be used to estimate undrained shear strength in soft to medium-stiff clays because of these factors.

Baguelin, et al. (1972) found that disturbance caused by insertion of the pressuremeter resulted in an increase in the SBPM measured shear strength. This effect is caused by distortion of the shape of the pressuremeter curve due to disturbance. The greater the thickness the disturbed annulus of soil was around the probe, the higher the measured shear strength. This effect was denoted as the "strength paradox" since, in contrast, disturbance tends to reduce apparent strength from other types of undrained field and laboratory tests.

With regard to probe length, Yeung and Carter (1990) have expanded on the work of Borsetto et al. (1983) to develop a theoretical correction method for SBPM undrained shear strength to account for the membrane end effects of the Cambridge Insitu version of the SBPM. The need for correction of SBPM undrained shear strength values is that the probe does not have a length to width ratio small enough such that true plane strain conditions exist. Because plane strain conditions are assumed in the derivations of the various SBPM shear strength analysis methods currently in use, Yeung and Carter indicate that some correction should be made to adjust the resulting value of undrained shear strength. Yeung and Carter's correction consists of the following empirical equation, derived from the results of finite element modeling:

$$s_u/s_{um} = 0.65 + 0.06 \log_{10}(G/s_u) \quad (\text{Eq 2-33})$$

where: s_u/s_{um} = the ratio of the corrected (s_u) to
 Gibson and Anderson determined (s_{um})
 undrained shear strength.
 G = elastic shear modulus, calculated from
 the slope of the unload/reload curve.

Yeung and Carter indicate that with known values of s_{um} and G , the equation can be iteratively solved to determine a corrected value of undrained shear strength. The researchers indicate that the equation has only been verified for clay deposits with G/s_u ratios between 7.5 and 375. Even with their correction, the researchers indicate that at an English test site, the adjusted value of undrained shear strength was somewhat higher than that measured by the field vane. This was attributed to other effects, such as mode of shear, or partial drainage during shear.

Fukagawa, et al. (1990) have used FEM methods to study the effect of partial drainage during "undrained" pressuremeter expansion. The authors found that partial drainage has the effect of making the pressuremeter expansion (shear) occur along a stress path that intersects the effective failure envelope at a higher shear value, thus resulting in an overestimation of strength.

Prapaharan, Chameau, Altschaeffl and Holtz (1990) have investigated the affect of disturbance on the SBPM measurement of undrained shear strength. Their research indicated that the remolded annulus of soil which results from disturbance during deployment of the SBPM can result in an overestimation of shear strength by as much as 100 percent. In their paper, the results of other researchers is discussed. It was indicated that SBPM tests in San Francisco Bay mud and Porto Tolle clay yield undrained shear strength values in reasonable agreement with some laboratory measurements, particularly simple shear and cubical shear tests. However, SBPM tests in Drammen clay, Onsey clay and Boston Blue clay all yield undrained shear strength values well in excess of

laboratory measurements. It was interestingly noted by Prapaharan, et al. that the failure strain in triaxial compression for the SBPM tested deposits with reasonable SBPM shear strengths was 1.8 percent or above. The SBPM tested deposits with triaxial compression failure strains of about 1.3 percent or less resulted in overestimated undrained shear strength. The conclusion was that soils exhibiting failure at lower strains (anisotropic or strain softening soils) seem most susceptible to overestimation of undrained shear strength.

Based on the findings of the mentioned researchers, it is clear that in most cases, the measured values of undrained shear strength from the SBPM are not suitable at this time for direct use in design. However, with continued research, appropriate corrections may be developed to make SBPM shear strength more useful. Currently, SBPM shear strength may have a use in measuring the trend of shear strength variation with depth, soil behavior and stress history.

2.5 Soil Moduli

Data obtained from the SBPM can be used to determine the shear modulus and elastic modulus. Figure 2-14 indicates methods for determination of the different moduli from the pressuremeter expansion and stress-strain curves. The pressuremeter stress-strain curve is generated by use of the sub-tangent method as described in Section 2.4.2. Also shown on Figure 2-14, for comparison, is the elastic modulus determined from a triaxial shear test.

Determination of initial tangent shear modulus, G_i , at the initial part of the pressuremeter curve, with a high degree of accuracy, is generally difficult. This is due to the fact that the initial part of the curve is rapidly changing in slope. It has been found that the initial tangent shear modulus is best determined by small cyclic strain loadings (Mair and Woods, 1987). The G_i can also be determined as part of the Denby and Clough (1978) shear strength method, as described in Section 2.4.3. The unload/reload shear modulus, G_w , is determined by performing an unload/reload cycle during the pressuremeter test or,

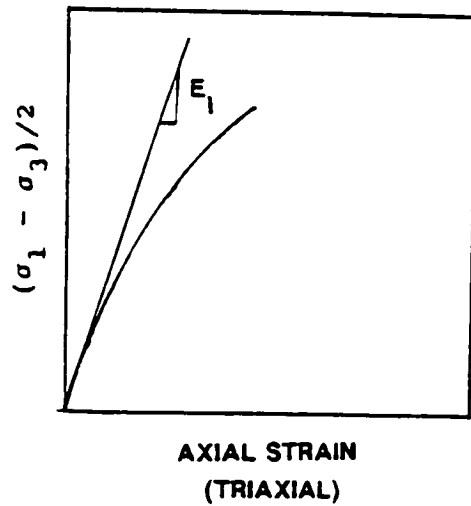
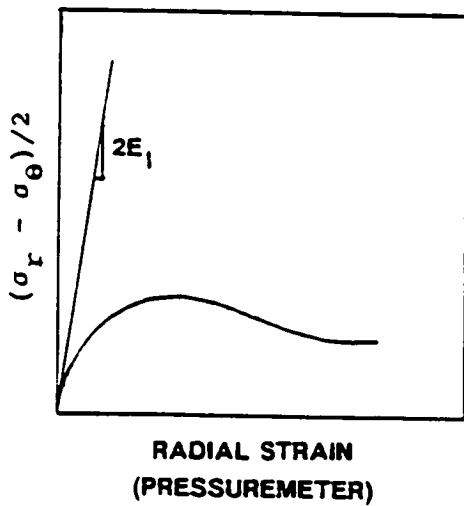
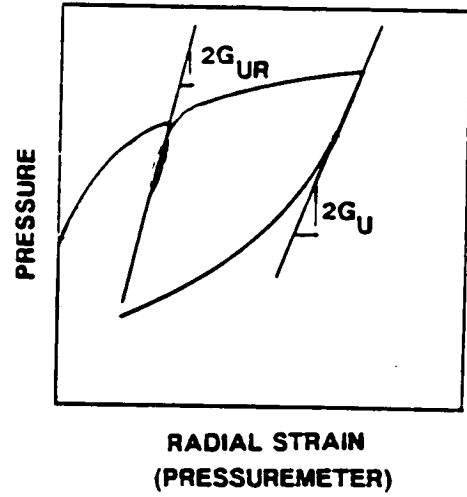
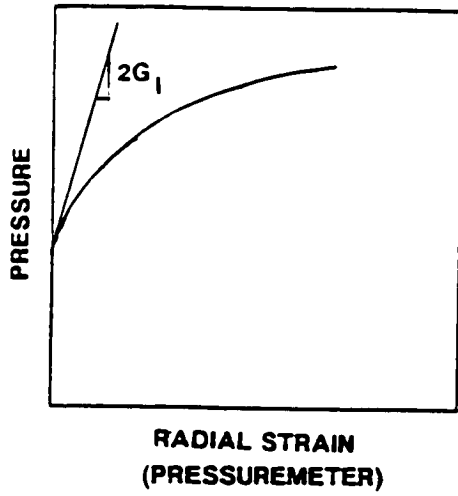


Figure 2-14 Moduli Obtained from Pressuremeter and Triaxial Tests (adapted from Benoit, 1983)

alternatively, by a reload/unload cycle during unloading of a completed test. Wroth (1982), however, warns that during unload/reload, the pressure should not be reduced more than $2s_u$, otherwise failure of the soil in extension could occur. Mair and Woods (1987) indicate that because true elasto-plastic soil behavior is not generally observed, the unload/reload loop should actually be kept smaller than $2s_u$.

Hughes (1982) has indicated that in clays, expansion should be stopped and the rate of pore pressure change allowed to equilibrate prior to performing an unload/reload (or reload/unload) cycle. Hughes says the need for this is that if the rate of pore pressure change is not equilibrated with the trend of stress change, strain will result on transecting yield surfaces and plastic deformation will occur. Equilibration of pore pressure change would result in the stress path remaining on stationary yield surfaces which would result in elastic deformation and a true G_w value. Hughes indicated that linearity (non-hysteresis) is an indication of the quality of the unload/reload cycle with respect to the accuracy of G_w implied. It has also been found by Wroth (1982) that shear modulus is affected by the percent strain at which the unload/reload cycle is made. Drainage which occurs during the "undrained" expansion likely results in a small increase in G_w with the radial strain at which the unload/reload is performed.

Determination of the elastic modulus can be made from the stress-strain curve obtained by the sub-tangent method, as indicated on Figure 2-14. The initial tangent and secant moduli can be determined, however, determination of the initial tangent modulus is difficult because of poor initial curve definition. Jamiolkowski (1980) found that the elastic modulus measured by an undrained SBPM test is on the order of 2 to 3 times that measured in undrained triaxial compression on Porto Tolle clay. This is thought to be due to the fact that modulus is highly sensitive to disturbance which occurs during sampling and trimming. The modulus determined by a triaxial test would be expected to be less than that from an SBPM test. In this same study, it is reported that the L/D

ratio of the probe itself can affect soil modulus values, with an L/D of 4 yielding a modulus 15 to 30 percent larger than that with L/D of 2.

Lacasse et al. (1990), indicates that the SBPM determined shear modulus, G , is at present considered to be the most reliable of any method. This has been corroborated by back-calculated modulus from plate load tests which compare very well with the G_w measured by the SBPM (Clough et al., 1990). The shear modulus measured by the SBPM is a large strain G , and not appropriate to machine foundation design which is dependent on very low strains.

Fahey and Jewell (1990) have determined that friction in the strain arm system of the Cambridge SBPM can affect measurement of G . The measurement error is particularly evident in stiff soils, and becomes less significant in softer soils. Fahey and Jewell recommend redesigning the strain arm system to reduce friction, or alternatively to correct for the friction based on laboratory measurements if the values of measured modulus are above 1,000,000 psf.

2.6 Horizontal Coefficient of Consolidation

Clarke, Carter, and Wroth (1979) have devised a method for determining the horizontal coefficient of consolidation (c_h) using the SBPM. The method involves utilization of test data from a holding test. A holding test can be conducted during a standard expansion test, when radial strain is at about 9 or 10 percent. The test is carried out by holding the membrane strain constant at a selected strain arm and measuring the decay of pore pressure with time. The Clarke, et al. (1979) method requires values of G_w and s_v from the earlier portion of a pressuremeter curve. When approximately 10 percent radial strain is achieved during an SBPM test, the total pressure is adjusted to maintain a fixed value of strain on a particular strain measuring arm. The effective stress data resulting from holding of strain can be reduced to obtain the decay of excess pore pressure data versus time. These data are plotted as indicated on Figure 2-15. The elapsed time when the excess pore pressure has dissipated to exactly half of the initial excess

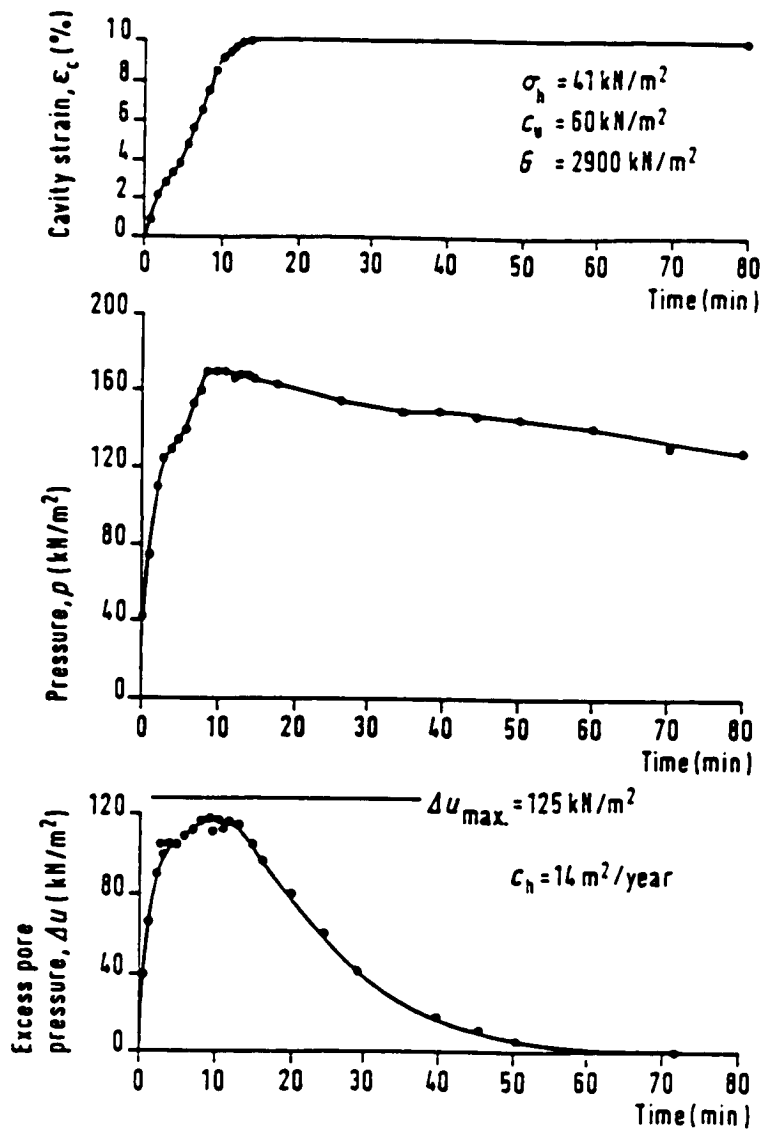


Figure 2-15 Determination of t_{90} From Holding Test (after Clarke, Carter and Wroth, 1979)

pore pressure at the start of strain holding is t_{50} , the time required for 50 percent consolidation to occur.

Randolph and Wroth (1979) obtained a closed-form solution for the time dependence of excess pore pressure around driven piles. This relationship is dependent on undrained shear strength (s_u) and is graphically presented on Figure 2-16. Note that c_v in the figure is equivalent to s_u . Knowing the maximum pore pressure (u_{max}) and undrained shear strength (s_u or c_v), the ratio of these two parameters allows determination of T_{50} (the consolidation time factor) from Figure 2-16. The theoretical value of u_{max} can be computed by the following equation, based on the work of Gibson and Anderson (1961) and presented by Clarke, Carter, and Wroth (1979):

$$u_{max} = s_u \ln[(G/s_u) (\Delta v/v)] \quad (\text{Eq 2-34})$$

where: $\Delta v/v = 1 - [1/(1+\epsilon)]^2$
 $\epsilon =$ strain at which holding test was conducted
 $\Delta v/v =$ volumetric strain

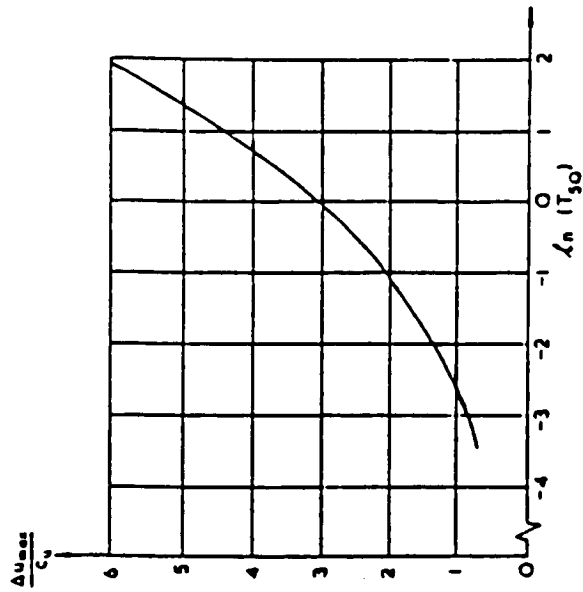
Computing the theoretical value of u_{max} provides a basis of comparison for evaluation of the reasonability of the measured value. The maximum pore pressure, u_{max} , occurs at the membrane soil interface as indicated on Figure 2-16. Once T_{50} is determined from Figure 2-16, c_h can be determined by:

$$c_h = (T_{50} r_m^2)/t_{50} \quad (\text{Eq 2-35})$$

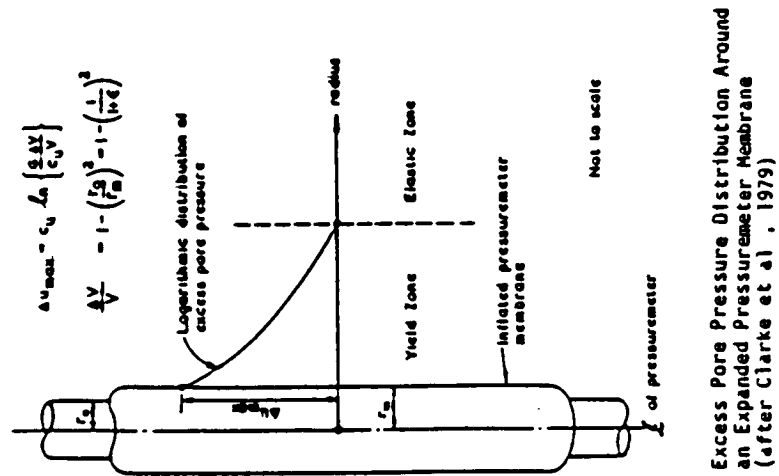
where: $r_m =$ radius of the expanded membrane

From c_h , the horizontal hydraulic conductivity, k_h , can be estimated by an equation presented by Clarke, Carter and Wroth (1979):

$$c_h = (k_h/\gamma_w) 2G [(1-\mu^2)/(1-2\mu)] \quad (\text{Eq 2-36})$$



Time for 50 Percent Excess Pore Pressure Dissipation at the Soil-Membrane Interface (after Randolph and Wroth, 1979)



Excess Pore Pressure Distribution Around an Expanded Pressuremeter Membrane (after Clarke et al., 1979)

Figure 2-16 Pore Pressures Adjacent to SBPM During Holding Test and Determination of T_{50}

where: γ_w = the unit weight of pore water
 μ = Poisson's ratio

Mair and Woods (1987) indicate that use of the SBPM holding test to measure c_v is dependent on the ability of the SBPM to measure changes in pore pressure. Mair and Woods further indicate that comparison of SBPM c_v to c_v from consolidometer tests is not of much use because of potential anisotropy with respect to hydraulic conductivity in most natural deposits. Clarke, et al. found the method to yield promising results in stiff clays. Benoit (1983) conducted two holding tests at Hamilton AFB. These tests resulted in values of c_v which were 14 to 17 times c_v from conventional consolidometer tests, which may be reasonable, due to depositional layering. Lacasse (1986) indicated that holding tests are difficult to conduct in Norwegian clays, primarily because the low permeability of these soils results in long holding periods to allow at least 50 percent dissipation.

CHAPTER III

SBPM EQUIPMENT AND TESTING METHODS

3.1 SBPM Description

The pressuremeter used to conduct the field testing for the current research is a modified self-boring model constructed by Cambridge Insitu Limited. This pressuremeter is the English version of the SBPM and was shown on Figure 2-2. The modifications of the probe were designed by Dr. Jean Benoit, and include the use of 9 strain feeler arms (three each at the quarter points of the probe) to monitor membrane expansion, rather than the conventional three feelers at the midpoint of the probe. For testing, the probe was equipped with a thin (1/16-inch thick) adiprene membrane and a Chinese lantern. A Chinese lantern is a flexible protective cover constructed of thin, longitudinally mounted metal strips which mitigate damage to the rubber membrane during insertion or expansion. Such potential damage includes tearing or puncture by shells or rock fragments. The membranes and Chinese lanterns used for the research were manufactured by Cambridge Insitu.

3.2 Calibration of SBPM

Prior to testing, the probe is calibrated to determine appropriate factors for the conversion of the computer acquisitioned voltage data from the membrane strain feeler arms to strain in percent and pressure transducer data to units of pressure. As part of the research, significant laboratory testing was conducted to assess factors affecting these electronic measurements. The results of these tests are discussed in Appendix A. Also, as a part of the calibration process, the membrane and Chinese lantern were expanded to determine their combined stiffness. Conventionally, the membrane is expanded in air to about 10 percent radial strain. In this research, this calibration was conducted in a pressure chamber to simulate confining conditions as discussed in

Appendix A. The expansion is monitored by computer in a manner identical to running a field expansion test. The pressure at which the membrane lifts away from the probe body (lift-off) represents the value of lift-off membrane stiffness. Conventional practice has been to directly use this value of stiffness to correct the measured values of in situ horizontal stress. After lift-off, the membrane continues to stretch as it expands, and consequently, membrane stiffness increases with increasing strain. The shape of the resulting expansion curve from calibration for each strain feeler arm is fitted mathematically by a cubic spline method (Benoit, 1983) allowing digital computer correction (direct subtraction of stiffness) of actual field test curves.

Findings of the current research indicated that the order of lift-off of the strain arms and confinement seem to affect the magnitude of stiffness. As a result, an alternative to conventional stiffness correction was used for this research, as discussed in detail in Appendix A.

3.3 Drilling

Insertion of the SBPM for the tests discussed in this report was done using both cutting and jetting techniques. Atwood (1990), in companion research, has determined that provided the correct drilling parameters are utilized, both jetting and cutting result in similar test results. A schematic of the probe, setup for deployment by the cutting method, was shown on Figure 2-2. The conventional configuration for deployment of the SBPM by jetting was shown in the first frame of Figure 2-3. Prior to drilling each SBPM boring for this research, the orientation of the strain measuring arms was measured using a Brunton compass. The purpose of this was to try to resolve the compass direction of the principal stress in the horizontal plane based on the apparent stress anisotropy indicated by the lateral stress measurements of the SBPM. After this alignment, the probe was drilled to test depth. To maintain the orientation of the probe while adding drill rods during the drilling process, the drill rods attached to the probe were always locked

in the drill head to prevent rotation while adding subsequent rods. Also, drill rod joints were kept tightly torqued during drilling. As a precaution, the drill rods were chalked prior to tightening or loosening rod joints or the drill head so that the probe alignment could continuously be checked.

Twenty tests were inserted using the cutting method at Pease AFB in borings PMC1, PMC2, PMC3 and PMC4. Drilling Parameters for these tests are summarized on Table 3.1. The tests were advanced at a rate ranging from 1 to 4.7 inches per minute, and the chopping bit was setback 0.5 to 0.75 inches. Water was pumped at a rate of about 5 gallons per minute to flush the soil cuttings to the surface.

Thirty tests at Pease AFB and six tests at Hamilton AFB were advanced using jetting insertion techniques in Borings PMJ3, PMJ4, PMJ5, PMJ6, PMJ7, PMJ8, PMS1, HAM1 and HAM2. Drilling parameters for these tests are summarized on Table 3.2 for Pease AFB and Table 3.3 for Hamilton AFB. Two of the jetting tests at Pease AFB (in boring PMS1) were inserted using the new shower head jetting technique described in Chapter II. For the conventional jetting tests, the center of the water jet ports on the jetting tip were positioned from 0.75 to 1.0 inches above the leading edge of the shoe. For tests performed for this research, the probe was advanced at a rates between 3 to 10 inches per minute. Water was pumped to the probe jets at a flow of 15 to 30 gallons per minute. The jetting tip had 6 jetting orifices, each of 0.165 inch diameter, resulting in a flow velocity of 38 to 75 feet per second.

In addition to cutting and jetting insertions, 3 tests at Pease AFB and 1 test at Hamilton AFB were advanced to test depth by push-in techniques. The pressuremeter was inserted by full displacement (with a conical tip replacing the cutting shoe) and open ended. Test PMP2.1 was inserted with a conical tip, and tests PMP1.2, PMP1.2 and HAM2.5 were pushed open ended. The purpose of these tests was to observe the influence of inefficient cutting/displacement on pressuremeter results.

Whether advanced by cutting, jetting, or push-in techniques, once

TEST NUMBER	DEPTH TO MIDDLE ARMS (ft)	CHOPPING BIT SETBACK (*) (in.)	CUTTER ROTATION (rpm)	ADVANCE RATE (inch/min)	FLOW RATE (gpm)	DISSIPATION PERIOD (**) (min)	EXPANSION RATE (psi/min)
PMC1.1	8.1	0.5	65	4.75	5	40	2
PMC1.2	10.6	0.5	65	4.75	5	40	2
PMC1.3	13.1	0.5	65	0.8	5	40	2
PMC2.1	8.1	0.5	60	1.0	5	40	1-2
PMC2.2	10.6	0.5	60	1.0	5	40	2
PMC2.3H	13.1	0.75	60	1.0	5	40	2
PMC2.4	15.6	0.5	60-80	1.0	5	40	2
PMC3.1	8.1	0.5	60	1.0	5	40	2
PMC3.2H	10.6	0.5	60	1.0	5	1020	2
PMC3.3H	13.1	0.5	60	1.0	5	1200	2
PMC3.4H	16	0.75	60	2-5	5	2640	2
PMC3.5H	18.1	0.75	60-100	2.0	5	40	2
PMC3.6H	20.6	0.75	60-80	2.0	5	40	2
PMC4.1	7.6	0.5	60	2.0	5	40	2
PMC4.2	10.1	0.5	60	2.0	5	40	2
PMC4.3	12.6	0.5	60	2.0	5	40	2
PMC4.4	15.1	0.5	60	2.0	5	40	2
PMC4.5	17.6	0.5	60	2.0	5	40	2
PMC4.6	20.1	0.5	60	2.0	5	40	2
PMC4.7	22.6	0.5	60	2.0	5	40	2

(*) : Cutter position measured from the tip of the blade to bottom edge of the cutting shoe.

(**) : Dissipation Periods are measured from completion of insertion to beginning of expansion (+/- 5 to 10 min.).

Table 3-1 SBPM Cutting Insertion and Testing Parameters at Pease AFB (adapted from Atwood, 1990)

TEST NUMBER	DEPTH TO MIDDLE ARMS (ft)	JETTING TIP SETBACK (°) (in.)	JETTING VELOCITY AT ORIFICE (ft/sec)	ADVANCE RATE (inch/min)	FLOW RATE (gpm)	DISSIPATION PERIOD (**) (min)	EXPANSION RATE (psi/min)
PMJ3.2	9.6	.50	75	6.0	30	40	2
PMJ3.3	12.6	.50	75	3.0	30	40	2
PMJ3.4	15.6	.75	75	4.0	30	40	2
PMJ3.5	18.6	.75	75	4.0	30	40	2
PMJ3.6	21.6	.75	75	6.0	30	40	2
PMJ4.1	7.6	.75	75	4.0	30	40	2
PMJ4.2	10.6	.75	75	5.0	30	40	2
PMJ4.3	13.6	.75	75	5.0	30	40	2
PMJ4.4	16.6	.75	75	6.0	30	40	2
PMJ4.5	19.6	.75	50-75	6.0	20-30	40	2
PMJ4.6H	22.6	.75	63	6.0	25	40	2
PMJ4.7	25.1	.75	38-63	6.0	15-25	40	2
PMJ5.1	6.6	1.0	63	5.1	25	40	4
PMJ5.2	9.6	1.0	63	4.8	25	40	5
PMJ5.3	12.6	1.0	50-63	4.6	20-25	40	4
PMJ5.4	16.1	1.0	63	6.5	25	40	10
PMJ5.5	19.1	1.0	50	5.8	20	40	8
PMJ5.6	22.1	1.0	63	5.4	25	40	8
PMJ6.1	8.1	1.0	63	4.3	25	40	4
PMJ6.2	10.6	1.0	54	7.5	22	40	4
PMJ6.3	13.1	1.0	63	8.4	25	40	4
PMJ6.4H	15.6	1.0	63	10.0	25	40	4
PMJ7.1	7.6	1.0	63	5.5	25	40	4
PMJ7.2	10.1	1.0	63	7.0	25	40	4
PMJ7.3	12.6	1.0	63	8.1	25	40	4
PMJ7.4H	15.1	1.0	63	7.4	25	14400	4
PMJ8.1	8.1	1.0	63	6.4	25	40	4
PMJ8.2	11.1	1.0	63	10.0	25	40	4
PMJ8.3H	13.6	1.0	63	8.1	25	40	4
PMJ8.4	16.1	1.0	63	10.1	25	40	4
PMS1.1	11.1	NA	NA	8.6	25	40	4
PMS1.2	14.1	NA	NA	7.7	25	1440	NA

(*) : Jetting tip measured from centerline of orifice to bottom edge of the cutting shoe.

(**) : Dissipation Periods are measured from completion of insertion to beginning of expansion (+/- 5 to 10 min.).

Table 3-2 SBPM Jetting Insertion and Testing Parameters at Pease AFB (adapted from Atwood, 1990)

TEST NUMBER	DEPTH TO MIDDLE ARMS (ft)	JETTING TIP SETBACK (*) (in.)	JETTING VELOCITY AT ORIFICE (ft/sec)	ADVANCE RATE (inch/min)	FLOW RATE (gpm)	DISSIPATION PERIOD (**) (min)	EXPANSION RATE (psi/min)
HAM1.1	11.6	1.0	63	6.0	25	40	3
HAM1.2	14.6	1.0	63	7.5	25	40	3
HAM1.3	16.6	1.0	63	7.5	25	40	3
HAM2.1	11.6	1.0	63	9.0	25	40	3
HAM2.2	14.6	1.0	63	5.3	75	40	3
HAM2.3	16.6	1.0	63	8.5	25	40	3
HAM2.4H	19.1	1.0	63	9.0	25	40	3

(*) : Jetting tip measured from centerline of orifice to bottom edge of the cutting shoe.

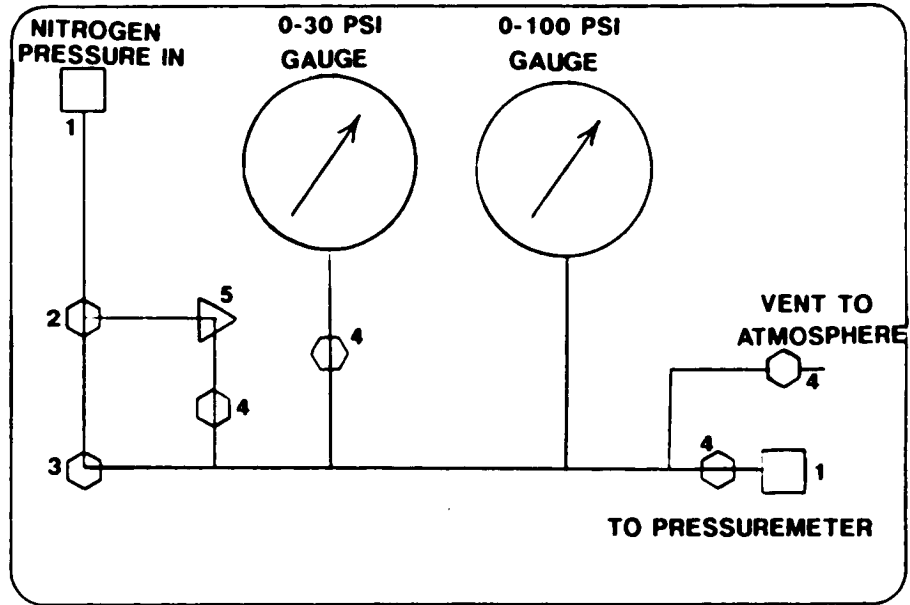
(**) : Dissipation Periods are measured from completion of insertion to beginning of expansion (+/- 5 to 10 min.).

Table 3-3 SBPM Jetting Insertion and Testing Parameters at Hamilton AFB (adapted from Atwood, 1990)

the probe was at test depth, the drilling was stopped and the excess pore pressure developed around the probe due to insertion allowed to dissipate to some extent. In previous research, dissipation periods of over 75 minutes (Benoit, 1983) to over 3 hours (Denby, 1978) have been observed prior to initiating an expansion test. Dissipation periods of such long duration greatly limit the viable cost effective use of the pressuremeter for general practice, so use of shorter dissipation periods and correction for excess pore pressure that persists at the beginning of the expansion test appears to be a practical alternative. For the current research, a dissipation period of between 30 and 45 minutes elapsed from insertion of the probe to test depth until lift-off of the membrane during expansion. Typically, during the first 30 minutes of the dissipation period, changes in the readings of the two effective stress cells, identified as "PPA" and "PPB", were monitored versus time. While at first glance it would appear that this monitoring might provide a means for determining when dissipation is complete, this is generally skewed for at least the first 20 minutes due to temperature equilibration. This equilibration is a consequence of the temperature difference between the drilling fluid and ambient ground temperature as well as changes of the ground temperature with depth, and is discussed in Appendix A.

3.4 Expansion

The probe was expanded in a stress controlled manner. A system of regulators, and needle valves in a control box (see Figure 3-1) at the ground surface was used to control the gas flow (bottled nitrogen) into and out of the probe. Nitrogen was used because it is a dry gas which mitigates condensation of water in the probe or measuring instruments. During a test, the membrane was expanded by gas flow which was controlled so as to increase the pressure within the probe at a rate of generally 2 to 4 psi per minute (about 1 to 4 percent radial strain per minute during shear), although a few tests in Boring PMJ5 were inflated at rates as fast as 8 to 10 psi per minute (up to 11 percent radial strain per



1. Quick Connect Fitting
2. Two-Way Valve
3. High Accuracy Needle Valve
4. One-Way Valve
5. Pressure Regulator

Figure 3-1 Pressure Control Panel

minute). Typically, expansion continued to about 6 to 10 percent radial strain, at which point, pressure increase was stopped. An unload-reload cycle was then performed by reducing the probe pressure about 5 psi at a rate of 2 to 4 psi per minute. Five psi was used in consideration of the findings of Wroth (1982) who indicated that probe pressure should never be decreased more than a pressure equal to twice the undrained shear strength of the soil to avoid failing the borehole wall in extension. The probe was then re-inflated at the same rate to a radial strain of about 12 or more percent. This unload-reload sequence was done to provide data for determination of shear modulus. Finally, the membrane was deflated completely at the same rate at which it was inflated (generally 2 to 4 psi per minute).

During SBPM testing conducted for this research, data from the probe were read and converted from analog voltage to digital output using an Isaac 2000 Analog to Digital Converter, and the digital output was recorded by a portable IBM compatible personal computer with a hard disk. Thirteen channels of information were recorded, including the nine strain arms (U1, U2, U3, M1, M2, M3, L1, L2, and L3) the total pressure cell (TP), two effective stress cells (PPA and PPB), and time (from the computer clock). The ISSAC polled the pressuremeter for readings at scan rates of from 5 to 250 microseconds, user selectable. The computer monitored the ISSAC digital output and was programmed to average every 5 to 25 readings from each channel, user selectable, so that disk output files were of manageable size. Averaging the ISSAC data resulted in the computer recording an averaged value for each channel 20 to 40 times per minute, dependent on the sampling time selected.

To obtain data to allow determination of the horizontal coefficient of consolidation, c_h , SBPM holding tests were conducted successfully in Borings PMC3.2, PMC3.3, PMC3.4, PMC3.5, PMC3.6, PMJ6.4 and PMJ8.4 at Pease AFB. A holding test is conducted during a standard expansion test, when radial strain is about 9 or 10 percent. The test is carried out by continuous adjustment of the total expansion pressure, such that a strain

arm is held at a constant value of strain and the change in effective stress (as indicated by effective stress cells PPA and/or PPB) is recorded with time. The strain must be held constant until the excess pore pressure indicated by PPA and/or PPB has decayed at least 50 percent of its initial value at the start of the holding phase. The length of a holding test was typically 1.5 to 2 hours at the Pease and Hamilton AFB test sites. For this research, pressure adjustments to maintain constant strain were made manually, however, other researchers (Clarke, Carter, and Wroth, 1979) have used servo-controlled pressure regulators to maintain a constant value of strain.

CHAPTER IV

FIELD TEST SITES

4.1 Introduction

The research presented in this dissertation includes field tests at two sites. The test sites are located at Pease AFB in Portsmouth, New Hampshire and Hamilton AFB in Novato, California, as indicated on Figure 4-1. This chapter discusses the conditions at both sites, previous research and/or engineering evaluation, and field and laboratory results from testing conducted for the current research.

4.2 Pease Air Force Base

The majority of the field work for this research was conducted at Pease Air Force Base. The Base is located about 50 miles north of Boston, Massachusetts, in the seacoast area of New Hampshire. The test site is adjacent to the Interstate I-95 Portsmouth Traffic Circle Interchange, on Pease Air Force Base property as indicated on Figure 4-2. The site was selected because it was adjacent to an area that had been the subject of extensive previous engineering evaluation for the construction of Interstate I-95.

4.2.1 Geology of Pease AFB Area

The geology of New England is greatly influenced by past glaciation during the Pleistocene Epoch (Strahler, 1988). The final glaciation, called the Wisconsin stage, started some fifty to seventy thousand years ago. During the peak of the Wisconsin glaciation, the ice sheet covered all of New England, and was up to 10,000 feet thick at some locations. At the same time, the oceans were 300 to 500 feet lower than present day sea level. The pressure under the ice was extremely high, and bedrock was depressed such that its surface elevation was significantly lower than present day elevations. After reaching its furthest advance, the ice sheet began to recede due to climatic changes. Glacial tills found

Self-Boring Pressuremeter Field Test Sites



Figure 4-1 Location of Field Test Sites

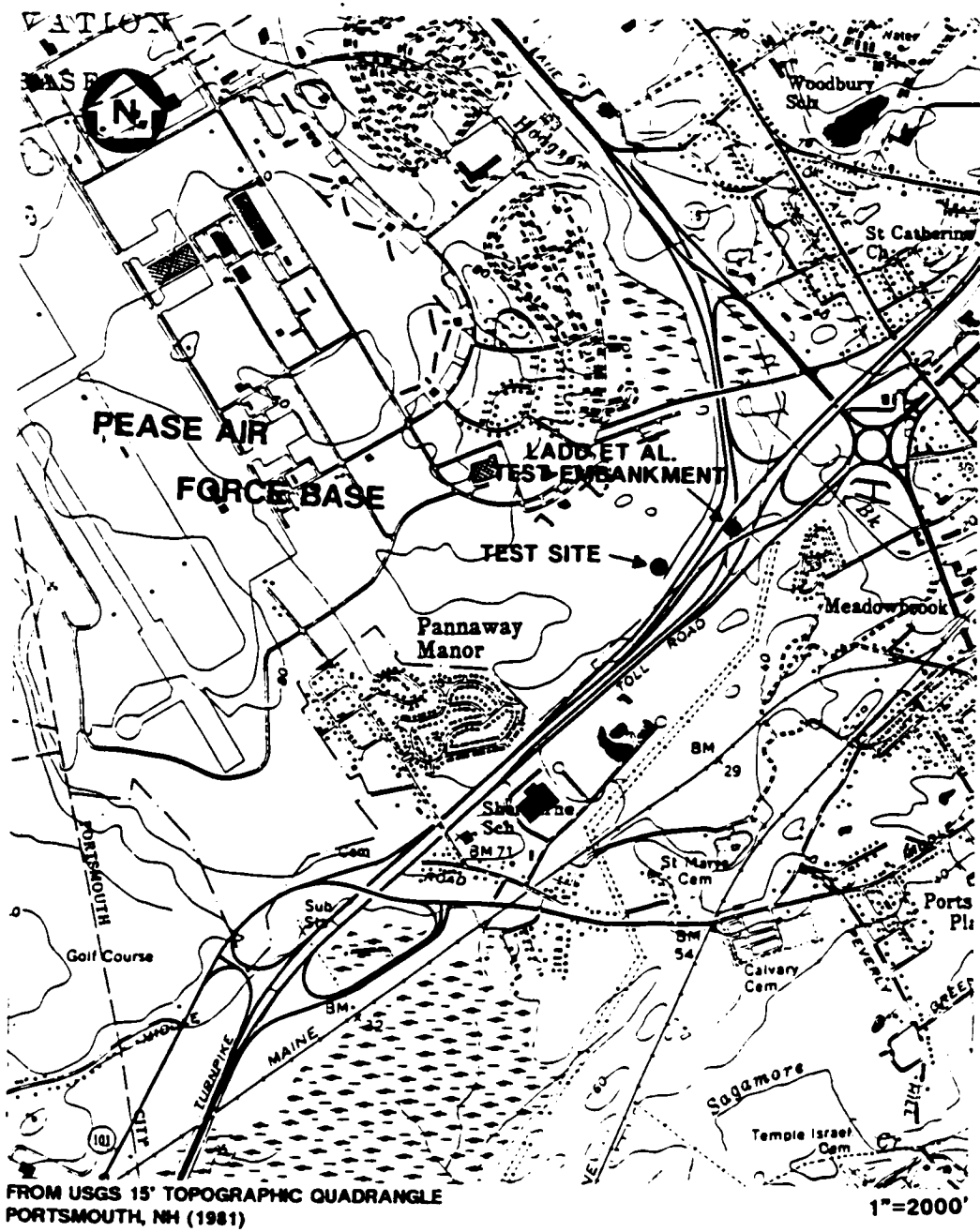


Figure 4-2 Site Location Map - Pease Air Force Base

in New England are a product of the gouging of the ice sheet against bedrock. Basal tills were deposited and over-ridden by the ice sheet, and are generally very dense as a result of the high pressure. Other till deposits, such as ablation tills can be less dense, deposited and formed at the edges of the ice sheet during recedance. As the ice sheet receded, areas of outwash deposits of soil formed. Outwash was formed by waterborne soil particles carried away from the glacier in melt water rivers. Such deposition caused sorting of materials, primarily a result of the velocity of the river carrying the soil particles. The larger particles generally settled out of the water relatively close to the glacier, where the flow velocities were still relatively fast. The finer clay and silt particles were generally carried much greater distances, to ultimate deposition in slow flow situations such as lakes or ocean bays. Some 10,000 to 15,000 years ago, after retreat of the glacier from the New Hampshire coast area, the bedrock had not yet rebounded in elevation from its depressed state during glaciation, however the oceans had recovered in elevation to levels closer to current sea level. As a result, the coastal areas that are presently land were inundated by sea water. At that time the Pease AFB site was below ocean level, and low energy deposition of fine grained silt and clay from the glacial outwash occurred through salt water, forming the silty clay deposit presently at the Pease AFB site. As time passed, the bedrock continued to rebound from the glaciation pressure, and eventually, the Pease site rose above sea level to its present day elevation.

4.2.2 Site Description

The test site at Pease AFB is adjacent to a 20 to 35 foot high embankment which was constructed in the late 1960's and early 1970's as part of the interchange shown on Figure 4-2 and 4-3. A small stream about 5 to 10 feet across exists at the embankment toe. On the other side of the stream, away from the embankment, a high pressure underground gas line exists, which restricted exploration efforts near its vicinity (the gas company requested that no explorations be made within about 20

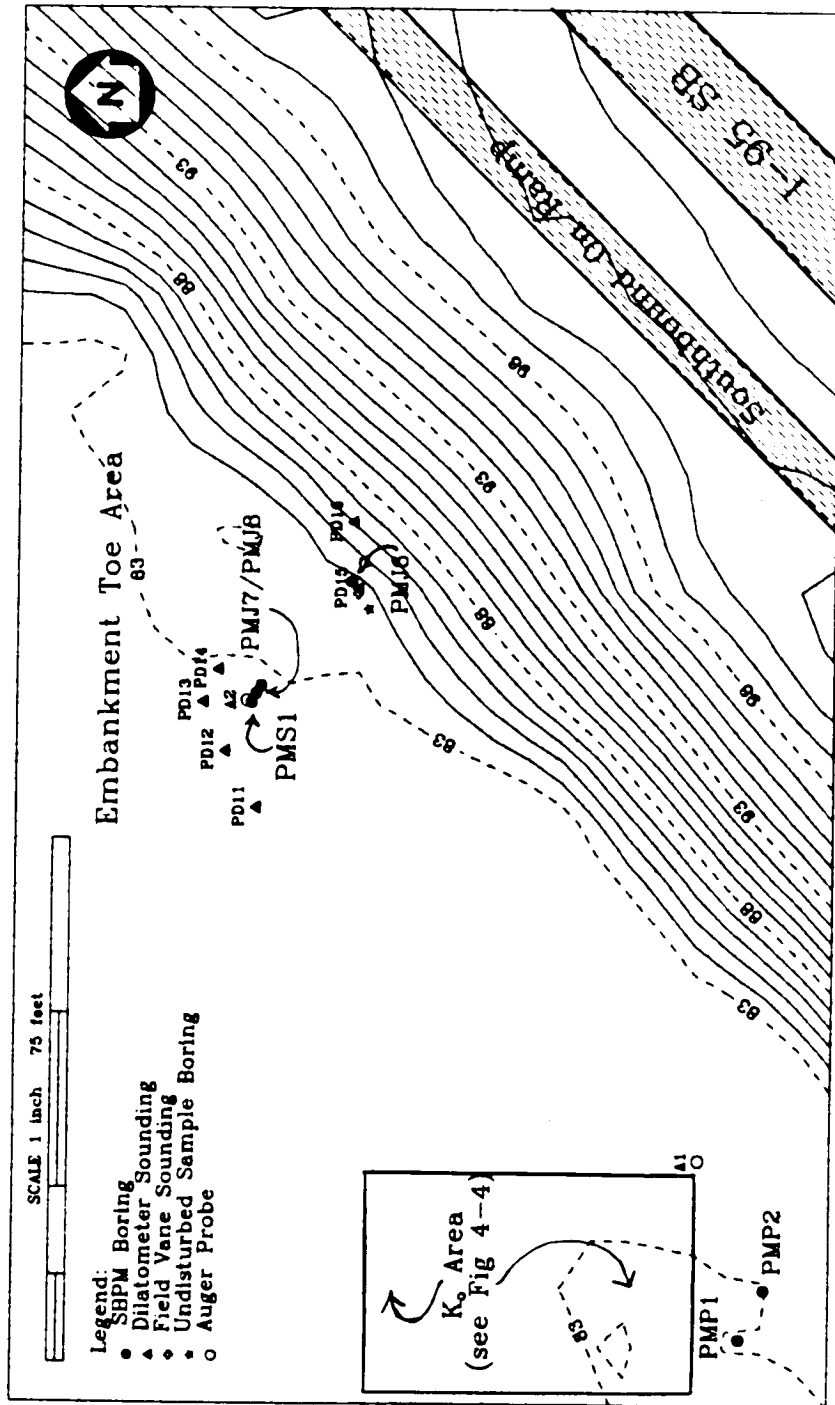


Figure 4-3 Pease Air Force Base Test Site

feet of the estimated location of the gas line alignment). Away from the embankment, the site is generally flat, open and swampy for a distance of about 260 feet, at which point, the swamp ends and a glacial till slope rises in a direction away from the highway embankment. Standing water (perched above the silty clay) is found over much of the site in depths ranging from 0 to 2 feet.

Based on the explorations made at the site for this project, subsurface conditions from the ground surface downward generally consist of about 1 foot of organic muck, about 0 to 1.5 feet of fine to medium sand, up to 25 feet of sensitive silty clay, ultimately underlain (as reported by Ladd, 1972, and Ladd, et al., 1972) by glacial till and bedrock. The depth to the bottom of the silty clay was found to range from about 6 feet (toward the embankment toe of slope near the Ko area) to 28 feet (at Ko area) in explorations made for the current research.

4.2.3 Index and Consolidation Properties from Previous Research

The silty clay has been the subject of previous research by Ladd (1972), and Ladd, Rixner and Gifford (1972) for construction of the adjacent Interstate I-95 embankments. Index properties of the silty clay determined for this previous work are summarized on Table 4-1. On the table, it can be seen that the natural moisture content of the silty clay is about 50 percent, which is significantly higher than the liquid limit. Also, the liquidity index was found to be 1.8 percent. The natural moisture content and indices indicate that the silty clay is likely very weak, and what strength it does possess is very sensitive to disturbance. A liquidity index above 1 indicates the natural moisture content of the soil is above the liquid limit and thus has a behavior similar to that of a highly viscous liquid.

Ladd (1972) indicated that the Atterberg limits are typical of marine illitic clays in New England. Ladd also found that the pore fluid salt concentrations of sodium chloride in the silty clay vary from 0.5 to 2 g/l, which is significantly less than sea water, through which deposition took place. This low concentration of sodium chloride

SUMMARY OF INDEX PROPERTIES PEASE AIR FORCE BASE TEST SITE		
INDEX PROPERTY	LADD (1972)	CURRENT RESEARCH
NATURAL WATER CONTENT (%)	50 ± 5%	42 ± 6.7%
LIQUID LIMIT (%)	35 ± 5%	34 ± 3.2%
PLASTIC LIMIT (%)	20 ± 1%	21 ± 1.9%
PLASTICITY INDEX (%)	15 ± 3%	13 ± 1.3%
LIQUIDITY INDEX (%)	1.8 ± 0.3%	2.1 ± 1.9%
TOTAL UNIT WEIGHT (pcf)	109	110 ± 3.2%
SPECIFIC GRAVITY	2.79 ± 0.01%	2.75 ± 0.04%

Table 4-1 Summary of Index Properties

suggests that the silty clay is highly sensitive due to leaching of the initially higher pore water salt concentrations.

During construction of the I-95 highway embankments, sand drains were used to speed consolidation of the underlying clay, and stage construction was used to mitigate slope failure during embankment placement. Ladd, et al. (1972) computed coefficient of consolidation values, both horizontal (c_h) and vertical (c_v), from piezometer and settlement observations made during construction. Areas both with and without sand drains were instrumented. At areas with sand drains, consolidation rate is governed mostly by horizontal drainage to the sand drain, and the computed coefficient of consolidation was assumed to be representative of c_h . At areas without sand drains, it was assumed that drainage was primarily vertical, so that the computed coefficient of consolidation was representative of c_v . The piezometer data is reported to have indicated c_v of about 0.1 to 0.25 ft²/day at areas without sand drains and c_h of 0.1 to 0.5 ft²/day at areas with sand drains. The value of c_h derived from the settlement data was less variable than that derived from the piezometer data, about 0.4 ft²/day. This wide range of values indicated by the data is attributed by Ladd, et al. to the existence of a partial drainage layer which was observed 13 to 14 feet below the ground surface. A similar layer was observed at a depth of 17 feet in some explorations in the Ko area during the current research. With consideration of the potential effects of the drainage layer, Ladd, et al. concluded that field c_h was likely about 0.27 ± 0.03 ft²/day, which was reportedly about 1.5 to 2.0 times the field c_v , estimated to be about 0.16 ± 0.04 ft²/day. Ladd, et al. indicated that the measured field values of c_h exceeded laboratory values of c_v by about 60 percent.

4.2.4 Field Testing and Sampling

The current research at the Pease Air Force Base site was generally limited to testing in and on samples of the silty clay. The silty clay consists of an upper stiff to medium crust which extends to a depth of

about 5 to 8 feet below the ground surface, becoming soft to very soft below that depth. Field testing at the site for the current research was conducted at two primary locations as indicated on Figure 4-3. The first area was located away from the highway embankment and is referred to as the "Ko area". A detailed layout of field tests at the K_0 area is presented as Figure 4-4. In general, the K_0 area was located about 120 to 150 feet away from the toe of the highway embankment. The area is believed to be outside of the stress influence of the embankment based on results of the finite element analysis performed for the current research and the fact that the clay is very thin at the embankment toe closest to the K_0 area, as indicated by an auger boring (designated as A1 on Figure 4-3) which encountered only 6 feet of clay.

Because the silty clay at the embankment toe nearest the K_0 area was too thin to provide a useful test area, attempts were made to find an area adjacent to the toe of the embankment where the clay deposit was thicker. Another hand auger sounding (A2 on Figure 4-3) was made about 280 feet northeast of A1, and encountered silty clay to a depth of about 18 feet. Since the silty clay deposit at this sounding was substantially thicker than at A1, this new area was selected to attempt measurement of the stress influence of the embankment. This area is designated as the "toe area" on Figure 4-3.

4.2.4.1 Undisturbed Sampling - Twenty-seven 3-inch thin-wall piston samples were obtained at the site in four boring locations as indicated on Figure 4-3 and 4-4. Borings U1, U2, and U3 were made at a locations 120 to 150 feet from the toe of the embankment. Boring U4 was made at the toe area next to the highway embankment. The samples were obtained to perform laboratory tests to determine index and engineering properties of the silty clay.

Piston sampling was performed using an Acker 3-inch diameter piston sampler. The sampler was actuated using "spaghetti rods" which are $\frac{1}{4}$ -inch inner rods contained within the AW rod drill string. To obtain a sample, a 4-inch hole was hand augered to sample depth, and the sampler

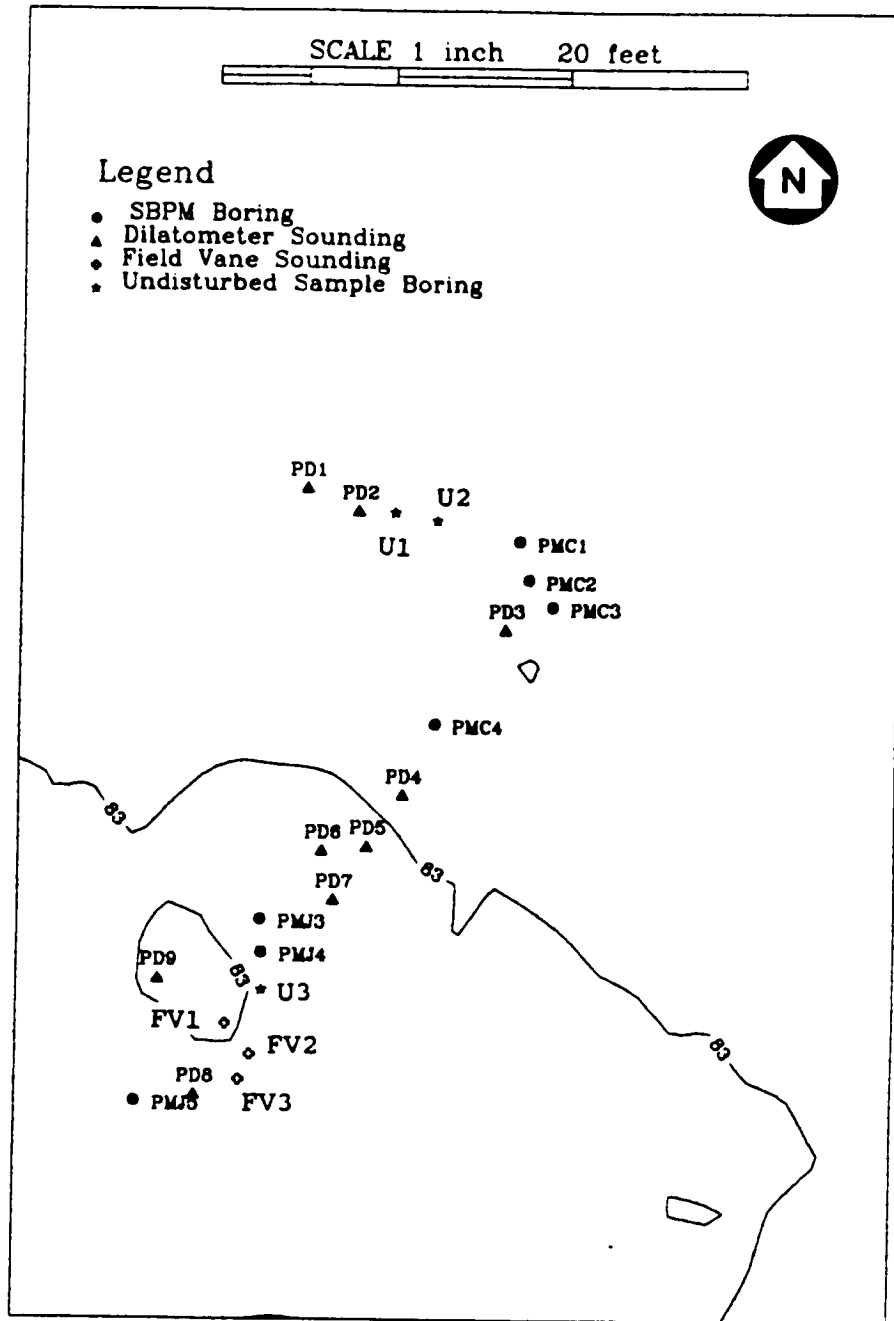


Figure 4-4 Pease Air Force Base K. Area

was lowered into the hole. The tube was then pushed into the soil, generally by hand, while the piston was held stationary by the spaghetti rods which were secured to the drill rig. Once extended 24 inches, the drill rods were clamped in the drill chuck and the pore pressures were allowed to dissipate for a period of about 10 minutes. The rods were then unclamped and torqued to shear the soil at the bottom of the sample tube. The tube was then carefully raised to the surface. At no time during sampling was the full gravity force of the drill string allowed to push on the sample or piston.

When each thin-wall tube sample was brought to the surface, it was carefully marked, sealed with bee's wax, capped, labeled and transported vertically back to the laboratory. The samples were stored in a cool, temperature controlled room until used for testing. Prior to testing, the tubes were carefully cut with a tube cutter, and samples smoothly extruded in the same direction as they were sampled.

4.2.4.2 Field Vane Testing - Twenty-six field vane tests were performed for the current research in four separate soundings at the Pease test site. The locations of the soundings are indicated on Figures 4-3 and 4-4; three soundings were made 120 to 125 feet away from the embankment at the Ko area, and one was made at the toe of the embankment. The tests were made with a Geonor field vane borer apparatus, using vanes with a height to width ratio of 2. Two different square end vanes were used; a smaller vane (55 mm diam. x 110 mm height) in the stiffer upper crust; and a larger (65 mm diam. x 130 mm height) vane in the softer, lower portion of the silty clay deposit. The tests were conducted in accordance with ASTM specification D-2573. Uncorrected results of field vane testing are presented on Figures 4-5 and 4-6.

Undrained shear strength is often normalized by dividing the value of undrained shear strength, s_u , by the effective vertical overburden pressure, p' , acting on the element of soil being tested, yielding the ratio s_u/p' . It was observed that the s_u/p' ratio indicated by the vane in the normally consolidated soil was about 0.23 to 0.26. A comparison

**SELF-BORING PRESSUREMETER RESEARCH - PEASE AIR FORCE BASE
SOIL PROFILE AT K₀ TEST AREA**

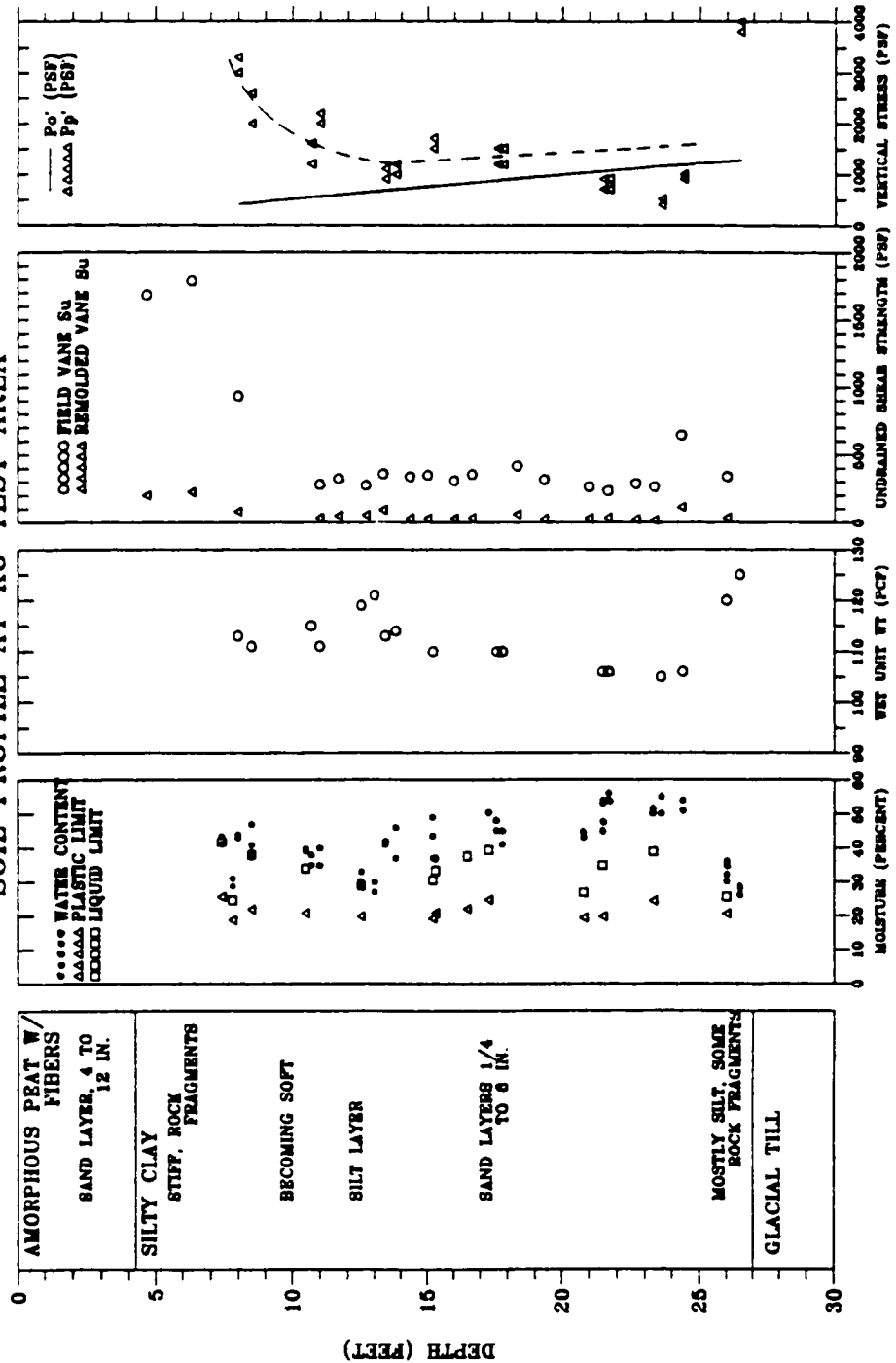


Figure 4-5 Profile at Pease AFB K₀ Area

SELF-BORING PRESSUREMETER RESEARCH - PEASE AIR FORCE BASE
SOIL PROFILE AT EMBANKMENT TOE

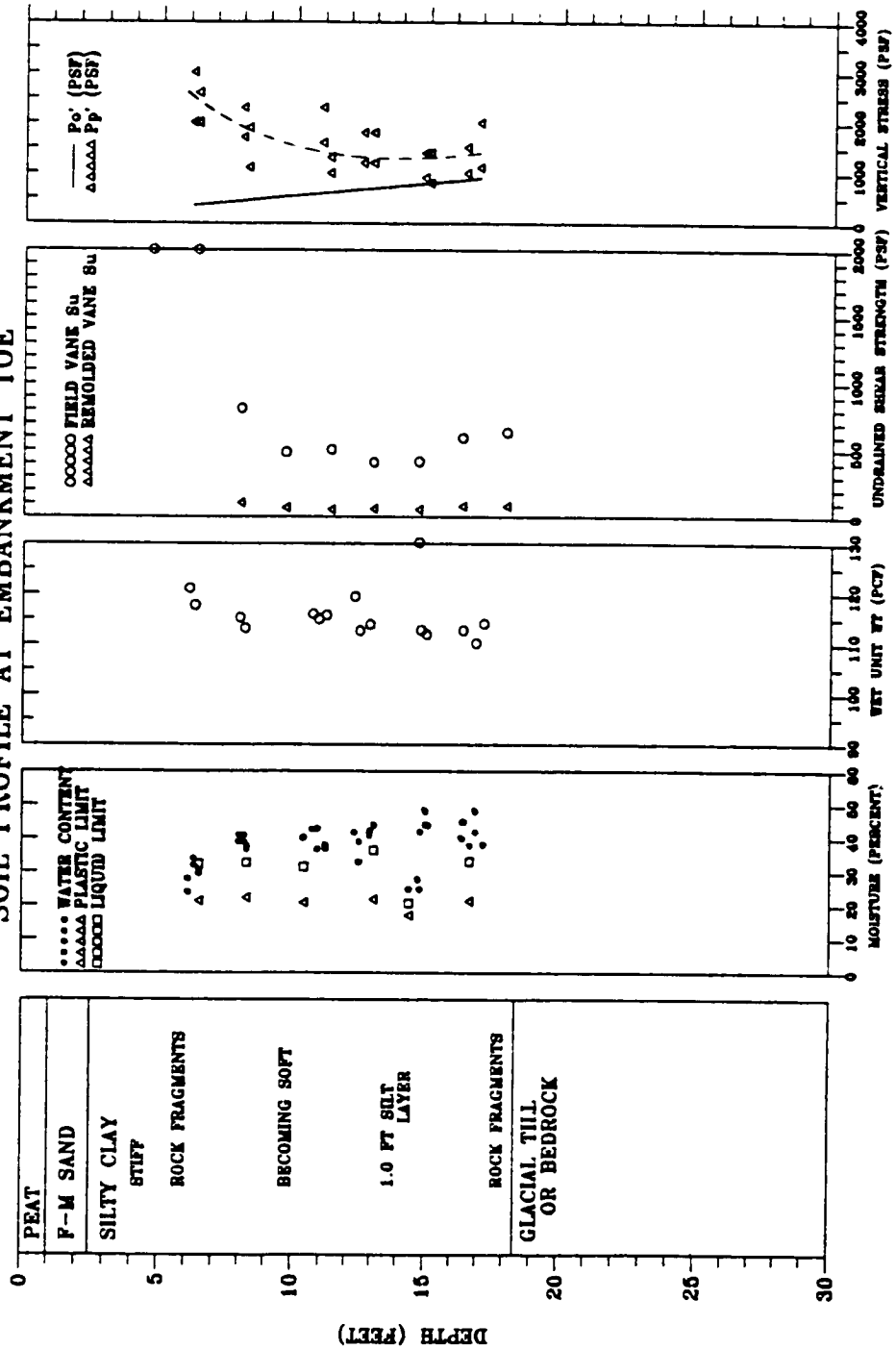


Figure 4-6 Profile at Pease AFB Embankment Toe Area

of the uncorrected field vane strength measured at the K₀ area during the current research to that measured by Ladd, et al. (1972) is presented on Figure 4-7. The figure indicates the undrained field vane shear strengths measured for the current research were generally similar to that measured by Ladd (1972) below a depth of about 20 feet. Above this depth, however, the vane strength measured during the current research at the K₀ area was about 10 to 80 percent higher than that measured by Ladd. At the embankment toe, the measured shear strength was on the order of up to 100 percent greater than that measured by Ladd. Higher shear strengths would be expected at the toe, however, results similar to Ladd's were expected at the K₀ area. An explanation can be found in that the area of the silty clay deposit tested by the current research had significantly lower moisture content (42 versus 50 percent, see Table 4-1) than that tested by Ladd. A statistical T-test (described in Section 4.2.5.1) indicated that the current and previous mean moisture contents were from different populations. A lower moisture content as indicated by the current research translates into a lower void ratio and thus a higher shear strength.

4.2.4.3 Self-Boring Pressuremeter Testing - Sixty-seven SBPM tests were conducted at the Pease Air Force Base Site. These tests were conducted in 15 borings, located as indicated on Figure 4-3 and 4-4. Logs of the pressuremeter borings are presented in Appendix D. General procedures and equipment used for drilling and testing were discussed in Chapter III.

The tests were conducted at the toe and K₀ areas. Testing at the K₀ area included borings PMC 1, 2, 3 and 4, and PMJ 1, 2, 3, 4, and 5. PMJ 1 and 2 were borings used to determine appropriate jetting insertion parameters and resulted in unreliable test results. Three push-in (borings PMP1 and 2) pressuremeter tests were carried out near the K₀ area, about halfway to the toe of the slope as indicated on Figure 4-3.

Testing at the toe of the slope included borings PMJ 6, 7 and 8 and PMS 1. PMJ 6 was made at the toe of the highway embankment and the other

**PEASE AIR FORCE BASE
FIELD VANE UNDRAINED SHEAR STRENGTH**

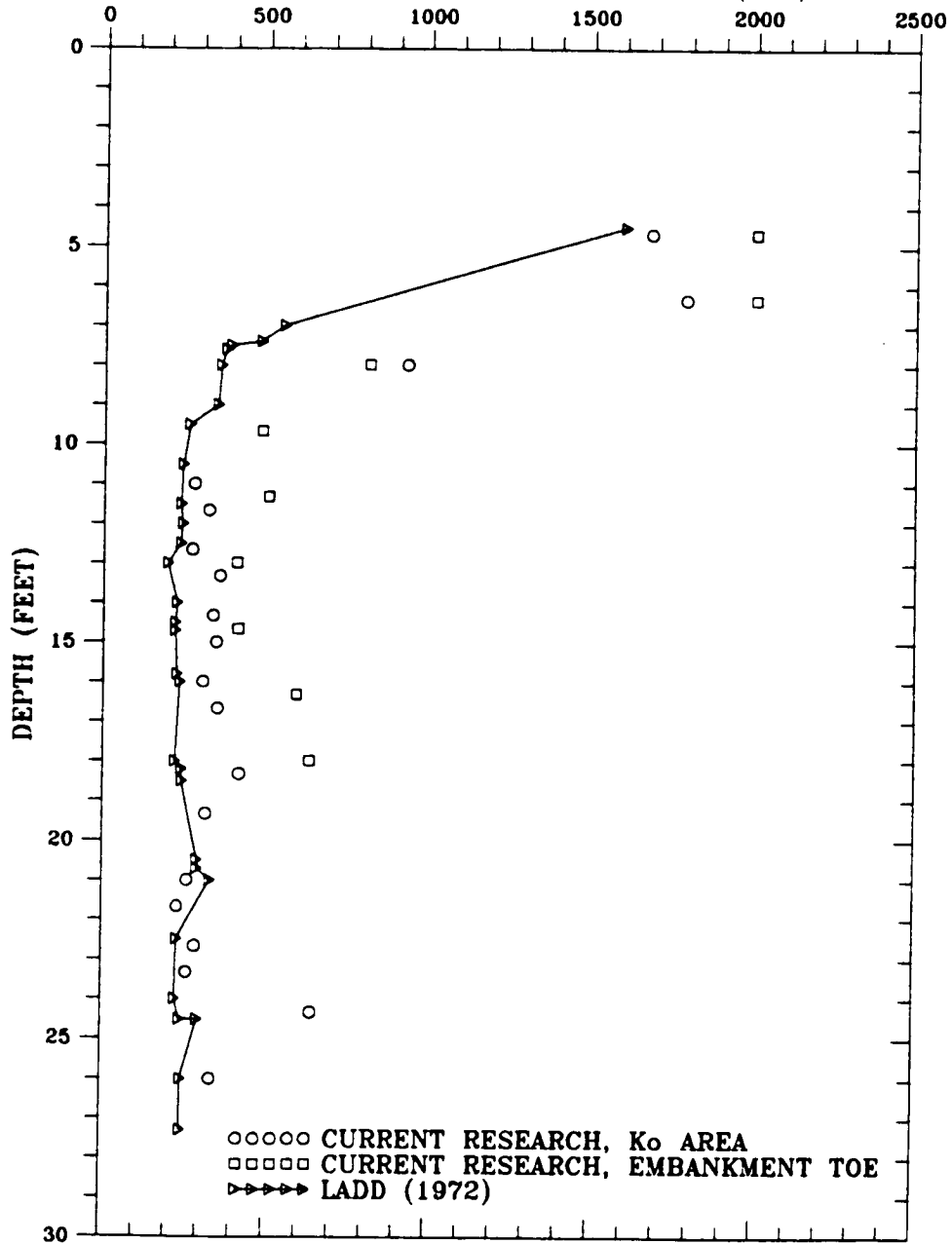


Figure 4-7 Profile of Field Shear Vane Strength

borings were made progressively further away from the embankment. Boring PMS 1 was furthest from the toe (about 80 feet) and was made using the new "shower head" jetting method. The results of these SBPM tests are described in detail in the following chapters.

4.2.4.4 Flat Dilatometer Testing - Concurrent with the subject research, Nejame (1991) conducted several dilatometer (DMT) soundings at the site. The results of the soundings are useful for consideration in the subject research for profiling, time rate of consolidation parameters (insertion pore pressure dissipation) and for estimation of the hydrostatic pressure profile.

With respect to profiling, the dilatometer I_d parameter is useful. The I_d parameter is determined from the dilatometer test "A" and "B" readings. The A reading is the pressure required to just lift the dilatometer membrane away from contact with the blade body. The B reading is the pressure required to further expand the membrane a distance of 1 millimeter. From the A and B readings, P_0 and P_1 are respectively determined by correcting for membrane stiffness. In order to determine I_d , an estimate of the hydrostatic pressure at a test location, u_0 , is required, and the following equation is used:

$$I_d = \frac{P_1 - P_0}{P_0 - u_0} \quad (\text{Eq 4-1})$$

Research has found that soil behavior can be classified by the following ranges of I_d (Marchetti, 1986, and ASTM, 1986):

Material	I_d
sand	3.3+
sandy silt	1.8-3.3
silty sand	1.2-1.8
silt	0.9-1.2
silty clay	0.6-0.9
clayey silt	0.35-0.6
clay	0.1-0.35

Dilatometer I_v profiles directly adjacent (generally within 5 to 10 feet) of SBPM borings are presented in Appendix D. Figure 4-8 is presented as an example of such a plot for SBPM boring PMC3. The purpose of these plots is to help resolve SBPM anomalies due to strata variations at intervals tested by specific SBPM tests.

The horizontal coefficient of consolidation can be predicted from a dilatometer dissipation test. A dissipation test can be conducted two different ways. First, after pushing the dilatometer to a particular test depth, repeated "A" readings are made with time and is referred to as a DMTA dissipation test (Marchetti and Totani, 1989). These readings are plotted versus the log of time, forming a curve similar in appearance to a deflection-log time curve from a consolidation test. From this curve, t_{50} (the time for 50 percent dissipation to occur) can be estimated. Knowing t_{50} , a determination of c_h can be made. Alternatively, repeated measurements of a third dilatometer parameter, the "C" readings are made with time (Schmertmann, 1988, and Robertson, 1988). After pressurization to obtain the A and B readings, the dilatometer membrane is deflated. The "C" reading is the pressure at which the membrane recontacts the dilatometer blade during deflation. This test is referred to as a DMTC dissipation test. Table 4-2 presents c_h values determined by Nejame (1991) from the dilatometer data. The table indicates that c_h derived from the dilatometer data ranged widely, varying from 0.03 to 5.9 ft²/day. These values are compared to those measured by consolidation and SBPM tests in Chapter VII. Compared to the data of Ladd, et al. (1972), the Robertson method seems to yield c_h values about the same to an order of magnitude larger, while the c_h values by the Schmertmann and Marchetti methods are about the same to about an order of magnitude less than those reported by Ladd.

The distribution of hydrostatic head can also be roughly estimated from dilatometer dissipation data. The final dissipated "C" value determined from the C-dissipation test has been observed (Luttenegger and Kabir, 1988) to be generally a function of the hydrostatic pressure at

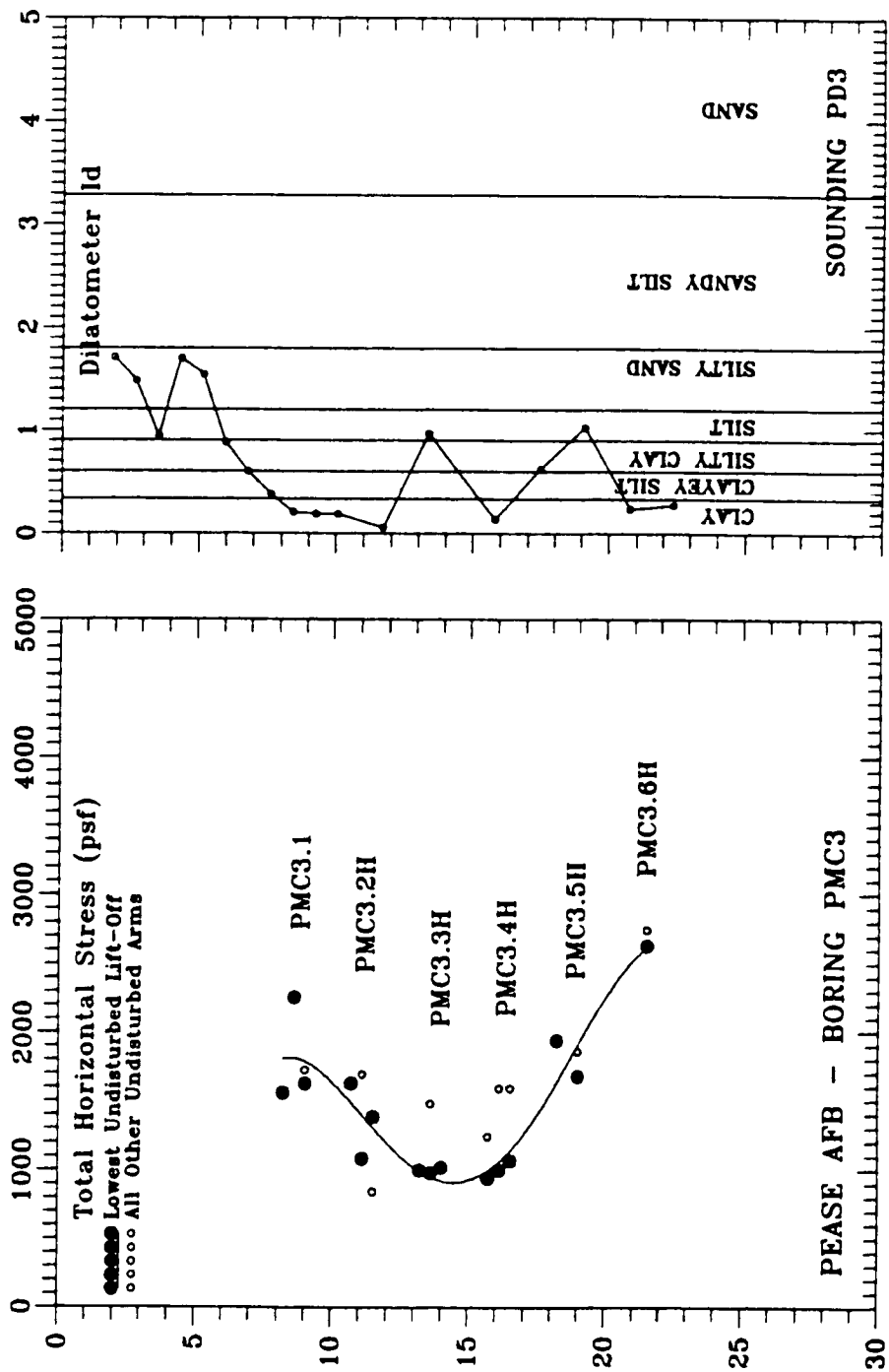


Figure 4-8 Profile of I_p and Horizontal Stress, PMC3

DILATOMETER c_h RESULTS OF NEJAME (1991)			
DEPTH (feet)	SCHMERTMANN(1988) cv. (ft ² /DAY)	ROBERTSON(1988) cv. (ft ² /DAY)	MARCHETTI(1989) cv. (ft ² /DAY)
8.4	0.06	0.62	0.03
9.3	0.22	1.63	0.13
10.1	0.08	0.69	0.04
11.7	0.05	0.55	0.03
13.4	0.17	1.26	0.04
14.2	0.07	0.77	NA
15.8	0.12	1.07	0.05
17.5	0.50	3.55	0.14
19.1	0.99	5.13	0.06
20.7	0.66	5.90	0.14
22.4	0.99	5.50	0.28

Table 4-2 Summary of Dilatometer c_h Values (after Nejame, 1991)

the test depth. Figure 4-9 presents a plot of the Pease test site dissipated C-readings with depth. A hydrostatic profile line, computed assuming the phreatic surface consistent with the ground surface, is also plotted on the figure. As can be seen, the dilatometer dissipated C-readings show some scatter, but have an overall trend that is generally consistent with the hydrostatic profile line. The scatter in the data is believed to be a result of error due to the indirect nature of the measurement, however, one measurement at a 19 foot depth seems to indicate a measured head about 300 psf (5 feet of head) less than the hydrostatic line. The I_p profile presented on Figure 4-8 indicates a silt layer at this depth. It is interesting to note, the SBPM test conducted closest to this low reading of static pore pressure (PMC3.6H) measured an excess pore pressure after insertion which was also less than the hydrostatic line indicated on Figure 4-9 by about 700 psf. This was an anomaly, since most tests inserted by the cutting method resulted in excess pore pressure above the hydrostatic line indicated on figure, and may lend some credence to the low head measured by the dilatometer. Further, Ladd, et al. (1972) alluded to a drainage layer that was implied due to their measured distribution of the horizontal coefficient of consolidation, c_h , across the soil profile. Aside from this anomaly, however, the dissipated dilatometer C-reading method is within, on average, ± 119 psf (about 2 feet of pressure head) of the assumed hydrostatic profile line shown on Figure 4-9.

4.2.4.5 Pneumatic Piezometers - Four pneumatic piezometers were installed in SBPM boring PMJ5 (piezometers P-1.1 and P-1.2) and in piston sample boring B-3 (piezometers P-2.1 and P-2.2). The piezometers were manufactured by Slope Indicator Co. of Seattle, Washington (Model 51417800) and were enclosed in pervious canvas bags filled with Ottawa sand. Prior to installation, the piezometers and sand bags were saturated in a bucket of water. These instruments were sealed in an approximately 1-foot thick layer of Ottawa sand which was sealed into the borehole using bentonite pellets. The depth of installation and

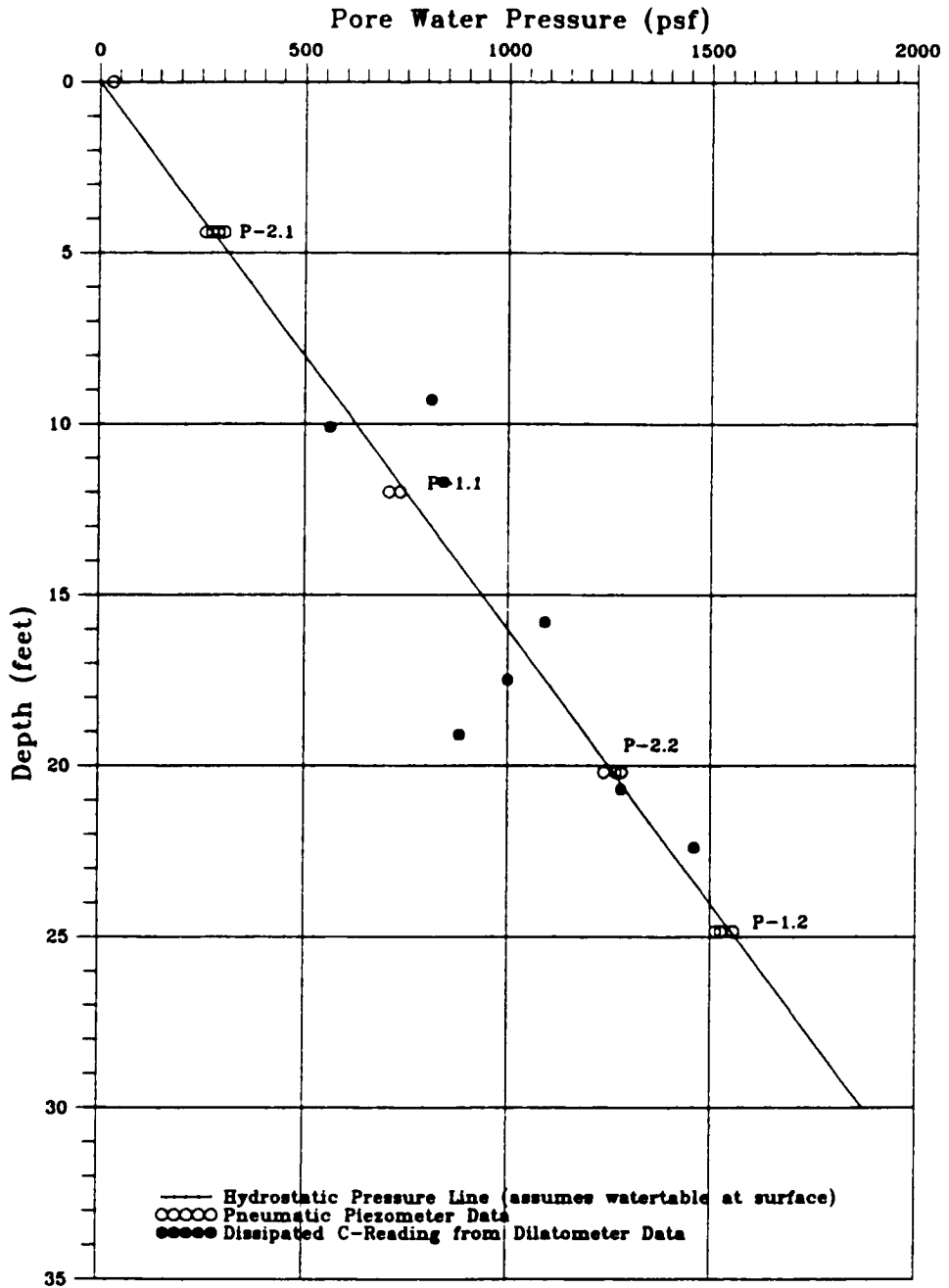


Figure 4-9 Summary of Pore Water Pressure Measurements at Pease AFB K_0 Area

subsequent porewater pressure readings are indicated on Figure 4-9. The porewater pressure levels indicated by the piezometers were observed over the course of a year, and were found, within the error of measurement of the piezometer reading equipment and installation measurement error (about 0.5 feet of water), to indicate that the static pore pressure distribution at the site is generally hydrostatic from the ground surface. No sign of a "drainage layer" as indicated by the dissipated dilatometer C-readings (discussed in the previous section) can be observed, however, it is noted that the piezometers are located more than 60 feet away from the dilatometer sounding.

As can be seen on Figure 4-9, there was standing water above the ground surface at the piezometer location. With the implied distribution of hydrostatic pressure from the ground surface, the standing water suggests a downward gradient likely exists between the surface water and groundwater within the silty clay deposit.

4.2.5 Laboratory Testing

Laboratory testing of the silty clay was performed for the current research to verify previously determined properties. Laboratory testing included isotropic (ICU) and anisotropic (ACU) consolidated-undrained triaxial tests, one-dimensional consolidation tests, Atterberg limits, specific gravity and moisture content determinations. The findings of this testing are in general agreement with the results of Ladd (1972) and Ladd, et al. (1972), with the exception of the natural moisture content, as will be discussed.

4.2.5.1 Index Properties - Index properties determined for the current research are summarized on Table 4-1 along with data determined previously by Ladd, et al. (1972). Based on the results of these tests, the silty clay at the site has a Unified Soil Classification of CL, or a silty clay of low plasticity. Index testing was conducted in general compliance with ASTM Standards. In general, it appears the index properties are in good agreement. However, the moisture content of the clay determined by the current research is on average about 8 percentage

points lower than the average reported by Ladd. The data of Ladd were statistically compared to that from the current research to confirm the apparent trends. Using a T-test procedure, it was verified that except for moisture content, there is no evidence to suggest that the mean values of the index properties measured during the current research are different than the mean values reported by Ladd. A level of significance of 0.5% was assumed for determination of the critical value of T. While it might be expected that the moisture content at the toe of the embankment would be lower than that measured by Ladd due to consolidation under the constructed embankment, it would have been expected that the moisture content at the K_0 area would be similar to the findings of Ladd. A reason for the difference may be due to the relative thicknesses of the portions of the clay deposit tested by the previous and current research. The area of the clay deposit tested by Ladd was on the order of 30 to 40 feet thick. The deposit tested by the current research was 30 to 50 percent thinner. Assuming variations in thickness result in varying degrees of desiccation, greater desiccation at the area of the current research may be responsible for the observed differences.

Soil profiles including results of laboratory and field tests conducted for the current research have been presented on Figures 4-5 and 4-6. Figure 4-5 represents conditions away from the influence of the embankment (K_0 area) and Figure 4-6 represents conditions at the embankment toe (toe area). It can be seen that below the crust, and at a given depth, the shear strength near the toe is from 5 to 35 percent higher than at the location away from the embankment, indicating that stress increase due to the embankment and the resulting consolidation has apparently increased the shear strength of the silty clay. However, little influence of the embankment construction on moisture content can be seen; moisture content at the embankment toe appears to be about the same as that at the K_0 area. It should be noted that the toe area is within 200 feet of one of the major exploration/test sample locations reported by Ladd, et al. (1972), while the K_0 area was more on the order

of 600 to 800 feet away. The observation of little difference in the moisture content between the toe area and the K_0 area may be because the pre-embankment construction moisture content of the clay at the toe area was closer to the moisture content determined by Ladd than that at the K_0 area.

4.2.5.2 One-Dimensional Consolidation Tests - Twenty-nine one-dimensional consolidation tests were performed as part of the current research. The tests were conducted in general accordance with ASTM specification D-2435 on samples trimmed from 3-inch undisturbed thin-walled piston samples obtained during the field testing. The samples were trimmed using a sharp bevel-edge 2.5 inch ID cutting ring which doubled as a confining ring during the test. The ring was carefully and smoothly pressed into the soil sample, and trimmings saved for moisture content determination. The trimmed test sample contained in the ring was 2.5-inches in diameter and 1-inch in height. Samples were trimmed so that their axis of compression and drainage was oriented both vertically (V-Series tests) and horizontally (H-Series tests). The V-series tests were made primarily to assess the stress history of the silty clay deposit, while the H-series tests were made to determine the horizontal coefficient of consolidation, c_h , for comparison with c_v values determined by SBPM hold tests, which is discussed in Chapter VII.

The testing was conducted in two compressed air Carrol-Warner consolidometers. Deflection was measured by an LVDT and recorded by a personal computer via a data acquisition system. Loads were applied maintaining a load-increment ratio of 1, meaning successive loads were double the previous load. Load was applied in the following increments: .25, .5, 1.0, 2.0, 4.0, 8.0 ksf, followed by an unload-reload cycle. After reloading to 8.0 ksf, additional loads of 16.0 and 32.0 ksf were applied, followed by final unloading. In general, virgin loads were maintained for at least 24 hours to assure a good definition of the end of primary consolidation. Reload or unload increments were sometimes maintained for lesser times since primary consolidation in these cases

generally occurred at significantly shorter time than virgin compression.

A summary of consolidation and related index property data is presented on Table 4-3. Table 4-4 presents stress history data resulting from analysis of the test data. A plot of the log of the overconsolidation ratio (OCR, the ratio of the maximum past pressure to the existing vertical effective overburden pressure) versus normalized shear strength (s_u/p') is presented in Figure 4-10. The error bars indicate the range in OCR due to uncertainty of determination of the maximum past effective stress from the consolidation test data. The maximum past pressure was determined from e-log p' curves using the Casagrande (1936) construction. The results reflect the stiffer "clay crust" (maximum past pressure of about 2000 to 3500 psf) in the upper portion of the deposit due to desiccation and the softer underlying clay (maximum past pressure generally less than 2000 psf) with depth. This stiffness difference can be observed on the plots of maximum past effective stress with depth on Figures 4-5 and 4-6. From the tests with the axis of compression oriented vertically, the compression index, C_c , varied from about 0.17 in siltier samples to up to 0.59 in the softer clays. The recompression index, C_r , was about an order of magnitude less, ranging from 0.01 to 0.08. The consolidation characteristics and stress history measured for the current research were generally similar to those reported by Ladd, et al. (1972).

Figures 4-11 and 4-12 are plots of the vertical and horizontal coefficient of consolidation, c_v and c_h , respectively, with depth. Data from the dilatometer dissipation tests as well as data from Ladd, et al. (1972), both described previously, are included on the figure. As can be seen on both figures, for data from the current research, values from virgin compression are about an order of magnitude less than the unload/reload values. From comparison of the two figures, it can also be seen that there is essentially no difference between the magnitude of c_v and c_h from the current research at a given depth and loading condition, however, a slight decrease is observed in both with depth.

PEASE AIR FORCE BASE SUMMARY OF ONE DIMENSIONAL COMPRESSION DATA															
TEST ID	BORING	SAMPLE	AXIS OF COMPRESSION	DEPTH (FEET)	UNIFIED CLASSIFICATION	MOISTURE CONTENT(%)	PL (%)	LL (%)	UNIT WT		INITIAL VOID RATIO	COEF OF COMP. C _c	COEF OF RECOMP. C _r	COEFFICIENT OF CONSOLIDATION	
									WET (PCF)	DRY (PCF)				ch (ft ² /day)	cv (ft ² /day)
1	U2	UD-7	VERT	15.2	CL	36.6-49.4	20.8	33.4	110.0	80.3	1.06	0.590	0.035	0.20	1.09
2	U2	UD-7	HORZ	13.4	CL	40.6-42.3	20.8	33.4	113.4	79.9	1.13	0.310	0.023	0.29	1.00
3	U2	UD-7	VERT	13.8	CL	37.0-46.4	20.8	33.4	113.9	82.2	1.06	0.333	0.023	0.40	0.96
4	U2	UD-6	VERT	13.0	ML-CL	26.7-29.7	20.0	28.9	121.3	94.0	0.78	0.170	0.021	0.26	1.05
5	U2	UD-6	HORZ	12.5	ML-CL	32.6-33.1	20.0	28.9	118.8	90.0	0.89	0.170	0.018	0.17	0.63
6	U2	UD-2	VERT	8.0	CL	42.7-44.1	21.1	34.1	113.1	79.1	1.17	0.445	0.035	0.20	0.40
7	U2	UD-2	HORZ	8.5	CL	40.7-46.9	22.1	34.1	111.4	78.4	1.13	0.580	0.040	1.09	0.72
8	U2	UD-3	HORZ	10.7	CL	35.0-38.4	20.9	34.0	115.4	83.4	1.04	0.330	0.030	0.49	1.06
9	U2	UD-3	VERT	11.0	CL	35.4-40.4	20.9	34.0	110.6	81.3	1.00	0.410	0.030	0.40	0.53
A	U3	UD-9	VERT	26.5	ML-CL	26.4-28.1	20.6	25.5	125.0	97.7	0.72	0.100	0.060	0.79	1.24
B	U3	UD-9	HORZ	26.0	ML-CL	30.3-32.0	20.6	25.5	120.0	91.0	0.85	0.170	0.010	0.19	4.76
C	U3	UD-7	HORZ	21.5	CL	53.4-53.6	19.7	34.8	106.0	68.8	1.44	0.400	0.020	0.88	1.04
D	U3	UD-7	VERT	21.7	CL	53.7-56.3	19.7	34.8	106.0	68.8	1.44	0.560	0.035	0.36	2.20
E	U3	UD-5	VERT	17.8	CL	38.6-44.9	24.7	39.4	109.4	75.5	1.22	0.360	0.020	0.19	1.16
F	U3	UD-5	HORZ	17.6	CL	44.8-47.9	24.7	39.4	110.4	74.6	1.27	0.440	0.035	0.11	0.89
G	U3	UD-8	VERT	23.6	CL	47.3-55.0	24.3	38.8	105.2	67.9	1.50	0.360	0.030	0.24	2.48
H	U3	UD-8	HORZ	24.4	CL	50.8-53.8	24.3	38.8	105.9	68.8	1.44	0.380	0.025	0.11	0.89
I	U4	UD-2	HORZ	8.2	CL	39.3-41.1	22.4	32.8	113.2	80.2	1.13	0.310	0.030	0.24	2.48
J	U4	UD-2	VERT	8.0	CL	38.8-41.0	22.4	32.8	115.3	81.8	1.13	0.280	0.030	0.23	1.37
K	U4	UD-1	HORZ	6.3	CL	32.0-34.1	21.4	32.4	117.7	89.2	0.89	0.160	0.025	2.14	7.35
L	U4	UD-1	VERT	6.1	CL	24.5-28.3	21.4	32.4	121.1	94.6	0.79	0.110	0.010	15.27	21.68
M	U4	UD-6	VERT	16.9	CL	42.3-48.1	21.3	33.2	110.3	74.6	1.32	0.480	0.035	0.19	2.34
N	U4	UD-6	HORZ	16.4	CL	40.9-44.9	21.3	33.2	112.8	77.8	1.22	0.330	0.020	0.25	1.96
O	U4	UD-4	HORZ	12.9	CL	41.4-42.2	21.8	34.5	114.0	80.7	1.13	0.370	0.025	0.33	3.11
P	U4	UD-4	VERT	12.5	CL	33.5-38.6	21.8	34.5	112.7	78.7	1.17	0.400	0.025	0.22	1.27
Q	U4	UD-5	VERT	14.8	ML-CL	41.0-42.3	17.1	20.7	112.8	79.3	1.17	0.330	0.020	0.22	2.99
R	U4	UD-5	HORZ	15.0	ML-CL	44.0-47.8	17.1	20.7	112.0	77.8	1.22	0.330	0.030	0.14	1.15
S	U4	UD-3	HORZ	11.2	CL	37.0-37.6	20.9	31.5	115.6	84.2	1.04	0.360	0.020	0.70	5.72
T	U4	UD-3	VERT	10.9	CL	37.2-43.0	20.9	31.5	115.0	83.2	1.04	0.370	0.025	3.24	2.41

Table 4-3 Summary of Compressibility Data

PEASE AIR FORCE BASE SUMMARY OF CONSOLIDATION TEST STRESS HISTORY DATA													
TEST ID	BORING	SAMPLE	AXIS OF COMPRESSION	DEPTH (FEET)	UNIFIED CLASSIFICATION	MAX EFF. PAST PRESSURE (PSF)		OVERBORN PRES (PSF)	SHEAR STRENGTH (PSF)	OVERCONSOLIDATION RATIO		NORMALIZED STRENGTH, S _w /P	
						MIN	MAX			MIN	MAX		
1	U2	UD-7	VERT	15.2	CL	1000	2000	772	350	1.30	2.59	0.45	
2	U2	UD-7	HORZ	13.4	CL	700	1000	643	340	1.02	1.46	0.53	
3	U2	UD-7	VERT	13.8	CL	900	1100	703	340	1.28	1.56	0.51	
4	U2	UD-6	VERT	13.0	ML-CL	2000	3000	663	340	3.02	4.32	0.54	
5	U2	UD-6	HORZ	12.5	ML-CL	500	600	637	340	0.78	0.94	0.57	
6	U2	UD-2	VERT	8.0	CL	2600	3500	408	930	6.37	8.58	2.28	
7	U2	UD-2	HORZ	8.5	CL	2000	2700	433	930	4.62	6.24	2.15	
8	U2	UD-3	HORZ	10.7	CL	1000	1700	546	280	1.83	3.11	0.51	
9	U2	UD-3	VERT	11.0	CL	2000	2200	561	280	3.37	3.92	0.50	
A	U3	UD-9	VERT	26.5	ML-CL	3000	3500	1284	340	2.34	2.73	0.26	
B	U3	UD-9	HORZ	26.0	ML-CL	300	500	1262	340	0.24	0.40	0.27	
C	U3	UD-7	HORZ	21.5	CL	700	1000	1064	270	0.66	0.94	0.25	
D	U3	UD-7	VERT	21.7	CL	700	1000	1073	270	0.63	0.93	0.25	
E	U3	UD-5	VERT	17.8	CL	1000	1600	896	355	1.12	1.79	0.40	
F	U3	UD-5	HORZ	17.6	CL	1200	2000	887	355	1.35	2.25	0.40	
G	U3	UD-8	VERT	23.6	CL	300	500	1156	265	0.26	0.43	0.23	
H	U3	UD-8	HORZ	24.4	CL	800	1200	1183	310	0.68	1.01	0.26	
I	U4	UD-2	HORZ	8.2	CL	1100	1900	456	800	2.41	4.17	1.75	
J	U4	UD-2	VERT	8.0	CL	1700	2300	446	850	3.81	5.16	1.91	
K	U4	UD-1	HORZ	6.3	CL	2000	2600	363	2000	5.51	7.16	3.51	
L	U4	UD-1	VERT	6.1	CL	2000	3000	352	2000	5.68	8.52	5.68	
M	U4	UD-6	VERT	16.9	CL	1100	2000	891	600	1.23	2.34	0.87	
N	U4	UD-6	HORZ	16.4	CL	1000	1500	866	580	1.15	1.75	0.87	
O	U4	UD-4	HORZ	12.9	CL	1200	1800	693	440	1.73	2.60	0.83	
P	U4	UD-4	VERT	12.5	CL	1200	1800	673	450	1.78	2.67	0.87	
Q	U4	UD-3	VERT	14.8	ML-CL	900	1400	790	410	1.14	1.77	0.52	
R	U4	UD-3	HORZ	15.0	ML-CL	800	1400	800	450	1.00	1.73	0.54	
S	U4	UD-3	HORZ	11.2	CL	1000	1500	607	500	1.63	2.14	0.82	
T	U4	UD-3	VERT	10.9	CL	1600	2300	592	500	2.70	3.89	0.84	

Table 4-4 Summary of Stress History Data

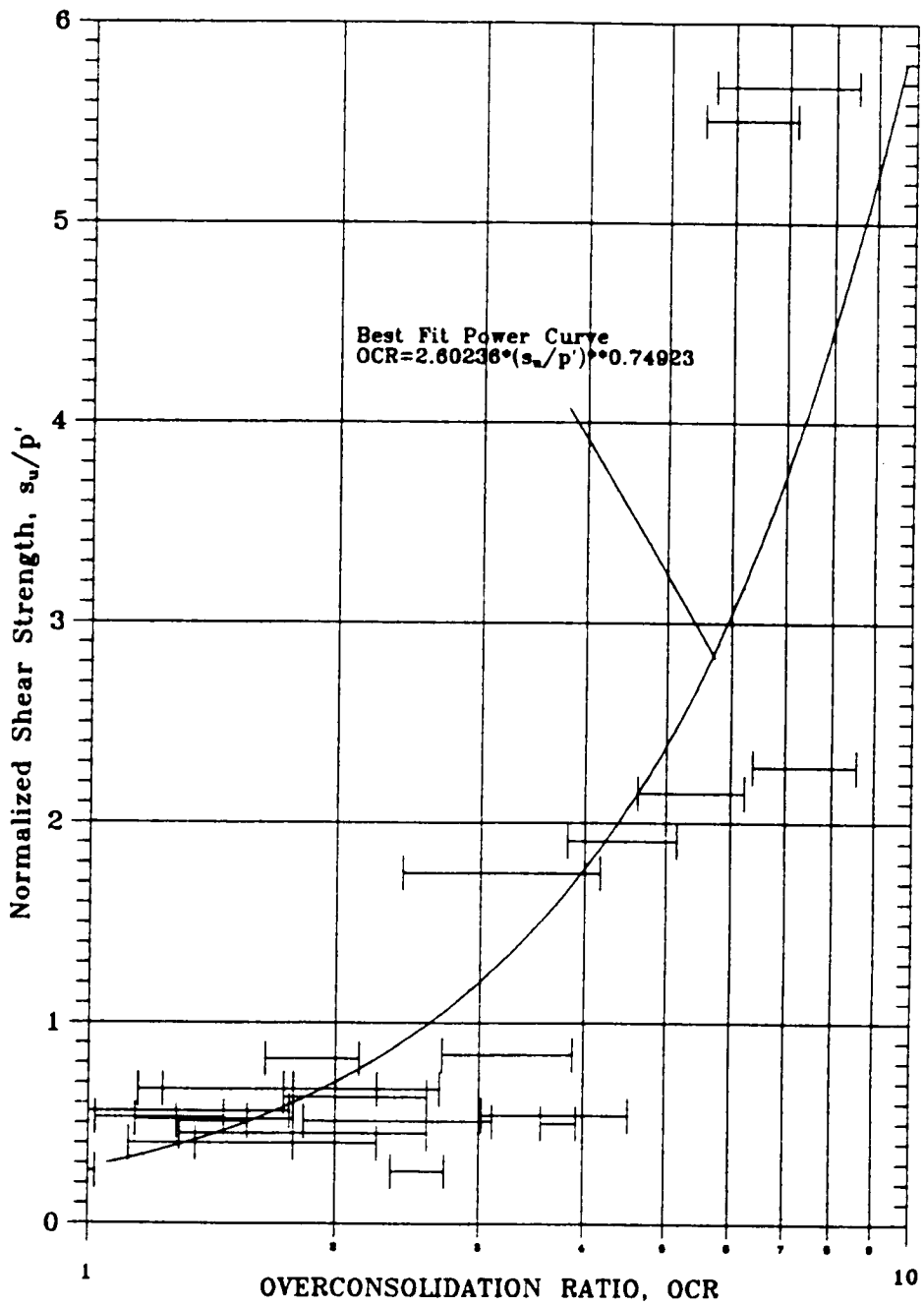


Figure 4-10 OCR Versus Normalized Shear Strength

PEASE AIR FORCE BASE
CONSOLIDATION TEST RESULTS

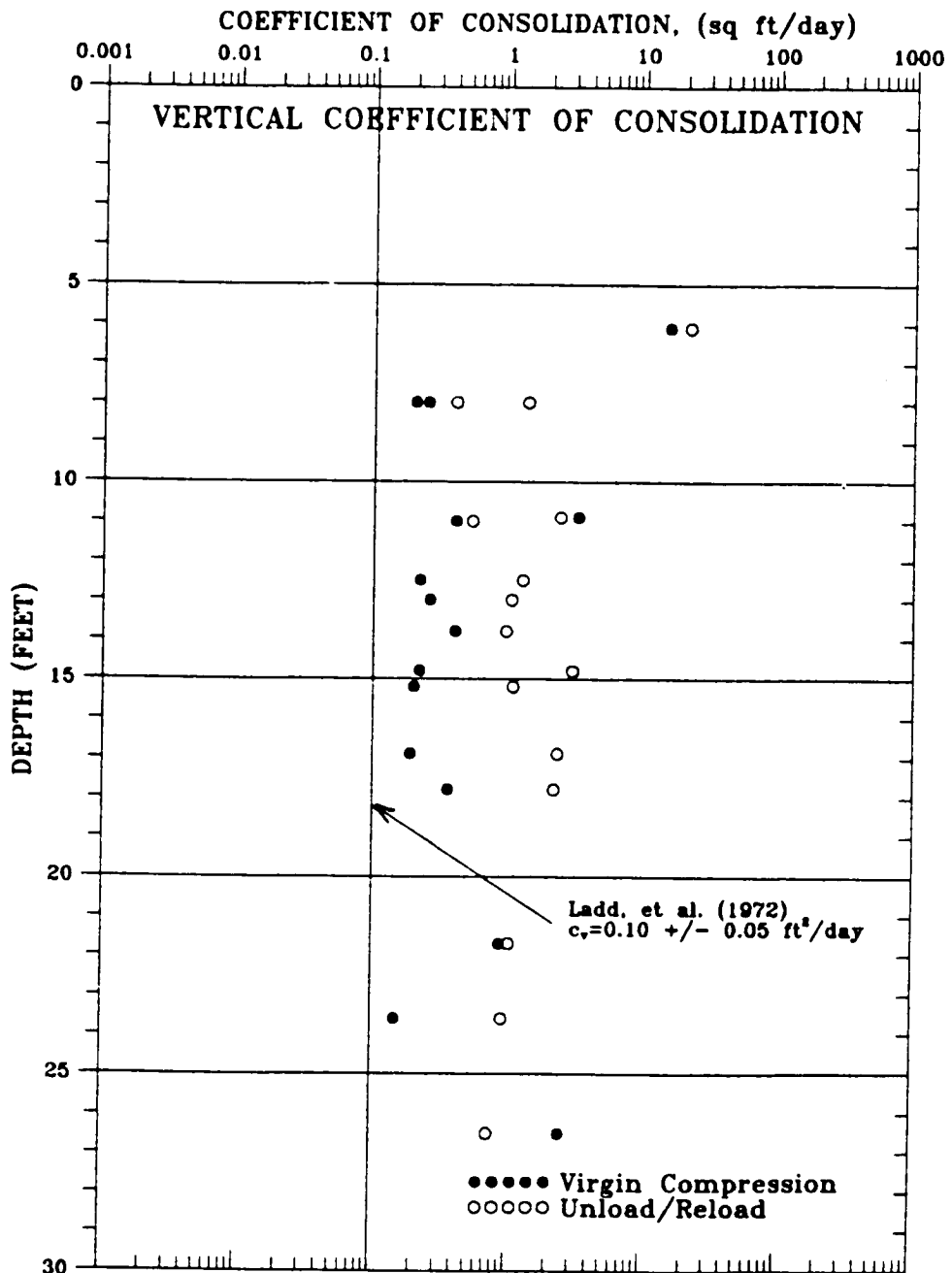


Figure 4-11 Vertical Coefficient of Consolidation

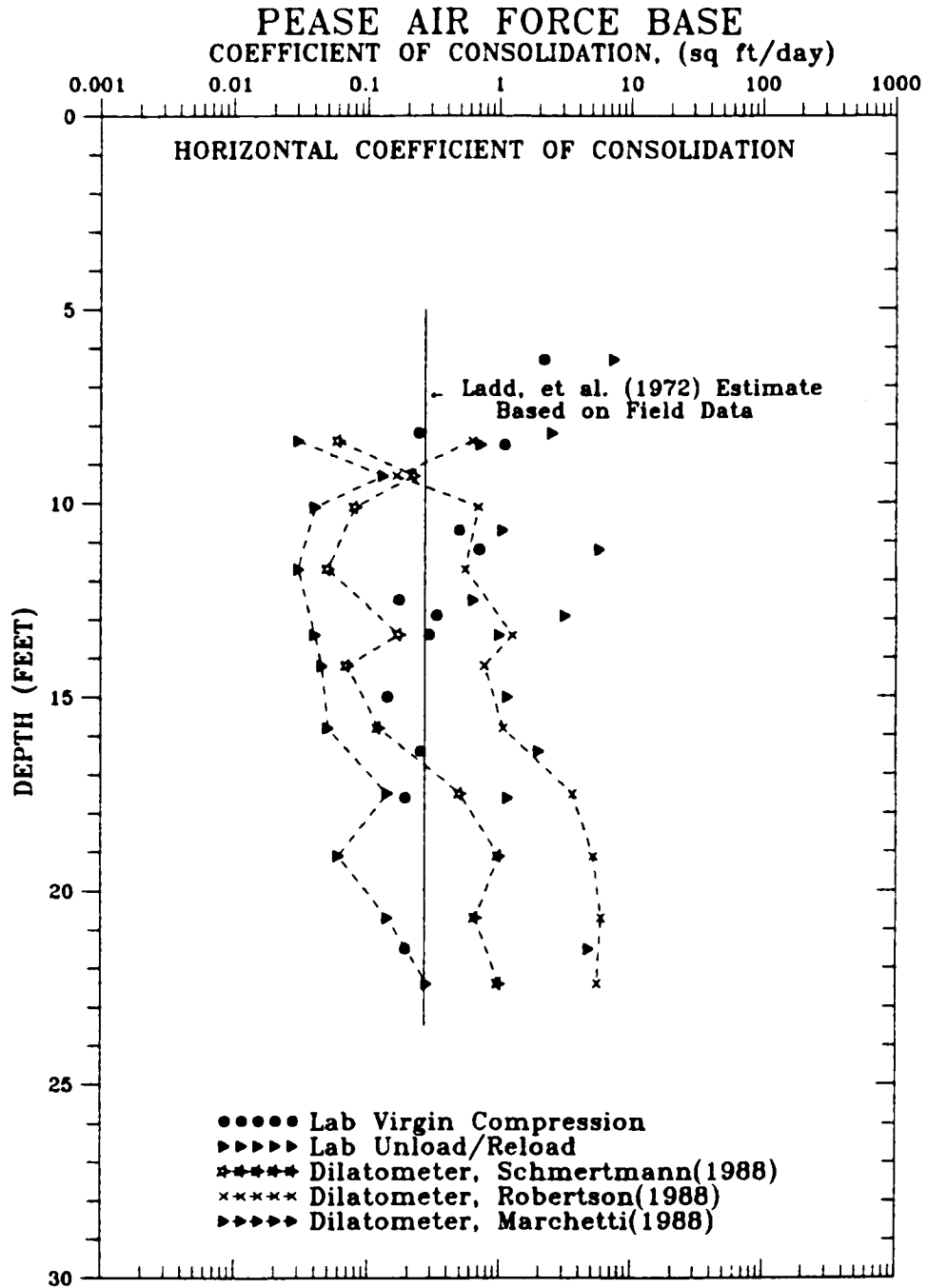


Figure 4-12 Horizontal Coefficient of Consolidation

As indicated earlier, Ladd, et al. noted that field measured c_v was generally 1.5 to 2 times field c_u . The reason that the lab results indicate that c_v is about the same as c_u is likely due to the fact that the laboratory samples are too small to contain the macro drainage layers which are actually present in the field, and have a major influence on the field measured values. In general, laboratory measured c_v and c_u were about 0.01 to 1 ft²/day for the softer, deeper portion of the deposit, and up to about 10 ft²/day in the stiff upper crust.

4.2.5.3 C-U Triaxial Testing - Ten consolidated-undrained (CU) triaxial shear tests were performed for the current research, three by the writer and seven by Jones (1988). The tests were designated AJ1 through AJ7 and RCF1, RCF2 and RCF5. Four of the tests conducted by Jones (AJ1 through AJ4) were stage tests conducted on one sample. All except one of the reported tests were isotropically consolidated, undrained shear tests (ICU). One test (RCF5) was an anisotropically consolidated, undrained shear test (ACU), with a ratio of horizontal to vertical effective consolidation stress of 0.5. The tests were performed in general accordance with the proposed ASTM standard for CU triaxial tests (not yet accepted at the time of testing). The CU tests conducted by the writer included computer data acquisition of strain, pore pressure and axial load. The tests were performed by first fully consolidating the specimen to the desired stress condition. Shearing did not commence until a measured Skempton (1954) B-value of about 0.95 or more was achieved. Shearing was conducted at a rate which would achieve failure at a time equivalent to 10 times t_{50} after initiation of shear, in accordance with the proposed ASTM standard. This was equivalent to failing the sample at about 24 hours or a strain rate of about 0.00005 inches/minute. The writer's tests were generally of 3 to 6 day duration. Tests by Jones were somewhat shorter in duration, about 12 to 24 hours with a strain rate of 0.0001 to 0.00005 inches/minute, however little difference was observed by the two different sets of tests. A summary of the results of the triaxial testing is presented on Table 4-5.

Effective stress paths for the tests are presented as Figures 4-13 and 4-14 for normally (including the ACU test) and overconsolidated tests, respectively. As can be seen, the normally consolidated ICU tests resulted in an effective angle of internal friction, (ϕ') of about 21.3 degrees and the overconsolidated tests resulted in a ϕ' of about 25.1 degrees with a cohesion intercept of about 200 psf. The ACU test on a normally consolidated sample indicated a ϕ' of about 30.6 degrees.

Six consolidated-undrained triaxial tests conducted for design of the highway embankments are included on Table 4-5 (Haley and Aldrich, 1968). These tests included 5 isotropically consolidated, and one anisotropically consolidated shear test. The anisotropically consolidated test was consolidated under a $K_0=0.6$ stress condition. Ladd indicates the ICU tests yielded a ϕ' of about 21°, which compares well with the findings of the present research, while the K_0 test indicated a ϕ' of 31.5°. The K_0 ϕ' was thought by Ladd (1972) to be high, possibly a result of friction in the test apparatus, however, that value was only about a degree more than that measured by the ACU test performed for the present research, indicating that Ladd's measured value may be reasonable.

With regard to normalized shear strength ratios, the ICU tests performed for the current research resulted in s_u/p' ratios of 0.18 to 0.25 compared to Ladd's 0.23 to 0.25. This is in reasonable agreement with s_u/p' from the field vane tests conducted for the current research, which indicated a range of 0.23 to 0.26. The ratio for the ACU test, RCF5, was 0.310. Ladd (1972) indicated that the s_u/p' ratios for plane strain active and plane strain passive K_0 tests was 0.295 and 0.13, respectively. Direct simple shear testing was reported to have yielded an s_u/p' value of 0.20.

The pore pressure parameter "A" (Skempton, 1954) at failure, A_f , was found to vary from 0.75 to 1.25 for ICU tests performed for the current research and 0.69 to 1.05 by previous tests performed for construction

PEASE AIR FORCE BASE												
SUMMARY OF TRIAXIAL TESTS FOR CURRENT RESEARCH												
TEST	BORING	DEPTH (feet)	% MOISTURE		CONSOLE PRES (psf)	K _o	OCR	FAILURE STRAIN (%)	UNDRAINED SHEAR STRENGTH (psf)	NORMALIZED STRENGTH, Su/p'	Af	φ'(c=0) (degrees)
			INITIAL	FINAL								
AJ1	B-3	22.0	33.8	NA	1440	1.0	1.3	1.1	446	0.310	0.89	22.5
AJ2	B-3	22.0	NA	NA	2880	1.0	1.0	1.4	691	0.240	1.25	21.3
AJ3	B-3	22.0	NA	NA	4320	1.0	1.0	1.4	1094	0.250	1.13	21.3
AJ4	B-3	22.0	NA	45.0	1080	1.0	3.0	5.0	922	0.850	0.13	27.1
AJ5	B-2	8.5	38.1	37.6	1253	1.0	2.4	3.0	1165	0.640	0.25	35.3
AJ6	B-2	16.5	43.7	42.1	1253	1.0	2.0	1.0	677	0.350	0.59	38.7
AJ7	B-2	14.5	45.3	47.7	626	1.0	2.0	3.0	418	0.400	0.40	37.3
RCF1	B-3	13.4	43.6	34.9	1526	1.0	1.0	0.9	893	0.247	0.75	22.5
RCF2	B-3	13.8	38.4	29.8	2578	1.0	1.0	1.6	1037	0.187	0.86	19.5
RCF5	B-4	13.0	34.5	25.0	2880	0.5	1.0	1.7	1310	0.310	0.56	30.6

PORTSMOUTH TRAFFIC CIRCLE												
SUMMARY OF TRIAXIAL TESTS FOR NHDPWH I-95 CONSTRUCTION												
TEST	BORING	DEPTH (feet)	% MOISTURE		CONSOLE PRES (psf)	K _o	OCR	FAILURE STRAIN (%)	UNDRAINED SHEAR STRENGTH (psf)	NORMALIZED STRENGTH, Su/p'	Af	φ'(c=0) (degrees)
			INITIAL	FINAL								
CIUC1	2A	12.1	59.5	46.9	1977	1.0	1.0	1.3	635	0.321	0.69	20
CIUC2	3A	17.7	38.7	29.9	4095	1.0	1.0	2	1146	0.280	0.86	21.5
CIUC3	3A	18.0	52.7	41	1977	1.0	1.0	2.5	604	0.305	0.87	19.8
CIUC5	3B	25.8	37.1	30.5	2217	1.0	1.0	1.6	573	0.258	1.05	21
CIUC6	3B	25.8	38.8	27.8	4519	1.0	1.0	2.1	1137	0.252	NA	19.9
CAUC1	3B	25.8	37.3	29.5	2683	0.6	1.0	0.5	755	0.281	1.53	23.8

Table 4-5 Summary of Triaxial Tests

PEASE AIR FORCE BASE - CU TRIAXIAL COMPRESSION TESTS
 GRAY SILTY CLAY - NORMALLY CONSOLIDATED TESTS

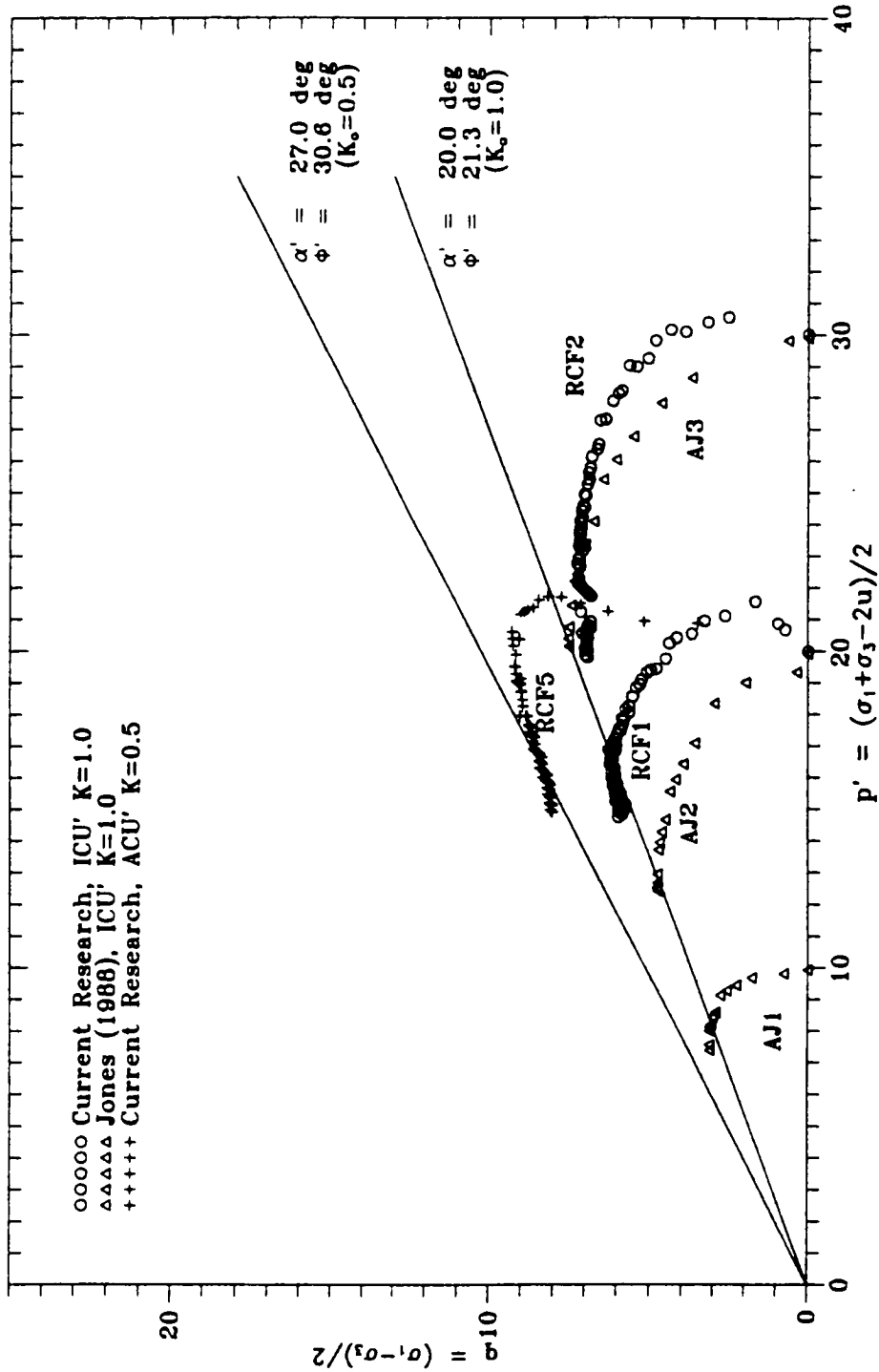


Figure 4-13 CU Triaxial Stress Paths - Normally Consolidated

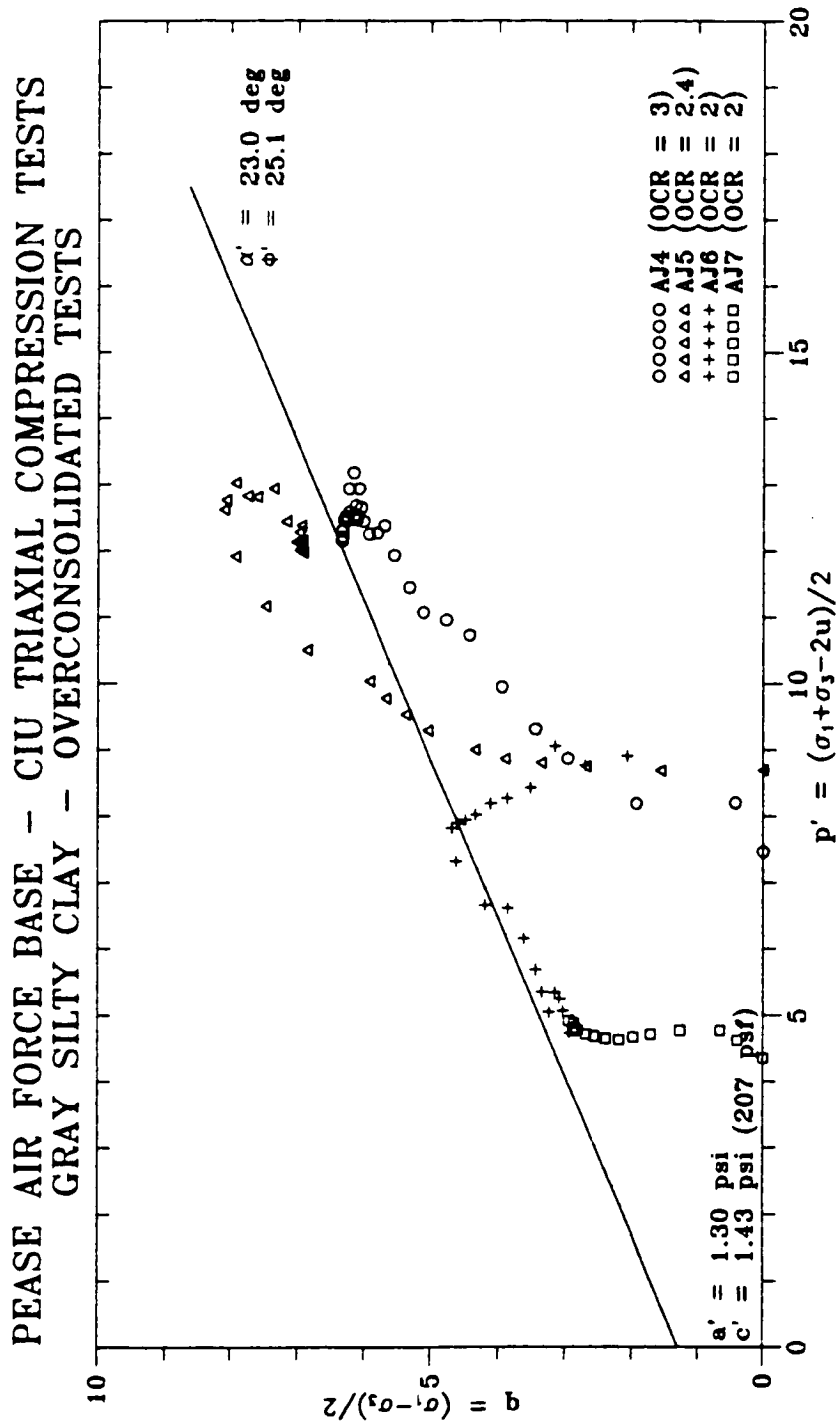


Figure 4-14 CU Triaxial Stress Paths - Overconsolidated

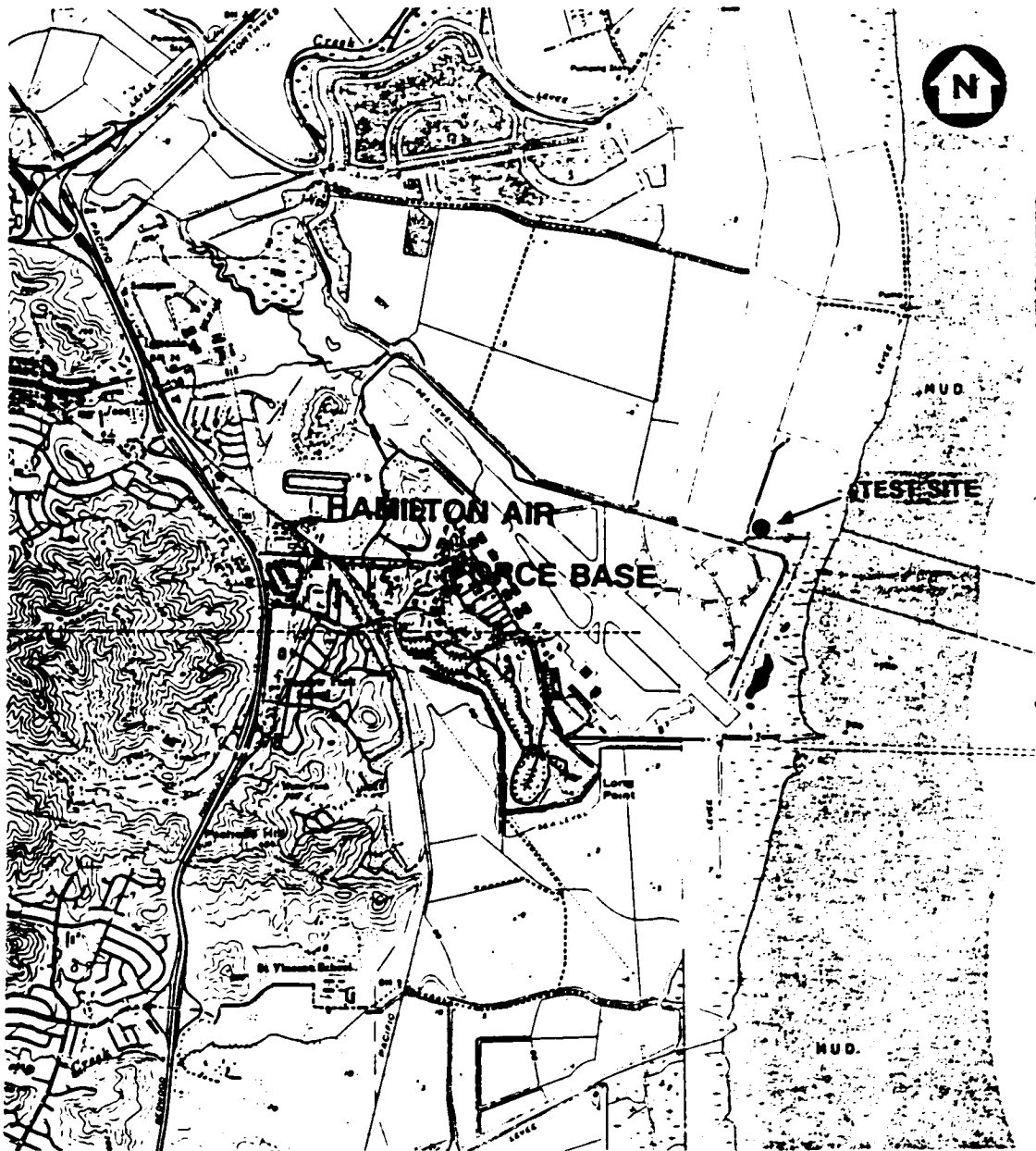
of the highway embankment. Holtz and Kovacks (1981) indicate that normally consolidated clays generally have A_v values of 0.5 to 1.0 while highly sensitive clays can have A_v values of from 0.75 to 1.5, which fits the range of values measured by the current and previous research. Tests conducted for the current research on overconsolidated soils resulted in lower A_v values, ranging from 0.13 to 0.59, which reflects the increased stiffness of these samples.

4.3 Hamilton Air Force Base

A portion of the field testing for this research was conducted at Hamilton Air Force Base, which is situated on northern San Francisco Bay in Novato, California, as shown on Figure 4-15, approximately 30 miles north of San Francisco. The test site is located on the Base, as indicated on Figure 4-15, and was selected because of the wealth of investigative work which has been performed in the past. That work included subsurface exploration, sampling, and testing by the USGS, the University of California at Berkeley, and Stanford University.

4.3.1 Geology

The geology of the San Francisco Bay sediments has been studied previously by Trask and Ralston (1951) and Treasher (1961) and more recently by Helley and Lajoie (1979). San Francisco Bay is a basin connected to the Pacific Ocean via the Golden Gate Channel. The bay is separated from the ocean by the Coastal Ridge to the west and is bordered by the Berkeley Hills to the east. The area is transected by several active faults, including the San Andreas, Hayward, and Calaveras zones. Soil deposits that exist over much of the bay area are the result of sedimentation. These sediments were derived from parent rock by weathering and geologic processes in the hill areas, and were transported down to the bay by stream and river flow. Between about 50,000 to 70,000 years ago, the oceans were significantly lower as a result of Pleistocene glaciation in the northern latitudes. Helley and Lajoie indicate that during the glaciation, sea level was 300 to 400 feet below the present elevation. At that time, the bay was primarily fresh water and



FROM USGS 15' TOPOGRAPHIC QUADRANGLES
 NOVATO, CALIF (1980) AND PETALUMA POINT, CALIF (1980) 1"=1200'

Figure 4-15 Site Location Map - Hamilton Air Force Base

deposition was generally more lacustrine in character. At the end of the last glaciation, some 15,000 years ago, the sea level began to rise quickly. The bay became saline about 10,000 to 11,000 years ago, and deposition became marine in character. This later marine deposition was responsible for the younger sediments which are the subject of the current research.

The bay sediments consist of five Quaternary formations summarized on Figure 4-16. These sediments are underlain by a Jurassic graywacke bedrock formation. The sediment which was the focus of the present research was the upper portion of the Young Bay Mud. This deposit is described as a silty clay to clayey silt with minor amounts of organic material, fine grained sand, and some shell lenses. Previous analyses have indicated the presence of montmorillonite, kaolinite, vermiculite, mica, hydrous mica, chlorite, and quartz. This wide mixture of materials is thought to be due, in part, to the extreme linear movement, measurable in terms of miles, that has occurred along faults in the bay area during the last 10,000 to 15,000 years. This movement has resulted in a number of different parent rock types to be within erosional vicinity of the bay, and thus influencing the composition of the sediment.

4.3.2 Site Description

The test site is located about 1000 feet away from the nearest perimeter dike which separates the airfield from the sea. A schematic map of the test site is presented on Figure 4-17. The site is generally level, grass covered, and is about 2 feet below mean sea level datum. The schematic shows the locations of previous explorations and soundings at the site, as well as those made for the current research. Denby (1978) indicated the USGS drilled a 90-foot deep boring at the location of the "Sample Borehole" on Figure 4-17. Figure 4-16 is a log of that boring. Samples from the boring indicated that the site is underlain, from the ground surface downward, by a desiccated zone of about 8-foot thickness, Young Bay Mud to a depth of about 58 feet, alluvial clay (Posey Formation) to about 77 feet, and finally Old Bay Mud, in which the

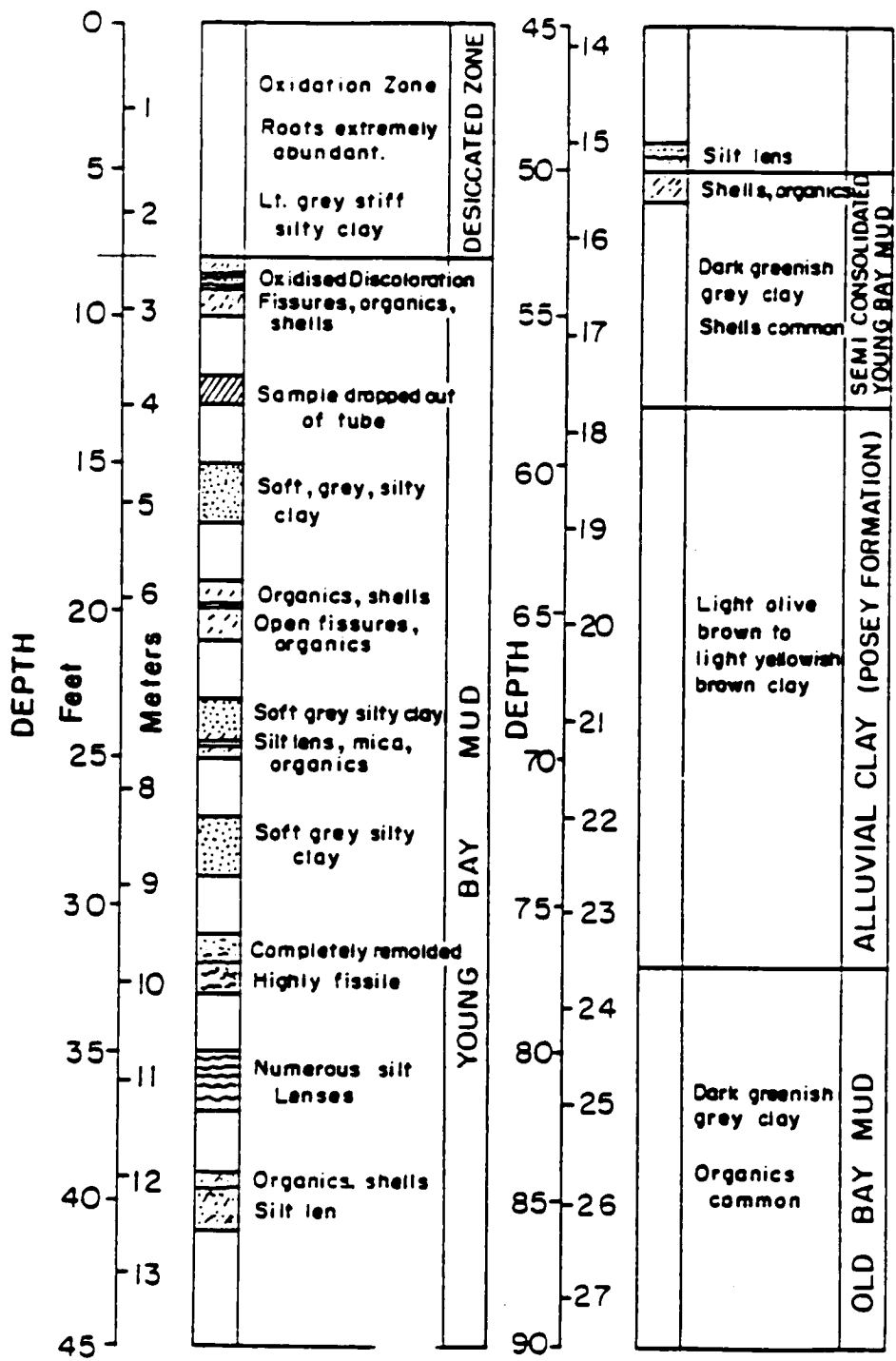
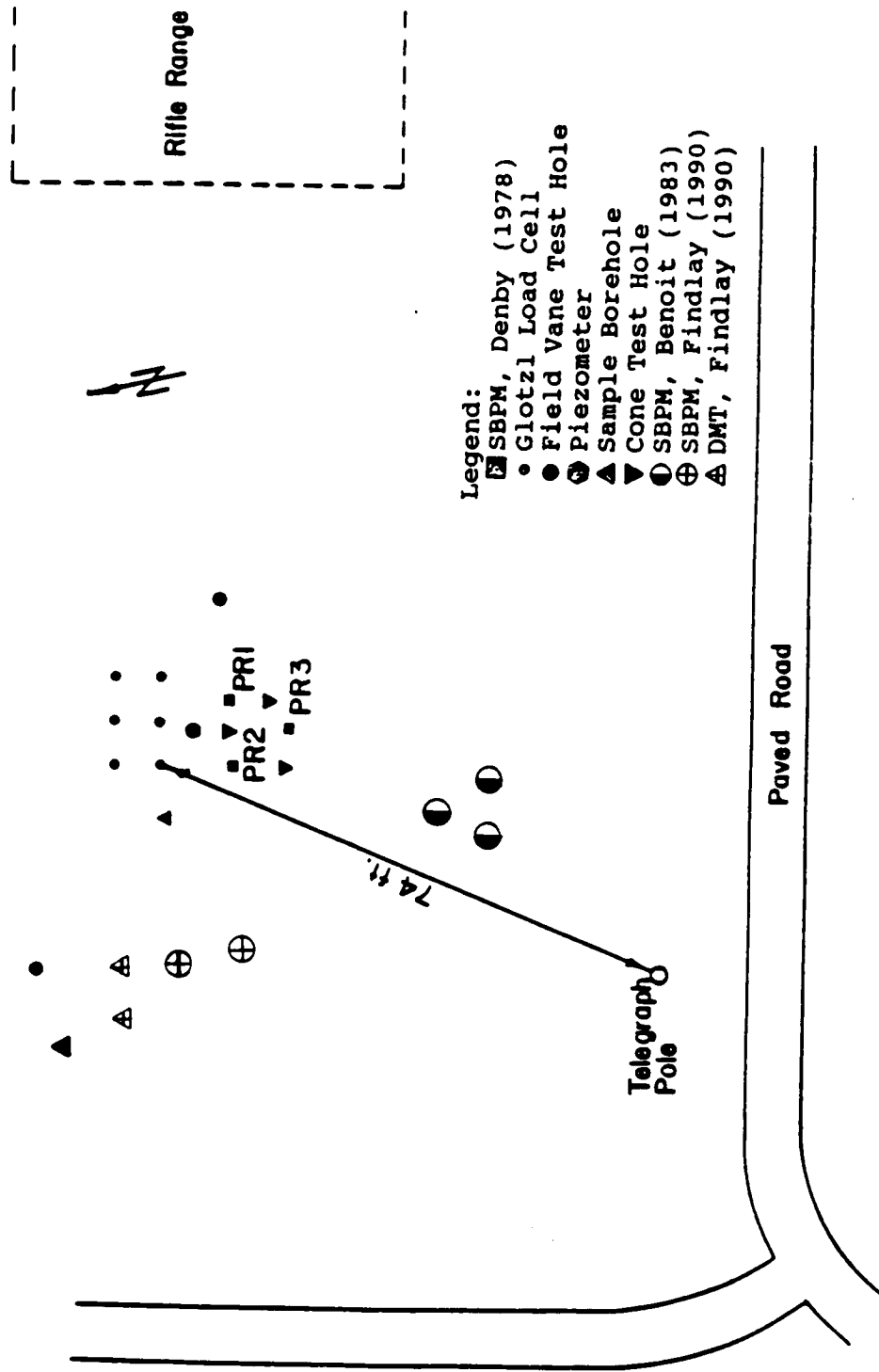


Figure 4-16 Log of USGS Boring at Hamilton AFB (after Denby, 1978)



- Legend:
- SBPM, Denby (1978)
 - Glotzl Load Cell
 - Field Vane Test Hole
 - ⊕ Piezometer
 - ▲ Sample Borehole
 - ▼ Cone Test Hole
 - ⊙ SBPM, Benoit (1983)
 - ⊕ SBPM, Findlay (1990)
 - ▲ DMT, Findlay (1990)

Figure 4-17 Schematic Plan of Hamilton AFB Test Site (after Denby, 1978)

boring was terminated. Benoit (1983) reported that the water table fluctuated from 2 to 7 feet below the ground surface during his field work. The water level was observed to be 6.0 feet below the ground surface during the current research in April of 1989.

4.3.3 Engineering Properties from Previous Research

Engineering properties of the site have been summarized by Bonaparte and Mitchell (1979), Denby (1978), and Benoit (1983). Figure 4-18 presents a profile of moisture content, Atterberg limits, and stress history of the site to a depth of about 50 feet. Atterberg limits from the previous work generally range from 40 to 45 and 85 to 90 percent for the plastic limit and liquid limit, respectively. The water content is generally slightly above the liquid limit, at an almost constant (below the desiccated zone) 90 percent. Based on the Atterberg limits, the soil is a silty clay of high plasticity (MH to CH by the Unified Soil Classification). Grain size analysis indicates that approximately 43.7 percent of the Young Bay Mud is smaller than the 2-micron upper clay size limit. A tabular summary of the properties of Young Bay Mud at Hamilton Air Force Base is presented as Table 4-6. This table indicates that the soil is highly compressible, with a compression index of from 1.2 to 1.8, with a recompression index of about one-tenth of the compression index (0.10 to 0.15). The coefficient of consolidation (c_v), ranged from 8 to 10 ft²/year.

Strength properties have been well documented. Effective stress ϕ' angles have been measured by laboratory tests to range from 31° to 38°, depending on the mode of failure, the highest values for vertical plane strain CU tests and lowest for consolidated drained tests. The undrained strength ratio, s_u/p' , has been calculated to range from 0.31 to 0.42 from field and laboratory test data, also dependent on the shearing mode. The lowest value of s_u/p' was measured by field vane testing (0.31 to 0.32), and the highest measured values (0.40) were by self-boring pressuremeter tests. Extrapolations of ICU tests to an OCR of 1.1 to 1.5 reportedly (Denby, 1978) produce comparable s_u/p' values to

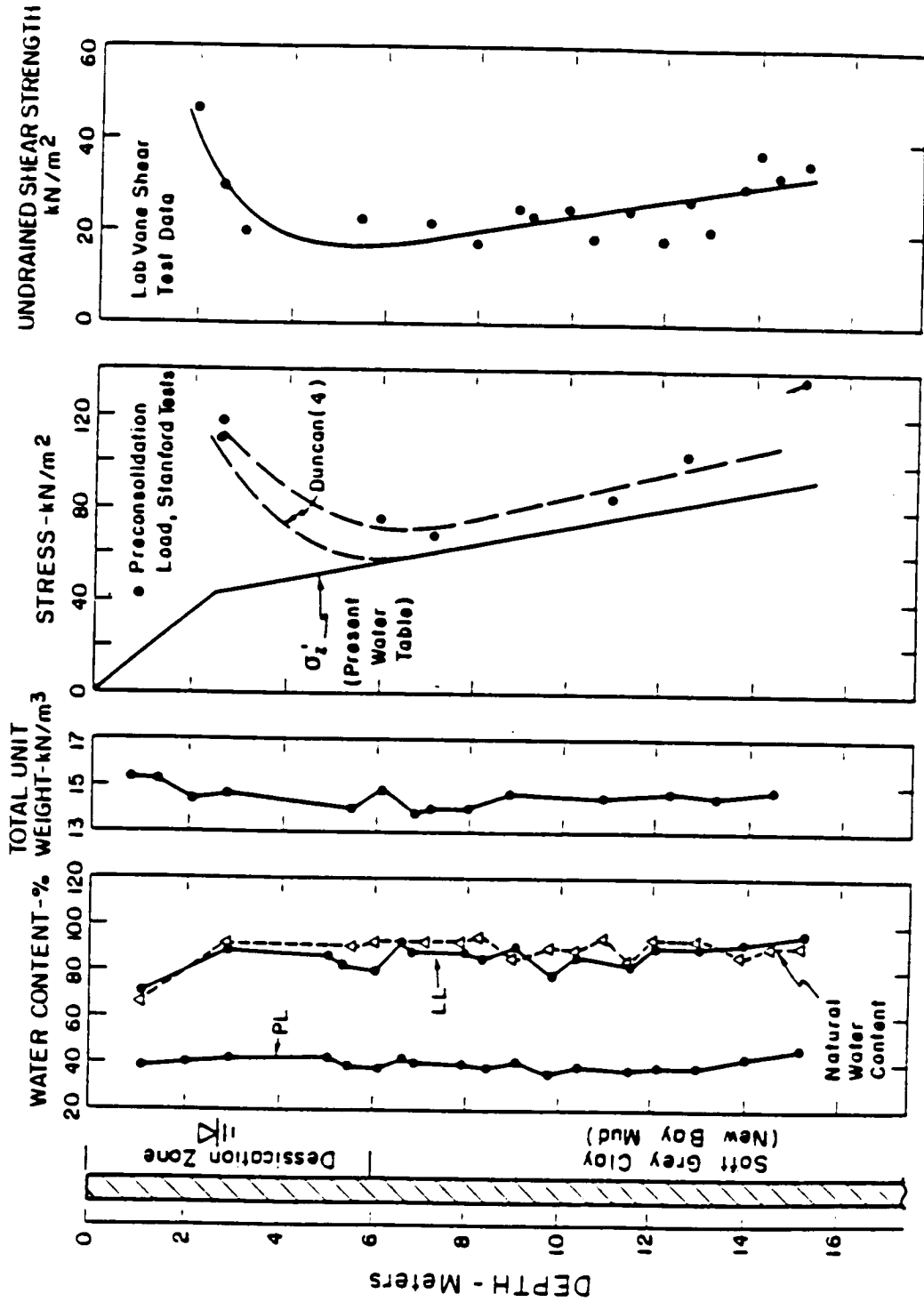


Figure 4-18 Hamilton AFB Test Site Soil Property Profile (after Clough and Denby, 1980)

Property	Value
Thickness of Deposit	55-58 feet
Saturated Unit Weight	94 pcf
Natural Water Content	90%
Liquid Limit	88%
Plasticity Index	40%
Liquidity Index	1%
Organic Content (Total Carbon)	1.5%
Compression Index, C_c	
Just Past P_p'	1.2-1.8
For $P' > 4000-6000$ psf	0.8-0.9
Recompression Index, C_r	0.1-0.15
Coefficient of Secondary Compression, C_a	0.01-0.02
Coefficient of Consolidation, C_v	8-10 ft ² /year
Effective Friction Angle, ϕ'	
CU Triaxial	32.5°-35°
Plane Strain Vertical CU	38°
Plane Strain Horizontal CU	35°
CD	31°
Undrained Strength Ratio S_u/p'	
ICU'	0.34
ACU' (K_o)	0.35
UU	0.32
Field Vane	0.31-0.32
Cone Penetrometer	0.31-0.32
Self-Boring Pressuremeter (Denby, 1978)	0.40
ICU extrapolated to OCR = 1.1 to 1.5	0.36-0.42
Plane Strain Vertical	0.29
Plane Strain Horizontal	0.37

Table 4-6 Summary of Soil Properties (after Bonaparte and Mitchell, 1979)

those indicated by self-boring pressuremeter tests. Figure 4-19 presents shear strength data measured by Denby (1978) and Benoit (1983). As can be seen, the shear strengths measured by both researchers appear to follow the same trend. As a result of this repeatability, it is concluded that the fact that the highest measured undrained shear strength values result from self-boring pressuremeter tests is not an anomaly.

Mitchell and Lunne (1977) installed Glötzl load cells at three separate depths at the Hamilton test site. The load cells indicated lateral stresses varying from 1300 psf (at 11 feet deep) to 2160 psf (at 23 feet deep) and K_0 values of from 0.70 to 1.02. Denby measured SBPM lateral stresses which suggested K_0 values of about 0.8 at 9.5 feet and about 0.48 between 18 to 30 feet. Benoit (1978) found similar results from SBPM testing. Lacerda (1976) suggested a K_0 value of 0.58 was appropriate for depths ranging from 20 to 25 feet based on laboratory tests to investigate the influence of stress relaxation in Young Bay Mud on K_0 .

The pore pressure parameter at failure, A_r (Skempton, 1954) has been measured by laboratory and field tests made in Hamilton Young Bay Mud. Duncan (1965) reported A_r from 0.91 to 1.18 on plane strain compression tests, and 0.65 to 0.75 for extension tests. Benoit reported that Sinram (1982) conducted cubical box tests to simulate pressuremeter testing and reported A_r values from 0.51 for OCR=1 to 0.44 for OCR=1.2. For SBPM tests, Denby (1978) and Benoit (1983) reported an average value of about 0.3.

4.3.4 Field Investigation for Present Research

Field investigation for this research included two self-boring pressuremeter borings. The locations of these borings are indicated on Figure 4-17. The explorations were made under the direction of Craig Findlay and Mike Atwood by RNL Enterprises, Inc. of Dillon Beach, California and Mike Bennett of the USGS, Menlo Park, California. The borings were designated as Ham 1 and Ham 2, and yielded a total of 9

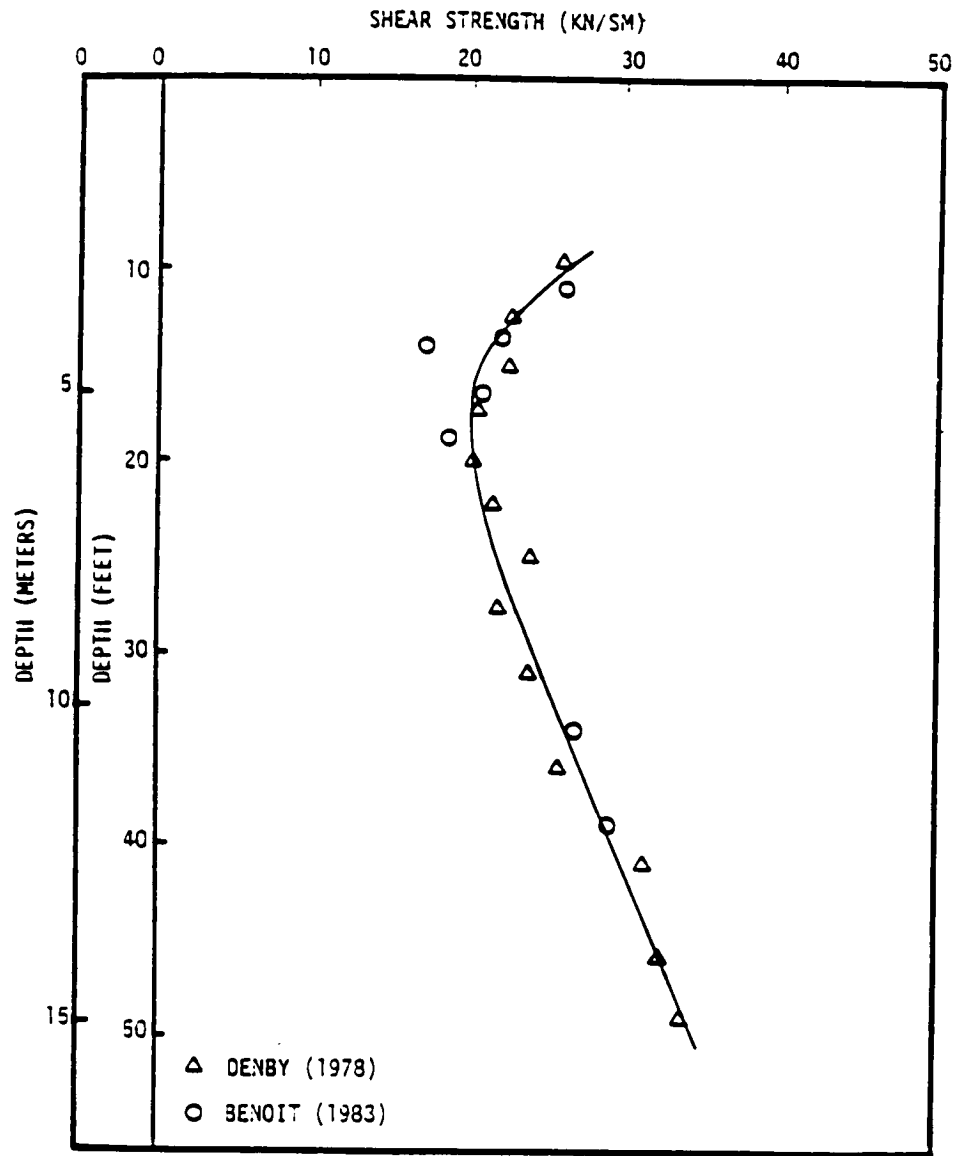


Figure 4-19 SBPM Shear Strength Profile from Previous Research (after Benoit, 1983)

tests. The borings were advanced to depths of 17.5 to 21.5 feet respectively. Self-boring pressuremeter tests were performed at depths ranging from 11.5 to 21.5 feet. Tests included 7 standard expansion tests, advanced by the jetting insertion method. The tests were denoted HAM1.1, through HAM1.3, and HAM2.1, through HAM2.4. After testing of HAM2.4, the membrane was re-expanded. This re-expansion was designated HAM2.4R. The final test (HAM2.5) was inserted by open-ended pushing, with no jetting. Insertion and test parameters were presented in Chapter III.

In addition to the SBPM tests, two dilatometer soundings were made at the test site for the current research at the locations indicated on Figure 4-17. The results of these soundings are not presented herein, however, they have been presented by Benoit, et al. (1990).

CHAPTER V

FINITE ELEMENT ANALYSIS

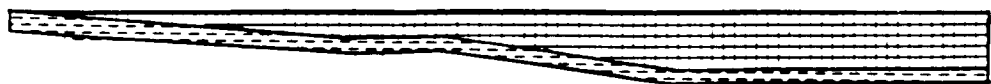
5.1 Introduction

Measurement of in situ horizontal stress is a primary use of the SBPM. At Hamilton AFB, previous researchers installed Glötzl stress cells in an effort to measure a "true" in situ horizontal stress. Those measurements gave an accepted basis of comparison for SBPM tests performed by Denby (1978) and Benoit (1983) and for tests conducted at Hamilton AFB as part of the current research. However, at the Pease AFB site, no such previous measurements of in situ lateral stress are available. Also, at the Pease test area adjacent to the Interstate I-95 highway embankment (toe area), stresses from the embankment preclude estimation of horizontal stress based on empirical K_0 methods. Because of the lack of horizontal stress data, and the non- K_0 conditions at the embankment toe, finite element modeling of the Pease AFB test site was conducted to simulate the stress history of the site in order to estimate the stress effects of the embankment. In situ stresses at the Pease AFB site would likely be representative of K_0 conditions at some distance away from the highway embankment and be influenced by an increasing amount approaching the embankment. To assess these changing effects, an interpretive site cross-section was developed that passes through the highway embankment, through the toe test area, extending outward and away from the highway embankment, as indicated on Figure 5-1.

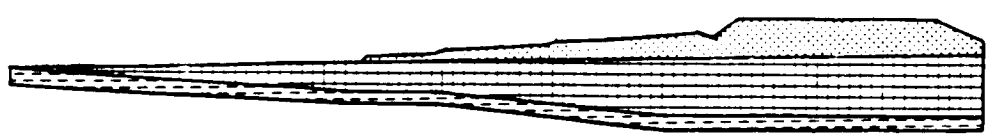
To model the cross-section such that the stress history is as close as possible to actual field conditions, it is necessary to understand the design considerations and construction sequence of the highway embankment. As a part of the design of the highway embankment, a test embankment (Ladd, 1972) was constructed about 1000 feet northeast of the SBPM site as previously indicated on Figure 4-2. This test embankment

←
→
Modeled By FEM

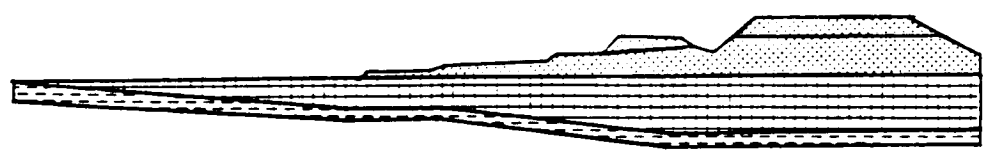
←
→
Not Modeled



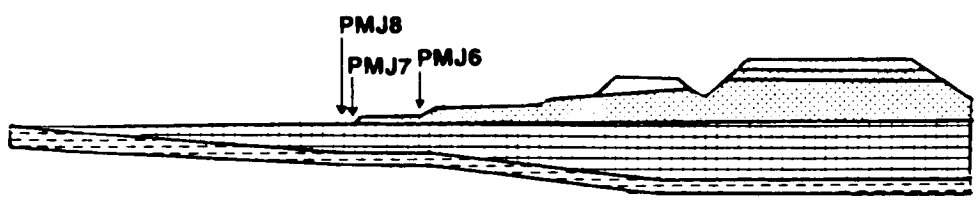
Initial Conditions



Phase I



Phase II



Finished Embankment

Fill
Silty Clay
Glacial Till/Bedrock

Approximate Scale:
 Vertical: 1"=90'
 Horizontal: 1"=140'

Figure 5-1 Stage Construction Sequence of I-95 Highway Embankment

was progressively increased in height until failure occurred. The test embankment indicated that if the planned highway embankment were placed all at once, failure of the foundation soils would likely have resulted. Consequently, the highway embankment was constructed in stages, such that only a portion of the full height was initially placed and consolidation of the underlying silty clay allowed to occur under the increased stress state. A waiting period of one year was observed to allow excess pore pressures within the silty clay to dissipate, thus allowing consolidation to occur. This consolidation had the effect of increasing the strength of the native silty clay, allowing additional embankment fill to be placed without instability.

Ladd, et al. (1972) described the stage construction sequence of the embankment. Based on this description, as well as by review of New Hampshire Department of Public Works and Highways (NHDPWH) construction drawings and the work of Israel (1987), the following sequence was used to construct the embankment adjacent to the test site.

First, between September 1968 and June, 1969, the site was grubbed, a 3 to 5-foot thick sand drainage blanket was placed, and sand drains were installed through the silty clay prior to embankment placement to decrease the waiting period between filling stages. The sand drains effectively reduced the drainage path which allowed the excess pore pressures to dissipate at a faster rate. After sand drain installation, the first stage of filling (Phase I) occurred between May and October of 1969. At the cross-section of Figure 5-1 this amounted to a maximum fill height of 19 feet.

Between May and August of 1970, filling for Phase II proceeded. The extent of Phase II filling is indicated on Figure 5-1. The maximum height of the embankment at the completion of Phase II was 24 feet at the depicted location.

Starting in April of 1971, the surcharge portions of Phases I and II fills were removed to finished grade. In September of 1972, the construction was completed and the highway was opened. Note on Figure

5-1 that SBPM boring PMJ6 is located at the present toe of slope. PMJ7 and PMJ8 are located at the toe of the construction sand blanket, about 55 feet from the present day embankment toe.

To predict in situ horizontal stress changes in the native silty clay at the site, the above construction sequence was simulated using finite element analysis. Two different finite element algorithms were used, namely, SOILSTRUCT and JFEST. Each of these analyses are described in the following sections.

5.2 SOILSTRUCT

5.2.1 Description of the Program

SOILSTRUCT was originally developed by G. Wayne Clough (1969) and was later modified by several of his students. The version of the program used for this research was adapted for operation under MS-DOS by the writer, compiled using Microsoft Fortran Version 5.1. The program was executed on a 20 mhz 80386 personal computer with a math coprocessor. The program simulates embankment construction assuming plane strain conditions. Soil behavior is considered isotropic and non-linear in stress-strain response. Stress-strain non-linearity is modeled by hyperbolic curve fitting of stress-strain curves at varying confinement, and both drained or undrained conditions can be simulated. The hyperbolic stress-strain model is that developed by Duncan and Chang (1970).

Soil elements in SOILSTRUCT have 4 external corner nodes, with an internal fifth node. The element is considered subparametric because geometry is defined by the external nodes, while displacement functions include the fifth internal node. This fifth internal node is used to improve flexural response of the element. Output includes displacements computed at each node, and stress is computed for each element.

5.2.2 Derivation of Input Parameters

In the Duncan and Chang (1970) hyperbolic model used in SOILSTRUCT, stress-strain behavior is represented by varying E_t (tangent modulus) and $(\sigma_1 - \sigma_3)_{\infty}$ (ultimate stress difference) with confining pressure. The

ultimate stress difference is an asymptotic value defined by the hyperbolic curve used to model an actual stress-strain curve. Because actual soil failure generally occurs at a stress difference that is smaller than this asymptotic value, the hyperbolic curve does not typically model failure accurately. To better model failure, the stress ratio, R_f , was developed by Duncan and Chang (1970) to relate the ultimate stress difference, $(\sigma_1 - \sigma_3)_{\infty}$, to the stress difference at failure, $(\sigma_1 - \sigma_3)_f$:

$$(\sigma_1 - \sigma_3)_f = R_f (\sigma_1 - \sigma_3)_{\infty} \quad (\text{Eq 5-1})$$

Duncan and Chang (1970) derived the following equation to define E_i at varying stress conditions:

$$E_i = \left[1 - \frac{R_f(1 - \sin\phi')(\sigma_1 - \sigma_3)}{2c' \cos\phi' + 2\sigma_3 \sin\phi'} \right]^2 K_p \left(\frac{\sigma_3}{p_a} \right)^n \quad (\text{Eq 5-2})$$

Where:

K = modulus parameter governing load behavior (relates initial modulus of elasticity to σ_3);

K_u = modulus parameter governing unload/reload behavior (relates unload/reload modulus of elasticity to σ_3);

n = modulus parameter governing load and unload/reload behavior (relates E_i and E_u to σ_3);

c' = cohesion intercept;

ϕ' = friction angle;

R_f = failure ratio (relates the ultimate deviator stress to the deviator stress at failure);

p_a = atmospheric pressure.

Techniques used to determine the hyperbolic stress-strain parameters which can be used for input into SOILSTRUCT have been presented by Wong and Duncan (1974). By these techniques, the hyperbolic parameters can be derived using two different schemes: 1) consolidated-drained (CD) or unconsolidated-undrained (UU) triaxial data,

or 2) one-dimensional consolidation and consolidated-undrained (CU) triaxial (with pore-pressure measurement) test data. The second method was used because CU tests and consolidation tests were performed for this research. Determination of the hyperbolic stress-strain parameters for the marine silty clay deposit using this method is subsequently described in details:

- Step 1 The cohesion, c' , and the friction angle, ϕ' , are determined using laboratory CU triaxial compression test stress paths. Figure 4-13 and 4-14 in Chapter IV show these parameters for the stiff (overconsolidated) and soft (normally consolidated) silty clay at the site. It was assumed that the stiff soil parameters represented the upper 9 feet of the silty clay deposit and the soft clay parameters governed clay behavior below this depth.
- Step 2 Deviator stress versus axial strain is plotted for the CU tests on Figure 5-2. For each stress-strain curve, the values of deviator stress and axial strain which correspond to 70 and 95 percent of the failure strength are determined.
- Step 3 The failure ratio, R_f for each test can be determined by plotting axial strain divided by the deviator stress versus axial strain (two points for each test, at 70 and 95 percent of failure strength) as shown on Figure 5-3. A straight line is drawn through each pair of values. The inverse of the slope (b) of each line is equivalent to the uncorrected hyperbolic ultimate deviator stress. R_f is equal to the uncorrected hyperbolic ultimate deviator stress divided by the deviator stress at test failure. The R_f value typically used for finite element analysis is the average of the values from all of the tests. For this research, a computer program developed by Wong and Duncan (1974) was used which computationally performs this analysis. Input into this program includes the CU stress-strain data at 70 and 95

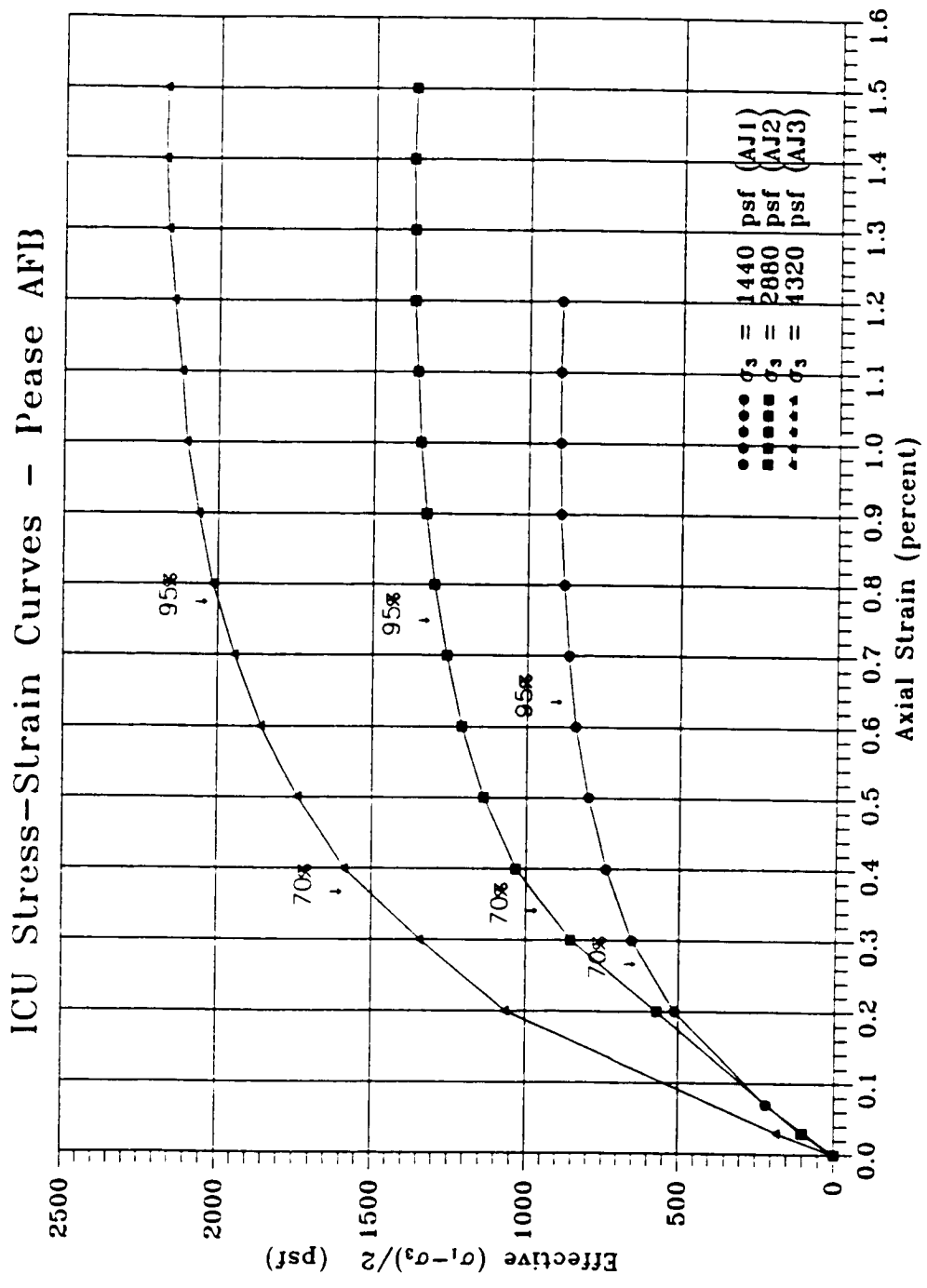


Figure 5-2 Axial Strain at 70 and 95 Percent Shear Strength

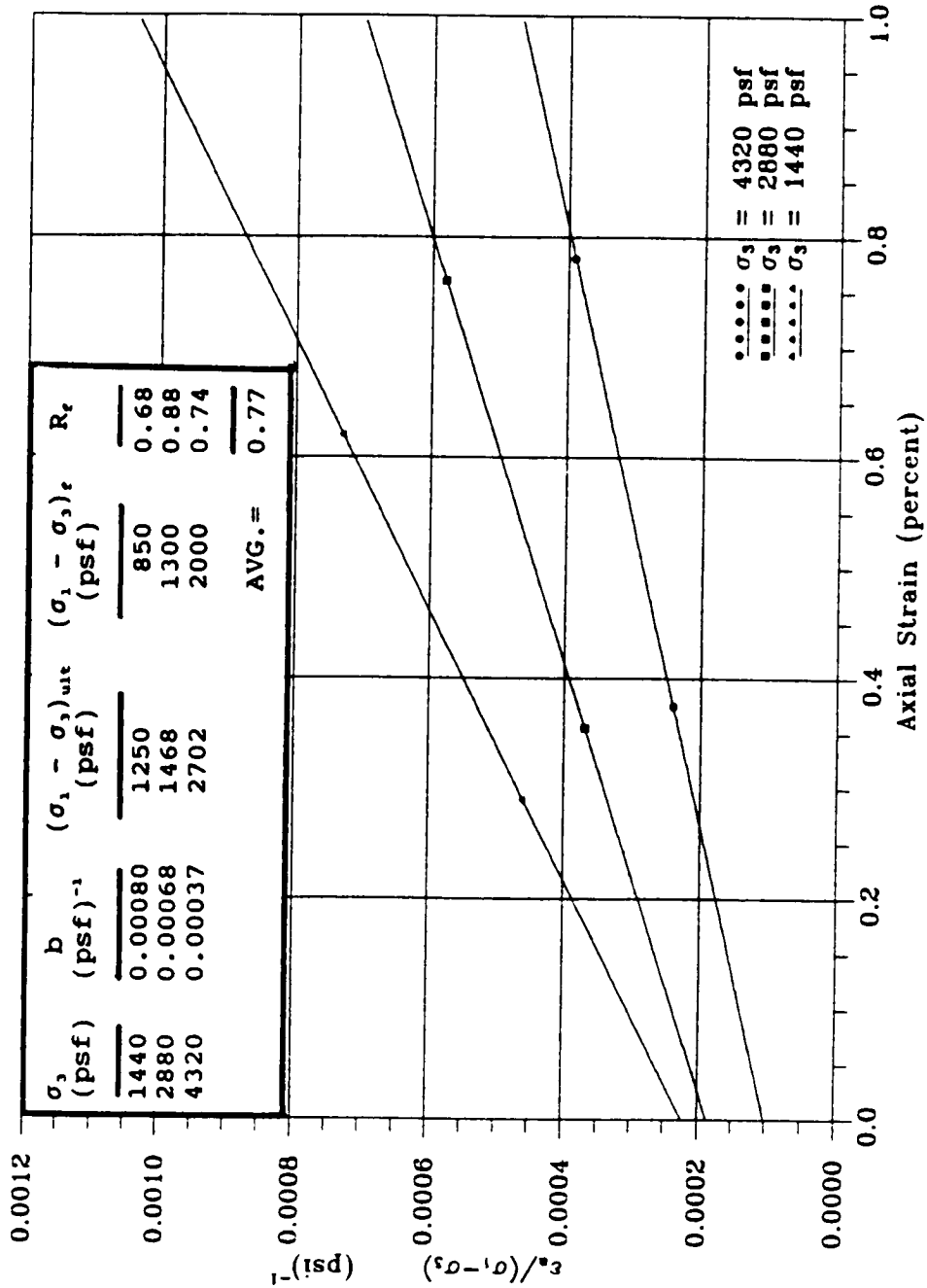


Figure 5-3 Determination of Failure Ratio, R_f

percent of failure, Φ' , c' , σ_3 , and the principal stress difference at failure.

Step 4 The data from consolidation tests are used to derive K and n as follows:

First, E_i is determined using data from the primary loading portion of the consolidation curve and the following equation:

$$E_i = \frac{\frac{p(1+e_0)}{\Delta e} \left[1 - \frac{2(K_0)^2}{(1+K_0)} \right]}{\left[1 - \frac{p(1+K_0)R_f}{K_0 p (\tan^2(45+\Phi/2) - 1) + 2c' \tan(45+\Phi/2)} \right]^2} \quad (\text{Eq 5-3})$$

where:

- E_i = initial tangent modulus
- Δp = increment of pressure in the consolidation test
- Δe = decrease in void ratio corresponding with Δp
- e_0 = void ratio at the beginning of the increment
- K_0 = coefficient of earth pressure at rest (see Figure 2-4)
- p = average pressure during increment
- c' = cohesion (effective stress strength parameter)
- Φ' = angle of internal friction (effective stress strength parameter)
- R_f = failure ratio

Values of E_i normalized to atmospheric pressure (P_a) for different load increments are plotted (log-log) against corresponding values of normalized σ_3 , and a line is drawn through the plotted points (see Figure 5-4) to determine K and n . K is the E_i/P_a intercept, and n is the slope of the

PEASE AIR FORCE BASE HYPERBOLIC STRESS-STRAIN PARAMETERS

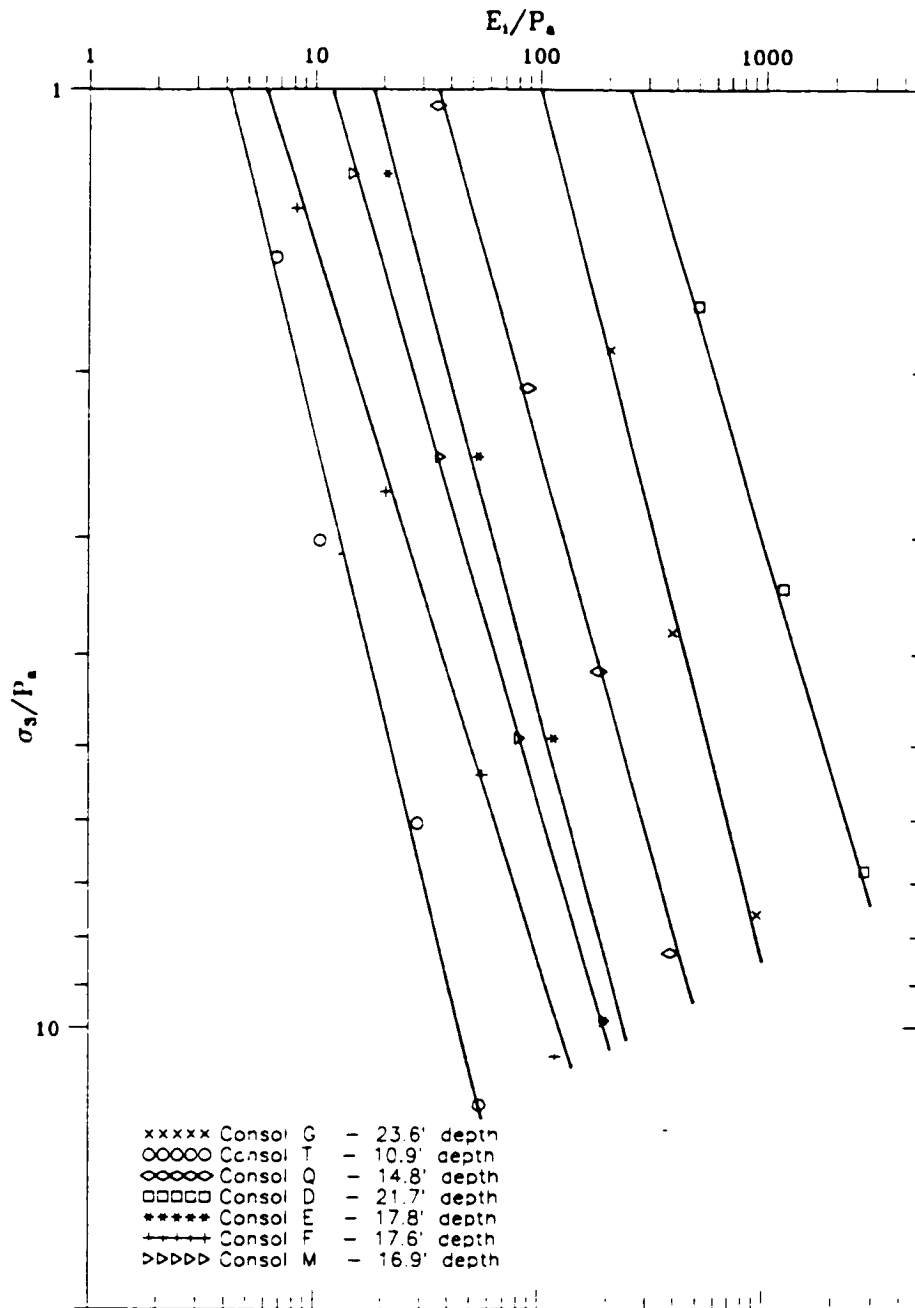


Figure 5-4 Determination of Normalized Initial Tangent Modulus, E_1

resulting line. The values of σ_3 for the plot are determined using:

$$\sigma_3 = K_o p \quad (\text{Eq 5-4})$$

Step 5 Finally, K_w is determined. For its determination, E_w must first be computed from the following equation, using data from the unload-reload portions of the consolidation curves:

$$E_w = \frac{\Delta p(1+e_o)}{\Delta e} \left[1 - \frac{2 (K_o^\Delta)^2}{(1 + K_o^\Delta)} \right] \quad (\text{Eq 5-5})$$

where: K_o^Δ = is the ratio of change in lateral stress to change in vertical stress during unloading in a consolidation test. The ratio is determined using Figure 5-5 and the plasticity index of the soil of interest.

K_w is then determined from:

$$K_w = \frac{E_w}{\frac{\sigma_3}{Pa} \left(\frac{\quad}{Pa} \right)} \quad (\text{Eq 5-6})$$

A tabulation of the hyperbolic parameters for the soft and stiff silty clay at the test site determined from the laboratory data is presented on Table 5-1. Table 5-1 indicates K_o in the crustal portions of the silty clay, based on Brooker and Ireland (1965) OCR and plasticity relationships, was estimated to be on the order of 1.5 to 2.0. As will be discussed in Chapter IX, K_o in the upper crust was measured to be as high as 7 at a depth of about 6.5 feet, which can be extrapolated to even higher values at shallower depth. To start with modeled stresses similar to those measured by the SBPM at the K_o area as the initial condition, the SBPM measured values of K_o in the crustal soils were used. SBPM measured values of K_o in the softer underlying silty clay were similar to Brooker

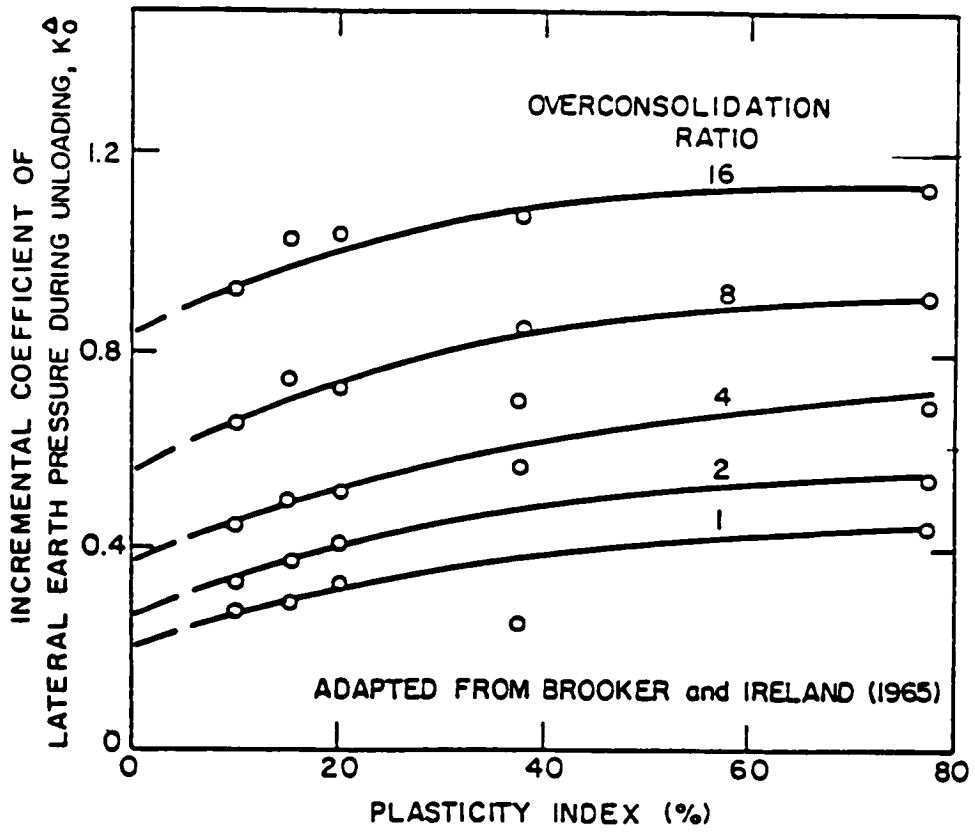


Figure 5-5 Incremental Coefficient of Lateral Earth Pressure During Unloading

SUMMARY OF HYPERBOLIC PARAMETERS
PEASE AIR FORCE BASE

Soil Type	Total Unit Weight (pcf)	R _f	K _o	φ' (deg)	c' (psf)	n	K	K _{ur}
Stiff Silty Clay	115	0.80 ±.08	1.5- 2.0	25.1	207	1.12 ±.14	164.4 ±69.0	197.3 ±69.0
Soft Silty Clay	109	0.79 ±.09	0.5- 0.6	21.3	0	1.12 ±.14	53.1 ±68.8	197.3 ±68.8
Granular Fill	125	0.73	1.0	45.0	0	0.50	640.0	768.0
Glacial Till	136	0.80	1.0	33.0	620	0.37	700.0	840.0

Table 5-1 Summary of Hyperbolic Parameters

and Ireland measured values.

Because testing was not conducted on the embankment fill and glacial till soils as part of the research, hyperbolic parameters had to be estimated for these soils. Boscardin, Selig, Lin and Yang (1990) have presented hyperbolic parameters for fill soils, based on ASTM T-99 determined relative density and the Unified Soil Classification System. A summary of their recommended hyperbolic stress-strain parameters is presented in Table 5-2. Field observation of the embankment fill material at the site indicates that it could be classified using the Unified Soil Classification as "GW", or a widely-graded gravel-sand mixture with little to no fines. Because the fill was placed with compactive effort, the material was assumed to be dense, with a relative density of between 90 and 95 percent of maximum dry density, based on typical NHDPWH requirements of embankment construction. Table 5-1 included the embankment fill hyperbolic parameters selected for analysis based on interpretation between the 90 and 95 percent maximum dry density values for GW soil presented by Boscardin, et al.

Hyperbolic stress-strain parameters for the glacial till underlying the marine silty clay at the Pease test site were selected based on a review of data presented by Wong and Duncan (1974) for a number of similar soils at numerous sites. The selected parameters are also presented on Table 5-1.

5.2.3 FEM Mesh and Construction Sequence

The FEM mesh used for the SOILSTRUCT analysis is presented on Figure 5-6. The mesh was configured to allow embankment placement to be simulated using identical construction steps as were used for actual construction. The mesh geometry was based on: 1) the findings of subsurface explorations made for the research as well as those made for the embankment construction as described by Ladd (1972) and Ladd, et al. (1972); 2) the results of transit survey of the site; and 3) NHDPWH construction drawings for the highway embankment. The mesh was refined in the area of the SBPM tests to provide a reasonable resolution, and was

Soil type (1)	T-99 (%) (2)	K (3)	" (4)	R_f (5)	c (kPa) (6)	ϕ_o (°) (7)	$\Delta\phi$ (°) (8)
SW	95	950	0.60	0.70	0	48	8
	90	640	0.43	0.75	0	42	4
	85	450	0.35	0.80	0	38	2
	80	320	0.35	0.83	0	36	1
ML	61	54	0.85	0.90	0	29	0
	95	440	0.40	0.95	28	34	0
	90	200	0.26	0.89	24	32	0
	85	110	0.25	0.85	21	30	0
CL	80	75	0.25	0.80	17	28	0
	49	16	0.95	0.55	0	23	0
	95	120	0.45	1.00	62	15	4
	90	75	0.54	0.94	48	17	7
	85	50	0.60	0.90	41	18	8
	80	35	0.66	0.87	35	19	8.5
	45	16	0.95	0.75	0	23	11

Note: 1 psi = 6.9 kPa.

Table 5-2 Hyperbolic Parameters for Fill Materials (After Boscardin, et al., 1990)

PEASE AIR FORCE BASE TEST SITE
SOILSTRUCT FEM MESH

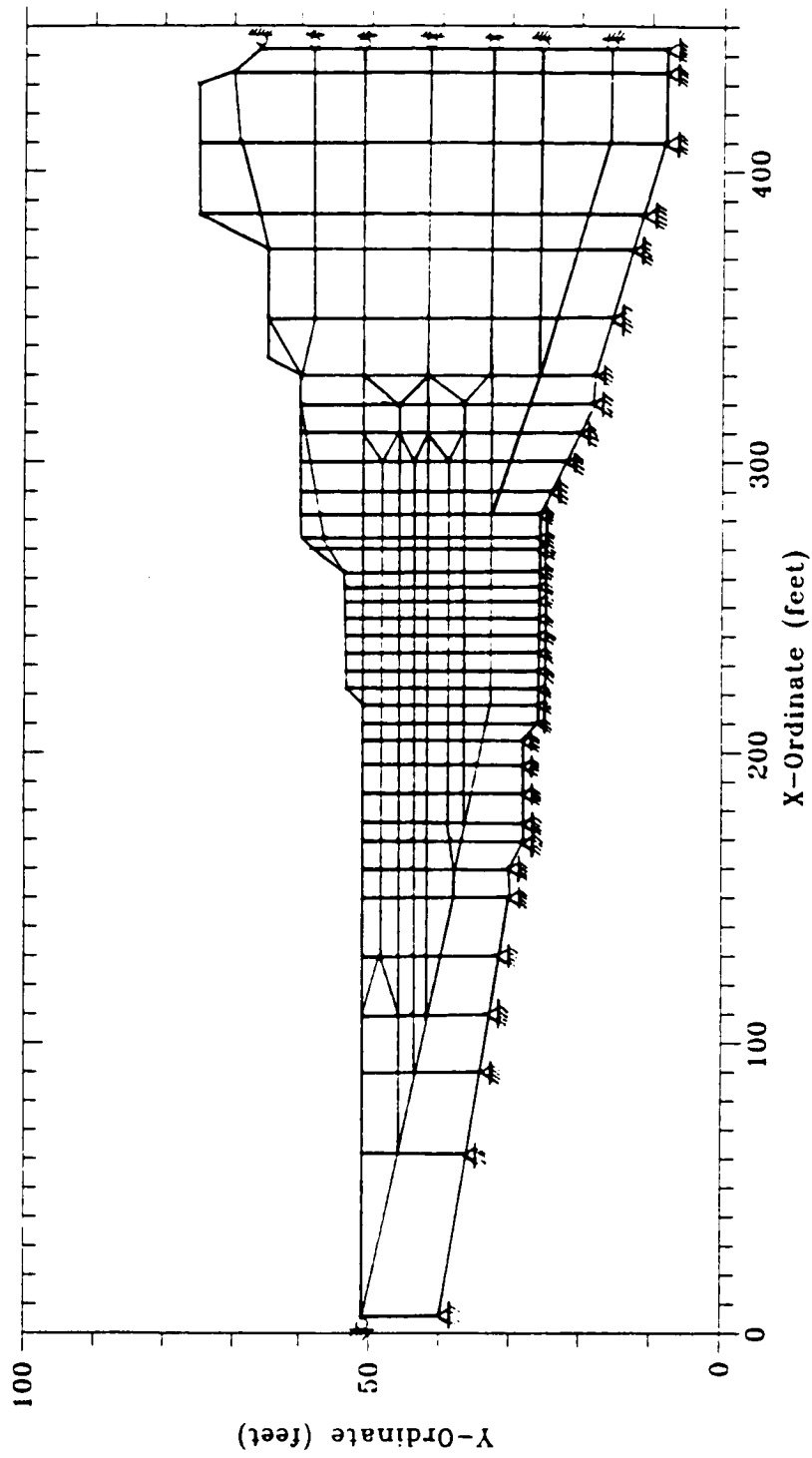


Figure 5-6 SOILSTRUCT Finite Element Mesh

made coarser with distance away from that area. The embankment fill was modeled in one to three layers. The silty clay was modeled by seven layers in the area of the SBPM tests. Rather than defining the bottom of the silty clay as the bottom of the mesh, a single layer of till was utilized, below the silty clay unit. This was recommended by Israel (1987) to mitigate stiffness effects of having a fixed mesh boundary at the bottom of the silty clay.

As previously shown on Figure 5-1, only a segment of the highway embankment was modeled, based on the findings of Israel (1987). Israel modeled a nearby portion of the same highway embankment for preliminary work at the test site. Several different size meshes were used and it was determined that modeling only a portion of the highway embankment (similar in size to the mesh for this research) had no adverse effect on the stresses calculated at the test area.

For analysis, SOILSTRUCT was run using four construction steps. The first and second steps involved placing the sand blanket and Stage I filling. The third step represented Stage II filling. Finally, the fourth step was the removal of the surcharge soil to finished grade. The cross-sections presented on Figure 5-1 depict each of these construction stages.

5.2.4 SOILSTRUCT Results

The purpose of the SOILSTRUCT FEM analysis was to compute the horizontal stress changes at the end of construction (long term, drained conditions) as a basis for comparison with the findings of the SBPM tests. Toward that end, only the FEM computed initial horizontal stresses and horizontal stresses after construction step 4 (removal of the surcharge soils) are of interest. Figure 5-7 presents profiles of horizontal stress, both before and after embankment filling at the modeled locations of borings PMJ6, PMJ7, and PMJ8. Only one plot is presented for borings PMJ7 and PMJ8 since they were drilled within 5 feet of each other and computed stress changes between the two borings were negligible. The computed horizontal stresses at each of the boring

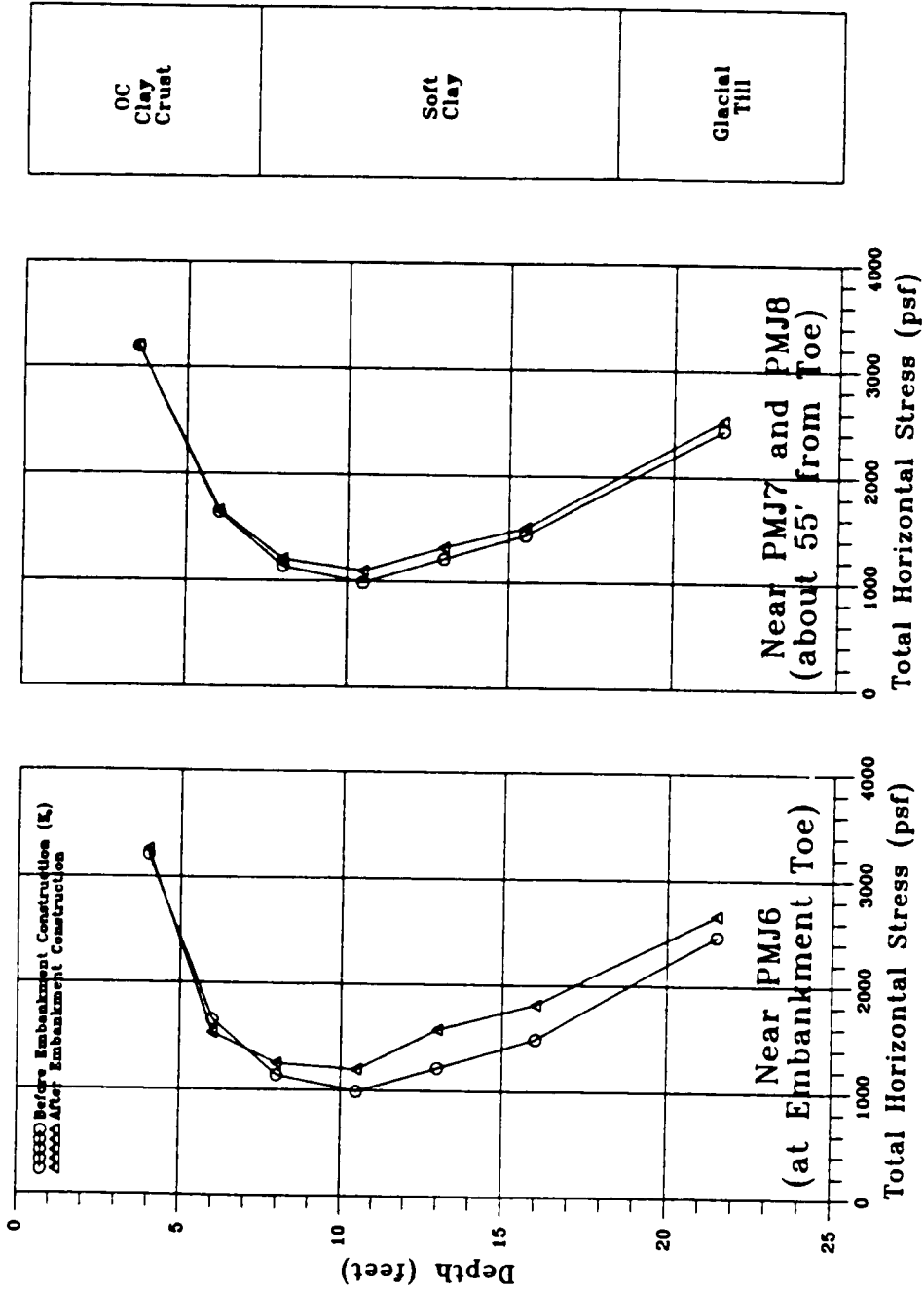


Figure 5-7 SOILSTRUCT Computed Horizontal Stresses Due To Embankment Load

locations are used as a basis of comparison to those measured by SBPM tests in Chapter IV. As can be seen by examination of the figure, the increase in horizontal stress was generally greater in the softer clay below a depth of about 6 to 8 feet than in the upper, overconsolidated crust of the deposit. At the toe (PMJ6), the stress increase due to the embankment construction is about 400 psf or less in the soft clay and essentially zero in the upper stiff clay. Away from the embankment, at PMJ7 and PMJ8, the stress increase was less, about 100 psf or less in the soft clay. It is noted that the computed stress increase at PMJ7 and PMJ8 is within the resolution of the SBPM's stress measurement ability, however, at the toe of the embankment (PMJ6) the computed stress change is sufficiently large so that it is expected that the SBPM would be able to detect the stress increase due to embankment construction.

Based on the results of the FEM analysis, Figure 5-8 presents a plot of the percentage increase in stress due to construction of the highway embankment since the initial, pre-construction stress condition, at the modeled location of PMJ6, 7 and 8. The figure indicates that the expected stress change due to embankment construction is about 30 percent or less at the embankment toe and about 10 percent or less at the location of PMJ7 and PMJ8, a distance of 55 feet from the embankment toe.

5.3 JFEST

5.3.1 Description of the Program

JFEST is an acronym for "Johnston-Finno Elasto-plastic Soil-Tunnel Interaction". The program was initially developed by Johnston (1981) and at the time was called PEPCO (Program for Elasto-Plastic Consolidation). Finno (1983) modified the program by adding a predictor-corrector algorithm, a non-linear elastic soil model (Duncan and Chang, 1970), improved interface elements, and other features. Both researchers used the program to model consolidation around shield tunnels in cohesive soils. The program has been successfully used to evaluate embankment construction stress and consolidation problems (Poepsel and Kavazanjian, 1984). JFEST has a number of stress-strain models which can be used,

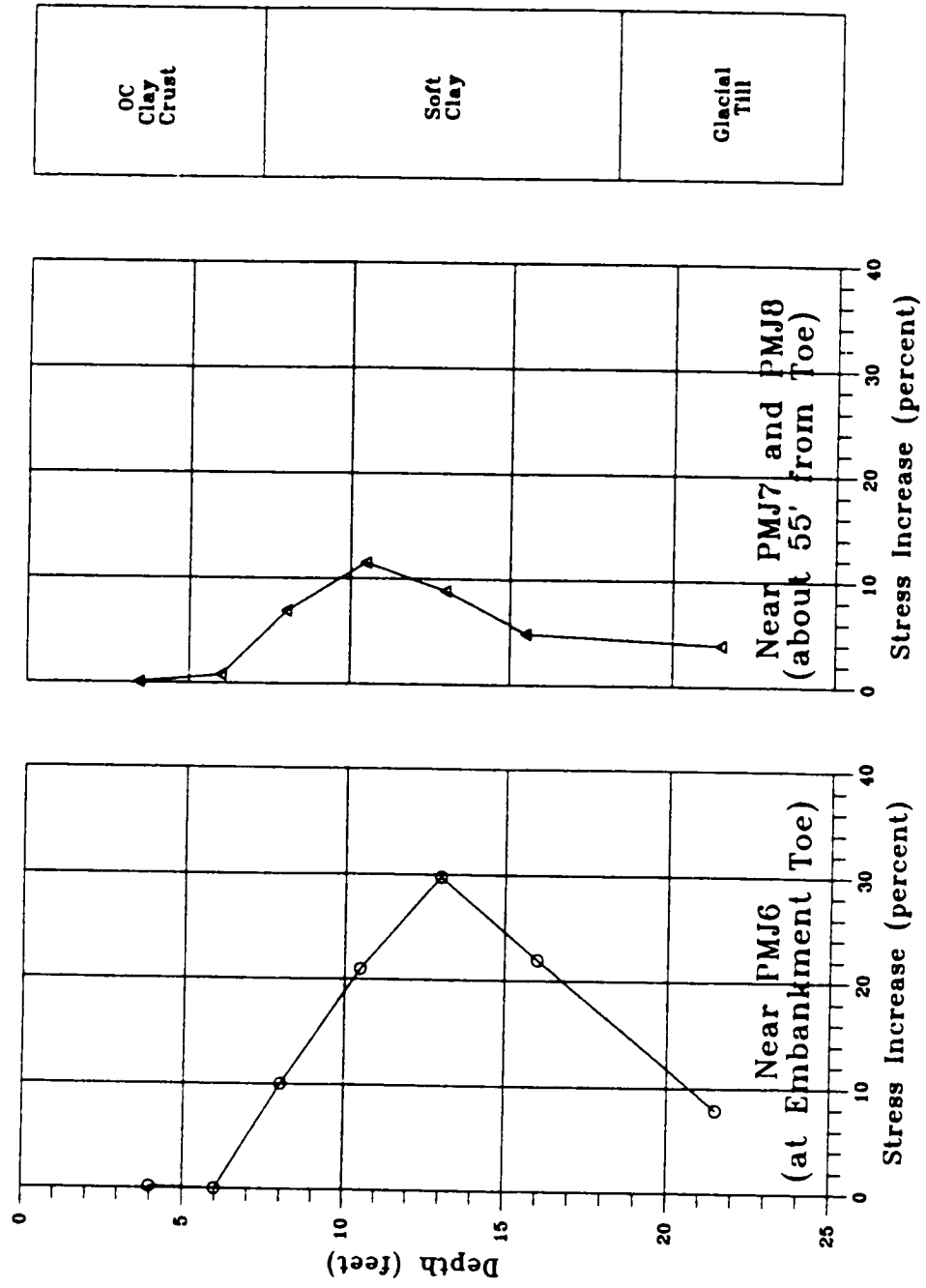


Figure 5-8 SOILSTRUCT Computed Percent Horizontal Stress Increase Due To Embankment Load

including linear-elastic, non-linear hyperbolic stress-strain (Duncan and Chang, 1970), and elasto-plastic analysis using the modified Cam-Clay model (Roscoe and Burland, 1968). The Cam-Clay model employs a plastic strain yield surface mechanism (see Figure 5-9) for simulation of plastic strain after yield and strain hardening. This yield model, coupled with a time rate of consolidation routine, allows JFEST to be used to simulate consolidation. Isotropic and anisotropic, drained and undrained soil behavior can be modeled. JFEST uses four or eight node isoparametric elements. With eight node elements, displacements are computed at the corners, and stresses are calculated at four program generated internal nodes.

5.3.2 Derivation of Input Parameters

The modified Cam-Clay model is used as a constitutive model in program JFEST. Because Cam-Clay is an elasto-plastic model, and because theoretical interpretation of SBPM data assumes elasto-plastic behavior, it is of interest to determine predictions of lateral stress at the Pease AFB toe area based on this model. However, it should be noted that the modified Cam-Clay model is intended to model soils wet of critical (normally to lightly overconsolidated). As a result, modeling highly overconsolidated soils can not be expected to yield realistic results. The basic Cam-Clay parameters used in JFEST are shown on Figure 5-10 and are described as follows:

λ = the slope of the virgin portion of the e - $\ln p'$ plot (isotropic compression line) determined from isotropic consolidation in a standard triaxial cell. Atkinson and Bransby (1978) indicated that the slope of the one-dimensional compression e - $\ln p'$ plot from a standard consolidation test is essentially parallel to the isotropic compression line, and can also be used.

κ = the slope of the load-unload portion of the e - $\ln p'$ plot (swell line) from isotropic compression or a one-dimensional consolidation test.

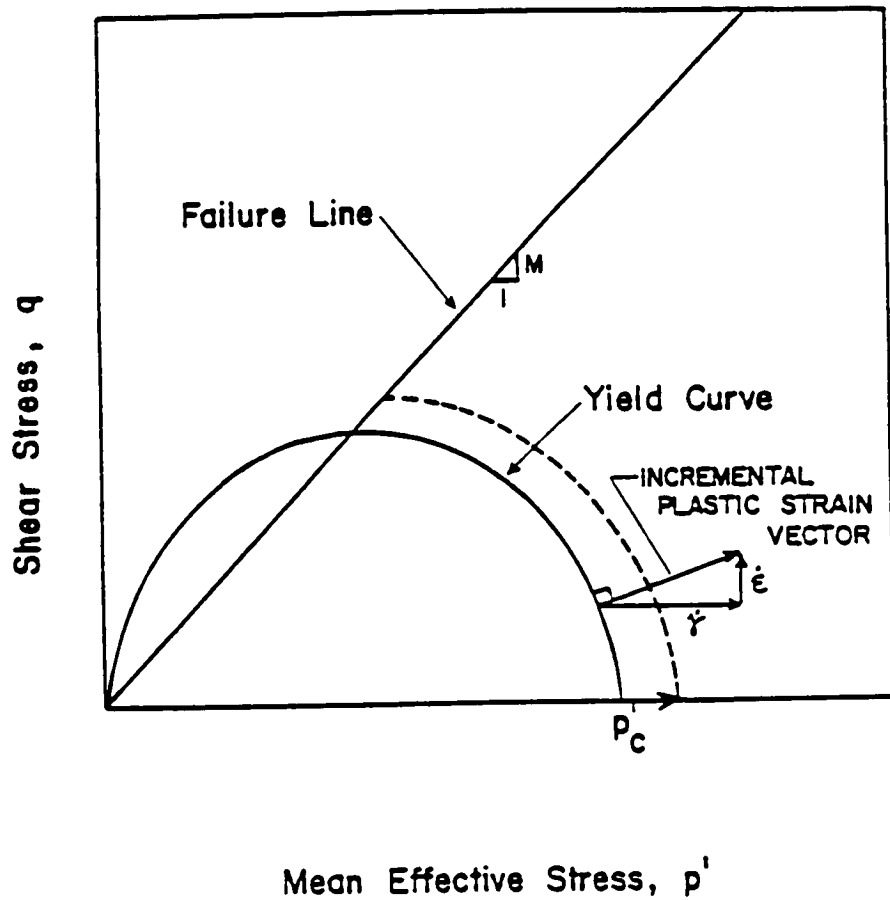


Figure 5-9 Cam-Clay Model (after Poepfel and Kavazanjian, 1984)

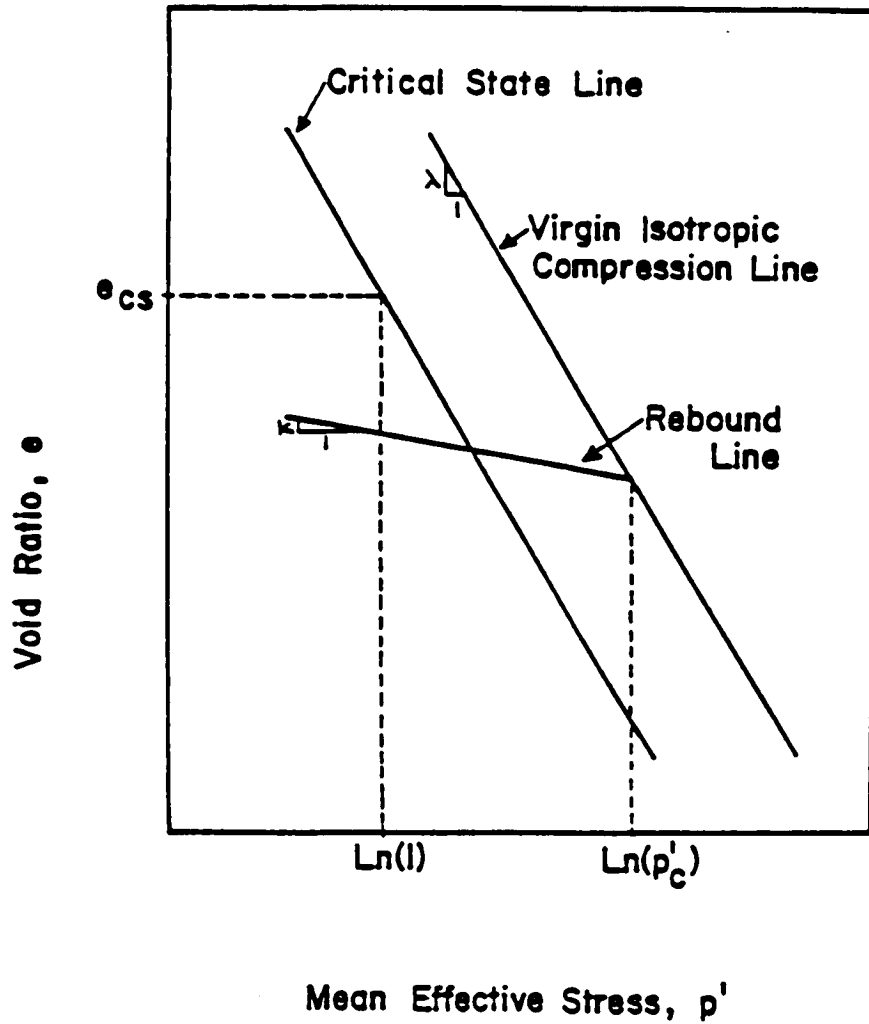


Figure 5-10 Definition of Cam-Clay Parameters
(after Poepel and Kavazanjian, 1984)

- e_{cs} = the critical state void ratio at unit stress ($\ln p = 1.0$).
- G_i = the initial shear modulus. This parameter can be estimated by multiplying the undrained shear strength by the modulus multiplier (Mitchell, 1977) or can be determined from SBPM test data.
- M = the slope of the critical state line. M is a function of ϕ' from drained triaxial shear test results. An equation for M is given by:

$$M = \frac{6 \sin \phi'}{3 - \sin \phi'} \quad (\text{Eq 5-7})$$

- c/p = ratio of the undrained shear strength to the effective vertical overburden pressure.
- k = coefficient of hydraulic conductivity.

For JFEST analysis, the above parameters were generally determined by laboratory or field measurements. Table 5-3 summarizes the values input. The e - $\ln p'$ slopes were determined by linear regression of standard one-dimensional consolidation test results. The critical state void ratio, e_{cs} , was determined by plotting consolidation test results as indicated on Figure 5-11. The slope of the critical state line, M , was determined using Equation 5-7, and assuming a ϕ' of 21.3 and 25.1 degrees for the soft and stiff silty clay, respectively, based on ICU' tests. The initial shear modulus was based on the results of SBPM tests. The unit weight and c/p ratio were based on test results discussed in Chapter II. Hydraulic conductivity was assumed based on results of triaxial permeameter tests on similar clay in the region.

5.3.3 FEM Mesh and Construction Sequence

The mesh used for JFEST analysis of the Pease Toe Area is presented on Figure 5-12. As can be seen, no embankment section is included. This is because JFEST models embankments as surface tractions or loads. For each construction step, the appropriate surface load must be manually

Parameter	Stiff Silty Clay	Soft Silty Clay
k, Slope of Swell Line	0.011	0.013
λ , Slope of Isotropic Compression Line	0.124	0.182
e_{cc} , Void Ratio at Critical State Under Unit Pressure	2.67	2.67
M, Slope of Critical State Line	0.827	0.990
G_i , Initial Shear Modulus (psf)	230,000	140,000
γ , Wet Unit Weight (pcf)	109	115
c/p, Normalized Shear Strength	5.0 to 1.0 (decrease w/ depth)	1.0 to 0.25
k_v , vertical coefficient of hydraulic conductivity (ft/day)	2.83×10^{-4}	2.83×10^{-4}
k_h , horizontal coefficient of hydraulic conductivity (ft/day)	2.83×10^{-2}	2.83×10^{-2}

Table 5-3 Summary of Cam Clay Properties for JFEST Input

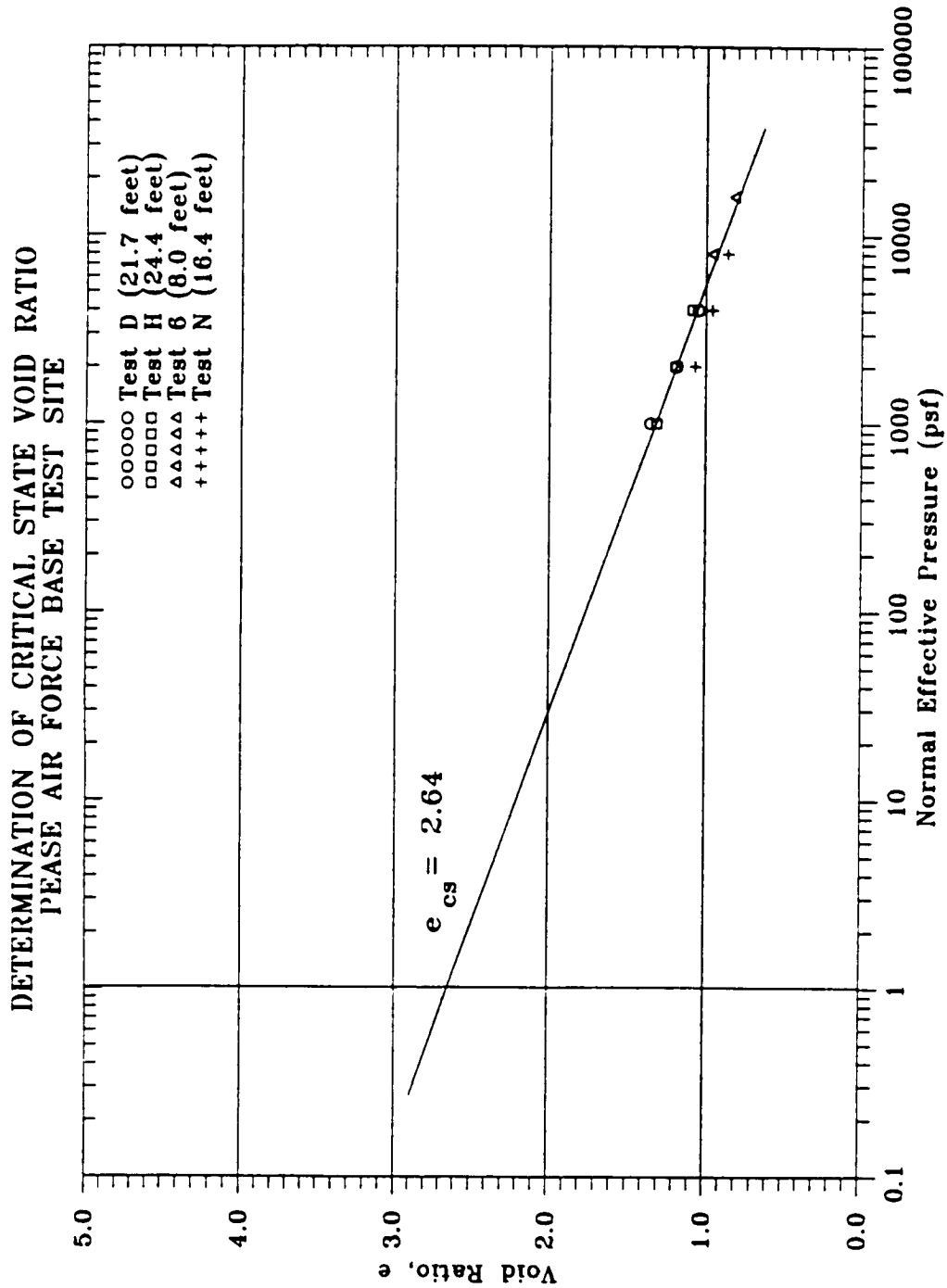


Figure 5-11 Determination of Critical State Void Ratio

PEASE AIR FORCE BASE TEST SITE
JFEST FEM MESH

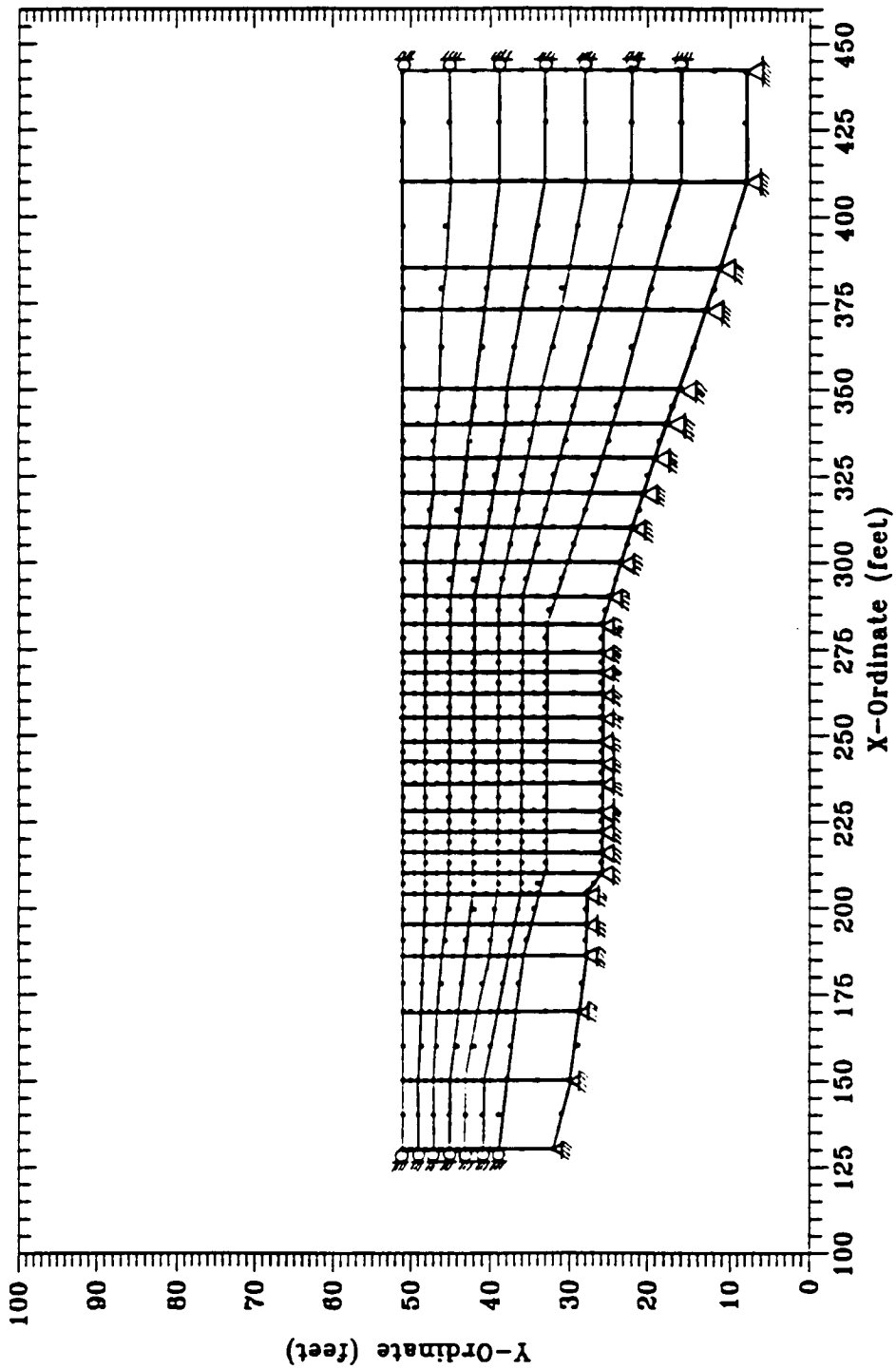


Figure 5-12 JFEST Finite Element Mesh

computed based on the unit weight of the embankment material (assumed to be 125 pounds per cubic foot) and the thickness of the embankment at the nodal location of the surface traction. The sequence of staged embankment construction has been described in Section 5.1. JFEST was used to model Phase I and II loadings, followed by unloading to finished grade. Surface tractions at each surface node in the embankment area were computed for each of these three construction steps. As indicated previously, JFEST can constitutively model soil consolidation. This requires a time-step analysis. The time units used were days. Embankment placement, surcharging and removal were simulated in the actual time frame used for construction.

5.3.4 JFEST Results

As with SOILSTRUCT, only the initial horizontal stresses before embankment construction and the long term post-embankment construction stresses are of interest for comparison with the SBPM test results. Figure 5-13 presents computed total horizontal stress at the location of PMJ6 and PMJ7/PMJ8. As can be seen, the horizontal stress increase as a result of the embankment construction is computed to be about 750 psf or less at PMJ6 and about 300 psf or less at PMJ7/PMJ8. These stress increases are about 2 to 3 times greater than the stress increases predicted by SOILSTRUCT (see Figure 5-7). The results of JFEST, in contrast to the results of SOILSTRUCT, suggest that the stress increase due to construction at PMJ7/PMJ8 should be large enough to be discernible by the SBPM.

Figure 5-14 presents the percent increase of the total horizontal stress after embankment construction from the initial stress conditions. The total horizontal stresses at the location of PMJ6 and PMJ7/PMJ8 are predicted to be up to 74 and 30 percent, respectively, greater than the initial stresses.

5.4 Comparison of SOILSTRUCT and JFEST Results

The previous sections have indicated differences between the values of horizontal stress computed by SOILSTRUCT and JFEST FEM modeling of the

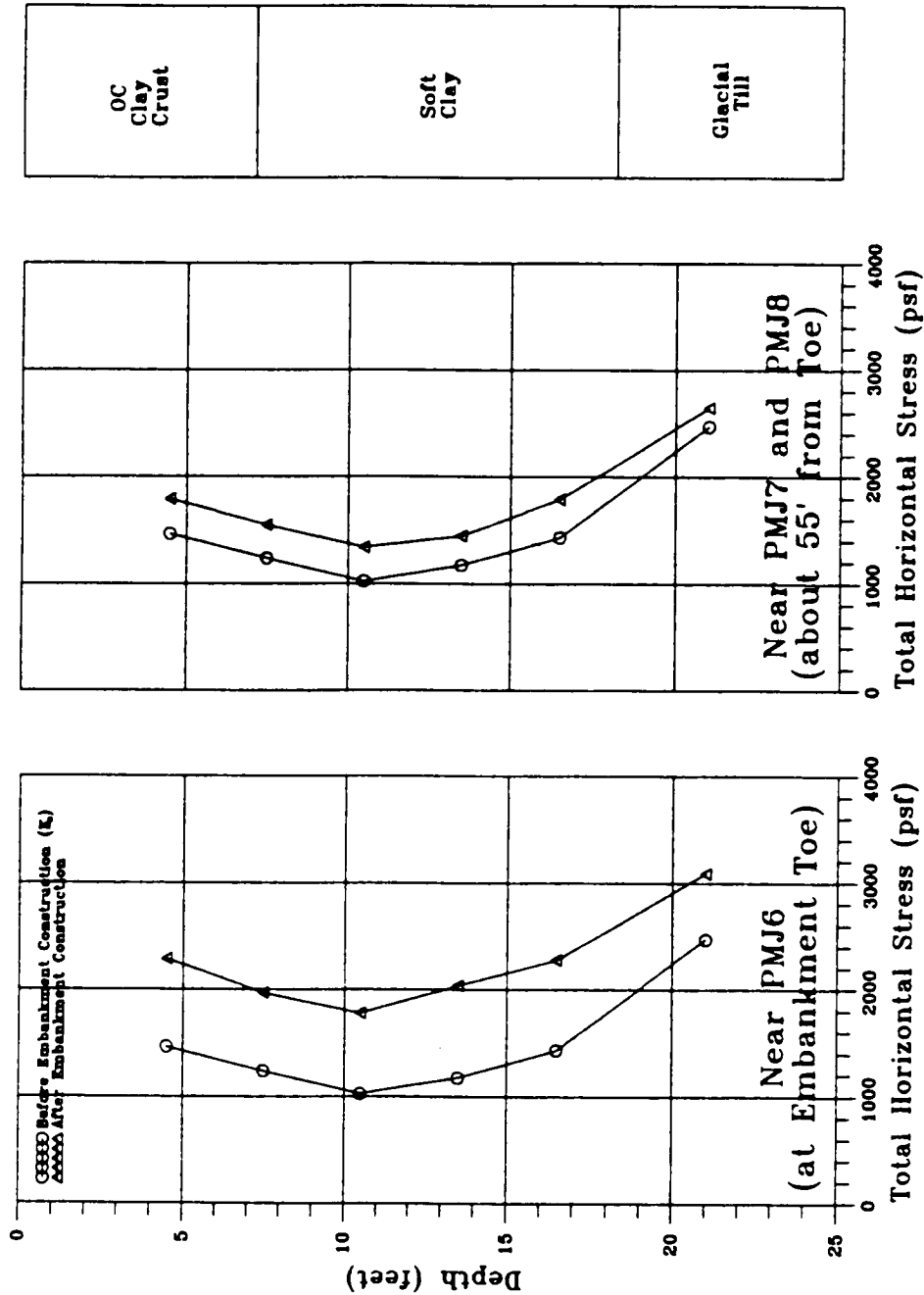


Figure 5-13 JFEST Computed Horizontal Stresses Due to Embankment Load

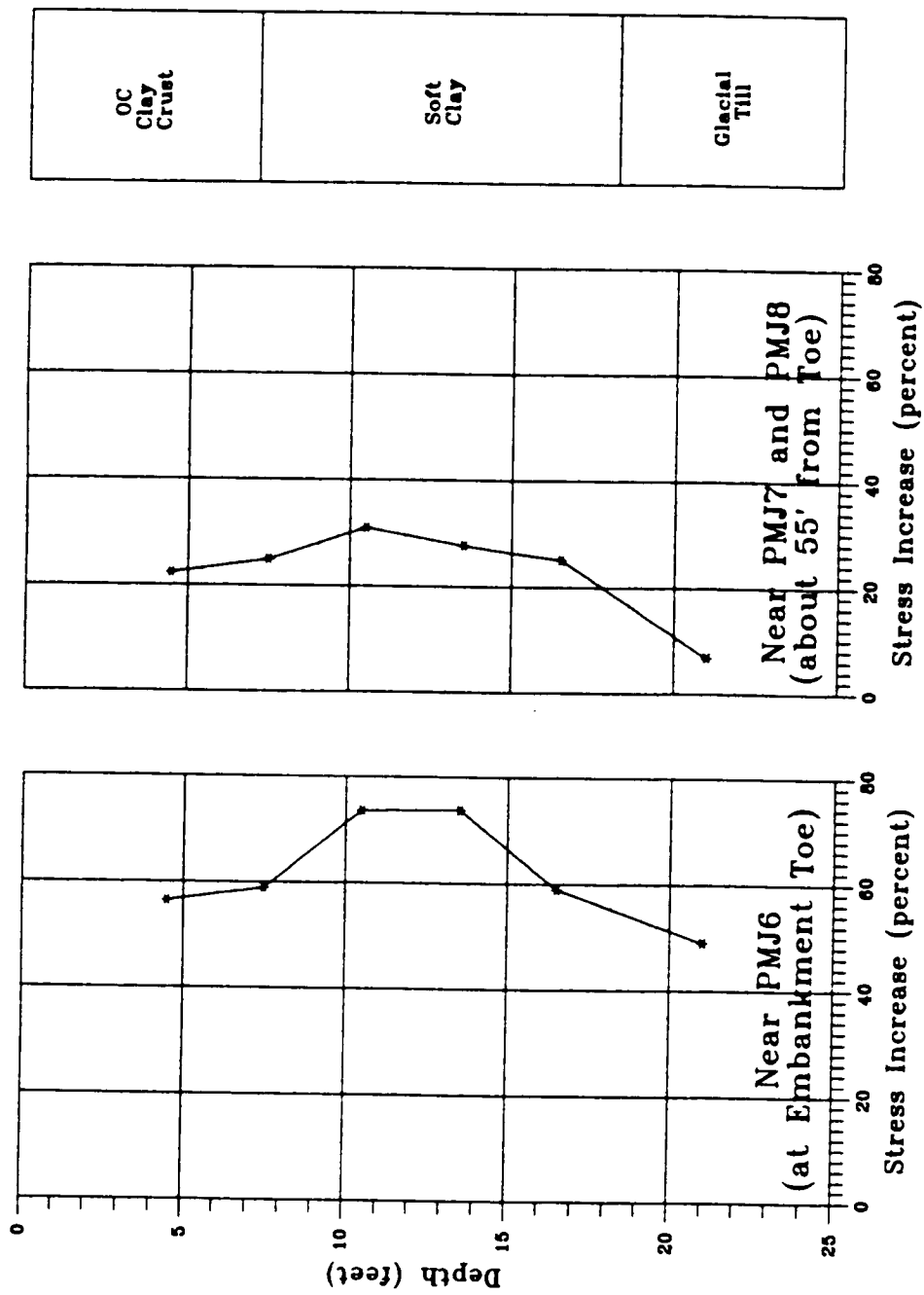


Figure 5-14 JFEST Computed Percent Horizontal Stress Increase Due To Embankment Load

embankment construction. As a basis of further comparison, Figure 5-15 is a plot of the total horizontal stress after embankment construction as a percentage of the initial stress versus distance from the embankment toe (location of PMJ6). Note that the 3 to 5 foot thick sand blanket placed prior to embankment construction extends about 55 feet from the toe of slope (to the location of PMJ7/PMJ8). Both analyses indicate a trend of decreasing stress change with distance from the embankment toe, with a major break in the rate of stress change with distance about 70 feet from the toe (about 15 feet beyond the end of the sand blanket).

The SOILSTRUCT results on Figure 5-15 suggest that the stress effects due to the embankment fill extend about 75 feet from the toe of the embankment (20 feet from the edge of the sand blanket). At this distance, stress increase in the soft silty clay was less than about 5 percent due to embankment construction. In contrast, the JFEST results suggest that the stress effects extend about 110 feet from the toe (55 feet from the edge of the sand blanket). Under and just beyond the sand blanket, both analyses indicate that the greatest percent of stress change (12 to 74 percent) occurred at mid depth of the soil profile (10 to 13 feet deep), and the least stress change (0 to 56 percent) occurred in the upper stiff clay crust and underlying glacial till. Further beyond the sand blanket, SOILSTRUCT indicates the same profile of stress change as below the sand blanket, however JFEST suggests the greatest stress change occurs within the upper 10 feet of the silty clay profile.

The differences in the results of the two FEM algorithms can be attributed to the differences in the soil models employed. As indicated earlier in this chapter, the Cam-Clay model on which JFEST is based is appropriate for soils wet of critical, which are soils that are normally consolidated to lightly overconsolidated. Because of the Cam-Clay model is based on elasto-plastic behavior and models void ratio changes due to changes in stress state, Cam-Clay might be expected to model the underlying soft silty clay better than SOILSTRUCT. However, the upper clay crust is desiccated and highly overconsolidated, and the Cam-Clay

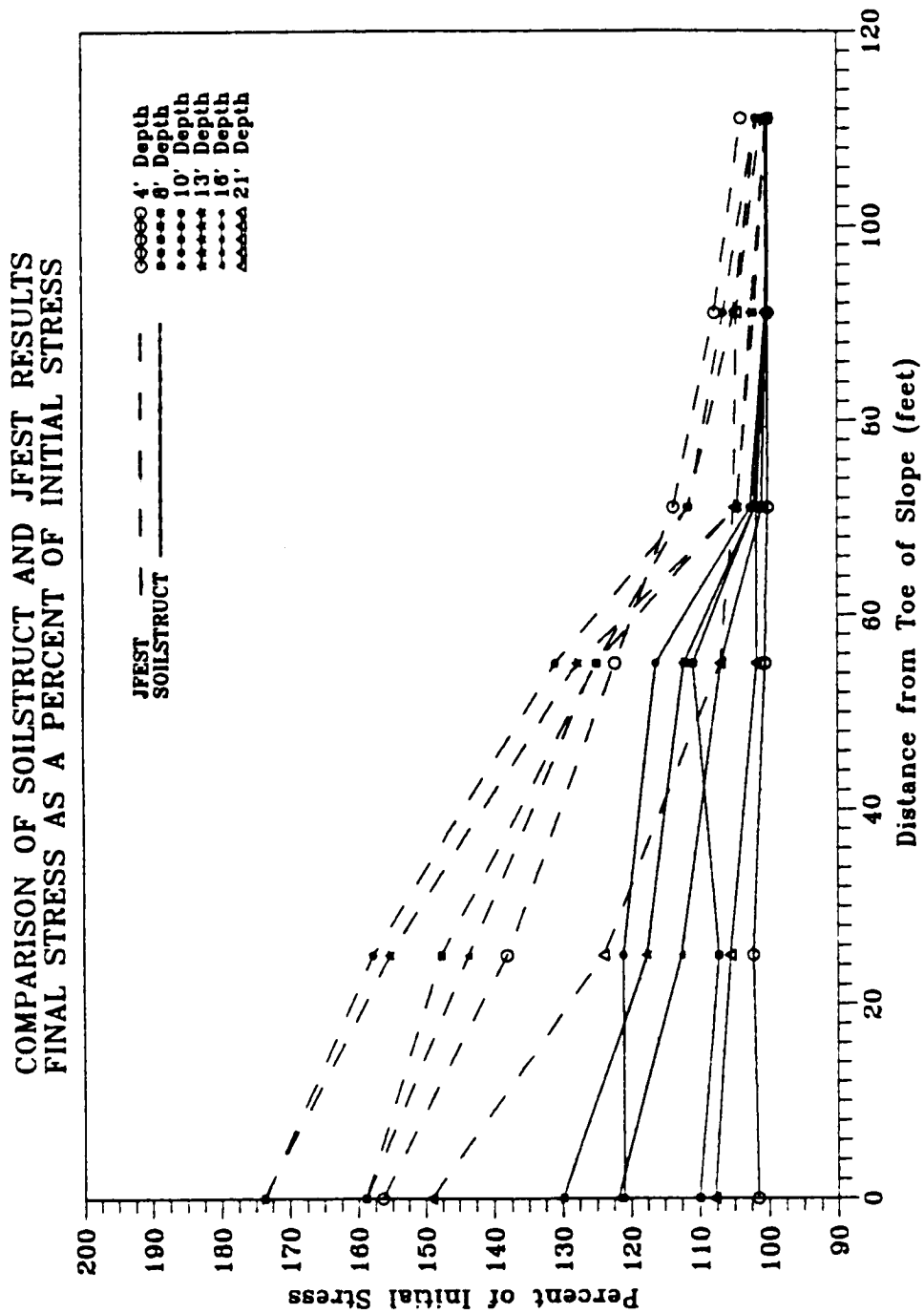


Figure 5-15 Comparison of SOILSTRUCT and JFEST Computed Horizontal Stress Increase Due to Embankment Load Versus Distance from Embankment Toe

model is theoretically less appropriate than SOILSTRUCT for this soil. As a result, it would be expected that the results of SOILSTRUCT would be more meaningful for the upper clay crust.

CHAPTER VI

TEST RESULTS: MEASUREMENT OF IN SITU STRESS

6.1 Introduction

This chapter discusses how the raw SBPM horizontal stress measurements were culled of data exhibiting soil disturbance and corrected for excess pore pressure caused by deployment of the probe to test depth. Following this discussion, the results of SBPM horizontal stress measurements at the Pease and Hamilton AFB test sites are presented and discussed. A later section in this chapter discusses use of the SBPM total horizontal stress measurements to estimate stress anisotropy in the horizontal plane.

6.2 Assessment of Horizontal Stress Results

Benoit (1983) and others found that disturbance can have profound effects on the shape of the pressuremeter curve and can lead to measurement of horizontal stresses which are not representative of actual in situ conditions. Also, excess pore pressure has been found to exist after deployment. Consideration of both disturbance and excess pore pressure are necessary to obtain total horizontal stress values which are representative of undisturbed in situ ground conditions.

6.2.1 Assessment of Test Results Affected by Disturbance

Determination of whether or not a pressuremeter curve is affected by disturbance is typically made by inspection. Inspection consists of observing if a pressuremeter curve deviates from the classic shape of a test with minimal disturbance. As a basis for comparison in studying the effects of soil disturbance on measured horizontal stress, a typical expansion curve from a test conducted in undisturbed soil is presented on Figure 6-1. The loading portion of the undisturbed test curve is initially steep after lift-off, progressively flatter (monotonic) with strain. The loading portion has a high degree of curvature and is

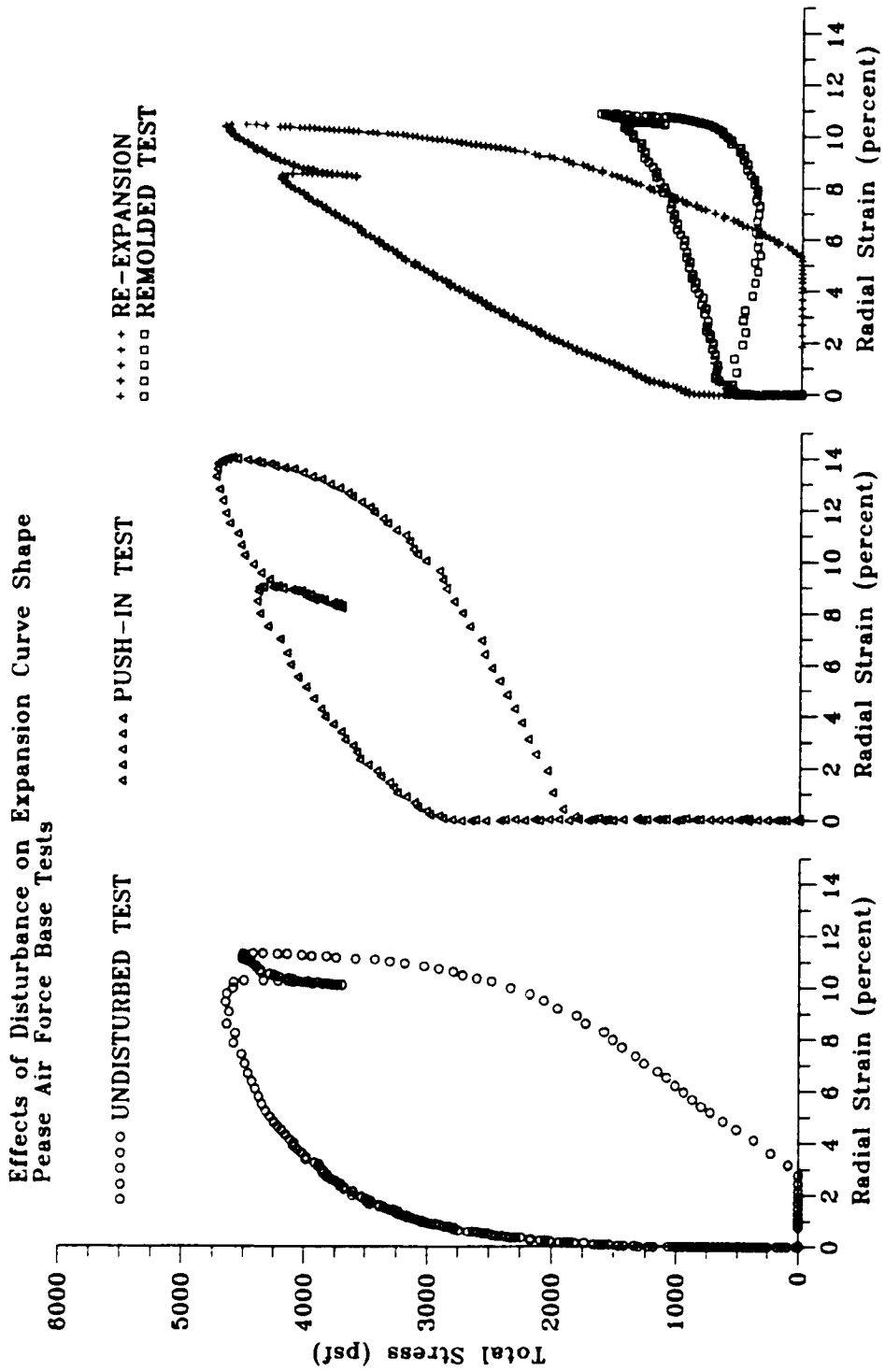


Figure 6-1 Typical SBPM Pressuremeter Curves

smooth. A profile of total horizontal stress measured by SBPM tests at Pease AFB in soil with a K_0 stress condition which appear (by inspection) to be undisturbed is included on Figure 6-2. These values have been found to be representative of in situ total horizontal stress by comparison with the profile of horizontal stress predicted by empirical methods.

A few pressuremeter tests experienced washing away ("wash-boring") of soil material outside of the pressuremeter membrane during deployment causing significant remolding of the soil. This was evidenced by the fact that the pressuremeter was found to be blocked by soil internally, a consequence of ineffective cutting/jetting. This blockage made the only possible route for the jetting water to be around the outside of the probe. An expansion curve for such a test is presented on Figure 6-1, and indicates that after lift-off, the membrane experienced a relatively large amount of strain with little stress increase, resulting from remolding of the soil cavity. Clearly, such a test shows disturbance by comparison with the monotonic undisturbed expansion curve on the same figure. Figure 6-2 presents values of horizontal stress with depth for a few remolded expansion curves. It can be seen that these lateral stresses are generally about or within the error of measurement of the hydrostatic stress line, well below actual in situ horizontal stress.

A few re-expansions were conducted in soil zones that had already been tested. Such tests included PMC3.5R, PMJ3.2R, PMJ3.4R, PMJ4.2R and HAM2.4R. A typical expansion curve for a re-expansion test is presented on Figure 6-1. This curve also exhibits a deviation from the undisturbed curve in that after lift-off, the re-expansion curve is generally steeper (except at small radial strain), and is almost linear, with only a slight curvature. Total horizontal stress measured during re-expansions at different depths are indicated on Figure 6-2. The measured stresses are on the order of hydrostatic stress or within the error of measurement, well below actual in situ total horizontal stress as indicated by the undisturbed results on the same figure. This suggests a void filled with

EFFECTS OF DISTURBANCE ON MEASURED HORIZONTAL STRESS
 TOTAL HORIZONTAL STRESS (PSF)

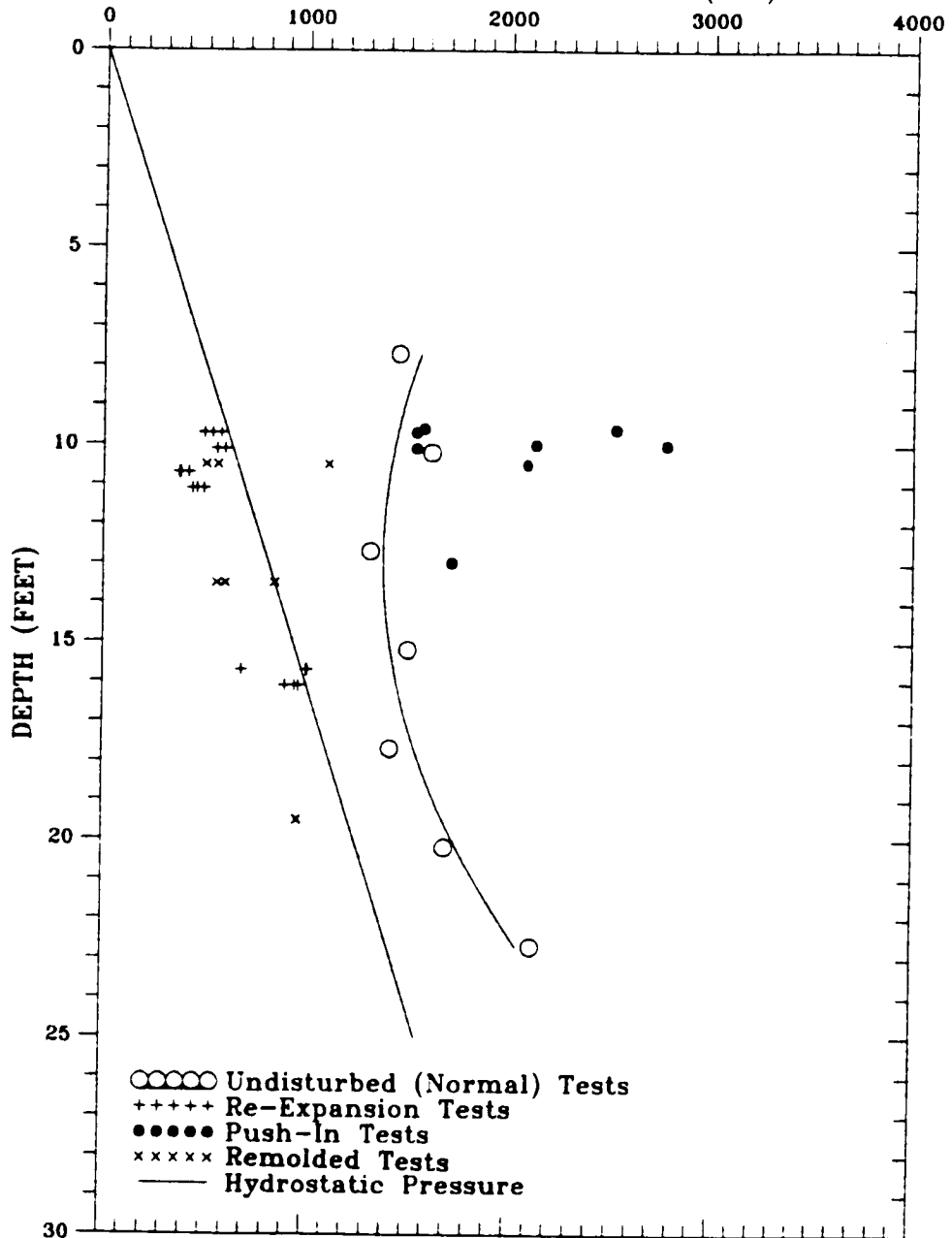


Figure 6-2 Effects of Disturbance on Measured Horizontal Stress

water likely exists adjacent to the probe.

Three push-in tests were performed at the Pease K₁ site and one at Hamilton AFB. An expansion curve from a push-in test is presented on Figure 6-1. As can be seen, the load portion of the curve is initially less steep, with less curvature than an undisturbed curve. While the push-in curve depicted on Figure 6-1 is representative of "fully developed" push-in disturbance, several of the push-in test curves were more difficult to discern from undisturbed tests (see the pressuremeter curves for tests PMP1.1, 1.2, 2.1 and HAM2.5P in Appendix C). The horizontal stresses indicated by the push-in tests are plotted with depth on Figure 6-2. As can be seen, the indicated horizontal stresses from push-in tests are generally higher than the undisturbed test data, although there is some overlap. This overlap is further evidence of the difficulty in discerning some push-in test curves from undisturbed test curves.

It is thought that normal pressuremeter tests can suffer to some extent from one or more of the above discussed disturbance effects. Push-in and remolding type disturbance could occur due to improper cutting/jetting insertion. Encountering a shell or stone during deployment could also cause disturbance. Both of these types of disturbance could also occur if the longitudinal axis of the probe were not perfectly aligned with the direction of drilling.

While remolding disturbance can be observed by inspection, push-in type disturbance can be more difficult to detect and evaluation of disturbed tests becomes somewhat subjective. In an attempt to decrease the subjectivity, a numerical method to assess test quality was developed, as subsequently discussed.

Tabulations of stresses at various radial strains for several undisturbed, re-expanded and push-in tests are presented respectively on Tables 6-1, 2 and 3 and 4. The total expansion pressure at lift-off, 1 percent radial strain and 5 percent radial strain are listed on these tables. The intent of selecting stresses at these radial strains was to

COMPUTATION OF DISTURBANCE RATIO UNDISTURBED TESTS IN K ₀ CONDITION				
TEST ARM	STRESS @ LIFT-OFF (psf)	STRESS @ 1% STRN (psf)	STRESS @ 5% STRN (psf)	DISTURB- ANCE RATIO, Cd
<u>PEASE AFB:</u>				
PMC2.1,M1	1801	3700	5550	0.34
PMC3.1,M1	1775	4000	5300	0.42
PMC4.3,M1	1362	3200	4300	0.43
PMC4.6,M1	1424	3300	5200	0.36
PMC4.7,M1	1871	3800	5200	0.37
PMC4.6,M2	1860	4000	5000	0.43
PMC4.7,M2	1871	3700	5150	0.36
PMC2.1,M3	1354	3300	5200	0.37
PMC4.7,M3	1378	3400	5050	0.40
PMJ3.4,M1	1724	3300	5050	0.31
PMJ5.5,M1	2323	3800	4750	0.31
PMJ5.6,M1	1798	3300	4600	0.33
PMJ3.4,M2	1783	3500	5000	0.34
PMJ4.1,M2	1927	3400	5300	0.28
PMJ5.5,M2	1757	3800	4800	0.43
PMJ5.6,M2	1326	3450	4700	0.45
PMJ3.4,M3	1822	3700	4950	0.38
PMJ4.1,M3	1312	3100	5200	0.34
PMJ5.5,M3	1994	3800	5050	0.36
PMJ5.6,M3	1736	3550	4800	0.38
			<u>AVERAGE =</u>	0.37
			<u>STD.DEV.=</u>	0.04
<u>HAMILTON AFB:</u>				
HAM1.2,M1	1892	2400	2900	0.18
HAM1.3,M1	1540	2100	2700	0.21
HAM2.1,M1	1383	2000	2700	0.23
HAM2.3,M1	1579	2050	2600	0.18
HAM1.1,M2	1913	2550	2850	0.22
HAM2.1,M2	1250	2000	2750	0.27
HAM2.3,M2	1661	2300	2625	0.24
HAM1.1,M3	1994	2550	3100	0.18
HAM1.2,M3	1955	2500	3000	0.18
HAM1.3,M3	1407	2100	2800	0.25
HAM2.3,M3	1661	2200	2775	0.19
			<u>AVERAGE =</u>	0.21
			<u>STD.DEV.=</u>	0.03

Table 6-1 Disturbance Ratio for K₀ Undisturbed Tests

COMPUTATION OF DISTURBANCE RATIO UNDISTURBED TESTS, PEASE EMBANKMENT TOE SITE				
TEST, ARM	STRESS @ LIFT-OFF (psf)	STRESS @ 1% STRN (psf)	STRESS @ 5% STRN (psf)	DISTURB- ANCE RATIO, Cd
PMJ6.1,M1	2086	3900	5100	0.36
PMJ6.2,M1	1798	3100	3800	0.34
PMJ6.3,M1	1919	3400	4200	0.35
PMJ6.4H,M1	2015	3400	4300	0.32
PMJ6.1,M2	1931	3900	5000	0.39
PMJ6.2,M2	1759	3100	3750	0.36
PMJ6.3,M2	1815	3500	4200	0.40
PMJ6.4H,M2	1636	3400	4200	0.42
PMJ6.1,M3	1899	3900	5100	0.39
PMJ6.2,M3	1759	3200	4000	0.36
PMJ6.3,M3	1796	3450	4200	0.39
PMJ6.4H,M3	1686	3400	4500	0.38
			AVERAGE=	0.37
			STD.DEV.=	0.03

Table 6-2 Disturbance Ratio for Non-K, Undisturbed Tests

COMPUTATION OF DISTURBANCE RATIO PUSH-IN TESTS				
TEST, ARM	STRESS @ LIFT-OFF (psf)	STRESS @ 1% STRN (psf)	STRESS @ 5% STRN (psf)	DISTURB- ANCE RATIO, Cd
PEASE AFB:				
PMP1.1,M1	1768	2550	4000	0.20
PMP1.1,L2	2347	3000	4000	0.16
PMP1.1,L3	2989	3300	4200	0.07
PMP1.2,M1	2788	3200	4000	0.10
PMP1.2,M2	2814	3400	4000	0.15
PMP1.2,M3	2814	3450	4250	0.15
PMP1.2,L2	2769	3300	4000	0.13
PMP1.2,L3	3148	3400	3800	0.07
PMP2.1,M1	3180	3550	4300	0.09
PMP2.1,M2	3076	4000	5000	0.18
PMP2.1,L2	3122	3800	4600	0.15
PMP2.1,L3	3726	4200	4800	0.10
			AVERAGE =	0.13
			STD.DEV. =	0.04
HAMILTON AFB:				
HAM2.5P,U1	2636	3000	3500	0.10
HAM2.5P,M1	2914	3200	3700	0.08
HAM2.5P,M2	2914	3200	3600	0.08
HAM2.5P,M3	2832	3100	3600	0.07
HAM2.5P,L1	3010	3300	3900	0.07
HAM2.5P,L2	2934	3200	3650	0.07
HAM2.5P,L3	2950	3200	3700	0.07
			AVERAGE =	0.08
			STD.DEV. =	0.01

Table 6-3 Disturbance Ratio for Push-In Tests

COMPUTATION OF DISTURBANCE RATIO RE-EXPANSION TESTS				
TEST, ARM	STRESS @ LIFT-OFF (psf)	STRESS @ 1% STRN (psf)	STRESS @ 5% STRN (psf)	DISTURB- ANCE RATIO, Cd
PEASE AFB:				
PMC3.5R,M1	1082	1600	3200	0.16
PMJ3.2R,M1	415	800	2500	0.15
PMJ3.4R,M1	691	1450	3200	0.24
PMC4.2R,M1	409	1200	3650	0.22
PMC3.5R,M2	940	1800	3450	0.25
PMJ3.2R,M2	415	1500	2500	0.43
PMJ3.4R,M2	738	1500	3100	0.25
PMC4.2R,M2	375	1200	3000	0.28
PMC3.5R,M3	934	1400	2800	0.17
PMJ3.2R,M3	455	1000	1950	0.28
PMJ3.4R,M3	757	1550	3000	0.26
PMC4.2R,M3	353	1550	2900	0.41
			<u>AVERAGE =</u>	0.26
			<u>STD. DEV. =</u>	0.08
HAMILTON AFB:				
HAM2.4R,M1	819	1000	2250	0.08
HAM2.4R,M2	874	1300	2250	0.19
HAM2.4R,M3	856	1200	2400	0.14
			<u>AVERAGE =</u>	0.14
			<u>STD. DEV. =</u>	0.04

Table 6-4 Disturbance Ratio for Re-Expansion Tests

compile representative stresses before, near and after failure. Since the curve shape of each type of disturbance varies in slope and curvature to some extent before and after failure, it follows that a ratio of the above three stresses could be derived to differentiate the different types of disturbance. Several different ratios consisting of various combinations of stress at lift-off, 1 percent and 5 percent radial strain were computed to determine one that would best yield a recognizable difference between undisturbed, re-expansion and push-in influenced pressuremeter curves. The best definition of the difference between test curves seems to be obtained using the following ratio, hereafter denoted as C_d , the "disturbance ratio":

$$C_d = (\sigma_{1\%} - \sigma_b) / \sigma_{5\%} \quad (\text{Eq 6-1})$$

where: C_d = disturbance ratio
 σ_b = total stress at lift-off (psf)
 $\sigma_{1\%}$ = total stress at 1% radial strain (psf)
 $\sigma_{5\%}$ = total stress at 5% radial strain (psf)

Table 6-1 presents computed C_d values for 20 undisturbed expansion curves from the Pease K_0 area and 11 curves from undisturbed tests at Hamilton AFB. The range of C_d (plus or minus one standard deviation) for undisturbed tests was 0.37 ± 0.04 and 0.21 ± 0.03 for Pease and Hamilton AFB, respectively. This difference in values between the two sites seems to indicate that soil type has an influence on C_d , and thus the shape of the pressuremeter curve. To see if non- K_0 conditions affect the ratio, stress data from undisturbed (based on inspection) tests conducted at the embankment (PMJ6) at the Pease site were compiled on Table 6-2. The average C_d ratio at the toe site was 0.37 ± 0.03 . A T-test with pooled standard deviations and an assumed significance level of 0.5% (0.25% in each of the two tails of the test) indicates that there is no evidence suggesting the Pease embankment site has an average C_d that is different from the Pease K_0 average. This suggests the ratio of vertical to

horizontal effective stress has little influence on the value of C_d .

Computed C_d values from push-in tests are presented on Table 6-3. The range in the ratio was found to be 0.13 ± 0.04 at Pease AFB and 0.08 ± 0.01 for the pressuremeter curves from one test at Hamilton AFB. The fact that the disturbance ratios for push-in tests are significantly less than those for undisturbed tests indicates that the disturbance ratio could be useful in numerically differentiating between undisturbed tests and those affected by push-in disturbance. To statistically test to see if the C_d ratio could distinguish between undisturbed and push-in pressuremeter tests, the mean value of C_d and the standard deviation of the mean value of C_d from samples of both types of tests were compared using a T-test. A null hypothesis that the values of undisturbed and push-in tests were from the same population was made, and the standard deviations from the undisturbed and push-in tests were pooled. A significance level of 0.5% was assumed. The T-test confirmed the null hypothesis, indicating that there is no evidence to suggest that the undisturbed and push-in means are from the same population. This gives statistical credence for the viable use of the C_d ratio to differentiate between push-in and undisturbed tests.

Table 6-4 is a tabulation of C_d for re-expansion tests. The average ratio of the listed tests was found to be 0.26 ± 0.08 at Pease AFB, and 0.14 ± 0.04 from limited data obtained at Hamilton AFB. The average C_d for re-expansion lies between that for undisturbed and push-in tests, making the ratio less useful for assessing re-expansion influenced pressuremeter curves. Fortunately, this form of disturbance is not expected to be found in typical field results. Even if such disturbance were to occur, it is usually distinguishable by inspection.

For the current research, all pressuremeter curves were assessed for disturbance. Tables summarizing the results of this assessment are presented in Appendix B. The assessment was done in two phases. The first phase was accomplished by inspection. This was done because a

pressuremeter curve with slight remolding disturbance or a slight void in the soil adjacent to the membrane could a yield disturbance ratio within the range considered representative of undisturbed tests. All curves exhibiting disturbed shape characteristics by inspection were denoted by "NA" under the C_c column on the tables in Appendix B. After assessment by inspection, C_c was computed for each of the remaining curves. These computed values were compared to the average undisturbed C_c values (Tables 6-1 and 6-2) for the respective test site. All computed C_c values within two standard deviations of the average undisturbed C_c values were considered undisturbed tests and are labeled "Good" on the tables presented in Appendix B. All tests outside of this range were considered suspect of disturbance and are labeled "Fair" on the tables. In the subsequent chapters of this dissertation, tests assessed to be "Good" on the tables presented in Appendix B are considered to be representative of tests made in zones of undisturbed soil.

Because of the differences of C_c between the Pease and Hamilton AFB sites, some baseline testing would be required to use the method at other soft clay sites. Further research using data from several different sites might result in determination of a relationship of the ratio with some soil index property.

6.2.2 Correction for Excess Pore Pressures Due to Insertion

Excess pore pressures due to deployment of the SBPM generally persists for a considerable time after completion of drilling. For fine-grained soils such as those found at the Pease and Hamilton test sites, pressuremeter holding tests and dilatometer dissipation tests have indicated that it may take several hours for pore pressure to completely dissipate. Such excess pore pressure existing at the start of an expansion test will effect the magnitude of measured total horizontal stress. Because it is usually not practical to wait for complete dissipation of pore pressures prior to expansion of the pressuremeter, it was the practice of this research to measure the excess pore pressure at the beginning of the expansion test for use in correction of the

measured total horizontal stress during data reduction. Because of the need to allow temperature equalization of the probe after drilling, as discussed in Appendix A, the expansion test typically commenced about 30 to 40 minutes after drilling the probe to test depth. Correction of the measured horizontal stress was done by simply subtracting the measured excess pore pressure.

6.3 In Situ Horizontal Stress

Horizontal stress was determined for this research using the inspection method. Using this method, the lift-off portion of the uncorrected pressuremeter curve is observed to determine the precise pressure at which the membrane lifts away from the probe. This pressure is the lift-off pressure or the apparent horizontal stress, and must be corrected for membrane stiffness. A new membrane stiffness correction method which considers the order of strain arm lift-off in the field test was derived and employed to improve horizontal stress measurement accuracy. This method is described in detail in Appendix A. Along with stiffness correction, measured total horizontal stress data was culled of disturbed test data by the method that has been discussed in the previous sections of this chapter.

In addition to stiffness correction and disturbance culling, the apparent horizontal stress may require correction for excess pore pressure due to insertion if an expansion test is conducted before such excess pore pressures fully dissipate. A method to assess this excess pore pressure was derived and employed for the current research, since expansion generally commenced about 40 minutes after deployment to allow sufficient time for temperature adjustment of the SBPM to the surrounding soil (experiments involving time for temperature adjustment of the SBPM are discussed in Appendix A). Holding tests conducted for this research indicated that the excess pore pressure due to insertion was likely only about half dissipated after 40 minutes. The correction method derived involves indirect consideration of temperature differences between the SBPM calibration and in-ground test environments and is discussed in

detail in Appendix A.

After processing of the data, the difference between the minimum and maximum horizontal stress measured at individual strain arms on a particular arm tier was on average about 100 to 250 psf as indicated by the fourth degree polynomial best-fit lines on Figure 6-3 for data from the Pease AFB K₁ site. It has been speculated that this difference could be a result of stress anisotropy in the horizontal plane, as will be discussed in a later section of this chapter; however, it is noted that this difference is about equal to the error of measurement of the SBPM equipment, about 150 to 200 psf (see Appendix A).

Previous researchers (Denby, 1978, Benoit, 1983 and others) have reported total horizontal stress based on an "electronic average" of the three arms on a standard SBPM. This electronic average is not a true average, and lift-off is defined when the first strain arm begins to move, rather than an average lift-off of all three arms. As a result, previous research has essentially defined in situ total horizontal stress as being equivalent to that indicated by the first strain arm to lift-off, or, in other words, the lowest measured total stress at lift away from the body of the probe during membrane inflation.

6.3.1 In Situ Horizontal Stress At Pease AFB

At Pease AFB, no previous measurements of in situ horizontal stress exist. As a basis for assessing the in situ horizontal stress measurements at Pease, both empirical methods and finite element analyses were utilized. Empirical methods were used to estimate horizontal stress at the K₁ area, and finite element methods have been used to assess lateral stresses at the embankment toe area. The FEM method is particularly useful as a comparison with the trends of measured stress indicated by the SBPM with respect to embankment effects and distance from the embankment. The following subsections discuss the comparison of expected lateral stress by empirical and FEM methods with those actually measured by the SBPM.

6.3.1.1 Pease K₁ Area - The results of finite element analyses

PEASE AIR FORCE BASE SBPM MEASURED HORIZONTAL STRESS

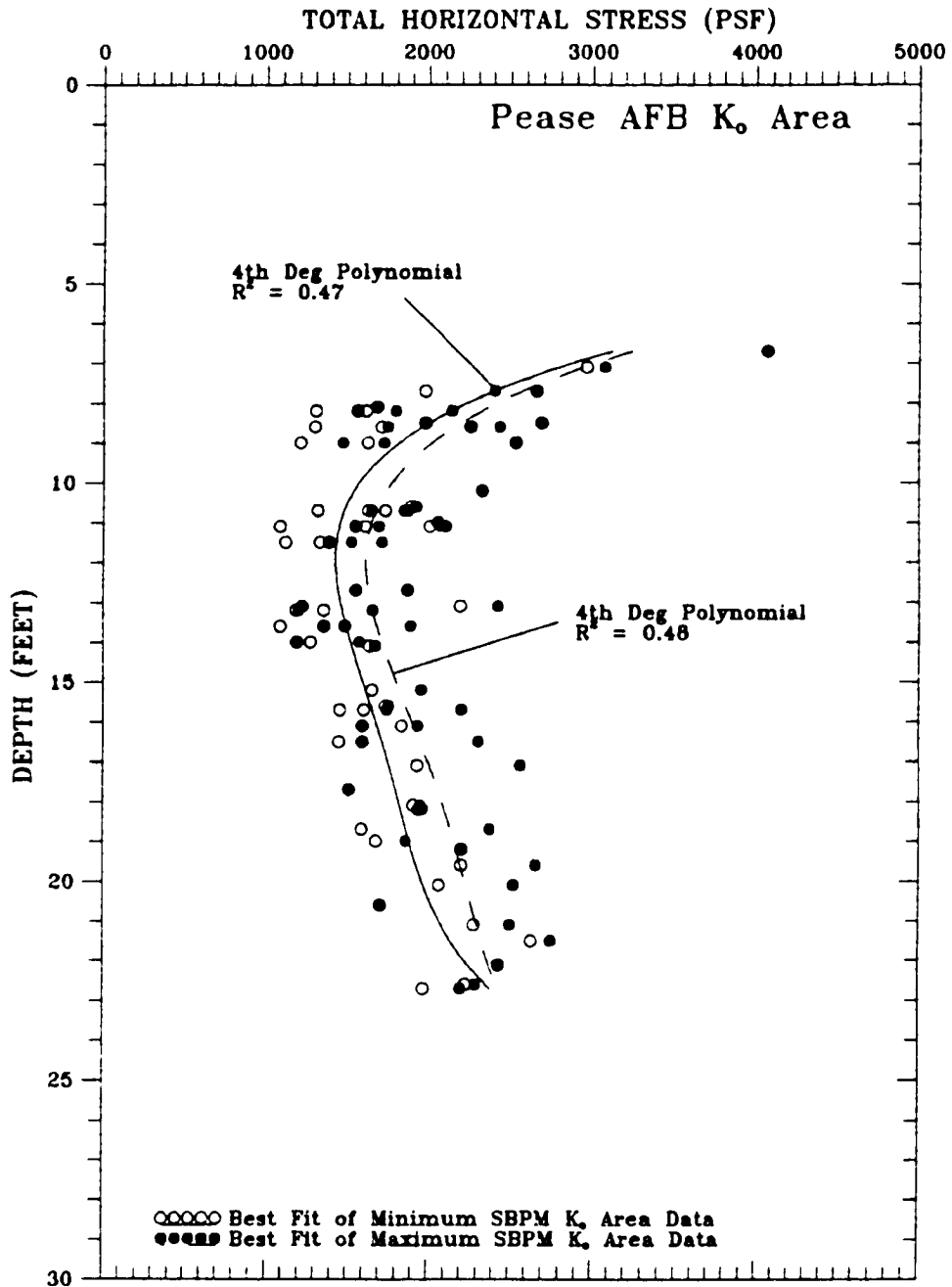


Figure 6-3 Minimum and Maximum Total Horizontal Stress Profiles at Pease AFB

described in Chapter V indicate that the Pease K_0 area is outside of the influence of the stress effects of the highway embankment, and as a result, horizontal stresses at this area are expected to be representative of at-rest K_0 earth pressure conditions. Table 6-5 summarizes the horizontal stresses measured at the Pease K_0 area during the current research. The measured excess pore pressures due to insertion are included in the last column of the table. It is noted that the horizontal stress results on this table are corrected for excess pore pressure due to insertion, but have not been culled for disturbance.

Figure 6-4 is a plot of SBPM measured total horizontal stress with depth for undisturbed lift-offs at the K_0 area. The measured horizontal stress plotted represents the lowest measured undisturbed value on a particular tier of arms and is seen to range from about 1500 to 4000 psf in the stiff upper crust of the clay to about 1000 to 2500 psf in the softer, underlying portion of the clay deposit. A fourth degree polynomial best-fit curve through the data has been included. Also indicated on the figure is the predicted horizontal stress based on an empirical estimate of K_0 by a method developed by Brooker and Ireland (1965). Good agreement between the lower bound of the SBPM measured values and the profile predicted by the Brooker and Ireland method can be observed below a depth of about 12 feet. Above a depth of 12 feet, in the stiffer clay crust, the SBPM tends to measure higher horizontal stresses, up to about 400 percent or more than the Brooker and Ireland (1965) method. This suggests that the effects of desiccation may tend to create higher apparent horizontal stresses than is generally accounted for by the OCR versus plasticity relationship of Brooker and Ireland (1965).

Profiles of total horizontal stress for each boring in the K_0 Area (PMC 1, 2, 3, and 4; and PMJ 3, 4, and 5) are presented in Appendix D. Adjacent to each of these profiles are profiles of dilatometer I_p values. As discussed in Chapter IV, I_p values can be used to characterize soil

**MEASURED TOTAL HORIZONTAL STRESS
SUMMARY OF TEST RESULTS - PEASE AIR FORCE BASE K₀ AREA**

TEST	DEPTH (feet)	MEASURED HORIZONTAL STRESS			EXCESS
		ARM 1 (psf)	ARM 2 (psf)	ARM 3 (psf)	PORE PRESSURE (psf)
<u>UPPER ARMS:</u>					
PMC1.1	8.2	2432	1794	1303	-47
PMC1.2	10.7	1731	1872	549	177
PMC1.3	13.2	1654	1353	903	-90
PMC2.1	8.2	2139	1613	676	56
PMC2.2	10.7	1846	1315	570	122
PMC2.3H	13.2	1179	1195	750	178
PMC2.4	15.7	1741	1602	546	347
PMC3.1	8.2	2151	1558	814	349
PMC3.2H	10.7	1648	1627	229	422
PMC3.3H	13.2	996	1018	245	487
PMC3.4H	15.7	1244	943	-32	885
<u>MIDDLE ARMS:</u>					
PMC1.1	8.6	2435	5175	1707	-47
PMC1.2	11.1	1610	2622	474	177
PMC1.3	13.6	1353	2960	943	-90
PMC2.1	8.6	1745	3395	1298	56
PMC2.2	11.1	1547	2974	372	122
PMC2.3H	13.6	1085	2638	675	178
PMC2.4	16.1	1116	3136	587	347
PMC3.1	8.6	2253	3427	1541	349
PMC3.2H	11.1	1083	1921	269	422
PMC3.3H	13.6	977	1726	285	487
PMC3.4H	16.1	1000	1561	619	885
<u>LOWER ARMS:</u>					
PMC1.1	9.0	1546	4239	1628	-47
PMC1.2	11.5	1328	2184	1023	177
PMC1.3	14.0	1573	2215	813	-90
PMC2.1	9.0	1207	2766	1297	56
PMC2.2	11.5	1117	1895	934	122
PMC2.3H	14.0	684	1859	698	178
PMC2.4	16.5	1447	2890	1378	347
PMC3.1	9.0	1624	3262	1890	349
PMC3.2H	11.5	841	1654	1014	422
PMC3.3H	14.0	1018	1322	777	487
PMC3.4H	16.5	1067	2212	2232	885

Table 6-5 Summary of Horizontal Stresses Measured at Pease K₀ Area

**MEASURED TOTAL HORIZONTAL STRESS
SUMMARY OF TEST RESULTS - PEASE AIR FORCE BASE K₀ AREA**

<u>TEST</u>	<u>DEPTH</u> <u>(feet)</u>	<u>MEASURED HORIZONTAL STRESS</u>			<u>EXCESS</u> <u>PORE</u> <u>PRESSURE</u> <u>(psf)</u>
		<u>ARM 1</u> <u>(psf)</u>	<u>ARM 2</u> <u>(psf)</u>	<u>ARM 3</u> <u>(psf)</u>	
<u>UPPER ARMS:</u>					
PMC3.5H	18.2	1961	1940	1188	230
PMC3.5R	18.2	-155	-155	-110	1044
PMC3.6H	20.7	1969	1835	1905	-740
PMC4.1	7.7	2659	1540	1412	-156
PMC4.2	10.2	2324	1475	1475	47
PMC4.3	12.7	1551	1072	1096	144
PMC4.4	15.2	1954	1652	1123	95
PMC4.5	17.7	1510	1380	1145	152
PMC4.6	20.2	2133	1509	1180	157
PMC4.7	22.7	2198	2098	1971	93
<u>MIDDLE ARMS:</u>					
PMC3.5H	18.6	1719	2787	1228	230
PMC3.5R	18.6	38	-104	-110	1044
PMC3.6H	21.1	2447	3515	2279	-740
PMC4.1	8.1	1436	1372	826	-156
PMC4.2	10.6	1921	1890	1250	47
PMC4.3	13.1	1218	1199	743	144
PMC4.4	15.6	1733	1752	839	95
PMC4.5	18.1	1948	1907	943	152
PMC4.6	20.6	1267	1703	1059	157
PMC4.7	23.1	1778	1778	1285	93
<u>LOWER ARMS:</u>					
PMC3.5H	19.0	1678	1859	784	230
PMC3.5R	19.0	-64	-85	-110	1044
PMC3.6H	21.5	2633	2748	2279	-740
PMC4.1	8.5	1472	726	2689	-156
PMC4.2	11.0	973	1008	2052	47
PMC4.3	13.5	669	836	1259	144
PMC4.4	16.0	839	1087	2276	95
PMC4.5	18.5	1070	1132	2139	152
PMC4.6	21.0	1111	1193	2133	157
PMC4.7	23.5	1486	1452	2884	93

Table 6-5 (Continued) Summary of Horizontal Stresses Measured at Pease K₀ Area

MEASURED TOTAL HORIZONTAL STRESS
SUMMARY OF TEST RESULTS - PEASE AIR FORCE BASE K₀ AREA

TEST	DEPTH (feet)	MEASURED HORIZONTAL STRESS			EXCESS PORE PRESSURE (psf)
		ARM 1 (psf)	ARM 2 (psf)	ARM 3 (psf)	
<u>UPPER ARMS:</u>					
PMJ3.2	9.7	709	494	706	-110
PMJ3.4	15.7	1454	2200	1735	-111
PMJ3.5	18.7	2377	980	1591	-6
PMJ3.6	21.7	1890	996	1805	59
PMJ4.1	7.7	2404	1977	1348	-334
PMJ4.2	10.7	1256	585	1075	-55
PMJ4.2R	10.7	378	378	418	-84
PMJ4.3	13.7	1569	1985	1473	-43
PMJ4.4	16.7	1398	1350	1401	-70
PMJ4.5	19.7	2081	1733	1781	10
<u>MIDDLE ARMS:</u>					
PMJ3.2	10.1	514	559	555	-110
PMJ3.4	16.1	1835	1894	1933	-111
PMJ3.5	19.1	2862	1069	2399	-6
PMJ3.6	22.1	2455	1319	2434	59
PMJ4.1	8.1	703	2261	1679	-334
PMJ4.2	11.1	1110	2004	2104	-55
PMJ4.2R	11.1	493	459	437	-84
PMJ4.3	14.1	1542	1671	1635	-43
PMJ4.4	17.1	1932	1897	2563	-70
PMJ4.5	20.1	2064	2280	2523	10
<u>LOWER ARMS:</u>					
PMJ3.2	10.5	502	559	1109	-110
PMJ3.4	16.5	964	1051	2600	-111
PMJ3.5	19.5	963	963	3669	-6
PMJ3.6	22.5	1117	1083	2999	59
PMJ4.1	8.5	541	1977	3351	-334
PMJ4.2	11.5	464	914	2749	-55
PMJ4.2R	11.5	436	476	801	-84
PMJ4.3	14.5	1588	1225	2818	-43
PMJ4.4	17.5	1946	1831	3491	-70
PMJ4.5	20.5	2130	1817	3048	10

Table 6-5 (Continued) Summary of Horizontal Stresses Measured at Pease K₀ Area

**MEASURED TOTAL HORIZONTAL STRESS
SUMMARY OF TEST RESULTS - PEASE AIR FORCE BASE K₀ AREA**

<u>TEST</u>	<u>DEPTH</u> <u>(feet)</u>	<u>MEASURED HORIZONTAL STRESS</u>			<u>EXCESS</u> <u>PORE</u> <u>PRESSURE</u> <u>(psf)</u>
		<u>ARM 1</u> <u>(psf)</u>	<u>ARM 2</u> <u>(psf)</u>	<u>ARM 3</u> <u>(psf)</u>	
<u>UPPER ARMS:</u>					
PMJ5.1	6.7	4377	4067	4067	-194
PMJ5.2	9.7	2516	2633	2326	-1015
PMJ5.3	12.7	1869	1552	2080	-736
PMJ5.4	16.2	1964	1579	2093	-258
PMJ5.5	19.2	2312	2202	1711	-445
PMJ5.6	22.2	2376	2465	1772	-490
<u>MIDDLE ARMS:</u>					
PMJ5.1	7.1	4142	3071	2962	-194
PMJ5.2	10.1	2133	2056	2416	-1015
PMJ5.3	13.1	2426	2194	2239	-736
PMJ5.4	16.6	1510	1767	1702	-258
PMJ5.5	19.6	2659	2202	2248	-445
PMJ5.6	22.6	2288	1816	2226	-490
<u>LOWER ARMS:</u>					
PMJ5.1	7.5	1814	3711	3360	-194
PMJ5.2	10.5	2576	3428	3430	-1015
PMJ5.3	13.5	1553	2528	2863	-736
PMJ5.4	17.0	2208	2157	3051	-258
PMJ5.5	20.0	2202	2889	3333	-445
PMJ5.6	23.0	1659	2367	3518	-490

Table 6-5 (Continued) Summary of Horizontal Stresses Measured at Pease K₀ Area

PEASE AIR FORCE BASE K_0 AREA

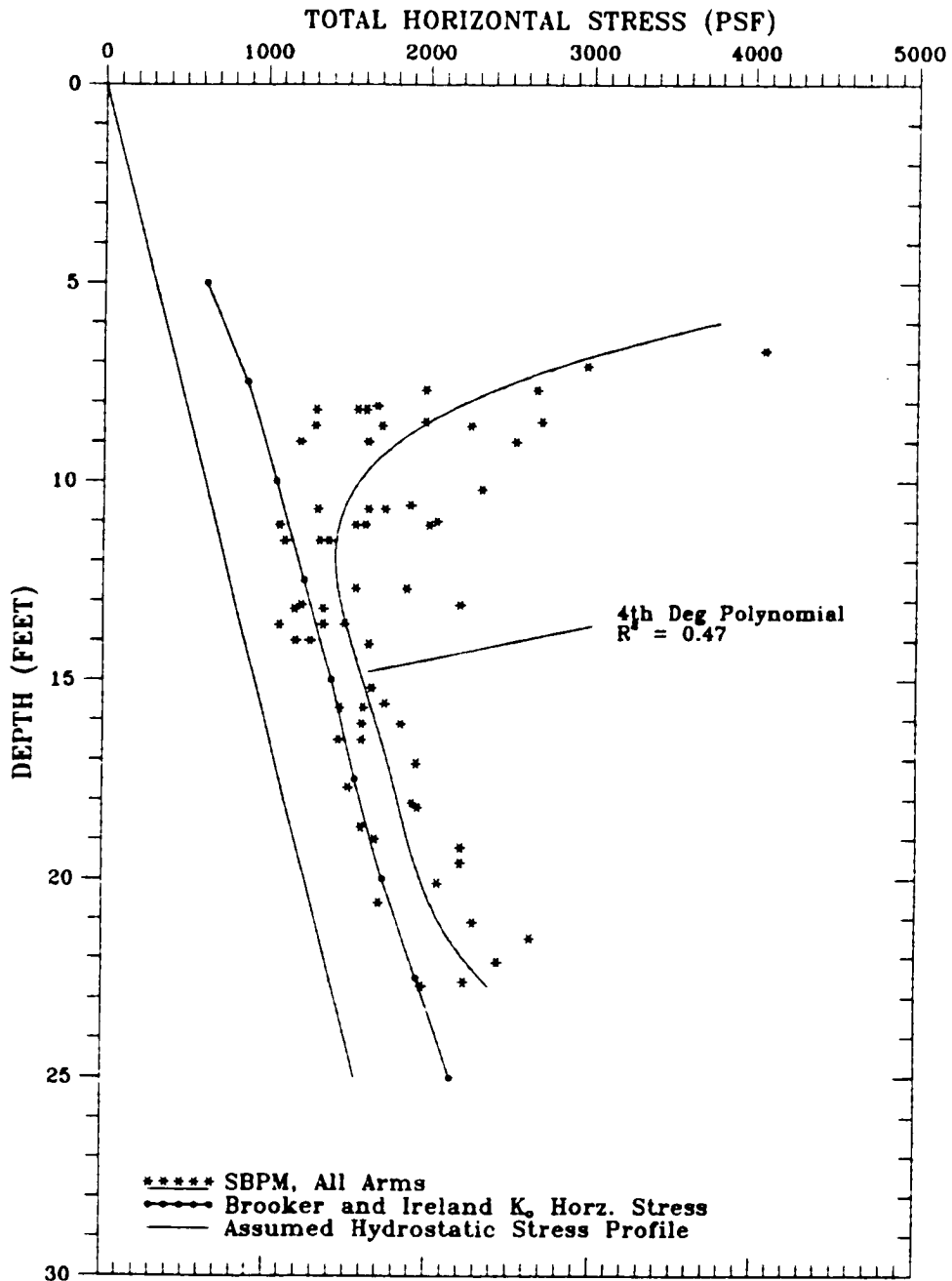


Figure 6-4 Pease AFB K_0 Area SBPM Total Horizontal Stress Profile

behavior, and thus give an indication of the soil type each pressuremeter test was conducted in. The intent of these plots was to help resolve any anomalies in the horizontal stress profiles. Figure 6-5 is presented as an example of one of the plots. As can be seen on the figure, tests PMC3.5 and PMC3.6 measured higher than expected horizontal stress. In the case of these tests, the plots of dilatometer I_p values suggests that silt layers may exist below a depth of 10 feet in the vicinity of boring PMC3. It is possible that similar layers at PMC3 could have resulted in these elevated stresses although the depth relationship between PMC3 and the I_p plot are not exact. Similar layers were not generally observed in other dilatometer profiles.

Figure 6-6 is a profile of K_0 values estimated from the SBPM total horizontal stress values of Figure 6-4. Values of K_0 estimated by the Brooker and Ireland (1965) method are also included on the profile. In the softer portion of the marine silty clay deposit, below a depth of about 12 feet, the SBPM estimated K_0 values range from about 0.5 to 1.0. The minimum value of 0.5 seems to be in agreement with the estimated K_0 profile estimated by the Brooker and Ireland (1965) method. Above a depth of 12 feet, the SBPM estimated K_0 ranges from about 0.5 to 1.0 at 12 feet, increasing to about 7.5 at a depth of 6.5 feet. A 4th degree polynomial best fit of the SBPM K_0 values is included on Figure 6-6, and indicates the average SBPM K_0 value in the softer clay is about 30 to 50 percent larger than K_0 predicted by the Brooker and Ireland method. These results suggest that the lowest K_0 values indicated by undisturbed SBPM tests are likely most representative of in situ K_0 .

6.3.1.2 Pease Embankment Toe Area - At the Pease AFB embankment toe, three SBPM jetting borings, PMJ6, PMJ7, and PMJ8 were drilled at progressively greater distances from the highway embankment (see Figure 4-3). PMJ6 was made at the toe of the highway embankment. PMJ7 and PMJ8 were made about 52 and 57 feet from the toe, respectively. Since PMJ7 and PMJ8 were drilled within 5 feet of each other, they are considered

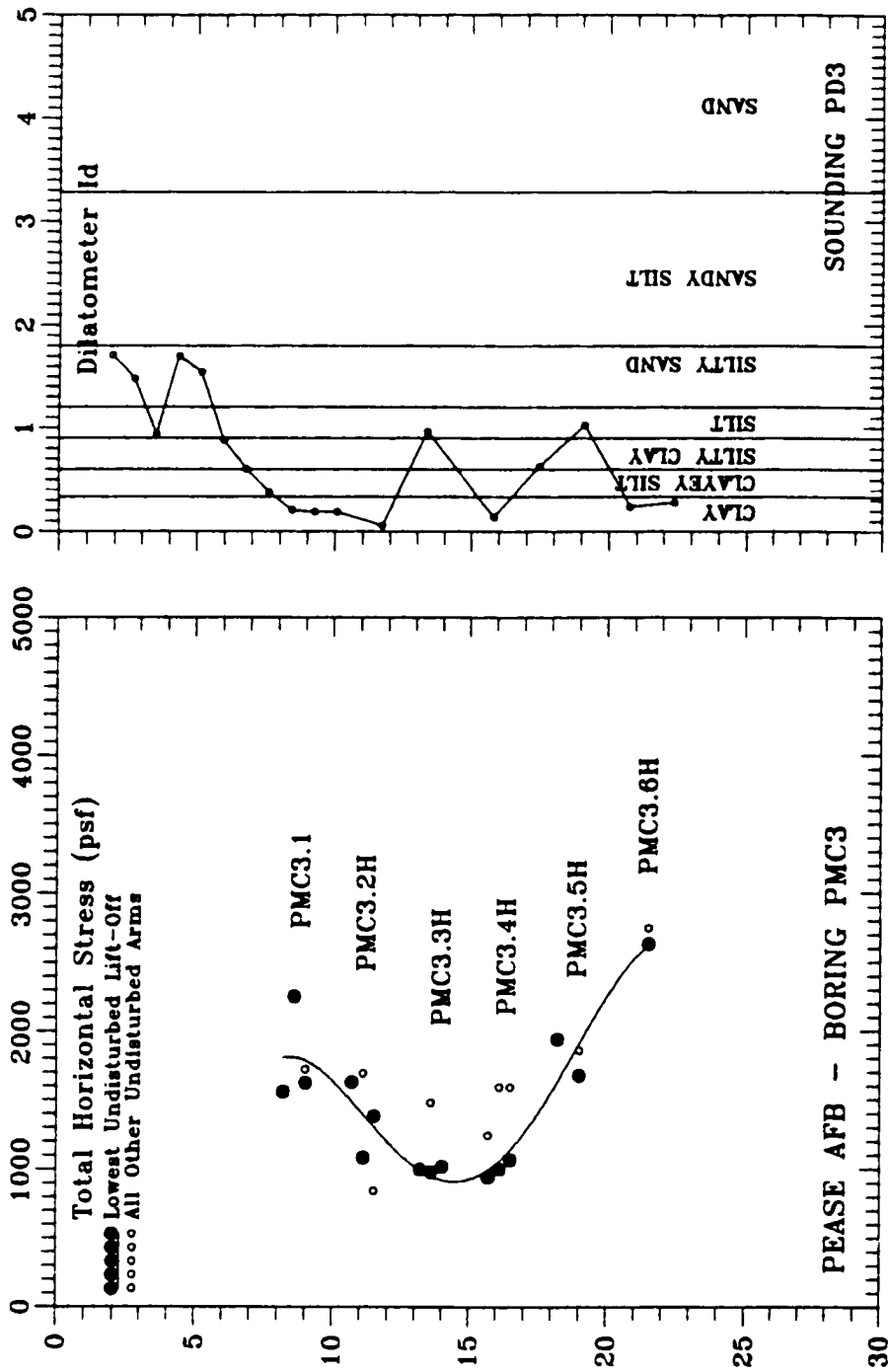


Figure 6-5 I_p and Horizontal Stress Profile, PMC3

PEASE AIR FORCE BASE K_0 AREA

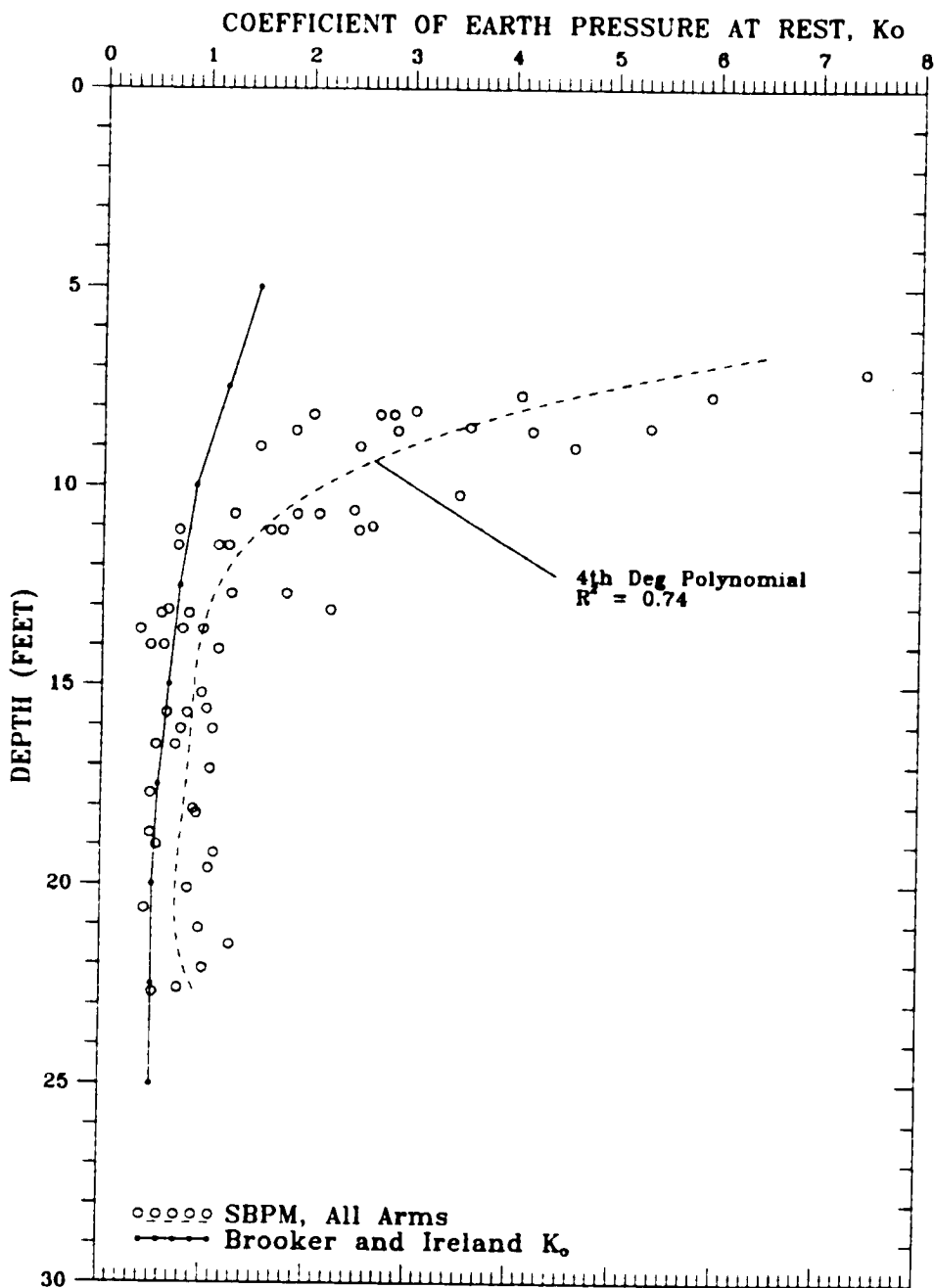


Figure 6-6 Pease AFB SBPM Profile of K_0 .

to represent measurements at a single location 55 feet from the toe of the highway embankment in the subsequent discussion in this section. A summary of all the lateral stress measurements from the SBPM tests conducted at these locations are presented on Table 6-6. Note that this data has been corrected for measured excess pore pressure, but has not been culled of data subject to disturbance. Profiles of horizontal stress culled of disturbed data for each of PMJ6, PMJ7 and PMJ8 along with dilatometer I_p profiles are included in Appendix D. The I_p profiles indicate that the soft zone of the silty clay is relatively homogeneous at the embankment toe area.

Intuitively, lateral stresses measured at the Pease AFB toe area would be expected to exhibit decreasing stress effects of the highway embankment proportional with distance away from the embankment. This intuition is verified by the results of the FEM analysis presented in Chapter V which indicated similar findings. Construction of the highway embankment has been shown by the FEM analyses in Chapter V to result in horizontal stresses within the native soils adjacent to the highway embankment which are greater than those measured in the K_0 condition assumed to exist prior to highway construction.

Figure 6-7 presents a profile of the minimum and maximum horizontal stresses (not principal stresses) measured at SBPM boring PMJ6. Note that PMJ6 is located at the toe of the highway embankment. The horizontal stresses on Figure 6-7 were culled of disturbed data. Also included on the figure for comparison are fourth degree polynomial best-fit curves of the minimum and maximum undisturbed stresses measured at the K_0 area (Figure 6-3). It can be seen that the minimum and maximum horizontal stress profiles at the toe are roughly 300 to 1000 psf higher than that indicated by the best-fits curve from the K_0 area. This suggests that the effect of the highway embankment seems to increase the measured horizontal stress over K_0 conditions. Also, the difference between the minimum and maximum measured stress is generally larger at the toe (up to about 700 psf) suggesting a greater degree of stress

**MEASURED TOTAL HORIZONTAL STRESS
SUMMARY OF TEST RESULTS - PEASE AIR FORCE BASE TOE AREA**

<u>TEST</u>	<u>DEPTH</u> <u>(feet)</u>	<u>MEASURED HORIZONTAL STRESS</u>			<u>EXCESS</u>
		<u>ARM 1</u> <u>(psf)</u>	<u>ARM 2</u> <u>(psf)</u>	<u>ARM 3</u> <u>(psf)</u>	<u>PORE</u> <u>PRESSURE</u> <u>(psf)</u>
<u>UPPER ARMS:</u> PMJ6.1	8.2	3213	2481	1666	-774
PMJ6.2	10.7	2448	2326	2184	-722
PMJ6.3	13.2	2530	2589	2036	-670
PMJ6.4	15.7	2683	2805	2188	-566
PMJ7.1	7.2	935	1801	1718	-379
PMJ7.2	9.7	882	1326	1326	-230
PMJ7.3	12.2	2087	2142	1301	-132
PMJ7.4	14.7	1616	815	1365	-37
PMJ8.1	7.7	2596	2658	2015	-47
PMJ8.2	10.7	705	1478	633	-56
PMJ8.3	13.2	1118	1368	441	136
PMJ8.4	15.7	1411	1066	744	-80
<u>MIDDLE ARMS:</u> PMJ6.1	8.6	2860	2705	2673	-774
PMJ6.2	11.1	2520	2481	2481	-722
PMJ6.3	13.6	2589	2485	2466	-670
PMJ6.4	16.1	2581	2202	2252	-566
PMJ7.1	7.6	1809	1448	1526	-379
PMJ7.2	10.1	1403	1011	960	-230
PMJ7.3	12.6	2181	2244	1184	-132
PMJ7.4	15.1	NA	932	1052	-37
PMJ8.1	8.1	2283	2377	575	-47
PMJ8.2	11.1	1299	1572	727	-56
PMJ8.3	13.6	1263	1192	628	136
PMJ8.4	16.1	1276	1316	837	-80
<u>LOWER ARMS:</u> PMJ6.1	9.0	2705	2500	3117	-774
PMJ6.2	11.5	2390	2280	2833	-722
PMJ6.3	14.0	2498	2228	2749	-670
PMJ6.4	16.5	2555	2349	2934	-566
PMJ7.1	8.0	1539	1507	1352	-379
PMJ7.2	10.5	1724	1345	1267	-230
PMJ7.3	13.0	1693	1711	1382	-132
PMJ7.4	15.5	935	854	1028	-37
PMJ8.1	8.5	1576	1678	653	-47
PMJ8.2	11.5	1299	1353	689	-56
PMJ8.3	14.0	1223	1200	688	136
PMJ8.4	16.5	1097	1151	828	-80

Table 6-6 Summary of Horizontal Stresses Measured at Pease AFB Embankment Toe Area

PEASE AIR FORCE BASE
TOTAL HORIZONTAL STRESS (PSF)

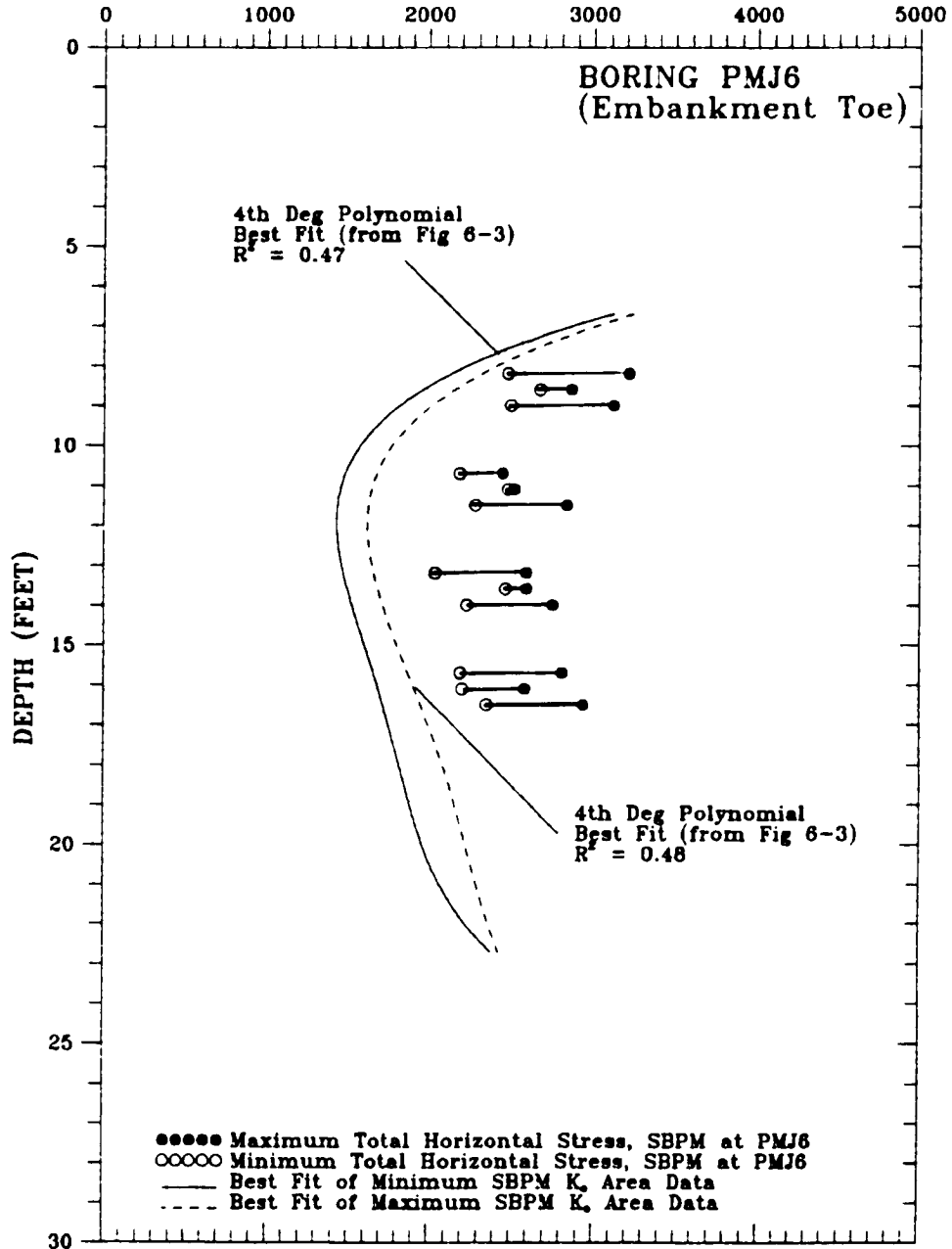


Figure 6-7 Minimum and Maximum Measured Total Horizontal Stress at PMJ6 Compared to K_0 Area

anisotropy than was observed at the K_0 area.

The higher lateral stress at the embankment toe results in ratios of horizontal to vertical stress (K) that are significantly higher than those observed at the K_0 toe area. Based on the results from all arms of PMJ6, K was found to range from 1.56 to 5.68 with a mean value of 3.28 \pm a standard deviation of 1.36. This is compared to a K_0 value of about 0.5 in the soft clay at the Pease K_0 area.

Figure 6-8 presents a similar plot to that presented on Figure 6-7, except that data from PMJ7/PMJ8 is presented rather than the data from PMJ6. Figure 6-8 indicates that the minimum and maximum total horizontal stresses at PMJ7/PMJ8 are roughly 200 to 300 psf less than those measured at the K_0 area. This could indicate some difference in the K_0 conditions that were originally at the embankment toe area (prior to embankment construction) and those currently existing at the K_0 test area. It was noted in Chapter IV that a lower average moisture content was measured at the K_0 test area than was measured by Ladd, et al. (1972) at the embankment construction area. The lower horizontal stresses and higher pre-construction moisture content at the embankment area tend to indicate that there was probably some depositional, stress history and/or degree of desiccation differences between the highway embankment area and the K_0 test area. It is noted that Figure 6-8, based on the difference between minimum and maximum horizontal stress, indicates less stress anisotropy in the horizontal plane than at PMJ6.

Figure 6-9 is a profile of the minimum undisturbed SBPM measured total horizontal stress from all the arm tiers at the toe of the highway embankment (PMJ6). Also included on the profile are the predicted total horizontal stresses after embankment construction from both SOILSTRUCT and JFEST FEM analyses. The magnitude of SBPM measurements of total horizontal stress are generally the same or up to about 30 percent greater than those predicted by JFEST, and up to 100 percent greater than those predicted by SOILSTRUCT. Agreement with the FEM method seems to

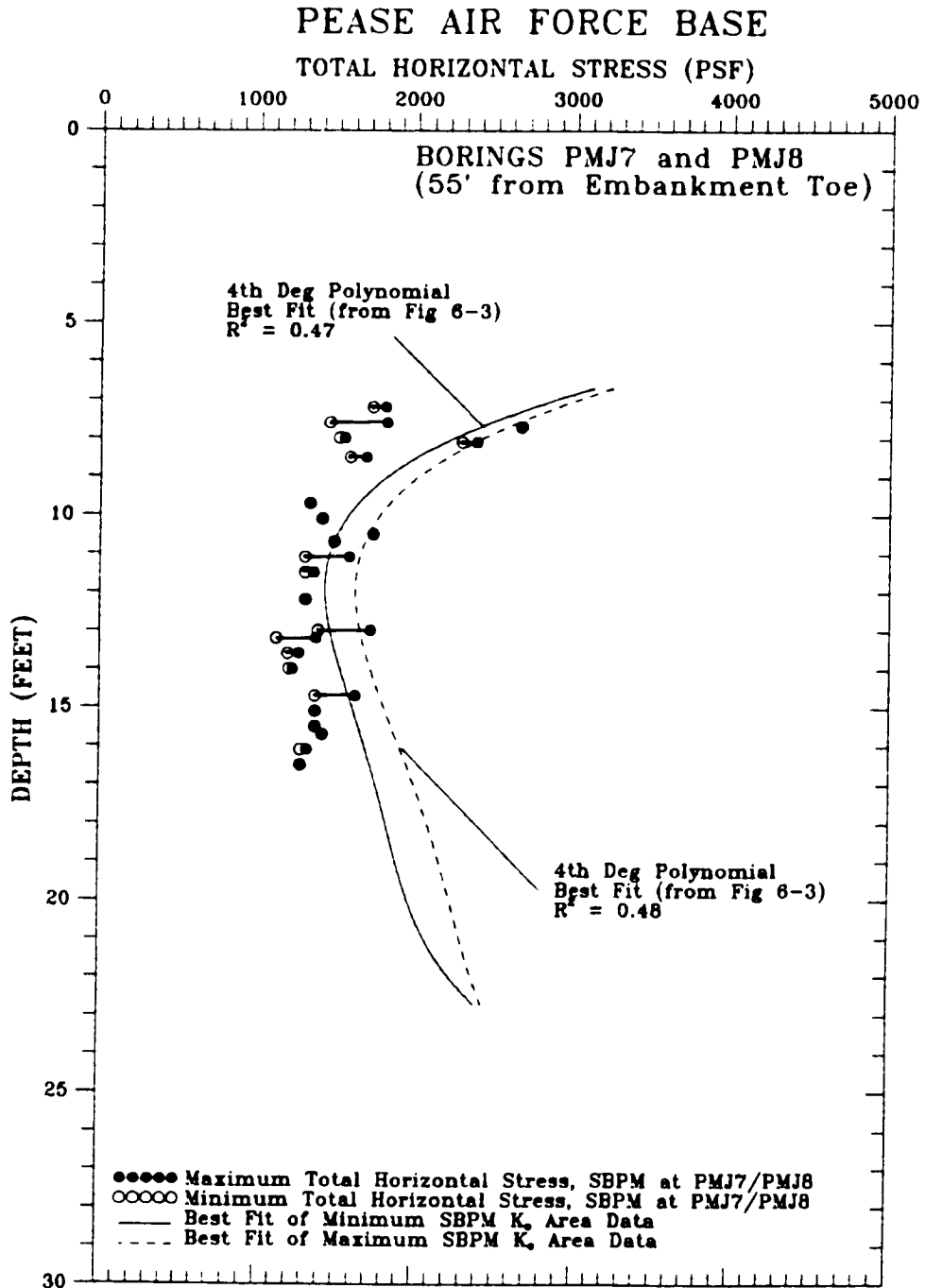


Figure 6-8 Minimum and Maximum Measured Total Horizontal Stress at PMJ7/PMJ8 Compared to K_0 Area

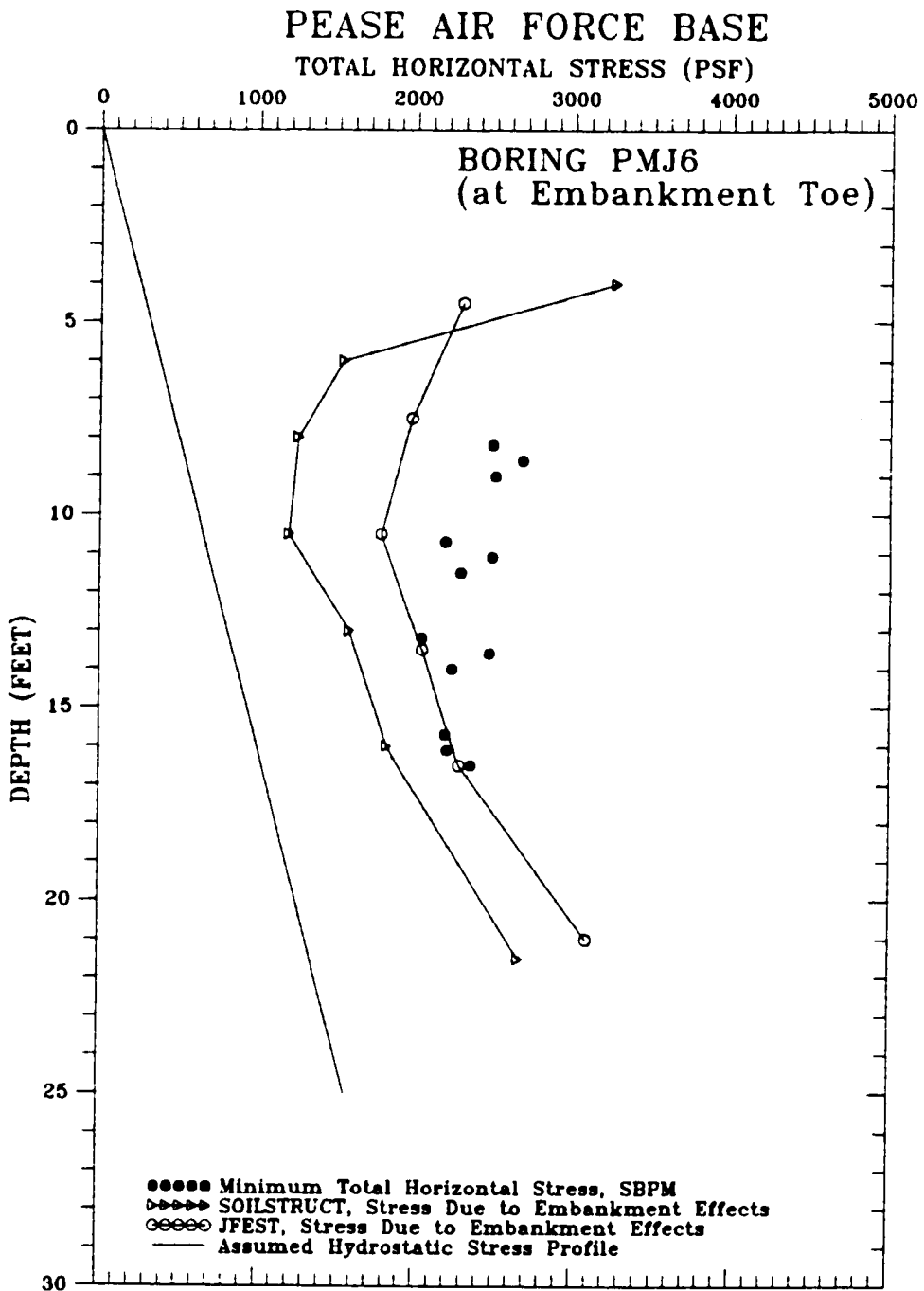


Figure 6-9 Comparison of PMJ6 Measured Horizontal Stress to FEM Predictions

be best in the lower portion of the clay deposit, below 12 foot depth. The greatest deviation between the SBPM and FEM values seems to be in the upper stiff portions of the clay deposit.

Figure 6-10 presents a profile of SBPM measured maximum total horizontal stress 55 feet from the toe of the embankment, the location of borings PMJ7/PMJ8. The profile indicates relatively good agreement between the SBPM measured values and both SOILSTRUCT and JFEST, although overall, agreement seems better with JFEST. In the upper crust of the clay, the SBPM values are up to 60 percent larger than those predicted by FEM.

Figure 6-11 presents a comparison of the measured total horizontal stress at PMJ6 and PMJ7/PMJ8 to illustrate the measured decrease of horizontal stress with distance from the highway embankment. The stress difference between the boring locations is about 900 psf. Also, since stresses at PMJ7/PMJ8 are similar to those at the K_v area, the SBPM indicated difference in horizontal stress between PMJ6 and PMJ7/PMJ8 represents an amount equal to or slightly less than the effect of embankment construction. Based on this, Figure 6-12 is a plot of percent stress change from initial conditions due to embankment construction. As can be seen, the SBPM measurements in the underlying soft clay at PMJ6 are more similar to the results of JFEST in terms of percent stress increase from initial conditions than SOILSTRUCT. SOILSTRUCT predicted a 10 to 30 percent stress increase at the embankment toe while JFEST predicted a 50 to 74 percent increase. The SBPM data on the figure indicates approximately 70 to 100 percent increase in horizontal stress over initial conditions in the soft clay.

6.3.2 In Situ Stress at Hamilton AFB

At the Hamilton AFB site, Mitchell and Lunne (1977) used Glötzl load cells to measure horizontal in situ stress. Later, Denby (1978) and Benoit (1983) performed SBPM tests at the site. The results of these previous SBPM studies have been compared to the Glötzl load cell findings on Figure 6-13. Both SBPM researchers determined horizontal stress by

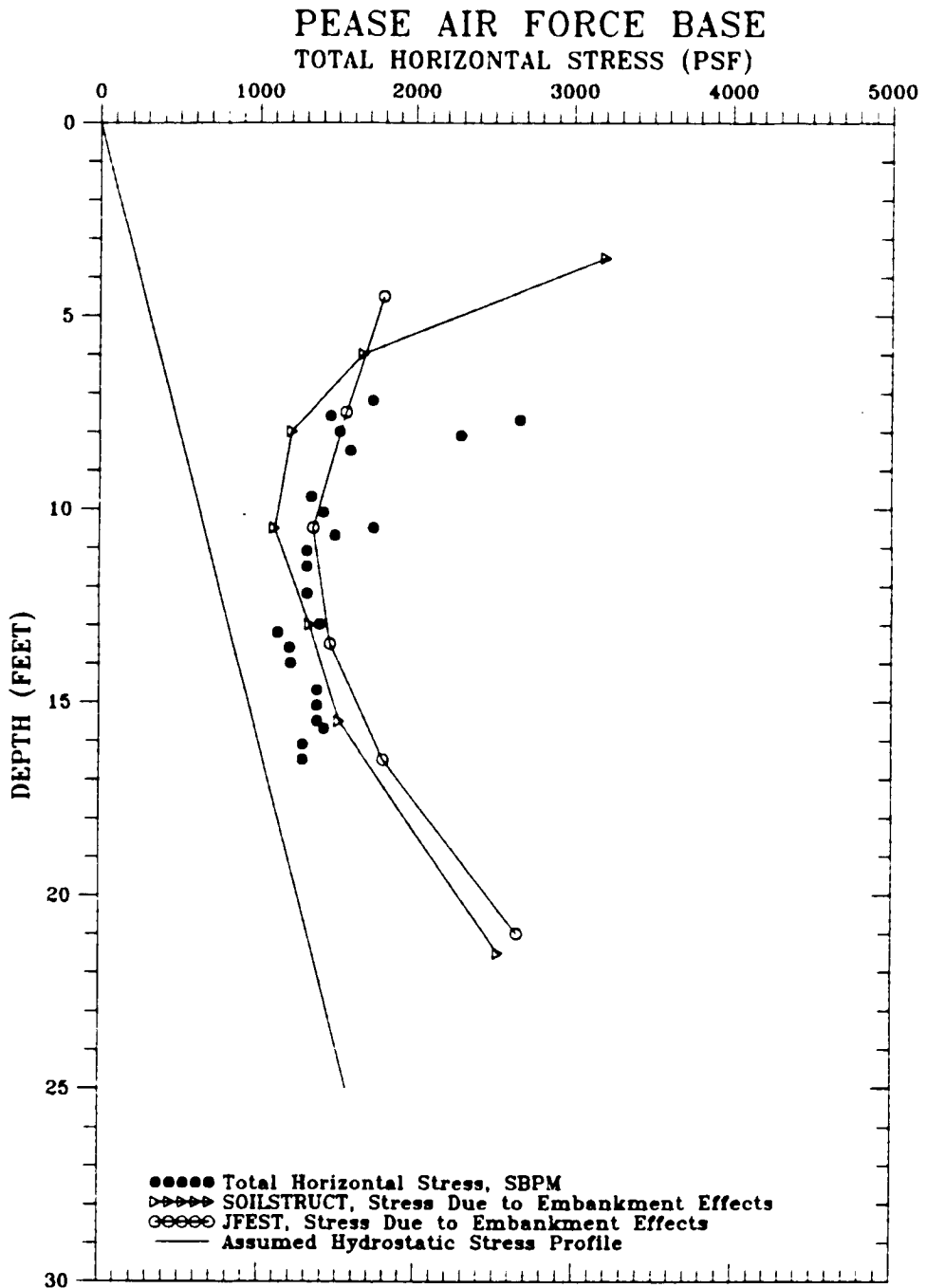


Figure 6-10 Comparison of PMJ7/PMJ8 Measured Horizontal Stress to FEM Predictions

PEASE AIR FORCE BASE SBPM MEASURED HORIZONTAL STRESS

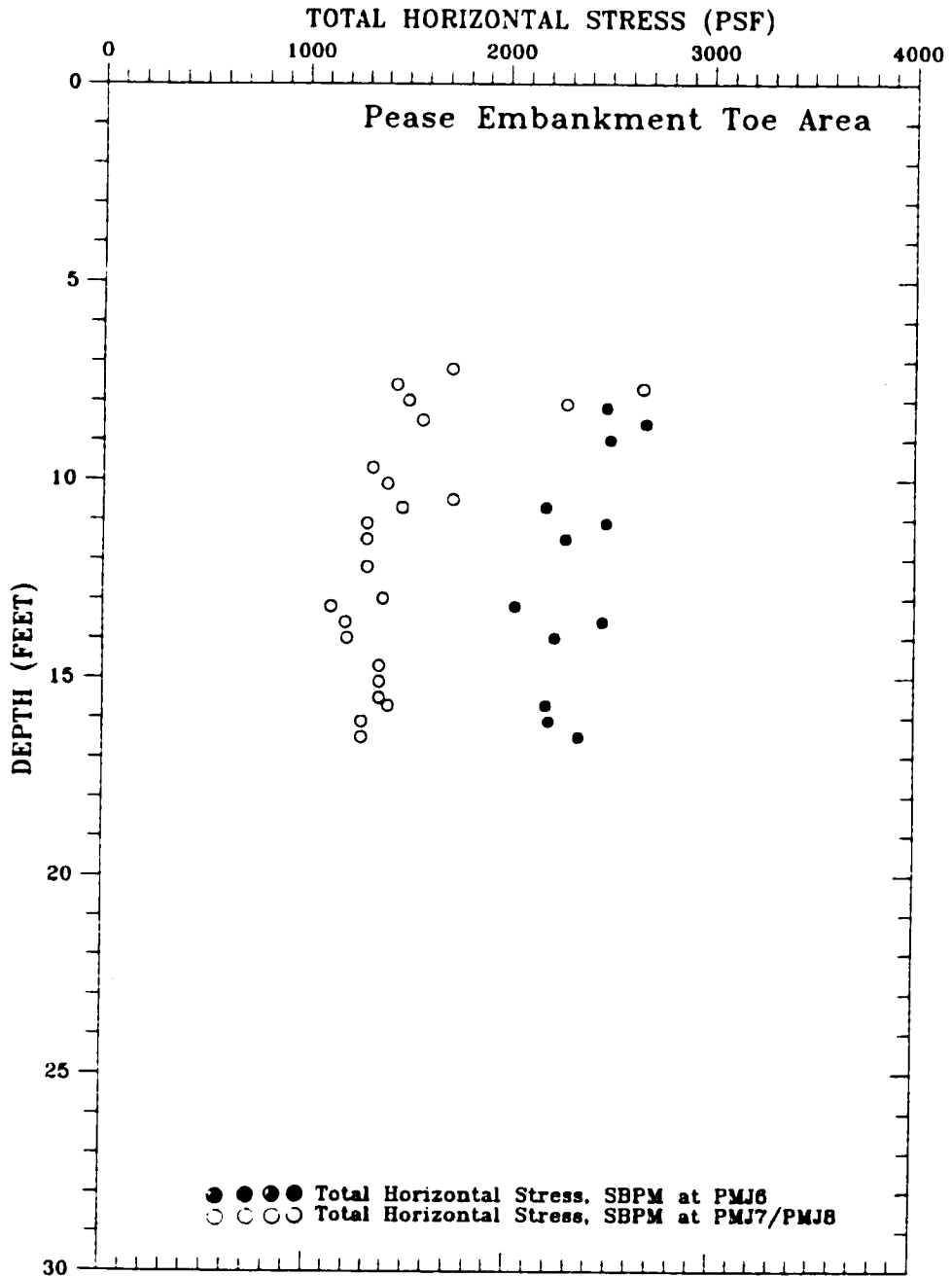


Figure 6-11 Stress Decrease With Distance From Toe of Highway Embankment

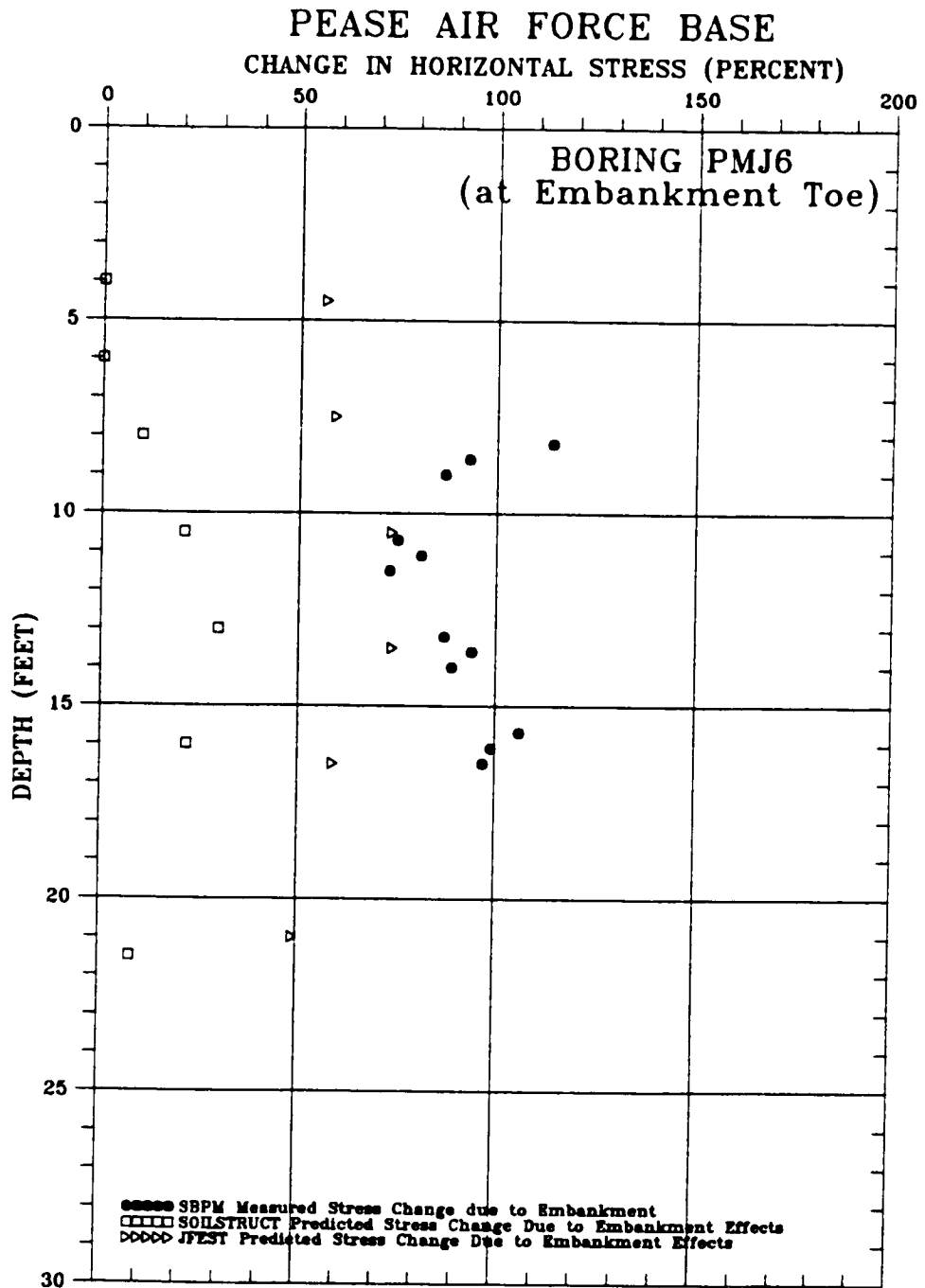


Figure 6-12 Percent Increase in Total Horizontal Stress at Toe Due to Embankment Construction

the inspection method. Additionally, Denby had to correct his data for arm compliance (apparent strain arm movement prior to lift-off), which, for his probe model was substantially greater than that for Benoit's (1983) and the present version of the SBPM. Within the range of depths tested by the SBPM, the horizontal stress profile indicated by the total pressure cells is slightly higher than that indicated by the SBPM data, likely a result of the push-in disturbance of the total pressure cells. Note that the Glötzl cell data of Mitchell and Lunne (1977) has been corrected using the Todd and Charles (1983) correction method. The differences between the results of Denby (1978) and Benoit (1983) on Figure 6-13 were reportedly (by Benoit, 1983) up to 10 percent in the normally consolidated zone (below a depth of about 15 feet) and up to 100 percent in the desiccated upper crust. Benoit indicated that similar drilling procedures to Denby were used, and attributes the differences to improvements in the strain measuring arms, and data acquisition. It should be noted that Denby's results were obtained by an SBPM system which was rather primitive by today's standards, in that far fewer data points were obtained as compared to the computer data acquisition techniques used by Benoit and the current research. Based on this sophistication difference, the consistency of Denby's data is more likely a result of the greater subjectivity in data interpretation than is afforded with the significantly larger amounts of data yielded by the more recent advances in high speed data acquisition techniques.

Figure 6-14 presents a profile of K_v for both the Glötzl pressure cell and SBPM. Denby (1978) indicated that the values of K_v estimated from his SBPM test results were in general agreement with a K_v value of 0.58 extrapolated by La Serda (1978) using data from special K_v consolidation tests performed on samples of Bay Mud from between 20 and 25 foot depth. Also, Denby reported that K_v values predicted by empirical methods, using the pressuremeter ϕ' and ϕ' obtained by SHANSEP triaxial tests ($\phi'=30^\circ$ in both cases) agreed well with the Hamilton SBPM K_v values. Benoit (1983) also derived SBPM K_v values which have been included on

HAMILTON AIR FORCE BASE

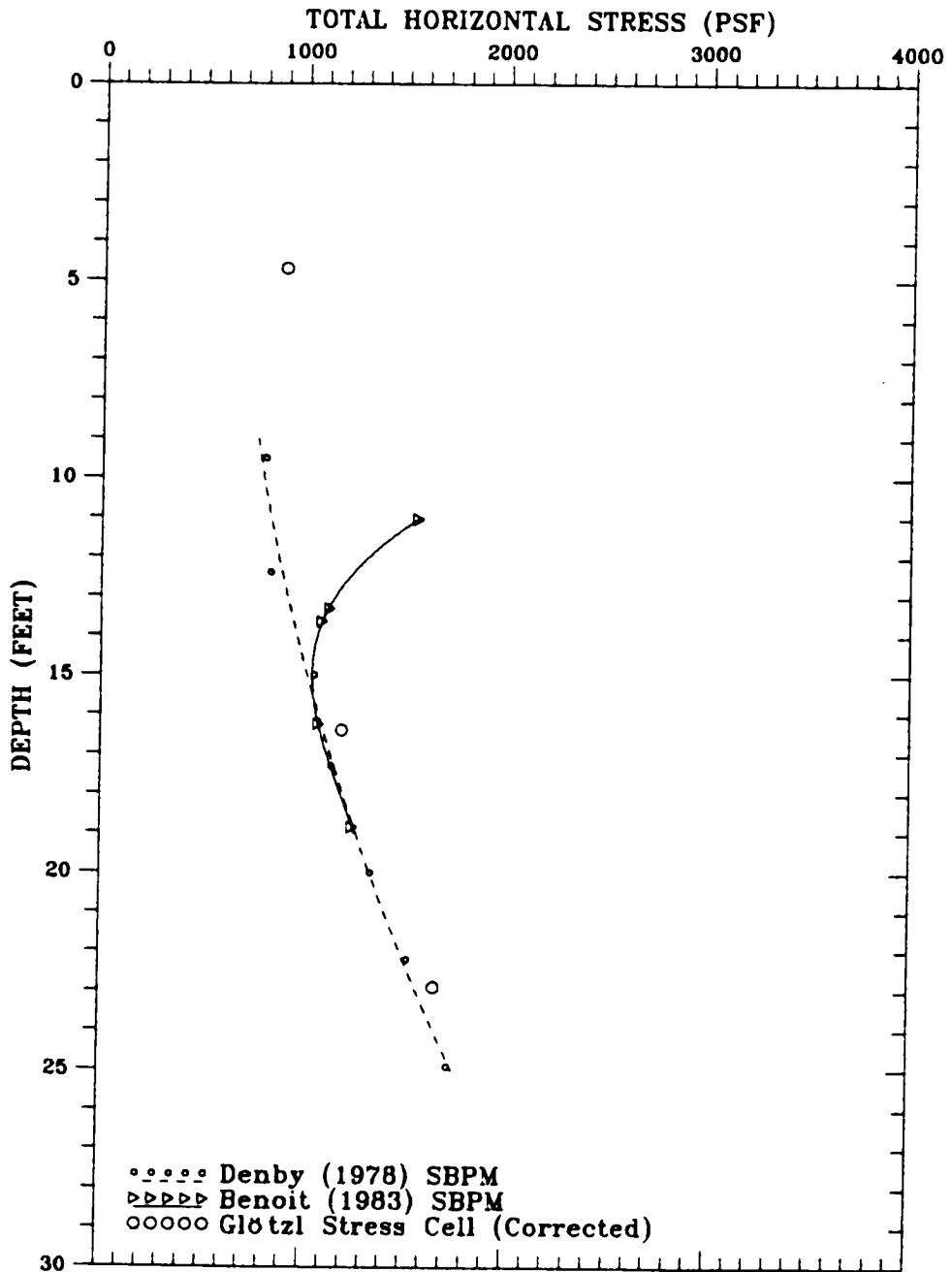


Figure 6-13 Total Horizontal Stress at Hamilton AFB From Previous Research

HAMILTON AIR FORCE BASE

COEFFICIENT OF EARTH PRESSURE AT REST, K_0

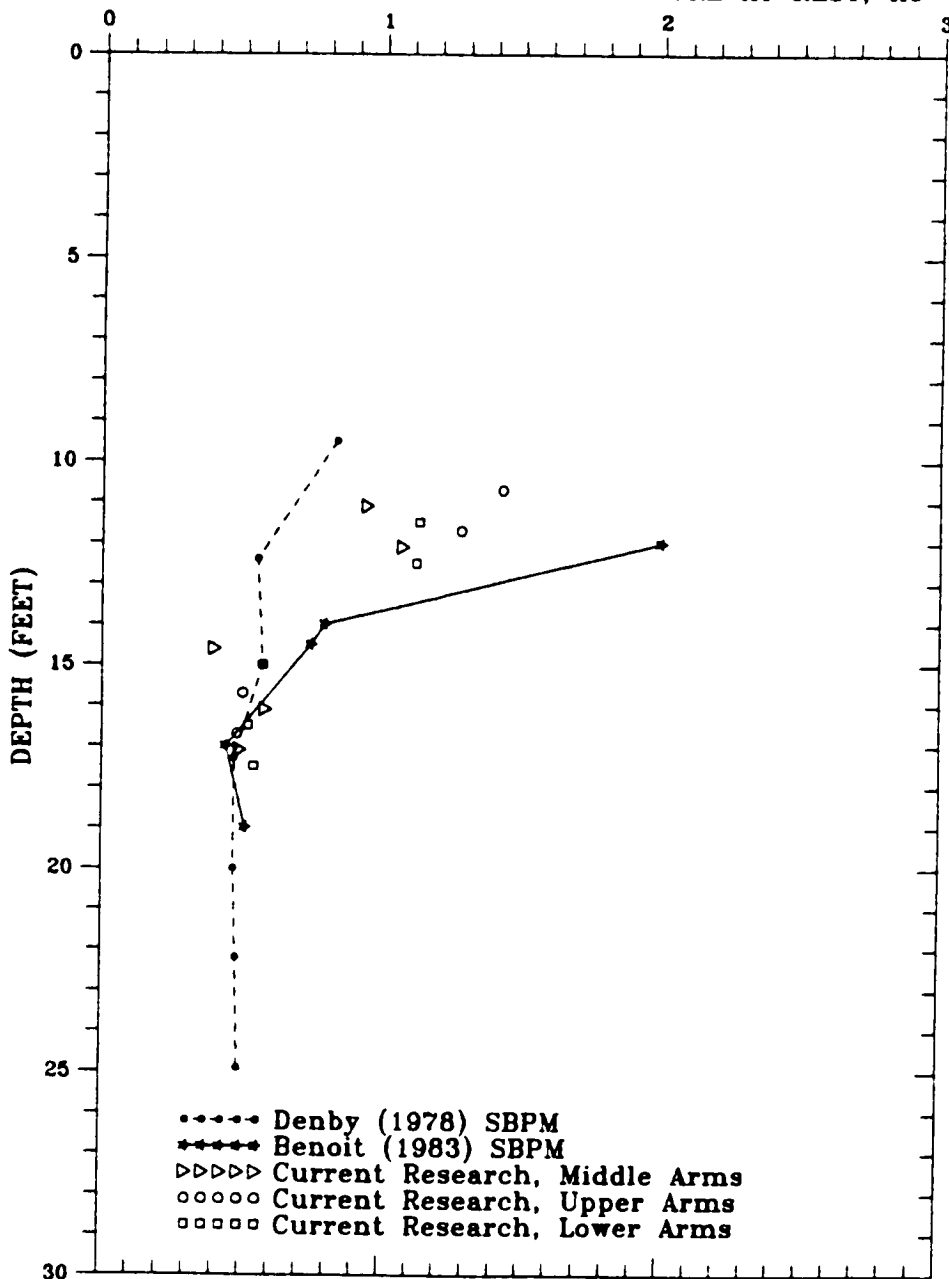


Figure 6-14 K_0 Profile at Hamilton AFB

Figure 6-14. Those K_v values are in general agreement with those of Denby (1978) below a depth of about 15 feet, however were up to 200 percent greater above that depth.

Two SBPM borings (HAM1 and HAM2) were carried out for the current research at the Hamilton AFB site. Table 6-7 is a tabulation of the measured horizontal stresses for the nine SBPM pressuremeter tests performed in these borings, corrected for the measured excess pore pressure at the start of expansion. The excess pore pressure measured at the beginning of the expansion test is indicated in the last column on the table. The tabulated values have not been culled for disturbance. The lowest measured horizontal stress from the tests judged to be undisturbed on each tier of arms are plotted with depth on Figure 6-15. The figure also includes the data of Denby (1978) and Benoit (1983). As can be seen, the data above a depth of 18 feet seems to be within the error of measurement of the SBPM or lie between the results of Denby and Benoit. The data of Benoit (1983) and Denby (1978) were not corrected for excess pore pressure resulting from deployment. However, both previous researchers allowed significant time to elapse (up to three hours or more) and it is likely any excess pore pressure was substantially dissipated. The consistency of the results from the current and previous SBPM programs indicate that the SBPM is capable of relatively repeatable measurements of horizontal stress and also indicates the importance of correcting for deployment excess pore pressures if they exist.

Below 18 feet, test HAM2.4H for the current research measured stresses about 50 percent in excess of those measures by Denby and Benoit, however, this test (labeled "Test subject to push-in disturbance" on the figure) was found to be subject to push-in disturbance. After completion of this test, the membrane was re-expanded into the tested soil zone, and the resulting data is labeled "re-expansion" on Figure 6-15. It appears that the measured lateral stress of the re-expansion is roughly equivalent (within the error of measurement) to hydrostatic

**MEASURED TOTAL HORIZONTAL STRESS
SUMMARY OF TEST RESULTS - HAMILTON AIR FORCE BASE**

<u>TEST</u>	<u>DEPTH</u> <u>(feet)</u>	<u>MEASURED HORIZONTAL STRESS</u>			<u>EXCESS</u> <u>PORE</u> <u>PRESSURE</u> <u>(psf)</u>
		<u>ARM 1</u> <u>(psf)</u>	<u>ARM 2</u> <u>(psf)</u>	<u>ARM 3</u> <u>(psf)</u>	
<u>UPPER ARMS:</u>					
HAM1.1	11.7	1324	1347	1306	725
HAM1.2	14.2	2040	2040	2127	530
HAM1.3	16.7	1103	1196	826	265
HAM2.1	10.7	1314	868	709	382
HAM2.2	13.2	1032	1113	1168	568
HAM2.3	15.7	990	990	1039	522
HAM2.4H	18.2	1776	1683	1132	194
HAM2.4R	18.2	441	398	441	280
HAM2.5P	20.7	2333	2004	1219	303
<u>MIDDLE ARMS:</u>					
HAM1.1	12.1	1245	1188	1269	725
HAM1.2	14.6	1362	874	1425	530
HAM1.3	17.1	1275	904	1142	265
HAM2.1	11.1	1001	868	435	382
HAM2.2	13.6	1207	445	565	568
HAM2.3	16.1	1057	1139	1139	522
HAM2.4H	18.6	1867	1867	1759	194
HAM2.4R	18.6	539	594	576	280
HAM2.5P	21.1	2611	2611	2529	303
<u>LOWER ARMS:</u>					
HAM1.1	12.5	1267	1426	1480	725
HAM1.2	15.0	522	798	1049	530
HAM1.3	17.5	1377	1218	1549	265
HAM2.1	11.5	1179	1338	1510	382
HAM2.2	14.0	698	760	562	568
HAM2.3	16.5	1117	1225	1225	522
HAM2.4H	19.0	1915	1816	1838	194
HAM2.4R	19.0	654	594	578	280
HAM2.5P	21.5	2707	2631	2647	303

Table 6-7 Summary of Horizontal Stresses Measured at Hamilton AFB

HAMILTON AIR FORCE BASE

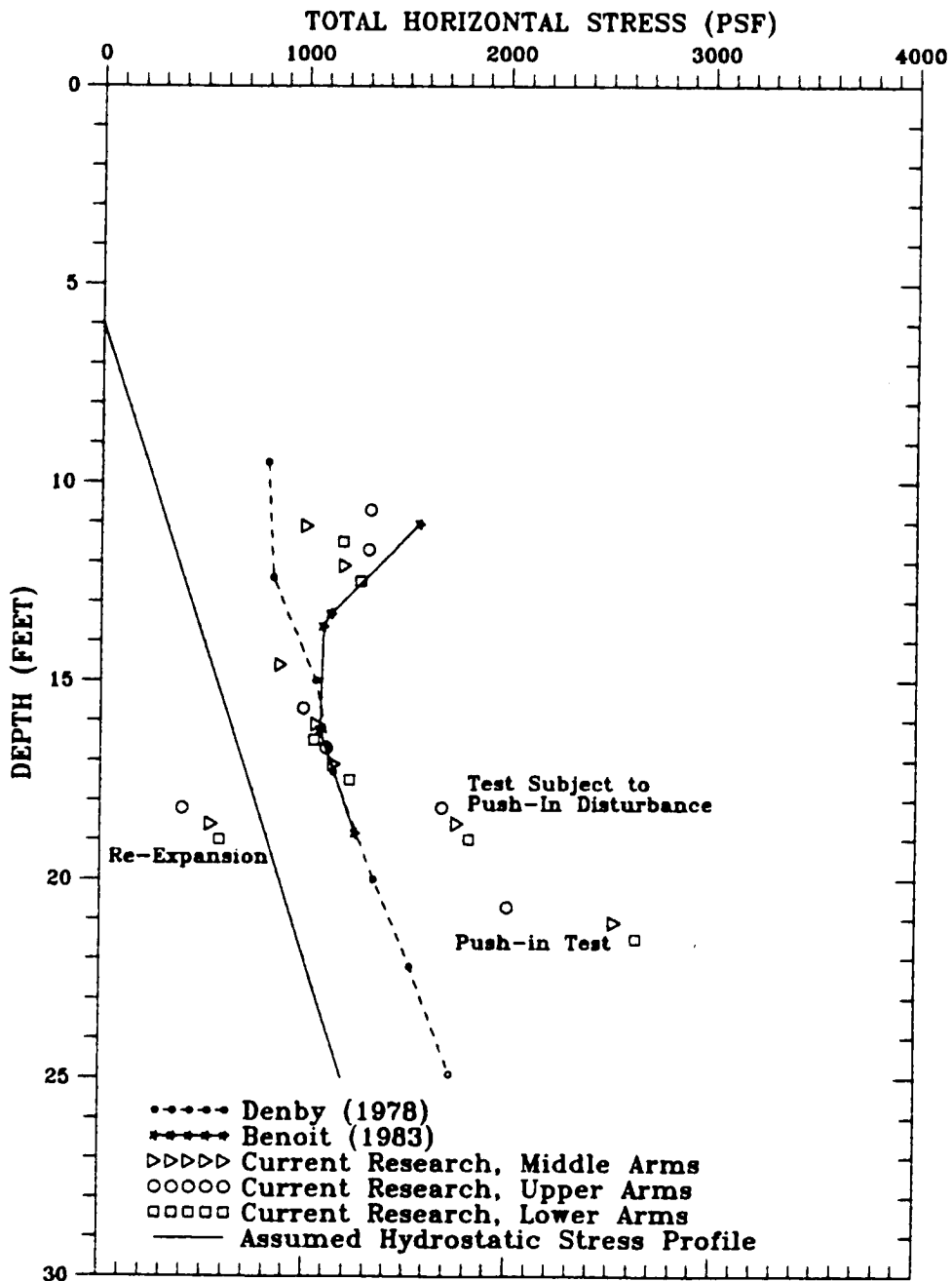


Figure 6-15 SBPM Total Horizontal Stress at Hamilton AFB

stress, a finding similar to that at Pease AFB. A push-in test was conducted at the site, and is labeled on the figure. The push-in test exhibited lateral stress about 40 to 80 percent greater than the undisturbed values measured by the previous researchers, indicating that soil displacement/disturbance tends to increase lateral stress.

Figure 6-14 includes K_h values determined from the horizontal stress measurements presented on Figure 6-15 for the current research. Again, the computed values of K_h for the current research are generally between or within the error of measurement of the results of Benoit (1983) and Denby (1978).

Figure 6-16 is a plot with depth of horizontal stresses measured by all 3 strain arms for undisturbed tests conducted by Benoit (1983). Also included on the plot are the horizontal stresses measured by all strain arms (upper, middle, and lower) from undisturbed tests conducted for the current research. Horizontal stresses from pressuremeter curves determined to be disturbed by inspection or numerical assessment have been omitted. Also, the results of push-in and re-expansion tests are labeled. The undisturbed results of both Benoit (1983) and the current research seem to be in general agreement within the error of measurement.

6.4 Stress Anisotropy in the Horizontal Plane

A method for determining the magnitude and direction of the major principal stress in the horizontal plane from SBPM data was described in Chapter II. This method, derived by Dalton and Hawkins (1982), was reportedly relatively insensitive to errors in measurement of the horizontal stress of up to 10 percent. As has been seen in an earlier section of this chapter, disturbance can result in deviations of significantly more than 10 percent. As a consequence, only data which appears to be undisturbed by inspection and numerical assessment were used in the current research for computation of the principal stress magnitude and direction. Use of only undisturbed data for computing the principal stresses implies that the expansion curves from all three arms on an arm tier would have to be undisturbed in order for a particular

HAMILTON AIR FORCE BASE

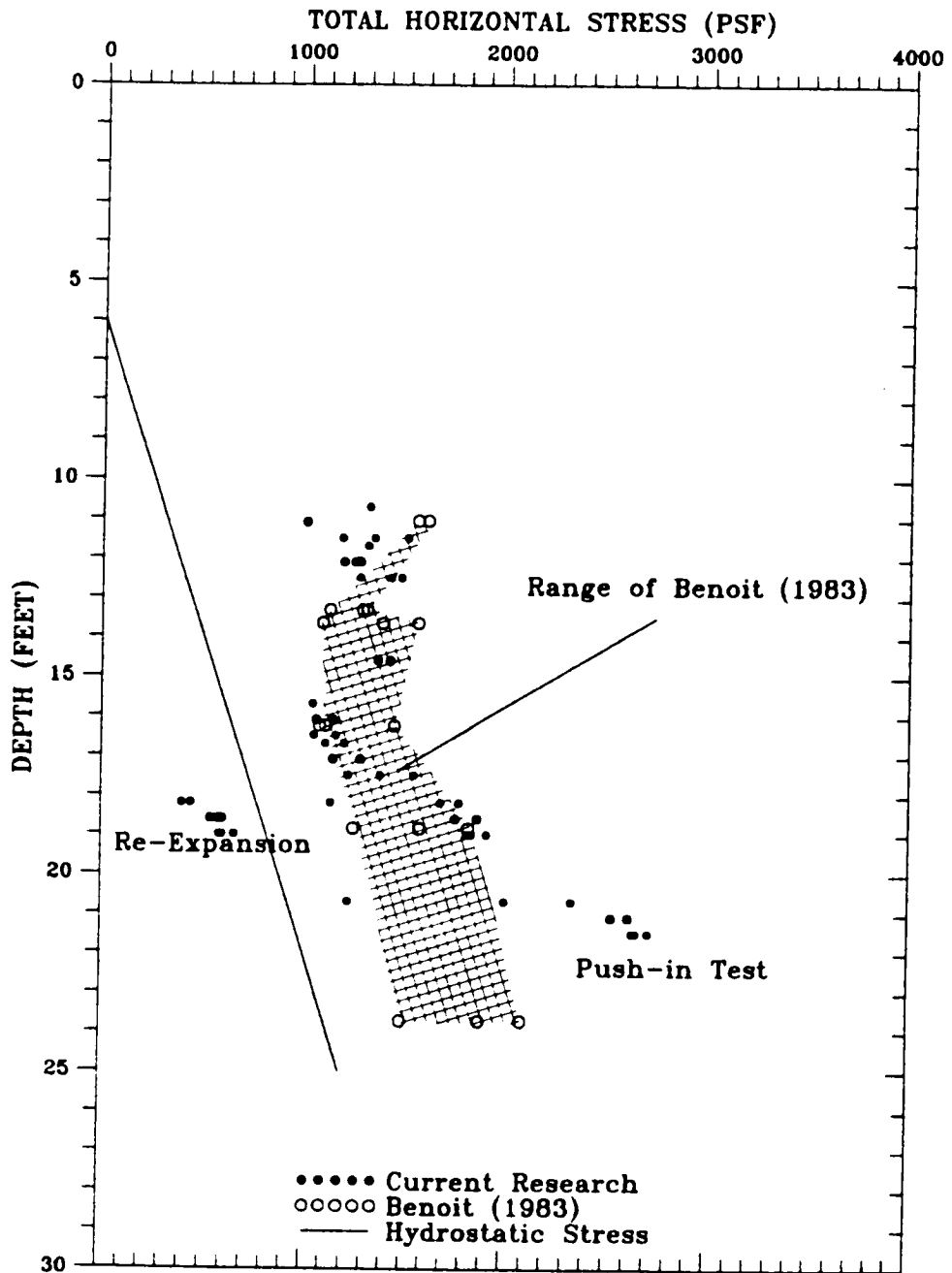


Figure 6-16 Horizontal Stress From All Arms Compared to Benoit (1983)

test to be useful for determination of the magnitude and direction of principal stresses. The tendency for all three strain arms to be undisturbed was found to be more the exception than the rule in K_0 conditions. A significantly higher percentage of tests seem to qualify as eligible for principal stress determination at the non- K_0 Pease Toe area. An explanation for this may be that the significantly higher confinement pressure around the probe resulting from the relatively higher lateral stress which has been found to exist at the Pease toe site may result in less "play" between the pressuremeter and surrounding soil during drilling, and thus less drilling disturbance. Higher lateral pressure would also reduce the significance of measurement errors.

The magnitude of the excess pore pressure at the start of an expansion test has an impact on the magnitude of measured horizontal stress. The middle arm tier is located within an inch or two of the effective stress cells, and it is reasonable to assume that pore pressures measured by the cells are fairly representative of the pore pressure at that arm tier; however, the upper and lower arm tiers are located further from the effective stress cells and it is suspected that variation in pore pressure between the upper/lower arms and the effective stress cell is likely, which would induce measurement error. As a result, consideration of the magnitude and direction of the principal stresses for the present research was limited to the middle arm tier.

6.4.1 Pease AFB Embankment Toe Area

The embankment toe at Pease AFB presents an excellent opportunity to see if the SBPM is capable of measuring stress anisotropy in the horizontal plane because the stress imposed by the weight of fill placed for the highway embankment dictates that the direction of the major principal stress will essentially be perpendicular to the axis of the embankment. This is an advantage over a K_0 area, where the direction of the major principal stress would generally be unknown. Also, as has already been noted, a higher percentage of the tests seem to result in three undisturbed lift-offs on more arm tiers at the embankment toe than

the Hamilton and Pease K₀ areas.

Figure 6-17 presents a profile of the horizontal stress measured by each of the middle strain arms at the embankment toe. Similar to the findings of Dalton and Hawkins (1982) and Benoit and Clough (1986), the sequence of strain arm lift-off seems to be relatively consistent in all tests made within the boring. Strain arm M2 and M3 generally lift-off simultaneously, prior to strain arm M1 lift-off. The horizontal stress indicated by arm M1 is about 10 to over 100 percent larger than the other two arms. It is noted that strain arm M1 is oriented in the direction of the major principal stress, normal to the axis of the highway embankment. As such, it is no surprise that M1 would lift-off at a higher horizontal stress than the other two arms.

Figure 6-18 presents a profile of the major and minor principal stresses computed from the SBPM tests made at the embankment toe using the Dalton and Hawkins (1982) method. The Major principal stress is about 5 to 25 percent larger than the minor principal stress (range of 50 to 500 psf). The Dalton and Hawkins method also provides a means of determining the direction of the major principal stress. Figure 6-19 is a plot of the direction of the major principal stress computed for the middle tier strain arms at the embankment toe. As can be seen, the results are extremely consistent, indicating the principal stress is oriented at about 323 ± 2.6 degrees clockwise from north. The direction of the major principal stress computed for the middle arms of boring PMJ6 are plotted in plan view on Figure 6-20. This direction is almost exactly consistent with a 325 degree strike perpendicular to the axis of the embankment, the expected orientation of the major principal stress resulting from the stress effects of the embankment construction.

Since PMJ7/PMJ8 seem to be just within the effects of the highway embankment as indicated by the FEM analysis of Chapter V, it is of interest to see what the direction of the major principal stress is at that location. However, as a result of a lump of soil that collected under the Chinese lantern, all the data from Arms U3, M3 and L3 in boring

PEASE AIR FORCE BASE TOE AREA
TOTAL HORIZONTAL STRESS (PSF)

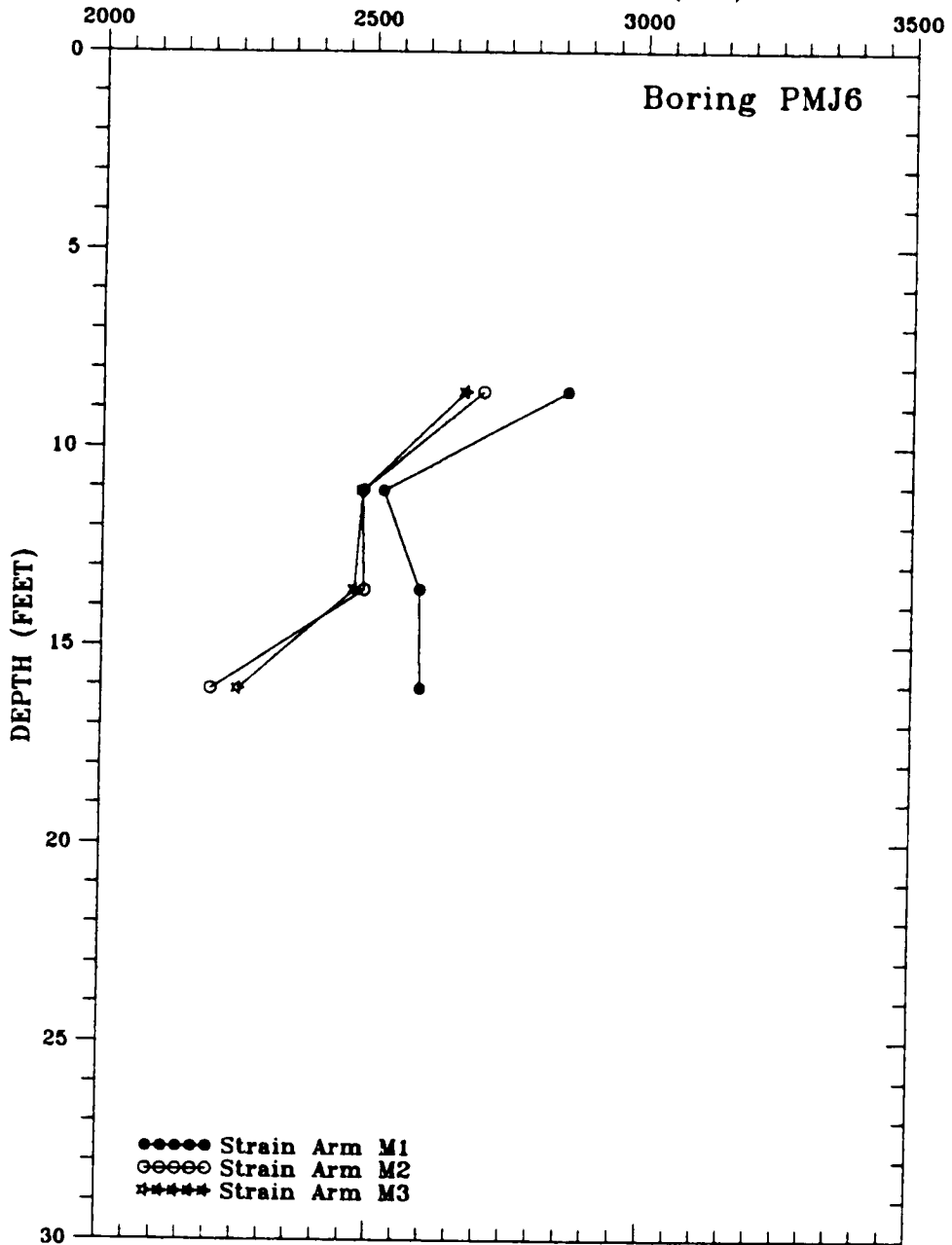


Figure 6-17 Horizontal Stress Results From All Middle Arms at Highway Embankment Toe

PEASE AIR FORCE BASE TOE AREA
TOTAL HORIZONTAL STRESS (PSF)

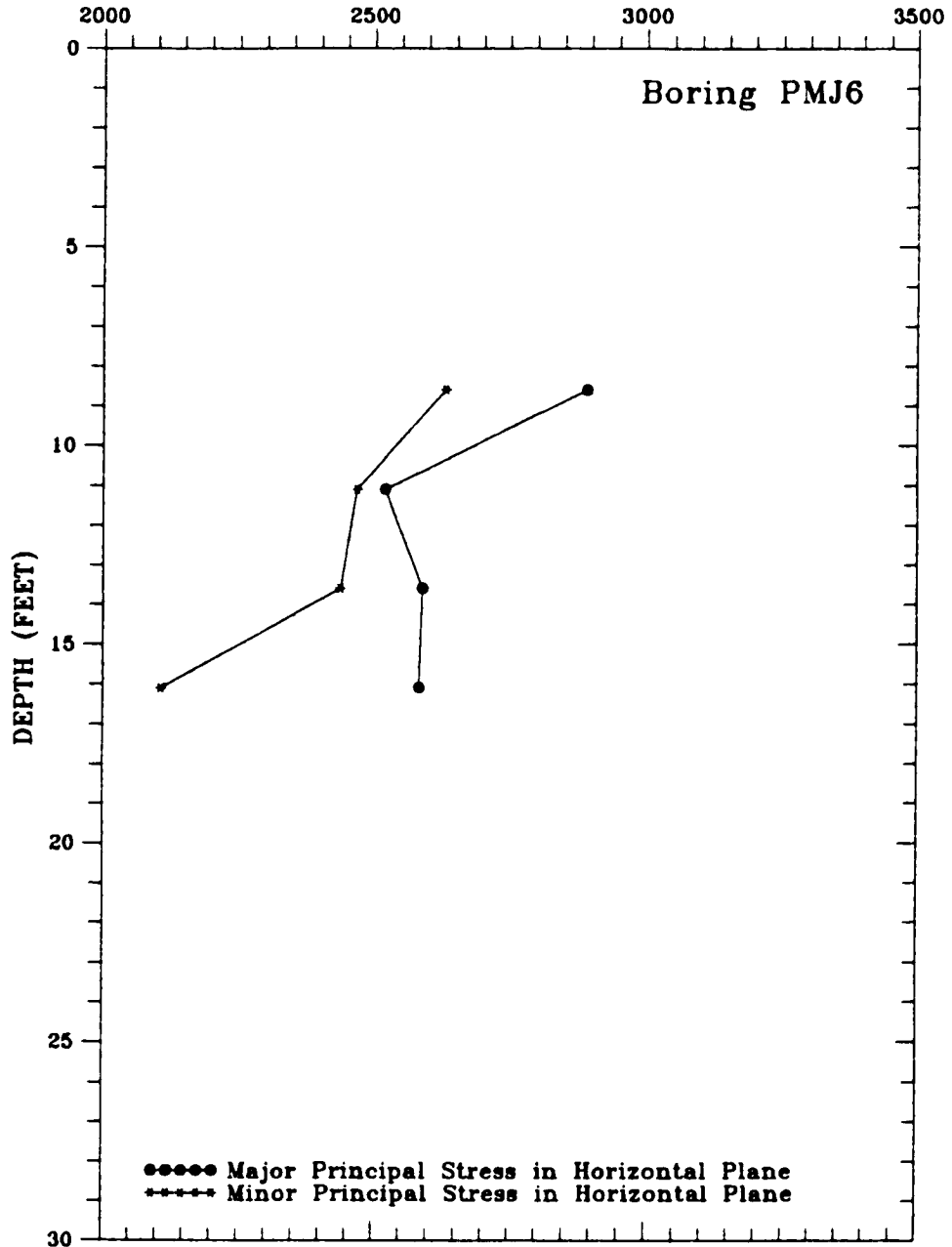


Figure 6-18 Principal Stresses From Middle Arms at the Highway Embankment Toe

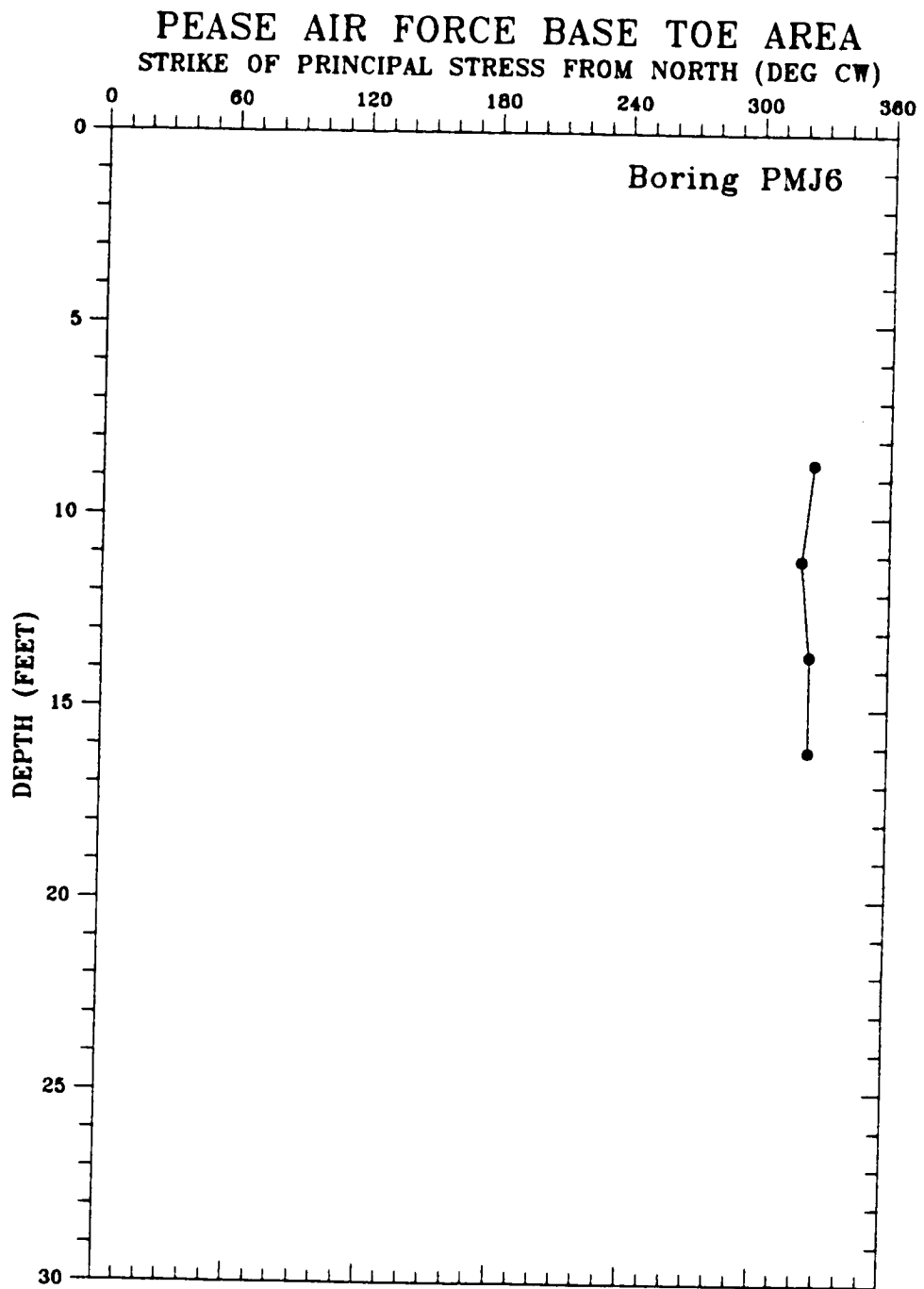


Figure 6-19 Direction of Major Principal Stress at the Highway Embankment Toe

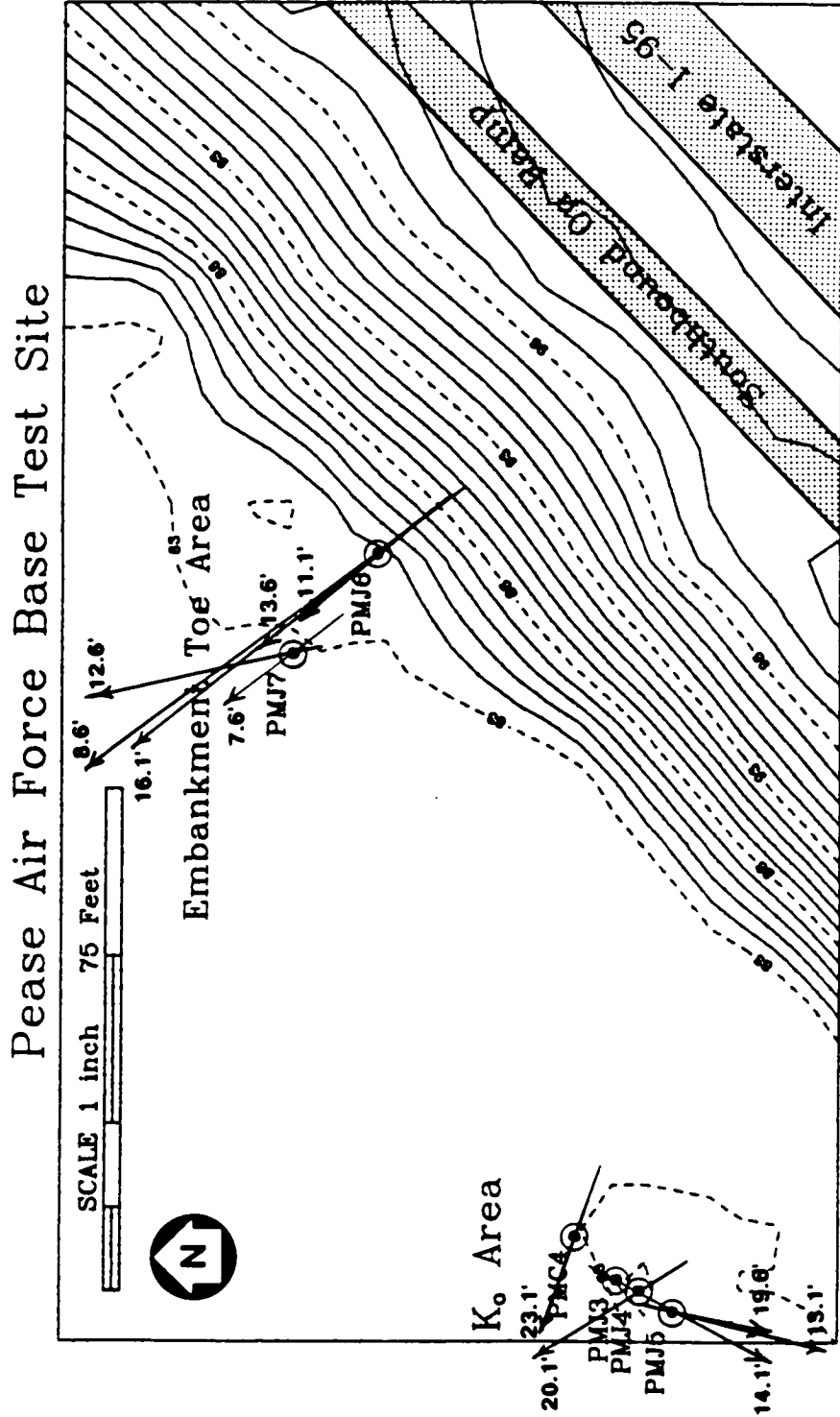


Figure 6-20 Plan View of Principal Stress Orientation at Pease AFB Test Sites

PMJ8 showed signs of disturbance and had to be discarded. Only Test PMJ7.1 and PMJ7.3 were found to be usable out of boring PMJ7 after culling disturbed data. The direction of the major principal stress is indicated in plan view on Figure 6-20. The six usable tests of PMJ6 and PMJ7 suggest, within a standard deviation of 10.6 degrees, that the major principal stress is oriented in a direction striking 327.8 degrees clockwise from north. This is consistent with the expected orientation of the major principal stress due to the embankment effects although the standard deviation is larger than that computed for the results from PMJ6 alone. The larger standard deviation may be due to the fact that the embankment effects are significantly less at PMJ7. The consistency of the results at the highway embankment toe seems to indicate that the SBPM is capable of measuring the orientation of the major principal stress in a non- K_0 situation (e.g. in soft clay below the toe of an embankment).

6.4.2 Pease AFB K_0 Area

At the Pease K_0 area, SBPM tests in which all three middle arms appear to be unaffected by disturbance included only tests PMC4.7, PMC3.4, PMJ4.5, PMJ5.3 and PMJ5.5. A profile of the maximum and minimum principal stresses from these tests is presented on Figure 6-21. The difference between the major and minor principal stress indicated on the figure ranges from 100 to 600 psf. This indicates that the major principal stress is 10 to 50 percent larger than the minor principal stress. In general, this range appears to be greater than that observed at the embankment toe (Figure 6-18), implying greater stress anisotropy at the K_0 area. This appears to be in conflict with Figures 6-3 and 6-7, which indicated greater difference between the maximum and minimum horizontal stress at the embankment toe. Based on the FEM modeling with respect to the initial and post construction stresses, and the fact that the Pease K_0 clay deposit was formed by marine deposition, it would be expected that the K_0 area would have a lesser degree of stress anisotropy than the embankment toe, therefore, the tests exhibiting large stress difference on Figure 6-21 are suspect. One explanation for the findings

**PEASE AIR FORCE BASE K_0 AREA
MAX AND MIN PRINCIPAL STRESSES
TOTAL HORIZONTAL STRESS (PSF)**

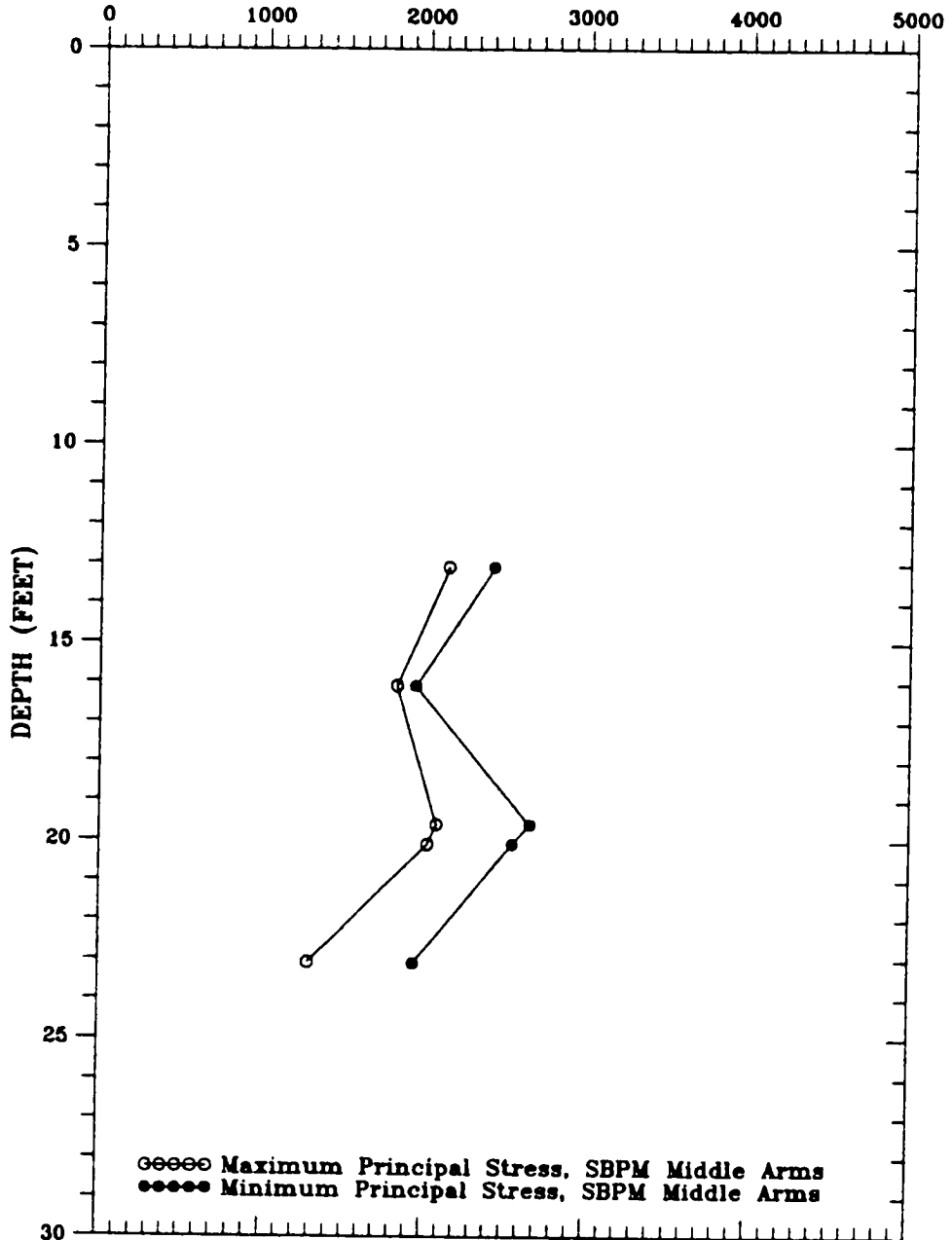


Figure 6-21 Profile of Minimum and Maximum Principal Stresses at Pease K_0 Area

of the relatively large degree of stress anisotropy in some of the tests on Figure 6-21 may be that even the apparently "undisturbed" tests depicted on the figure suffer from disturbance to some degree. To illustrate the effect of disturbance on the principal stress difference, Figure 6-22 presents the minimum and maximum principal stresses computed from all of the SBPM results at the K_0 area. Third and fourth degree polynomial best-fit lines through both data indicate an average principal stress difference of about 1000 psf or more, significantly larger than indicated by the "undisturbed" results on Figure 6-21. This indicates that disturbance has the effect of increasing the apparent principal stress difference indicated by the SBPM.

Based on the observation that disturbance seems to result in increased stress anisotropy, and the fact that there is no apparent reason why K_0 anisotropy would be greater than that at the embankment toe, it can be concluded that even the "undisturbed" K_0 tests likely suffer from some degree of disturbance. It may be that insufficient lateral confinement exists in the shallow depth K_0 conditions tested at Pease AFB to allow SBPM deployment without some degree of disturbance, and thus the principal stresses can, in generally, not be accurately determined. Also, the horizontal stresses measured at the K_0 area are, at worst, only 5 times larger than the error of measurement of the SBPM equipment. This greatly increased the significance of measurement error over that at the embankment toe. These factors suggest that the actual in situ horizontal stress anisotropy may be significantly smaller than is indicated by the SBPM measurements.

Based on the Dalton and Hawkins method, the compass orientations of the major principal stress in the horizontal plane for the undisturbed tests are plotted with depth on Figure 6-23. As can be seen on the figure, the computed direction varied from about 193 to 324 degrees clockwise from magnetic north, a range of 131 degrees. This resolves into an average direction of 242 degrees clockwise from north, with a standard deviation of ± 60 degrees. Compared to the results at the

**PEASE AIR FORCE BASE K₀ AREA
MAX AND MIN PRINCIPAL STRESSES
TOTAL HORIZONTAL STRESS (PSF)**

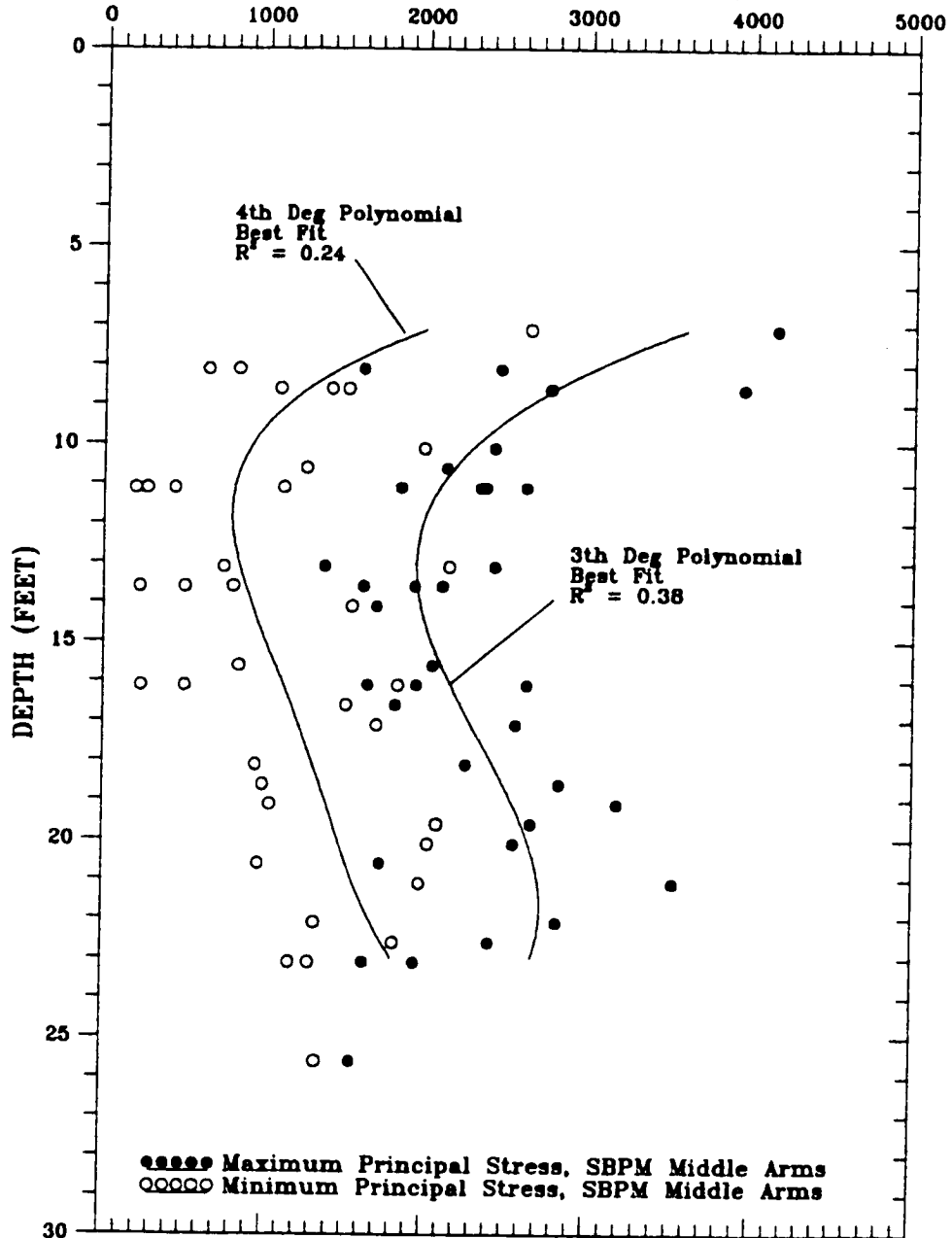


Figure 6-22 Minimum and Maximum Principal Stresses From All Tests at Pease K₀ Area

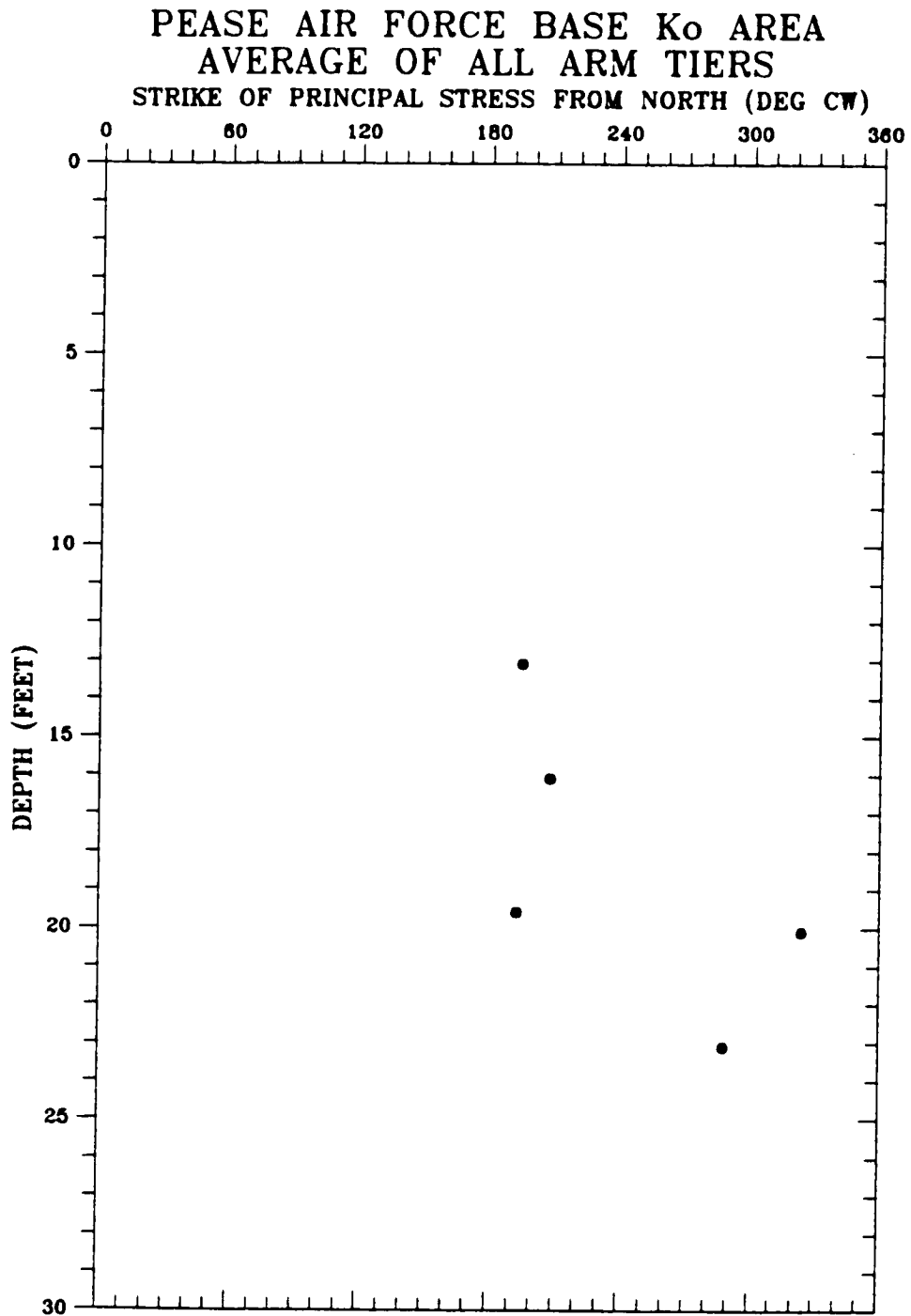


Figure 6-23 Profile of Direction of Maximum Principal Stress at Pease K₀ Area

embankment toe, this seems to indicate that a consistent direction of the major principal stress was not determined at the K_0 area, which is not surprising considering the foregoing discussion regarding the large principal stress difference at the K_0 area; however, the randomness of the direction of the major principal stress in the K_0 stress condition could also be, at least partially, the result of a number of geologic factors. Deposition of the soil was likely not wholly uniform, and forces due to shifting flow channels or sloped surfaces could have influenced the stress history of the deposit in an apparently random way. Also, the surface of the strata directly below the silty clay deposit is known to be extremely variable from location to location, which could have caused variable lateral wedging during self-weight consolidation after deposition. This lateral wedging could cause variable lateral stresses. In addition, it is possible that variable tectonic forces and/or forces caused by desiccation of the crust could have induced randomness to the direction of the major principal stresses.

6.4.3 Hamilton AFB Site

The Dalton and Hawkins (1982) technique for determining the magnitude and direction of the maximum principal stress in the horizontal plane was used by Benoit (1983) at the Hamilton AFB site. Benoit noted the tendency for a particular strain arm to lift-off first for the tests made in a particular borehole. This tendency was noted for each of two boreholes made for Benoit's research. Because the tendency was observed for different strain arms in each borehole, mechanical effects were discounted. Benoit indicated that a difference between the major and minor principal stress of 20 percent or more was generally observed. The major and minor principal stresses reported by Benoit and Clough (1986) within the depth of testing of the current research are included on Figure 6-24. The Dalton and Hawkins (1982) computed principal stresses from undisturbed tests for the current research are also included on Figure 6-24. Similar principal stress differences between the current and previous research are seen, generally about 50 to 600 psf, and the

HAMILTON AIR FORCE BASE

TOTAL HORIZONTAL STRESS (PSF)

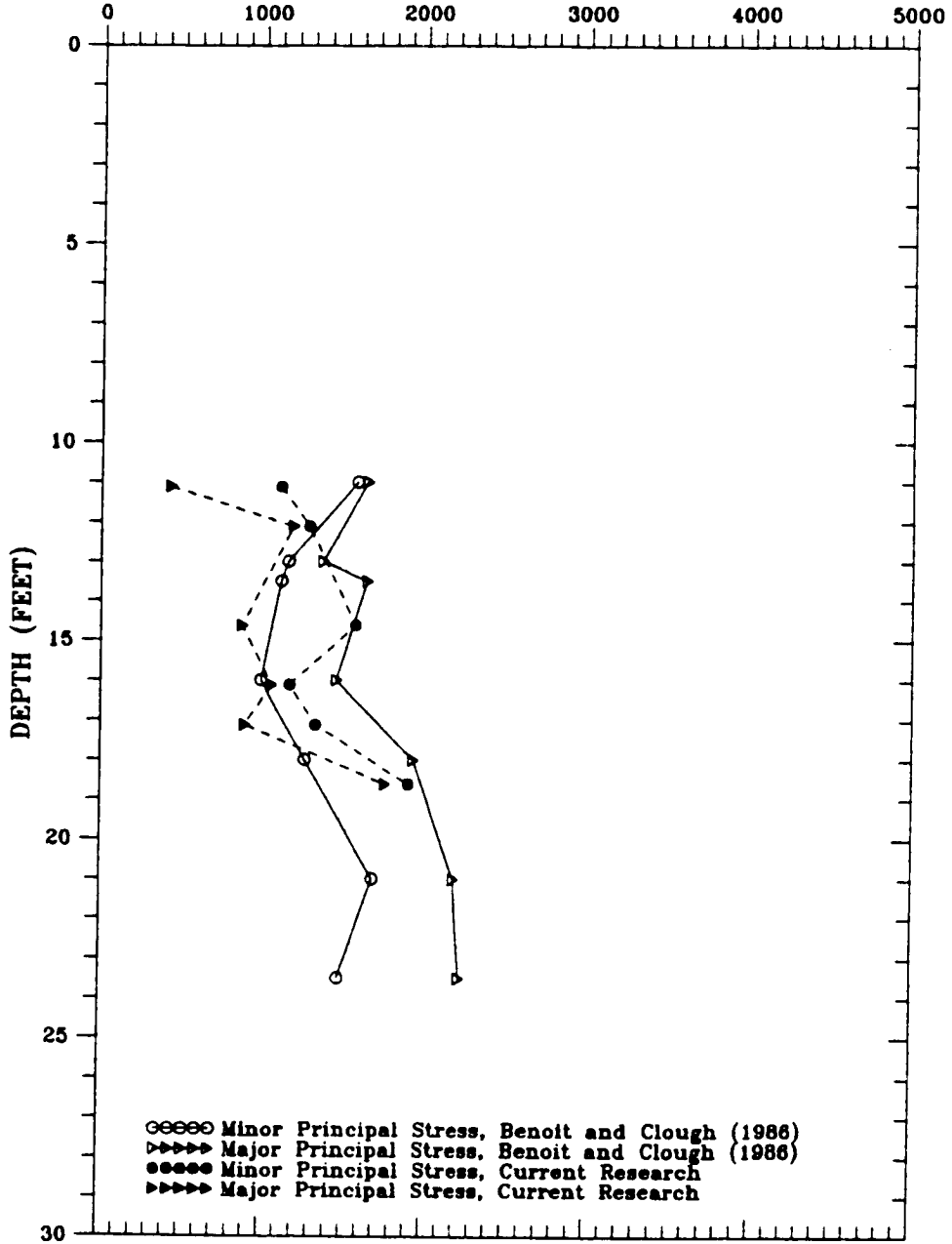


Figure 6-24 Major and Minor Principal Stress at Hamilton AFB

data appears to be relatively consistent in magnitude. It is noted that the principal stress difference is very similar to that observed at the Pease AFB K_0 area, and seems to be a relatively large stress difference, considering K_0 deposition.

Benoit (1983) estimated the compass orientation the probe in two of his borings by the position of the umbilical instrumentation cable taped to the drill rods in photographs made during his field work. While this does not provide an extremely accurate means of assessing the direction of orientation, it is interesting to plot the resulting strike of the major principal stress as a comparison with the current research. This is done on Figure 6-25. As can be seen, Benoit's (1983) data provides a fairly consistent orientation of the major principal stress within a particular boring, but varies up to 80 degrees between borings. The results of the current research are also included on Figure 6-25. Tests HAM2.1 and HAM1.3 agree well with Benoit's boring JAB-4. The other tests conducted for this research do not seem to coincide with Benoit's data. Again, as with the Pease K_0 data, there seems to be a randomness to the orientation of the major principal stress in the K_0 conditions, likely due to a combination of disturbance, measurement error, and deposition related randomness in actual in situ stresses.

6.5 Summary

This chapter has reviewed considerations in the assessment of SBPM in situ horizontal stress, including consideration of the effects of disturbance. The chapter also discussed SBPM measured stresses at the Pease and Hamilton AFB test sites and investigated the use of the SBPM to measure stress changes and stress anisotropy.

Disturbance was found to have a variable effect on measured horizontal stress. Remolding and disturbance due to encountering a shell or rock during deployment tend to create a void adjacent to the probe which results in a measured horizontal stress less than would be measured within in situ undisturbed conditions. Re-expansion of the SBPM membrane in soil that was already tested also indicated a horizontal stress less

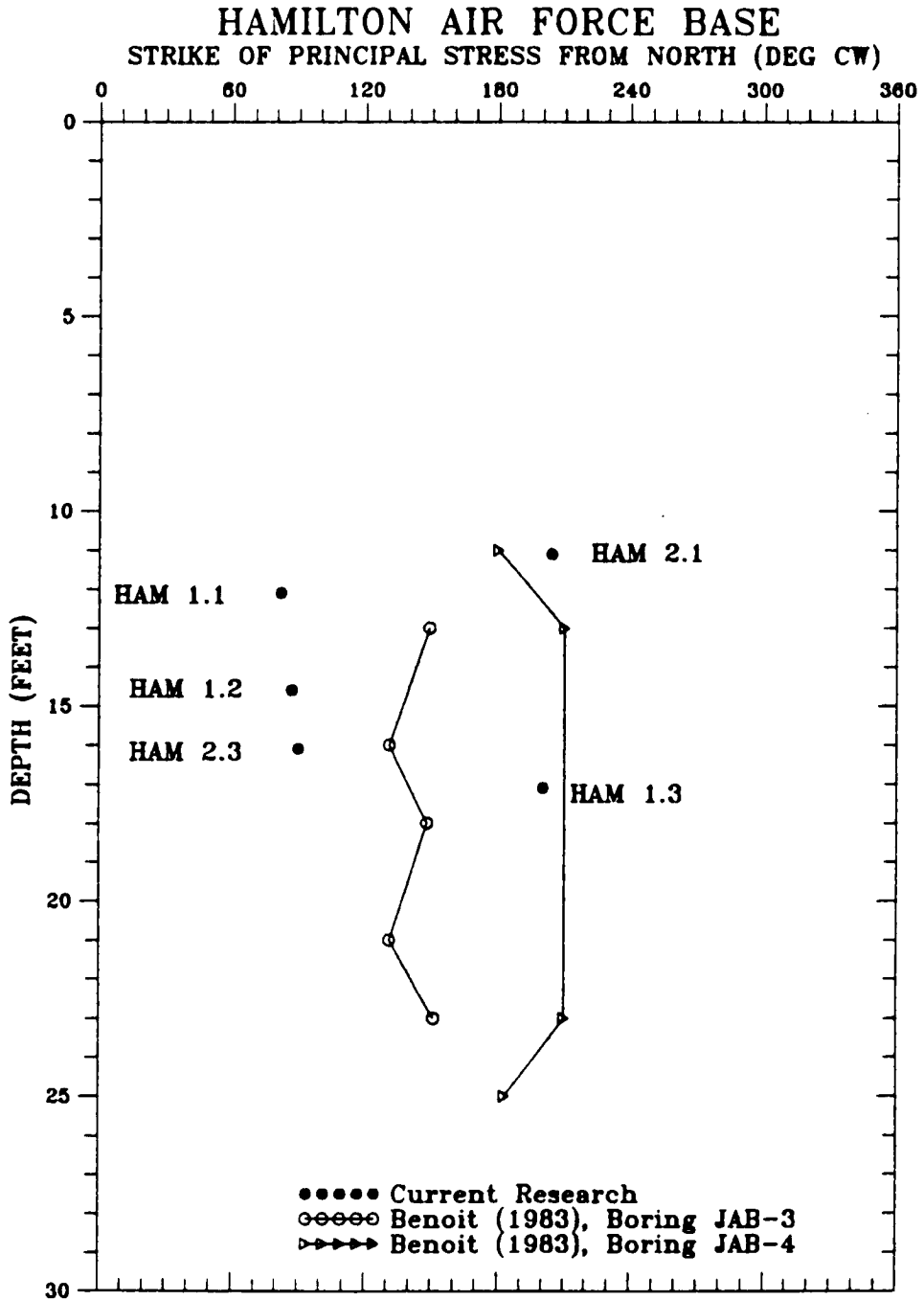


Figure 6-25 Strike of Major Principal Stress at Hamilton AFB

than in situ undisturbed conditions. Push-in tests, conversely, measured horizontal stresses that were the same or larger than those measured in undisturbed soil, likely due to the pre-stressing effect of push-in disturbance. Comparison of the shapes of the pressuremeter curves from tests with various forms and degrees of disturbance led to development of a new ratio, C_d , the disturbance ratio. The ratio seems to be effective in mathematically differentiating between the different forms of disturbance. As a result of the findings with regard to disturbance effects on the pressuremeter curves, both visual inspection and numerical assessment of the pressuremeter curves were employed to cull the horizontal stress results which were subject to disturbance. These methods were found to work well, yielding profiles of horizontal stress which appear reasonable and consistent. The C_d ratio was found to be sensitive to soil type, but not stress condition.

Additionally, the research found that the accuracy of the measured stress is dependent on correction for the magnitude of residual excess pore pressure due to insertion of the probe to test depth, unless several hours are allowed to elapse between drilling and expansion.

The SBPM has been shown to be useful in measurement of in situ horizontal stress at two K_0 test sites. The minimum measured horizontal stress indicated by a strain arm tier at results at Pease AFB compares well, within the error of measurement, with empirical methods, and the results at Hamilton AFB compare well with previous SBPM test programs (Denby, 1978 and Benoit, 1983). The research has demonstrated that the SBPM can be used to measure stress changes in a soft sensitive clay foundation soil with distance from a filled embankment. The SBPM yielded similar trends in stress increases to those predicted by FEM methods with distance away from an embankment.

In regard to the orientation of stress anisotropy in the horizontal plane, the technique suggested by Dalton and Hawkins (1982) was used to compute the magnitude and direction of the principal stresses at Pease and Hamilton AFB. Excellent agreement was observed between the

anticipated and measured direction of the major principal stress at the Pease embankment toe; however, the direction of the principal stress at both K₀ sites appear to be relatively random. It is suspected that the inability of the SBPM to measure a consistent direction of the major principal stress at the K₀ areas is a result of a combination of effects, including the difficulty of deploying the SBPM in soft clays at shallow depths (low confinement) without causing disturbance, error of measurement being large compared to the actual principal stress difference, and actual randomness of the principal stress orientation due to depositional, consolidation, and/or other geologic forces.

CHAPTER VII

TEST RESULTS: MEASUREMENT OF STRESS-STRAIN BEHAVIOR

7.1 Introduction

The results of the SBPM can be theoretically analyzed to determine various parameters which describe the stress-strain behavior of soils. This chapter presents results of such analyses on the SBPM data from Pease and Hamilton AFB. Results presented and discussed include stress paths, shear strength (s_u , Φ'), shear modulus (G), failure ratio (R_f), and Skempton "A" parameter at failure. The horizontal coefficient of consolidation (c_h) is also discussed.

7.2 SBPM Stress Paths

Plotting the total horizontal stress path from an SBPM test can be done to observe soil behavior. Figure 7-1 shows an idealized elasto-plastic stress path. If soil response is elasto-plastic, the stress path will essentially be vertical during elastic shear, and then horizontal after failure, in a direction of increasing p . Observation of the degree of conformance to elasto-plastic behavior is important, because it may be an indicator of whether certain analysis methods, such as the SBPM shear strength reduction methods which are based on an elasto-plastic assumption, are appropriate.

Based on the observed shape of stress paths of tests made for the current research, it was concluded that the stress paths from "undisturbed" tests conducted at both sites conform reasonably to elasto-plastic behavior before failure, however, after failure, deviation from the idealized elasto-plastic stress path was typical. Examples of stress paths from undisturbed tests are presented on Figure 7-1. The "humped" character of the horizontal portion of the stress path is a result of the spline curve fitting method, and it is believed the overall trend of the stress path is more representative of apparent SBPM shear behavior rather

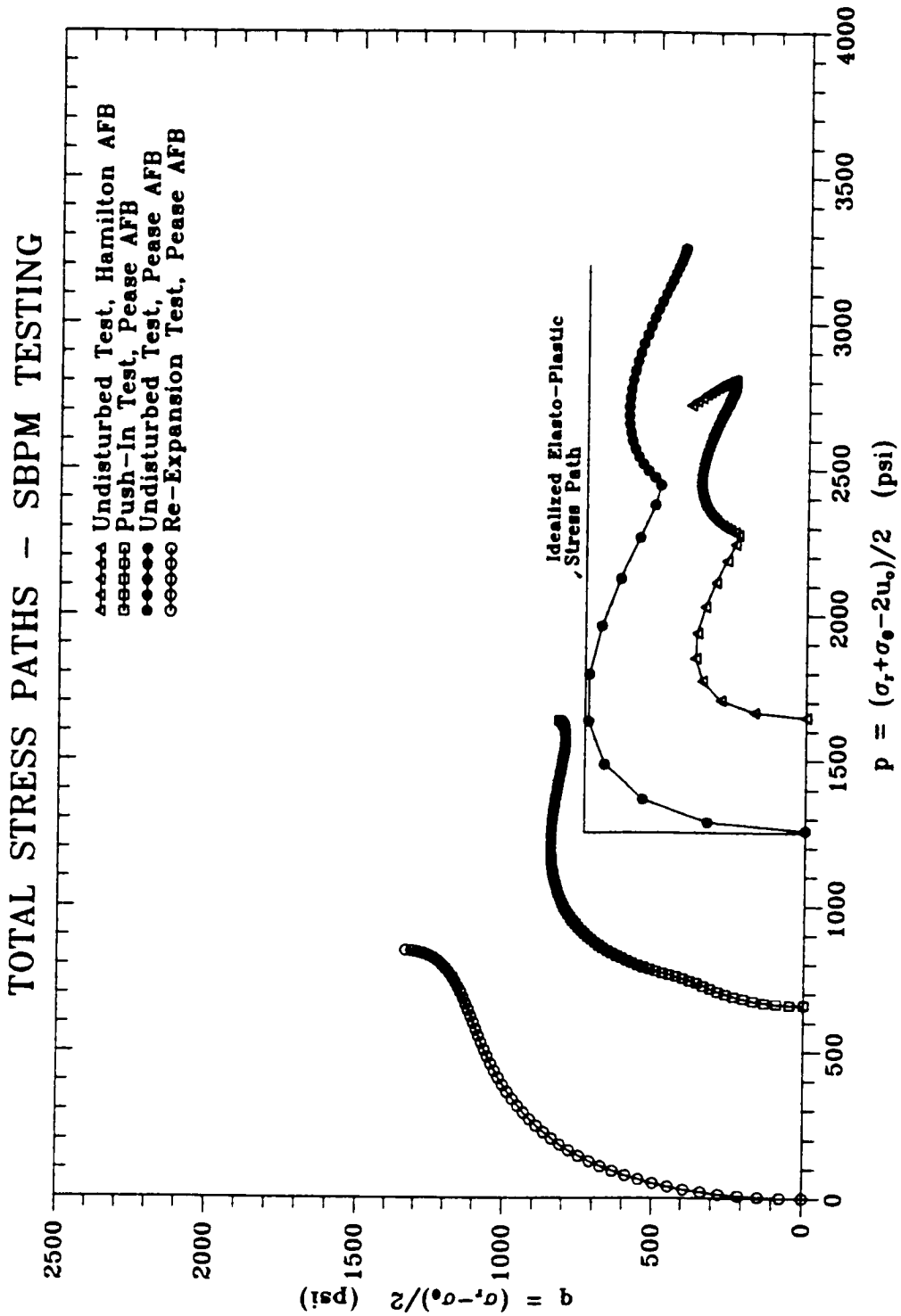


Figure 7-1 Typical Total Stress Paths

than the more local humps. The figure indicates that undisturbed test stress paths seem to exhibit strain softening after failure at Pease AFB. At Hamilton AFB, the overall trend of q appears to be more horizontal with increasing p than observed at Pease AFB, indicating apparently better conformance to elasto-plastic behavior; however, it is noted that in some instances, strain hardening was observed in some tests.

To investigate the effects of disturbance on the SBPM total stress path, stress paths from both re-expansion and push-in tests were examined. Representative stress paths from each of these two types of tests are shown on Figure 7-1. The re-expansion curve is from a test conducted within a zone of soil that was previously tested. As can be seen, the curve shape for the re-expansion test seems to exhibit strain hardening after failure, although it is noted that some curves exhibited strain softening. Also, at maximum test strain (about 10 to 15 percent radial strain) it was observed that the re-expansion stress path approaches the same maximum magnitude of q experienced by the undisturbed test conducted previously in the same zone of soil; however, for the undisturbed test, the maximum q occurs at a much lower strain level. For the push-in tests, pure plastic behavior or strain hardening was typically observed.

As can be seen, the effects of disturbance on the stress path can be subtle and require a good understanding as to what the shape of an undisturbed stress path resembles. If the undisturbed stress path conforms well to elasto-plastic behavior, and the disturbed tests do not, assessment of disturbance using the stress path may be useful. However, with soils such as those at Pease AFB that exhibit strain softening, it was a finding of the current research that disturbance is likely better assessed by examination of the pressuremeter curve as described in Chapter VI.

The effective stress path can be plotted to determine the effective angle of internal friction, ϕ' , as was shown on Figure 2-10. Figure 7-2 presents effective stress paths derived from Pease AFB tests. For some

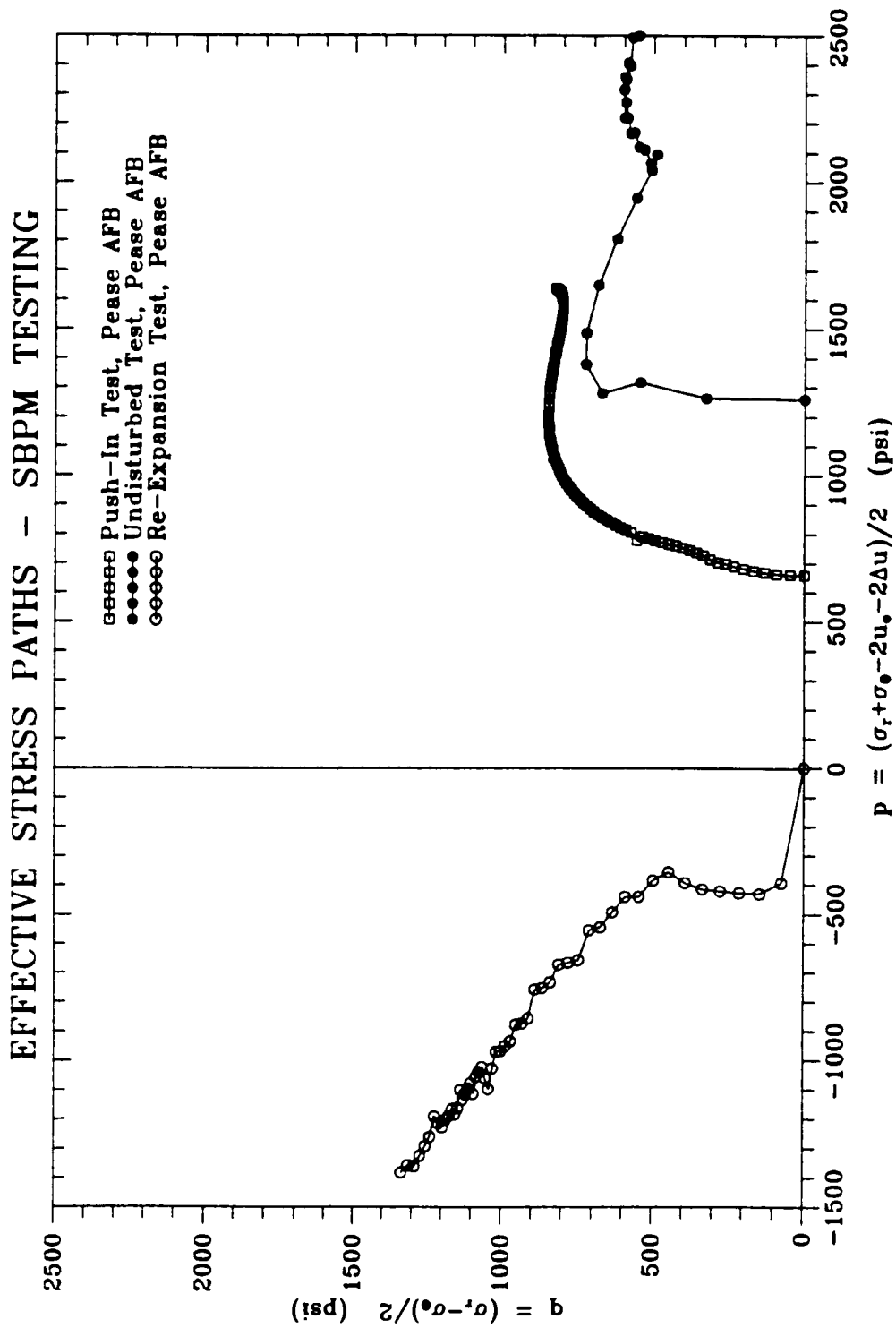


Figure 7-2 Typical Effective Stress Paths

undisturbed tests, it was observed that stress paths can enter negative p space. This has been previously observed by Baguelin, et al. (1973) and Wood and Wroth (1977). A stress path in negative p space is indicative of significant tensile tangential effective stresses. Mair and Wood (1987) indicate that such an occurrence is possible if fissures are not present, and negative pore pressure can be sustained by clay to a sufficient magnitude to keep the effective tangential stress compressive. Fissures were not observed in the Pease AFB silty clay. It is interesting to note that the stress paths from Hamilton AFB and at the Pease Embankment toe were entirely within positive p space.

At the Pease K_0 area, in tests where the SBPM effective stress path remained in positive p space, the minimum implied ϕ' was found to be about 32° . At the Pease embankment toe area, SBPM ϕ' was found to be $26.9 \pm 11.4^\circ$. In general, these values are higher than have been observed in normally consolidated CU triaxial tests (19.5° to 22.5° at Pease AFB). However, the Pease embankment toe range of SBPM ϕ' overlaps the value of ϕ' (30.6°) from a CU triaxial test conducted for this research on a sample consolidated under a $K_0 = 0.5$ stress condition.

At Hamilton AFB, the ϕ' computed from SBPM tests conducted for the current research was $27.8 \pm 10.6^\circ$. In general, this ϕ' represents a wide range which brackets the ϕ' that has been observed in normally consolidated CU triaxial tests conducted by previous researchers (32.5° to 35° at Hamilton AFB) as described in Chapter IV. Using the SBPM, Benoit (1983) measured a ϕ' of 16° to 24° at Hamilton AFB which was reportedly lower than CU triaxial tests, but within the range of SBPM measured values for the current research.

Figure 7-2 includes effective stress paths for re-expansion and push-in tests. In general, re-expansion tests were observed to developed very high pore pressures during shear and entered negative p space, indicating tensile effective tangential stresses develop during shear. The high pore pressure in re-expansion likely result from the inability of the previously tested soil zone to resist the applied shear stress.

This stress is transferred to the confined pore water, resulting in apparent tensile stress between the soil particles. Conversely, it was noted that push-in tests seem to generate relatively low, and even negative pore pressures during shear. This is likely related to the fact that the push-in tests performed for the current research had relatively high excess pore pressures due to insertion (1000 to 2000 psf). In general, the effective stress paths from push-in tests seem to be similar to or even higher than (in terms of p) total push-in stress paths. The relatively low pore pressure generation resulting during expansion in a push-in test may be due to hydraulic fracture of the tested soil zone. Hydraulic fracture would limit the maximum pore pressure that could occur to that equivalent to the minimum in situ horizontal stress.

7.3 Undrained Shear Strength

Various methods for determining undrained shear strength were discussed in Chapter II. For the current research, the Ménard (1956), Gibson and Anderson (1961), Baguelin, et al. (1972), and Denby and Clough (1980) methods have been used.

The Gibson and Anderson method as shown on Figure 7-3 was found to yield a "broken-back" line with two slopes in many instances. The change in slope was generally around 4 to 5 percent volumetric strain (about 2.1 to 2.6 percent radial strain) at Pease AFB. As will be discussed, the soft Pease AFB clay generally fails at low strain. Therefore, at Pease AFB, undrained shear strength was determined using the Gibson and Anderson method at volumetric strain ranges of a relatively low 2 to 5 percent volumetric strain as well as a higher strain range of 5 to 10 percent. At Hamilton AFB, the Bay Mud fails at a relatively higher strain, so only the 5 to 10 percent volumetric strain range is appropriate for shear strength determination, since the clay is generally in an elastic stress state at the lower strain range.

The results of a method used to correct membrane end effects, developed by Yeung and Carter (1990), was also examined. This method can be used to adjust computed SBPM shear strength values to account for the

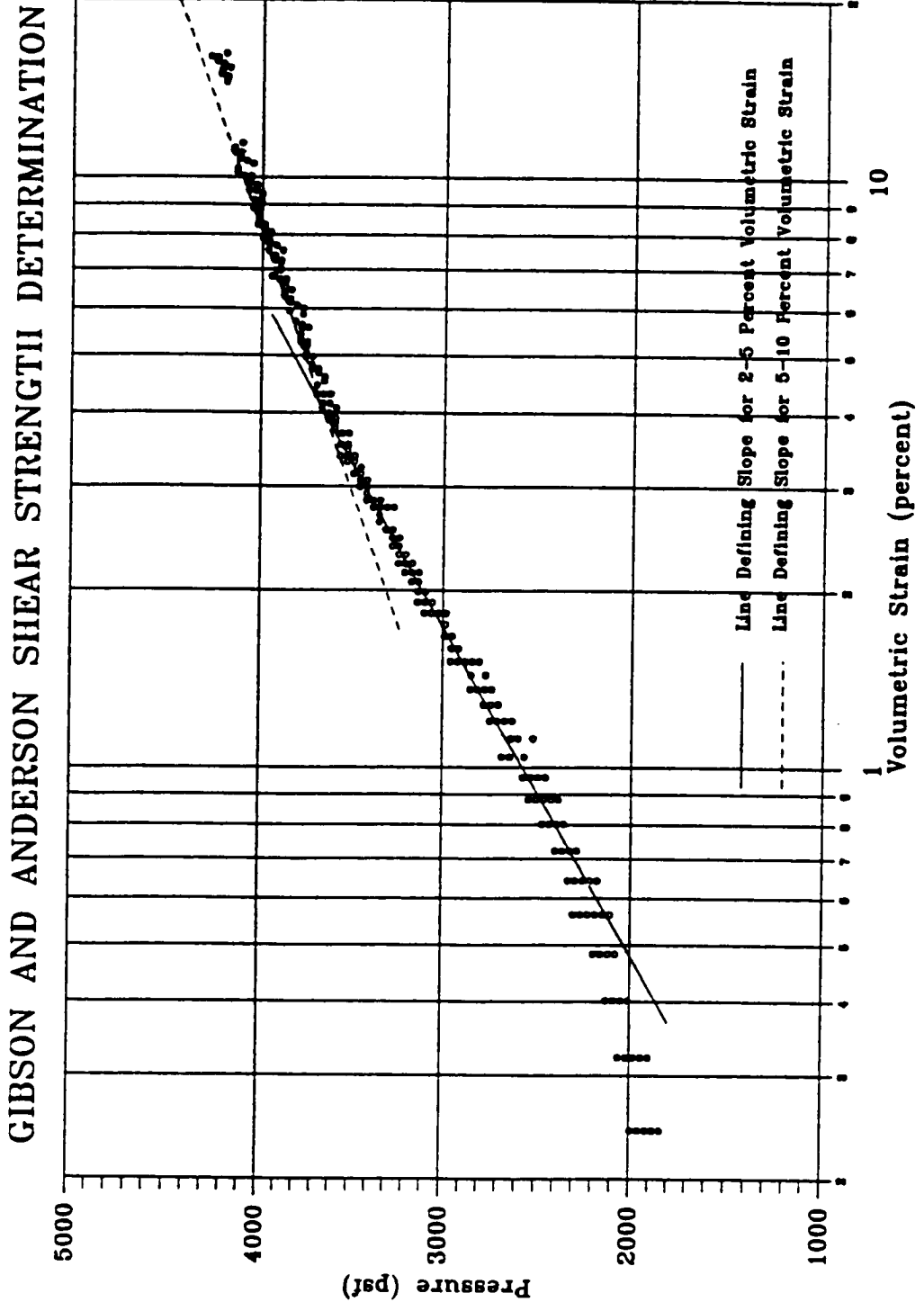


Figure 7-3 Typical Gibson and Anderson (1961) Shear Strength Determination Plot

limited length of the probe which causes deviation from the plane strain conditions assumed in analysis of shear strength.

7.3.1 Shear Strength at Pease AFB K_0 Site

7.3.1.1 Comparison of Methods - Figure 7-4 presents a profile of undrained shear strength versus depth for SBPM boring PMC4, which was conducted at the Pease AFB K_0 site. The figure is a comparison of the results of the Gibson and Anderson, sub-tangent, and Denby and Clough methods. The SBPM shear strength values presented are an average of the shear strength indicated by all three of the middle tier strain measuring arms. PMC4 was chosen because it is the deepest boring in the K_0 area and yielded results which are considered typical of the conditions at the K_0 area. Also included on the figure are uncorrected undrained shear strength data from Geonor field vane tests performed at the K_0 site.

As indicated on Figure 7-4, undrained shear strength determined by the SBPM below 10 foot depth ranged from 650 to 1100 psf, which is more than 60 to 200 percent greater than that determined by the field vane. In general, the highest shear strength values are from the sub-tangent method, and the lowest values generally result from the Gibson and Anderson method, at volumetric strains between 5 to 10 percent (radial strains between 2.6 and 5.4 percent). Shear strength determined by the Denby and Clough method and Gibson and Anderson method between 2 and 5 percent volumetric strain are generally between the upper and lower boundaries of SBPM undrained shear strength formed by the sub-tangent and 5 to 10 percent volumetric strain Gibson & Anderson values. The Denby and Clough method shear strength appeared to be more variable than the other three methods, widely fluctuating in its position between the highest and lowest shear strength value at a given depth. The 5 to 10 percent Gibson & Anderson values are consistently in closest agreement to the results of the field vane, in trend and magnitude, however they are in excess of the field vane values by about 120 percent.

Above a depth of 10 feet, Figure 7-4 indicates the SBPM shear strength values are 25 to 80 percent greater than the vane shear data,

PEASE AIR FORCE BASE UNDRAINED SHEAR STRENGTH

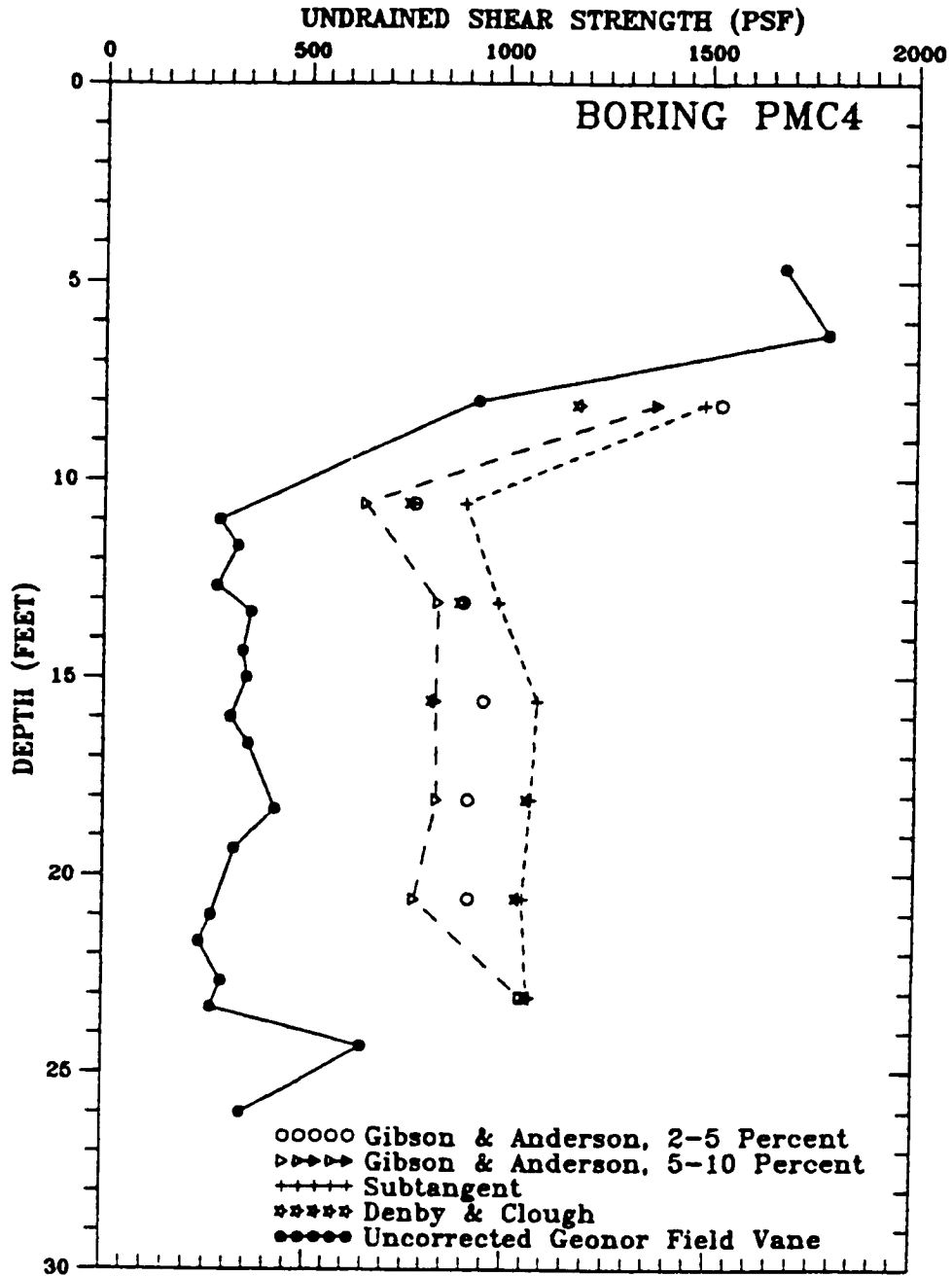


Figure 7-4 Undrained Shear Strength Profile at Pease K₀ Area

indicating a better comparison with vane data than was found in the softer, underlying clay. In the case of the upper stiff clays, it was found that the Denby and Clough method yielded values closest to the field vane results.

Figure 7-5 presents a comparison of the Gibson and Anderson shear strength from each of the middle arms as well as the averaged values indicated on Figure 7-4. The range of the Gibson and Anderson 5 to 10 percent values are shaded with vertical lines, while the range of the 2 to 5 percent values are shaded with dots. Note the overlap of the dots and lines. The range of the 5 to 10 percent values is consistently smaller at a given depth than the range of the 2 to 5 percent values. Also, the 5 to 10 percent shear strength is smaller at a given depth, implying the 5 to 10 percent data is a more consistent measurement of the SBPM undrained shear strength than the 2 to 5 percent data and provides results which are closer to the field vane measurements.

Because of the closest agreement between the vane results and the Gibson and Anderson 5 to 10 percent shear strength values, only those results are considered in the subsequent discussion of shear strength at Pease AFB. Further, because Baguelin, et al. (1978) demonstrated that disturbance can cause overestimation of the undrained shear strength ("strength paradox" effect), the lowest value of shear strength indicated by the three middle arms from expansion curves judged to be "undisturbed" (see Section 9.2.1) will be adopted as the representative SBPM undrained shear strength.

As discussed previously, Yeung and Carter derived a method for correcting SBPM undrained shear values for error caused by the limited length of the probe which result in deviation from assumed plane strain conditions. Figure 7-6 presents a profile of Gibson and Anderson 5 to 10 percent volumetric strain data both corrected and uncorrected for the effects of deviation from plane strain conditions. Included on the figure are the Geonor field vane and ICU triaxial (based on the consolidation test maximum effective past vertical pressure profile,

PEASE AIR FORCE BASE UNDRAINED SHEAR STRENGTH

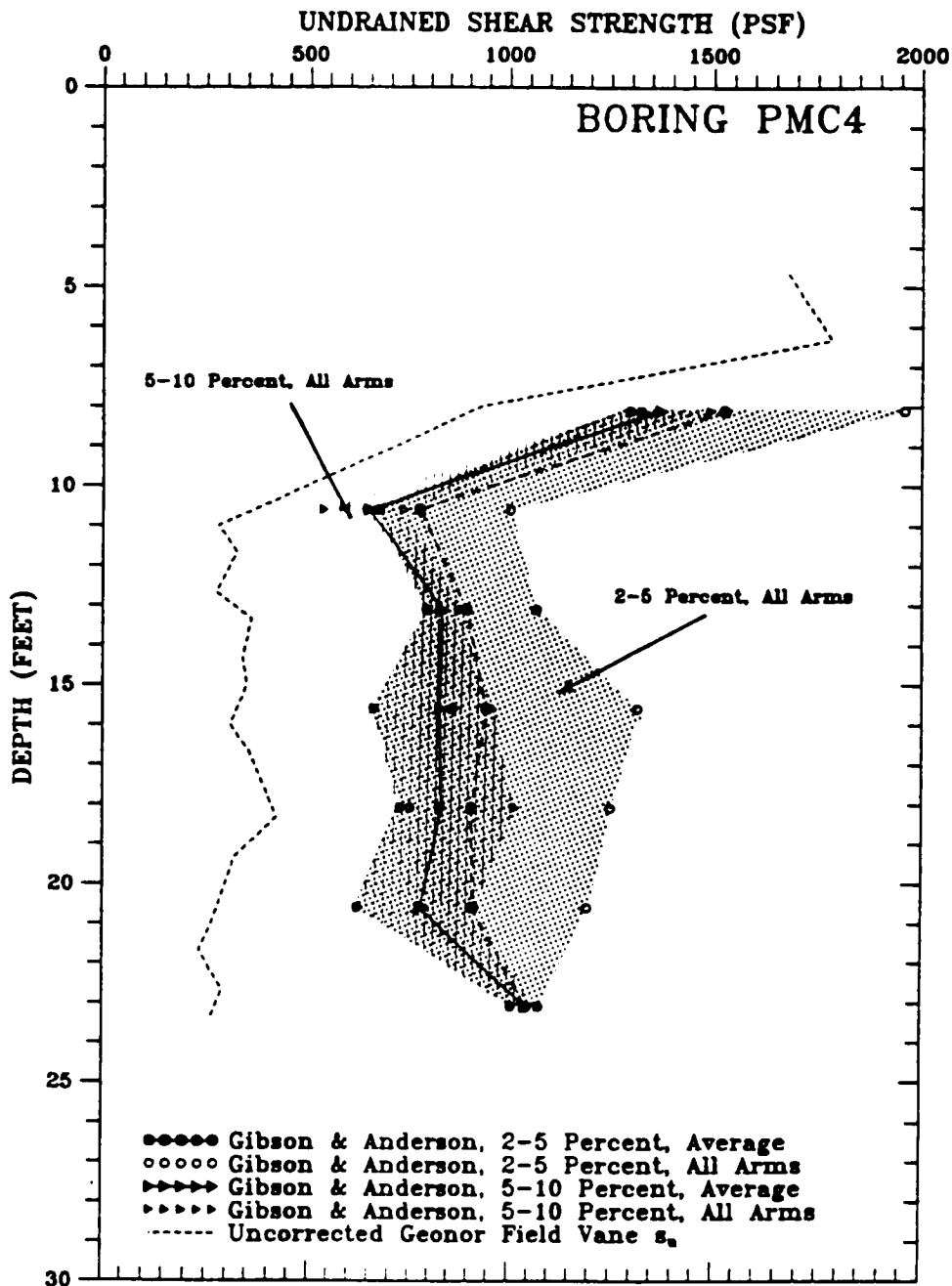


Figure 7-5 Comparison of Gibson and Anderson 5 to 10 and 2 to 5 Percent Volumetric Strain Results at K_0 Area

PEASE AIR FORCE BASE UNDRAINED SHEAR STRENGTH

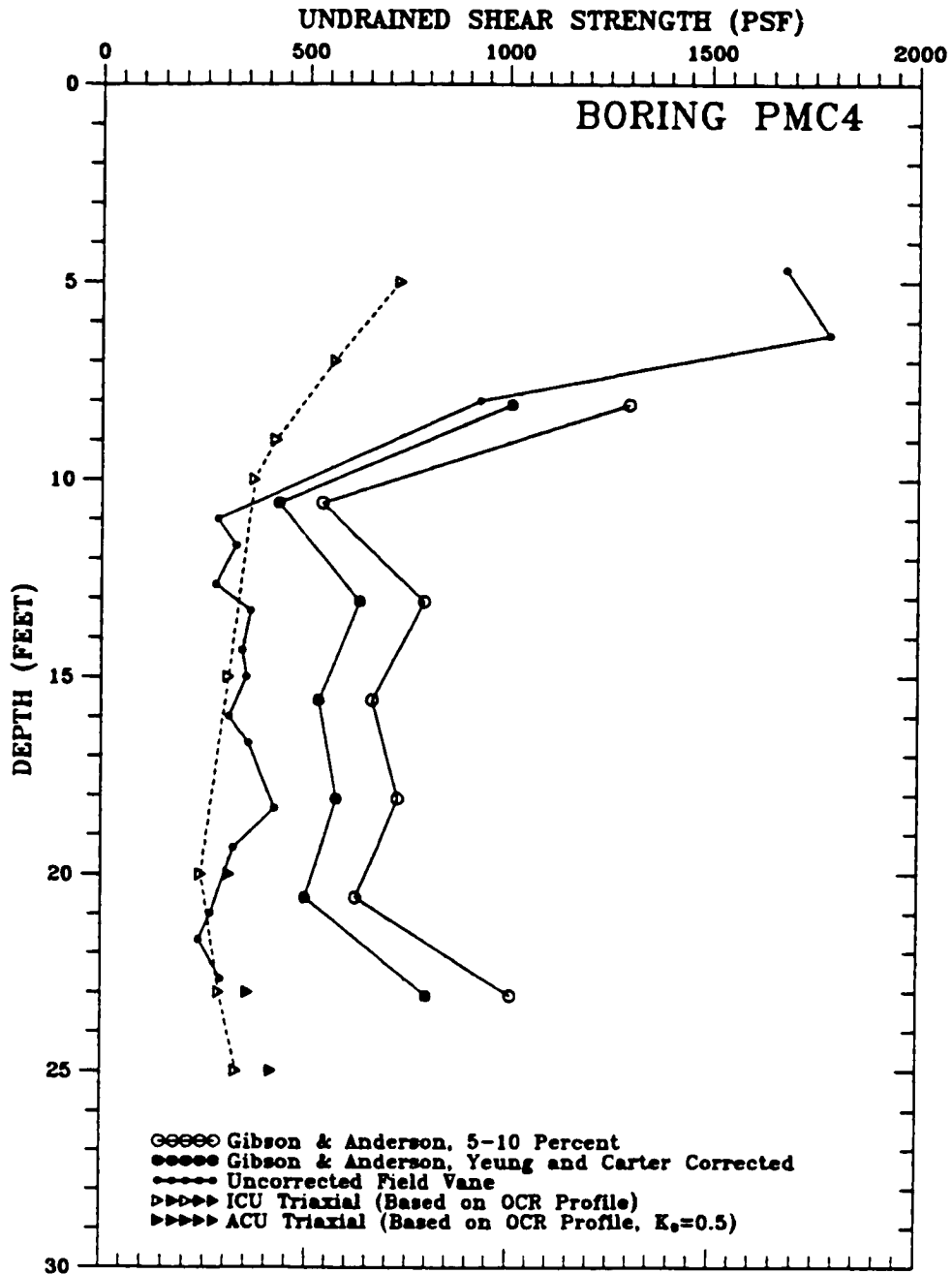


Figure 7-6 Comparison of Shear Strength Corrected and Uncorrected by Yeung and Carter Method at K_0 Area

Figure 4-5) measured undrained shear strength values. The Yeung and Carter correction reduces the SBPM shear strength about 20 percent, which is about 40 to 100 percent greater than the uncorrected vane shear and ICU triaxial values in the soft, lower portions of the silty clay deposit. In the upper, stiffer portion of the clay deposit, the corrected SBPM shear strength was only about 10 percent greater than the field vane values, but 10 to 100 percent greater than the ICU triaxial test values. This indicates that the Yeung and Carter (1990) correction seems to improve results, although they are still significantly higher than that indicated by other test methods.

7.3.1.2 Effect of Failure Strain and Disturbance - A possible explanation for the closer agreement between the vane and SBPM shear strength of the upper stiff clay in comparison with the soft clay may be related to the percent strain at which the silty clay fails, and the effect of disturbance on SBPM measured shear strength as is discussed in the following paragraphs.

Figure 7-7 presents a plot of the strain at failure versus OCR from ICU triaxial tests made for the current research. A general trend of increasing strain at failure versus increasing OCR can be observed. The low strain at failure for one of the tests depicted on the figure at an OCR (overconsolidation ratio) of 2 may have been due to a weakening of the failure plane due to disturbance. A best-fit line plotted through the data suggests the average failure strain is about 1 percent for normally consolidated soil to about 5 percent for an OCR of about 3. This general trend may be a consequence of the fact that the in situ soft soils have been leached of their original pore water salt ions (described in Chapter IV) which has essentially created a very sensitive "card house" structure in the fabric of the clay, and strength is a function of tenuous inter-particle forces or cohesion. Small strains tend to cause this "card house" structure to collapse, resulting in failure. The "card structure" in the stiffer, upper clay has been collapsed due to desiccation, and strength is derived more by a frictional mechanism that

**PEASE AIR FORCE BASE
RESULTS OF LABORATORY CU TRIAXIAL TESTS
OVERCONSOLIDATION RATIO (OCR)**

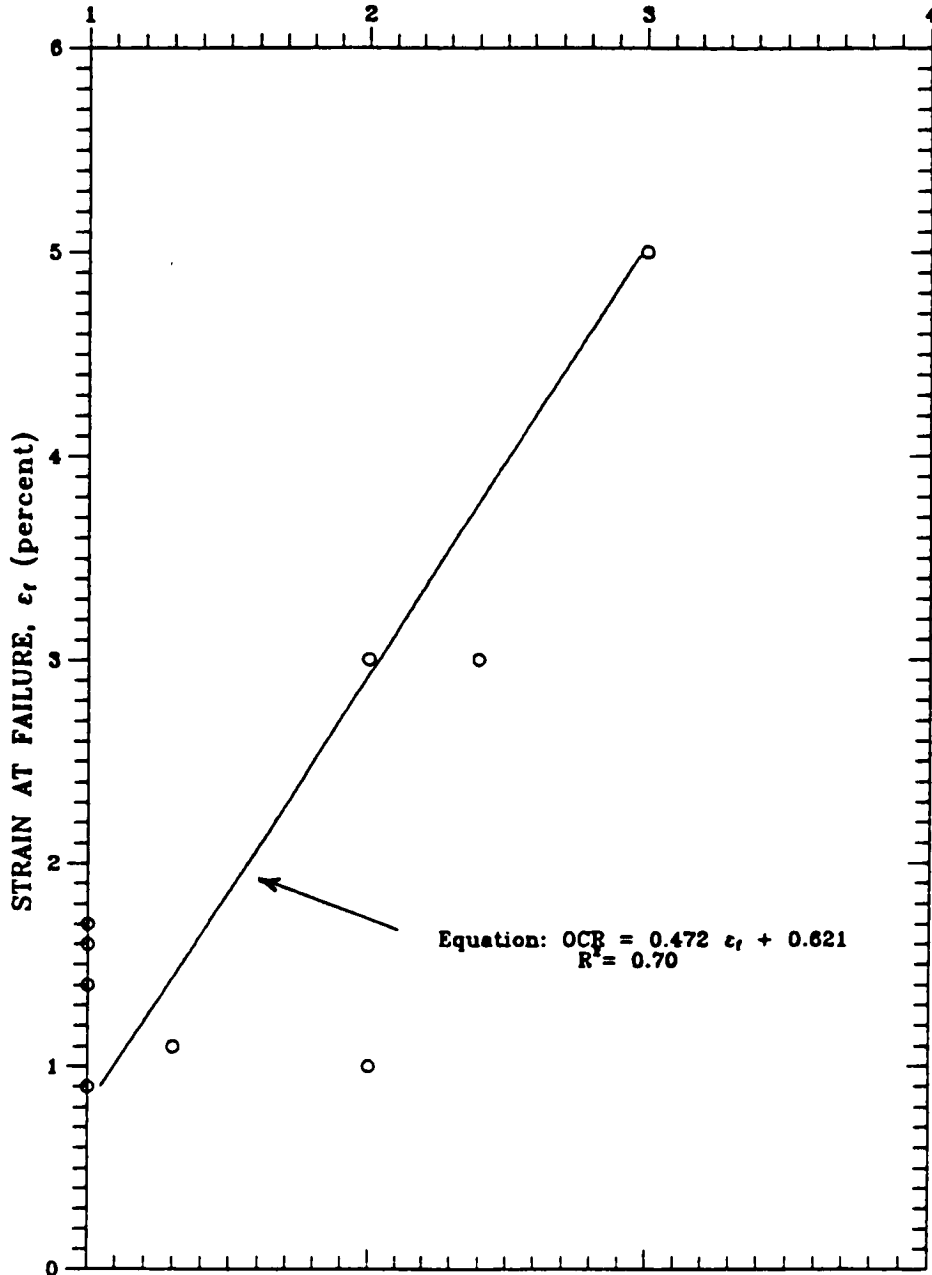


Figure 7-7 Triaxial Failure Strain Versus OCR for Pease AFB Silty Clay

peaks at some higher strain than the soft clay card house strength mechanism.

The concept that shear strength is the result of different strength mechanisms that mobilize at different strains was discussed by Lambe (1960). At least two components of strength seem to occur in clays. At low strains, strength is the result of inter-particle attractions (cohesion). After sufficient strain has occurred, cohesion is overcome and dilatancy and/or inter-granular friction/interlocking are responsible for shear strength. The softer Pease AFB clays appear to generally fail at lower strain, suggesting that the cohesion component, resulting from the "card house structure" is responsible for the peak strength. The lower residual strength that typically follows at higher strain is likely to result of intergranular friction. Conversely, the Hamilton AFB Bay Mud achieves peak strength at higher strain, and typically does not seem to strain soften like the Pease AFB clay does. This suggests Bay Mud peak strength is more the result of intergranular friction, and that the peak frictional strength is higher than that due to cohesive forces.

Push-in disturbance is thought to form in a thin annulus around the SBPM probe during deployment. Based on Equation 2-34, and assuming: $G = 140,000$ psf, $s_v = 400$ psf, and $u_{max} = 400$ psf; the thickness of the disturbance annulus can be computed to be equal to about 0.5 percent radial strain. Interestingly, stress-strain curves from SBPM tests in the soft Pease AFB silty clay derived by the sub-tangent method typically indicated peak shear strength at a similar radial strain. In the stiff crustal clays at Pease AFB, shear failure indicated by the sub-tangent method stress-strain curves was on the order of 1.5 to 3.0 percent radial strain. Based on the foregoing discussion, it could be inferred that the Pease AFB soft silty clay is so sensitive to disturbance, that is, peak SBPM shear strength is mobilized at such a low strain level, that inserting the SBPM into very soft sensitive soils may be impossible without causing disturbance within an annulus equivalent to the radial strain at which peak SBPM strength is mobilized. This disturbed annulus

would tend to cause the pressuremeter curve to become somewhat flattened, as depicted on Figure 7-8. While the disturbed curve is initially less steep than the undisturbed curve, it is steeper during failure, resulting in the shear strength for the disturbed curve being larger than that from an undisturbed pressuremeter curve. This is an explanation for the so-called "strength paradox". Since the peak strength derived by the stiff crustal silty clay is more a result of frictional component of shear strength that is not mobilized until relatively higher strains occur (5 percent axial strain in the CU triaxial tests and 1.5 to 3.0 percent radial strain in SBPM tests), insertion disturbance strains were not sufficient to affect the pressuremeter curve curvature in the strain range where peak strength is mobilized.

The relationship of triaxial strain at failure and SBPM disturbance effects on shear strength has been previously noted by Prapaharan, et al. (1990), and is discussed in Chapter II. However, those authors did not relate SBPM failure strains and "strength paradox" to the idea of shear strength components as discussed herein, but rather simply noted the fact that the SBPM seems to measure reasonable shear strength values in soils that fail at higher strain.

7.3.1.3 Results of Push-In Tests - Figure 7-9 presents data from push-in tests conducted at the K_0 area. It is seen on the figure that the SBPM shear strength values are generally up to 150 percent higher than the field vane shear values. The magnitude of the SBPM push-in strength values at a given depth are about the same as those from undisturbed tests, except for the 2 to 5 percent Gibson and Anderson shear strength values. It is also interesting to note that the 2 to 5 percent Gibson and Anderson shear strength values for push-in tests are generally less than the 5 to 10 percent value, which is the reverse of what was observed for undisturbed tests. A reason for this could be that the prestressed soil around the push-in test is still in an elastic state at 2 to 5 percent volumetric strain, with failure occurring at relatively higher strain within the 5 to 10 percent range.

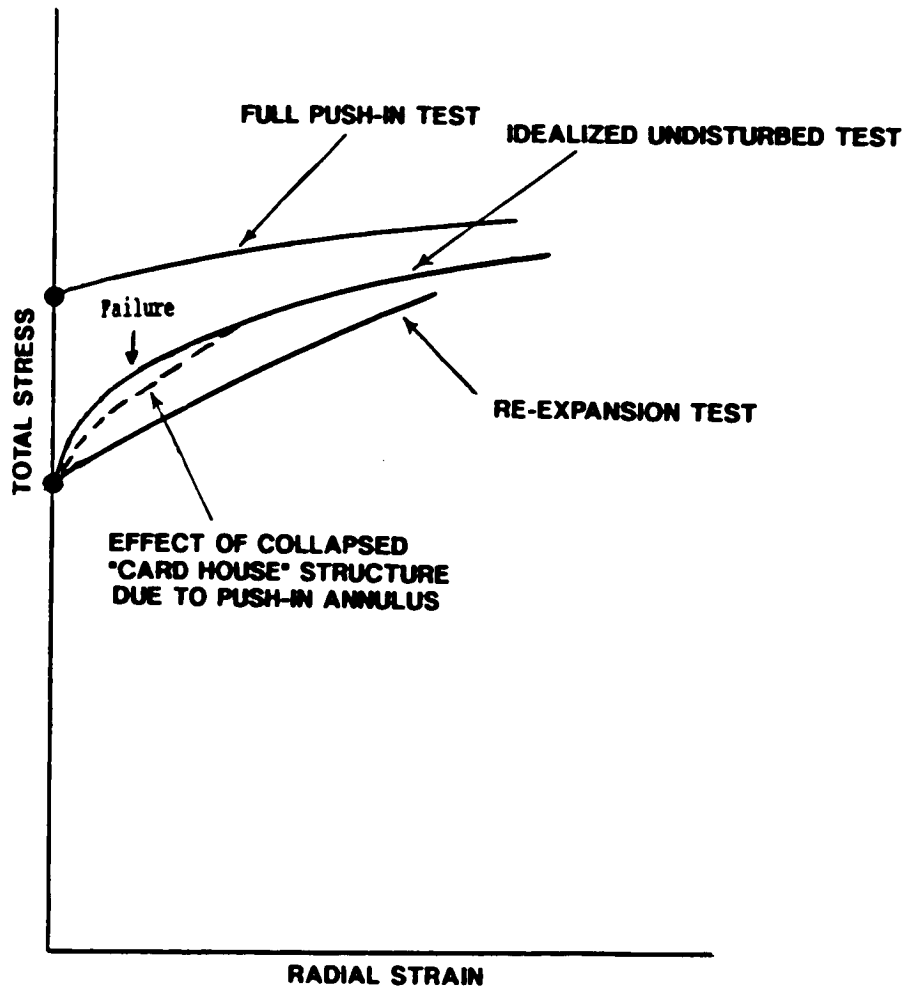


Figure 7-8 Effect of Insertion Disturbance on Pressuremeter Curve

PEASE AIR FORCE BASE UNDRAINED SHEAR STRENGTH

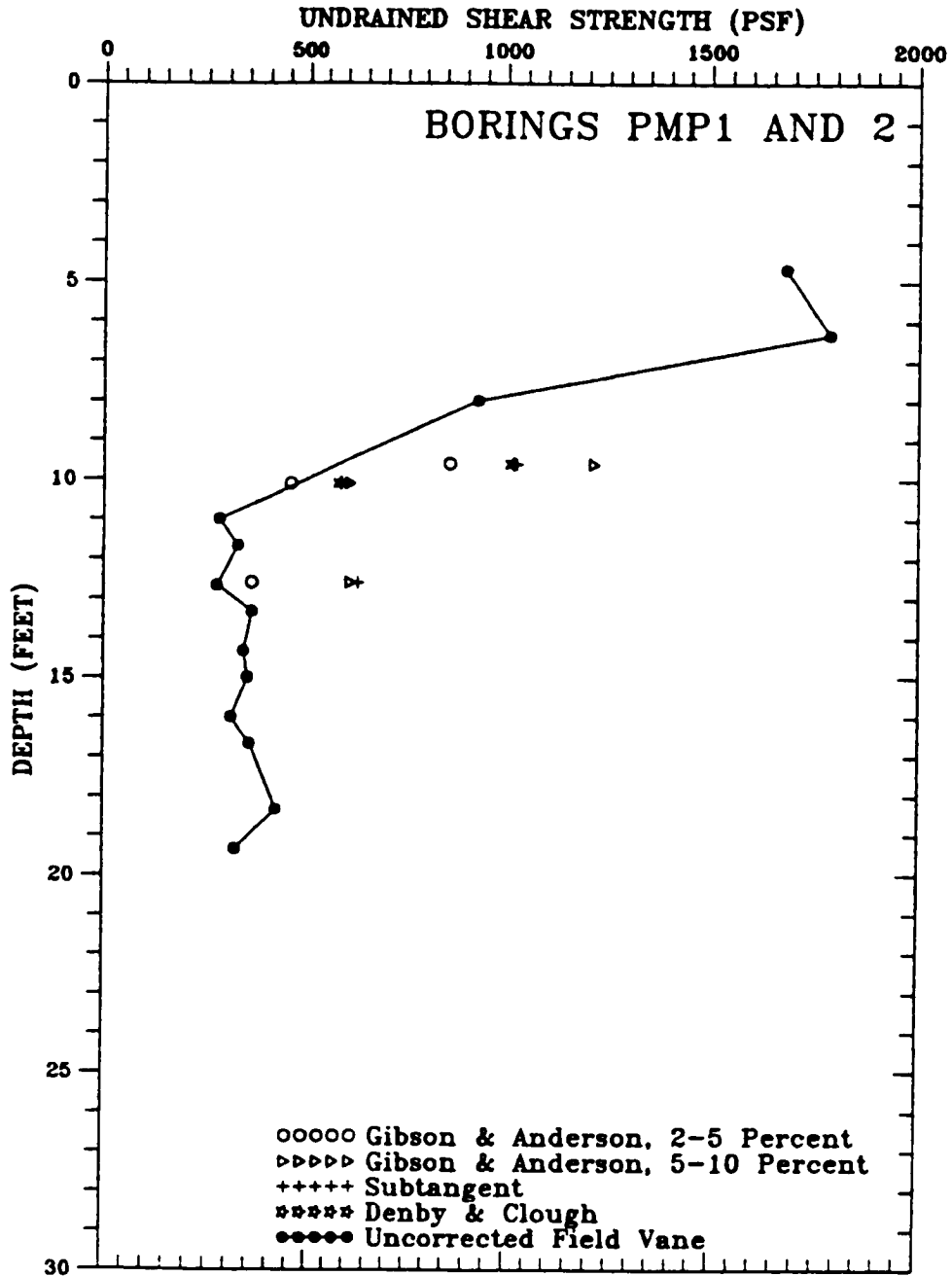


Figure 7-9 Push-In Shear Strength at Pease AFB

7.3.1.4 Effect of Inflation/Radial Strain Rate - In general, SBPM tests conducted for the current research were performed at inflation rates of 2 to 4 psi per minute. The use of this inflation rate was based on the findings of previous research regarding expansion rate (Benoit, 1983). This inflation rate resulted in radial strain rates of generally less than about 1 to 4 percent per minute. Boring PMJ5 included tests with higher inflation rates (up to 10 psi per minute) which resulted in radial strain rates of up to over 11 percent per minute, as indicated on Figure 7-10. These faster inflation rates were employed to observe the effects of increased strain rate on shear strength.

It was of interest to see if an increase in radial strain rate would result in increased shear strength. The radial strain rate was measured between 5 and 10 percent strain, the same range as the Gibson and Anderson Shear strength values indicated on the figure. Figure 7-10 includes the results of all the middle arms, and it can be seen that within a particular test, the radial strain rate at each arm can be significantly different from the strain rate at the other arms, indicating the membrane does not necessarily strain outward at a constant rate around the probe. With regard to the shear strength, little effect of varying strain rate within a given test can be seen, although there is admittedly not very much data on which to make this conclusion. While a distinct increase in shear strength due to increasing strain rate was not observed at Pease AFB, there is evidence from previous research that inflation rate may have an effect on SBPM measured shear strength. Benoit (1983) noted an increase in measured shear strength of 15 percent at radial strain rates in excess of 1 percent per minute in San Francisco Bay Mud at Hamilton AFB. Benoit (1983) also found that very slow strain rates could result in an increase in measured shear strength, likely due to drainage and consolidation during testing.

7.3.1.5 Ménard Method - Ménard (1956) presented an empirical method for estimating undrained shear strength given the lift-off pressure, the limit pressure and a coefficient "N". The "N" coefficient has been

PEASE AIR FORCE BASE UNDRAINED SHEAR STRENGTH

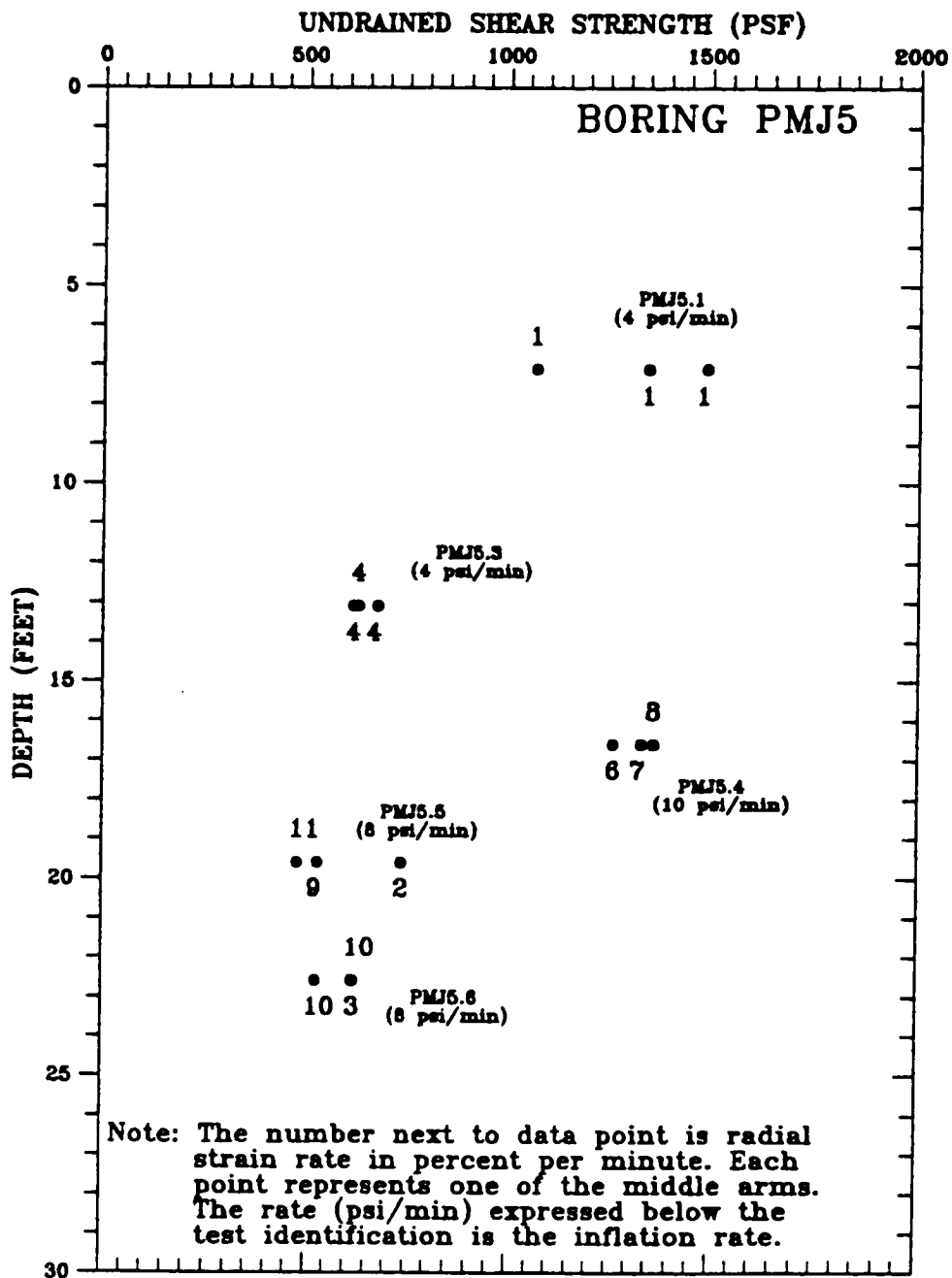


Figure 7-10 Effect of Strain Rate on Measured Undrained Shear Strength

discussed in Chapter II and is essentially an empirical calibration factor that correlates the difference between limit pressure and lift-off pressure to undrained shear strength. Ménard indicated that this value is typically between 4 and 6. Hughes (1982) has suggested that for the Cambridge SBPM, the total pressure at 10 percent radial strain could be used in lieu of the limit pressure. Based on the total pressure at 10 percent radial strain, the "N" value which correlates the Pease K_0 SBPM data to the uncorrected field vane data was found to be 11.3 ± 1.72 . This value is significantly larger than the normal range indicated by Ménard, and is an additional indicator that the SBPM pressuremeter curves at the K_0 area suffer from the so-called "strength paradox" due to insertion disturbance.

7.3.2 Shear Strength at Pease AFB Embankment Toe Site

7.3.2.1 Trend of s_u with Distance from Embankment - The 5 to 10 percent Gibson and Anderson undrained shear strength values derived from SBPM data at the Pease Embankment Toe (PMJ6) are indicated on Figure 7-11. Also presented on the figure for comparison are similar data from the K_0 area (PMC4). In Chapter IV, it was shown that the vane shear strength profile at the Pease Embankment toe was larger in magnitude than that at the K_0 site. This trend is what would be expected because the consolidating effect of the highway embankment would increase shear strength over K_0 conditions. However, as can be seen on Figure 7-11, the SBPM indicates lower strength at the embankment toe than at the K_0 area. In Chapter IV, it was indicated that the soil profiles at the K_0 area and the embankment toe may have been somewhat different in moisture content and initial K_0 stress condition due to depositional, stress history or desiccation conditions. To investigate if such a profile difference could result in the measurement of decreased shear strength at the embankment toe, it is of interest to compare the SBPM shear strength profiles of PMJ6 at the toe and PMJ7/PMJ8 located about 55 feet from the toe of the highway embankment. Such a comparison is presented on Figure

PEASE AIR FORCE BASE UNDRAINED SHEAR STRENGTH

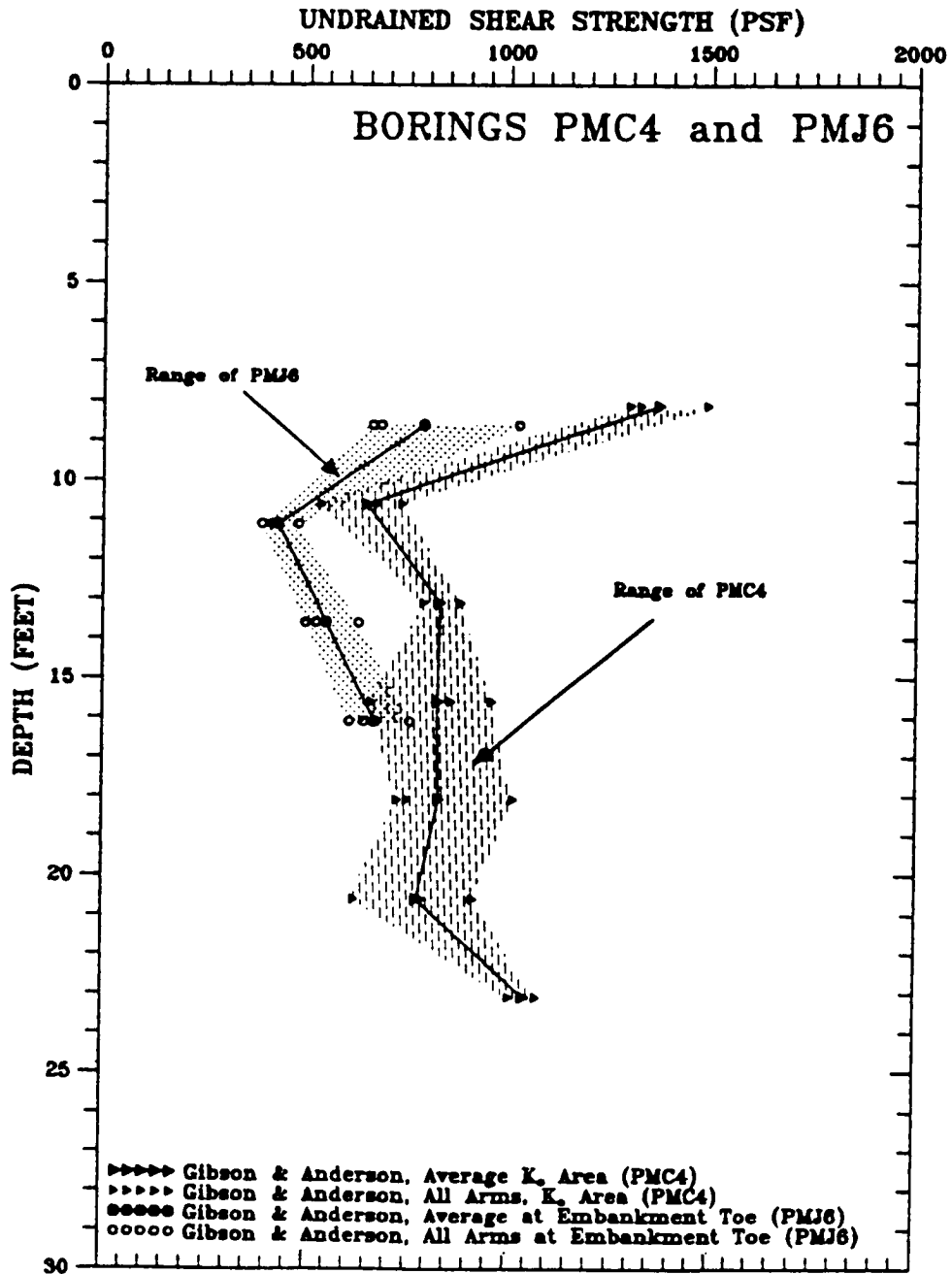


Figure 7-11 Comparison of SBPM Shear Strength Profiles at Pease Embankment Toe and K_c Area

7-12. As can be seen, higher shear strength is predicted at PMJ7/PMJ8 rather than at PMJ6. This, along with the comparison with the K_0 data presented on Figure 7-11 indicates that stress condition may affect the ability of the SBPM to measure undrained shear strength.

Analysis of pressuremeter data for shear strength considers only tangential (σ_θ) and radial (σ_r) stress, and not overburden pressure (σ_v). Wood and Wroth (1977) conducted some true triaxial laboratory tests to assess the effect of neglecting σ_v in the analysis of pressuremeter data. They found that during shear along a stress path similar to that of an SBPM test, σ_θ and σ_r quickly become the principal stresses and failure can be considered to be governed by σ_θ and σ_r alone. The authors concluded that the findings lend credibility to analysis of SBPM tests on clays where $K_0 < 1.0$. However, they further state that response during shear is likely elastic rather than elasto-plastic for clays in which K_0 were greater than:

$$K_0 > 1/(1 - \sin \phi') \quad (\text{Eq 7-1})$$

For such soils, the authors indicate that conventional pressuremeter analysis considering elasto-plastic conditions is not proven. For the Pease AFB clay, ϕ' from ICU tests is about 21 degrees. Using Equation 7-1, this would yield a critical value of K_0 equal to 1.56. At the embankment toe, (PMJ6) the ratio of effective horizontal to vertical stresses, based on the SBPM measured values of horizontal stress presented in Chapter VI ranges from 1.56 to 5.68, with an average of 3.28 and a standard deviation of 1.36. This is well above the critical value indicated by Equation 7-1 and indicates that conventional elasto-plastic analysis is likely not appropriate at the embankment toe. This may be a possible explanation for why the SBPM computed shear strength values deviate from the expected trend of increasing with proximity to the embankment.

PEASE AIR FORCE BASE UNDRAINED SHEAR STRENGTH

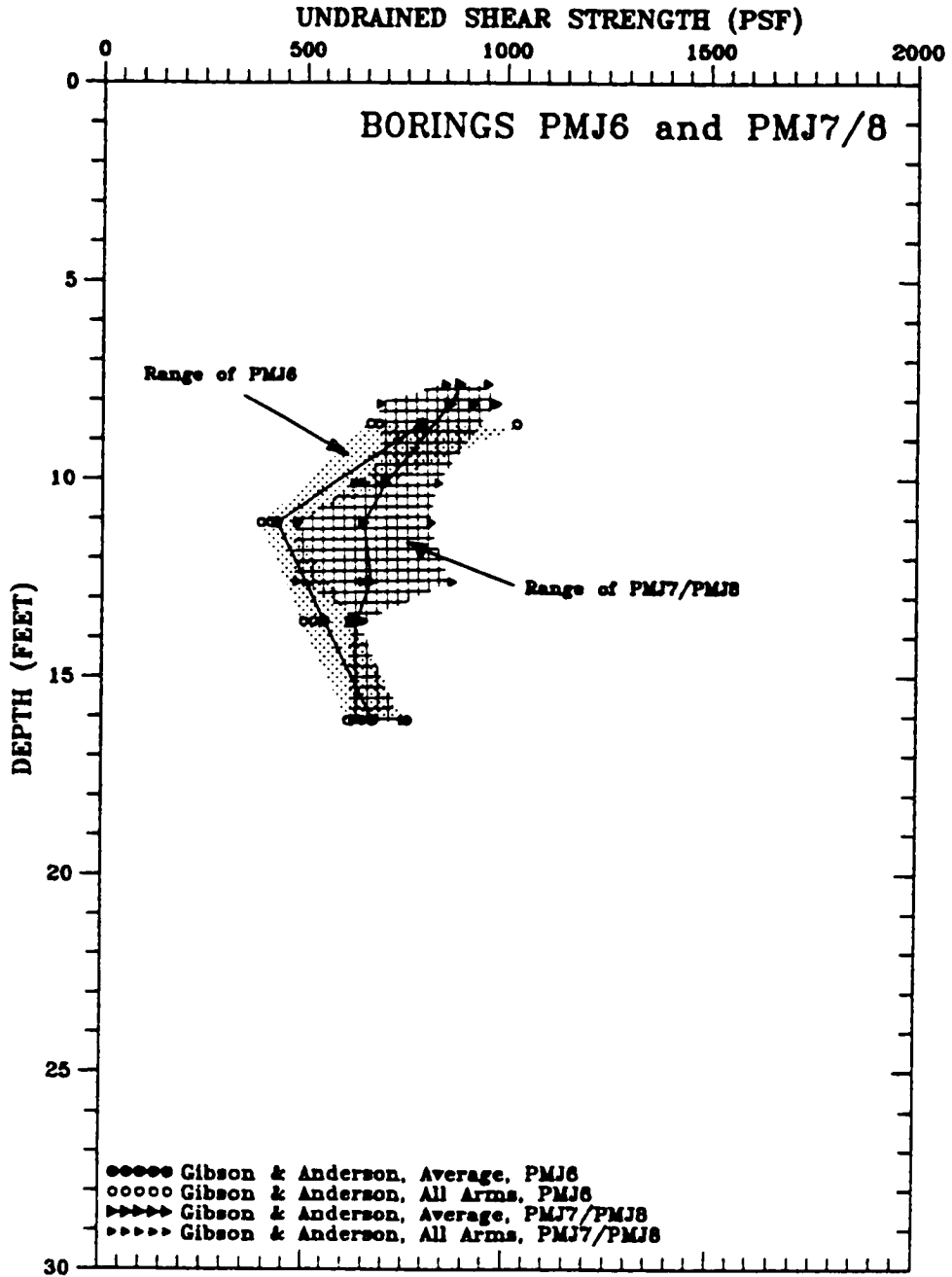


Figure 7-12 Comparison of SBPM Shear Strength Profiles at PMJ6 and PMJ7/PMJ8

7.3.2.2 Ménard Method at Embankment Toe - The Ménard (1956) "N" coefficient was determined for the toe area, and found to be 4.95 ± 0.67 . This is less than at the K_v area and is similar to the findings of Hughes (1982), who indicated that this value would be around 5 using the Ménard method and the pressure at 10 percent strain rather than the limit pressure.

7.3.2.3 Shear Strength from Shower Head Insertion - Test PMS1.1 was deployed using the new shower head jetting technique described in Chapter II. This test was made in boring PMS1, within a 10 foot radius of borings PMJ7 and PMJ8. Because of this close proximity, a shear strength profile similar to that at PMJ7 and PMJ8 would be expected. PMS1.1 was conducted at a depth of 11.1 feet. PMJ7.2 and PMJ8.2 were conducted at a similar depth of 10.1 and 11.1 feet, respectively. The following is a tabulation of resulting shear strengths:

<u>Method</u>	<u>SBPM Undrained Shear Strength (psf)</u>		
	<u>PMS1.1</u>	<u>PMJ7.2</u>	<u>PMJ8.2</u>
G&A, 5 to 10% strain:	530-930	622-835	643-817
Sub-tangent:	740-840	755-1170	780-940
Denby-Clough:	725-735	641-1064	641-758

Based on the results of tests PMS1.1, PMJ7.2 and PMJ8.2, the measured range of shear strength for tests inserted by conventional jetting generally coincides with that for the test inserted using the new shower head. This single test indicates that the shower head appears to be a promising method of insertion, however more research is necessary to optimize and perfect its use.

7.3.3 Shear Strength at Hamilton AFB

7.3.3.1 Comparison of Methods - Previous research (Denby, 1978) has compared the different SBPM shear strength determination methods and found that for San Francisco Bay Mud, the Gibson and Anderson method did not seem to yield consistent results, reportedly due to the non-linear

deformational behavior of the soil. The sub-tangent method yielded results that were generally lower than those obtained by the Denby and Clough method. The SBPM data of Benoit (1983) has been analyzed by the sub-tangent and Gibson and Anderson methods. Gibson and Anderson shear strength values determined by Benoit have been plotted on Figure 7-13, and contrary to the findings of Denby (1978) seem to yield consistent results. It should be noted that Denby's (1978) and Benoit's (1983) shear strength values were determined on pressuremeter curves derived from an electronic average of the three strain measuring arms. It is difficult to predict what the pressuremeter curve that results from an electronic average would resemble since curvature would be affected by complicating factors of differing lift-off stresses. It is speculated that electronic averaging tends to make the curve steeper at greater radial strain (and thus steeper at failure) than an unaveraged curve, and as a consequence, it might be expected that shear strength would be larger. Benoit's sub-tangent values are not included on Figure 7-13; however, they were on the order of 10 percent less than the electronic average Gibson and Anderson values. Figure 7-13 includes a profile of undrained shear strength from the field vane (Mitchell and Lunne, 1977). As can be seen, Benoit's electronic average Gibson and Anderson shear strength values were on the order of 0 to 50 percent larger than the field vane. It is noted that Benoit's (1983) sub-tangent values were virtually equal to the field vane data.

Figure 7-13 includes a profile of the Gibson and Anderson 5-10 percent volumetric strain undrained shear strength values for tests conducted at Hamilton AFB for the current research. The range of values measured from each of the middle strain measuring arms as well as the average of the arms at each test depth are included. As can be seen, the range of undisturbed Gibson and Anderson results from all the middle arms from the current research are generally about equal to or up to about 50 percent less than the field vane values. The average of all of the middle arms for each test from the current research are about 0 to 15

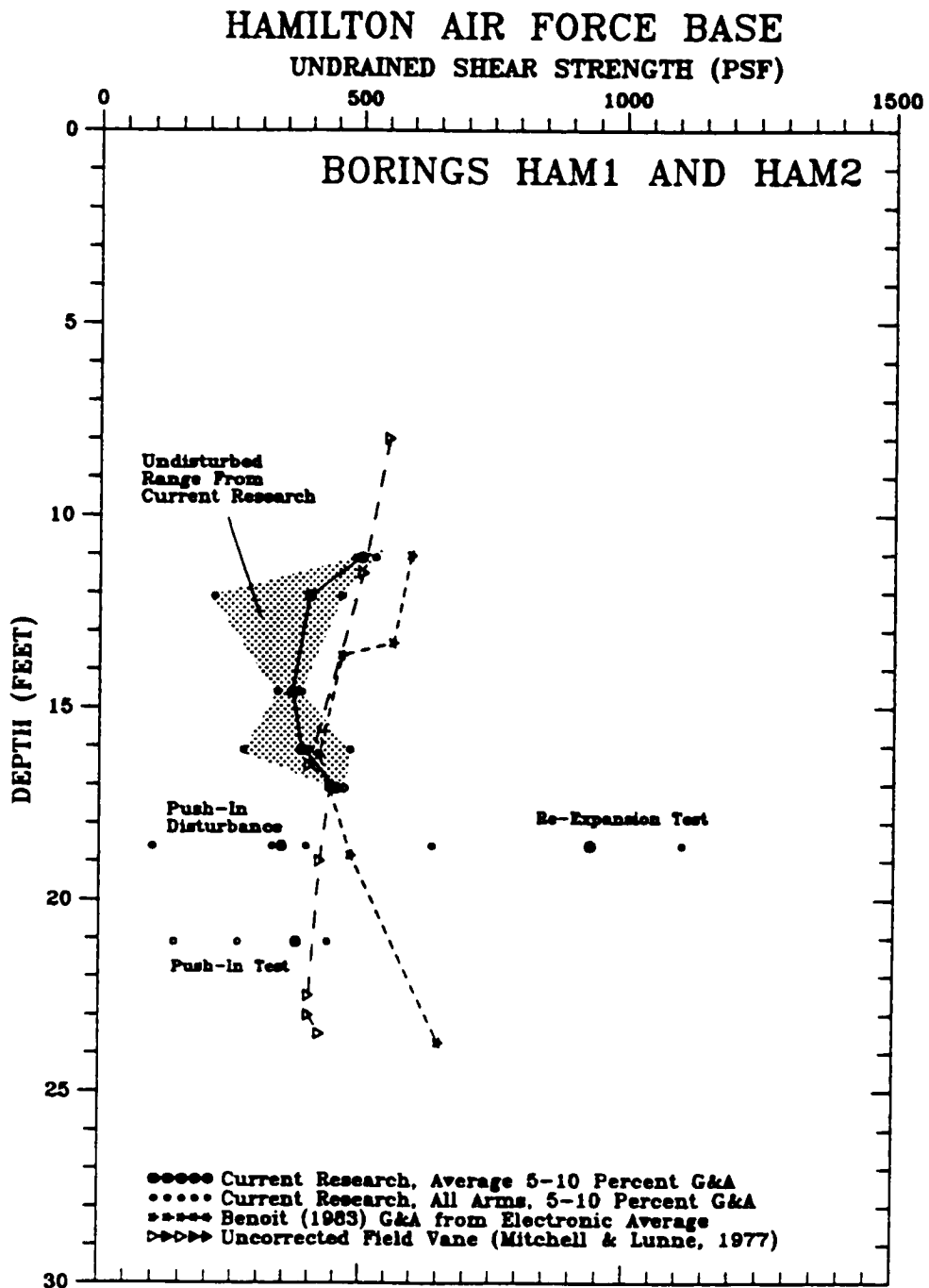


Figure 7-13 Shear Strength at Hamilton AFB

percent less than the field vane values. Interestingly, the 2 to 5 percent Gibson and Anderson values for Hamilton AFB are consistently less than or equal to the 5 to 10 percent values which is the reverse finding at Pease AFB. This is likely due to the fact that the 2 to 5 percent shear strength values at Hamilton AFB are reflective of elastic rather than peak strength, since peak strength occurs relatively higher strain in comparison with the Pease AFB soft clay. In common with the Pease AFB findings, however, the 5 to 10 percent values were found to be in closer agreement with the vane shear results.

Undrained shear strength was also determined for the current research by the sub-tangent and Denby and Clough methods. Figure 7-14 presents the shear strength indicated by the middle arms for the Denby and Clough and sub-tangent methods. For the current research, both methods yield essentially the same shear strength value within about 5 percent. These values were found to be about 0 to 15 percent less than the vane strength profile and the Benoit (1983) Gibson and Anderson shear strength values, but were about equal to the sub-tangent values of Benoit (1983).

Chapter II discussed the observation that SBPM measured undrained shear strength has often been found to be in excess of that measured by other in situ and laboratory tests. The reasons for this over-estimation included several potential factors, such as installation disturbance, partial drainage, strain rate effects, among others. Borsetto, et al. indicate that for a probe diameter to length ratio of 1:6, an overprediction of undrained shear strength of 22 percent could be expected. Yeung and Carter (1990) developed a correction method as has been discussed previously. Application of the Yeung and Carter correction to the Hamilton AFB data would cause it to be less than the uncorrected vane values. It has been stated in Chapter II that based on the mode of shear, it would have been expected that the SBPM shear strength would be somewhat larger than the vane shear value. In the absence of any effects that might be expected to cause the pressuremeter

HAMILTON AIR FORCE BASE

UNDRAINED SHEAR STRENGTH (PSF)

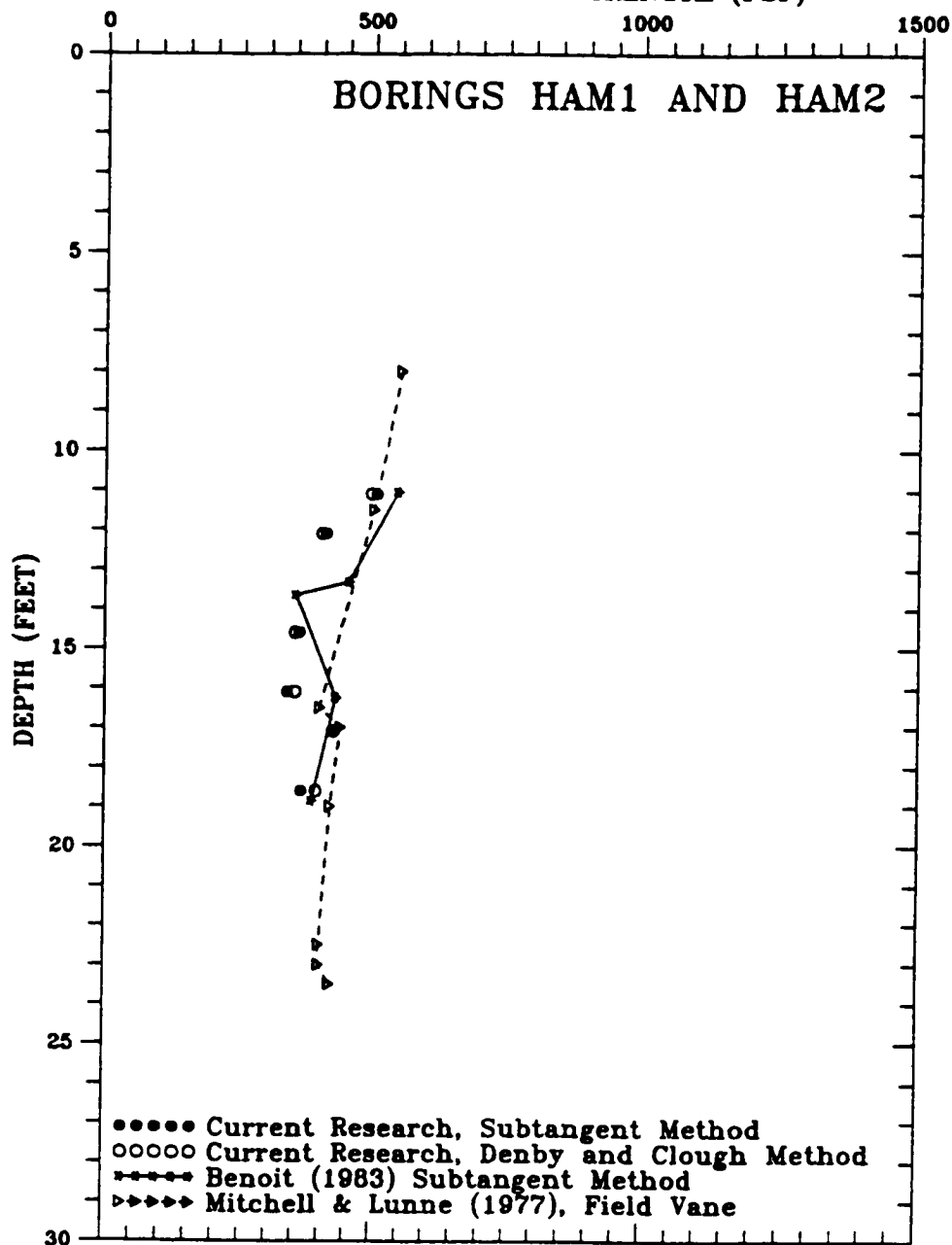


Figure 7-14 Sub-Tangent and Denby and Clough Method SBPM Shear Strength at Hamilton AFB

to underestimate shear strength (e.g. slow strain rate, K_v greater than 1), this may indicate that violation of the plane strain assumption due to the limited length of the Cambridge probe does not seem to significantly affect SBPM shear strength measurement in the Hamilton AFB Bay Mud.

In consideration of the fairly good agreement of the uncorrected SBPM data with the field vane results, it is interesting to note that the failure strain of CU triaxial tests conducted on the material have been reported (Bonaparte and Mitchell, 1979) to range from about 1.8 to 3.2 percent. Also, SBPM stress-strain curves for the current research derived by the sub-tangent method suggest shear failure generally occurs at a radial strain of 2 percent or more. This lends credence to strain at failure being related to whether "strength paradox" is observed or not. This also suggests that peak strength of Bay Mud seems to be a result of frictional rather than cohesive strength mechanisms, which seems to be the reverse of the soft silty clay at Pease AFB.

7.3.3.2 Push-In and Re-Expansion Results - One push-in and one re-expansion test were conducted at Hamilton AFB. For the push-in test, the probe was inserted open-ended. The push-in test indicated undrained shear strength values which were generally less than the uncorrected field vane data. The uncorrected Gibson and Anderson strength values are presented on Figure 7-13 and range from 0 to 70 percent lower than the uncorrected vane data. Also included on the figure is a test with push-in disturbance due to inefficient jetting which resulted in a similar range of shear strengths. The shear strength indicated by the average of all of the arms for the push-in test and the test found to be subject to push-in disturbance seem to be consistent in magnitude with the results from undisturbed tests. This was a finding similar to that at Pease AFB. However, this finding seems to be the reverse of the findings of Benoit (1983), who found that inefficient cutting seemed to cause an increase in the measured SBPM shear strength. One possibility for this may have to do with the fact that significant excess pore pressure due

to insertion was present during expansion of the push-in tests conducted for this research due to the relatively shorter dissipation periods observed compared to Benoit (1983). The higher pore pressures would be expected to reduce strength.

A re-expansion test is also depicted on Figure 7-13. As seen at Pease AFB, the undrained shear strength resulting from a re-expansion pressuremeter curve was up to several hundred percent higher than the undisturbed test conducted at the same depth.

7.3.3.3 Ménard Method at Hamilton AFB - The Ménard (1956) "N" value was determined for the current research for all the undisturbed middle strain arm pressuremeter curves. "N" was found to be about 3.2 ± 0.6 . This was slightly smaller than that found by Benoit (1983), which was 4.3 ± 0.5 . This difference is likely due to the difference between the pressuremeter curve indicated by the electronic average used by Benoit (1983) and the individual strain arm curves used for the current research.

7.4 Shear Modulus

The method for determining the elastic shear modulus has been discussed in Chapter II. For the current research, both the initial (G_i) and the unload/reload (G_w) moduli were calculated. The initial shear modulus was determined by the Denby and Clough (1978) method. The unload/reload modulus was assessed by graphical enlargement of the unload/reload loop of the pressuremeter curve. Such enlargement allows all individual data points to be considered in the assessment of G_w .

7.4.1 Shear Modulus at Pease AFB K_0 Area

Figure 7-15 presents a profile of the unload/reload modulus, G_w , at SBPM boring PMC4, located within the K_0 area. The profile seems to generally follow the stress history of the deposit. The modulus was found to be about 200,000 psf in the stiff upper crust of the clay deposit, and generally between 100,000 and 200,000 psf in the softer, lower clay. Another observation that can be made is that the lowest value of the modulus at a given depth seems to consistently be indicated

PEASE AIR FORCE BASE
 MEASURED SHEAR MODULUS - K₀ TEST AREA
 UNLOAD/RELOAD SHEAR MODULUS, G_{ur} (PSF)

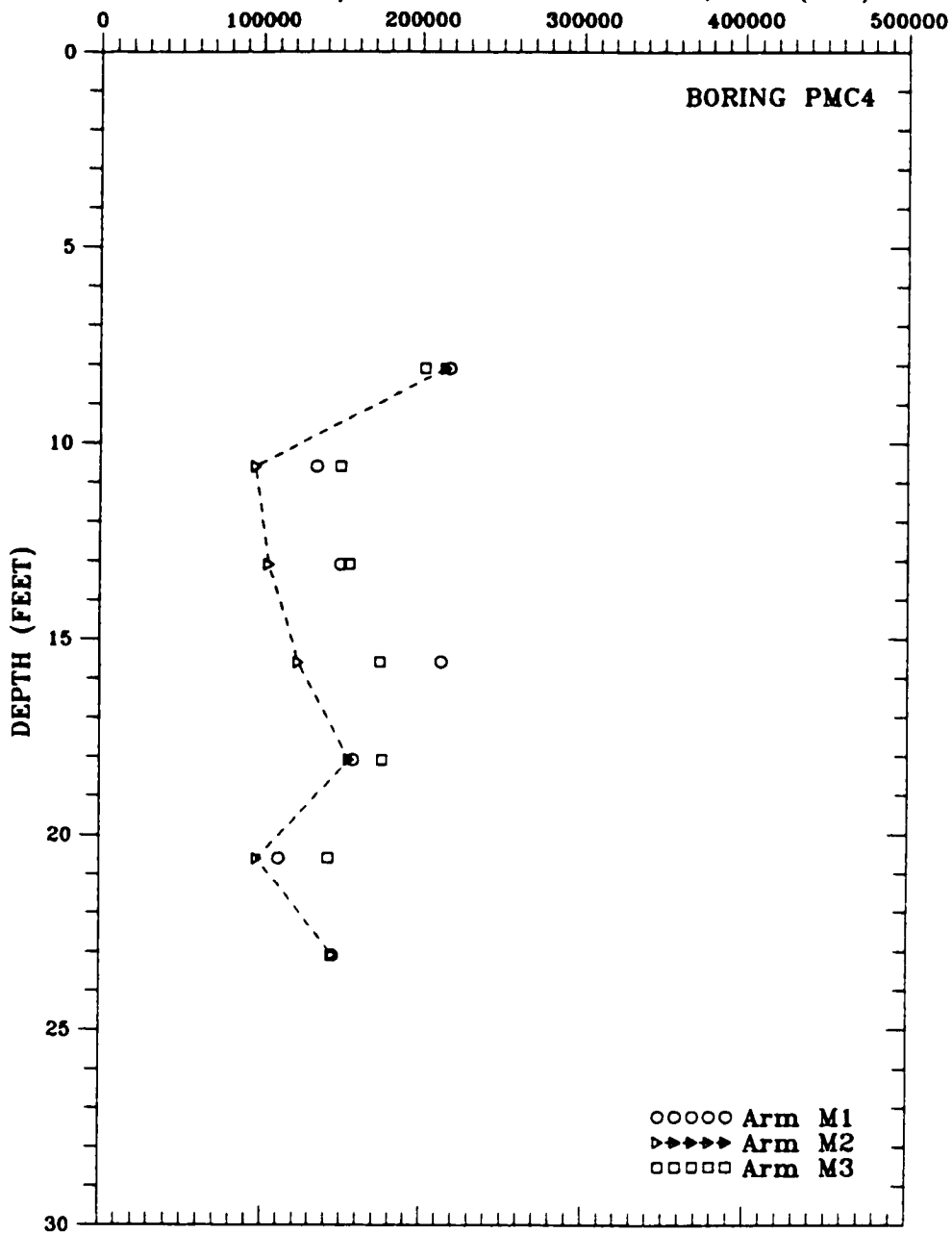


Figure 7-15 Unload/Reload Modulus Profile at Pease K₀ Area

by strain arm M2. The value indicated by M2 is up to 30 percent less than the shear modulus indicated by the other two arms. This may indicate that anisotropy with respect to the shear modulus may exist in a K_0 condition. It could also be a result of uncalibrated friction in the Cambridge SBPM strain arm system similar to that noted by Fahey and Jewell (1990).

Wroth (1982) has indicated that shear modulus in saturated clays would likely increase with increasing strain at which the unload-reload cycle commences due to partial drainage and thus consolidation during the test. The amount of drainage that occurs during a test can not be quantified, so this effect can not be corrected. However, another factor with respect to conventional data analysis likely has a compensating effect. Mair and Wood (1987) indicate that the unload/reload modulus is defined by:

$$G_w = 1/2(p/p_0)(dp/d\epsilon) \quad (\text{Eq 7-2})$$

where: p = expansion pressure at which the unload/reload cycle is initiated
 p_0 = horizontal stress
 $dp/d\epsilon$ = slope of the unload/reload loop

Mair and Wood (1987) indicate that the p/p_0 term is typically neglected in practice because at small radial strains, p/p_0 is nearly equal to 1. However, at large radial strains, the term becomes greater than 1, (potentially up to 2 or more at strains of 10 percent) and negligence can result in an apparent value which is smaller than actual value of G_w . In an attempt to assess the effects of drainage during testing and negligence of the p/p_0 term, Figure 7-16 presents a plot of the data from PMC4 with and without the p/p_0 term as a function of strain at unloading. As can be seen, the data which includes the p/p_0 term shows a trend of increasing G_w with strain, indicating that Wroth's alleged drainage during expansion likely is occurring, although significant scatter is

PEASE AIR FORCE BASE
 MEASURED SHEAR MODULUS - K₀ TEST AREA
 UNLOAD/RELOAD SHEAR MODULUS, Gur (PSF)

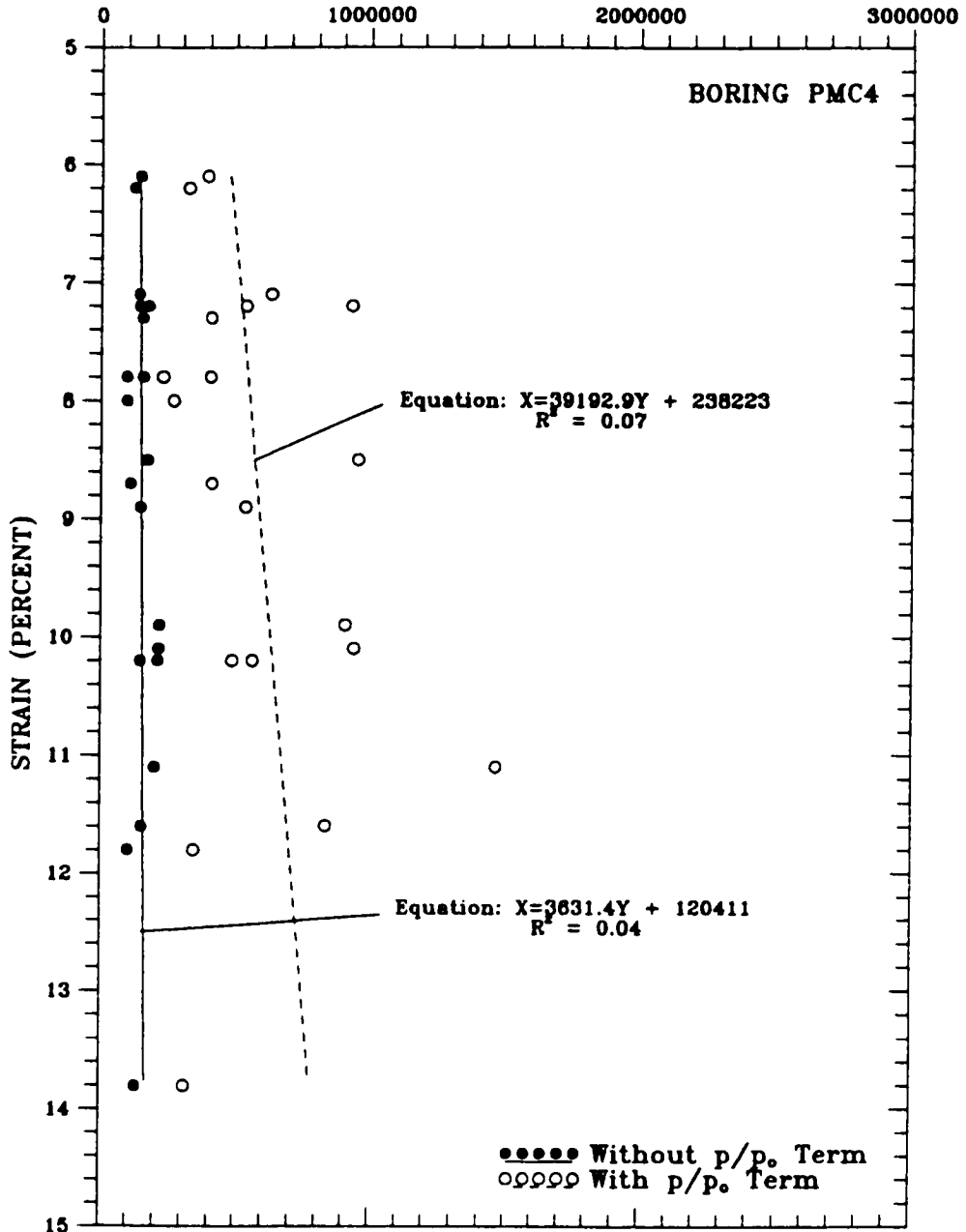


Figure 7-16 Unload/Reload Modulus Versus Radial Strain at Pease K₀ Area

noted. Also, the G_w including the p/p_o term is about 200 to 400 percent greater than that without the term, although it appears that both tend to converge at low strain. The scatter in G_w that includes the p/p_o term is likely the result of both varying drainage conditions (layering effects) and disturbance effects on the apparent value of p_o . Since the data on Figure 7-16 that does not include the p/p_o term shows essentially no trend with depth and significantly less scatter, it appears that drainage during expansion and failure to correct for p/p_o are fairly compensating effects. This may be the reason that neglecting both effects has been acceptable practice in previous SBPM work. The p/p_o term is neglected for the remainder of this discussion.

The pressuremeter curves from the current research indicate that the radial strain at which an unload/reload loop occurs for different arms on a particular tier of arms can be different. Differences of 4 or 5 percent were commonly observed, although some unload/reload loops occur at essentially the same radial strain on a particular arm tier. The left frame of Figure 7-17 presents a profile of the SBPM measured G_w from boring PMC4. Adjacent to each data point on the figure is a number which indicates the percent radial strain at which the unload/reload loop occurred. Review of this profile indicates that there seems to be no obvious trend of the magnitude of radial strain on the measured value of G_w . Similar G_w values resulted at radial strains of 6.1 to 13.8 percent, the range of strains at which unload/reload loops were conducted in PMC4. However, for the tests on the figure, there seems to be a trend where greater unload/reload strain differences tend to result in greater shear modulus scatter. To investigate this further, the right frame of Figure 7-17 is a plot of the difference between the radial strains at which an unload/reload loop occurs in a particular test versus the range in the resulting values of G_w . This plot includes only the soft clay data from the K_o area (below about 10 foot depth), and does not include push-in, wash-boring or re-expansion data. Although there is some scatter, the

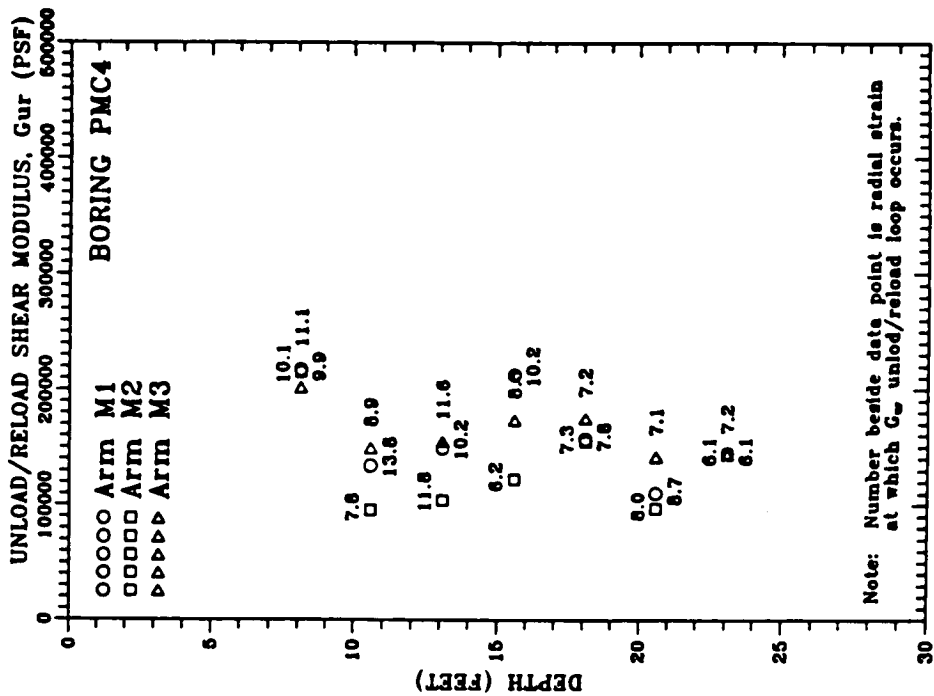
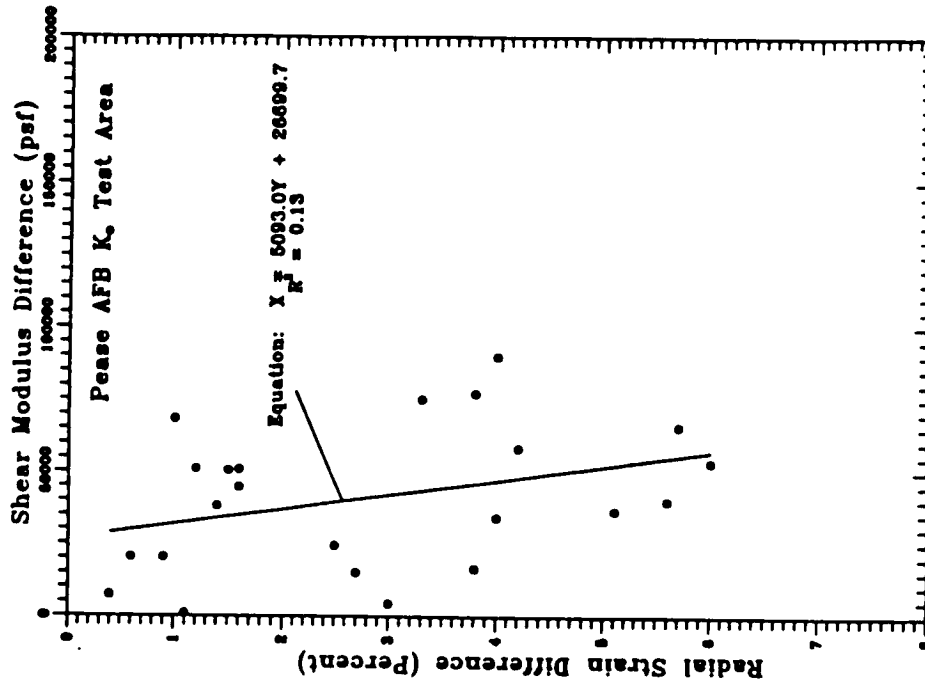


Figure 7-17 Effect of Radial Strain at Which G_{ur} is Determined Within a Particular Test

best-fit line on the figure indicates a trend of increasing difference between the maximum and minimum G_w with increasing difference between the minimum and maximum radial strain at which the unload/reload loop occur. This indicates non-radial strains may induce error into the measurement of shear modulus. The reason for this is not clear, but concentric radial strain during SBPM shear is one of the basic assumptions in theoretical analysis of pressuremeter cavity expansion. Figure 7-18 presents unload/reload shear modulus values for push-in and re-expansion tests as well as the shear modulus values from the undisturbed tests at the K_0 area. As can be seen, the push-in tests yield modulus values which are generally 10 to 80 percent below the best-fit of the undisturbed test values. The reason for this may be due to the fact that extremely high initial excess pore pressure results from push-in insertion (up to 1800 psf observed). This excess pore pressure causes a temporary reduction in soil strength that potentially persists into the expansion test phase because of the relatively short dissipation period observed during the current research. This reduction in strength likely allows plastic strains to occur during the unload/reload loop, resulting in a flatter average slope to the loop and thus lower G_w . Had the excess pore pressure been allowed to dissipate prior to push-in expansion, it may be that the G_w measured may have been similar to or greater than that of an undisturbed test.

Re-expansion tests, which are also indicated on the left frame of Figure 7-18, are tests conducted within a zone of soil which has already been sheared. G_w from re-expansion tests seem to be on the high side of the range of values from undisturbed tests, probably a result of strength increase due to consolidation that likely occurred when the soil zone was originally sheared.

The right frame of Figure 7-18 presents the G_w data from all of the undisturbed tests at the K_0 area plotted against the radial strain at which the unload/reload loop was performed. The data from undisturbed tests do not seem to show any significant trend with increasing strain,

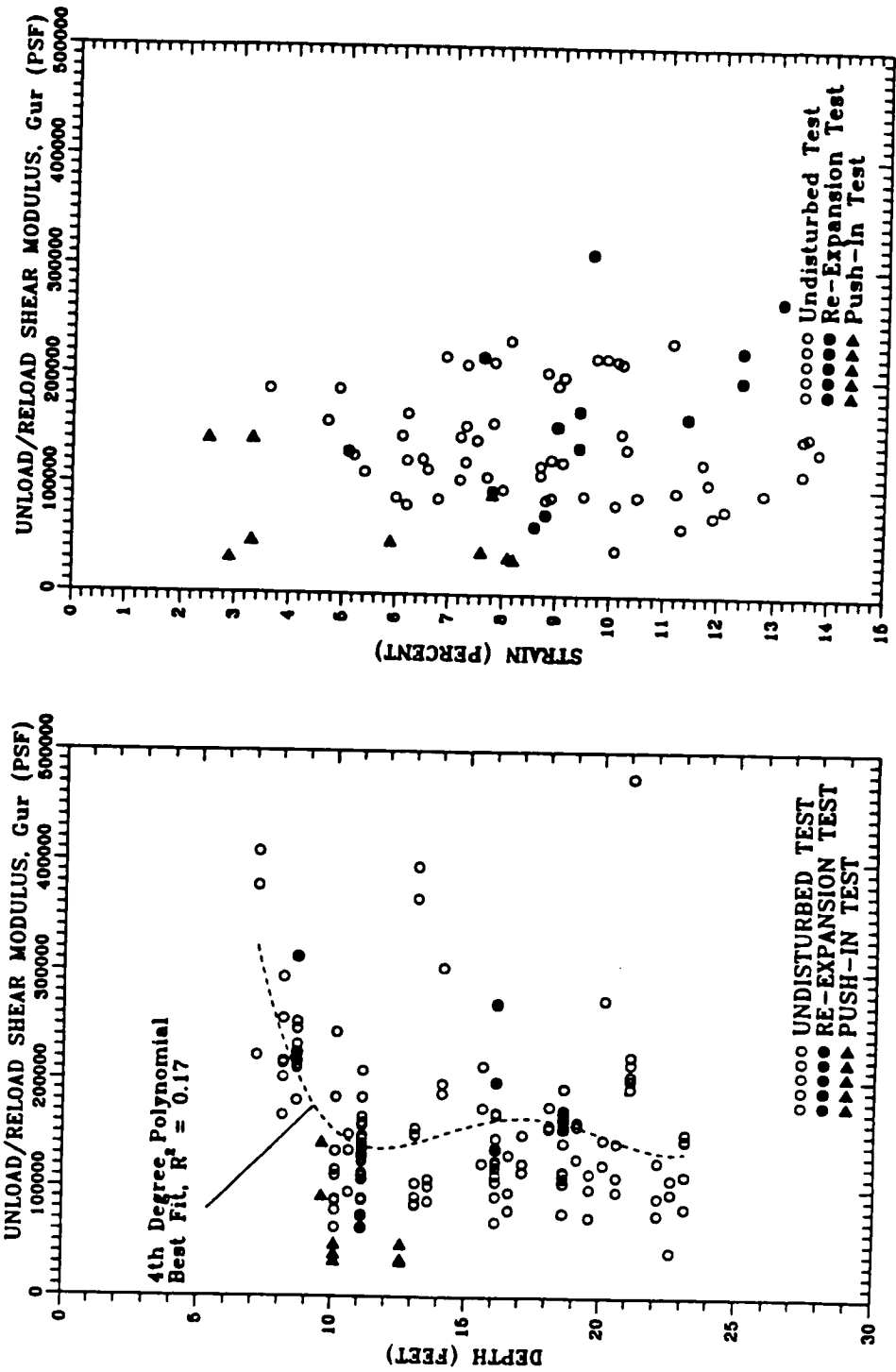


Figure 7-18 G_{ur} From All Borings at Pease K_0 Area

likely due to the compensating effects of drainage and negligence of p/p_0 as discussed previously. Interestingly, the re-expansion data seems to indicate increasing shear modulus with strain. This could be an effect of drainage and consolidation occurring in increasing amounts at increasing radial strain. The effect might occur at a faster rate in re-expansion than in an undisturbed tests for a similar reason that unload/reload in a consolidation test results in a larger c_v than does virgin compression. A larger c_v implies larger hydraulic conductivity, and thus faster dissipation of excess pore pressures during the assumed undrained expansion. Push-in tests do not seem to indicate any significant trend in G_u versus radial strain on the right frame of Figure 7-18.

Figure 7-19 presents a profile of the Denby and Clough method initial shear modulus values from PMC4. Also included on the figure are the G_u values from undisturbed tests for comparison. On average, it can be seen that G_i tends to be slightly greater than G_u , although there is some overlap. G_i is determined at low strain and would be expected to be larger than G_u .

As a basis of comparison for the SBPM G_i measured at the K_0 test area, it is interesting to consider the results of previous research near the Pease test site. Ladd (1972) reported undrained E_u/s_u values extrapolated from CK_U' shear tests on the order of 865 to 1950 between depths of 5 to 25 feet, where E_u represents the initial undrained Young's Modulus. Ladd (1972) also indicated that based on the results of the test embankment constructed near the test area, E_u/s_u was estimated to be on the order of 2000. Assuming elastic behavior, if Poisson's ratio is assumed to be 0.5, then 1/3 of Young' modulus is equal to the shear modulus. Based on this, SBPM G_i divided by the uncorrected field vane shear strength can be multiplied by 3 to obtain SBPM E_u/s_u . Considering average measured G_i values in SBPM boring PMC4, SBPM E_u/s_u was computed to range from 999 to 2000 between 5 and 25 foot depth, or about equal to

PEASE AIR FORCE BASE
 MEASURED SHEAR MODULUS - K₀ TEST AREA
 SHEAR MODULUS, (PSF)

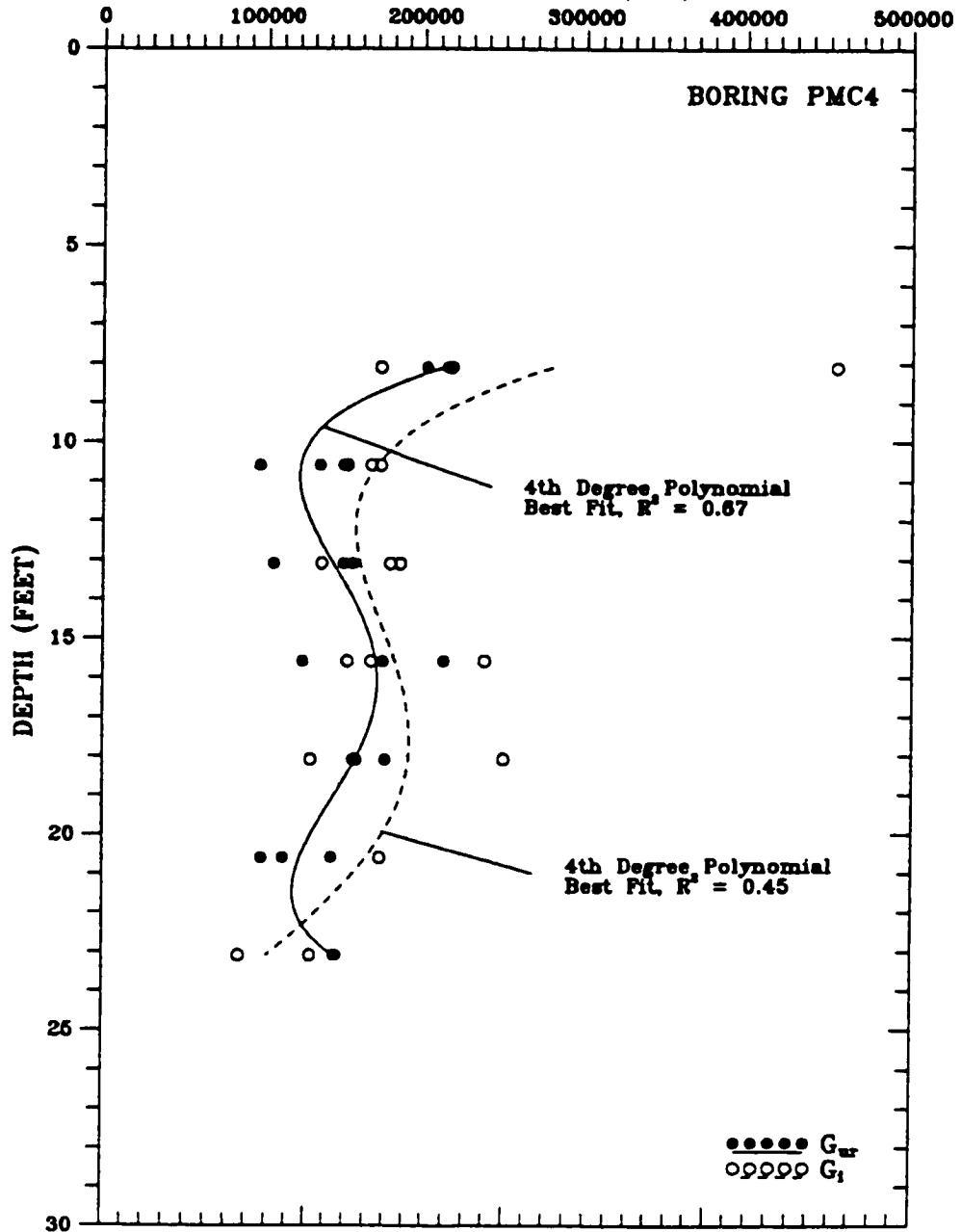


Figure 7-19 Profile of G₁ and G_{cr} at Pease K₀ Area

that indicated by Ladd based on laboratory and field data. This indicates that SBPM G_i measurements may be in general agreement with high quality laboratory test results and field observations.

7.4.2 Shear Modulus at Pease AFB Embankment Toe

At the embankment toe, above a depth of about 12 feet, the left frame of Figure 7-20 indicates an unload-reload modulus on the order of 200,000 psf in the stiff clay crust, and decreasing to about 100,000 psf at a depth of about 12 feet and below. The values of the modulus at a given depth are generally less than those observed at the K_0 area by about 15 to 50 percent.

The left frame of Figure 7-20 indicates that there is no apparent difference in the measured value of G_w at PMJ6 and PMJ7/PMJ8. This suggests that the embankment construction seems to have had little effect on the magnitude of G_w . Further, the differences in shear modulus between the borings near the embankment toe and the K_0 area may be due more to differences in moisture content and depositional history rather than the effects of the embankment construction, as has been discussed earlier with respect to vane shear strength.

Unload-reload modulus versus strain at which the unload-reload cycle is performed is plotted on the right frame of Figure 7-20 for borings PMJ6 and PMJ7/PMJ8. In general, the data does not seem to indicate any significant trends with strain. Also, both the results from PMJ6 and PMJ7/PMJ8 seem to yield similar results.

Denby and Clough initial shear modulus values, G_i , interpreted from the toe data are plotted versus depth on Figure 7-21. Also included on the plot are values of G_w . The value of the initial modulus is about the same as or up to 30 percent greater than the unload-reload modulus. This finding is similar to that at the K_0 area.

7.4.3 Shear Modulus at Hamilton AFB

The left frame of Figure 7-22 presents a profile of G_w with depth determined for the current research at Hamilton AFB. A trend of

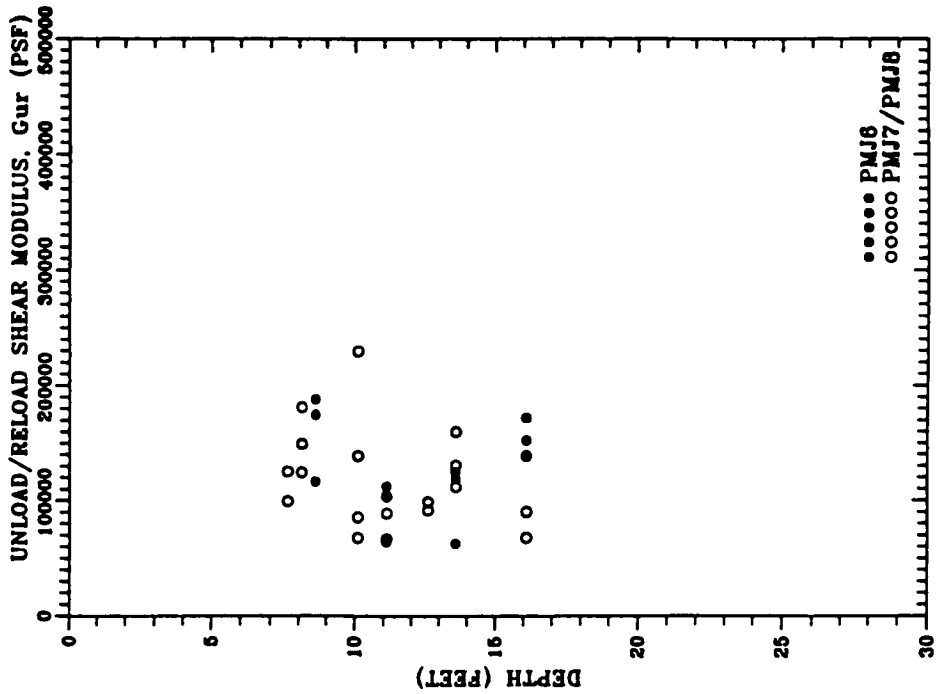
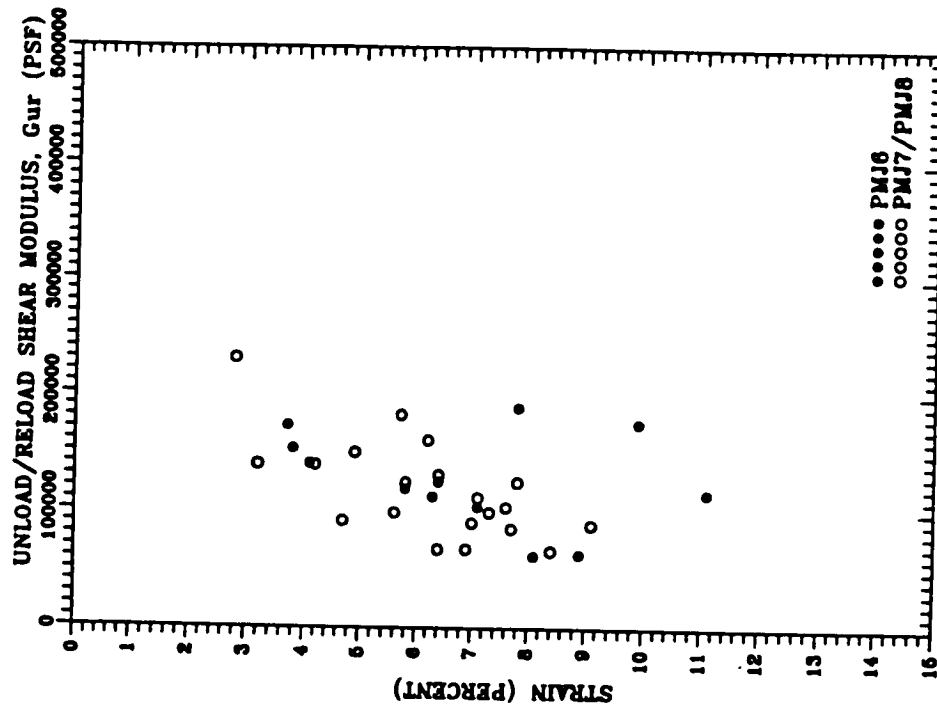


Figure 7-20 G_{ur} at Pease Embankment Toe Area

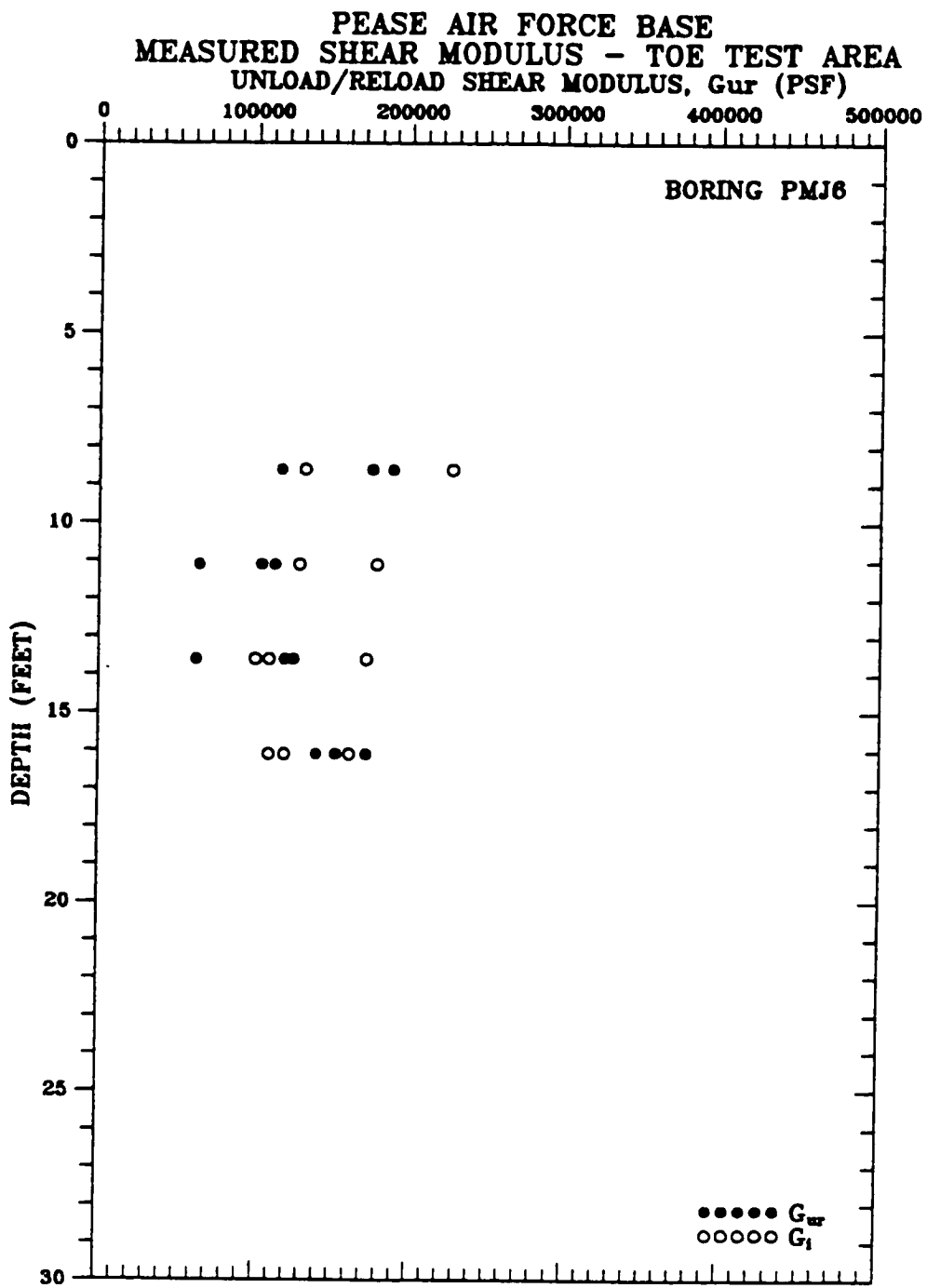


Figure 7-21 Profile of G_1 and G_{ur} at Pease Embankment Toe Area

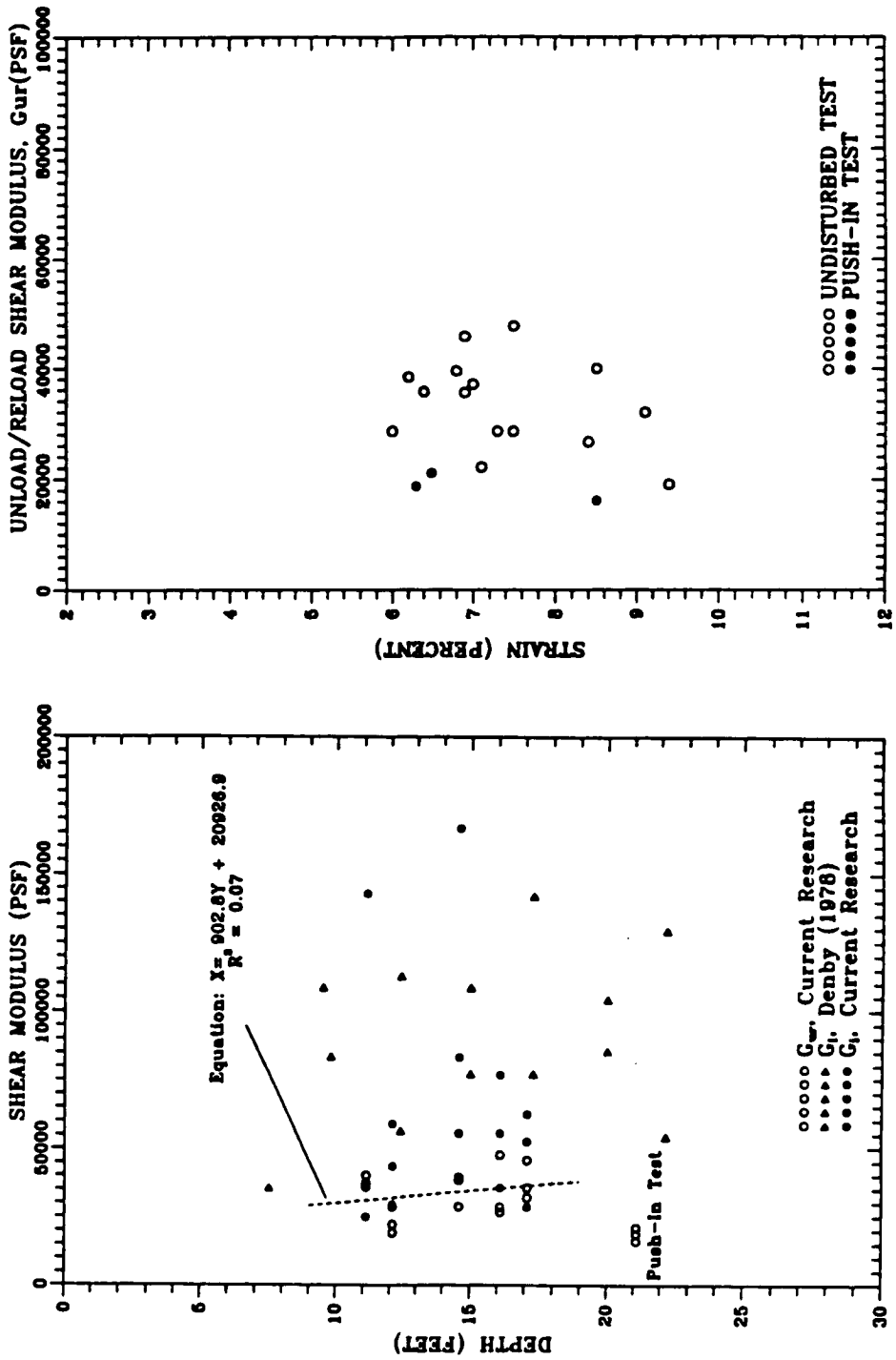


Figure 7-22 Shear Modulus at Hamilton AFB

increasing shear modulus with depth can be seen, which follows the general trend of the vane shear strength profile for the site. The measured value of G_w at Hamilton AFB is about 30,000 psf plus or minus about 10,000 psf. Benoit (1983) conducted unload/reload loops in a few SBPM tests. The slope of these loops indicated a shear modulus of about 54,000 to 107,000 psf. This is at least 100 percent greater than measured for the current research. However, Benoit conducted his tests with unload/reload loops at a depths of at least 40 feet, which was about twice as deep as the tests conducted for the current research. The larger modulus values might be anticipated based on the observation that shear modulus seems to increase with depth at the Hamilton AFB site. They might also be larger due to the consolidation effects of Benoit's (1983) longer dissipation periods prior to testing which would result in less plastic strain and thus higher G_w .

The right frame of Figure 7-22 includes a plot of the G_w data plotted against the radial strain at which it was measured. The figure indicates no particular trend with radial strain, which is consistent with the findings at the Pease K₁ area, and indicates that the effects of drainage during expansion on G_w were likely compensated by neglecting the p/p_0 ratio in Equation 7-2 at Hamilton AFB. Figure 7-22 includes the results from a push-in test. As can be seen, push-in disturbance tends to cause the shear modulus to be smaller than corresponding undisturbed tests by an average of about 50 percent, a finding that was similar to the finding at Pease AFB.

The left frame of Figure 7-22 presents the results of the initial shear modulus determined by the Denby and Clough reduction method for the current research, as well as that determined by Denby (1978). Both sets of data exhibit considerable scatter compared to the G_w data, and are observed to range from about 30,000 to 170,000 psf. This is up to about 5 times greater than the G_w measured values, although the lower values of G_i are consistent in magnitude with the G_w profile.

7.5 R_f by Denby and Clough Method

As described in Chapter II, the failure ratio, R_f , is a curve fitting parameter used in the hyperbolic constitutive model described by Duncan and Chang (1970) which is used in many FEM methods. In this research, the failure ratio was determined by the Denby and Clough shear strength method.

From laboratory tests conducted during this research program, R_f at Pease AFB for the soft silty clay was found to be about 0.79 ± 0.09 . Denby (1978) indicated that R_f for San Francisco Bay Mud was on the order of 0.85 to 0.95. Wong and Duncan (1974) indicate that R_f for soft plastic clays would typically be expected to be around 0.9, with a value of 0.6 for more overconsolidated materials. Denby (1978) indicated that R_f could be used as a measure of disturbance in soft, normally consolidated clays such as San Francisco Bay Mud; a low R_f would be indicative of disturbance.

R_f values determined at the Pease and Hamilton AFB sites from SBPM data using the Denby and Clough method are plotted with depth on Figure 7-23 for the Pease K_0 , Pease embankment toe and Hamilton AFB sites. SBPM determined R_f at the Pease K_0 area generally range from 0.4 to 0.75, with an average value of 0.52 ± 0.24 . The upper range of the SBPM data seems to be in agreement with the findings of the triaxial shear tests conducted for this research. However, the average SBPM value of R_f at the K_0 area is less than the triaxial shear data suggests. The reason the SBPM R_f value was significantly lower than that determined by laboratory testing is not clear; however, because the shape of the expansion curve has a major impact on both SBPM determined shear strength and R_f , it is likely that the "strength paradox" that seems to affect the K_0 area shear strengths also causes under-estimation of R_f .

At the Pease embankment toe site, the magnitude of R_f was about 20 percent less than that observed at the K_0 area, and R_f at PMJ6 was

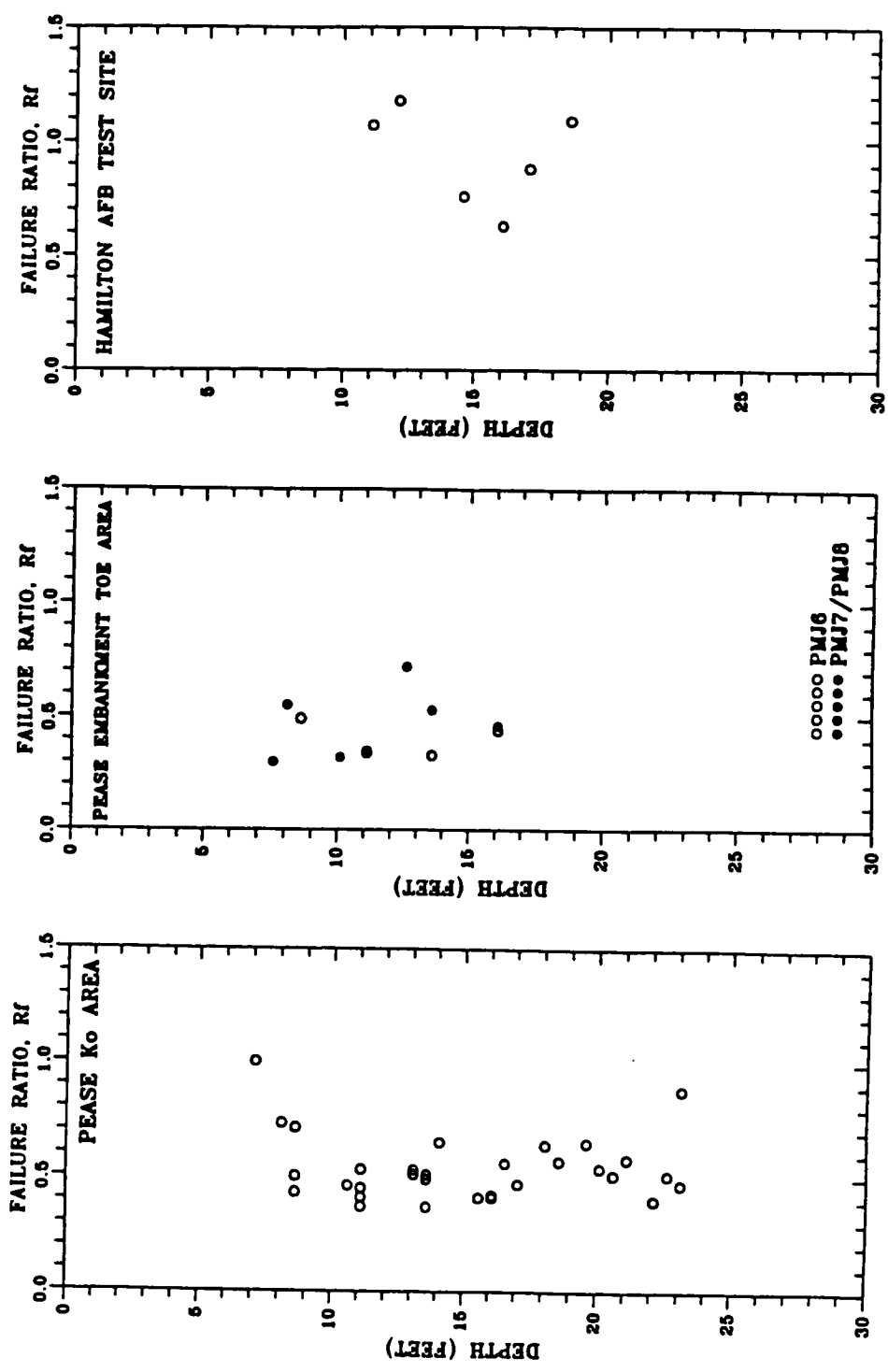


Figure 7-23 R_f Profiles at Current Research Test Sites

generally less than R_f at PMJ7/PMJ8. This may be an effect of the high ratio of horizontal to vertical effective stress at the embankment which has been shown to affect shear strength values.

At Hamilton AFB, the value of R_f measured by SBPM tests for the current research was 0.94 ± 0.39 . This value is similar to that measured by Denby (0.7 to 0.95), and is in the range predicted by CU triaxial tests (0.85 to 0.95). The relatively good agreement between the values of R_f measured by the SBPM and CU triaxial tests at Hamilton AFB further supports the relationship of strain at failure to the ability of the SBPM to measure shear strength parameters.

7.6 Skempton "A" Parameter at Failure

The Skempton (1954) "A" parameter at failure, A_f , is useful in predicting pore pressures which might occur when soil begins to yield. Assuming the polar coordinates of the SBPM, excess pore pressure due to shear can be predicted by Skempton's equation:

$$\Delta u = B \Delta \sigma_v + A(\Delta \sigma_s - \Delta \sigma_v) \quad (\text{Eq 7-3})$$

Further assuming saturation ($B=1$) for the condition at failure, the equation reduces to:

$$A_f = (\Delta u - \Delta \sigma_v) / (\Delta \sigma_s - \Delta \sigma_v) \quad (\text{Eq 7-4})$$

Previously at Hamilton AFB, Denby (1978) measured A_f of about 0.3 from SBPM tests. Benoit (1984) measured a range of from -0.08 to 0.52, but generally between 0.2 and 0.4. These values were significantly below those measured by CU triaxial tests on Bay Mud, which were generally above 0.5. Benoit (1983) references cubic shear tests by Sinram (1982) which simulated the stress path of the SBPM test, and yielded A_f values of about 0.44, closer to the A_f of the SBPM, and indicating A_f is likely stress path dependent. At Pease AFB, A_f indicated by CU triaxial tests

for the current research and the previous embankment construction ranged from 0.69 to 1.25.

A_v values measured by the SBPM during the current research at the Pease and Hamilton AFB sites from undisturbed tests from borings PMC4, PMJ6 and HAM1 are summarized on Table 7-1. The data indicates that SBPM A_v at Hamilton AFB was 0.49 ± 0.16 , which is in general agreement with the range previously measured with the SBPM by Denby (1978) and Benoit (1984). SBPM A_v at Pease AFB K_0 area was 0.55 ± 0.16 , which was generally less than that indicated by the CU triaxial tests. The trend of SBPM A_v being less than that from CU triaxial tests is similar to that observed at Hamilton AFB. At the Pease embankment toe area, SBPM A_v was found to be 0.37 ± 0.09 . A T-test with pooled standard deviation was conducted to see if there was a statistical difference between the SBPM A_v values measured at the toe and the K_0 Area. A level of significance of 0.5% was assumed for determination of the critical value of T. The results of the test indicate that there is no evidence that the mean value of A_v from the K_0 area and the embankment toe are from the same population. This difference in A_v suggests the high horizontal to vertical effective stress ratio at the embankment toe affects A_v . This is likely a result of the fact that A_v is determined from data derived by an analysis assuming elasto-plastic behavior (sub-tangent method). It was shown previously in this chapter that the ratio of the effective horizontal to vertical stress at the embankment toe area was outside of the range of values where elasto-plastic soil response would be expected.

7.7 Consolidation Parameters

The SBPM can be used to determine the horizontal coefficient of consolidation, c_h . Clarke, et al. (1979) and Benoit and Clough (1986) have indicated that the SBPM c_h values tend to be higher than those measured vertically by one-dimensional consolidation tests, and may be more consistent with field performance.

Eight holding tests were performed at Pease AFB. For most of the

BORING	STRAIN ARM	DEPTH (feet)	A _f
PMC4.2	M1	10.6	0.42
	M2	10.6	0.43
PMC4.3	M1	13.1	0.61
PMC4.4	M1	15.6	0.46
	M2	15.6	0.75
PMC4.5	M1	18.1	0.38
	M2	18.1	0.41
PMC4.6	M2	20.6	0.83
PMC4.7	M1	23.1	0.50
	M2	23.1	0.74
PMJ6.1	M1	8.6	0.26
	M2	8.6	0.20
	M3	8.6	0.27
PMJ6.2	M1	11.1	0.40
	M2	11.1	0.34
	M3	11.1	0.38
PMJ6.3	M1	13.6	0.42
	M2	13.6	0.34
	M3	13.6	0.35
PMJ6.4H	M1	16.1	0.51
	M2	16.1	0.45
	M3	16.1	0.49
HAM1.1	M1	12.1	0.66
	M2	12.1	0.62
	M3	12.1	0.54
HAM1.2	M1	14.6	0.36
	M3	14.6	0.23
HAM1.3	M1	17.1	0.57
	M2	17.1	0.32
	M3	17.1	0.65

Table 7-1 Summary of Computed SBPM A_f Values

tests, only effective stress cell PPB was functioning properly. In two of the tests, PPA was working because the experimental high-air entry porcelain stone was replaced with a conventional brass stone. Table 7-2 is a summary of the tests performed at Pease AFB. Plots of the dissipation of excess pore pressure versus time from the hold tests are included in Appendix C. The intermittent zero pore pressure values at the early time portions of some of the plots in the appendix are a result of the fact that the version of SOSAP used to reduce the data forced a zero value of pore pressure if strain arm M1 had not moved. Noise in the M1 output caused the program to intermittently print the actual non-zero values of pore pressure. The results of one holding test, test PMC3.2 are presented on Figure 7-24, and include plots of radial strain, total stress and excess pore pressure with time.

As was previously discussed, an estimate of field c_v is available as a result of the previous work of Ladd (1972) and Ladd, et al. (1972) from observation of sand drain/settlement performance during construction of the Portsmouth I-95 Interchange. These researchers concluded that actual field c_v was about 0.27 ± 0.03 ft²/day, and that c_v was likely about 1.5 to 2.0 times greater than c_v measured in the laboratory.

The current research included performance of 29 consolidation tests on undisturbed samples of the Pease silty clay. The test samples were oriented with the axis of compression both vertical and horizontal to determine both c_v and c_h . As was discussed in Chapter IV, a ratio of c_h to c_v of about 1.0 was observed based on the results of consolidation tests, indicating a fairly isotropic silty clay. The macro effects of major sand/silt layers, however, are not represented by the relatively small samples used for standard consolidation tests which consisted of fairly homogeneous silty clay, and it is believed that the ratio of about 2 to 1 suggested by Ladd is more appropriate. Values of c_v and c_h vary from about 0.1 ft²/day for virgin loading to about 1.0 ft²/day for unload/reload.

Table 7-2 presents a summary of the c_v values determined at Pease

SUMMARY OF SBPM HORIZONTAL COEFFICIENT OF CONSOLIDATION VALUES									
Test Designation	Depth (Feet)	G, SBPM (psf)	Su, SBPM (psf)	Radial Strain Held (in/in)	Umax measured (psf)	Umax estimated (Eq 2-34) (psf)	160 (Mln)	SBPM T60	SBPM ch (in/day)
PMC3.2H PPB	11.1	99117	457	0.085	1580	1593	74	1.36	0.66
PMC3.3H PPB	13.6	121735	554	0.099	2120	2012	23.5	1.82	2.40
PMC3.4H PPB	16.1	168855	569	0.136	4680	2391	28.5	19.87	23.04
PMC3.5H PPB	18.6	98739	514	0.125	4900	1900	25	35.08	45.46
PMC3.6H PPB	21.1	211488	727	0.109	4500	2905	28	7.40	8.32
PMJ4.6H PPB	23.1	335915	1035	0.072	2545	3872	18.5	0.64	1.02
PMJ6.4H PPA	16.1	153101	534	0.061	1315	1851	39	0.64	0.47
PMJ6.4H PPB	16.1	153101	534	0.061	1860	1851	29	1.43	1.42
PMJ8.3H PPA	13.6	98849	493	0.092	2200	1714	16.5	2.76	5.11

Table 7-2 Summary of SBPM C_h Measurements

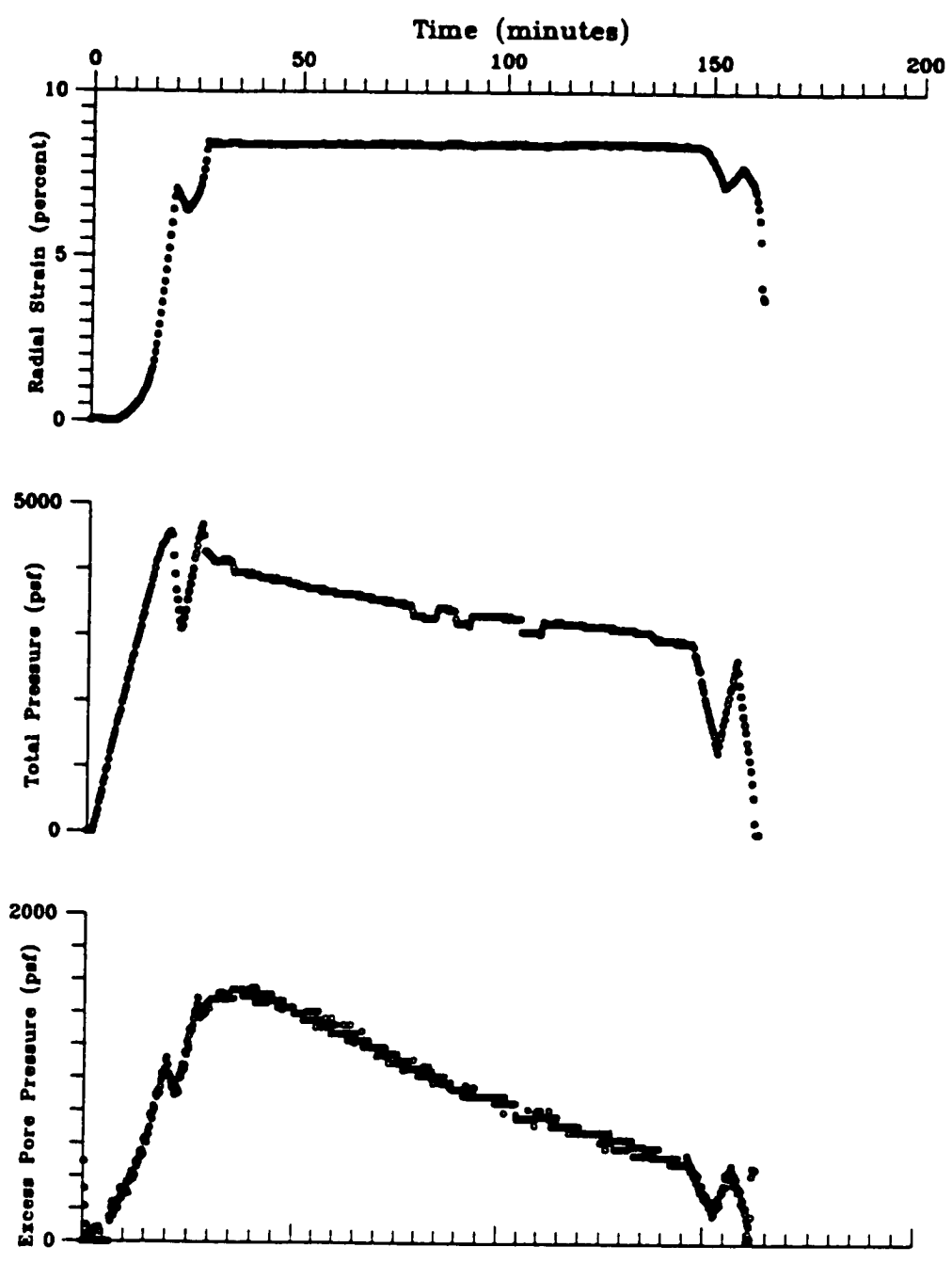


Figure 7-24 Results of Holding Test PMC3.2H

AFB by the SBPM holding tests using Equation 2-35. These values were computed using s_u and G_u determined from the pressuremeter curve prior to the holding portion of the SBPM test, as recommended by Clarke, et al. (1979). As can be seen on the table, the SBPM computed c_v values for tests PMC3.4H, PMC3.5H and PMC3.6H are significantly higher than measured by the other holding tests. Examination of the dilatometer I_p profile made adjacent to boring PMC3 (Figure 4-8) indicates some significant silt layers are present in the depth range of these three tests. Silt typically has a hydraulic conductivity that is an order of magnitude or more greater than clay, and would allow faster dissipation of excess pore pressures, resulting in higher c_v .

Considering only the tests that appear to have been conducted in homogenous clay, absent of significant drainage layers, the average value of c_v of the holding tests was 1.83 ± 1.75 ft²/day. This is roughly an order of magnitude larger than c_v and c_h for virgin loading indicated by the consolidation tests, and roughly equal to c_v and c_h during the unload/reload portions of the consolidation tests. The SBPM computed values of c_v indicated on Table 7-2 were determined using minimum Gibson and Anderson undrained shear strength values. These values were determined between 5 and 10 percent volumetric strain and have been corrected for probe shortness using the Yeung and Carter (1990) method (note that Clarke, et al. did not use such a correction). If uncorrected vane shear strength values are used instead of the SBPM shear strength values described, c_v is significantly less consistent and increased by 60 to 800 percent. In agreement with the recommendation of Clarke, et al., it appears that SBPM determined values of s_u should be used rather than field vane values.

Figure 7-25 is a profile of the Table 7-2 measured c_v values in homogeneous clay plotted with depth. Included on the plot are the results of Nejame (1991) from dilatometer dissipation tests. The dilatometer data was analyzed by Nejame using three different techniques

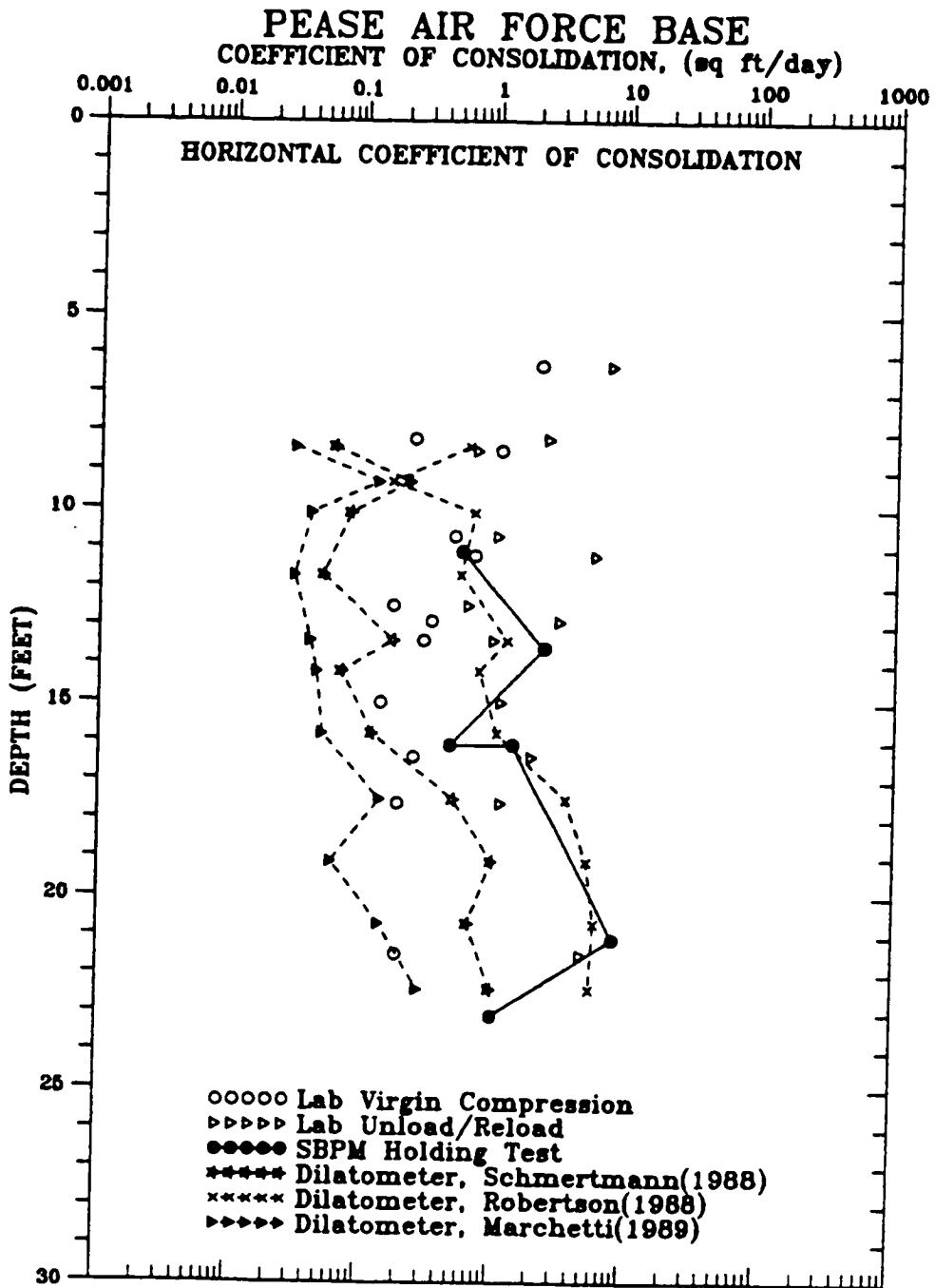


Figure 7-25 Profile of Horizontal Coefficient of Consolidation

which included Schmertmann (1988), Robertson, et al. (1988) and Marchetti and Totani (1989). As can be seen, the Marchetti, et al. and Schmertmann methods yield c_v values which are generally smaller than those indicated by virgin load consolidation results. The Robertson et. al. method seems to yield results which are generally consistent with those from the SBPM holding tests.

Ladd, et al. (1972) estimated field c_v based on settlement and piezometer observations of highway embankments constructed near the Pease AFB test site. As indicated in Chapter IV, Ladd, et al. (1972) measured laboratory c_v values which were about half of those measured by the current research. With this difference in c_v , a direct comparison between c_v estimated by the field observations of Ladd, et al. and those measured during the current research using the SBPM is not appropriate. However, a comparison of the trend in difference between the laboratory measured c_v compared to field c_v is of interest. Ladd, et al. (1972) reported a field estimated c_v of about 1.5 to 2 times their laboratory values of c_v . For the current research, the SBPM c_v was about 2 to 4 times the laboratory measured values of virgin loading c_v . This indicates the difference between the SBPM c_v and laboratory c_v is only slightly larger than the trend reported by Ladd, et al. (1972), and suggests that the SBPM can provide a reasonable measure of in situ c_v . Clarke, et al., (1978) indicate that a slight amount of drainage during membrane expansion (consolidation) may account for SBPM measured c_v values being larger than laboratory measured values, although soil layering effect are likely a more important factor.

7.8 Summary

With respect to shear strength determination method, that posed by Gibson and Anderson (1961) seems to yield the best results. Use of the method to analyze data between 5 and 10 percent volumetric strain (about 2.1 to 5.4 percent radial strain) seems to yield values of shear strength that are consistently the closest to the values of field vane shear

strength at Pease AFB, however, the difference is still large. At Hamilton AFB, all the SBPM methods used resulted in similar shear strength values. Comparisons were made between use of the average shear strength measured on all three middle strain arms versus use of the lowest values of shear strength. Which of these values work better varied between the two test sites. The minimum shear strength values were still about 120 percent larger than the vane shear strength at Pease AFB. At Hamilton AFB, the average values result in an SBPM shear strength about 0 to 15 percent less than field vane measured strength. Application of the Yeung and Carter correction for the limited length of the probe to the Gibson and Anderson shear strength values resulted in shear strengths from 10 to 100 percent larger than the vane shear strength at Pease AFB, which was an improved correlation over the uncorrected results. Application of this correction to the Hamilton AFB data would result in shear strength values that are less than the field vane values.

The SBPM appears to yield the most reasonable shear strength results in soils with triaxial axial strain at failure greater than about 1.5 to 2.0 percent, or greater than about 1 percent radial strain as indicated by the sub-tangent stress-strain curve. Clays with peak strength mobilized at relatively low strain seem to exhibit the so called "strength paradox" of higher apparent strength due to disturbance.

Another observation of the current research is that the increased horizontal stress at the highway embankment toe seems to have an impact on SBPM measured shear strength. SBPM shear strengths at the toe of the embankment were significantly less than that measured in a K_0 condition, likely a result of the fact that the ratio of horizontal to vertical stress was outside of the range where elasto-plastic behavior can be assumed.

The failure ratio, derived from SBPM data was found to be reasonable at Hamilton AFB and generally low at Pease AFB compared to CU triaxial results. Plots of stress paths from both sites indicates that

the soils at Pease and Hamilton AFB seem to generally follow an idealized elastic stress path prior to failure provided the soil tested is not disturbed. After failure, strain softening at Pease AFB is typically observed and strain hardening or pure plastic behavior was observed at Hamilton AFB. This suggests some deviation from the assumed elasto-plastic behavior of stress-strain analysis.

A_v was determined from the SBPM data. In general, SBPM A_v seems to be less than that indicated by conventional CU triaxial tests at Pease and Hamilton AFB. Benoit (1983) indicated that this was likely the case at Hamilton AFB due to the differing stress paths of SBPM and triaxial tests.

Shear modulus, both unload/reload (G_w) and initial (G_i) were computed from the SBPM data. SBPM G_i was found to be in reasonable agreement with the results of Ladd's (1972) E_v/s_v data, using uncorrected field vane shear strength and assuming a Poisson's ratio of 0.5 and elastic behavior to convert G_i to E_v . SBPM Shear modulus was generally found to follow the trend of shear strength with depth. Little trend was observed in plots of G_w versus radial strain at which G_w was determined, likely due to the compensating effects of drainage/consolidation during expansion and the generally accepted practice of neglecting the stress level. A trend of increasing scatter of G_w was observed when the difference in radial strain at which the unload/reload loop occurred between strain arms within a particular test increased. The cause of this is not clear, but may be an effect of membrane stiffness, mechanical and/or strain arm response.

A tendency for a particular arm in a boring to have the lowest G_w was also observed. This is similar to the findings of previous researchers with respect to horizontal stress. However, based on the previous observation pertaining to increased scatter due to non-radial strain, additional research is necessary to clarify if this finding has any potential application to determination of anisotropy in the

horizontal plane.

Several holding tests were conducted at Pease AFB and the results compared to laboratory consolidation tests, dilatometer dissipation tests, and field observations made previously with regard to sand drain performance during construction of the adjacent highway embankments. The SBPM holding tests seem to result in c_v values which may be slightly higher than actual field conditions, and about 2 to 4 times greater than laboratory measurements of c_v . The difference between the SBPM and laboratory values is only slightly greater than the field observations by Ladd, et al. (1972), indicating the SBPM may yield reasonable measurements of in situ c_v . SBPM c_v values seem to compare best to the Robertson dilatometer dissipation method, with the dilatometer methods of Schmertmann and Marchetti yielding c_v values at or below laboratory determined values.

CHAPTER VIII

FINDINGS SPECIFIC TO THE 9-ARM SBPM

8.1 Introduction

This chapter presents observations made with regard to test results from the 9-arm version of the SBPM used for this research which would not otherwise be available using the conventional 3-arm SBPM. These observations include, as will be subsequently discussed:

- o Trend of soil strength/stiffness with depth based on maximum radial strain occurring during a test,
- o Horizontal stress implied by the upper and lower arms in comparison with the middle arms,
- o Shear strength implied by the upper and lower arms in comparison with the middle arms,
- o Unload/reload shear modulus implied by the upper and lower arms in comparison with the middle arms, and
- o Validity of the plane strain and axisymmetric assumptions.

8.2 Trend of Soil Strength and Stiffness with Depth

During the research, it was observed that the difference in the maximum radial strain that occurred during a test between the upper, middle and lower strain arms had a general trend consistent with the shear strength profile of the soil deposit. This trend might intuitively be expected because soil elements under a given stress condition would be expected to strain increasing amounts with decreasing shear strength. To illustrate this observation, PMC4 is selected because this boring extends deeper than most other borings and has a high percentage of good quality expansion curves. The maximum radial strain for each strain measuring arm during expansion tests made in boring PMC4 are presented on Table 8-1. Also shown in the far right column on the table is the average maximum strain for each arm tier. This is the arithmetic average

BORING PMC4						
TEST	ARM TIER	DEPTH (feet)	MAXIMUM TEST STRAIN (%)			
			SIDE 1	SIDE 2	SIDE 3	AVERAGE
4.1	UPPER	7.7	9.5	10.2	8.9	9.5 ± 0.5
	MIDDLE	8.1	12.5	12.7	13.7	13.0 ± 0.5
	LOWER	8.5	14.1	12.5	18.0	13.3 ± 2.3
4.2	UPPER	10.2	12.0	10.1	7.4	9.8 ± 1.9
	MIDDLE	10.6	15.6	10.0	8.6	11.4 ± 3.0
	LOWER	11.0	16.3	9.0	15.1	13.5 ± 3.2
4.3	UPPER	12.7	13.8	13.8	18.0	13.8 ± 2.0
	MIDDLE	13.1	11.1	13.0	12.7	12.3 ± 0.8
	LOWER	13.5	12.2	18.0	11.1	11.7 ± 3.0
4.4	UPPER	15.2	14.3	10.7	9.6	11.5 ± 2.0
	MIDDLE	15.6	13.2	8.0	11.0	10.7 ± 2.1
	LOWER	16.0	10.2	7.2	8.9	8.8 ± 1.2
4.5	UPPER	17.7	10.2	12.6	10.0	10.9 ± 1.2
	MIDDLE	18.1	10.2	9.8	9.5	9.8 ± 0.3
	LOWER	18.5	10.7	9.4	9.1	9.7 ± 0.7
4.6	UPPER	20.2	6.8	7.3	7.6	7.2 ± 0.3
	MIDDLE	20.6	10.4	9.8	8.6	9.6 ± 0.7
	LOWER	21.0	12.9	10.7	11.4	11.7 ± 0.9
4.7	UPPER	22.7	8.4	9.9	12.0	10.1 ± 1.5
	MIDDLE	23.1	7.9	7.9	9.0	8.3 ± 0.5
	LOWER	23.5	12.2	18.0	13.2	12.7 ± 2.5

Table 8-1 Summary of Maximum Test Strains for PMC4

of the maximum strain occurring at each of the three strain feeler arms on the particular tier. As can be seen, the average maximum strain typically varies to some degree for each arm tier within a particular test. In general, the three tiers of arms monitored in each expansion test offer a means of assessing the trend of change in shear strength with depth. For example, if the maximum test strain is observed to be increasing from the upper arm tier to the lower arm tier, the soil deposit in the test zone would be expected to have a decreasing shear strength with depth. If the maximum test strain were decreasing from the upper arms to the lower arms, the shear strength would apparently be increasing with depth. If no maximum strain trend were observed, then the deposit in the test zone would have a constant strength with depth or possibly be at an inflection point in shear strength variation with depth. Figure 8-1 is a graphic illustration of the use of the maximum test strain trend to predict the trend of shear strength with depth. The left side of the figure presents the uncorrected field vane strength versus depth measured at the Pease K₂ test area. A line has been fitted through the data to indicate the trend of shear strength variation with depth. As can be seen, the soil profile is somewhat complex, with zones of decreasing and increasing shear strength dependent on stress history, desiccation, and possibly deposition period. On the right side of the figure, three horizontal lines have been drawn directly to the left of each test designation (PMC4.1, PMC4.2, etc.). The upper most line for each test represents the maximum average strain occurring in the upper tier of arms. The middle line represents the middle arm average, and the lower line the lower arm average. The relative length of the lines is indicative of the amount of total test strain that was observed at the respective arm tier. Within a particular test, the lines (upper, middle and lower) can be compared to assess the trend in the maximum test strain with depth. To the left of each test's three lines, a descriptor of the interpreted trend of shear strength with increasing depth, based on examination of the relative length of the lines, is given. Comparing

**PEASE AIR FORCE BASE
FIELD VANE UNDRAINED SHEAR STRENGTH**

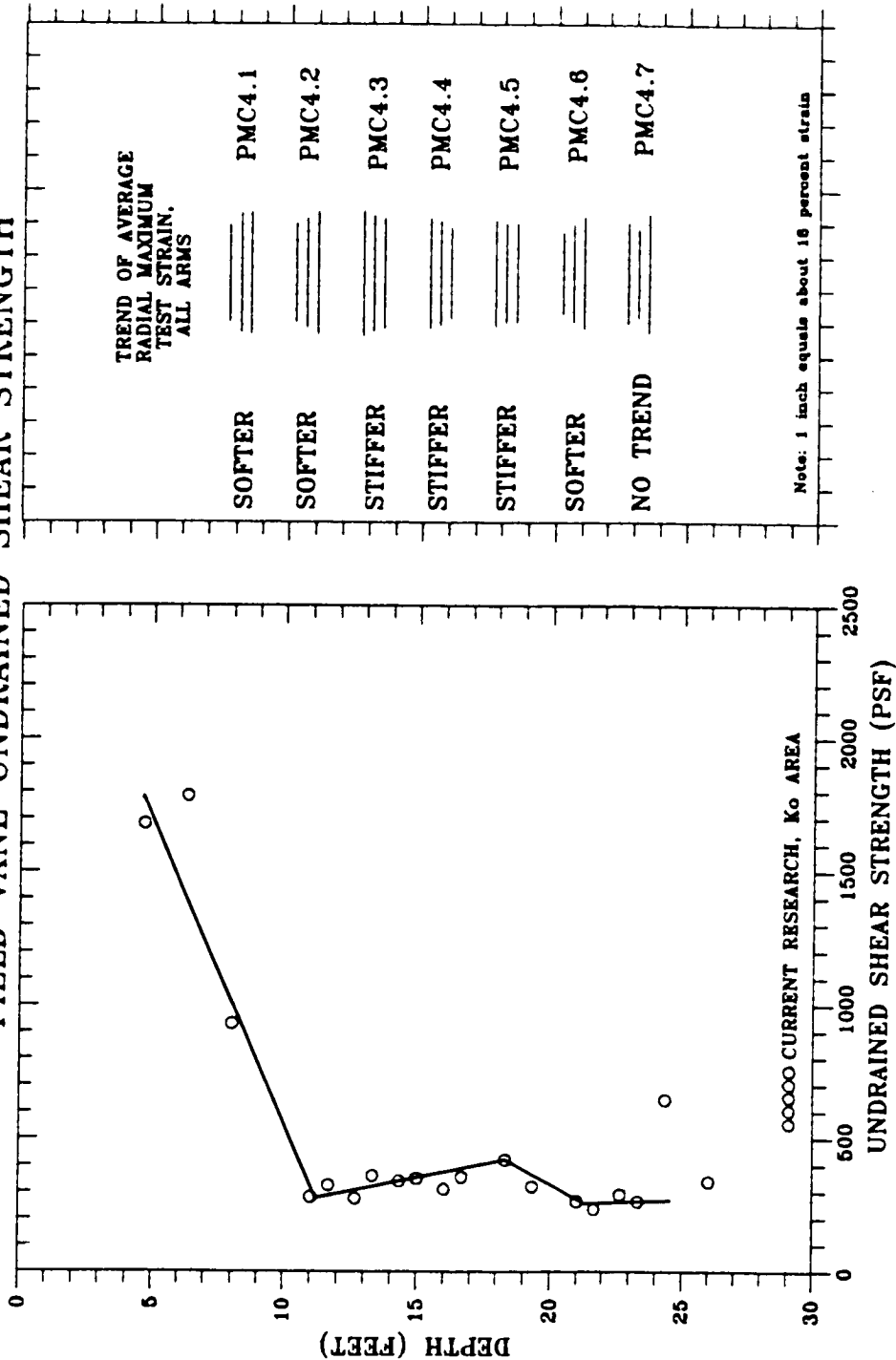


Figure 8-1 Use of Trend of Maximum Test Strain to Predict Trend of Shear Strength Versus Depth

this descriptor to the uncorrected vane shear strength, it can be seen that the trend of shear strength with depth can be correctly deduced based on the trend of the maximum test strain between the tiers of arms in a particular test. The ability to interpret the trend of shear strength with depth has value in understanding the stress history of a site and assessing the quality and validity of the SBPM test results, at least in terms of trend.

Prior to using the average strain from each tier to assess trend of shear strength with depth, the strain indicated by the three arms on a particular side of the probe was used. While this approach also seems to be usable to assess the trend of shear strength with depth, it was found that the use of the average of the arms on a particular tier tends to yield more consistent results. The reason for this is likely that the use of the average strain tends to attenuate the influence of varying amounts of insertion disturbance at each of the strain arms on a particular tier.

8.3 Horizontal Stress from Upper/Lower Arms

Consideration of the total horizontal stress from the upper, lower and middle arm tiers was included the assessment of lateral horizontal stress presented in Chapter VI. By examination of the trends indicated by the plots of horizontal stress versus depth in that chapter, nothing definitive can be said with respect to the middle arms being a better measurement of total horizontal stress than the upper or lower tier arms. Intuitively, this is not surprising, since any constraints of the membrane ends would be accounted for by membrane stiffness calibration. However, the pore pressure transducers, located closest to the middle tier of arms, may have an influence on horizontal stress measurements. The pore pressure transducers are located about 2 inches from the middle arms, 3 inches from the upper arms and about 7 inches from the lower arms. Because insertion pore pressures likely vary along the length of the probe, correction of horizontal stress indicated by the upper and lower tier arms would be expected to be subject to greater error by

virtue of that greater distance from the pore pressure transducers than the middle arms. This would also be expected to be true for pore pressure measurements made after lift-off. As a result, it would appear to be prudent to limit effective stress considerations to the middle arms.

While it appears prudent, based on our current understanding of pore pressure distribution along the probe, to limit effective stress considerations to the middle strain arms, an interesting observation was made of data from several tests. Wroth (1980) described a method for determining in situ horizontal stress which involves plotting TP (volts) versus PPB (volts), as indicated on Figure 8-2. Based on Wroth's method, lift-off (horizontal stress) is defined as the TP value at the break ("A" on the figure) in the resulting plotted line. TP values at lift-off of all 9 strain arms are also included on the figure. Notice that the first arm to lift-off (arm L1) occurs just prior to the break in the TP versus PPB plot. The observation indicates the effective stress transducer can measure pore pressure increase from an upper or lower arm, before a middle arm lifts. This suggests that pore pressures seem to transmit quickly along the face of the probe, which seems to be at odds with the concerns stated in the previous paragraph. It is not known if this effect is limited to the use of the Chinese Lantern, whose metal strip construction may enhance pore pressure transmission or if it would also be observed with just an adiprene membrane (no Chinese lantern). The implication of this pore pressure generation is that each strain arm lifting subsequent to the first lift-off of the membrane will be influenced by excess pore pressure resulting from the first lift-off. Such excess pore pressure would tend to make subsequent lifting strain arms indicate higher than in situ values of horizontal stress. This could explain the high degree of anisotropy measured in K_0 conditions by this and previous research. Development of a correction method for this effect could lead to better horizontal stress and horizontal stress anisotropy measurement and is recommended for future research.

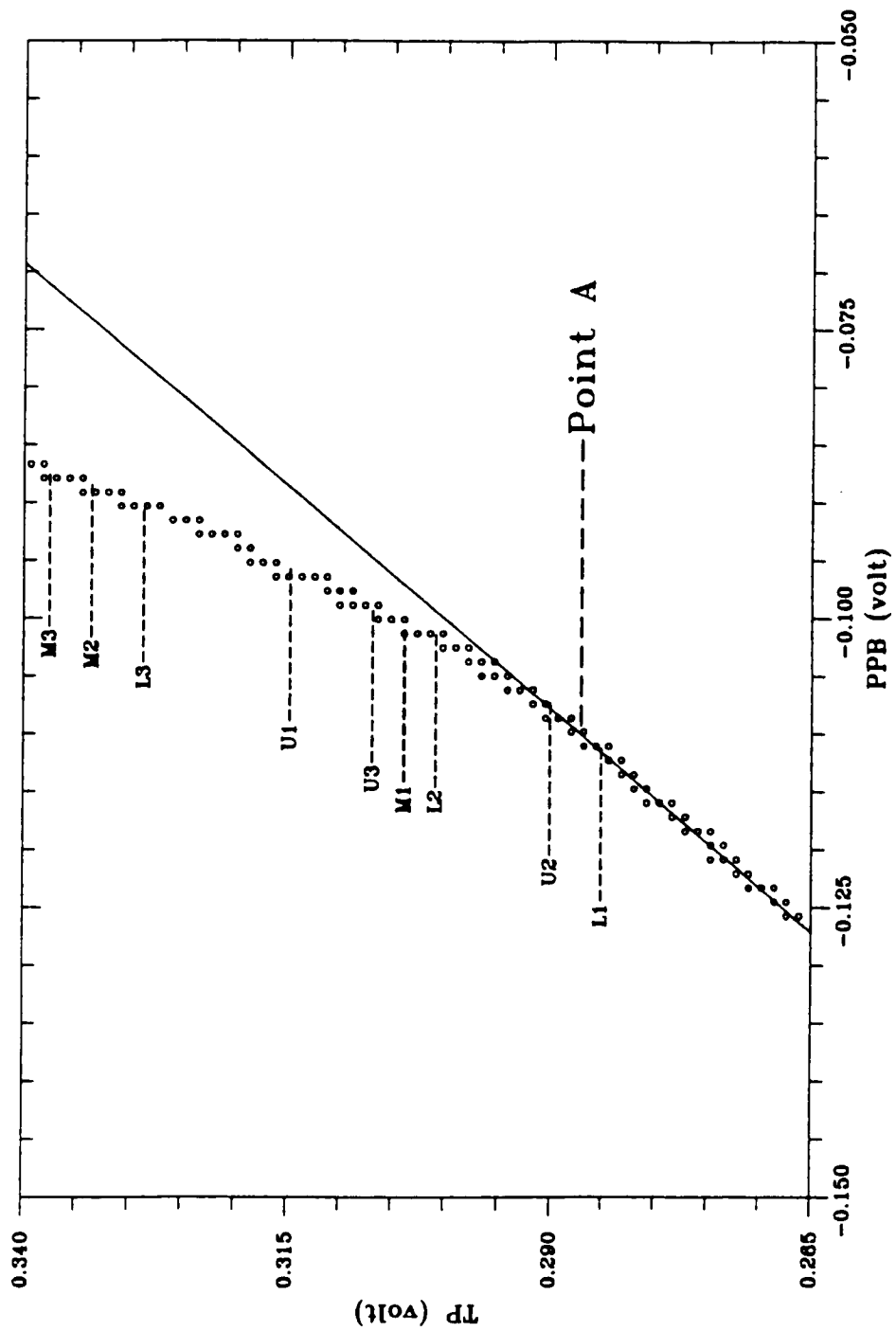


Figure 8-2 Typical Plot of Field Test TP Versus PPB (Test PMC4.2)

Two other issues regarding potential effects of the probe on measured horizontal stress arose during the research. One was with regard to whether the pore pressure transducers would cause some local stiffness which might adversely affect the horizontal stress measurements at adjacent strain arms. The other issue was in regard to how the strain measuring arms were hung on the probe. At the middle and lower arms, the hinge is at the top of the strain arm and the measuring foot or feeler, which is in contact with the membrane, hangs downward. This configuration was depicted on Figure 2-2. The upper arms are hung in reverse, with the feeler at the top and the hinge near the bottom. The concern was whether gravity might have an influence on performance. Visual observation of the horizontal stress profiles measured by the SBPM over the course of the research did not indicate that any particular strain arm seemed to result in horizontal stress measurements which were consistently better or worse than any of the other arms, so it is reasoned that if either of these issues have an effect, it seems to be compensated by stiffness calibration of the membrane.

8.4 Undrained Shear Strength from Upper/Lower Arms

SBPM shear strength interpretation assumes that the probe is of sufficient length that plane strain conditions exist. However, Yeung and Carter (1990) have indicated that undrained shear strength values from the middle arms of the Cambridge SBPM are affected by the limited length of the probe. Further, these authors have presented a correction method to account for the limited probe length. The length to diameter (L/D) ratio at the middle arms is about 6.2. Because the upper and lower arms are closer to the axial limits of the probe, it follows that the effective L/D ratio is smaller (about 3.1), and the deviation from the plane strain assumption is greater. In order to assess if the smaller L/D ratio has a greater influence on the value of shear strength derived from the upper and/or lower arms, the shear strength from these arms was computed for the tests made in boring PMC4. The shear strength method used was the Gibson and Anderson method between 5 and 10 percent

volumetric strain. The Young and Carter correction was not applied since it is the trend in shear strength that is of interest in this comparison between arm tiers, rather than actual magnitude. Table 8-2 presents the computed shear strengths at all of the strain feeler arms for all of the tests conducted in Boring PMC4. The last column of the table is the numerical average of undrained shear strength for each arm tier. Figure 8-3 presents a plot of the calculated shear strength values at each strain feeler arm from Table 8-2 versus depth below the ground surface. As can be seen on the figure, no distinctive trend of the relative magnitude of shear strength between any of the arm tiers is apparent, however the plot does not provide a definitive means of comparison. A more definitive comparison is provided by Figure 8-4. On this figure, the ratio of the shear strength from the upper or lower arm to that from the middle arm is plotted for all the tests from Boring PMC4. No definite trend of the shear strength measured by the upper or lower arm being consistently larger or smaller than that measured at the middle arm can be seen. Based on this observation, non-plane strain effects do not appear to affect the interpreted shear strength at the upper or lower arms.

In boring PMC4, it was found that the strain arms on the lower arm tier had a tendency to have the smallest range in undrained shear strength. Based on the results indicated on Figure 8-3, the range in shear strength of the three arms on the lower tier averaged about 100 ± 62 psf, while the range for the upper and middle arms was 185 ± 97 and 208 ± 96 , respectively. This is consistent with the R^2 findings on Figure 8-4, which seem to indicate that the upper and middle arm shear strength values are more similar than the lower arm values. The reason for this is likely that insertion disturbance increases along the probe since the soil adjacent to the lower arms has only just contacted the SBPM while the soil adjacent to the middle and upper arms has been subject to a greater amount of friction (and thus disturbance) resulting from the passage of the lower parts of the probe during drilling.

SBPM UNDRAINED SHEAR STRENGTH GIBSON AND ANDERSON METHOD 5 TO 10 PERCENT RADIAL STRAIN					
TEST/TIER	DEPTH (feet)	ARMS 1 (psf)	ARMS 2 (psf)	ARMS 3 (psf)	AVERAGE (psf)
PMC4.1/U	7.7	1326	1500	1565	1464
/M	8.1	1300	1326	1491	1372
/L	8.5	1217	1348	1174	1246
PMC4.2/U	10.2	522	717	804	681
/M	10.6	535	674	735	648
/L	11	652	978	630	754
PMC4.3/U	12.7	696	804	783	761
/M	13.1	826	791	883	833
/L	13.5	1261	1174	1196	1210
PMC4.4/U	15.2	565	717	878	720
/M	15.6	661	861	961	828
/L	16	783	804	687	758
PMC4.5/U	17.7	804	761	826	797
/M	18.1	726	752	1017	832
/L	18.5	826	826	761	804
PMC4.6/U	20.2	652	717	804	725
/M	20.6	791	622	917	777
/L	21	674	761	674	703
PMC4.7/U	22.7	804	696	739	746
/M	23.1	1048	1009	1078	1045
/L	23.5	696	717	543	652

Table 8-2 Summary of Undrained Shear Strength From All 9 Arms
in Boring PMC4

PEASE AIR FORCE BASE UNDRAINED SHEAR STRENGTH

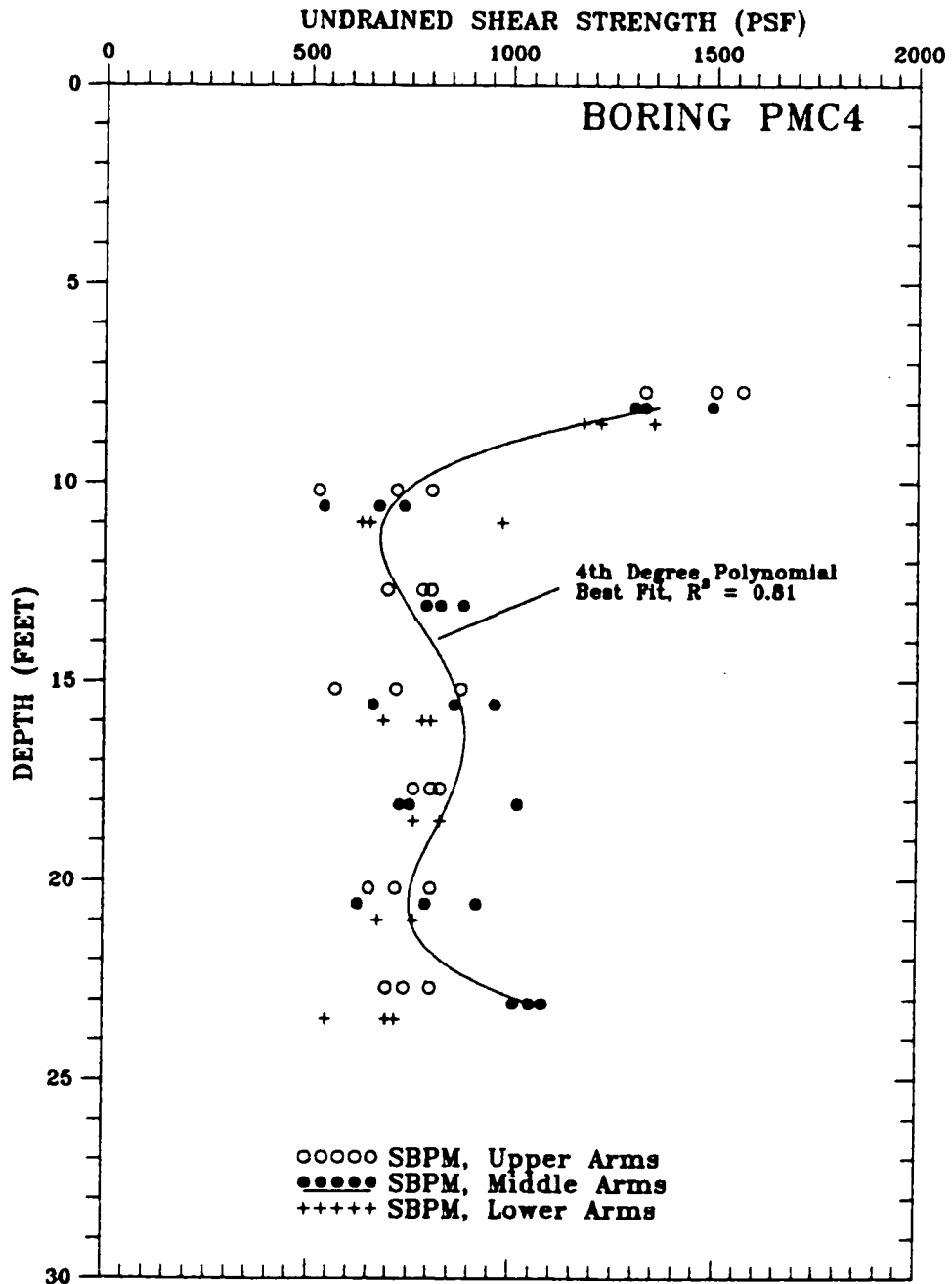


Figure 8-3 Profile of Shear Strength From All 9 Arms Versus Depth

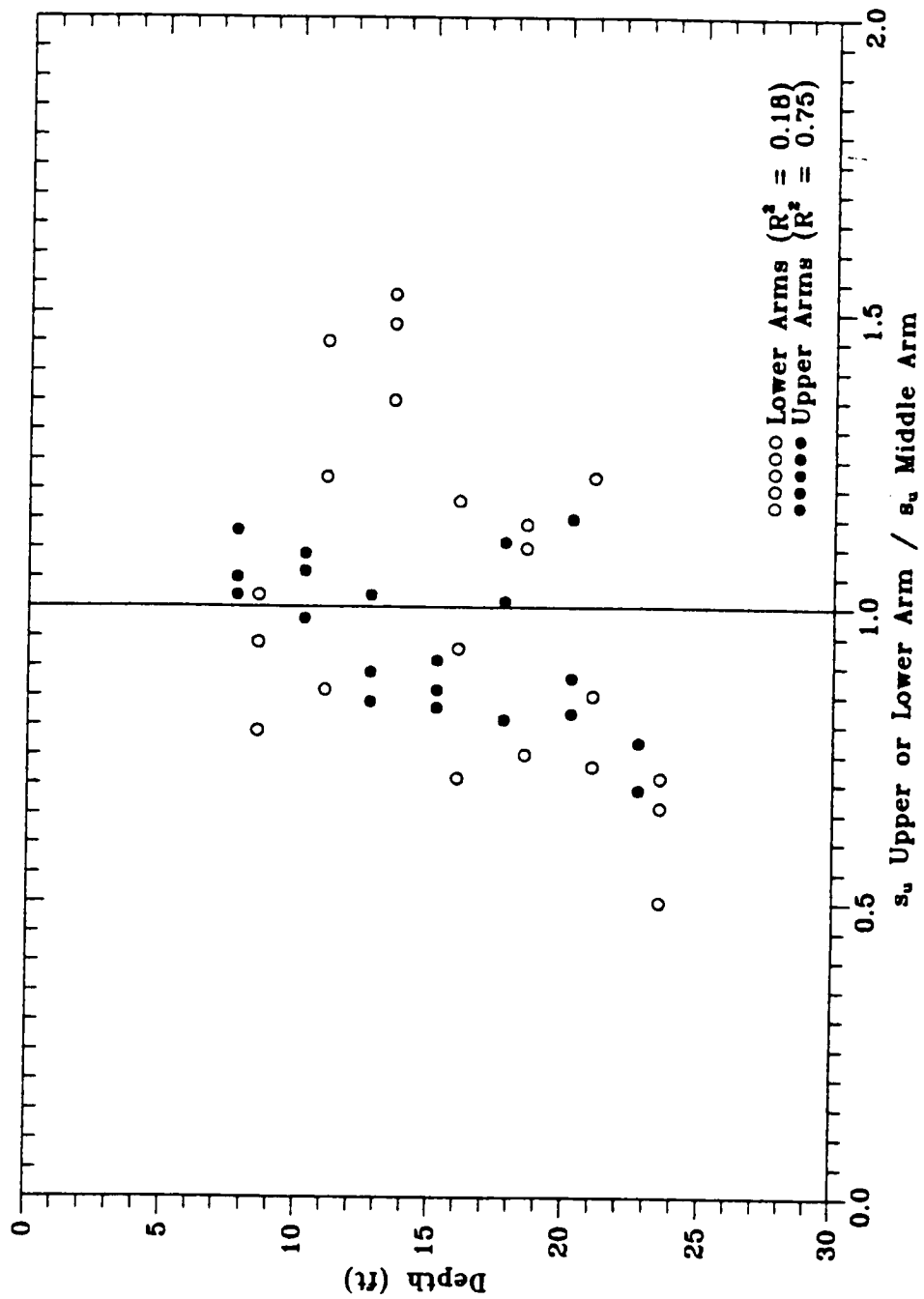


Figure 8-4 Ratio of s_u from Upper/Lower Arms to s_u from Middle Arms Versus Depth

With regard to any effects on undrained shear strength resulting from the location of the pore pressure transducers, the theoretical interpretation of undrained shear strength from SBPM data is generally based on the change in slope of the pressuremeter curve with increasing radial strain. The magnitude of the initial excess pore pressure due to insertion will not affect the shape or slope of the pressuremeter curve (assuming no drainage during expansion), it will only shift the curve up or down, and thus not affect the computed shear strength. However, pervious soil layers or preferential drainage paths occurring at the pore pressure transducer or alternatively at the upper or lower strain measuring arms would cause a miss-assessment of pore pressure during expansion and thus render the pore pressure measurements to be inappropriate for effective stress analysis.

8.5 Unload/Reload Modulus from Upper/Lower Arms

The results of PMC4 were examined to assess the unload/reload shear modulus, G_w , determined from the upper and lower strain arms in comparison with that determined from the middle arms. The unload/reload modulus was determined as described in Chapter II, from graphical enlargements of the unload/reload loops made during an expansion test. Table 8-3 presents the modulus values determined in boring PMC4. Figure 8-5 presents a plot of shear modulus versus depth. Individual tests are designated so that the upper, middle and lower arm data can be distinguished. As can be seen, G_w ranges between about 90,000 and 230,000 psf. No distinct trends between the results of the upper, middle or lower arms are apparent, however, it appears that the lower arm tier tends to have the smallest range (between 100,000 and 170,000 psf) of G_w values. The span of the lower arm G_w range (about 70,000 psf) is about 50 percent less than the span of the range of the upper arms (about 140,000 psf). The span of the range in values for the middle arms (about 120,000 psf) was about 86 percent of the upper arm range. This indicates that the span of the range in G_w increases with tier location up the probe. The reason for this is may be that insertion disturbance

PEASE AIR FORCE BASE							
TEST	DEPTH	ARM M1		ARM M2		ARM M3	
		STRAIN (%)	G (psf)	STRAIN (%)	G (psf)	STRAIN (%)	G (psf)
PMC4.1/U	7.7	7.6	232558	8.2	180180	7.4	909091
/M	8.1	9.9	217391	10.1	215054	11.1	202020
/L	8.5	10.5	136986	NA	NA	9.2	108108
PMC4.2/U	10.2	10.5	156250	8.8	104167	6.7	190476
/M	10.6	13.8	134228	7.8	95694	8.9	149254
/L	11	14.2	116279	8.8	124224	13.2	126582
PMC4.3/U	12.7	12.4	94340	12.4	77519	12.4	108696
/M	13.1	10.2	149254	11.8	104167	11.6	155039
/L	13.5	11.5	103093	NA	NA	10.2	85837
PMC4.4/U	15.2	11.0	117647	8.2	93897	7.5	185185
/M	15.6	10.2	212766	6.2	122699	8.5	173913
/L	16	7.9	156250	5.6	158730	6.8	166667
PMC4.5/U	17.7	7.8	100000	9.7	84746	7.7	130719
/M	18.1	7.8	157480	7.3	155039	7.2	175439
/L	18.5	8.2	114286	7.3	152672	6.9	112360
PMC4.6/U	20.2	5.5	128205	5.9	113636	6.3	129870
/M	20.6	8.7	110497	8.0	97087	7.1	141844
/L	21	10.3	100000	8.2	109290	8.8	109290
PMC4.7/U	22.7	5.8	229885	8.3	107527	6.9	200000
/M	23.1	6.1	144928	6.1	144928	7.2	143885
/L	23.5	8.3	121212	10.0	129032	8.8	114286

Table 8-3 Summary of G_{ur} From All 9 Arms in Boring PMC4

**PEASE AIR FORCE BASE
 MEASURED SHEAR MODULUS - BORING PMC 4
 UNLOAD/RELOAD SHEAR MODULUS, G_{ur} (PSF)**

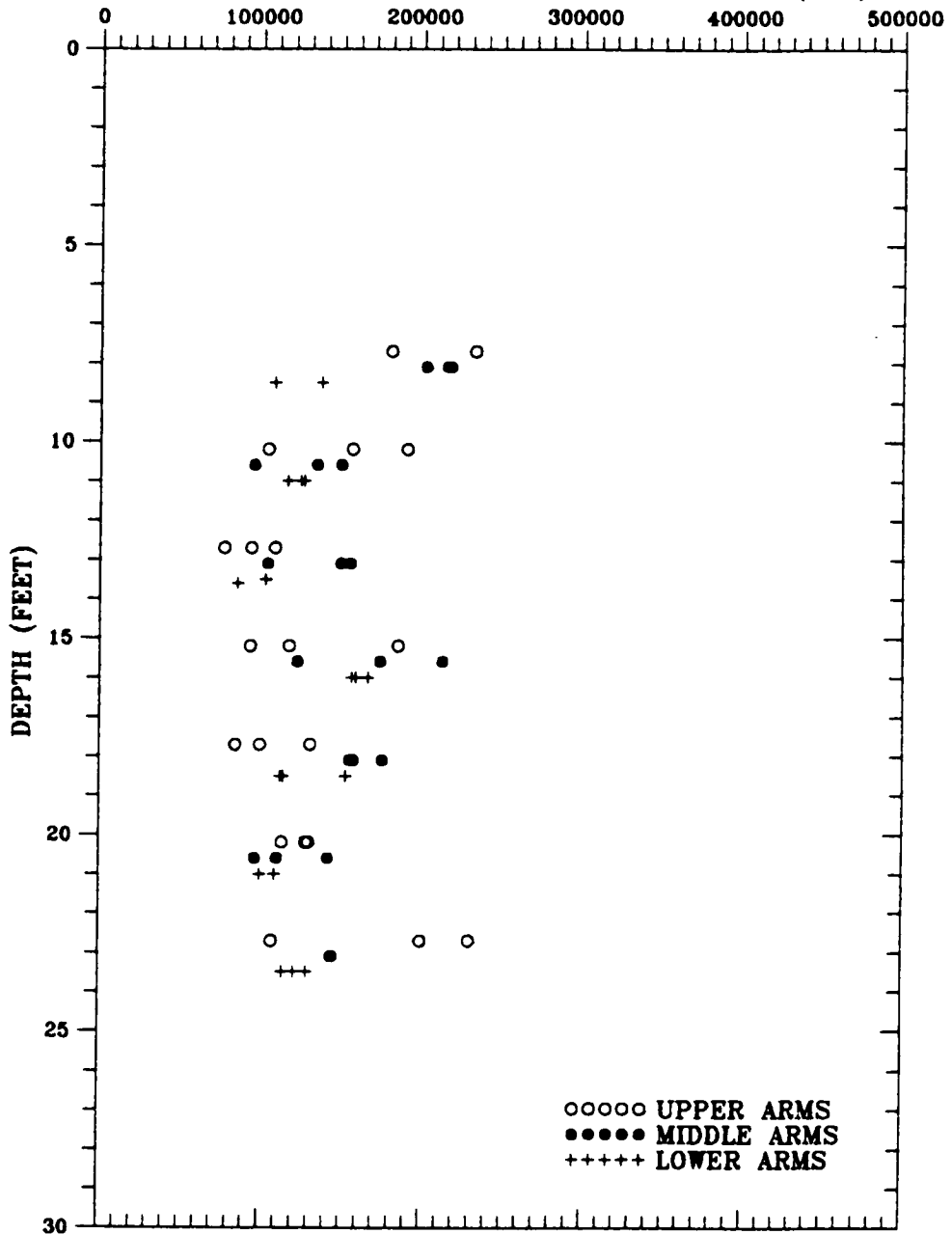


Figure 8-5 Profile of G_{ur} From All 9 Arms in Boring PMC4

increases up the probe since the soil adjacent to the lower arms has only just contacted the SBPM while the soil adjacent to the middle and upper arms has been subject to greater amounts of friction resulting from the passage of the lower parts of the probe during drilling.

Because the strain at which the unload/reload loop occurs at each arm is an independent variable, a plot of G_w versus the strain at which the unload reload loop occurred has been prepared as Figure 8-6. Modulus values from each arm tier have been distinguished by use of different symbols. It can again be seen that G_w from the lower arms has the least range, and G_w may tend to decrease with increasing strain. It also appears that G_w from the lower arms seems to tend toward the lower G_w bound of all the data. The lower G_w values at the lower arms could be due to higher excess insertion toward the bottom of the probe than exists in the soil along the upper portions of the probe. Such a pore pressure distribution has been determined to exist after insertion of the cone penetrometer, another in situ device (Baligh and Levadeux, 1986, Levadeux and Baligh, 1986). The smaller G_w values and smaller range in the values at the lower arms could also be a result of relatively less soil disturbance at the lower arm level compared to that at the progressively higher arms due to drilling vibration and side friction.

8.6 Plane Strain and Axisymmetric Assumptions

A basis of the theoretical analysis of SBPM data is that plane strain and axisymmetric stress conditions exist. Plane strain conditions imply that the length of the SBPM is very long with respect to its radius, and that all deformation occurs in a direction radially outward from the vertical axis of the SBPM, with no strain in an axial direction. With the SBPM, this implies that the probe is sufficiently long such that the finite probe length and membrane end effects do not constrain cavity expansion and that cavity expansion occurs radially, at the same rate at all locations along the membrane of the SBPM. The assumption of axisymmetric stresses assumes that the stress applied by the probe acts radially outward, the vector of the stress passing through the probe's

PEASE AIR FORCE BASE
 MEASURED SHEAR MODULUS - BORING PMC 4
 UNLOAD/RELOAD SHEAR MODULUS, G_{ur} (PSF)

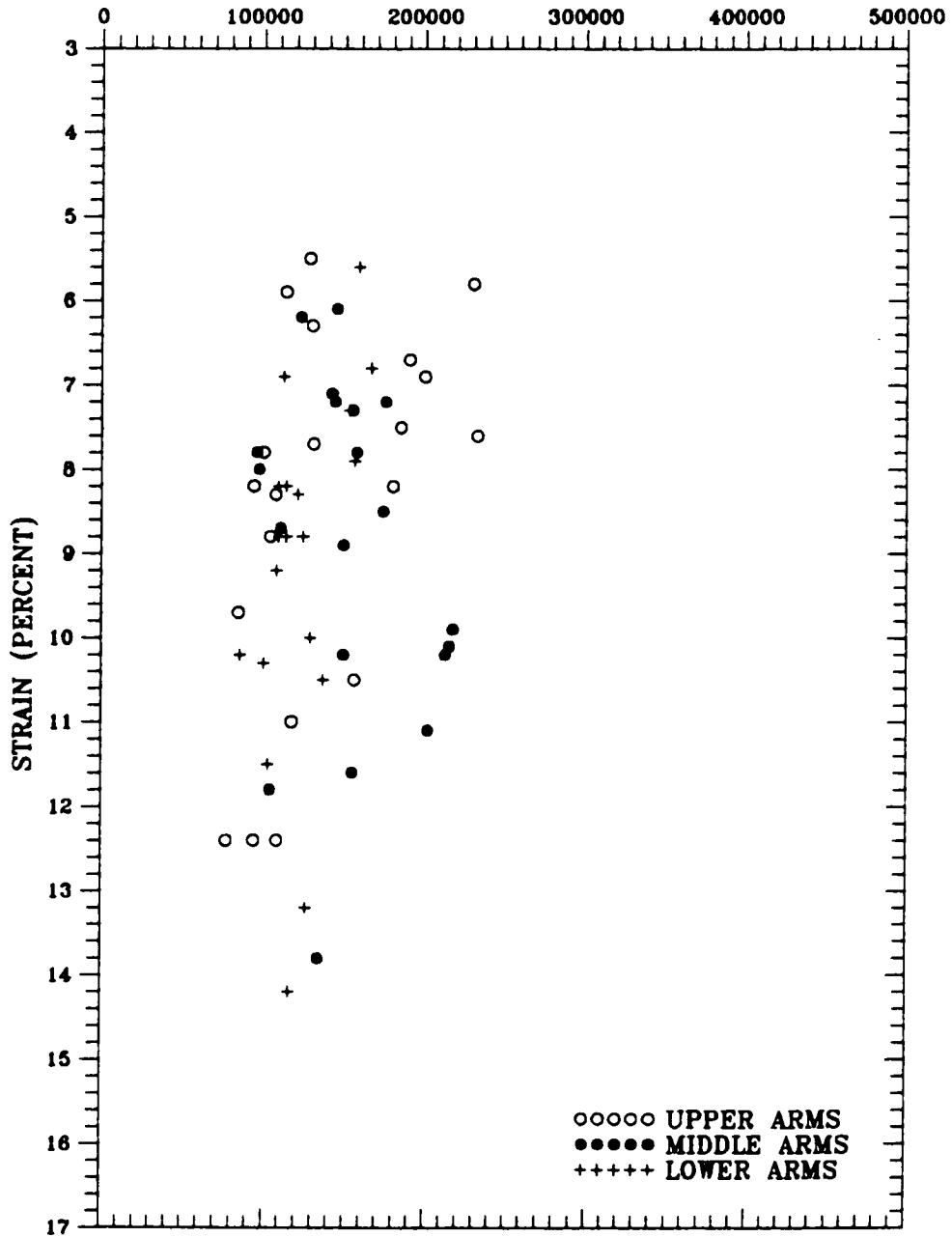


Figure 8-6 G_{ur} Versus Strain From All 9 Arms in Boring PMC4

geometric center.

With regard to probe length only, previous researchers, (Borsetto et al., 1983, and Yeung and Carter, 1990) have indicated that the Cambridge In Situ probe is too short in relation to its breadth (aspect ratio too low) for true plane strain conditions to exist. It has been stated that assuming plane strain conditions could lead to overprediction of undrained shear strength by as much as 22 percent for a probe length to diameter ratio (L/D ratio) of 6 (Borsetto, et al., 1983). However, two observations made during this research, subsequently discussed, suggest that deviation from plane strain conditions may have an influence that is less than thought by the previous researchers.

The first observation was that the undrained shear strength values measured at Hamilton AFB during the current and previous (Denby, 1978, and Benoit, 1983) research seems to be in agreement with shear strength measured by other methods. Application of the Yeung and Carter (1990) correction for non-plane strain conditions, as discussed in Chapter VII, causes a decided underestimation of undrained shear strength with the Hamilton data from the current research. As has been also been discussed in Chapter VII, the overestimation of shear strength at some test sites (such as Pease AFB) may have more to do with insertion disturbance than shortness of the probe.

The second observation which indicates deviation from plane strain conditions may have less influence than previously thought is apparent from examination of the additional data available due to the 9-arm nature of the probe used for the current research. If up to 22 percent overestimation of shear strength (at the probe mid-point, for L/D=6, based on Borsetto, et al. 1983) were possible due to the low aspect ratio of the probe, one would expect an increase in the overestimation of undrained shear strength from pressuremeter curves derived at locations closer to the ends of the pressuremeter, such as the upper and lower strain tracking arms on the 9-arm version of the probe. This is because toward the probe end, the plane strain assumption would be increasingly

violated. Since the upper and lower strain arms are approximately 5-inches from the membrane ends, and the probe is about 3.2-inches in diameter, an equivalent L/D ratio of about 3 can be rationalized for the upper and lower strain arms. The results of Borsetto, et al. (1983) can be linearly extrapolated to indicate that such an L/D ratio would result in about 31 percent overestimation in undrained shear strength, or almost 10 percent greater than that measured at the probe center, an amount which would be expected to be reflected in the results shown on Figure 8-3. Figure 8-3 includes the influence of varying shear strength with depth and side (likely anisotropy) of the pressuremeter. Considering these potential skewing effects, no distinct trend of increased strength at the upper or lower arms over the strength measured at the middle arms can be seen. While it is true that the shear strength measured by the SBPM at Pease AFB is significantly larger than that measured by other testing methods, it is believed that this is more a result of disturbance during insertion and other effects discussed in Chapter VII, rather than violation of the plane strain assumption. Although probe length certainly induces some violation of the plane strain assumption, the effect on shear strength may be less than previous researchers have indicated based on the similarity in the range of measured shear strength along the probe.

Based on the observations made for the current research, it has also been found that deformations parallel to the axis of the probe can occur, which is another violation of the plane strain assumption. The fact that varying amounts of strain occur across the face of the SBPM during expansion was demonstrated on Figure 8-1. This trend has been noted by Lien (1991) in stiff clays, as referenced by Clough, et al. (1990). In such cases, the membrane is not parallel to the probe axis after lift-off, and during a test, expansion is not perfectly radial away from the probe. The result of this expansion irregularity, as indicated on the upper half of Figure 8-7, is that soil strain has some component along the probe axis as well as in a radial direction. This axial

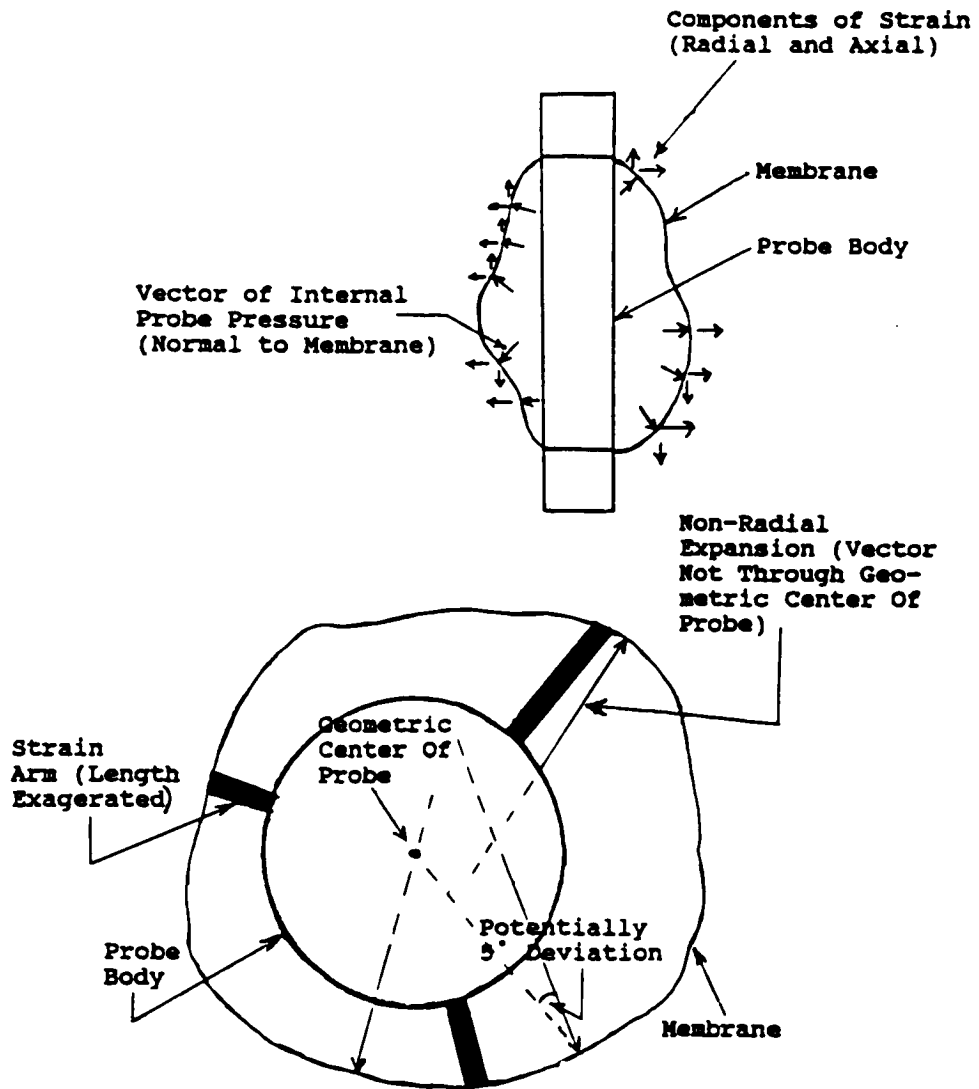


Figure 8-7 Non-Radial and Axial Components of Strain During SBPM Expansion

component would increase as greater difference in strains along the probe increase.

The observations of the current and previous research efforts, depicted on the bottom portion of Figure 8-7, also indicate that differing strains at each arm on a particular tier of arms can occur during a test. These differing strains indicate that strain occurring on a horizontal plane are not necessarily radial, which is a violation of the axisymmetric assumption of expansion made for theoretical interpretation. Also, these differing strains imply that differing strain rates also occur along and around the probe.

Assessment of the error induced by the violation of the plane strain and axisymmetric stress assumptions in actual SBPM test data is a complex issue. However, in a qualitative sense, the effect of the irregular strains can be rationalized. Non-radial and axial strains are not measured by the strain tracking arms which only measure radial strain. Since the occurrence of any strain requires energy, neglecting axial and non-radial strains would result in an overestimation of the energy required to cause the measured radial strain. This would tend to make the pressuremeter curve steeper, and thus an overestimation of undrained shear strength and shear modulus would result. This implies that stress anisotropy along the probe, which conceivably results in non-uniform membrane expansion, will tend to cause an overestimation of undrained shear strength using the SBPM. To roughly quantify the above overestimation, it is assumed that changes in pressure required to expand the membrane are proportional to the magnitude of measured shear strength. This assumption is thought to be valid since derivation of shear strength is based on the slope of the pressuremeter curve which is the change in pressure versus radial strain. Maximum difference in strain during a test between strain measuring arms has been observed on Table 8-1 to range from 0 to as much as 6 percent, out of a maximum radial strain of 7 to 16 percent for a test. This can result in a difference in the strain measured at any two strain arms of up to 60

percent. Based on a 60 percent difference between two adjacent strain measuring arms (one of them fully extended), and an approximately 3 inch distance between adjacent strain measuring arms, the pressure force normal to the expanding membrane can be as much as 6 degrees away from passing through the geometric center of the probe assuming a monotonic transition of strain between the two strain measuring arms. Resolving this into a percentage difference between the force normal to the membrane and the component of the force passing through the geometric center of the probe, yields about 1 percent difference. Based on the above assumption that the magnitude of shear strength and change in expansion stress are proportional, it appears that deviation of SBPM expansion from being truly radial only results in a small deviation in computed undrained shear strength. This approximate calculation indicates that non-radial pressuremeter expansion does not appear to induce significant error into calculation of undrained shear strength.

8.7 Summary

It has been demonstrated in this chapter that the trend of average maximum strain on the three strain arm tiers can be used to deduce the trend of shear strength variation with depth through a deposit. It was also observed that shear strength and shear modulus from each of the arm tiers yield similar results and that the upper and lower arms do not appear to be affected by their closer proximity to the constrained ends of the membrane. The lower arms may yield values of shear strength and shear modulus with less range in value than the upper and middle arms.

With regard to horizontal stress and stress anisotropy, an interesting pore pressure phenomenon was observed where the effective stress cell begins to measure excess pore pressure along the face of the probe as soon as any of the strain arms lift, indicating a rapid transmittal of pore pressure across the face of the probe. It was indicated that this could cause an overestimation in the horizontal stress indicated by the subsequently lifting arms, and thus greater apparent stress anisotropy.

The results of the 9-arm SBPM seem to imply that change in L/D ratio between the middle and upper/lower arms does not seem to affect the measured values of shear strength and shear modulus. This may indicate that the effects of deviation from plane strain conditions may not be as great as thought by previous researchers.

With respect to the validity of the radial symmetry assumption which is made in theoretical analysis of SBPM data, it appears that such a condition is commonly are not present in actual test data from the 9-arm pressuremeter. While the effect of violation of this assumption would be difficult to accurately quantify, particularly since the gradient of strain differences across the probe likely impacts the magnitude of the effect, it has been concluded that violation of axial symmetry assumption tends to cause only a minor overestimation of shear strength in typical tests in undisturbed, relatively homogenous soil.

CHAPTER IX

SUMMARY, CONCLUSIONS, AND RECOMMENDATIONS

9.1 Summary of Research Activities

The research summarized in this dissertation included review of the history and technology of the self-boring pressuremeter leading up to the current 9-strain arm version of the SBPM. The 9-arm device was used at two soft clay test sites, namely Pease and Hamilton Air Force Bases, located in Portsmouth, New Hampshire and Novato, California, respectively. These sites were selected because each was the subject of previous geotechnical research and/or construction performance monitoring. Beyond the field work, an extensive laboratory program to measure the engineering properties of the Pease Air Force Base silty marine clay was conducted, along with finite element analysis to predict stress changes which could occur in the non- K_0 environment at the toe of an existing highway embankment. A similar laboratory testing program was not conducted on the Hamilton AFB clay because of the volume and quality of previous laboratory and field testing results which were already available.

Laboratory experiments were conducted to determine factors which significantly influence the SBPM measurements. Also, the effects of SBPM membrane stiffness were studied by performing membrane expansions inside and out of a pressure chamber.

9.2 Summary of Research Findings

The research effort indicated the SBPM is useful in measuring in situ horizontal stress in soft clay in a K_0 stress condition. A K_0 stress condition exists in soil that is fully consolidated under its own weight (normally consolidated) and is away from the influence of a sloping ground surface or other external force. The SBPM is also useful in measuring horizontal stress and horizontal stress changes with distance

from a highway embankment supported on soft clay (non- K_0 stress condition). The SBPM indicated similar trends in percent lateral stress change to those predicted by an elasto-plastic FEM constitutive model (JFEST) and greater than those predicted by a hyperbolic FEM constitutive model (SOILSTRUCT). The SBPM is capable of measuring stress anisotropy in the horizontal plane under some conditions. The ability to measure stress anisotropy was quite definitive in the non- K_0 condition at the Pease embankment toe, where the principal stress was measured to strike perpendicular to the axis of the embankment. The results, however, were less definitive in the K_0 situations at both the Pease and Hamilton sites, where relatively large differences in the principal stresses were measured and the direction of the major principal stress was indicated to be variable. It is believed that the higher lateral stress at the Pease embankment toe resulted in less deployment disturbance than the relatively smaller confinement at the K_0 conditions tested. This was exemplified by the far fewer "disturbed" tests at the embankment toe area compared to the K_0 areas. It was shown that disturbance tends to increase the apparent difference between the major and minor principal stress. Also, it is believed that the actual in situ stress difference at the K_0 area is about equal to or smaller than the measurement accuracy of the SBPM, which likely affects the direction of the major principal stress. It should also be stated, however, that the apparent randomness in the direction of the major principal stress in a K_0 situation may be real, due to variations in deposition, consolidation effects resulting from variable deposit thickness, and/or tectonic effects.

SBPM shear strength was determined using the Gibson and Anderson, sub-tangent, and Denby and Clough methods. It was found that the SBPM over-estimated undrained shear strength (in comparison to other field and laboratory methods of shear strength measurement) in the soft silty clay at the Pease K_0 test site and measured reasonable values of undrained shear strength at Hamilton AFB and in the stiffer, silty clay crust at

Pease AFB. The Gibson and Anderson method, between 5 and 10 percent radial strain yielded undrained shear strength values closest to measured field vane values, although they were still up to 100 percent higher than uncorrected field vane and isotropically consolidated, undrained triaxial values in the soft clay at the Pease K₀ area. At Hamilton, all of the shear strength analysis methods seemed to yield reasonable results. While shear strength is not a unique value and is dependent on mode of shear, SBPM measured shear strength in the soft clay at Pease AFB is larger than can be rationalized.

One theory that is proposed by several researchers is that the probe deviates from plane strain conditions, as assumed in the analysis, which results in overestimation of undrained shear strength. Correction for non-plane strain conditions using the Yeung and Carter (1990) method helped at Pease AFB, however SBPM data corrected using the method was still significantly above field vane and isotropically consolidated, undrained triaxial values. Application of the Yeung and Carter correction to the Hamilton AFB data caused shear strength to be below previous isotropically consolidated, undrained triaxial and field vane values. Another reason for the Pease soft clay over-estimation is a function of higher sensitivity, evidenced by relatively low triaxial and SBPM strain at shear failure, and thus greater susceptibility to the so-called "strength paradox". It appears that the SBPM provided the most reasonable measurements of undrained shear strength when triaxial strain at failure, for the tested deposits, was in excess of about 1.5 to 2.0 percent and SBPM shear failure (as evidenced by the sub-tangent stress-strain curve) was greater than about 1.0 percent.

SBPM shear strength was also evaluated in a non-K₀ situation near the toe of an existing highway embankment. Although SBPM shear strength was expected to decrease with distance away from the toe, the reverse was observed. An explanation for this observation may be that the stress condition at the embankment toe was not appropriate for elasto-plastic analysis of SBPM data. The SBPM indicated the ratio of horizontal to

effective vertical stress at the toe of the embankment to be 3.28 ± 1.36 , which is above the upper limit given by Wood and Wroth (1977) as being applicable to conventional SBPM shear strength analysis. Less disturbance due to the higher confinement may also contribute to the lower shear strength measured at the embankment toe, however the trend appears to be far too consistent to be a result of disturbance alone.

With regard to SBPM measured shear modulus, several findings were made. The initial shear modulus evaluated by the Denby-Clough shear strength method was found to generally be larger than the unload/reload modulus. The unload/reload modulus was found to generally follow the trend of shear strength with depth. No significant trend was found in the unload/reload modulus versus the radial strain at which the modulus was evaluated. This lack of trend is thought to be due to the compensating effects of drainage during expansion and the generally accepted practice of neglecting the stress level correction in evaluating the unload/reload shear modulus.

There seems to be a trend of the unload/reload modulus to be smallest on a particular side of the probe. While this may hold some future potential for evaluation of stress anisotropy in the horizontal plane, additional evaluation will be necessary with regard to membrane stiffness and calibration of strain arm friction.

Several holding tests were conducted at Pease AFB to determine the horizontal coefficient of consolidation. The SBPM results were higher than virgin laboratory values by about an order of magnitude, but were reasoned to be similar to the value which would be expected under actual field conditions, based on comparison the field performance measurements made previously by others during construction of an adjacent highway embankment and in consideration of horizontal layer effects.

Results of the research using the 9-arm capability of the SBPM were also discussed. The trend of total average strain occurring on each of the three strain measuring arm tiers can be interpreted to determine trends of shear strength variation with depth. It was observed that

shear strength and shear modulus values measured on the upper and lower strain arm tiers seems to give similar results to those measured at the middle arms, however the values measured at the lower arms seem to be more consistent, with less scatter than the values measured by the middle and upper arms.

The 9-arm version of the SBPM allowed observation of a phenomenon where the effective stress cells measure excess pore pressure as soon as any portion of the membrane lifts away from the probe. This has implications on evaluation of horizontal stress and stress anisotropy, in that subsequently lifting arms will be affected by excess pore pressures generated during soil shear at the arms that have lifted previously. It is possible that these pore pressures are partly responsible for the large difference between the apparent major and minor principal stresses and scatter in the direction of the major principal stress noted by the present and previous research in K_0 soft clay deposits.

It was found that the plane strain and radial symmetry assumptions made for theoretical reduction of SBPM data are invalid to some extent, however it was concluded the error in measurement resulting from the invalidity of the assumptions is relatively small.

9.3 Conclusions Regarding SBPM Usage

- 1) Based on the findings of this research, it is concluded that the SBPM is useful for measurement of horizontal stress in soft clays; however, accuracy is critically dependent on frequent calibration. In the K_0 situation, the SBPM has provided measurements of horizontal stress in agreement with those measured by thin blade pressure cells and those estimated by empirical methods. In non- K_0 situations, such as at the toe of an embankment supported by a soft clay deposit, the SBPM provides one of the few rational methods of assessing in situ lateral stress.
- 2) The testing for this research was conducted at relatively shallow depth with total horizontal stress ranging from about 800 to 4000

psf. Based on this range of horizontal stresses, the measurement error (estimated to be about ± 150 to 200 psf) constituted about 5 to 25 percent of the measured horizontal stress. While 10 to 20 percent error might be acceptable for estimation of horizontal stress, errors greater than about 10 percent render estimation of the magnitude and direction of the major principal stress to be relatively inaccurate. As such, it is concluded that SBPM use should be limited to deposits where horizontal stress is large enough to render the significance of the measurement error of the system to be acceptable to the desired use of the measurement. It was observed that pressuremeter deployment seems to result in more disturbed tests in shallow depth K_u soft clay than in clay with larger lateral stress, such as that at the Pease embankment toe.

- 3) With regard to measurement of undrained shear strength and stress-strain parameters at the two test sites, SBPM shear strength should be used with caution and only in conjunction with values determined by other proven test methods. For this research, the SBPM worked best in deposits that fail at radial strains of more than about 1 percent as indicated by the sub-tangent stress-strain curve. Axial strains at failure from isotropically consolidated, undrained triaxial tests of 1.5 to 2.0 percent form a similar boundary. The portions of the deposits tested that fail at smaller strains suffer from the so-called "strength paradox" and result in SBPM shear strength values that are much higher than would be expected, even considering that shear strength is not a unique value and is dependent on the mode of shear. Also, it was observed that the existing SBPM elasto-plastic analysis methods are not applicable to a clay deposit below an embankment toe which has a high ratio of horizontal to vertical effective stress. The best measurements of SBPM undrained shear strength were obtained by using the Gibson and Anderson Method, considering the data between 5 and 10 percent volumetric strain. The 9-arm version of the SBPM was found to be

applicable to predicting the trend of shear strength with depth by comparison of the maximum test strain on the three arm tiers.

- 4) Data from the Pease K_v area indicates that the unload/reload shear modulus is most consistent if determined by the conventional practice of neglecting the stress level correction term. The effect of neglecting this term was essentially compensated by consolidation and drainage during expansion. Negligence of this term reduces scatter in modulus data caused by wide variability in measured lateral stress values from different strain arms within a particular test. Comparison of the values of unload/reload shear modulus determined by the SBPM was not made to other measurement methods in the current research, however, previous research has indicated that SBPM unload/reload shear modulus compares well to that indicated by plate load tests. Assuming elastic behavior and Poisson's ratio of 0.5, a comparison of the SBPM initial shear modulus was made to previous values of initial Young's modulus determined by laboratory tests and extrapolated from field observations of an embankment failure. The comparison indicated that the SBPM value of initial shear modulus is in general agreement with observed field and laboratory behavior.
- 5) The SBPM yielded values of horizontal coefficient of consolidation which were interpreted to be representative of in situ field conditions, particularly considering potential horizontal layer drainage effects.

9.4 Recommendations for Future Research

- 1) Pore pressure may be the single most important issue regarding SBPM testing, for both effective and total stress tests. Further research should address the following:
 - a) effect of excess pore pressure, which has been observed after the first strain arm lift-off, on the horizontal stress indicated by the subsequently lifting arms.
 - b) Distribution of excess pore pressure along the probe due to

insertion.

- c) Quantification of drainage during "undrained" shear, and its effect on stress-strain parameters.
- d) The potential for drainage along the probe face to exit into the borehole during a holding test. Verify if radial dissipation really governs.

Future research with respect to pore pressure should begin by replacement of the current strain gauge based effective stress cells with a direct measuring, low volume change, electrical pressure transducer system that is insensitive to temperature changes and can easily be deaired.

- 2) Cataloging of information from all available SBPM test sites to see if strain at failure is a reliable predictor of the applicability of the SBPM for use in measurement of undrained shear strength.
- 3) Effects of the actual in situ magnitude of horizontal stress on the tendency for insertion disturbance.
- 4) The effect of the ratio of horizontal to vertical effective stress on determination of stress-strain parameters, particularly when the ratio is greater than 1.0.
- 5) The applicability of the use of the variation of unload/reload modulus and/or undrained shear strength values indicated by each of the three strain measuring arms on a tier of arms to resolve the direction of the major principal stress in the horizontal plane. Such parameters may be less sensitive to disturbance effects than SBPM measured horizontal stress.

REFERENCES

- Arnold, M., (1981), "An Empirical Evaluation of Pressuremeter Test Data," Canadian Geotechnical Journal, Vol. 18, No. 3, pp.455-459.
- ASTM (1986) D-18.02.10, "Suggested Method for Performing Flat Dilatometer Test," ASTM, Philadelphia, Pa.
- Atkinson, J.H. and Bransby, R.L. (1978) The Mechanics of Soil. An Introduction to Critical State Soil Mechanics, McGraw-Hill Book Company (UK) Limited, Maidenhead, Berkshire, England.
- Atwood, M.J., (1990), "Investigation of Jetting Insertion Procedures for Rapidly Deploying a Self-Boring Pressuremeter in Soft Clays," Thesis Presented in Partial Fulfillment of the Requirements for the Masters Degree, University of New Hampshire, Durham, NH.
- Baguelin, F., Jézéquel, J-F., Lemée, E. and Le Mehaute, A., (1972), "Expansion of Cylindrical Probes in Cohesive Soils," Journal of Soil Mechanics and Foundation Division, ASCE, Vol. 98, No.SM11, pp. 1129-1142.
- Baguelin, F., Jézéquel, J-F., and Le Mehaute, A., (1974), "The Self-Boring Placement Method of Soil Characteristics Measurements," Proc. ASCE Specialty Conference on Subsurface Exploration for Underground Excavation and Heavy Construction, New England College, Henniker, NH.
- Baguelin, F., Jézéquel, J-F., and Shields, D.H., (1978), "The Pressuremeter and Foundation Engineering, Series on Rock and Soil Mechanics," Transactions of Technical Publications, Clausthal, West Germany.
- Benoit, J., (1983), "Analysis of Self-Boring Pressuremeter Tests in Soft Clay," A Thesis Presented in Partial Fulfillment of the Ph. D. Degree, Stanford University, Palo Alto, California.
- Benoit, J., and Clough, G.W., (1986a), "Principal Stresses Derived from Self-Boring Pressuremeter Tests in Soft Clay," Spec. Publ. 950: The Pressuremeter and Its Marine Applications, ASTM, 1986, pp. 137-148.
- Benoit, J., and Clough, G.W., (1986b), "Self-Boring Pressuremeter Tests in Soft Clay," Journal of Geotechnical Engineering, ASCE, Vol.112, No.1, 1986, pp 60-78.
- Benoit, J., NeJame, L.A., Atwood, M.J., and Findlay, R.C., (1990), "Dilatometer Lateral Stress Measurements in Soft Sensitive Clays," Proceedings of the 69th Annual Meeting of the Transportation Research Board, Washington, D.C.
- Baligh, M.M., and Levadoux, J.N., (1986), "Consolidation After Undrained Piezocone Penetration. II: Interpretation," Journal of the Geotechnical Engineering Division, ASCE, Vol. 112, No. 7, pp.727-745.
- Bonaparte, R, and Mitchell, J.K., (1979), "The Properties of San Francisco Bay Mud at Hamilton Air Force Base, California," Department of Civil Engineering, University of California, Berkeley.
- Borsetto, M., Imperato, L., Nova, R., Peano, A., (1983), "Effect of Pressuremeter of Finite Length in Soft Clay," Proc. International Symposium on Soil and Rock Investigation by In-Situ Testing, Paris.

- Boscardin, M.D., Selig, E.T., Lin, R-S, Yang, G-R, (1990), "Hyperbolic Parameters for Compacted Soils," *ASCE Journal of Geotechnical Engineering*, Vol. 116, No. 1.
- Brooker, E.W., and Ireland, H.O., (1965), "Earth Pressures at Rest Related to Stress History," *Canadian Geotechnical Journal*, Vol. II, No. 1, pp 1-15.
- Cadling, L., and Odenstad, S., (1950), "The Vane Borer, An Apparatus for Determining the Shear Strength of Clay Soils Directly in the Ground," *Royal Swedish Geotechnical Institute, Proceedings*, Vol.2, 1950, pp. 1-87.
- Campanella, R.G., and Robertson, P.K., (1981), "Applied Cone Research", *Symposium on Cone Penetration Testing and Experience*, *Geotechnical Engineering Division, ASCE*, October, 1981, pp. 343-362.
- Campanella, R.G., and Robertson, P.K., (1988), "Current Status of the Piezocone Test," *Proceedings of the First International Symposium on Penetration Testing, ISOPT-1, Orlando, Fla., J. De Ruiter, Ed.*, pp. 93-116.
- Clarke, B.G., Carter, J.P., and Wroth, C.P., (1979) "In-situ Determination of the Consolidation Characteristics of Saturated Clays," *Proc. 7th Eur. Conf. on Soil Mechanics and Foundation Engineering*, Vol. 2, Brighton, England, pp.207-211.
- Clarke, B.G. and Wroth, C.P. (1988) "Comparison Between Results from Flat Dilatometer and Self-Boring Pressuremeter Tests," *Proceedings of the Geotechnology Conference on Penetration Testing in the U.K., University of Birmingham*.
- Clough, G.W. and Denby, G.M., (1978), "Experience with the Cambridge Self-Boring Pressuremeter in the United States", *Proceedings of a Symposium on Site Exploration in Soft Ground Using In-Situ Techniques*, May, 1978, Alexandria, Va., *Federal Highway Administration*, final report dated January, 1980.
- Clough, G.W. and Denby, G.M., (1980), "Self-Boring Pressuremeter Study of San Francisco Bay Mud", *JGED, ASCE*, Vol. 106, No. GT1, pp45-63.
- Clough, G.W., Briaud, J.L., and Hughes, J.M.O. (1990) "The Development of Pressuremeter Testing," *Proceedings of the 3rd International Symposium on Pressuremeters, British Geotechnical Society, Oxford University*.
- Dalton, J.C.P. and Hawkins, P.G., (1982), "Fields of Stress - Some Measurements of the In-Situ Stress in a Meadow in the Cambridgeshire Countryside", *Ground Engineering*, Vol. 15, No.4.
- Denby, G.M., (1978), "Self-Boring Pressuremeter Study of the San Francisco Bay Mud", *A Thesis Presented in Partial Fulfillment of the Ph. D. Degree, Stanford University, Palo Alto, California*.
- Denby, G.M. and Clough, G.W., (1980), "Self-Boring Pressuremeter Tests in Clay", *Journal of the Geotechnical Engineering Division, ASCE*, Vol. 106, No. GT12, pp. 1369-1387.
- Duncan, J.M., and Chang, C-Y, (1970), "Nonlinear Analysis of Stress and Strain in Soils," *Journal of Soil Mechanics and Foundation. Division, ASCE*, Vol. 96, No. SM5.
- Fahey, M., and Jewell, R.J. (1990) "Effect of Pressuremeter Compliance on Measurement of Shear Modulus," *Proc. of the 3rd Int. Symposium on Pressuremeters, British Geotechnical Society, Oxford University*.

- Findlay, R.C. (1988) "Hydrostatic Pressure at a Soil-Structure Interface," Proceedings of the 2nd International Conference on Case Histories in Geotechnical Engineering, University of Missouri-Rolla, St. Louis.
- Fukagawa, R., Ohta, A.I., Iizuka, A., Nishihara, A., and Morita, Y., (1990) "Effects of Drainage on Interpretation of Pressuremeter Tests in Clay," Proc. of the 3rd Int. Symposium on Pressuremeters, British Geotechnical Society, Oxford University.
- Fung, Y.C., (1977) A First Course in Continuum Mechanics, Second Ed., Prentice-Hall, Inc., Englewood Cliffs, New Jersey.
- Gibson, R.E. and Anderson, W.F. (1961), "In-Situ Measurement of Soil Properties with the Pressuremeter," Civil Engineering and Public Works Review, 56, pp. 615-618.
- Haley and Aldrich, Inc., (1970), "Interim Report on Soil Engineering Studies for the Approach Embankments, Interstate Route 95, Portsmouth, NH," Report to the New Hampshire Department of Public Works and Highways.
- Handy, R.L., Remmes, B., Moldt, S., Luttenegger, A.J., and Trott, G., (1982), "In Situ Stress Determination by Iowa Stepped Blade," Journal of Geotechnical Engineering Division, ASCE, Vol. 108, No. GT11.
- Helley, E.J., and Lajoie, K.R., (1979), "Flatland Deposits of the San Francisco Bay Region, California - Their Geology and Engineering Properties, and Their Importance to Comprehensive Planning," USGS Geological Survey Professional Paper 943, US Government Printing Office, Washington, D.C.
- Holtz, R.D., and Kovacs, W.D., (1981), An Introduction to Geotechnical Engineering, Prentice-Hall.
- Hughes, J.M.O., (1973), "An Instrument for In-Situ Measurement of the Properties of Soft Clays," Ph.D. Dissertation, Cambridge University.
- Hughes, J.M.O., Wroth, C.P., and Windle, D., (1977), "Pressuremeter Tests in Sands," Geotechnique 27, No. 4, 455-477).
- Hughes, J.M.O., (1982), "Interpretation of Pressuremeter Tests for the Determination of the Elastic Shear Modulus," Proceedings of the Conference on Updating Subsurface Sampling of Soils and Rocks and Their In Situ Testing," Engineering Foundation, Santa Barbara, Calif.
- Hughes, J.M.O., Jefferies, M.G., and Morris, D.L., (1984), "Self-Boring Pressuremeter Testing in the Arctic Offshore", Proceedings of the Sixteenth Annual Offshore Technology Conference, Houston, Texas, pp. 255-264.
- Israel, M., (1987), "Finite Element Analysis to Determine Horizontal Stress Changes Due to Embankment Loading of a Soft Clay Foundation, I-95, Portsmouth, New Hampshire", A Project Paper for Master's Degree, University of New Hampshire, Durham, New Hampshire.
- Jáky, G., (1944), "The Coefficient of Earth Pressure at Rest," (In Hungarian), Magyar Mérnök és Építész Egylet Közönyve (Journal of the Society of Hungarian Architects and Engineers), Vol.78, No.22, pp.355-358.
- Jamiolkowski, M., Ladd, C.C., Germaine, J.T., and Lancellotta, R., (1975), "New Developments in Field and Laboratory Testing of Soils," Proc. of the 11th ICSMFE Conference, Vol.1, San Francisco.

- Jefferies, M.G., (1988), "Determination of Horizontal Geostatic Stress in Clay with Self-Bored Pressuremeter," Canadian Geotechnical Journal 25, 559-573.
- Johnston, P.R., (1981), "Finite Element Consolidation Analysis of Tunnel Behavior in Clay," A Thesis submitted in Partial Fulfillment of the Ph.D. Degree, Stanford University, California.
- Jones, A.J. (1989), Measurements of Acoustic Properties of Marine Clays in Triaxial Tests, A Project Paper for Master's Degree, University of New Hampshire, Durham, New Hampshire.
- Ktatorov, A.A., (1930), "Determination of Permissible Soil Pressure by Elastic Pile Method", Stroitel'naya Promyslennost, No. 3, pp 231-234.
- Lacasse, S., and Lunne, T., (1982), "In Situ Horizontal Stress from Pressuremeter Tests," Proc. of the Symposium on the Pressuremeter and its Marine Applications, Paris.
- Lacasse, S., (1986) "In Situ Site Investigation Techniques and Interpretation for Offshore Practice - Interpretation of the Pressuremeter Test," Norwegian Geotechnical Institute, September, 1986.
- Lacasse, S., D'Orazio, T.B., and Brandis, C, (1990) "Interpretation of Self-Boring and Push-In Pressuremeter Tests," Proc. of the 3rd Int. Symposium on Pressuremeters, British Geotechnical Society, Oxford University.
- Ladanyi, B., (1972), "In-Situ Determination of Undrained Stress Strain Behavior of Sensitive Clays with the Pressuremeter," Canadian Geotechnical Journal, 9, pp. 313-319.
- Ladd, C.C. and Luscher, U., (1965), "Engineering Properties of the Soil Underlying the MIT Campus," Research Report R65-68, Soils Publication 185, Department of Civil Engineering, MIT, Cambridge, Mass.
- Ladd, C.C., (1972), "Test Embankment on Sensitive Clay," ASCE Specialty Conference on Performance of Earth and Earth Supported Structures, Lafayette, Indiana, Vol I, Part I, pp. 101-128.
- Ladd, C.C., Rixner, J.J, and Gifford, D.G. (1972), "Performance of Embankments with Sand Drains on Sensitive Clay," ASCE Specialty Conference on Performance of Earth and Earth Supported Structures, Lafayette, Indiana, Vol I, Part I, pp. 211-242.
- Ladd., C.C., and Foott, R., (1977), "Foundation Design of Embankments on Varved Clays," U.S. Dept. of Transportation, FHA, Washington.
- Lambe, T.W. (1960) "A Mechanistic Picture of Shear Strength in Clay," Research Conference on Shear Strength of Cohesive Soils, ASCE, Boulder, Colo.
- Lamé, G., (1852), Le cons sur la théorie mathématique del'élasticite des corps solides", Paris, France.
- Lien, B., (1991), "Anisotropic Behavior and Cylinder Expansion of Pressuremeter in Stiff Soils," Thesis Submitted in Partial Fulfillment for the Ph.D. Degree, Virginia Polytechnic Institute and State University, Blacksburg, VA.
- Levadoux, J.N., and Baligh, M.M., (1986), "Consolidation After Undrained Piezocone Penetration. I: Prediction," Journal of the Geotechnical Engineering Division, ASCE, Vol. 112, No. 7, pp.707-726.

- Lunne, T., Christoffersen, H.P., and Tejelta, T.I., (1985), "Engineering Use of Piezocone Data in North Sea Clays," Proceedings of the XI ICSMFE, San Francisco.
- Lunne, T., Eidsmoen, T., Powell, J., and Quaterman, R., (1986), "Piezocone Testing in Overconsolidated Clays," Proc. 39th Canadian Geot. Conference, Ottawa, pp. 209-218.
- Lutenegger, A.J. and Timian, D.A., (1986), "In Situ Test with K_c Stepped Blade," Proc. of ASCE Spec. Conference on Use of In Situ Tests in Geotechnical Engineering, Blacksburg, VA.
- Lutenegger, A.J. (1988) "Current Status of the Marchetti Dilatometer Test," Proc. of the 1st Int Symposium on Penetration Testing, ISOPT-1, Orlando, Fla, J. de Ruiter, Ed., pp 136-155.
- Mair, R.J., and Wood, D.M., (1987), Pressuremeter Testing, Methods and Interpretation, Butterworths, London, England.
- Marchetti, S., (1975), "A New In Situ Test for the Measurement of Horizontal Soil Deformability," In Situ Measurement of Soil Properties, ASCE, Vol. 2, pp 225-259.
- Marchetti, S., (1981), "Insitu Tests by Flat Dilatometer," Journal of the Geotechnical Engineering Division, Vol. 107, No. GT6, pp.831- 837.
- Marchetti, S., and Totani, G. (1989), " C_u Evaluations from DMTA Dissipation Curves," 12th International Conference on Soil Mechanics and Foundation Engineering, Rio de Janeiro, Brazil.
- Massarsch, K.R., Holtz, R.D., Holm, B.G., and Fredrickson, A., (1975), "Measurement of Horizontal Stress", In Situ Measurement of Soil Properties, ASCE, Raleigh, NC., Vol. I, pp.266-286.
- Massarsch, K.R. (1979), "Lateral Earth Pressure in Normally Consolidated Clay," Proceedings of the Seventh European Conference on Soil Mechanics and Foundation Engineering, Brighton, England, Vol.2, pp 245-250.
- Mayne, P.W., and Kulhawy, F.H. (1982) " K_c -OCR Relationships in Soil," JGED, ASCE, Volume 108, No. GT6.
- Mayne, P.W., and Holtz, R.D., (1986), "Profiling Stress History by Piezocone Soundings," Soils and Foundations, 28 (1), 13 p.
- Mayu, P., (1987), "Determining Parameters For Stiff Residual Soils Using the Self-Boring Pressuremeter," A Thesis Presented in Partial Fulfillment of the Ph. D. Degree, Virginia Polytechnic Institute and State University, Blacksburg, Va.
- Ménard, L., (1956), "An Apparatus for Measuring the Strength of Soils in Place," M.Sc. Thesis, University of Illinois.
- Mitchell, J.K., and Lunne, T. (1977) Unpublished study of several in situ soil tests at H.A.F.B., University of California, Berkeley.
- Nejame, L.A., (1991), "Dilatometer Testing of the Marine Clay Deposit at Pease AFB, New Hampshire," Thesis Presented in Partial Fulfillment of the Requirements for the Masters Degree, University of New Hampshire, Durham, NH.
- Osaimi, A.E., and Clough, G.W, (1979), "Pore-Pressure Dissipation During Excavation", Journal of the Geotechnical Engineering Division, ASCE, pp.481-498.

- Palmer, A.C., (1972), "Undrained Plane-Strain Expansion of a Cylindrical Cavity in Clay: A Simple Interpretation of the Pressuremeter Test," *Geotechnique*, Vol. 22, No. 3, pp. 451-457.
- Poepsel, P., and Kavazanjian, E., (1984), "Elasto-Plastic Finite Element Analysis of the I-95 and Atchafalaya Embankment Foundations," Stanford Univ. Dept. of Civ. Eng., Geotechnical Report GT2.
- Powell, J.J.M., (1990), "A Comparison of Four Different Pressuremeters and Their Methods of Interpretation in Stiff, Heavily Overconsolidated Clay," Proc. of the 3rd Int. Symposium on Pressuremeters, British Geotechnical Society, Oxford University.
- Prapaharan, S., Chameau, J.L., Altschaeffl, A.G. and Holtz, R.D., (1990), "Effect of Disturbance on Pressuremeter Results in Clays", *Journal of Geotechnical Engineering*, ASCE, Vol. 116, No. 1, pp. 35-53.
- Prevost, J-H. and Hoeg, K., (1975), "Analysis of Pressuremeter in Strain-Softening Soil," *Journal of the Geotechnical Engineering Division*, ASCE, Vol. 101, No. GT8, pp.717-732.
- Robertson, P.K. and Campanella, R.G., (1983), "Interpretations of Cone Penetration Tests- Part 1 (Sand)," *Canadian Geotechnical Journal*, Vol. 20, No. 4.
- Robertson, P.K. and Campanella, R.G., (1986), "Guidelines for Use and Interpretation of the Electric Cone Penetration Test," Hogentogler and Company, Inc., 196 p.
- Robertson, P.K., Campanella, R.G., Gillespie, D., and By, T., (1988) "Excess Pore Pressure and the Flat Dilatometer Test," Proc. ISOPT-1, Orlando Fla., Vol. 1, pp 567-576.
- Roscoe, K.H., and Burland, J.B., (1968), "On the Generalized Stress-Strain Behavior of 'Wet' Clay," *Engineering Plasticity*, Cambridge University Press, Cambridge, pp. 535-609.
- Schmertmann, J.H., (1970), "Static Cone to Compute Static Settlement Over Sand," *Journal of Soil Mechanics and Foundation Division*, ASCE Vol. 96, No. 3.
- Schmertmann, J.H., (1977), "Guidelines for Cone Penetration Test - Performance and Design," FHWA-TS-78-209, US Department of Transportation, Federal Highway Administration.
- Schmertmann, J.H., (1986), "Suggested Method for Performing the Flat Dilatometer Test," *ASTM Geotechnical Journal*, June, 1986.
- Schmertmann, J.H., (1988), "The Coefficient of Consolidation Obtained from P2 Dissipation in the DMT," *Geotechnical Conference Sponsored by the Pennsylvania Dept of Transportation*.
- Schmidt, B., (1966), "Discussion of 'Earth Pressures at Rest Related to Stress History,'" *Canadian Geotechnical Journal*, Vol. III, No.4, pp. 239-242.
- Sivakugan, M., Holtz, R.D., and Chameau, J.L., (1988), "CKoUC Shear Strength of Normally Consolidated Clays from CIUC Tests", *Journal of Geotechnical Engineering*, ASCE, Vol. 114, No. 3.
- Skempton, A.W., (1954), "The Pore Pressure Coefficients A and B," *Geotechnique*, Vol. IV, pp 143-147.
- Stordal, A., (1985), "Shear Strength Parameters Obtained from

- Pressuremeter Tests", Eleventh International Conference, ICSMFE, San Francisco.
- Strahler, A.N., (1988), "A Geologists View of Cape Cod," Parnassus Imprints, Orleans, Massachusetts.
- Tedd, P., and Charles, J.A. (1983) "Evaluation of Push-In Pressure Results in Stiff Clay," Symposium International, Essais en Place In Situ Testing, Paris.
- Tevenas, F.A., Blanchette, G., Leroueil, S., Roy, M., and LaRochelle, P. (1975) "Difficulties in the In Situ Determination of K_v in Soft, Sensitive Clays," Proc. of ASCE Specialty Conf. on Insitu Measurement, Raleigh, N.C.
- Trask, P.D., and Rolston, J.W. (1951), "Engineering Geology of the San Francisco Bay, California," Geological Society of America, Bulletin, Vol. 62.
- Treasher, R.C., (1963), "Geology of the Sedimentary Deposits in San Francisco Bay," California Division of Mines and Geology, Special Report 82.
- Vesic, A.S., (1972) "Expansion of Cavities in Infinite Soil Mass," Journal of the Soil Mechanics and Foundation Design Division, ASCE, Vol. 98, No. SM3.
- Wardwell, R.E., Findlay, R.C., and Muzzy, M.W., (1988) "Seepage Effects on Sedimentation of Fly Ash Slurry," Hydraulic Fill Structures, American Society of Civil Engineers Special Publication No. 21, Fort Collins, Co.
- Wong, K.S., and Duncan, J.M., (1974), "Hyperbolic Stress-Strain Parameters for Nonlinear Finite Element Analysis of Stresses and Movements in Soil Masses," Univ. of Berkeley Dept. of Civil Eng. Report No. TE-74-3, Berkeley, Calif.
- Wood, D.M., and Wroth, C.P. (1977) "Some Laboratory Experiments Related to the Results of Pressuremeter Tests," Geotechnique, June.
- Wroth, C.P., (1975), "Insitu Measurement of Initial Stresses and Deformation Characteristics," Proceedings, In Situ Measurement of Soil Properties, ASCE, North Carolina, 1975.
- Wroth, C.P., (1980), "Cambridge In-Situ Probe," Proceedings of a Symposium on Site Exploration in Soft Ground Using In-Situ Techniques, May, 1978, Alexandria, Va., Federal Highway Administration, final report dated January, 1980.
- Wroth, C.P., (1982), "British Experience with the Self-Boring Pressuremeter," Symposium sur la Pressiometrie et ses Applications en Mer, L'Institut Francais du Petrole et les Laboratoires des Ponts et Chaussees, Paris.
- Yeung, S.K., and Carter, J.P., (1990), "Interpretation of Pressuremeter Test in Clay Allowing for Membrane End Effects and Material Non-Homogeneity," Proceedings of the 3rd International Symposium on Pressuremeters, British Geotechnical Society, Oxford University.

APPENDIX A
FACTORS INFLUENCING SBPM MEASUREMENTS

APPENDIX A

FACTORS INFLUENCING SBPM MEASUREMENTS

A.1 Introduction

The purpose of this appendix is to present the findings of research conducted to determine factors influencing measurements made with the Cambridge Insitu version of the SBPM. Factors assessed include barometric pressure, temperature, drift of calibration factors with time, membrane stiffness, inclination of the pressuremeter in the ground, and the surface load of the drill rig. The assessment of these factors resulted in the finding that some of the factors required correction during data reduction, namely, temperature influence on measured pore pressure, and membrane stiffness on measured horizontal stress. Improved methods of applying these corrections are discussed herein.

A.2 Factors Influencing Pore Pressure Measurements

A.2.1 Instrumentation of the SBPM

The pressure applied within the probe is measured by the total pressure transducer (TP) located inside the SBPM probe. Two additional transducers (PPA and PPB) are mounted to the SBPM membrane on opposite sides at the midpoint of the probe. PPA and PPB are differential transducers which sense both the pressure within the probe as well as the pressure just outside the membrane, at the membrane-soil interface. Assuming full saturation of the porous stone and cell cavity on the exterior side of these transducers, output from these membrane mounted transducers represents the difference between the internal probe and external soil pore water pressures. This is actually a measurement of effective stress, since the pore water pressure is automatically subtracted from the expansion pressure. Because of this, transducers PPA and PPB are referred to as effective stress cells or transducers. All of the transducers are circular strain gauges, mounted on flexible diaphragms, and measure pressure in terms of volts.

The configuration of a typical effective stress cell is exhibited on Figure A-1. For the subject research, two variations to this cell were used. The standard version, as supplied by Cambridge Insitu, is cell PPB. This cell consists of a strain gauge mounted on a steel diaphragm with a porous brass filter disk. The cell must be saturated prior to use by injecting de-aired water through a hole in the filter stone which is normally plugged with a small screw. The other cell, PPA, was modified in an attempt to improve on the pore pressure measuring system. The porous brass stone was replaced by a Coors porcelain, high pressure air entry stone. No de-airing plug was included in this model. The design was to de-air this cell by injecting pressurized de-aired water into the cell through an internal tube. Test results indicated that the system did not function properly, likely due to expansion/contraction of a plastic section of the internal de-airing tube inside the probe.

A.2.2 Conventional Computation of SBPM Pore Pressure

Computation of excess pore pressures which exist at the start of an SBPM test due to deployment requires consideration of a number of variables. Theoretically, the pore pressure at the membrane-soil interface can be deduced by converting the voltage readings from the total pressure transducer, TP, and the effective pressure transducers, PPA and PPB, to units of pressure. This is done by multiplying the voltage readings by the appropriate calibration factors which are determined as part of the calibration procedures of the SBPM prior to testing. Pore pressure can then be determined by the fact that the effective stress cells (PPA and PPB) measure the internal probe pressure

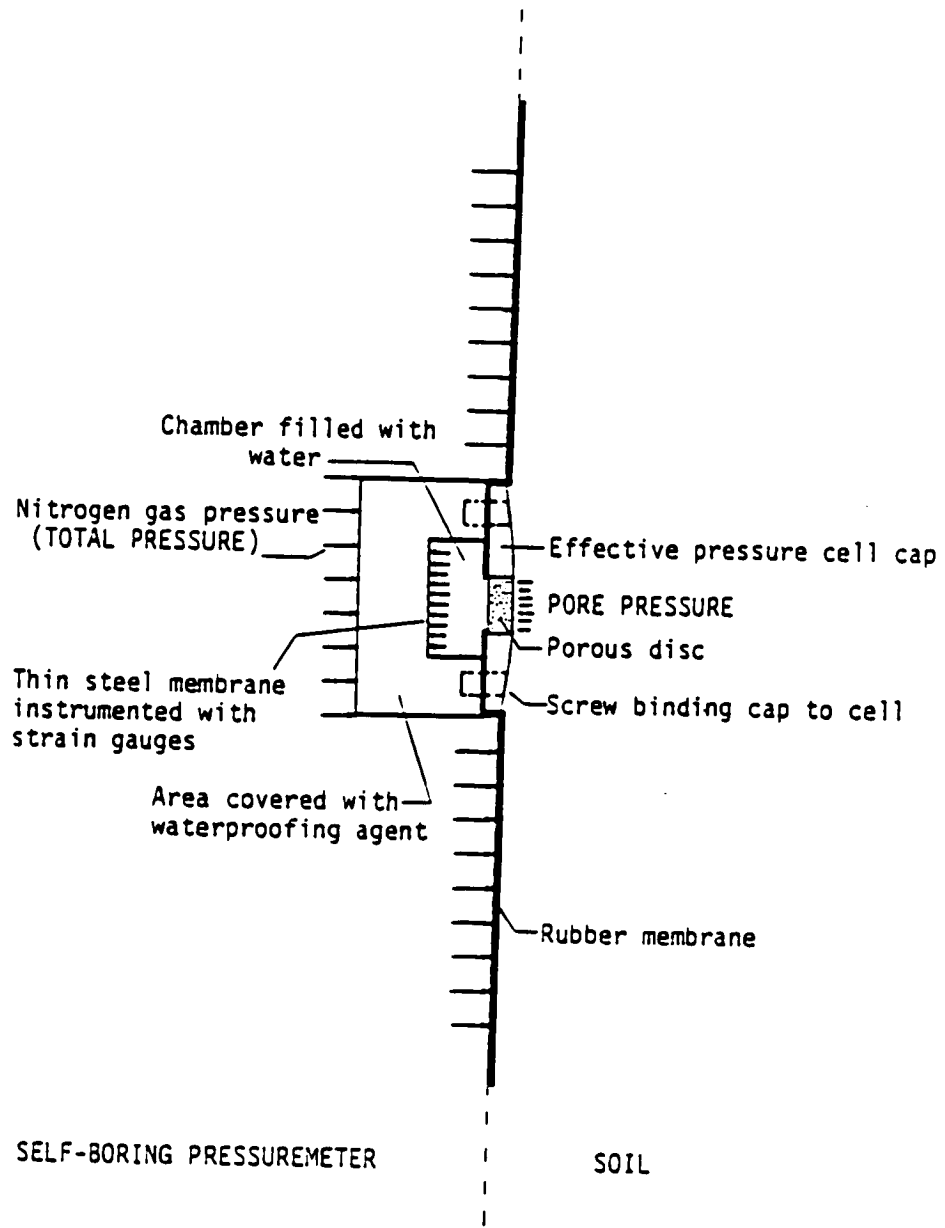


Figure A-1 Schematic of an Effective Stress Cell (after Benoit, 1983)

minus the pore pressure (u) outside of the probe:

$$\sigma_{ppm} \text{ (or } \sigma_{ppb}) = \sigma_p - u \quad (\text{Eq A-1})$$

where:

- σ_{ppm} = pressure measured by PPA
- σ_{ppb} = pressure measured by PPB
- σ_p = pressure measured by TP
- u = pore pressure

rearranging: $u = \sigma_p - \sigma_{ppm} \text{ (or } \sigma_{ppb}) \quad (\text{Eq A-2})$

Since the transducers are strain gauge based and output is in volts, the problem in conversion of TP, PPA and PPB to units of pressure requires an accurate knowledge of the voltage these transducers measure when the pressure each is sensing is atmospheric. It appears that this determination should be straightforward; the atmospheric pressure value of TP should be equal to the voltage measured prior to expansion, while the probe is vented. Also, similar "zero" voltages can be measured for PPA and PPB when the probe is at the ground surface. However, the findings of this research indicate that the zero voltage from test to test in a particular boring can vary. Table A-1 is a tabulation of conversion factors and output voltages for the tests conducted during this research. Examination of the Test Zero TP column (Column 9) of Table A-1 indicates the variability of the zero voltage. The variability from test boring to test boring is even greater. Generally, the range of variability amounted to about 200 psf for tests conducted within a particular borehole. Over the entire field program, however, the range of atmospheric pressure values of TP voltage amount to a range in measured pressure of over 1800 psf. Possible explanations for the shift in the atmospheric pressure value of TP include: standard measurement errors, changes in atmospheric pressure, temperature shift, changes in the transducer system resistivity with time, and possibly internal probe moisture, all of which are subsequently discussed.

A.2.3 Measurement Errors

The accuracy of the SBPM to measure relative pressure changes, assuming all other factors are constant (atmospheric pressure, temperature, grounding, etc.) was assessed from examination of initial portions of the raw test data, prior to probe pressurization. The following voltage and pressure resolutions were observed:

	Voltage Measurement Resolution (volt)	Pressure Measurement Resolution (psf)
TP	± 0.001	31-33
PPA	± 0.001	42-54
PPB	± 0.001	41-45

Since pore pressure is determined by subtraction of values of PPA or PPB and TP (see Equation A-2), the resolution error being additive, then the error in measurement of excess pore pressure could be about ±150 to ±200 psf. However, this measurement error is significantly less than the observed variation of the test zero value of TP on Table A-1, therefore other influences must come into play.

A.2.3.1 Influence of Atmospheric Pressure

Possibly the most obvious environmental factor which might be surmised to have an influence on the output from TP, PPA and PPB is fluctuation of atmospheric pressure. Since PPA and PPB measure the pressure differential outside and inside of the probe, it can be reasoned that atmospheric pressure changes would have no influence on the measured pressure if atmospheric pressure acts on both sides of the membrane.

Test Designation (1)	FROM CALIBRATION										Test Zero PPA (Volt) (10)	Test Zero PPB (Volt) (11)	Computed SIKpppac (Volt) (12)	Computed SIKppbac (Volt) (13)
	PPA Factor (psf/v) (2)	PPB Factor (psf/v) (3)	Surface		Surface PPB Zero (Volt) (6)	TP vs PPB Slope (v/v) (7)	TP vs PPA Slope (v/v) (8)	TP (Volt) (9)	Test Zero TP (Volt) (9)					
			Surface TP Zero (Volt) (4)	Surface PPA Zero (Volt) (5)										
PMC1.1	54090	45346	45346	0.260010	0.089111	-0.100090	0.707447	0.593084	0.261465	0.076904	-0.109863	0.089974	-0.099061	
PMC1.2	54090	45346	45346	0.260010	0.089111	-0.100090	0.707447	0.593084	0.261230	0.075684	-0.118408	0.089835	-0.099227	
PMC1.3	54090	45346	45346	0.260010	0.089111	-0.100090	0.707447	0.593084	0.261230	0.073242	-0.115967	0.089835	-0.099227	
PMC2.1	54090	45346	45346	0.260010	0.089111	-0.100090	0.707447	0.593084	0.261230	0.026855	-0.112305	0.089835	-0.099227	
PMC2.2	54090	45346	45346	0.260010	0.089111	-0.100090	0.707447	0.593084	0.261230	0.028076	-0.117188	0.089835	-0.099227	
PMC2.3H	54090	45346	45346	0.260010	0.089111	-0.100090	0.707447	0.593084	0.266113	0.043945	-0.118408	0.092731	-0.095772	
PMC2.4	54090	45346	45346	0.260010	0.089111	-0.100090	0.707447	0.593084	0.262451	0.042725	-0.128174	0.090559	-0.090363	
PMC3.1	54090	45346	45346	0.260010	0.089111	-0.100090	0.707447	0.593084	0.260010	0.029297	-0.119629	0.089111	-0.100090	
PMC3.2H	54090	45346	45346	0.260010	0.089111	-0.100090	0.707447	0.593084	0.263672	0.052490	-0.122070	0.091283	-0.097499	
PMC3.3H	54090	45346	45346	0.260010	0.089111	-0.100090	0.707447	0.593084	0.263672	0.057373	-0.126953	0.091283	-0.097499	
PMC3.4H	54090	45346	45346	0.260010	0.089111	-0.100090	0.707447	0.593084	0.263672	0.063477	-0.139160	0.091283	-0.097499	
PMC3.5H	54090	45346	45346	0.260010	0.089111	-0.100090	0.707447	0.593084	0.263672	0.059814	-0.128174	0.091283	-0.097499	
PMC3.5R	54090	45346	45346	0.260010	0.089111	-0.100090	0.707447	0.593084	0.264893	0.062256	-0.145264	0.092007	-0.096636	
PMC3.6H	54090	45346	45346	0.260010	0.089111	-0.100090	0.707447	0.593084	0.262451	0.061035	-0.111084	0.090559	-0.098363	
PMC4.1	53944	43744	43744	0.256348	0.090332	-0.117180	0.732285	0.594688	0.253906	0.081787	-0.126953	0.088800	-0.118968	
PMC4.2	53944	43744	43744	0.256348	0.090332	-0.117180	0.732285	0.594688	0.25127	0.076904	-0.134277	0.089606	-0.118074	
PMC4.3	53944	43744	43744	0.256348	0.090332	-0.117180	0.732285	0.594688	0.256348	0.078001	-0.139160	0.090332	-0.117180	
PMC4.4	53944	43744	43744	0.256348	0.090332	-0.117180	0.732285	0.594688	0.256348	0.078001	-0.141602	0.090332	-0.117180	
PMC4.5	53944	43744	43744	0.256348	0.090332	-0.117180	0.732285	0.594688	0.256348	0.067714	-0.146484	0.090332	-0.117180	
PMC4.6	53944	43744	43744	0.256348	0.090332	-0.117180	0.732285	0.594688	0.256348	0.063477	-0.150146	0.090332	-0.117180	
PMC4.7	53944	43744	43744	0.256348	0.090332	-0.117180	0.732285	0.594688	0.257568	0.061035	-0.151367	0.091058	-0.116287	

Table A-1 Excess Pore Pressure Variables

Test Designation (1)	FROM CALIBRATION										Test Zero TP (Volt) (9)	Test Zero PPA (Volt) (10)	Test Zero PPB (Volt) (11)	Computed SIOppac (Volt) (12)	Computed SIOppac (Volt) (13)
	PPA Factor (psi/v) (2)	PPB Factor (psi/v) (3)	Surface TP Zero (Volt) (4)	Surface PPA Zero (Volt) (5)	Surface PPB Zero (Volt) (6)	TP vs PPB Slope (%/v) (7)	TP vs PPA Slope (%/v) (8)	Test Zero							
								TP (Volt) (9)	PPA (Volt) (10)						
PMJ3.2	53944	43744	0.256348	0.090332	-0.117180	0.732285	0.594688	0.257568	0.076904	-0.128174	0.091058	-0.116287			
PMJ3.2R	53944	43744	0.256348	0.090332	-0.117180	0.732285	0.594688	0.260010	0.075684	-0.125732	0.092510	-0.114498			
PMJ3.3	53944	43744	0.256348	0.090332	-0.117180	0.732285	0.594688	0.258789	0.078125	-0.133057	0.091784	-0.115392			
PMJ3.4	53944	43744	0.256348	0.090332	-0.117180	0.732285	0.594688	0.257568	0.076904	-0.136719	0.091058	-0.116287			
PMJ3.4R	53944	43744	0.256348	0.090332	-0.117180	0.732285	0.594688	0.261230	0.068359	-0.131836	0.093235	-0.113605			
PMJ3.5	53944	43744	0.256348	0.090332	-0.117180	0.732285	0.594688	0.260010	0.072021	-0.141602	0.092510	-0.114498			
PMJ3.6	53944	43744	0.256348	0.090332	-0.117180	0.732285	0.594688	0.261230	0.065918	-0.146184	0.093235	-0.113605			
PMJ4.1	53944	43744	0.256348	0.090332	-0.117180	0.732285	0.594688	0.260010	0.074463	-0.118408	0.092510	-0.114498			
PMJ4.2	53944	43744	0.256348	0.090332	-0.117180	0.732285	0.594688	0.261230	0.074463	-0.128174	0.093235	-0.113605			
PMJ4.2R	53944	43744	0.256348	0.090332	-0.117180	0.732285	0.594688	0.263672	0.074463	-0.125732	0.094487	-0.118117			
PMJ4.3	53944	43744	0.256348	0.090332	-0.117180	0.732285	0.594688	0.262451	0.073242	-0.131836	0.093961	-0.112711			
PMJ4.4	53944	43744	0.256348	0.090332	-0.117180	0.732285	0.594688	0.262451	0.072021	-0.135498	0.093961	-0.112711			
PMJ4.5	53944	43744	0.256348	0.090332	-0.117180	0.732285	0.594688	0.262451	0.069280	-0.141602	0.093961	-0.112711			
PMJ4.6H	53944	43744	0.256348	0.090332	-0.117180	0.732285	0.594688	0.261230	0.058594	-0.145264	0.093235	-0.113605			
PMJ4.7	53944	43744	0.256348	0.090332	-0.117180	0.732285	0.594688	0.260010	0.052490	-0.150146	0.092510	-0.114498			
PMJ5.1	54819	42421	0.205078	0.091553	-0.184432	0.756212	0.585193	0.211182	0.085449	-0.185547	0.095125	-0.179816			
PMJ5.2	54819	42421	0.205078	0.091553	-0.184432	0.756212	0.585193	0.212402	0.095215	-0.169678	0.095839	-0.178894			
PMJ5.3	54819	42421	0.205078	0.091553	-0.184432	0.756212	0.585193	0.212402	0.083008	-0.180664	0.095839	-0.178894			
PMJ5.4	54819	42421	0.205078	0.091553	-0.184432	0.756212	0.585193	0.216064	0.076904	-0.194092	0.097982	-0.176124			
PMJ5.5	54819	42421	0.205078	0.091553	-0.184432	0.756212	0.585193	0.216064	0.076904	-0.194092	0.097982	-0.176124			
PMJ5.6	54819	42421	0.205078	0.091553	-0.184432	0.756212	0.585193	0.217285	0.076904	-0.196533	0.098696	-0.175201			
PMJ6.1	56229	42600	0.214844	0.089085	-0.183120	0.767255	0.571859	0.228271	0.076904	-0.187236	0.096763	-0.172818			
PMJ6.2	56229	42600	0.214844	0.089085	-0.183120	0.767255	0.571859	0.228271	0.080566	-0.172119	0.096763	-0.172818			
PMJ6.3	56229	42600	0.214844	0.089085	-0.183120	0.767255	0.571859	0.228271	0.076904	-0.177002	0.096763	-0.172818			
PMJ6.4H	56229	42600	0.214844	0.089085	-0.183120	0.767255	0.571859	0.228271	0.072021	-0.183105	0.096763	-0.172818			

Table A-1 (continued) Excess Pore Pressure Variables

Test Designation	FROM CALIBRATION										Test Zero PPA (Volt) (10)	Test Zero PPB (Volt) (11)	Computed SLOppbc (Volt) (12)	Computed SLOppbc (Volt) (13)
	PPA Factor (psi/v) (2)	PPB Factor (psi/v) (3)	Surface TP Zero (Volt) (4)	Surface PPA Zero (Volt) (5)	Surface PPB Zero (Volt) (6)	TP vs PPB Slope (v/v) (7)	TP vs PPA Slope (v/v) (8)	TP (Volt) (9)						
PM17.1	52523	41643	0.214844	0.092304	-0.160440	0.770354	0.610776	0.218506	0.087890	-0.159912	0.094541	-0.157619		
PM17.2	52523	41643	0.214844	0.092304	-0.160440	0.770354	0.610776	0.218506	0.093994	-0.167236	0.094541	-0.157619		
PM17.3	52523	41643	0.214844	0.092304	-0.160440	0.770354	0.610776	0.218506	0.097656	-0.173340	0.094541	-0.157619		
PM17.4H	53442	44650	0.225830	0.091503	-0.155500	0.767255	0.610776	0.225830	0.075684	-0.175781	0.091503	-0.155500		
PM18.1	47295	40764	0.214844	0.104980	-0.114740	0.786969	0.678298	0.213623	0.093994	-0.126953	0.104152	-0.115701		
PM18.2	47295	40764	0.214844	0.104980	-0.114740	0.786969	0.678298	0.216004	0.091553	-0.129393	0.103808	-0.113780		
PM18.3H	47295	40764	0.214844	0.104980	-0.114740	0.786969	0.678298	0.216004	0.085449	-0.137939	0.103808	-0.113780		
PM18.4	47295	40764	0.214844	0.104980	-0.114740	0.786969	0.678298	0.217285	0.083008	-0.135498	0.106636	-0.112819		
PMS1.1	42400	40366	0.218506	0.118408	-0.100090	0.794714	0.756593	0.218506	0.104980	-0.106201	0.118408	-0.100090		
PMS1.2	42400	40366	0.218506	0.118408	-0.100090	0.794714	0.756593	0.218506	0.101318	-0.128174	0.118408	-0.100090		
PMPI.1	54819	42421	0.205078	0.091553	-0.184432	0.756212	0.585193	0.220947	0.090332	-0.191650	0.100839	-0.172432		
PMPI.2	54819	42421	0.205078	0.091553	-0.184432	0.756212	0.585193	0.220947	0.090332	-0.224609	0.100839	-0.172432		
PMP2.1	54819	42421	0.205078	0.091553	-0.184432	0.756212	0.585193	0.220947	0.053711	-0.225830	0.100839	-0.172432		
HAM1.1	53442	44650	0.227051	0.091503	-0.156250	0.718477	0.600271	0.227051	0.069580	-0.181885	0.091503	-0.156250		
HAM1.2	53442	44650	0.227051	0.091503	-0.156250	0.718477	0.600271	0.227051	0.064697	-0.181885	0.091503	-0.156250		
HAM1.3	53442	44650	0.227051	0.091503	-0.156250	0.718477	0.600271	0.227051	0.072021	-0.179443	0.091503	-0.156250		
HAM2.1	53442	44650	0.227051	0.091503	-0.156250	0.718477	0.600271	0.225830	0.079346	-0.174561	0.090770	-0.157127		
HAM2.2	53442	44650	0.227051	0.091503	-0.156250	0.718477	0.600271	0.224609	0.078125	-0.183105	0.090037	-0.158005		
HAM2.3	53442	44650	0.227051	0.091503	-0.156250	0.718477	0.600271	0.224609	0.075684	-0.183547	0.090037	-0.158005		
HAM2.4H	53442	44650	0.227051	0.091503	-0.156250	0.718477	0.600271	0.229947	0.067139	-0.184326	0.087839	-0.160636		
HAM2.4R	53442	44650	0.227051	0.091503	-0.156250	0.718477	0.600271	0.227051	0.069580	-0.181885	0.091503	-0.156250		
HAM2.5P	53442	44650	0.227051	0.091503	-0.156250	0.718477	0.600271	0.225830	0.069580	-0.186768	0.090770	-0.157127		

Table A-1 (continued) Excess Pore Pressure Variables

Figure A-2 presents plots of PPA and PPB readings at different barometric pressures. The readings were taken on several different days. Barometric pressure at the time of the readings was obtained from a local meteorologic station (Pease Air Force Base). The probe was in a laboratory environment, at relatively constant temperature (about 20°C). As reasoned, it appears that atmospheric pressure has no visible influence on the output of PPA and PPB. However, in the ground, if the groundwater system adjacent to the probe was not affected by atmospheric pressure, and the probe was vented to atmosphere, it is conceivable that an effect could be measured by the transducers.

Voltage versus atmospheric pressure data is presented on Figure A-2 for the TP transducer. In contrast to PPA and PPB, a slight effect can be seen. The data indicates that as atmospheric pressure increases, the TP pressure measured increases. This appears reasonable because the TP transducer measures absolute pressure, rather than the differential pressure measured by the other two transducers. Further, it indicates that during testing in the ground, fluctuations in atmospheric pressure could affect the magnitude of measured lateral stress in the soil, however, since borings are usually completed on the same day, and on days when weather was fair, atmospheric pressure fluctuations are likely to be small.

The range of atmospheric pressure on Figure A-2 is about 0.60 inches of mercury. This converts to 42 psf. This indicates that fluctuations in atmospheric pressure will have, at most, a negligible influence on SBPM measurements. Further, the potential range in atmospheric pressure does not account for the observed range in the TP test zero voltage (Column 9) on Table A-1 which is measured when the transducer is sensing atmospheric pressure.

A.2.3.2 Influence of Temperature

The influence of temperature on the SBPM pressure transducer system was assessed in the laboratory. The probe was first placed in a 30 gallon tank filled with hot tap water, and temperature measurements monitored with time. Temperature measurements were taken by use of a standard laboratory thermometer ($\pm 1^\circ\text{C}$) in the water bath and by a temperature transducer built into the SBPM. The bath was frequently stirred to maintain a relatively constant temperature throughout the tank. Figure A-3 is a plot of probe and bath water temperature versus time after submersion of the SBPM. This plot indicates that the temperature equalization of the probe interior with the water bath took about 20 to 30 minutes.

During drilling of Pease AFB boring PMJ8 (in November), it was noticed that after drilling to each test depth, the temperature of the probe was about 9.5°C. After the dissipation period at each test depth, the probe warmed to about 12°C. It is believed that this temperature change was a result of the drilling fluid (surface water) being cooler than the ambient ground temperature. As a result, the use of a dissipation period for temperature adjustment of the probe is not only important upon first putting the probe into the ground, but also after drilling to each test depth because of the potential temperature differences of drilling fluid and the ground temperature.

After temperature equalization of the SBPM probe with the warm laboratory bath, periodic readings of TP, PPA and PPB were taken to see if temperature variation influenced voltage output. After the temperature of the bath had achieved room temperature (about 24 hours) some ice was added. The probe was again inserted into the bath, the probe temperature was allowed to equalize with the bath temperature (about 20 to 30 minutes) and readings of the transducers made as the bath warmed. Figure A-4 presents plots of probe temperature versus TP and PPA/PPB output voltage. As can be seen, there is an apparent shift in measured pressure (volts) with temperature. The range in output voltage and indicated pressure range over the imposed 20 degree Celsius range for the transducers is as follows:

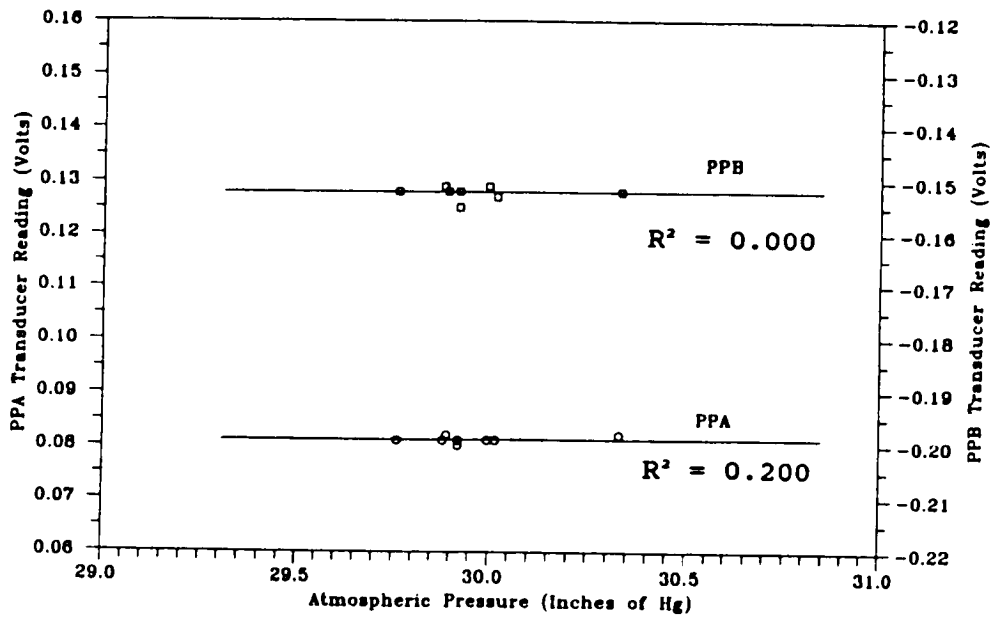
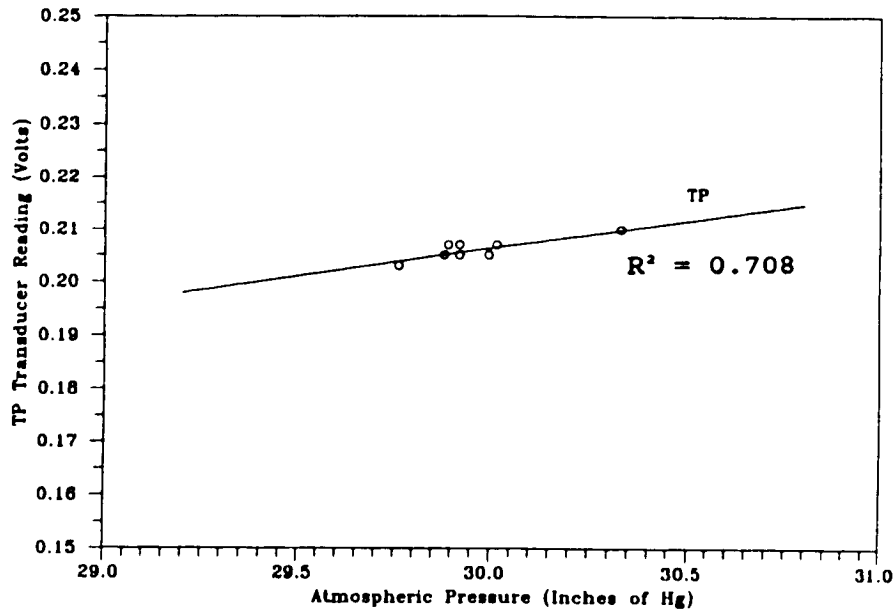


Figure A-2 TP, PPA and PPB Versus Barometric Pressure

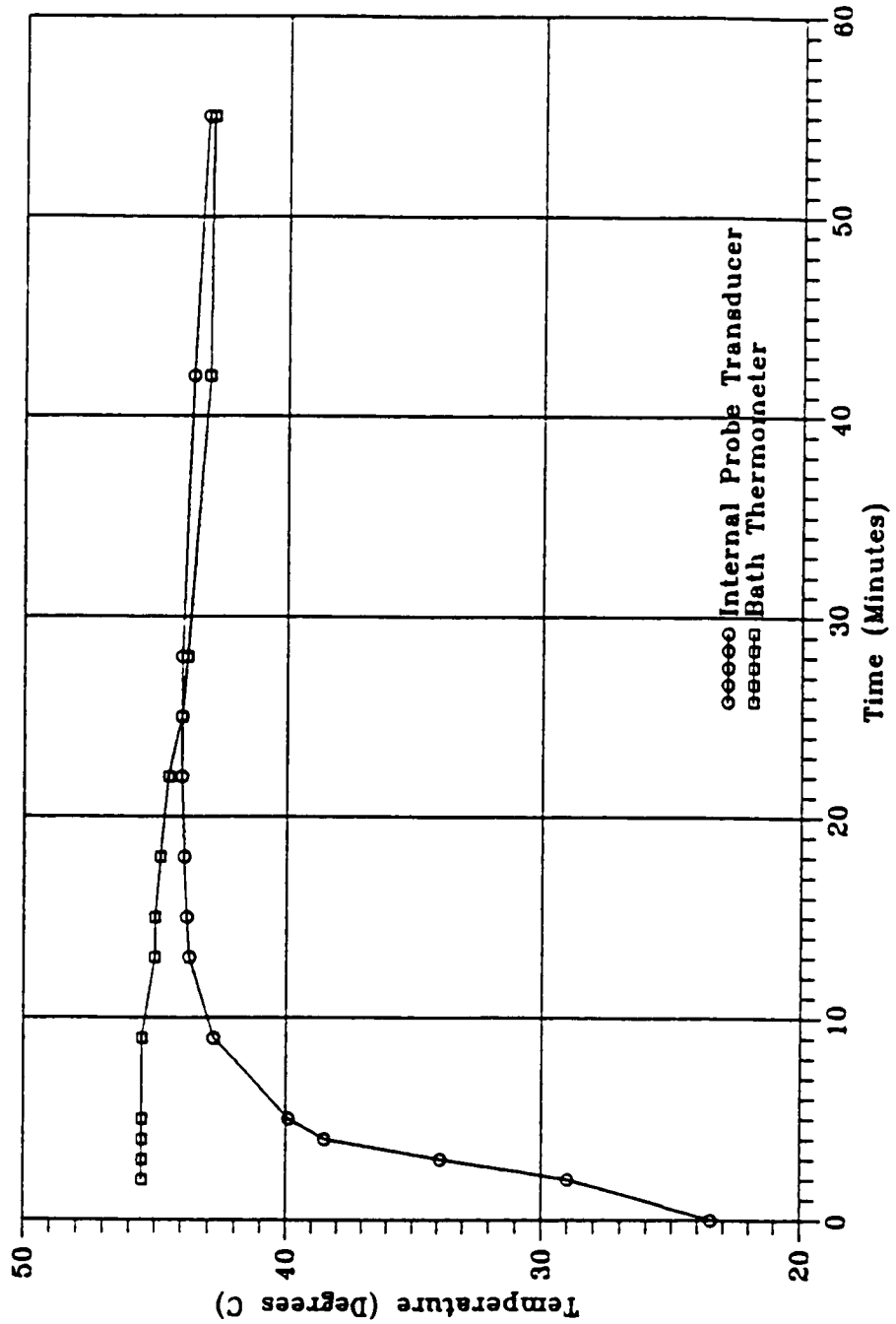


Figure A-3 Time for Temperature Adjustment of SBPM to Warm Bath

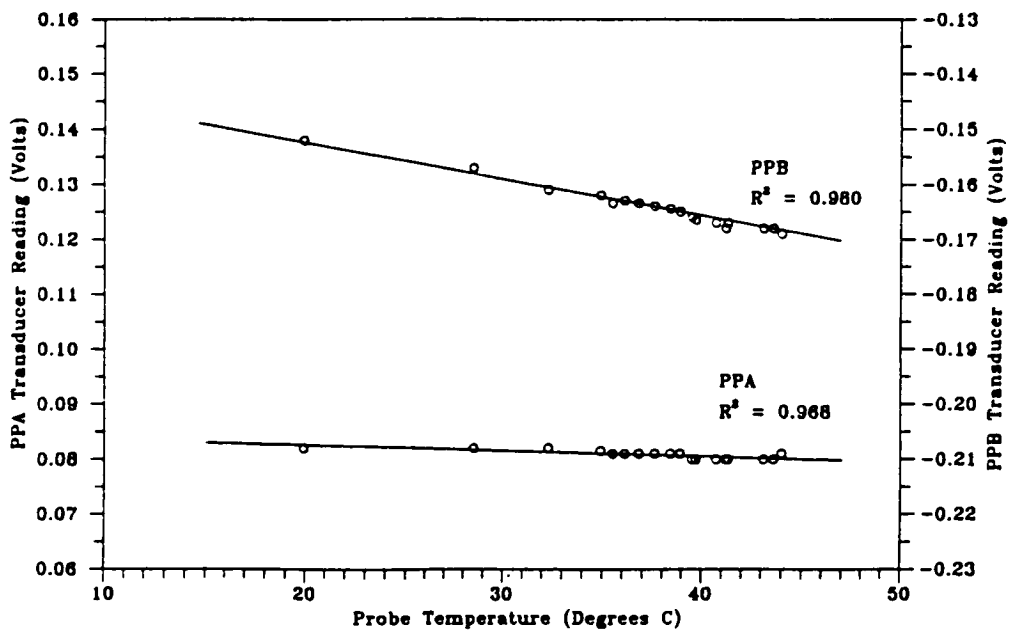
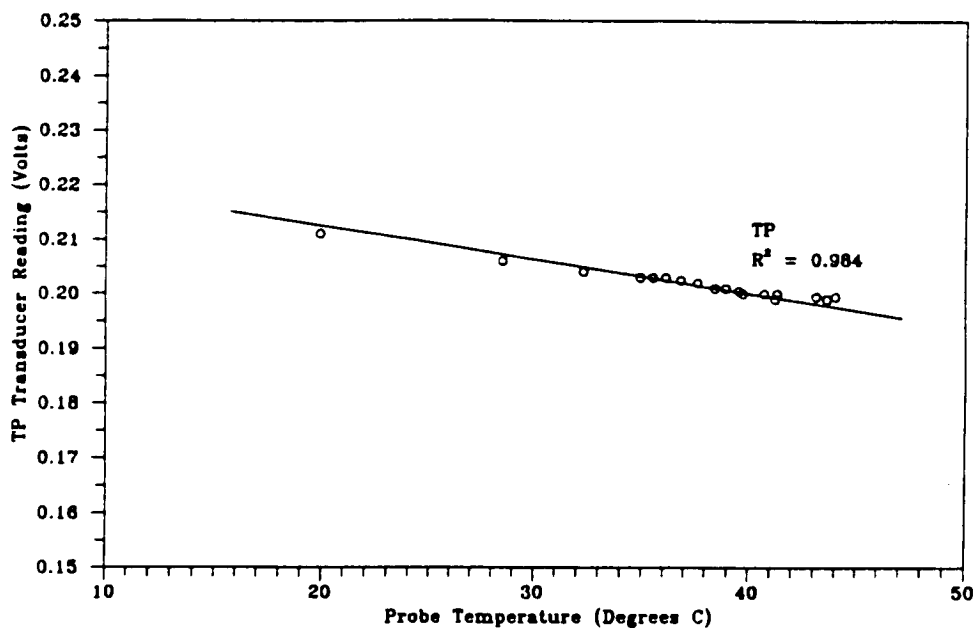


Figure A-4 TP, PPA and PPB Versus Probe Temperature

	Range of Voltage Over 20° C -----	Apparent Pressure Range Over 20° C -----
TP	0.015 v	± 500 psf
PPA	0.001 v	± 50 psf
PPB	0.015 v	± 600 psf

As can be seen, the response of TP and PPB is relatively similar compared to that of PPA. The significantly flatter response of PPA indicated on the above table can be observed on Figure A-4.

This range of apparent pressure due to temperature change brackets the kind of fluctuations observed in the test zero value of TP within a particular boring as indicated in Column 9 of Table A-1, but does not account for the fluctuation in test zero values observed over the entire research period. This indicates that another influence must exist.

A.2.3.3 Influence of System Resistance

During the SBPM research, the probe had to be dismantled and cleaned on occasion. The following lists the tests performed with respect to major dismantlings:

- Prior to First Dismantling: PMC1, 2, 3, and 4; and
PMJ3 and 4
- After First Dismantling: PMJ5, 6, and 7; PMP1 and 2
and HAM1 and 2
- After Second Dismantling: PMJ8 and PMS1

These three sets of tests will be denoted Series 1, 2 and 3, respectively. After dismantling and cleaning, shifts in the atmospheric zero value of TP were observed, as can be noted on Table A-1. Similar shifting occurred to the calibration "zero" values of PPA and PPB. It is theorized that this shifting was caused by low level grounding due to dirt and corrosion between wires mounted on the probe body and/or changes to the resistance values of the resistors due to aging or the weathering effects of moisture which has entered the probe. While the actual cause of these shifts was not determined, their consequences were examined. Figure A-5, a plot of the atmospheric zero value of TP versus that of PPB, was made from several calibration expansions performed during all three series of tests. Each data point is from a single calibration test. As can be seen, three groups of points emerge, each group representing a particular series of tests. The implication of this is that expansion calibrations used to reduce test data should be made frequently, ideally, on the same day as the SBPM test, in the field and using the identical equipment setup, and that the probe should be fully calibrated after every dismantling.

A.2.3.4 Influence of Internal Humidity

An additional effect was observed in the case where the probe was left in the ground for a long period of time. Boring PMC 3 was done over the course of 7 days; during the entire time, the probe was in the ground below the groundwater table. Calculated excess pore pressures (see Table A-2) suggested by these tests were up to almost 1000 psf, a value more on the order of the push-in tests PMP1.1, PMP1.2 and PMP2.1. Some of the PMC3 tests, namely 3.2, 3.3H, 3.4H and 3.5R were drilled on one day and tested on a subsequent day, with high excess pore pressures indicated at the start of the test. After an elapsed time of 24 hours or more, one would expect excess pore pressures to be substantially dissipated; holding tests conducted during the research indicated the time for dissipation of 50 percent of the excess pore pressure, t_{50} , on the order of 30 minutes or so. As a result, it is concluded that the computed excess pore pressures indicated for these tests are in error, likely due to some sort of drift that occurred due to the long time the probe was in the ground, possibly due to high humidity of the air within the probe. This humidity could have been caused by water seepage through the

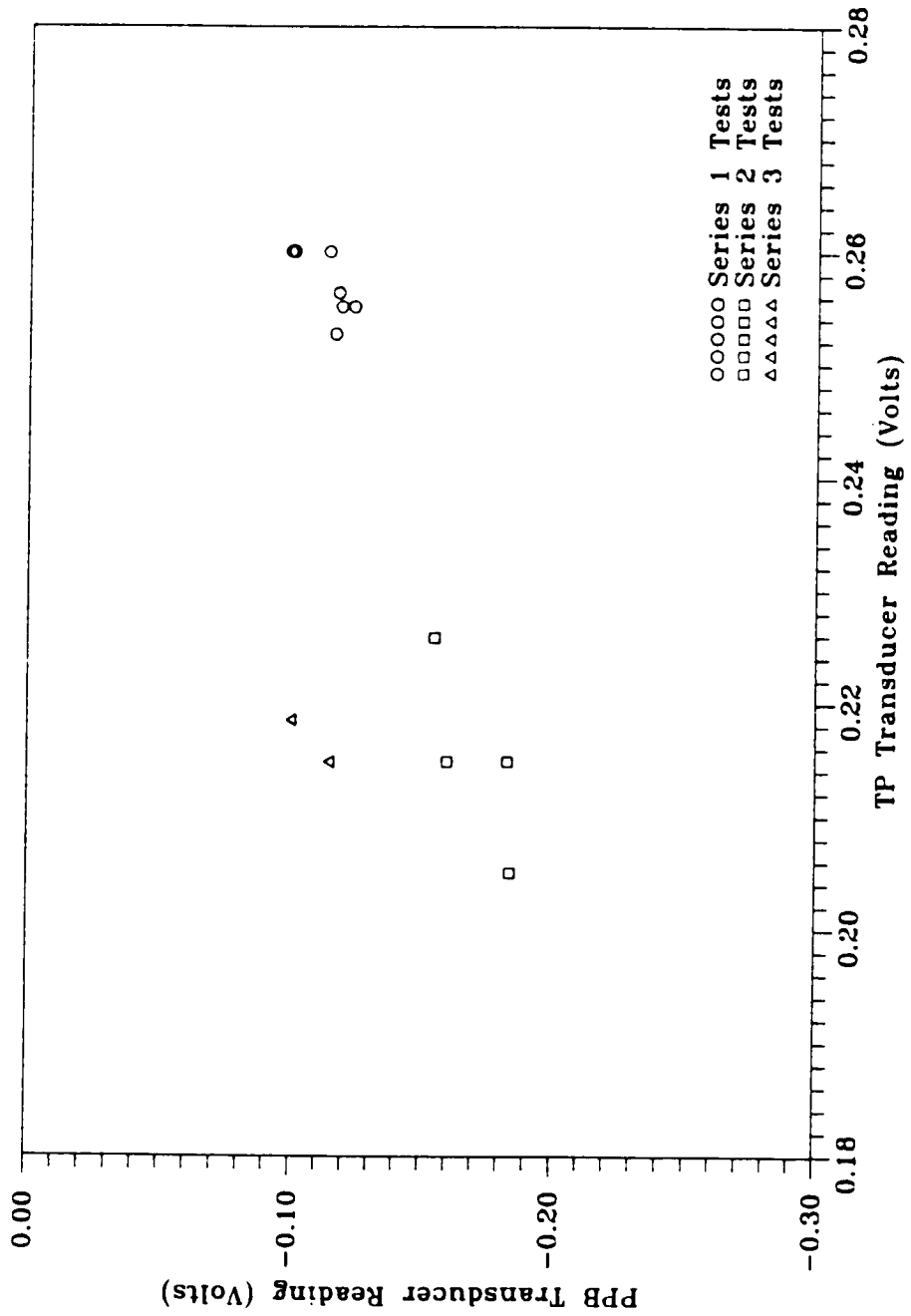


Figure A-5 TP Versus PPB at Atmospheric Pressure

Test Designation (1)	Estimated Uo @ PPB (psf) (2)	Rate of Insertion (in/min) (3)	U-Uo PPB (psf) (4)	Month Test Conducted (5)
PMC1.1	536.6	4.7	-47	May
PMC1.2	692.6	4.7	177	May
PMC1.3	848.6	0.8	-90	May
PMC2.1	536.6	1	56	Jun
PMC2.2	692.6	1	122	Jun
PMC2.3H	848.6	1	178	Jun
PMC2.4	1004.6	1	347	Jun
PMC3.1	536.6	1	349	Jun
PMC3.2H	692.6	1	422	Jun
PMC3.3H	848.6	1	487	Jun
PMC3.4H	1004.6	3.5	885	Jun
PMC3.5H	1160.6	2	230	Jun
PMC3.6H	1316.6	2	-740	Jun
PMC4.1	505.4	2	-154	Aug
PMC4.2	661.4	2	47	Aug
PMC4.3	817.4	2	144	Aug
PMC4.4	973.4	2	95	Aug
PMC4.5	1129.4	2	152	Aug
PMC4.6	1285.4	2	157	Aug
PMC4.7	1441.4	2	93	Aug
PMJ3.2	630.2	6	-110	Aug
PMJ3.2R	630.2	NA	-139	Aug
PMJ3.3	817.4	3	-45	Aug
PMJ3.4	1004.6	4	-111	Aug
PMJ3.4R	1004.6	NA	-207	Aug
PMJ3.5	1191.8	4	-6	Aug
PMJ3.6	1379.0	6	59	Aug
PMJ4.1	505.4	4	-334	Aug
PMJ4.2	692.6	5	-55	Aug
PMJ4.2R	692.6	NA	-84	Aug
PMJ4.3	879.8	5	-43	Aug
PMJ4.4	1067.0	6	-70	Aug
PMJ4.5	1254.2	6	10	Aug
PMJ4.6H	1441.4	6	-57	Aug
PMJ4.7	1597.4	6	-38	Aug

Table A-2 Summary of Computed Excess Pore Pressures

Test Designation (1)	Estimated U _o @ PPB (psf) (2)	Rate of Insertion (in/min) (3)	U-U _o PPB (psf) (4)	Month Test Conducted (5)
PMJ5.1	436.8	5.1	-194	Oct
PMJ5.2	624.0	4.8	-1015	Oct
PMJ5.3	811.2	4.6	-736	Oct
PMJ5.4	1020.2	6.5	-258	Oct
PMJ5.5	1207.4	5.8	-445	Oct
PMJ5.6	1394.6	5.4	-490	Oct
PMJ6.1	536.6	4.3	-774	Mar
PMJ6.2	692.6	7.5	-722	Mar
PMJ6.3	848.6	8.4	-670	Mar
PMJ6.4H	1004.6	10	-566	Mar
PMJ7.1	474.2	5.5	-379	May
PMJ7.2	630.2	7	-230	May
PMJ7.3	786.2	8.1	-132	May
PMJ7.4H	942.2	7.4	-37	May
PMJ8.1	505.4	6.4	-47	Nov
PMJ8.2	692.6	10	-56	Nov
PMJ8.3H	848.6	8.1	136	Nov
PMJ8.4	1004.6	10.1	-80	Nov
PMS1.1	692.6	8.6	-446	Nov
PMS1.2	879.8	7.7	254	Nov
PMP1.1	599.0	5.2	216	Nov
PMP1.2	786.2	4.7	1427	Nov
PMP2.1	630.2	4.2	1635	Nov
HAM1.1	458.6	6	725	Apr
HAM1.2	614.6	7.5	530	Apr
HAM1.3	770.6	7.5	265	Apr
HAM2.1	396.2	9	382	Apr
HAM2.2	552.2	5.3	568	Apr
HAM2.3	708.2	8.5	522	Apr
HAM2.4H	864.2	9	194	Apr
HAM2.4R	864.2	NA	280	Apr
HAM2.5P	1020.2	NA	303	Apr

Table A-2 (continued) Summary of Computed Excess Pore Pressures

membrane, governed by the permeability of the membrane material. Leakage through a tear or hole was ruled out because none were found and the probe resumed normal function after the probe was removed from the ground and the internal air was exchanged by test expansion. Tests in other borings that were drilled one day and tested on a subsequent day, such as PMC1.2, PMJ7.4H, PMJ8.3H and PMS1.2 have relatively lower computed pore pressures at the start of testing, at about the accuracy of measurement (200 psf).

A.2.3.5 Discussion

The factors that have an influence on pore pressure measurements discussed in this section fall into two groups: those that cause predictable changes in the zero values such as temperature and barometric pressure and those that cause unpredictable shifts such as occur when the probe is dismantled and cleaned or is in the ground for a long period of time.

The first group causes changes in the zero value which are predictable. Because barometric pressure has a small effect, it is neglected. Temperature variation, on the other hand, has a much more significant effect for which corrections must be made. The research found, if all other factors were constant, that a shift in temperature would cause a shift in the apparent pressure measured by PPB and TP. As a result, correction of transducer readings for temperature shifts need to be made as will be discussed in the next section.

The unpredictable shifts which occur due to dismantling and cleaning or long term below water table residence times are more difficult to account for. Between dismantlements, all systems of the probe must be calibrated. This will correct for shifts that occur due to resistivity changes. Also, an expansion calibration should be done at the beginning of each boring to account for possible grounding induced shifts which might occur due to differences in test setup. The best results are likely obtained when an expansion calibration is made with the probe attached to drilling rods in the drill chuck, with the cutting shoe touching the ground or groundwater (if surficial). Although it was not always the practice of this research, it would be beneficial to run a calibration at the completion of each boring also, in the event of large drift. As for long term drift due to the length of time the probe is in the ground, the only solution with the available equipment is avoidance. The best test results seem to be from borings that are completed the same day, or at least within a couple of days.

A.2.4 Determination of Excess Pore Pressures Due to Deployment

A.2.4.1 Description of the Method

As a result of the findings presented in Section A.2, a procedure for computation of excess pore pressure at the end of dissipation, prior to an expansion test is presented. The procedure neglects barometric changes and corrects for shifts in TP (vented to atmosphere) between the calibration expansion test and the actual in-ground test. The method assumes that the temperature response of the TP and PPA/PPB transducers are the same. This assumption results in about 100 psf error in computed pore pressure for a 20 degree shift in temperature for PPB. The error would have been much larger, however, for PPA, had it been used, since this transducer seems to shift a greater amount than TP. Using factors determined from expansion calibration of the pressuremeter, and estimating the hydrostatic pressure, u_0 , prior to insertion based on the depth below the water table, the pore pressure just prior to expansion sensed by the PPB transducer was computed as follows:

$$u = [(\sigma_{ppbc} - \sigma_{ppb0}) * PPB] - u_0 \quad (\text{Eq A-3})$$

where:

u = excess pore pressure just prior to expansion (psf).

σ_{ppbc} = computed PPB transducer output voltage at
at start of in-ground test based on shift of TP

between ground surface calibration and in-ground test (volt).

σ_{ppb0} = PPB transducer output voltage at start of in-ground test (volt).

PPB = The conversion factor of volts to psf (psf/volt) for the PPB transducer from SBPM calibration.

u_0 = hydrostatic pressure (psf).

All of the terms in Equation A-3 are self-explanatory except for σ_{ppbc} . σ_{ppbc} is the computed atmospheric pressure or "test zero" value of the PPB transducer for an in-ground test. The need for calculating this value is that the recorded test value at the beginning of an in-ground test includes pressure due to hydrostatic and excess insertion pore pressures, and thus is not an atmospheric pressure reading. For this research, the value was computed using a ratio determined from the results of the air expansion calibration. Using the results of the air expansion, a linear regression on the PPB transducer voltage versus TP transducer voltages was performed. The plotted data form a straight line, as indicated on Figure A-6, and the slope of the line can be determined. This slope is the variable M in Equation A-4 below. Knowing M, the data from an in situ test can now be used to determine σ_{ppbc} . The data required for this determination include σ_{tp0} , the voltage value of the TP transducer for the in-ground test with the probe vented to atmosphere as well as the test zero values (open to atmosphere) of the TP and PPB transducers from the surface calibration. These surface test zero values are denoted as σ_{tp0} and σ_{ppb0} (for the TP and PPB transducers, respectively) in the following equations, which can be used to determine σ_{ppbc} :

$$\text{slope} = M = \frac{dy}{dx} = \frac{\sigma_{ppbc} - \sigma_{ppb0}}{\sigma_{tp0} - \sigma_{tp0}} \quad (\text{Eq A-4})$$

Rearranging:

$$\sigma_{ppbc} = \sigma_{ppb0} + M (\sigma_{tp0} - \sigma_{tp0}) \quad (\text{Eq A-5})$$

This determination of σ_{ppbc} is the correction for the zero shift caused by the change in temperature at the ground surface to that at the test depth. This correction will yield an atmospheric pressure value of the PPB transducer in volts that is adjusted to eliminate the influence of excess pore pressure which is included in the value of σ_{ppb0} measured at the beginning of the in ground test.

A.2.4.2 Example Problem

It is useful to work through an example of the determination of excess pore pressure at the start of membrane expansion using the method outlined in the previous section. Using the data on Tables A-1 and A-2 for SBPM test PMCl.1 and Equation A-5:

$$\sigma_{ppbc} = \sigma_{ppb0} + M (\sigma_{tp0} - \sigma_{tp0})$$

excess pore pressure at the start of expansion (u) is found with the following values:

$$\sigma_{ppb0} = -0.10090 \text{ volt (Table A-1, Column 6)}$$

$$M = 0.707447 \text{ (Table A-1, Column 7)}$$

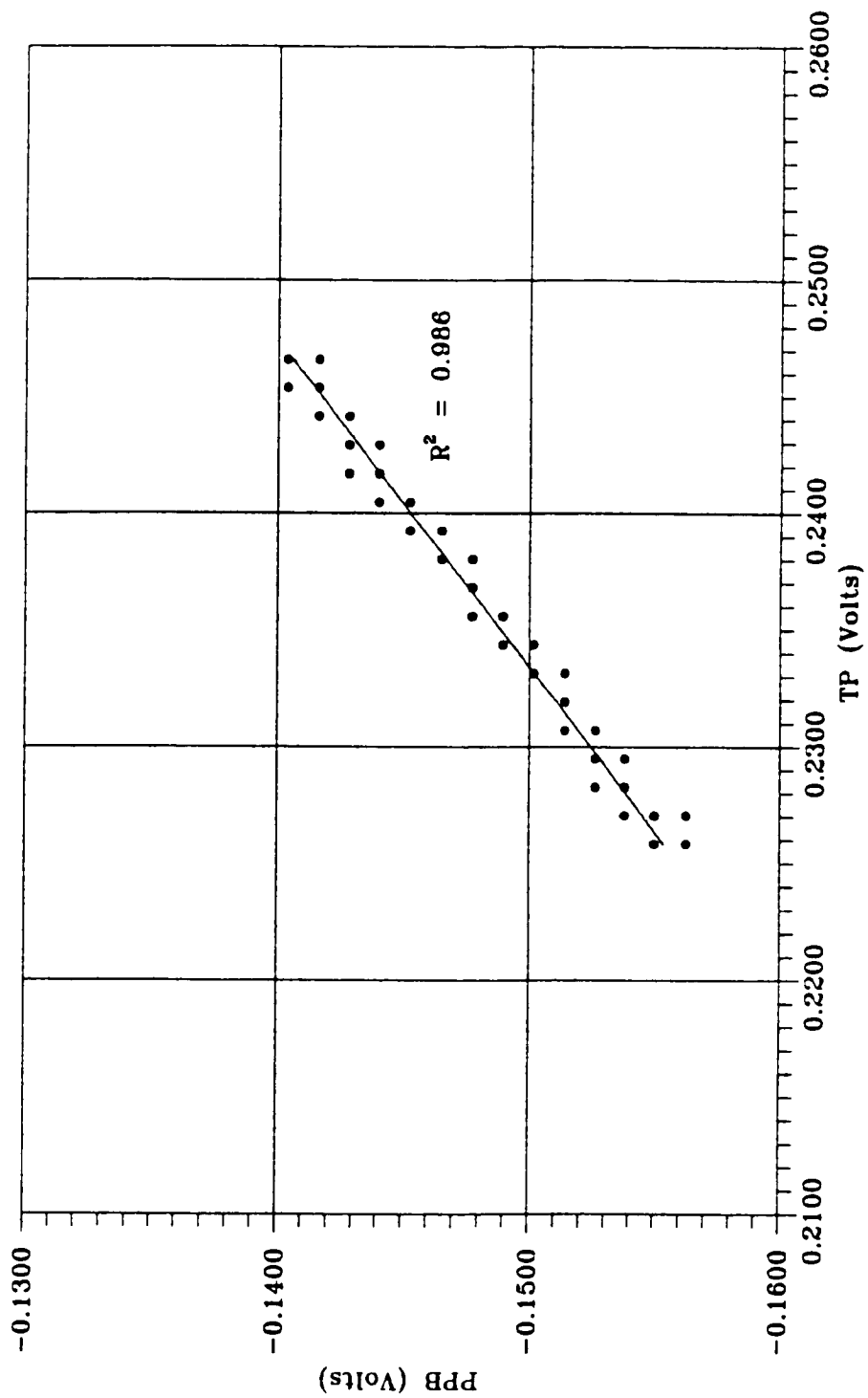


Figure A-6 Air Expansion, PPB vs TP

σ_{ps} = 0.261465 volt (from Table A-1, Column 9)

σ_{pso} = 0.260010 volt (Table A-1, Column 4)

$$\begin{aligned}\sigma_{ppbc} &= \sigma_{ppso} + M (\sigma_{ps} - \sigma_{pso}) \\ &= -0.100090 + 0.707447(0.261465 - 0.260010) \\ &= -0.099061 \text{ volt (Table A-1, Column 13)}\end{aligned}$$

PPB = 45346 psf (Table A-1, Column 3)

u_s = 536.6 psf (Table A-2, Column 2)

Inserting into Equation A-3:

$$\begin{aligned}u &= [(\sigma_{ppbc} - \sigma_{ppso}) * PPB] - u_s \\ u &= [(-0.099061 - (-0.109863)) * 33065] - 536.6 \\ u &= -47 \text{ psf (Table A-2, Column 4)}\end{aligned}$$

A.2.4.3 Excess Pore Pressure For Research Test Results

The fourth column of Table A-2 lists excess pore pressures just prior to the start of the expansion tests (about 30 to 40 minutes after deployment), determined using transducer PPB by the method outlined in Section A.3.1 for 68 pressuremeter tests. The table presents data obtained from tests conducted at Pease Air Force Base (PMC, PMJ, PMS and PMP series tests) as well as tests carried out at Hamilton Air Force Base (HAM series tests). As discussed previously, transducer PPA was an experimental model and did not function properly. On Table A-2 it can be seen that excess pore pressures resulting from cutting insertion (PMC series borings) are generally positive (with a few exceptions), and pore pressures from jetting (PMJ and HAM series borings) can be positive or negative. This is shown graphically for the Pease AFB data on Figure A-7.

Full displacement pressuremeter tests were conducted at the Pease Air Force Base test site for the subject research. As indicated by the excess pore pressure values presented on Table A-2 (PMP 1.1, 1.2, and 2.1), insertion pore pressures were positive, and with the exception of PMP1.1, were generally significantly higher than measured by cutting and jetting insertion methods. It is believed that PMP1.1 had lower excess pore pressure since it was the first of two consecutive tests that were pushed open ended. The cutting shoe was initially clear and empty, allowing soil to enter the probe as it was pushed, and minimizing soil displacement around the probe. Test PMP1.2, which was conducted below PMP1.1 (without removing the probe from the boring) was more likely representative of full displacement of soil around the probe since the cutting shoe was jammed with soil from the start of deployment to test depth. PMP2.1 was deployed with a cone tip which immediately caused soil displacement during deployment. The results of push-in tests PMP 1.2 and 2.1 are included on Figure A-7.

The observations of excess pore pressure just prior to the start of expansion testing are interesting in that it might be expected that pore pressures could be zero or positive due to SBPM deployment, however, it is not as immediately obvious why excess pore pressures would be negative (below hydrostatic pressure). An hypothesis of the mechanism of generation of excess pore pressures, both positive and negative, which occur during SBPM insertion might be formulated by examining the specific insertion processes.

In cutting, the probe is pushed slowly into the soil. As the soil enters the cutting shoe, it is cut by the chopping bit. The cuttings from the chopping bit are then washed to the surface by a low flow of water (generally 5 gallons per minute versus 20 gallons per minute for jetting). The potential stress relief caused by removal of the soil during cutting is balanced by a combination of the weight of the water column and the shear stresses in the soil plug within the cutting shoe. These shear stresses are caused by compression of the soil within the

PEASE AIR FORCE BASE SBPM TEST PROGRAM

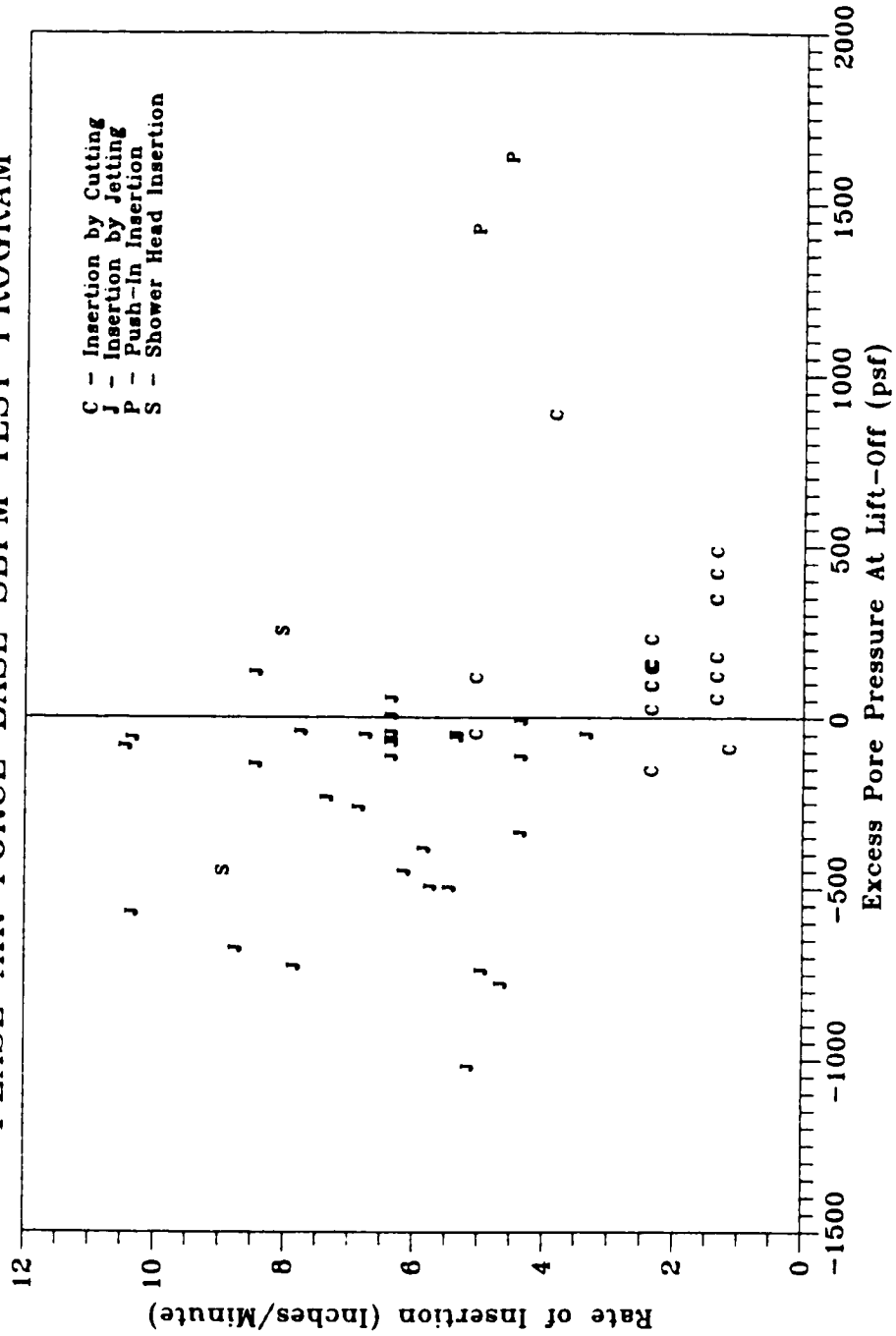


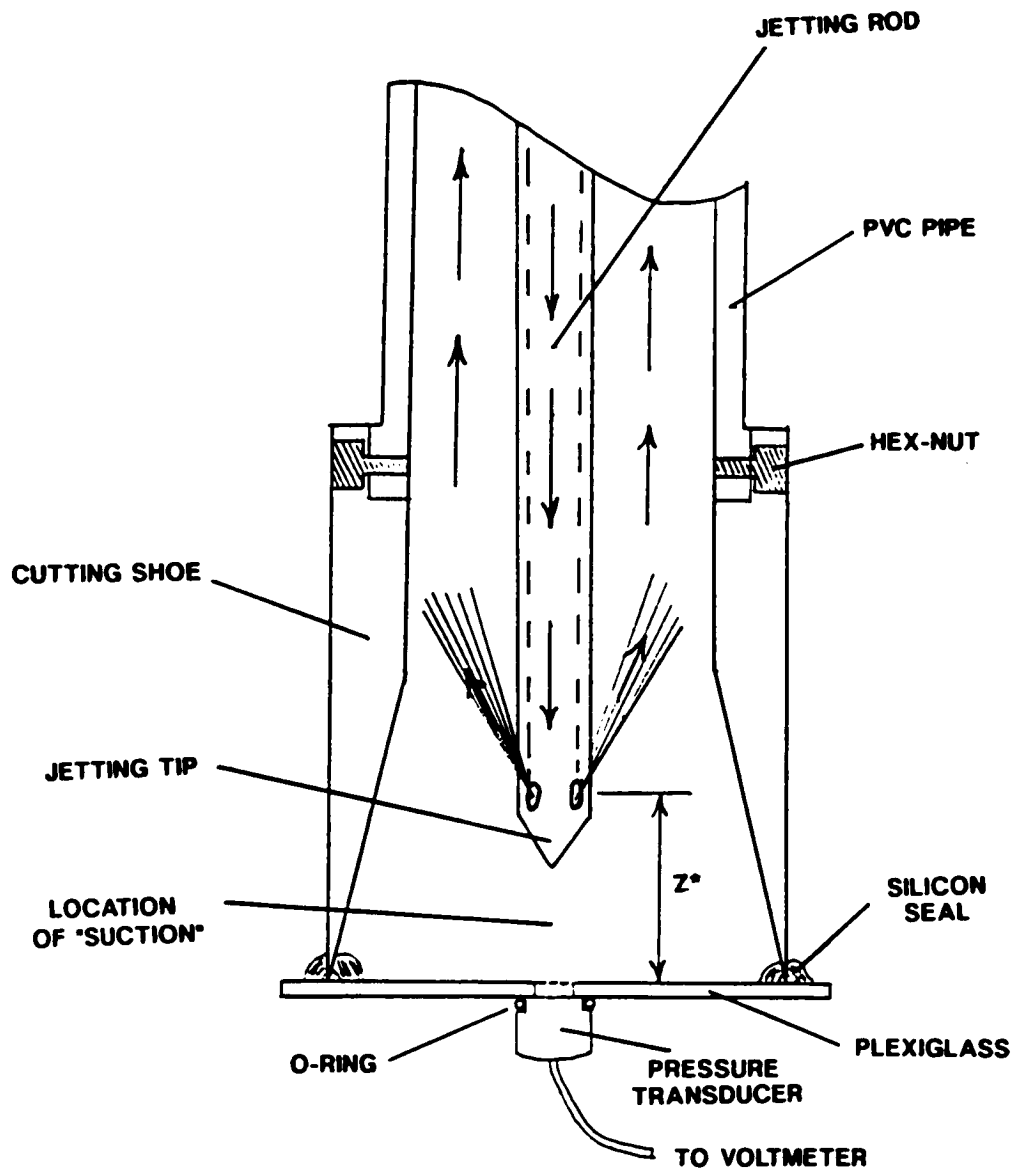
Figure A-7 Pore Pressure versus Insertion Rate

cutting shoe during forward advance of the probe. If cutting was inefficient, these shear stresses and the forward movement of the SBPM would tend to cause soil in front of the probe to displace around the probe (rather than cut or removed). Such displacement of soil outside of the cutting shoe causes shearing and thus positive excess pore pressures to develop. If cutting were over-efficient, it is conceivable that soil could yield into the cutting shoe.

In jetting insertion, the soil is cut by high velocity water jets. By the orientation of the jets, which are pointed up the probe, it is conceivable that below the jetting tip, a reduction in water pressure occurs which may be analogous to a vacuum aspirator connected to a water faucet, similar to those used to de-air a specific gravity picnometer bottle. The magnitude of this "suction" is likely dependent on the velocity of the jets. If the "suction" due to jetting were sufficiently high, stress relief (yield of the soil into the cutting shoe) in the soil just outside of the cutting shoe could result in generation of negative pore pressures similar to those observed during excavation of soft soils (Osaimi and Clough, 1979). Similar negative pore pressure could result from cutting insertion if soil were to yield into the cutting shoe, however, it would be expected that such occurrence would be less likely in the absence of jetting "suction". As is theorized for cutting, the tendency for stress relief is likely resisted by the shear stresses in the soil plug within the cutting shoe. If insertion were too slow, insufficient shear stress could develop within the cutting shoe and a greater amount of stress relief might result. As the rate of insertion is increased, greater shear stresses occur in the soil plug and the potential for soil yield into the pressuremeter shoe would conceivably be less. High negative pore pressure resulting from jetting or cutting insertion may indicate significant stress relief, and thus, too slow an insertion rate and, consequently, disturbance.

To determine if "suction" occurs below the jetting tip during the jetting insertion process, a laboratory experiment was conducted. The aim of the experiment was to see if a pressure reduction below the jetting tip actually occurs. A mock pressuremeter was constructed, using a cutting shoe and jetting rod as shown on Figure A-8. The body of the pressuremeter was simulated using a 2-inch inner diameter pvc pipe; this inner diameter is the same as that of the pressuremeter. An electrical pressure transducer was mounted to a plexiglass plate and attached to the bottom of the cutting shoe. Output of the pressure transducer was monitored by a standard voltmeter; the transducer/voltmeter system had an accuracy of about 0.001 volts, or ± 29 psf. Calibration of the pressure transducer was done using a test gauge, applying pressures both above and below atmospheric pressure, in the range from 30 psi above to 5 psi below atmospheric pressure, bracketing the range of pressures anticipated to be measured in the experiment.

Tests were conducted by pumping water down the jetting rod and up through the internal annulus of the mock pressuremeter. Flow was determined by measuring the time in seconds for 5-gallons of water to be expressed through the jetting system. A Wenner diaphragm pump was used, capable of outputting a maximum of 30 to 40 gpm. This was the same pump utilized for the Pease Air Force Base field testing, for which the pump was used to output about 15 to 25 gpm through the jetting system. This flow rate was found, in companion research, to be adequate for insertions with minimal associated soil disturbance (Atwood, 1990). Flows less than the above rate resulted in disturbance of the soil outside of the SBPM. The flow rates tested with the mock pressuremeter were randomly selected as 7, 11, 14, and 20 gpm. Resulting pressure transducer readings for each of the flow rates were measured for 4 different jetting tip set-backs (dimension "z" in Figure A-8, measured to the center of the jetting ports). Specifically, these jetting tip set-backs included 1/2-inch, 3/4-inch, 1-inch and between 1-inch and 6-inches. The measured pressure for each of these cases is indicated on Table A-3. The mock pressuremeter experiment does not exactly model the field condition, in that the plexiglass plate acts as an impervious boundary, while in



***NOTE: Z MEASURED TO CENTER OF JETTING PORT**

Figure A-8 Schematic of Mock Pressuremeter

actuality, no boundary exists. However, since the point of the experiment was to see if jetting could induce a suction which could facilitate yielding of the soil into the pressuremeter, inclusion of a boundary only precludes the soil reaction to the suction.

As can be seen from Table A-3, flows of less than 14 gpm through the jetting system appear to have no influence on measured pressure. At 14 gpm, if the tip is set back from the cutting shoe edge a distance of 3/4-inch or more, a pressure reduction, below static head resulted. At 20 gpm, pressure reduction appears to result regardless of the set-back, but the pressure reduction increases with set back up to about 1-inch. For set-backs greater than 1-inch, no additional pressure reduction was measured at a 20 gpm flow rate. These observations suggest that negative pore pressures (pressures less than hydrostatic) could result due to the jetting insertion process, provided sufficient flow is present (at least 14 gpm) and the effect seems to increase to a limited extent as the jetting tip is moved back from the cutting shoe edge.

Increased pressure reduction resulting from increased jetting tip set back (the "z" distance on Figure A-8, measured to the center of the jetting ports) indicated by the mock pressuremeter tests is consistent with the results of the jetting insertion tests made at Pease Air Force Base. Figure A-9 presents the resulting excess pore pressures at the just prior to the start of membrane expansion for insertions with "z" set-backs of 3/4-inch and 1-inch, plotted against insertion rate (inches per minute) to highlight the influence of insertion rate. As can be seen by comparing the two "z" set-backs, lower pore pressures result with greater "z" set-back at a given insertion rate. The plot also supports the theory that for jetting insertions, the rate of insertion has an affect on the resulting excess pore pressure. A general trend can be seen that the faster the insertion, the higher the resulting pore pressure. Figure A-9 also shows that if insertion rate is too slow, negative pore pressures (pressure below hydrostatic pressure) could result. This lends credence to the previously theorized inter-relationship of insertion rate, internal cutting shoe plug shear stresses, and jetting velocity.

A.3 Influence of Membrane Stiffness on SBPM Measurements

A.3.1 Introduction

Reduction of SBPM test data requires determination of membrane stiffness. Membrane stiffness is the force required to expand the membrane in the absence of other restraints. Membrane stiffness is generally measured by expanding the pressuremeter in air, and conventionally has two parts; a lift-off stiffness component and a component after lift-off that increases with increasing strain. The lift-off stiffness is defined as that pressure during an air expansion at which the membrane just lifts away from the pressuremeter body. The component after lift-off is determined by expanding the membrane well beyond lift-off to determine how membrane stiffness increases with radial strain. The measured values of increase in membrane stiffness with radial strain can be mathematically curve fitted so that the increase in stiffness above the lift-off stiffness can be defined at any radial strain to allow automation of correction of in situ SBPM test curves for membrane stiffness. The sum of the lift-off stiffness and increase in stiffness after lift-off are subtracted from each data point along a field expansion curve to determine the corrected pressuremeter curve. The components of stiffness and correction of a field expansion curve are illustrated on Figure A-10. The following subsections discuss the findings of the current research with respect to the two components of membrane stiffness.

A.3.2 Stiffness at Lift-off

The SBPM membranes used for this research were manufactured by Cambridge Insitu and were made of a rubber-like material called adiprene. The thickness of the membranes used was 1/16 of an inch. During this research, air expansions of the membrane (fitted on the SBPM) were made in a pressure chamber provided by Virginia Tech (Mayu, 1987). A schematic of this chamber is presented on Figure A-11. The membrane was

Flow Through Jetting Tip (gpm)	Velocity Through Jetting Tip (ft/sec)	"z" Setback (see Fig A-8) (inches)	Measured Deviation From Hydrostatic Pressure Below Jetting Tip (psf)
5	12.8	0.5	103
7	17.8	0.5	103
		0.75	103
		1	103
		1 to 6	103
11	27.7	0.5	103
		0.75	103
		1	103
		1 to 6	103
14	35.3	0.5	103
		0.75	0
		1	-103
		1 to 6	-103
20	50.4	0.5	-206
		0.75	-309
		1	-514
		1 to 6	-514

Table A-3 Summary of Mock Pressuremeter Results

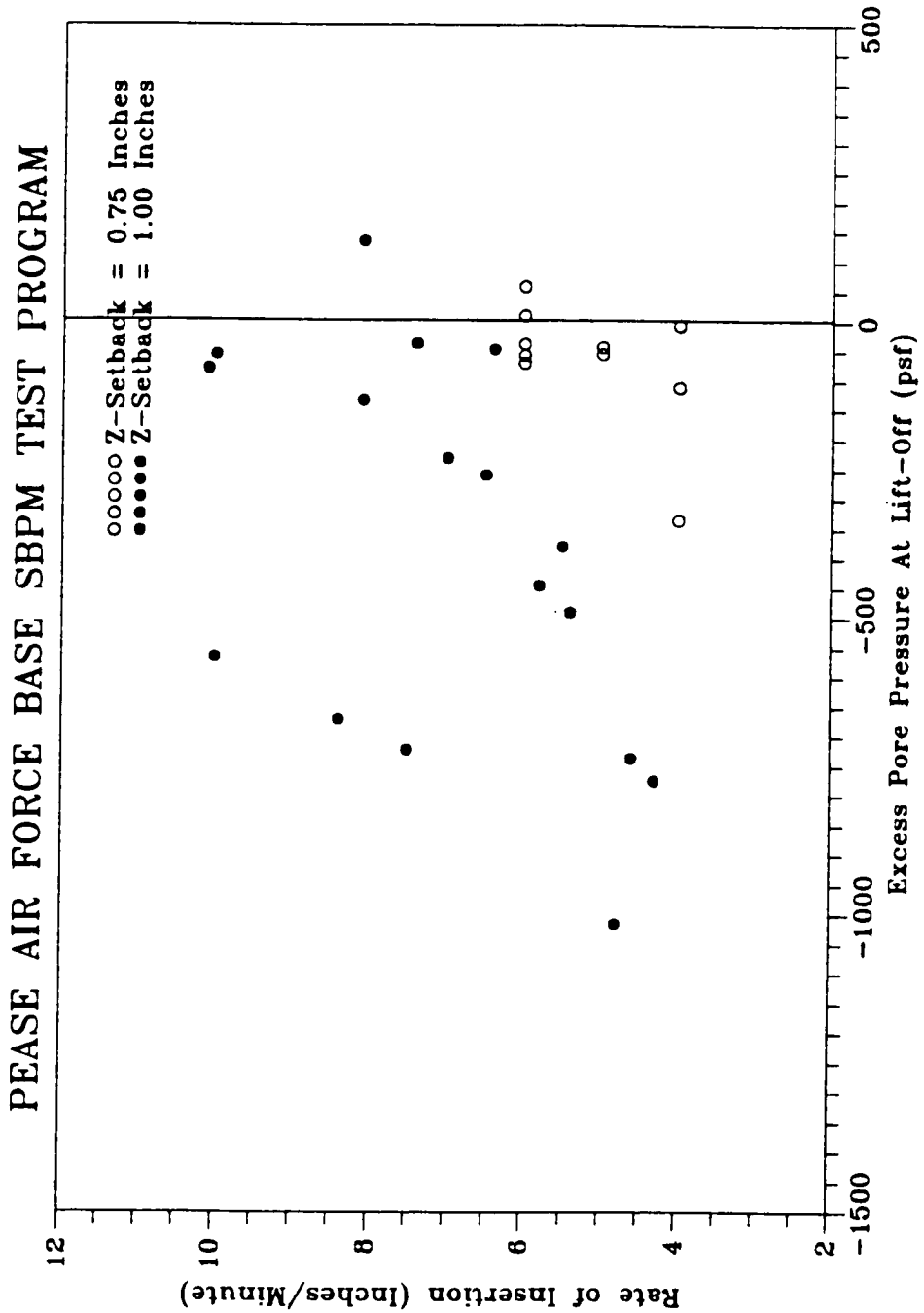


Figure A-9 Excess Pore Pressure Versus Insertion Rate

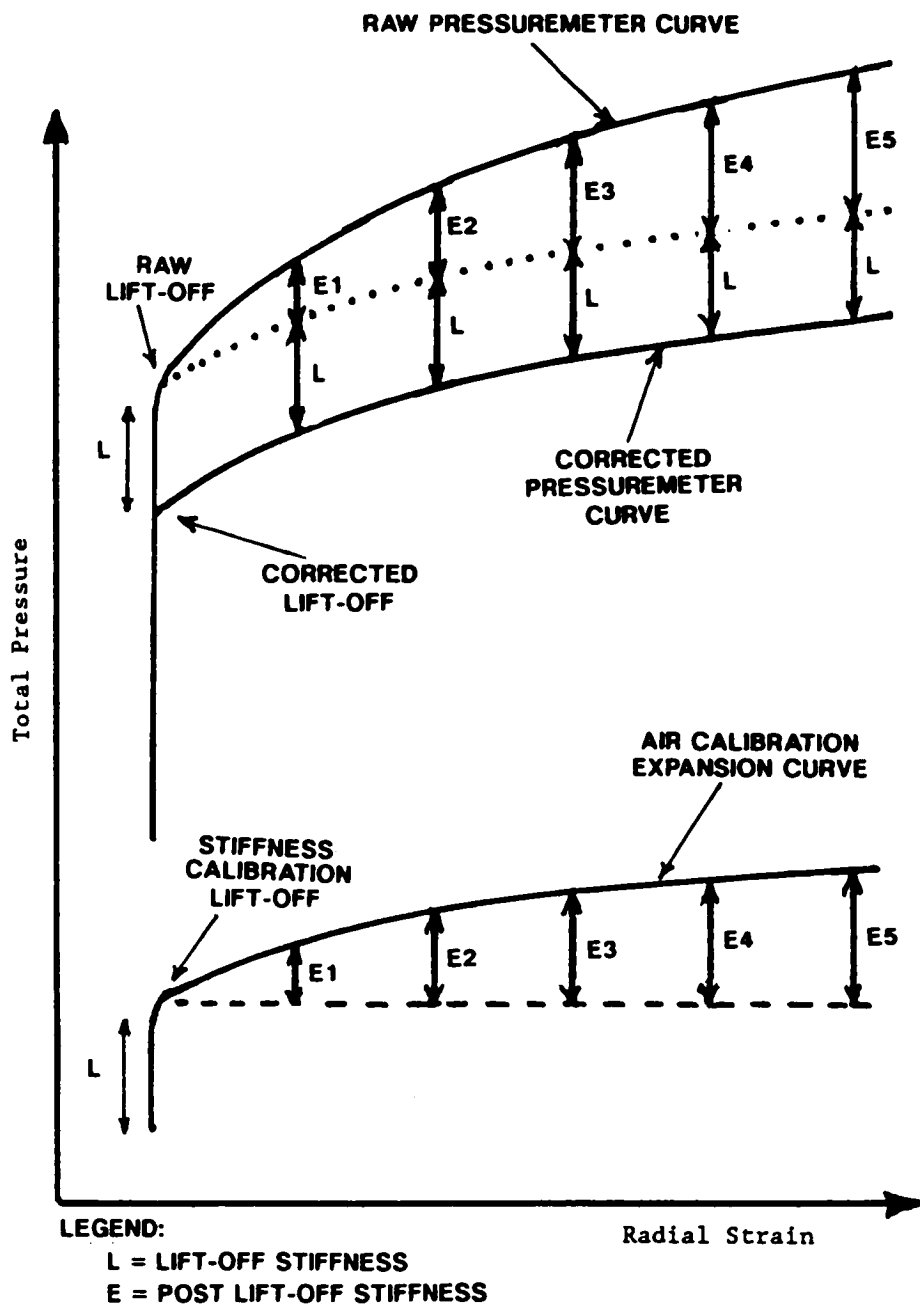


Figure A-10 Components of Stiffness Correction

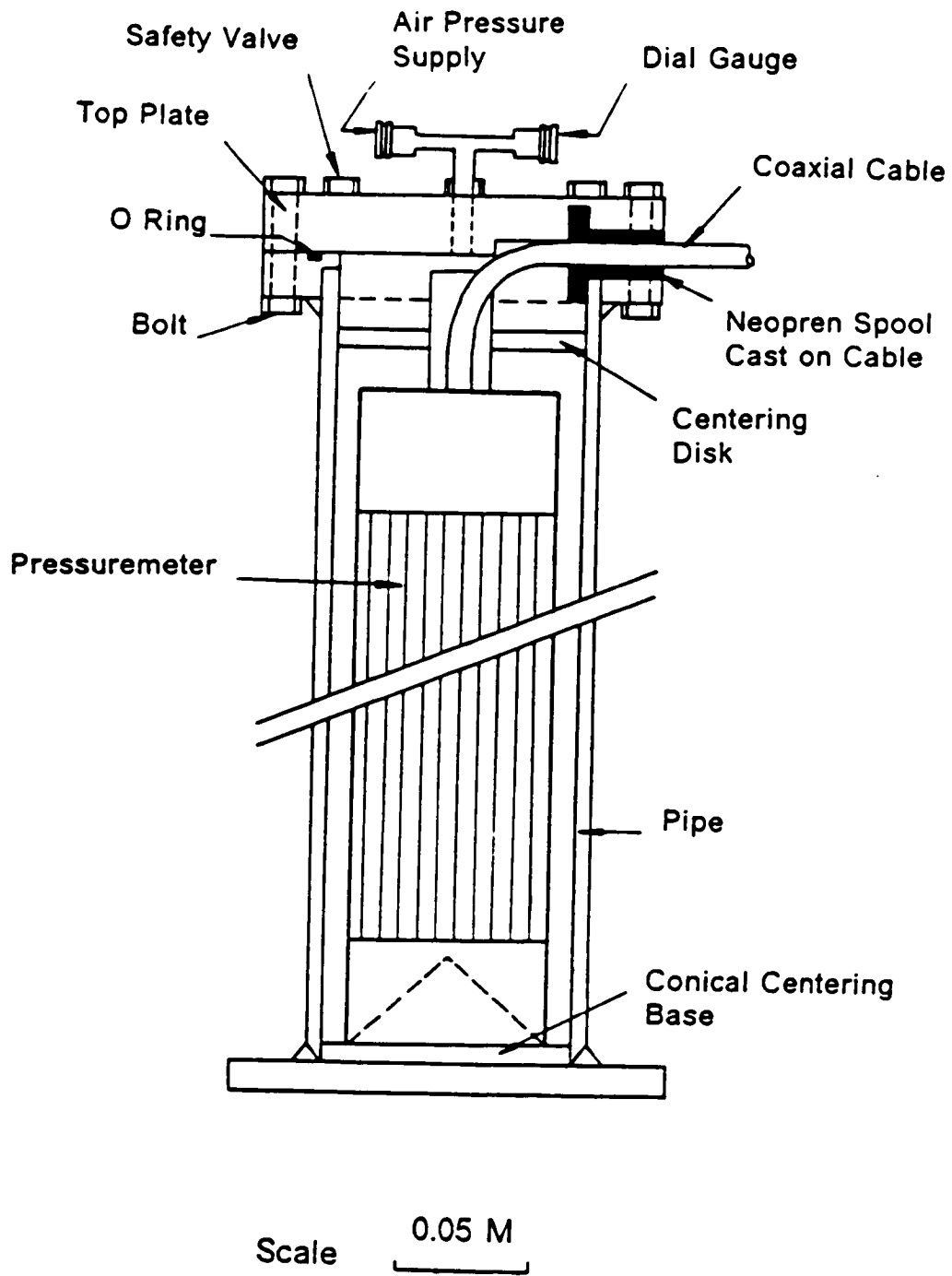


Figure A-11 Schematic of Pressuremeter Chamber (after Mayu, 1987)

expanded at different chamber pressures in an effort to determine the effect of confining pressure on membrane lift-off stiffness. Similar calibrations were performed in previous research by Mayu (1987). Mayu found that membrane stiffness at lift-off seemed to decrease with confining pressure. The results of chamber calibrations made for the current research for membrane stiffness versus confining pressure are presented on Figure A-12. This figure presents data for expansions made with the SBPM fitted with a thin membrane (no Chinese lantern) and indicates that stiffness increases with confinement, which is at odds with the findings of Mayu. Since Mayu performed his test expansions with a probe fitted with a Chinese lantern, it was thought that the trend of the difference in stiffness with confinement may have been due to the absence or presence of the Chinese lantern. To test this hypothesis, lift-off stiffness for test expansions made with an SBPM equipped with a thin membrane and a Chinese lantern were obtained and are presented on Figure A-13. This data also indicates a trend of increasing lift-off stiffness with confining pressure, again at odds with the findings of Mayu. No explanation for this difference is apparent.

Further examination of Figure A-13 reveals that rather than lifting at the same pressure value for a given chamber pressure, each arm experiences lift-off at different pressure values. Although the order of lift-off of the arms is relatively constant for a given tier with increasing confining pressure, the relative difference in total pressure between lift-offs on a given tier varies widely. This observation of irregular relative lift-off pressure indicates that there is likely another mechanism which affects lift-off stiffness other than just material differences (e.g. non-uniform thickness) from place to place across the membrane. As a result, it is useful to investigate this issue further.

The work of Lamé (1852), as reiterated by Stordal (1985), Vesic (1972) and others, indicated that the relationship of radial stress to the tangential stress in the wall of a thin cylinder is given by:

$$-\delta\sigma_{\theta} = \delta\sigma, \quad (\text{Eq A-6})$$

This equation indicates that hoop or tangential stress ($-\delta\sigma_{\theta}$, tension is negative in the equation) increases as the force within the hoop or radial stress ($\delta\sigma_r$) increases. It is believed that this equation applies directly to the pressuremeter membrane and thus membrane stiffness at lift-off. At the time of the first occurrence of lift-off on a particular tier of strain measuring arms, the membrane is forced to stretch slightly. This stretching increases the hoop stress and therefore, lift-off of the second arm will require a radial pressure somewhat higher than the first lift-off. Likewise, after the second lift-off, the membrane stretches some more, and the third lift-off requires a radial pressure that is higher than the first or second lift-offs.

For this research, an experiment was conducted in an attempt to verify the above theory using the SBPM equipped with a thin membrane and a Chinese lantern. After repeatedly expanding and deflating the membrane to remove any residual stiffness which might exist, several air calibrations were made controlling which strain arm could lift first. This was done by holding the membrane against the probe over 2/3 of the circumference with a stiff cardboard split-tube as indicated on Figure A-14. The pressure was increased until the arm in the unrestrained area lifted and the pressure recorded. This test was repeated three times for each arm, allowing each of the middle arms to be the unrestrained arm. The results are summarized on Table A-4. As can be seen for these "forced first lift-off" tests, the membrane stiffness was measured to range from 305 to 381 psf (a range of 76 psf) over all three arms. It is further noted that for all three expansions for each arm, the arm lifted at the same pressure, and arm M1 lifted at the highest pressure and M3 lifted at the lowest pressure.

Following the "forced first lift-off" expansions, three

SELF-BORING PRESSUREMETER TESTING
THIN MEMBRANE, NO CHINESE LANTERN

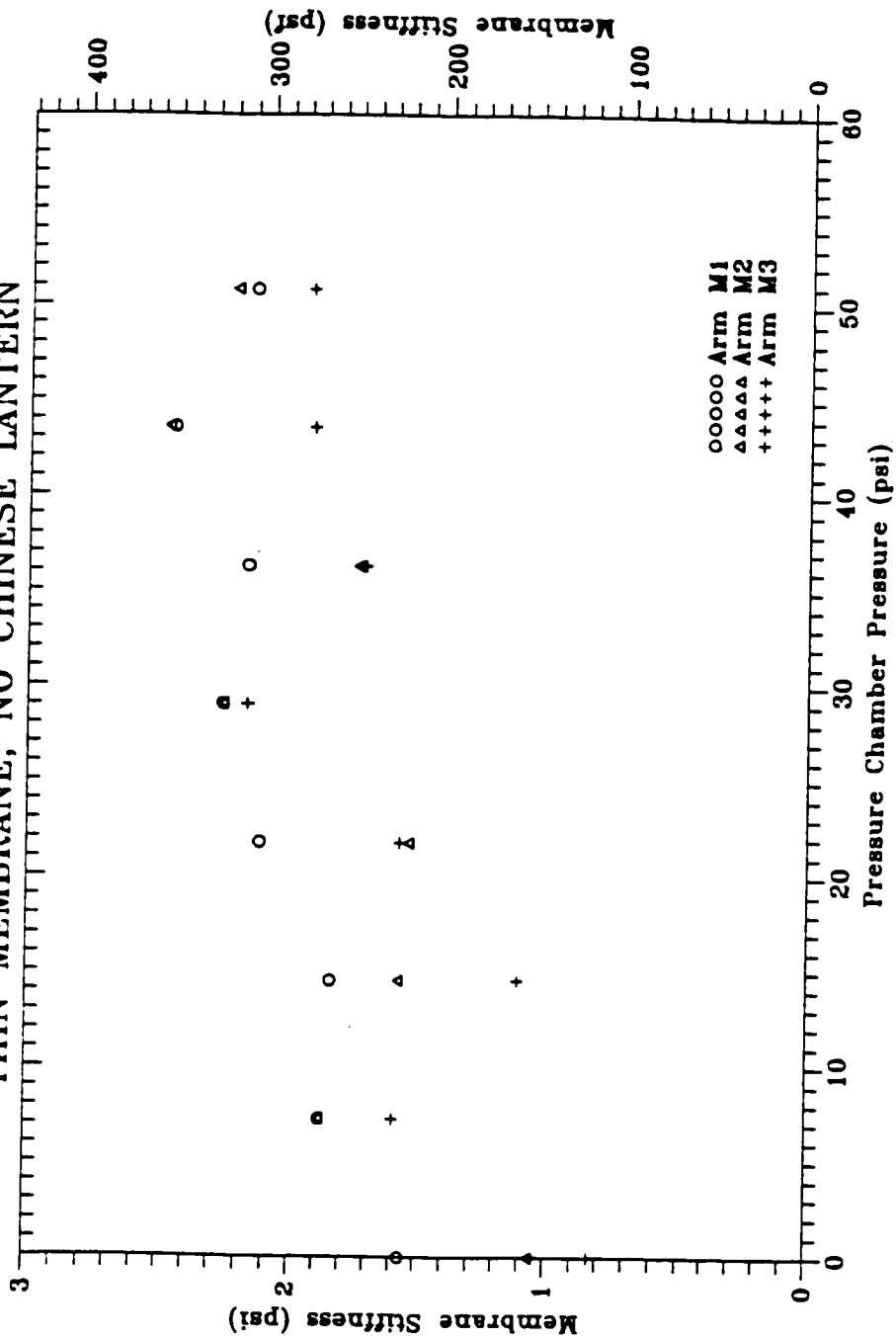


Figure A-12 Stiffness Effects of Confinement, No Chinese Lantern

**SELF-BORING PRESSUREMETER TESTING
THIN MEMBRANE, WITH CHINESE LANTERN**

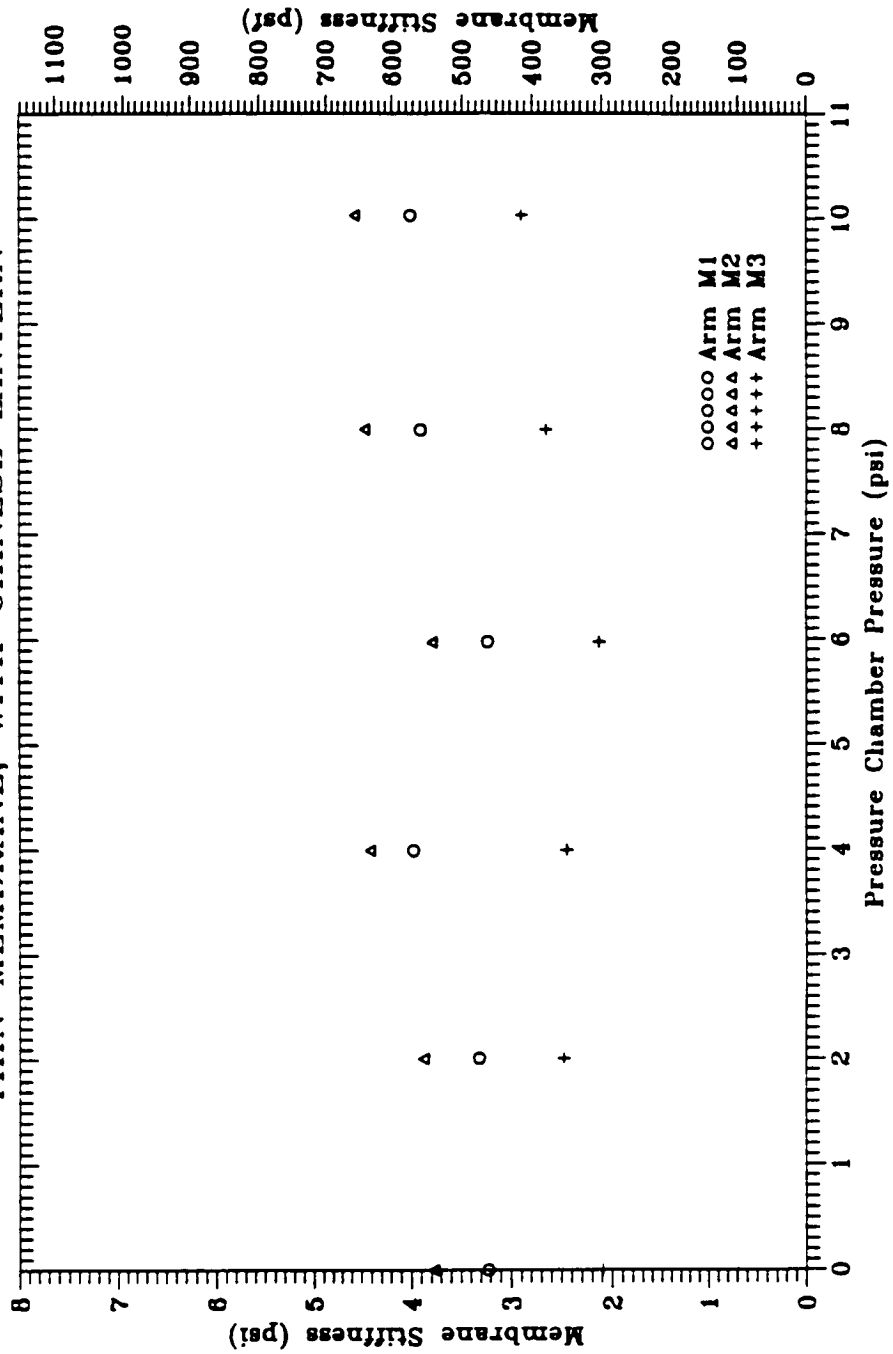


Figure A-13 Stiffness Effects of Confinement, With Chinese Lantern

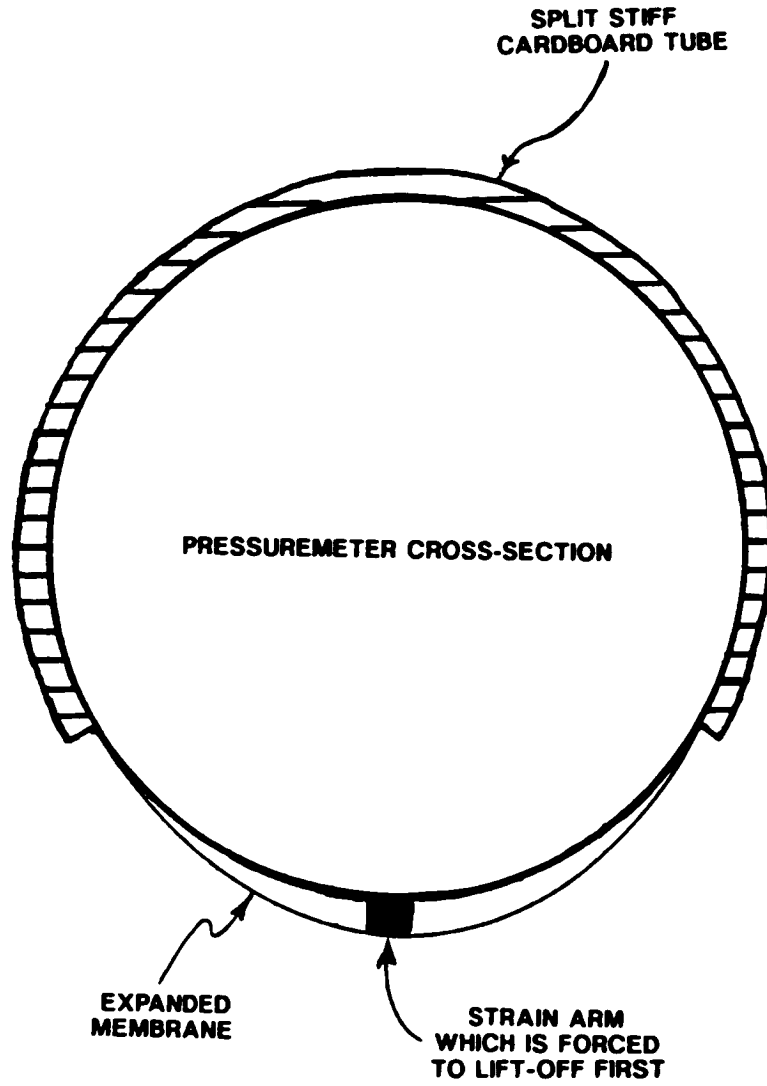


Figure A-14 Forced First Lift-Off

SELF-BORING PRESSUREMETER TESTING
 SUMMARY OF MEMBRANE STIFFNESS AT FORCED FIRST LIFTOFF
 THIN MEMBRANE, WITH CHINESE LANTERN
 -RCF- 2/5/90

FORCED FIRST LIFTOFF:			UNRESTRAINED LIFT-OFF:		
STRAIN ARM	MEMBRANE STIFFNESS (PSF)		STRAIN ARM	MEMBRANE STIFFNESS (PSF)	
M1	381		M1	419	
M1	381		M2	305	
M1	381		M3	191	
M2	343		M1	419	
M2	343		M2	305	
M2	343		M3	267	
M3	305		M1	419	
M3	305		M2	305	
M3	305		M3	267	
AVERAGE:	343	PSF	AVERAGE:	322	PSF
MAXIMUM:	381	PSF	MAXIMUM:	419	PSF
MINIMUM:	305	PSF	MINIMUM:	191	PSF
STD DEV:	31	PSF	STD DEV:	76	PSF
RANGE:	76	PSF	RANGE:	228	PSF

Table A-4 Summary of Membrane Stiffness Experiment

unrestrained expansions were made. The results of these tests are also summarized on Table A-4. For the unrestrained expansions, the stiffness was measured to range from 191 to 419 psf (a range of 228 psf). This range is similar to that observed on Figure A-13 for the chamber test. In addition, membrane stiffness seems to be dependent on the order of lift-off; the first lift-off was found to range from 191 to 267 psf, the second to be 305 psf, and the third to be 419 psf for the three separate expansions. It is noted again that arm M1 lifted at the highest pressure and M3 lifted at the lowest pressure.

The conclusion that can be drawn from the results of these two series of tests is that there seems to be two components of lift-off membrane stiffness. One attributable to the variation of membrane stiffness from arm to arm location; the other attributable to the order of lift-off.

The forced first lift-off tests summarized on Table A-4 remove the influence of the order of lift-off and are probably representative of the variation in stiffness over the membrane tested, particularly since the values were perfectly repeatable at each arm for three separate expansions. These tests indicate that the standard deviation of membrane stiffness from arm to arm was about 31 psf. This is a value which is at about the resolution of the measurement equipment, and as a result can be neglected without significant error.

The unrestrained expansions summarized on Table A-4 show a significantly higher range of lift-off pressures than the forced first lift-off expansions. These tests measured a lift-off membrane stiffness that included a combination of the influence of variation in membrane stiffness as well as the influence of increased stiffness due to the order of lift-off. The test results indicate a difference in stiffness from arm to arm that is about three times greater than that which would be attributable to material variations from location to location across the membrane as indicated by the forced first lift-off tests. This indicates that the order of lift-off appears to be the most important aspect of the variation in lift-off membrane stiffness of the membrane tested. The ratio of significance of membrane stiffness to order of lift-off will likely vary to some degree from membrane to membrane. However, since the membrane tested was randomly selected, and the membranes are manufactured in a controlled manner, there is little reason to believe that the results of testing additional membranes would yield greatly deviating results.

For in-ground testing, if the in situ horizontal stress anisotropy is significantly greater than the variation of stiffness of the membrane, the small differences in stiffness from location to location across a particular membrane will become insignificant with regard to which arm lifts first. If a different arm lifts first in the in-ground test than lifted first in the air expansion, direct application of the lift-off stiffness measured from an air expansion for a particular arm could result in an inappropriate stiffness correction, causing a potential error of plus or minus 200 psf (the typical measured range of stiffness from first to third lift-off as indicated on Figure A-13). Considering the range in lateral stresses measured during the research (about 500 to 2500 psf), this error could be significant, particularly in the measurement of stress anisotropy and predicting the orientation of the major principal stresses. As a result, it appears that the order of lift-off should be considered in correction of membrane lift-off stiffness as discussed in Section 7.4.

A.3.3 Membrane Stiffness After Lift-off

Expansion curves for an air expansion are shown on Figure A-15. A general trend is noted where the expansion curves seem to exhibit a loss of curvature and slope flattening with the order of lift-off. In other words, the first strain arm to lift-off has a calibration expansion curve that is steeper and more curved than the second and third lift-off arms. These observations imply that the order of lift-off affects the shape and slope of the post lift-off calibration curve.

The previous work of Mayu indicated that increasing confinement

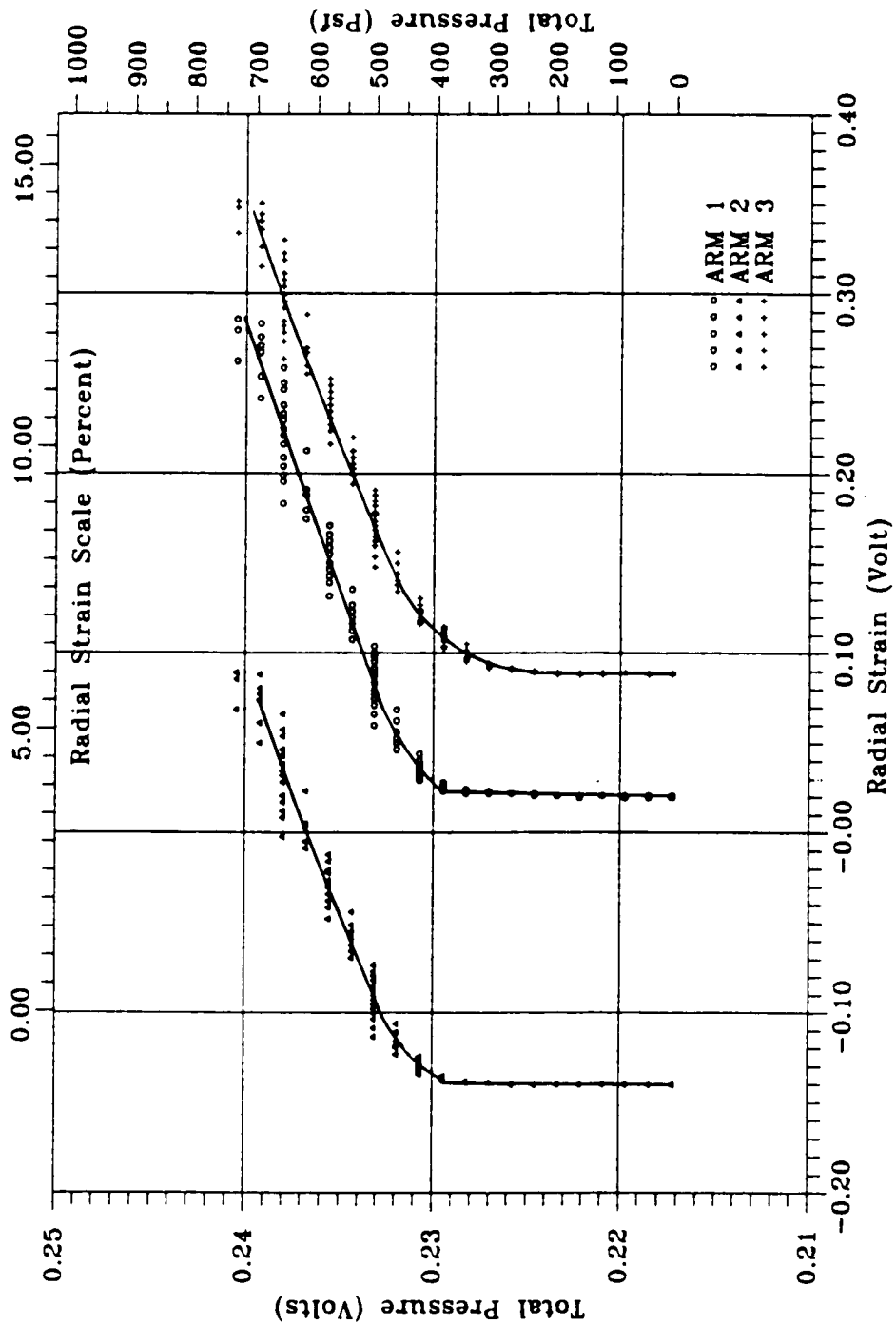


Figure A-15 Pressuremeter Curves for Typical Air Expansion

pressure had little effect on the slope of the stiffness expansion curve after lift-off. Figure A-16 presents the results of membrane expansions made in a pressure chamber configured as previously indicated in Figure A-11. The figure presents expansion curves at three different confining pressures, measured at middle strain arms M1, M2, and M3. As can be seen, the slopes of the post lift-off portions of the curves appear to be essentially identical, which indicates constant stiffness with increasing confining pressure and verifies the conclusion drawn by Mayu. It is further interesting to note, comparing this figure with the air expansions shown on Figure A-15, that the differences in slope exhibited between arms in unconfined expansions seems to disappear in a confined situation, and all the post lift-off curves in the confined situation have almost identical slopes, despite different lift-off stiffness. Also, it appears that the increased curvature of the first lift-off is reduced with confinement.

Another potential influence on post lift-off stiffness that may not be accounted for in air expansions may be friction between the soil and the membrane. To investigate this in a qualitative manner, the SBPM equipped with a thin membrane and a Chinese lantern was wrapped in a remnant of shag carpeting. The piece of carpet was taped radially, and the pile (soft) side was against the membrane. The purpose of this test was to provide some confinement and friction on the membrane surface to see if any shape changes occurred to the pressuremeter curve. The results of this expansion are presented on Figure A-17. As can be seen, the expansion curves are steeper due to the confinement of the carpet. More significant, however, is the fact that the increased curvature of the expansion curve of the first lifting arm observed with air calibrations has disappeared in the carpet expansion. This is an indication that post lift-off membrane stiffness in actual soil tests will be influenced by confinement and interface friction such that the more appropriate calibration curve to be used for correction of membrane stiffness is likely the second or third lift-off curve rather than the first, initially more curved, post lift-off expansion curve. Also, because of the apparent influence of confinement which seems to make the slope of the post lift-off curve more uniform, calibration expansions made in the pressure chamber are likely more appropriate for correction of post lift-off stiffness.

A.3.4 Method for Correcting Membrane Stiffness

A.3.4.1 Lift-Off Stiffness Correction

As a result of the findings presented in the previous sections, a new method of membrane stiffness was used for this research. This stiffness correction method is perhaps "overkill" for conventional testing in stiffer soils or at greater depths, however, it appears to be important for accurate determination of horizontal stress and/or horizontal stress anisotropy in soft soils at relatively shallow depth, which is the subject of this research. The lift-off stiffness correction method used for this research involved performing several air expansions in a pressure chamber, at various pressures in the range of the expected in situ test horizontal stresses. The plots presented on Figure A-16 for the middle strain tracking arms, as well as similar plots for the upper and lower arms were used to determine an appropriate stiffness correction based on the estimated horizontal stress condition of the tests. Rather than apply the stiffness measured at a particular arm during air expansion to correct the in-ground test data from that arm as has been past practice, the in-ground test data was observed to determine which arm on a particular tier of arms lifted off first, second and third. The lift-off stiffness measured in the air calibration for the first arm that lifted is applied to the in-ground test first lift-off, and so on for the second and third arms on a particular tier of arms. While this method neglects the differences in material stiffness across the membrane, it does account for the difference in lift-off stiffness due to the order of lift-off, which has been found to be the most significant component of lift-off membrane stiffness. For the subject research, the range of estimated in situ horizontal stress prior to field testing was

SELF-BORING PRESSUREMETER TESTING
THIN MEMBRANE, CHINESE LANTERN

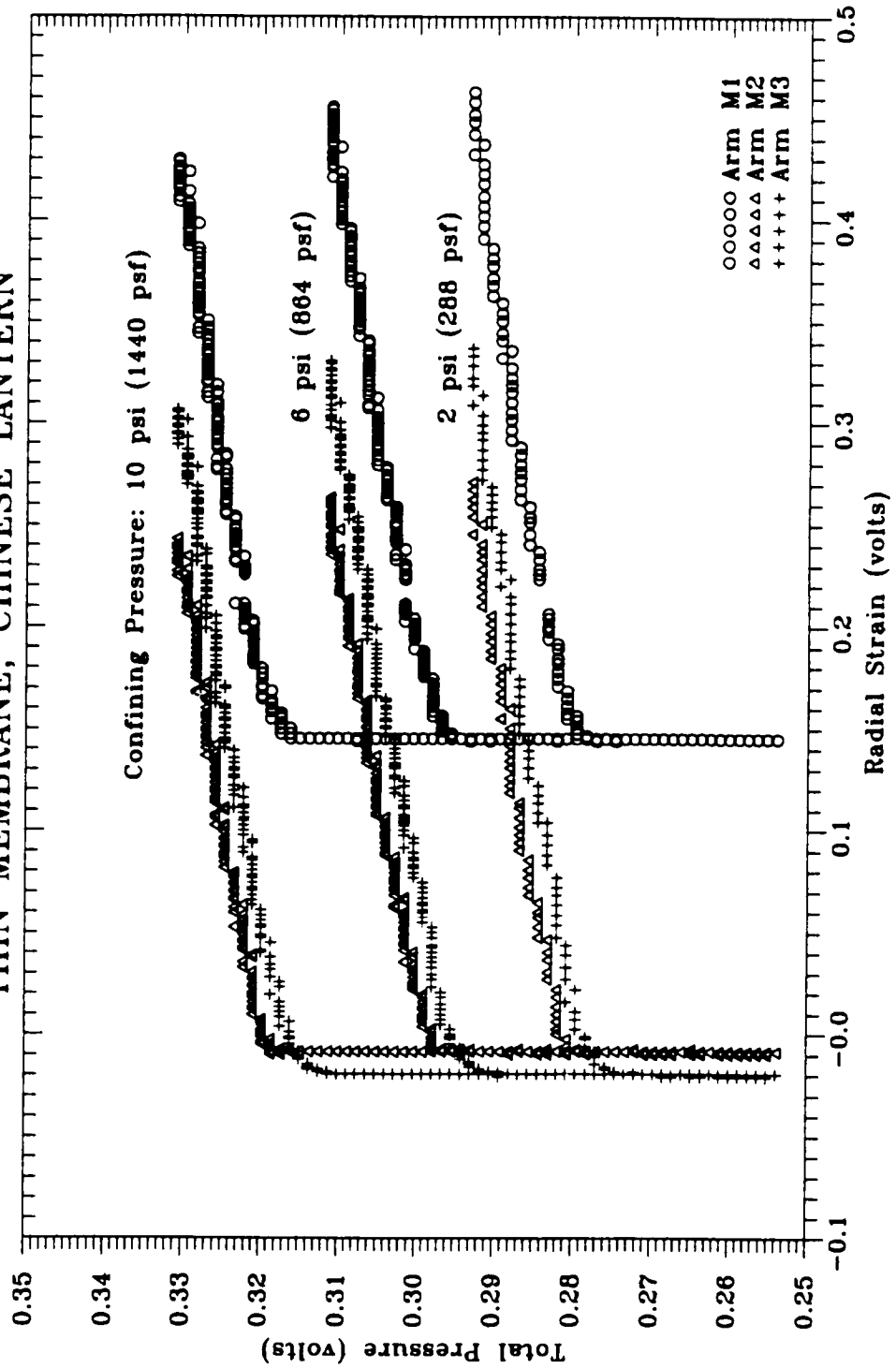


Figure A-16 Effects of Confinement Pressure

SELF-BORING PRESSUREMETER TESTING
THIN MEMBRANE, CHINESE LANTERN

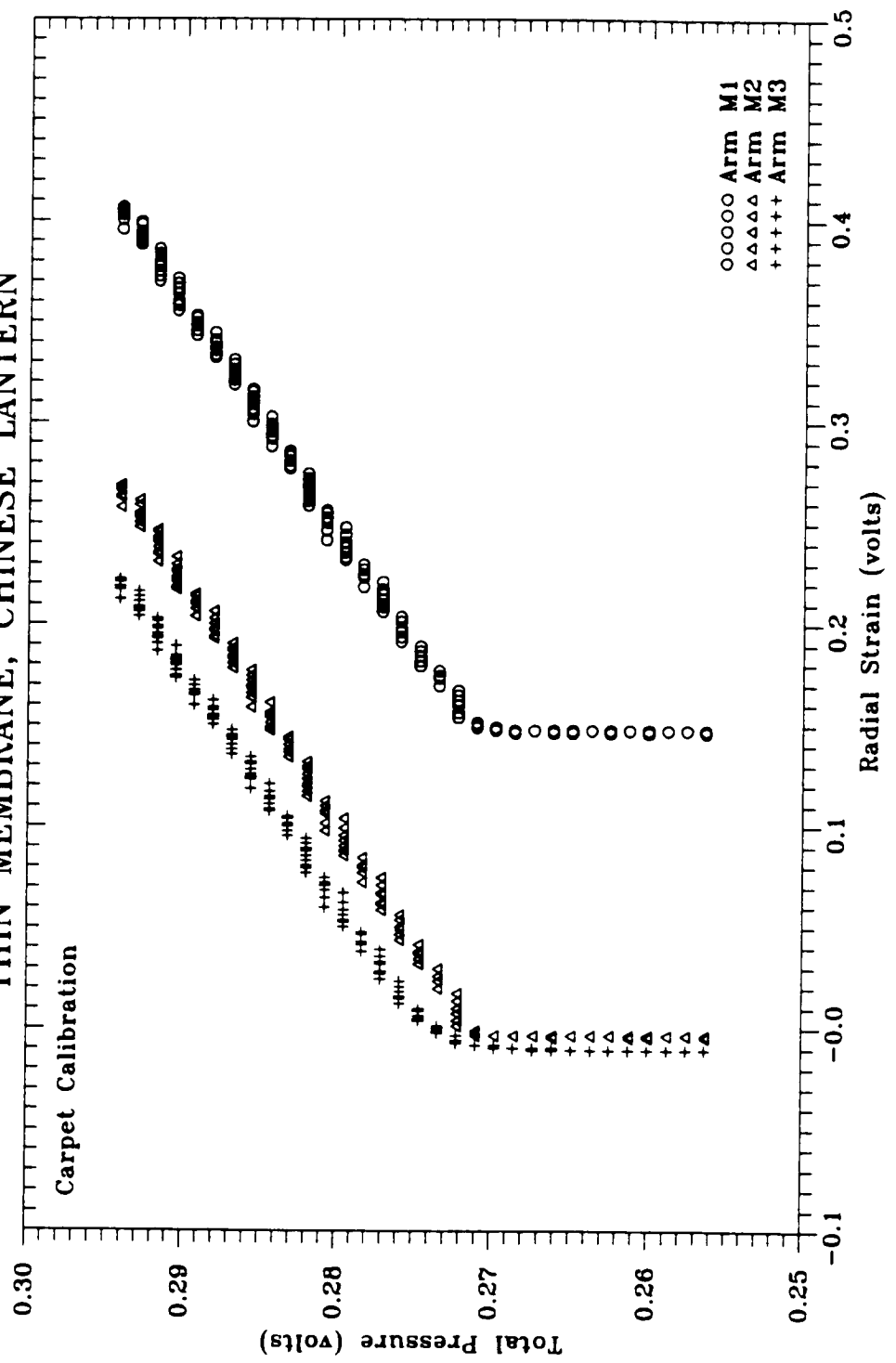


Figure A-17 Effects of Interface Friction

approximately 500 to 2500 psf (4 to 17 psi). Based on lift-off stiffness values derived from chamber calibrations at an estimated median in situ horizontal stress, the following stiffness corrections were applied for the subject research:

First Lift-off: 358 psf
Second Lift-off: 473 psf
Third Lift-off: 575 psf

A problem with applying this stiffness correction occurs where two arms on a particular tier of arms lift-off at approximately the same pressure. In such a case, it is reasoned that the stiffness applied to each of these arms would be an average of the stiffness that would normally be applied by the order of lift-off method described in the preceding paragraphs. For example, when two arms simultaneously (assumed ± 50 psf for this research) lift before the third arm lifts, a lift-off stiffness of $(358 \text{ psf} + 473 \text{ psf})/2 = 415$ psf is applied to the simultaneously lifting arms and 575 psf is applied to the third lifting arm. Similarly, when two arms simultaneously lift after another arm has lifted, a lift-off stiffness of 524 psf is applied to the simultaneously lifting arms and 358 psf is applied to the first lifting arm.

A.3.4.2 Post Lift-Off Stiffness Correction

For correction of post lift-off stiffness, the findings of Section 7.3 were considered. Because confinement and interface friction appear to mitigate the curvature observed just after lift-off for the first lifting strain arm on a given tier of arms, it can be reasoned that the first lift-off curves should not be used for stiffness correction. For this research, post lift-off stiffness was corrected for by use of a pressure chamber stiffness expansion curve which resulted from a second or third lift-off on a particular tier of arms. The magnitude of confinement does not appear to be a significant issue because of the finding that post lift-off stiffness does not seem to change with increasing confinement. However, expansion curves from a test made with a confinement of 1440 psf (10 psi) were used, which was within the range of in situ horizontal stresses measured during field testing. A post lift-off expansion curve was selected for each arm tier from these curves.

A.4 Drilling Rig Influence on SBPM Measurements

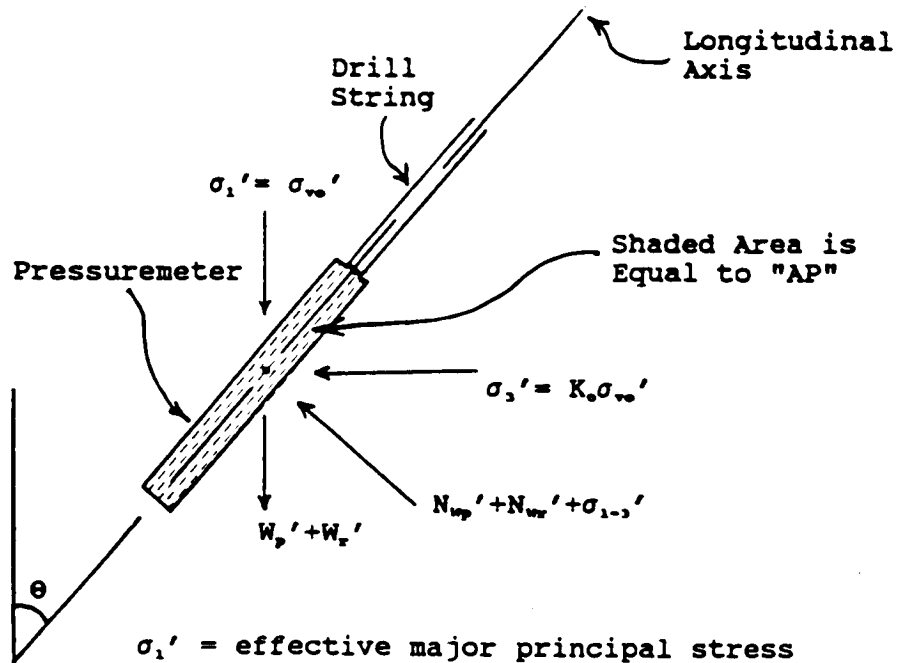
A.4.1 Introduction

During this research, two conditions imposed by the drilling equipment were noted which require consideration in order to assess the potential impact on the quality of the SBPM field test measurements. One condition was the fact that some drift of the drill string was likely to occur during drilling which could cause the SBPM to be out of plumb from vertical. Also, the drill rig and associated equipment imposed a surface load which could conceivably have some stress influence on the field measurements. The purpose of this chapter is to examine the degree to which these conditions affect SBPM lateral stress measurements.

A.4.2 Influence of SBPM Inclination

To assess the influence of probe inclination on the horizontal stress measured by the SBPM, a simplified free body diagram of the probe was drawn as indicated on the upper half of Figure A-18. The forces acting on the probe include vertical and horizontal soil pressures, and the net force of gravity on the probe. If K_v conditions are assumed, the vertical soil pressure can be estimated by multiplying the depth by the average unit weight of the soil, and the horizontal soil stress can be estimated by multiplying the vertical soil stress by an assumed K_h value. The gravity effect on the probe includes the net probe weight and net drill string weight, which are assumed to act at the centroid of the probe on the figure. The gravity effect will increase with depth, because the deeper the SBPM is below the ground surface, the more drill rods would be included in the drill string.

When the probe is vertical and suspended on the drill string from the drill rig, the weight vector is oriented parallel to the axis of the



- σ_1' = effective major principal stress
- σ_3' = effective minor principal stress
- σ_{vo}' = effective vertical stress
- σ_{1-3}' = effective stress between σ_1' and σ_3' due to SBPM inclination
- θ = inclination of SBPM from vertical
- W_p' = effective weight of pressuremeter
- W_r' = effective weight of drill string
- N_{vp}' = effective normal force on SBPM resulting from weight of the SBPM
- N_{vr}' = effective normal force on SBPM resulting from weight of the drill string
- AP = Area of longitudinal cross-section of the probe through the longitudinal axis

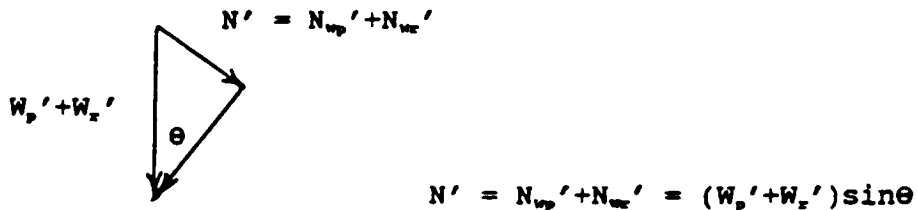


Figure A-18 Effect on σ_n' of SBPM Inclination

probe/drill string and has no influence on the measured lateral stress. The measured lateral stress, assuming K_0 conditions and K_0 less than 1.0, is σ_3' . However, if the probe is not vertical, a component of the weight of the probe/drill string, proportional to the angle of inclination, θ , tends to increase the stress on the face of the probe angled downward and decrease the stress on the upward angled face. The field of stress is no longer σ_3' on the upward and downward angled faces of the probe, but has a magnitude between σ_3' and σ_1' . Also, because the probe is not vertical, there is a differential hydrostatic stress around the probe at any point along the probe axis, again dependent on the angle of inclination of the probe. However, since this head difference only amounts to less than an inch for inclinations from vertical of 10 degrees or less, this differential hydrostatic stress can be neglected without creating any significant error.

The bottom half of Figure A-18 includes a resolution of the gravity effect or weight component of measured horizontal stress if the probe is inclined. The component N' is the normal force acting on the downward tilted probe face resulting from the weight of the probe and drill string. Because this weight will tend to deflect the soil on which the probe rests, it was assumed that the force acting on the upward tilted face of the probe would be decreased by N' . As indicated on the figure:

$$N' = (W_p' + W_d') \sin\theta \quad (\text{Eq A-7})$$

where: W_p' = weight of the pressuremeter
 W_d' = weight of the drill string
 θ = inclination of probe axis from vertical (degrees)

To resolve this force into a stress over the face of the probe, N' can be divided by AP , the area of the longitudinal cross section of the probe through the longitudinal axis.

The component of the SBPM measured lateral stress due to measurement of stresses outside of the horizontal plane when the probe is inclined is indicated on Figure A-18. Assuming σ_3' is the horizontal stress and σ_1' is the vertical stress, as the probe becomes more inclined, the measured stress on the upward and downward tilted sides of the probe will deviate from σ_3' and begin to increase toward σ_1' . This intermediate measured stress is termed σ_r' , and from the Mohr's circle on Figure A-19:

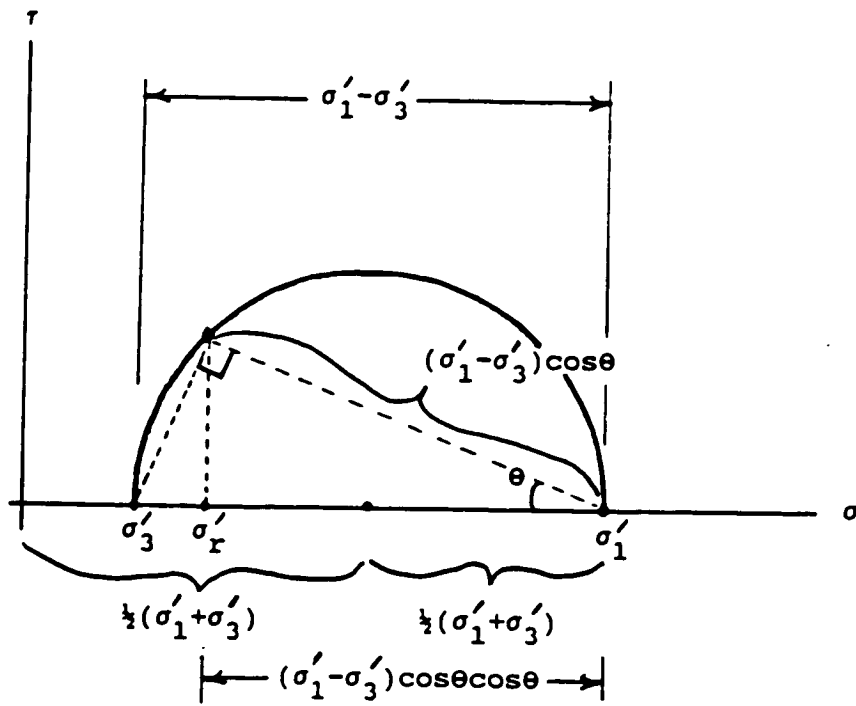
$$\sigma_r' = \sigma_1' - (\sigma_1' - \sigma_3') \cos^2\theta \quad (\text{Eq A-8})$$

Combining the gravity and stress rotation effects, the measured stress on the upward and downward tilted faces of the probe are:

$$\begin{aligned} \sigma_r', \text{ Upward} \\ \text{Tilted Face} &= \sigma_1' - (\sigma_1' - \sigma_3') \cos^2\theta - \left[\frac{(W_p' + W_d') \sin\theta}{AP} \right] \quad (\text{Eq A-9}) \end{aligned}$$

$$\begin{aligned} \sigma_r', \text{ Downward} \\ \text{Tilted Face} &= \sigma_1' - (\sigma_1' - \sigma_3') \cos^2\theta + \left[\frac{(W_p' + W_d') \sin\theta}{AP} \right] \quad (\text{Eq A-10}) \end{aligned}$$

To assess the influence of the angle of inclination on the SBPM measured lateral stress, Equations A-9 and A-10 were used to calculate the stress measured if the pressuremeter were inclined, and these computed stresses were compared to the estimated effective horizontal stress, σ_3' . Figure A-20 presents a plot of the maximum percent deviation from σ_3' that is predicted by Equations A-9 and A-10 for various inclinations and depths. K_0 was assumed to be equal to 0.5. As can be seen, the greater the inclination, the greater the error



$$\sigma'_r = \sigma'_1 - (\sigma'_1 - \sigma'_3) \cos^2 \theta$$

Figure A-19 Determination of σ'_r from Mohr's Circle

EFFECT OF SBPM INCLINATION ON MEASURED LATERAL STRESS

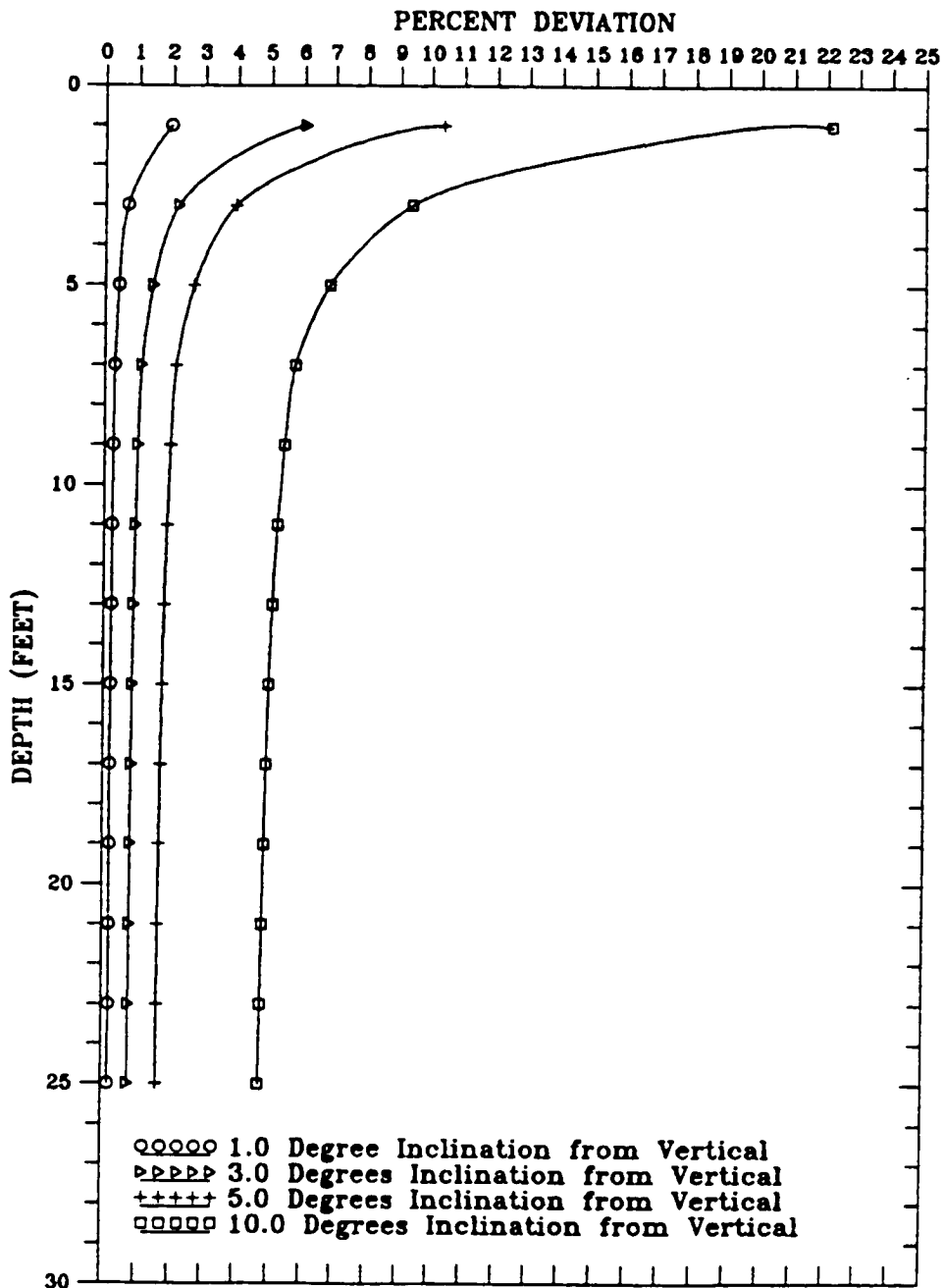


Figure A-20 Effect of SBPM Inclination on Measured Horizontal Stress

at a given depth. Also, the greatest error appears to occur at shallow depth. This is because the inclination component of the weight of the probe and drill string are a more significant portion of the measured lateral stress at shallow depth than at greater depth.

Computations were made for other K_v values, and a similar trend of decreasing percentage of error with depth was found. It was also observed that as K_v increased, the percentage of error decreased, as a result, the error indicated by Figure A-20 would be the maximum expected error assuming K_v of the soil is 0.5 or greater.

In the soils at Pease and Hamilton AFB, K_v is estimated to be about 0.5 or more. Also, tests were conducted at depths of 6.0 feet or more. Although the inclination of the probe at depth could not be determined, it is noted that the probe was plumbed vertical at the ground surface prior to drilling, so any inclination of the probe at test depth would be the result of drift of the drill string. Since the testing for this research was conducted at shallow depths (less than 30 feet), it seems reasonable to assume that the probe would not be out of vertical more than about 3 degrees at a depth of 6 feet and not more than 5 degrees at a depth of 15 or more feet. Based on these estimates and Figure A-20, the maximum error in lateral stress measurement resulting due to inclination of the SBPM is expected to be less than about 2 percent.

A.4.3 Influence of Drill Rig Weight

The effect of surface loading caused by the weight of the drill rig on SBPM measured lateral stress was investigated using the Boussinesq pressure distribution for continuous spread footings. The drill rig is supported on the ground by two wooden skids about 8-inches wide by about 8 feet long. Since the drill rig weighs less than about 2,000 pounds, it can be assumed that each skid imparts a force to the ground surface of 1,000 pounds or a pressure of 186 pounds per square foot. A schematic plan view of the skid location and the annulus of the SBPM borehole is presented on Figure A-21. Assuming symmetry and the fact that both skids will influence the stress sensed at an SBPM test location, the stress influence of only one skid was computed using Boussinesq theory, and that stress multiplied by two to account for both skids. The influence of the offset of the boring annulus from the plan location of the skids was also considered. According to Boussinesq theory and the above geometry, the vertical stress at a depth of 6 feet along the borehole annulus imparted by the drill rig is about 5 percent of the skid-ground surface contact stress or less than 9.3 pounds per square foot. Assuming a K_v of 2.0 at a depth of about 6 feet which represents the shallowest tests conducted during the research, the lateral stress imposed by the drill rig would be about 18 pounds per square foot, an amount considered negligible considering the lateral stress at this depth is about 1500 pounds per square foot or more. This would be an error of about 1 percent. The error becomes significantly less with depth since the stress imposed by the drill rig and K_v decrease quickly below a depth of 6 feet.

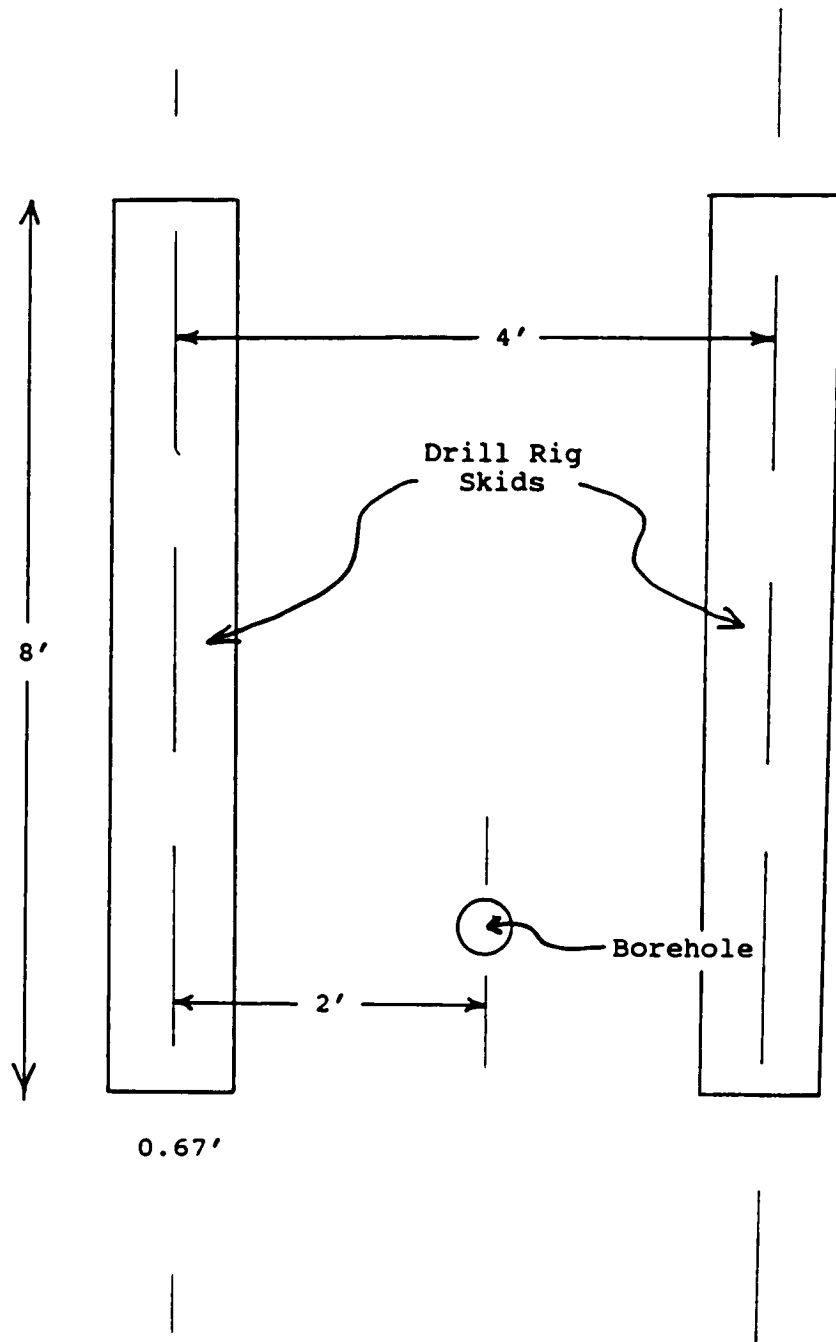


Figure A-21 Schematic Plan of Borehole and Drill Rig Skids

APPENDIX B
TABULATIONS OF CURVE RATING BY C_s METHOD

SBPM CURVE EVALUATION						
TEST DESIGN- ATION	ARM U1		ARM U2		ARM U3	
	DISTURB- ANCE RATIO, Cd	QUAL- ITY	DISTURB- ANCE RATIO, Cd	QUAL- ITY	DISTURB- ANCE RATIO, Cd	QUAL- ITY
PMC1.1	0.24	Fair	0.41	Good	0.37	Good
PMC1.2	0.37	Good	0.34	Good	NA	Fair
PMC1.3	0.35	Good	0.45	Good	NA	Fair
PMC2.1	0.27	Fair	0.42	Good	0.47	Fair
PMC2.2	0.33	Good	0.43	Good	0.56	Fair
PMC2.3H	0.37	Good	0.42	Good	0.46	Fair
PMC2.4	0.33	Good	0.43	Good	NA	Fair
PMC3.1	0.27	Fair	0.36	Good	NA	Fair
PMC3.2H	0.31	Good	0.33	Good	NA	Fair
PMC3.3H	0.40	Good	0.37	Good	0.48	Fair
PMC3.4H	0.31	Good	0.42	Good	NA	Fair
PMC3.5H	0.31	Good	0.32	Good	NA	Fair
PMC3.5R	0.25	Fair	NA	Fair	NA	Fair
PMC3.6H	0.36	Good	NA	Fair	NA	Fair
PMC4.1	0.29	Good	0.46	Fair	NA	Fair
PMC4.2	0.35	Good	NA	Fair	NA	Fair
PMC4.3	0.33	Good	0.46	Fair	NA	Fair
PMC4.4	0.36	Good	0.40	Good	NA	Fair
PMC4.5	0.45	Good	NA	Fair	NA	Fair
PMC4.6	0.40	Good	0.44	Good	NA	Fair
PMC4.7	0.32	Good	0.35	Good	0.37	Good
PMJ3.2	0.15	Fair	0.22	Fair	0.18	Fair
PMJ3.2R	0.15	Fair	0.08	Fair	0.07	Fair
PMJ3.3	NA	Fair	NA	Fair	NA	Fair
PMJ3.4	0.44	Good	0.38	Good	NA	Fair
PMJ3.4R	0.27	Fair	0.25	Fair	0.32	Good
PMJ3.5	0.31	Good	0.17	Fair	0.39	Good
PMJ3.6	0.26	Fair	NA	Fair	0.28	Fair
PMJ4.1	0.32	Good	0.37	Good	NA	Fair
PMJ4.2	NA	Fair	0.54	Fair	NA	Fair
PMJ4.2R	0.20	Fair	0.20	Fair	0.20	Fair
PMJ4.3	0.28	Fair	NA	Fair	0.28	Fair
PMJ4.4	0.30	Good	0.40	Good	0.36	Good
PMJ4.5	0.27	Fair	0.51	Fair	NA	Fair
PMJ4.6H	0.33	Good	NA	Fair	NA	Fair
PMJ4.7	NA	Fair	NA	Fair	NA	Fair

SBPM CURVE EVALUATION						
TEST DESIGN- ATION	ARM U1		ARM U2		ARM U3	
	DISTURB- ANCE RATIO, Cd	QUAL- ITY	DISTURB- ANCE RATIO, Cd	QUAL- ITY	DISTURB- ANCE RATIO, Cd	QUAL- ITY
PMJ5.1	NA	Fair	0.33	Good	NA	Fair
PMJ5.2	NA	Fair	0.25	Fair	NA	Fair
PMJ5.3	0.39	Good	0.45	Fair	NA	Fair
PMJ5.4	NA	Fair	0.28	Fair	NA	Fair
PMJ5.5	NA	Fair	0.34	Good	NA	Fair
PMJ5.6	0.27	Fair	0.16	Fair	0.46	Fair
PMJ6.1	0.29	Good	0.45	Good	0.58	Fair
PMJ6.2	0.36	Good	0.42	Good	0.43	Good
PMJ6.3	0.35	Good	0.36	Good	0.46	Good
PMJ6.4H	0.32	Good	0.30	Good	0.40	Good
PMJ7.1	NA	Fair	0.38	Good	0.43	Good
PMJ7.2	NA	Fair	0.41	Good	0.42	Good
PMJ7.3	0.28	Good	0.28	Good	0.38	Good
PMJ7.4H	NA	Fair	NA	Fair	NA	Fair
PMJ8.1	0.36	Good	0.35	Good	0.43	Good
PMJ8.2	NA	Fair	0.33	Good	NA	Fair
PMJ8.3H	0.39	Good	0.42	Good	NA	Fair
PMJ8.4	0.40	Good	NA	Fair	NA	Fair
PMS1.1	0.54	Fair	0.44	Good	NA	Fair
PMS1.2	NA	Fair	NA	Fair	NA	Fair
PMP1.1	0.20	Bad	0.25	Fair	0.25	Fair
PMP1.2	0.14	Bad	0.41	Good	0.08	Fair
PMP2.1	0.17	Bad	0.32	Good	0.04	Fair
HAM1.1	0.12	Fair	0.11	Fair	0.18	Good
HAM1.2	0.13	Fair	0.10	Fair	0.13	Fair
HAM1.3	0.32	Fair	0.21	Good	0.35	Fair
HAM2.1	0.20	Good	0.30	Fair	0.33	Fair
HAM2.2	NA	Fair	NA	Fair	NA	Fair
HAM2.3	0.21	Good	0.23	Good	0.24	Good
HAM2.4H	0.15	Fair	0.15	Fair	0.30	Fair
HAM2.4R	0.20	Good	0.07	Fair	0.01	Fair
HAM2.5P	0.10	Fair	0.20	Good	0.45	Fair

SBPM CURVE EVALUATION						
TEST DESIGNATION	ARM M1		ARM M2		ARM M3	
	DISTURBANCE RATIO, Cd	QUALITY	DISTURBANCE RATIO, Cd	QUALITY	DISTURBANCE RATIO, Cd	QUALITY
PMC1.1	0.33	Good	0.20	Fair	0.43	Good
PMC1.2	0.41	Good	0.34	Good	NA	Fair
PMC1.3	0.44	Good	0.29	Fair	NA	Fair
PMC2.1	0.34	Good	0.27	Fair	0.37	Good
PMC2.2	0.44	Good	0.24	Fair	NA	Fair
PMC2.3H	0.43	Good	0.31	Good	NA	Fair
PMC2.4	0.45	Good	0.28	Fair	NA	Fair
PMC3.1	0.42	Good	0.28	Fair	NA	Fair
PMC3.2H	0.41	Good	0.31	Good	NA	Fair
PMC3.3H	0.39	Good	0.31	Good	NA	Fair
PMC3.4H	0.42	Good	0.34	Good	NA	Fair
PMC3.5H	0.45	Fair	0.26	Fair	0.64	Fair
PMC3.5R	0.19	Fair	0.25	Fair	0.20	Fair
PMC3.6H	0.38	Good	0.20	Fair	0.27	Fair
PMC4.1	NA	Fair	0.48	Fair	NA	Fair
PMC4.2	0.40	Good	0.42	Good	NA	Fair
PMC4.3	0.43	Good	NA	Fair	NA	Fair
PMC4.4	0.40	Good	0.29	Good	NA	Fair
PMC4.5	0.43	Good	0.43	Good	NA	Fair
PMC4.6	0.36	Good	0.43	Good	NA	Fair
PMC4.7	0.37	Good	0.36	Good	0.40	Good
PMJ3.2	0.25	Fair	0.46	Fair	0.48	Fair
PMJ3.2R	0.15	Fair	0.33	Good	0.27	Fair
PMJ3.3	0.12	Fair	0.12	Fair	0.17	Fair
PMJ3.4	0.31	Good	0.34	Good	0.38	Good
PMJ3.4R	0.25	Fair	0.26	Fair	0.28	Fair
PMJ3.5	NA	Fair	0.18	Fair	0.28	Fair
PMJ3.6	0.30	Good	NA	Fair	0.31	Good
PMJ4.1	0.48	Fair	0.28	Fair	0.34	Good
PMJ4.2	0.49	Fair	0.42	Good	0.34	Good
PMJ4.2R	0.24	Fair	0.26	Fair	0.36	Good
PMJ4.3	0.48	Fair	0.45	Good	0.44	Good
PMJ4.4	0.42	Good	0.47	Fair	0.33	Good
PMJ4.5	0.33	Good	0.39	Good	0.34	Good
PMJ4.6H	0.40	Good	NA	Fair	0.34	Good
PMJ4.7	NA	Fair	NA	Fair	0.13	Fair

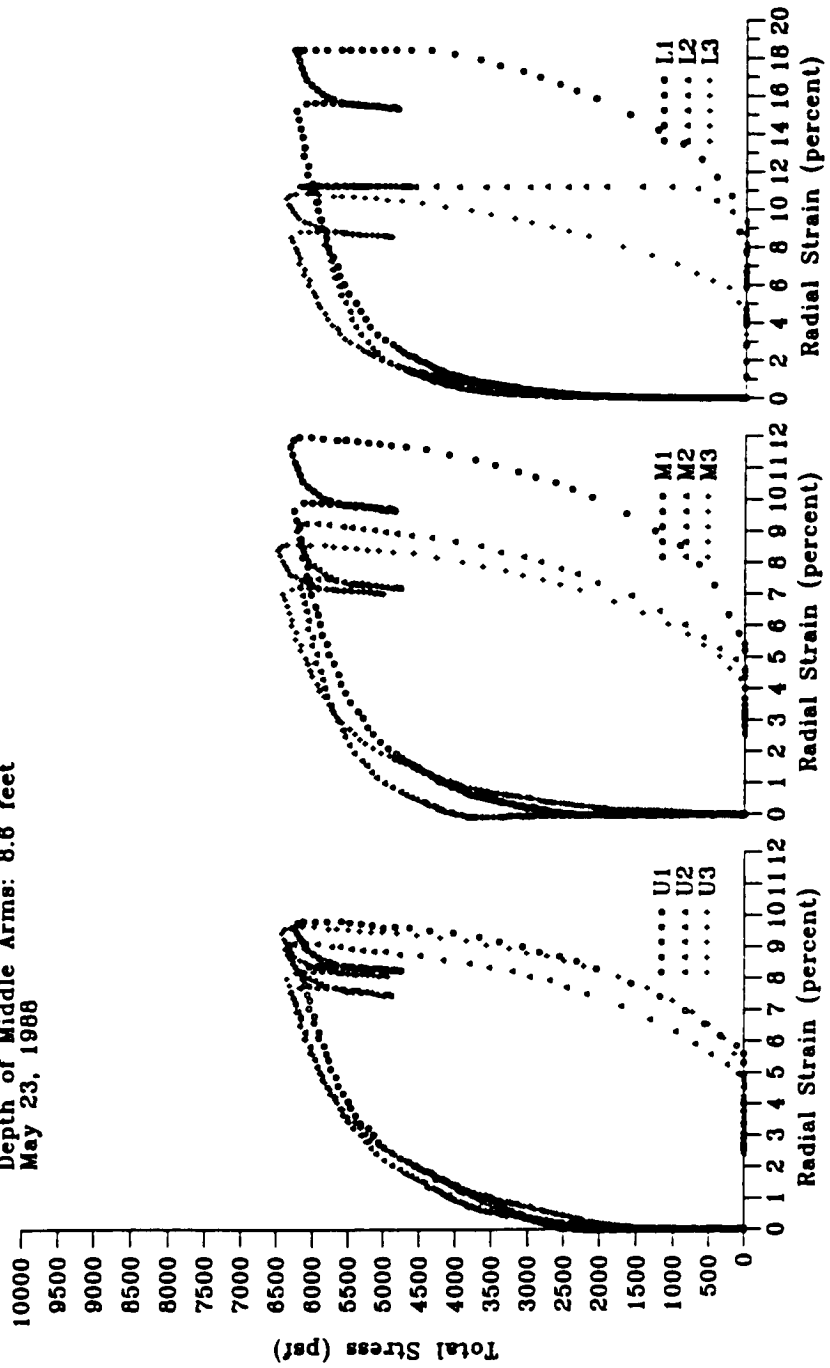
SBPM CURVE EVALUATION						
TEST DESIGNATION	ARM M1		ARM M2		ARM M3	
	DISTURBANCE RATIO, Cd	QUALITY	DISTURBANCE RATIO, Cd	QUALITY	DISTURBANCE RATIO, Cd	QUALITY
PMJ5.1	0.22	Fair	0.36	Good	0.31	Good
PMJ5.2	0.21	Fair	0.21	Fair	0.26	Fair
PMJ5.3	0.38	Good	0.44	Good	0.42	Good
PMJ5.4	0.27	Fair	NA	Fair	0.31	Good
PMJ5.5	0.31	Good	0.43	Good	0.36	Good
PMJ5.6	0.33	Good	0.45	Fair	0.38	Good
PMJ6.1	0.36	Good	0.39	Good	0.39	Good
PMJ6.2	0.34	Good	0.36	Good	0.36	Good
PMJ6.3	0.35	Good	0.40	Good	0.39	Good
PMJ6.4H	0.32	Good	0.42	Good	0.38	Good
PMJ7.1	0.42	Good	0.42	Good	0.44	Good
PMJ7.2	0.45	Good	0.45	Good	0.45	Good
PMJ7.3	0.37	Good	0.32	Good	0.38	Good
PMJ7.4H	NA	Fair	NA	Fair	NA	Fair
PMJ8.1	0.36	Good	0.39	Good	NA	Fair
PMJ8.2	0.43	Good	0.40	Good	NA	Fair
PMJ8.3H	0.41	Good	0.44	Good	NA	Fair
PMJ8.4	0.44	Good	0.37	Good	NA	Fair
PMS1.1	0.52	Fair	0.55	Fair	NA	Fair
PMS1.2	NA	Fair	NA	Fair	NA	Fair
PMP1.1	0.20	Fair	0.21	Fair	0.35	Good
PMP1.2	0.10	Fair	0.15	Fair	0.15	Fair
PMP2.1	0.09	Fair	0.18	Fair	0.23	Fair
HAM1.1	0.15	Good	0.22	Good	0.18	Good
HAM1.2	0.18	Good	0.26	Good	0.18	Good
HAM1.3	0.21	Good	0.26	Good	0.25	Good
HAM2.1	0.23	Good	0.27	Good	0.18	Good
HAM2.2	NA	Fair	NA	Fair	NA	Fair
HAM2.3	0.18	Good	0.24	Good	0.19	Good
HAM2.4H	0.14	Fair	0.15	Fair	0.14	Fair
HAM2.4R	0.19	Good	0.23	Good	0.16	Good
HAM2.5P	0.08	Fair	0.08	Fair	0.07	Fair

SBPM CURVE EVALUATION						
TEST DESIGN- ATION	ARM L1		ARM L2		ARM L3	
	DISTURB- ANCE RATIO, Cd	QUAL- ITY	DISTURB- ANCE RATIO, Cd	QUAL- ITY	DISTURB- ANCE RATIO, Cd	QUAL- ITY
PMC1.1	0.46	Fair	0.36	Good	0.44	Good
PMC1.2	0.45	Good	0.38	Good	0.49	Fair
PMC1.3	0.30	Good	0.43	Good	NA	Fair
PMC2.1	0.38	Good	0.40	Good	0.48	Fair
PMC2.2	0.42	Good	0.37	Good	0.54	Fair
PMC2.3H	0.50	Fair	0.39	Good	NA	Fair
PMC2.4	0.37	Good	0.32	Good	0.51	Fair
PMC3.1	0.36	Good	0.42	Good	0.46	Fair
PMC3.2H	0.41	Good	0.37	Good	0.53	Fair
PMC3.3H	0.33	Good	0.34	Good	NA	Fair
PMC3.4H	0.40	Good	0.30	Good	NA	Fair
PMC3.5H	0.33	Good	0.30	Good	0.47	Fair
PMC3.5R	0.10	Fair	0.08	Fair	0.10	Fair
PMC3.6H	0.34	Good	0.32	Good	0.28	Fair
PMC4.1	NA	Fair	0.55	Fair	0.30	Good
PMC4.2	0.52	Fair	NA	Fair	0.30	Good
PMC4.3	NA	Fair	0.23	Fair	0.21	Fair
PMC4.4	0.54	Fair	0.50	Fair	0.28	Fair
PMC4.5	0.50	Fair	0.53	Fair	0.29	Fair
PMC4.6	0.51	Fair	0.47	Fair	0.29	Fair
PMC4.7	0.46	Fair	0.45	Fair	0.23	Fair
PMJ3.2	0.17	Fair	0.18	Fair	0.18	Fair
PMJ3.2R	0.16	Fair	0.19	Fair	0.17	Fair
PMJ3.3	NA	Fair	NA	Fair	NA	Fair
PMJ3.4	NA	Fair	0.49	Fair	0.24	Fair
PMJ3.4R	0.21	Fair	0.32	Good	0.18	Fair
PMJ3.5	0.48	Fair	0.25	Fair	0.19	Fair
PMJ3.6	NA	Fair	NA	Fair	0.18	Fair
PMJ4.1	NA	Fair	0.40	Good	0.24	Fair
PMJ4.2	NA	Fair	0.59	Fair	0.23	Fair
PMJ4.2R	NA	Fair	0.32	Good	0.25	Fair
PMJ4.3	NA	Fair	0.53	Fair	0.21	Fair
PMJ4.4	NA	Fair	0.47	Fair	0.16	Fair
PMJ4.5	NA	Fair	NA	Fair	0.23	Fair
PMJ4.6H	NA	Fair	NA	Fair	0.23	Fair
PMJ4.7	NA	Fair	NA	Fair	NA	Fair

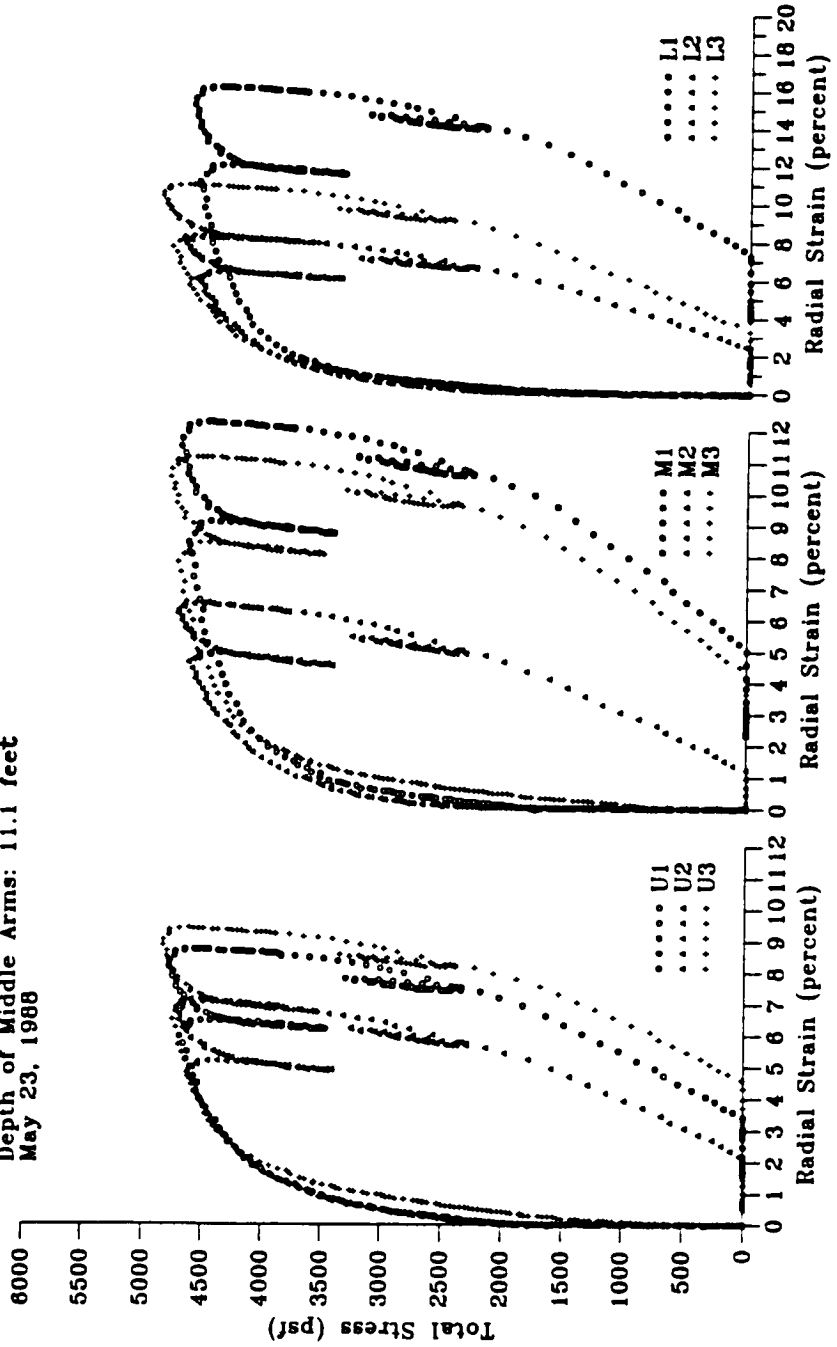
SBPM CURVE EVALUATION						
TEST DESIGNATION	ARM L1		ARM L2		ARM L3	
	DISTURBANCE RATIO, Cd	QUALITY	DISTURBANCE RATIO, Cd	QUALITY	DISTURBANCE RATIO, Cd	QUALITY
PMJ5.1	0.45	Fair	0.22	Fair	0.29	Good
PMJ5.2	0.41	Good	0.32	Good	0.25	Fair
PMJ5.3	NA	Fair	0.33	Good	0.26	Fair
PMJ5.4	0.31	Good	0.41	Good	0.24	Fair
PMJ5.5	0.41	Good	0.37	Good	0.23	Fair
PMJ5.6	0.45	Fair	0.40	Good	0.20	Fair
PMJ6.1	0.34	Good	0.38	Good	0.31	Good
PMJ6.2	0.34	Good	0.32	Good	0.29	Good
PMJ6.3	0.33	Good	0.39	Good	0.30	Good
PMJ6.4H	0.36	Good	0.41	Good	0.29	Good
PMJ7.1	0.44	Good	0.40	Good	NA	Fair
PMJ7.2	0.44	Good	NA	Fair	NA	Fair
PMJ7.3	0.38	Good	0.38	Good	0.33	Good
PMJ7.4H	NA	Fair	NA	Fair	NA	Fair
PMJ8.1	0.40	Good	0.42	Good	NA	Fair
PMJ8.2	0.45	Good	0.44	Good	NA	Fair
PMJ8.3H	0.43	Good	0.43	Good	NA	Fair
PMJ8.4	NA	Fair	NA	Fair	NA	Fair
PMS1.1	0.60	Fair	0.53	Fair	NA	Fair
PMS1.2	NA	Fair	NA	Fair	NA	Fair
PMP1.1	0.33	Good	0.16	Fair	0.07	Fair
PMP1.2	0.27	Fair	0.13	Fair	0.07	Fair
PMP2.1	0.30	Good	0.15	Fair	0.10	Fair
HAM1.1	0.22	Good	0.12	Fair	0.13	Fair
HAM1.2	0.40	Fair	0.21	Good	0.23	Good
HAM1.3	0.28	Fair	0.19	Good	0.17	Good
HAM2.1	0.34	Fair	0.25	Good	0.20	Good
HAM2.2	NA	Fair	NA	Fair	NA	Fair
HAM2.3	0.26	Good	0.20	Good	0.20	Good
HAM2.4H	0.15	Fair	0.13	Fair	0.15	Fair
HAM2.4R	0.21	Good	0.24	Good	0.23	Good
HAM2.5P	0.07	Fair	0.07	Fair	0.07	Fair

APPENDIX C
PLOTS OF SBPM RESULTS

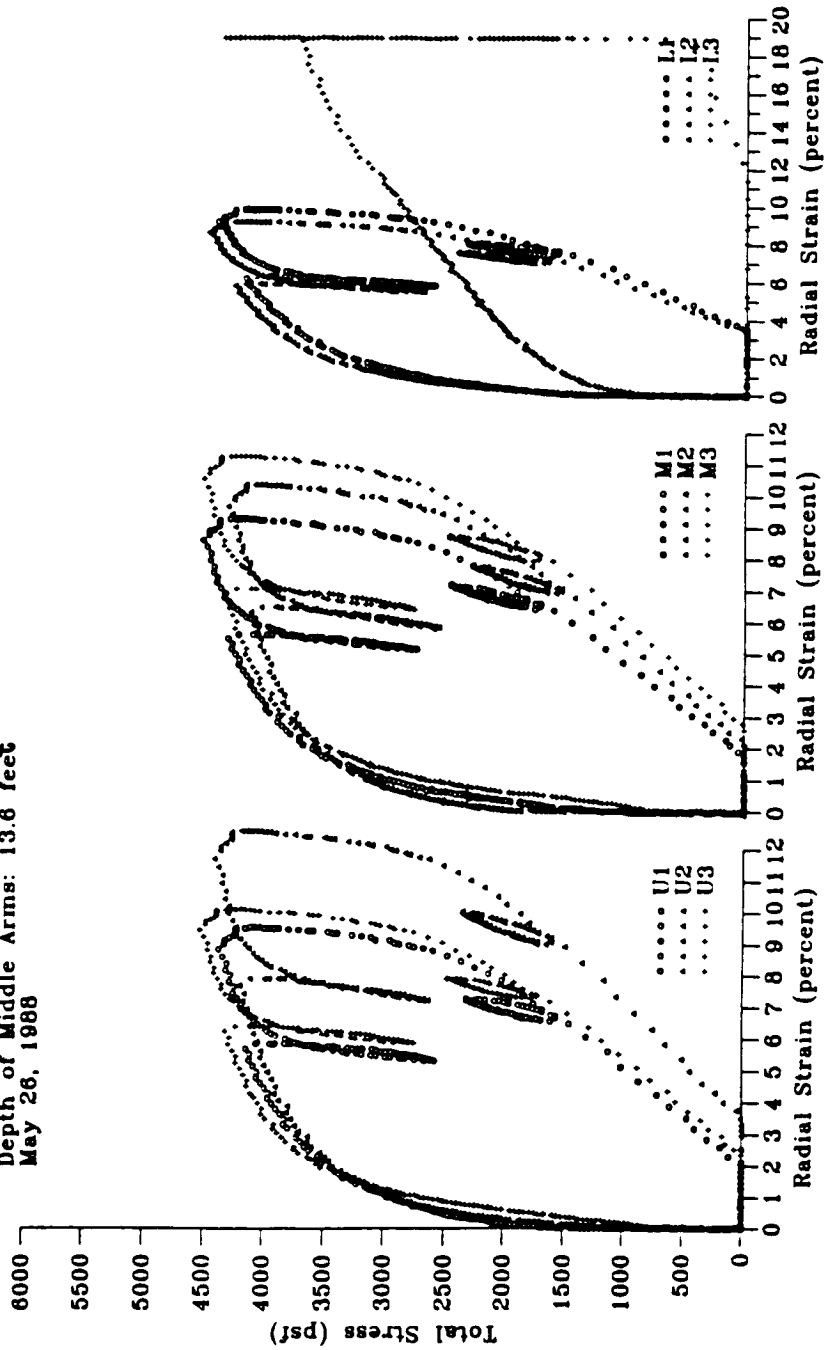
Test PMC 1.1 - Pease Air Force Base Site
 Depth of Middle Arms: 8.6 feet
 May 23, 1968



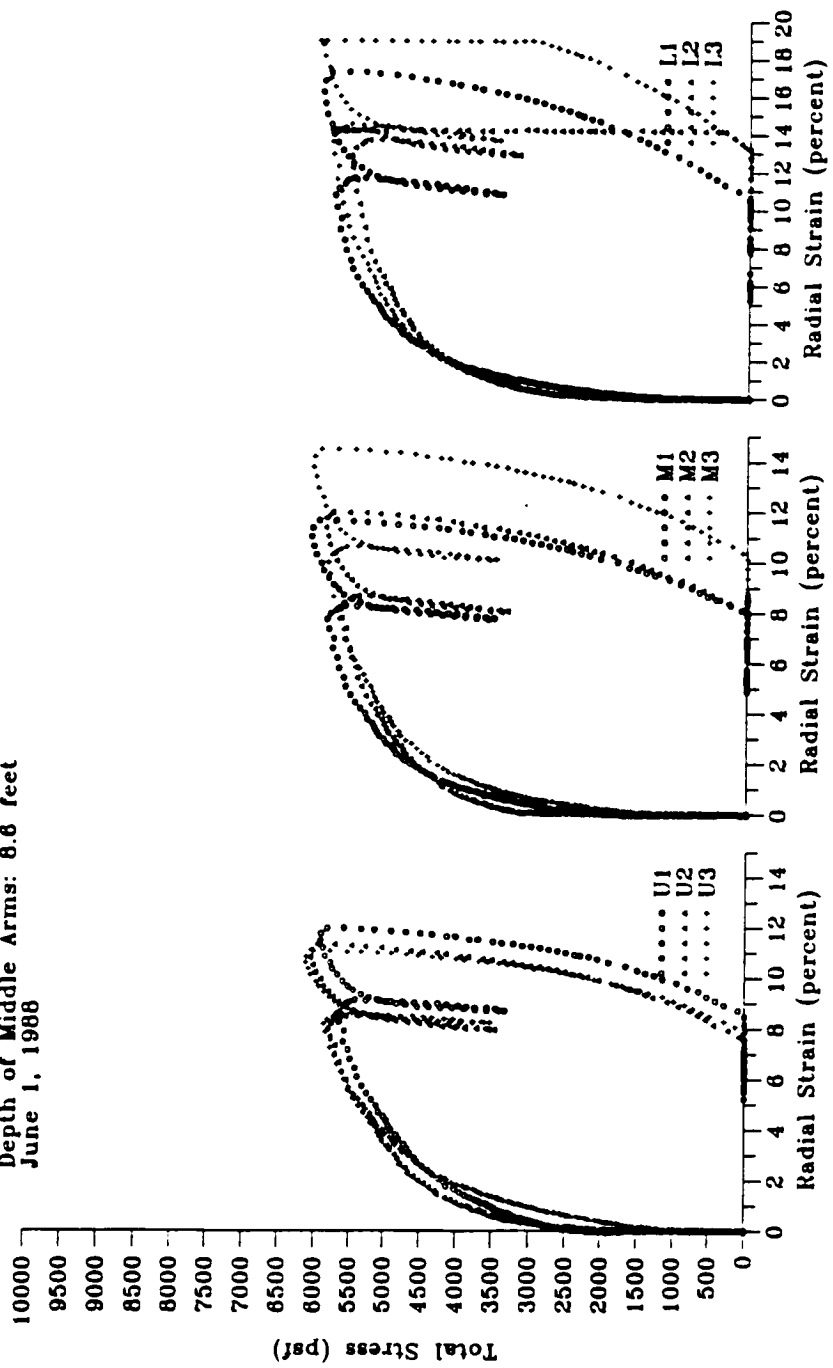
Test PMC 1.2 - Pease Air Force Base Site
 Depth of Middle Arms: 11.1 feet
 May 23, 1988



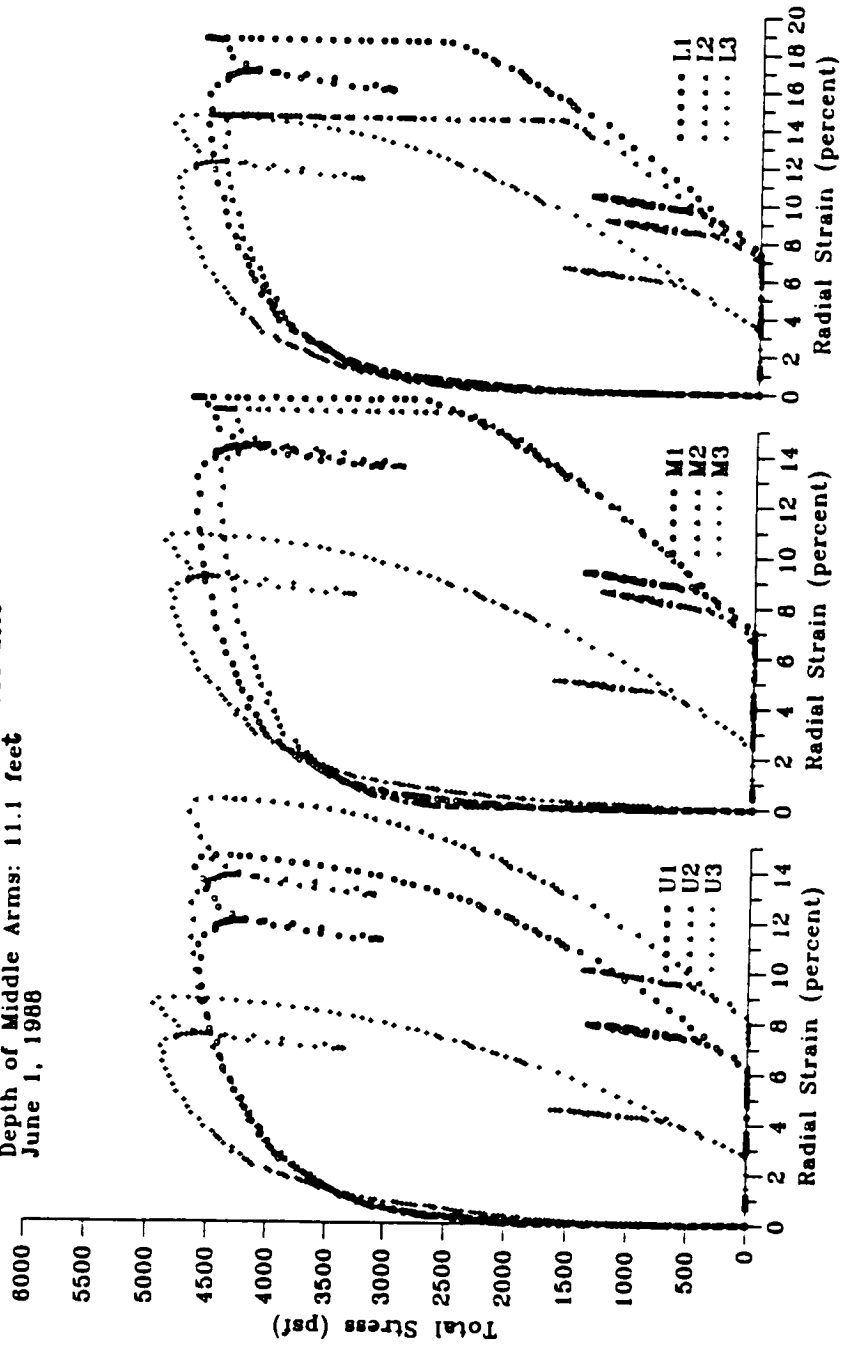
Test PMC 1.3 - Pease Air Force Base Site
 Depth of Middle Arms: 13.6 feet
 May 26, 1988



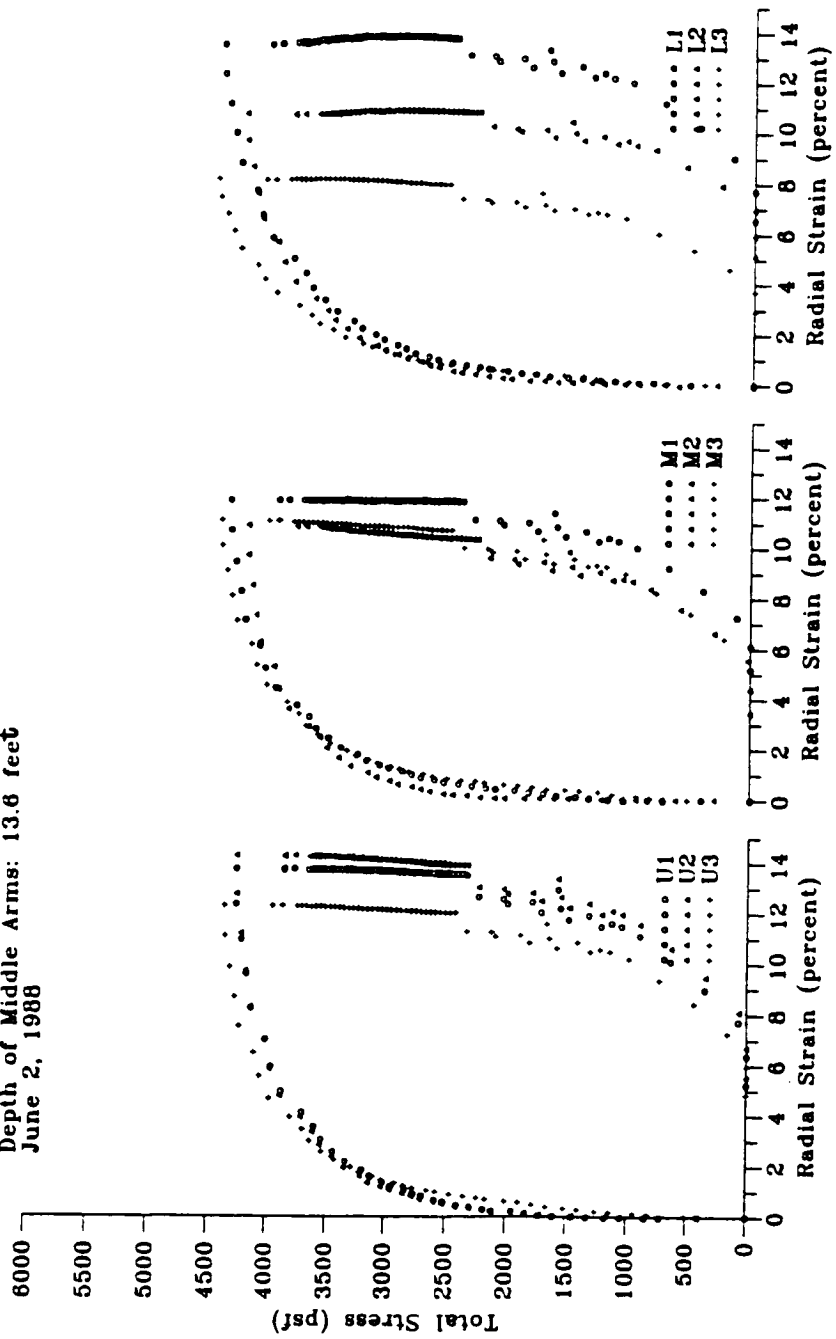
Test PMC 2.1 - Pease Air Force Base Site
 Depth of Middle Arms: 8.6 feet
 June 1, 1988



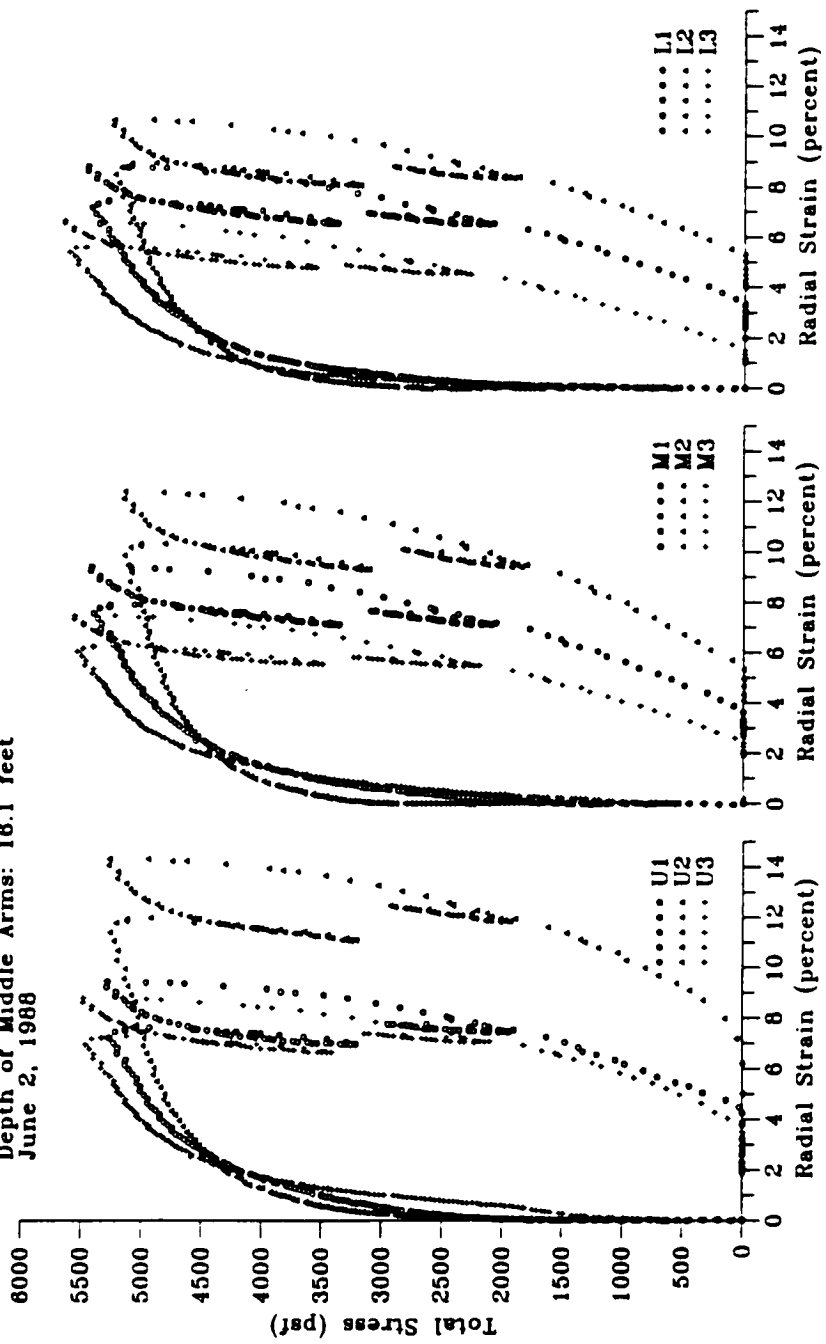
Test PMC 2.2 - Pease Air Force Base Site
 Depth of Middle Arms: 11.1 feet
 June 1, 1988



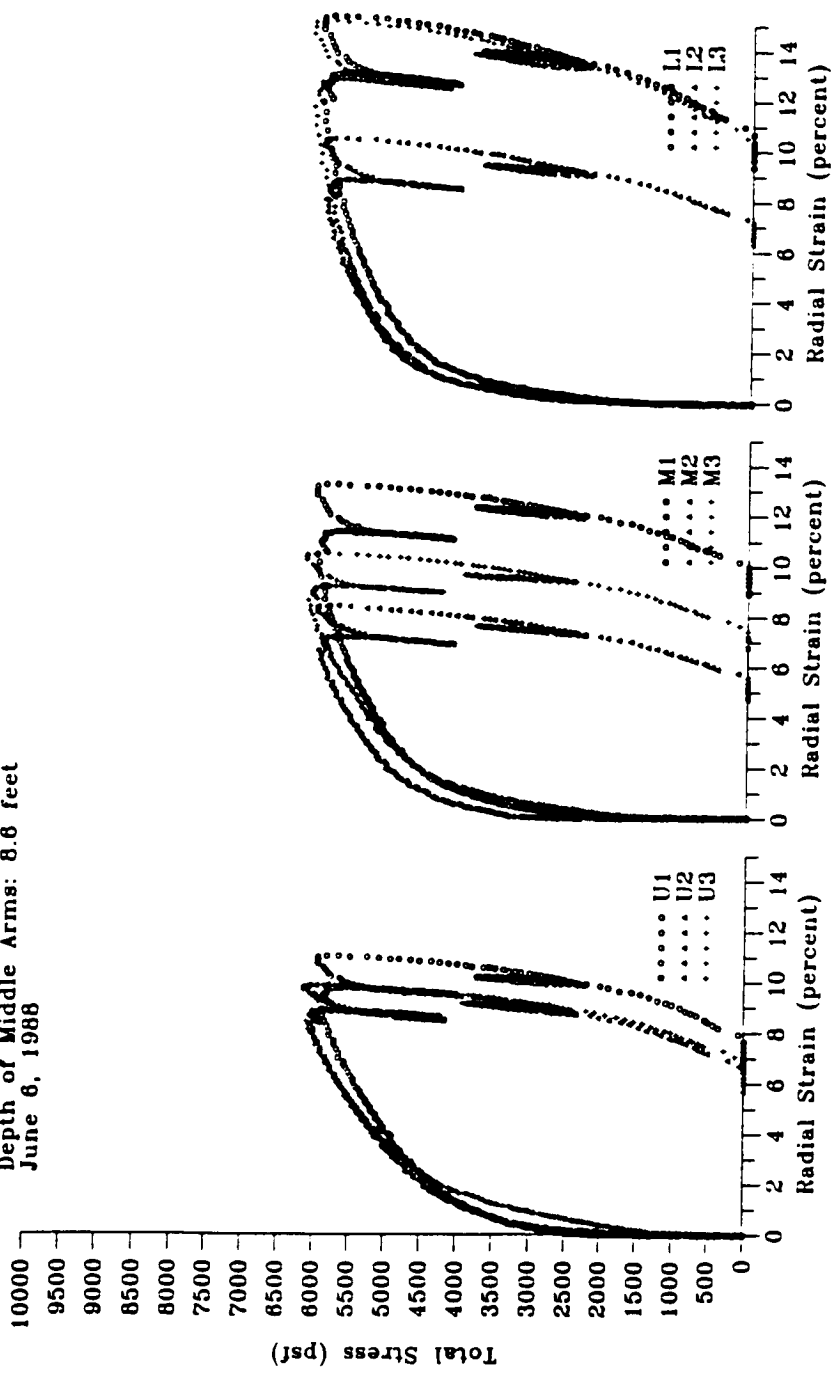
Test PMC 2.3II - Pease Air Force Base Site
 Depth of Middle Arms: 13.6 feet
 June 2, 1988



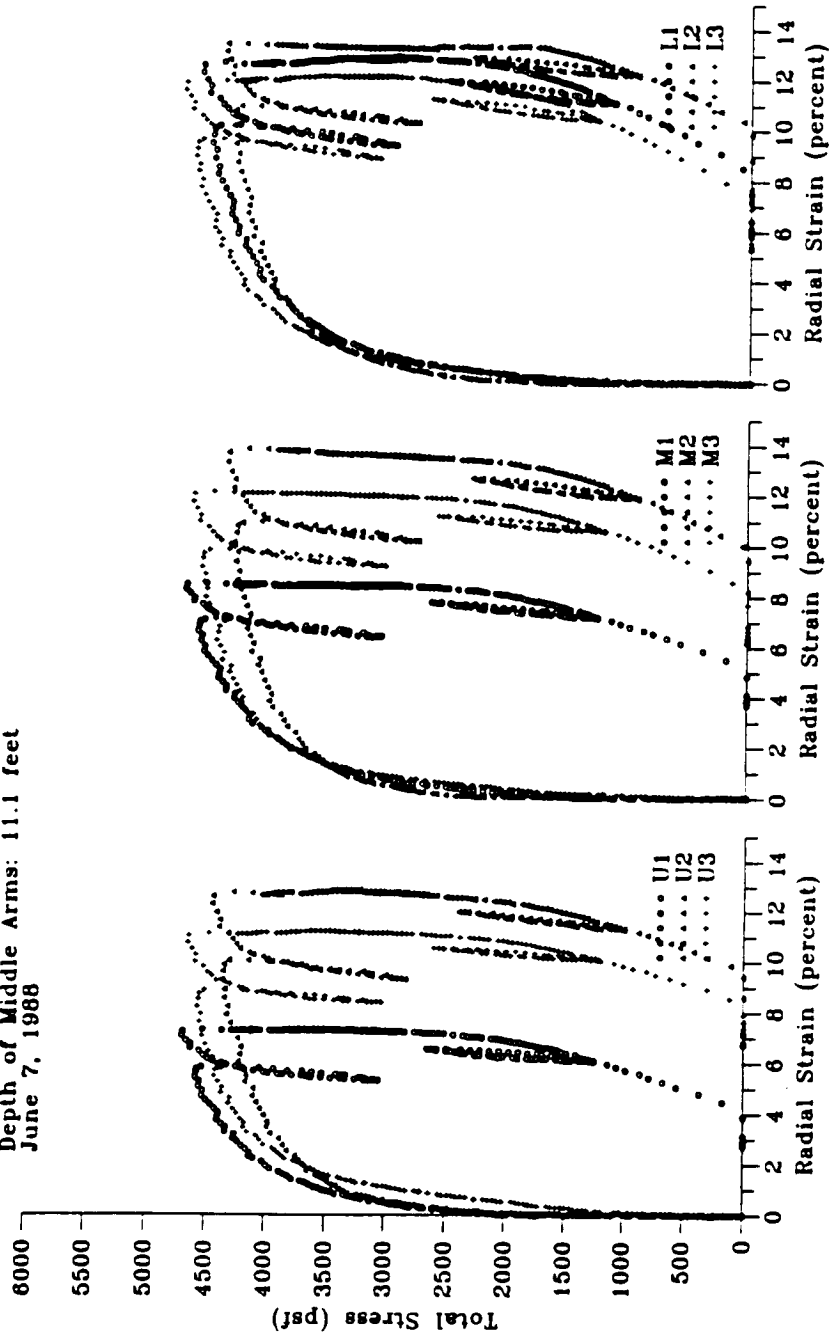
Test PMC 2.4 - Pease Air Force Base Site
 Depth of Middle Arms: 16.1 feet
 June 2, 1988



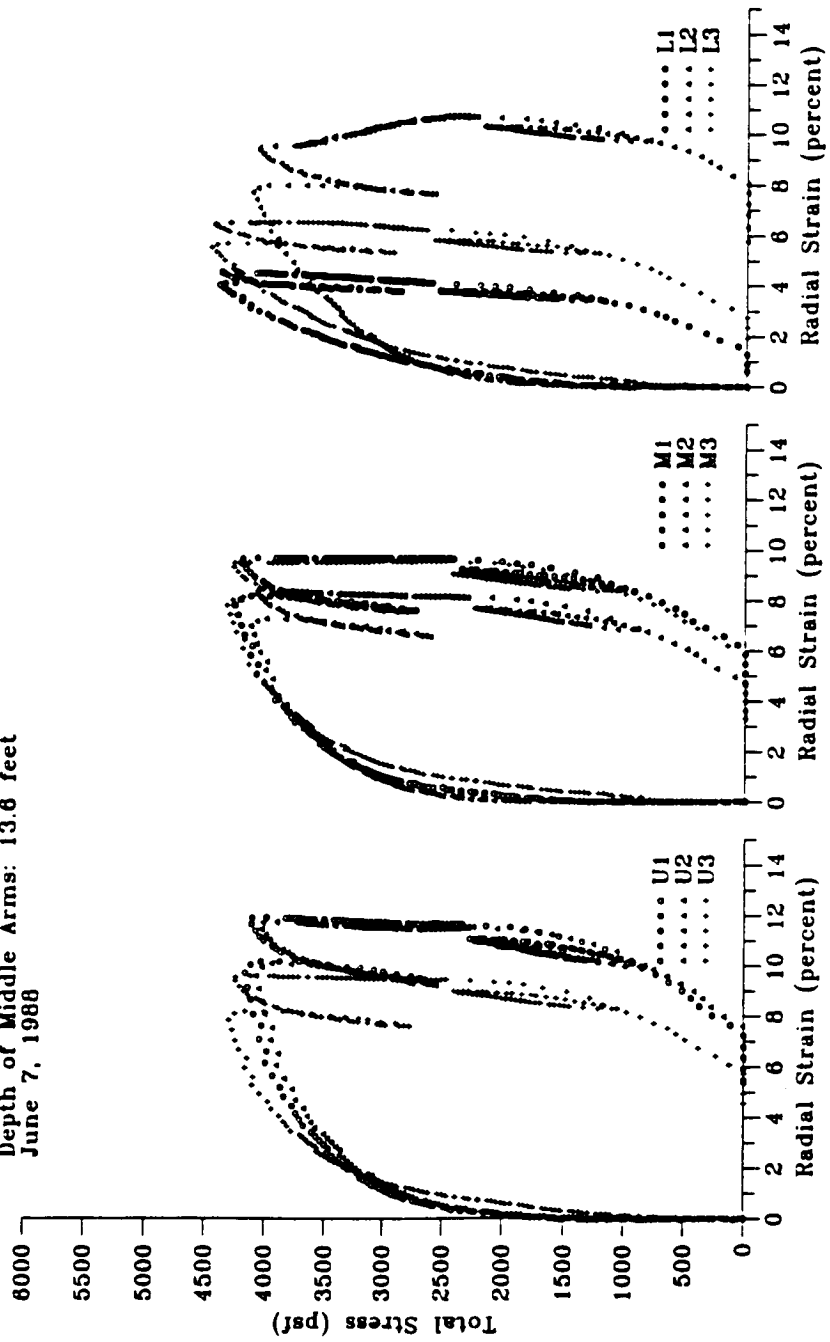
Test PMC 3.1 - Pease Air Force Base Site
 Depth of Middle Arms: 8.6 feet
 June 6, 1988



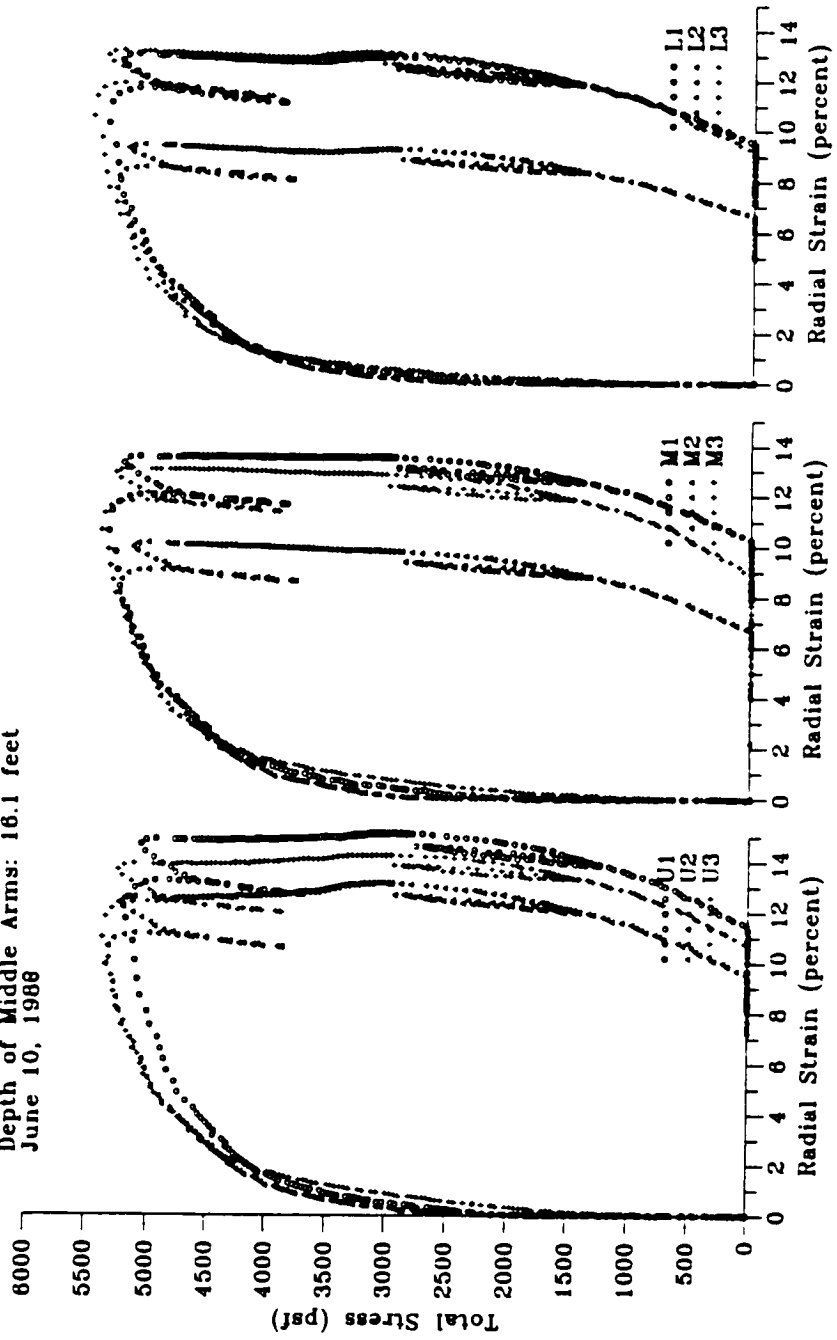
Test PMC 3.2II - Pease Air Force Base Site
Depth of Middle Arms: 11.1 feet
June 7, 1988



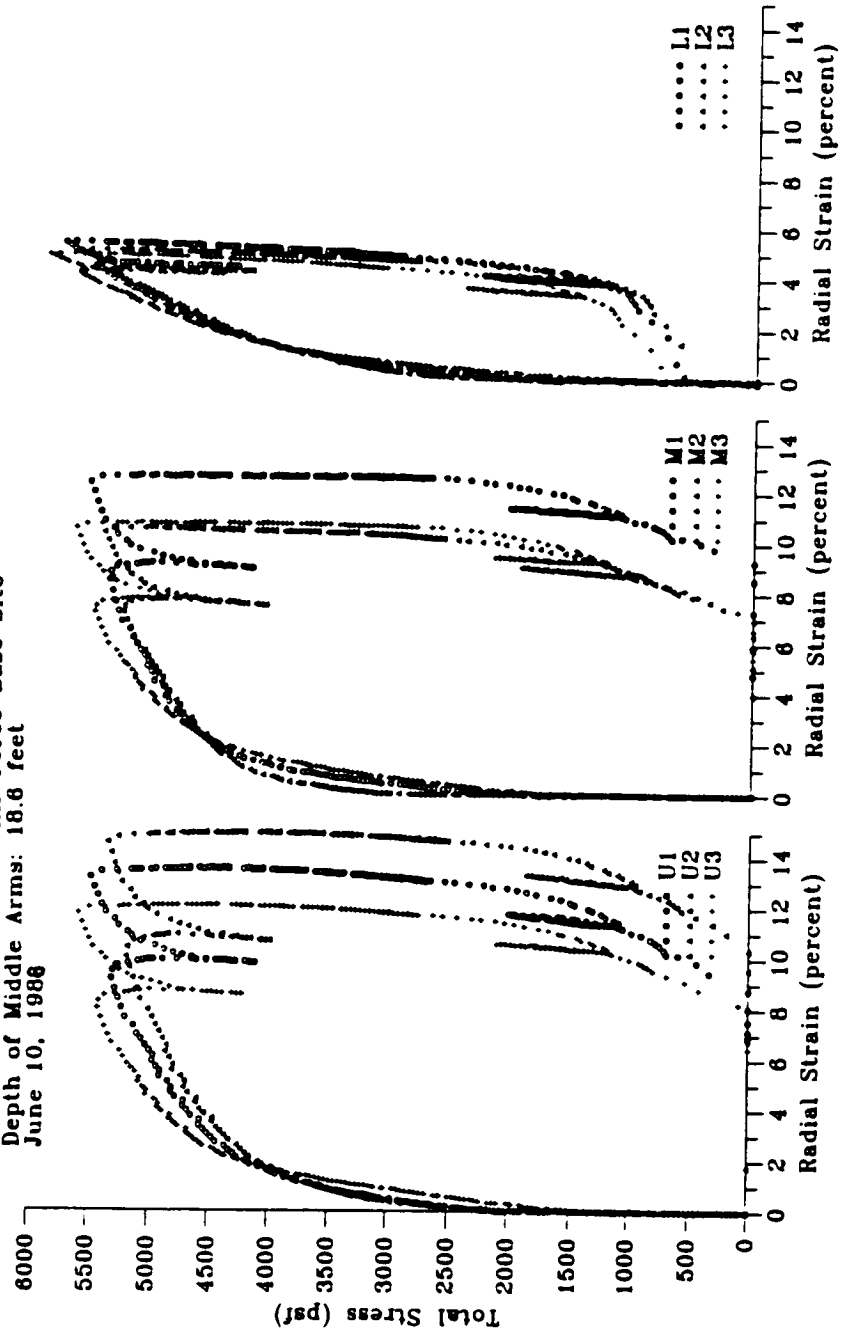
Test PMC 3.3H - Pease Air Force Base Site
 Depth of Middle Arms: 13.6 feet
 June 7, 1988



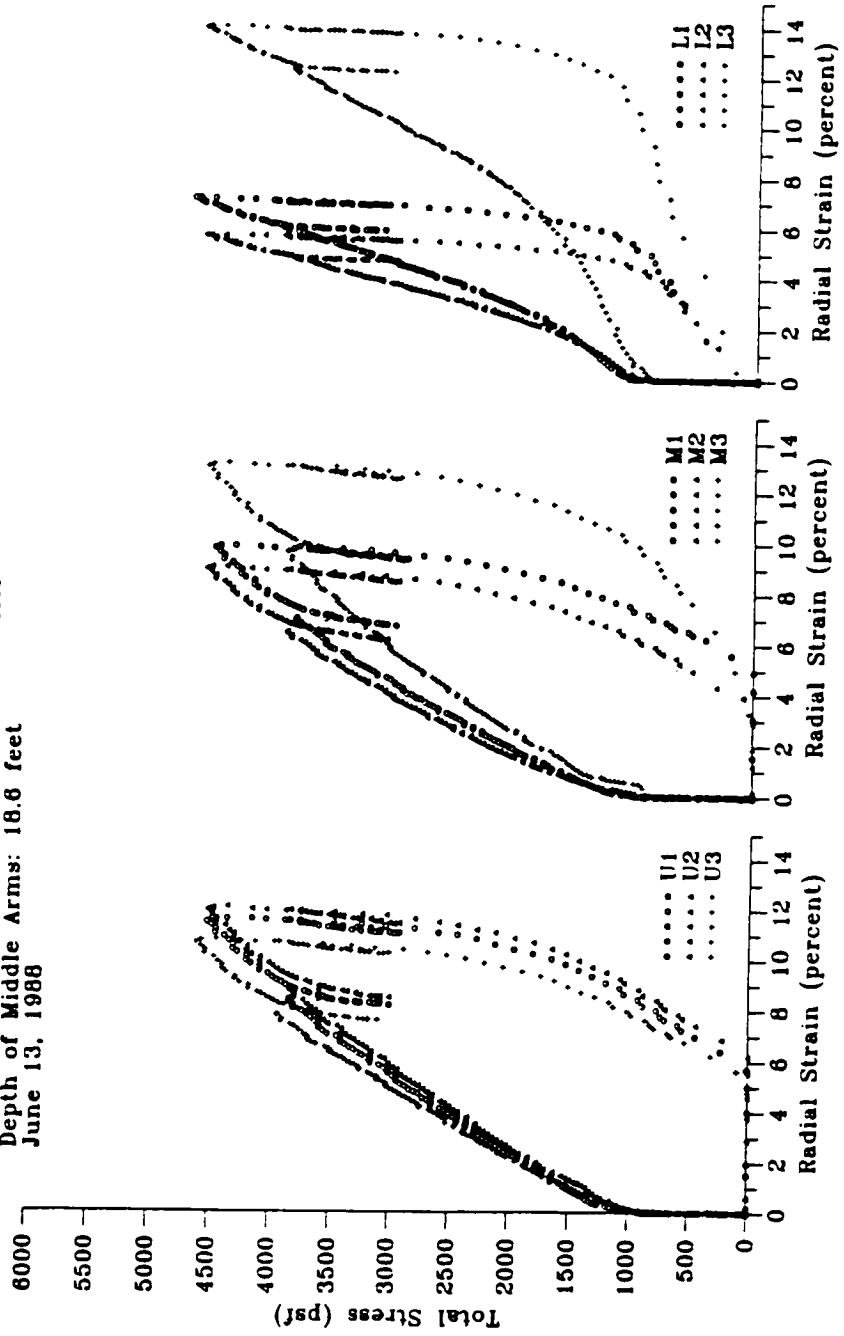
Test PMC 3.4H - Pease Air Force Base Site
Depth of Middle Arms: 16.1 feet
June 10, 1988



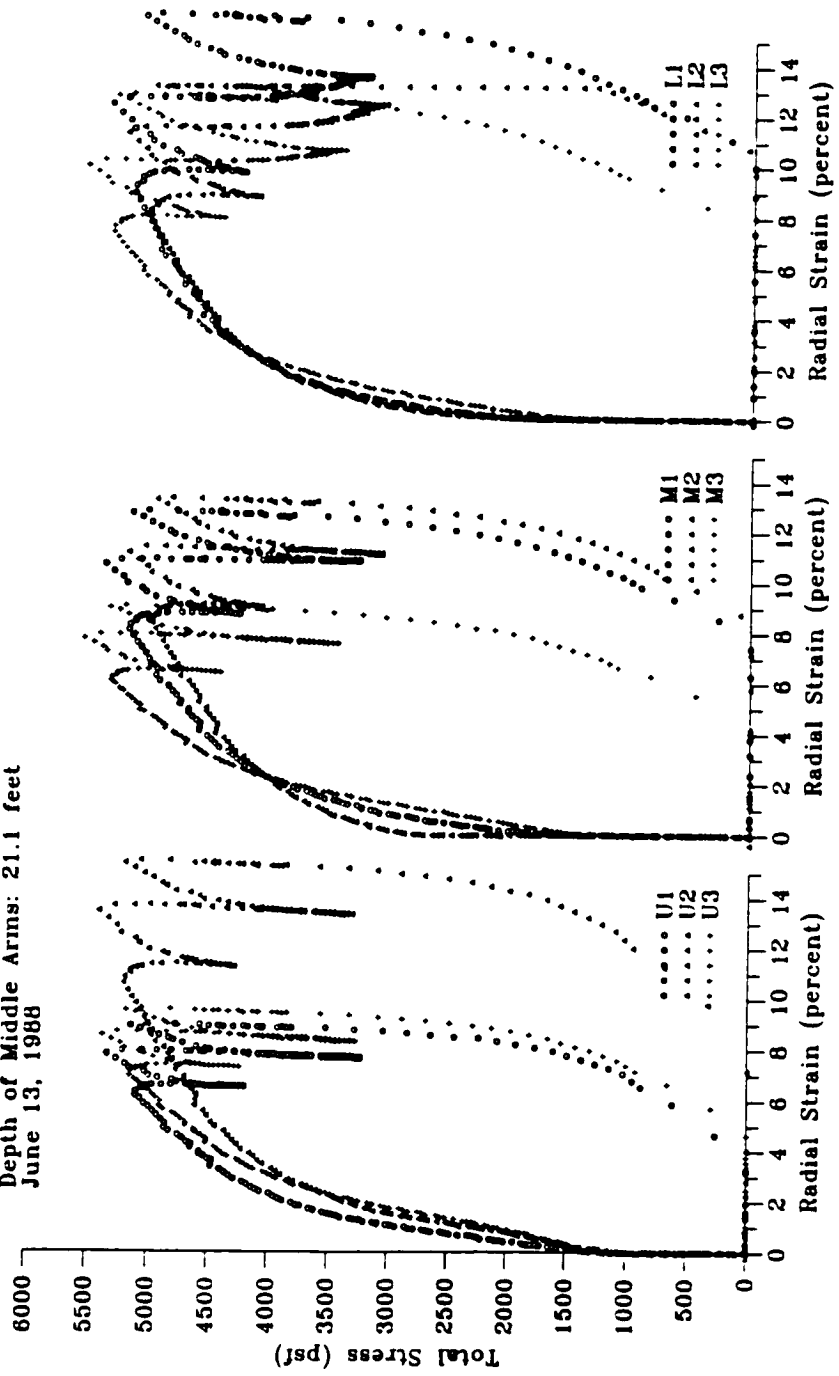
Test PMC 3.5II - Pease Air Force Base Site
 Depth of Middle Arms: 18.6 feet
 June 10, 1986



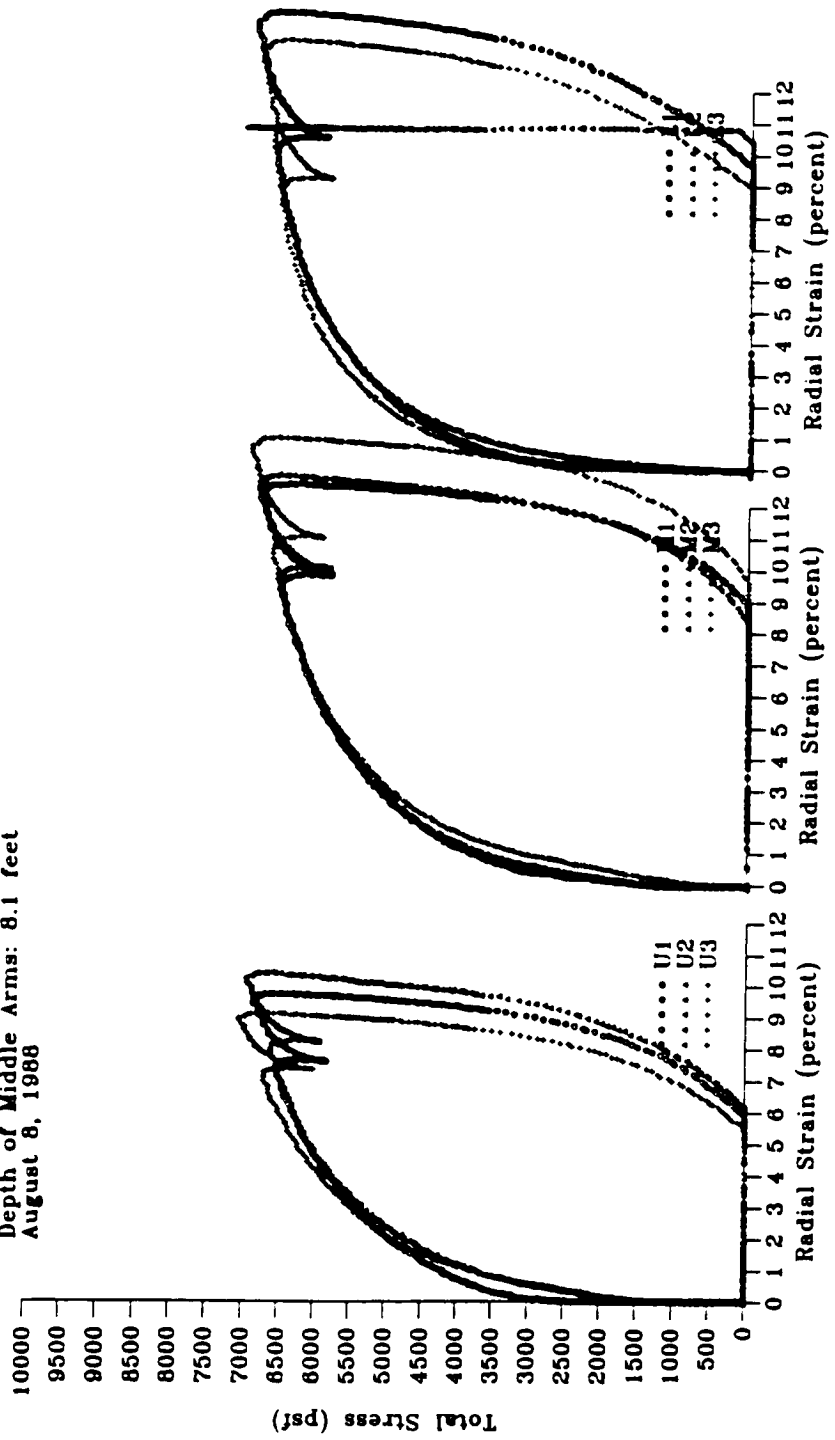
Test PMC 3.5R - Pease Air Force Base Site
 Depth of Middle Arms: 18.6 feet
 June 13, 1988



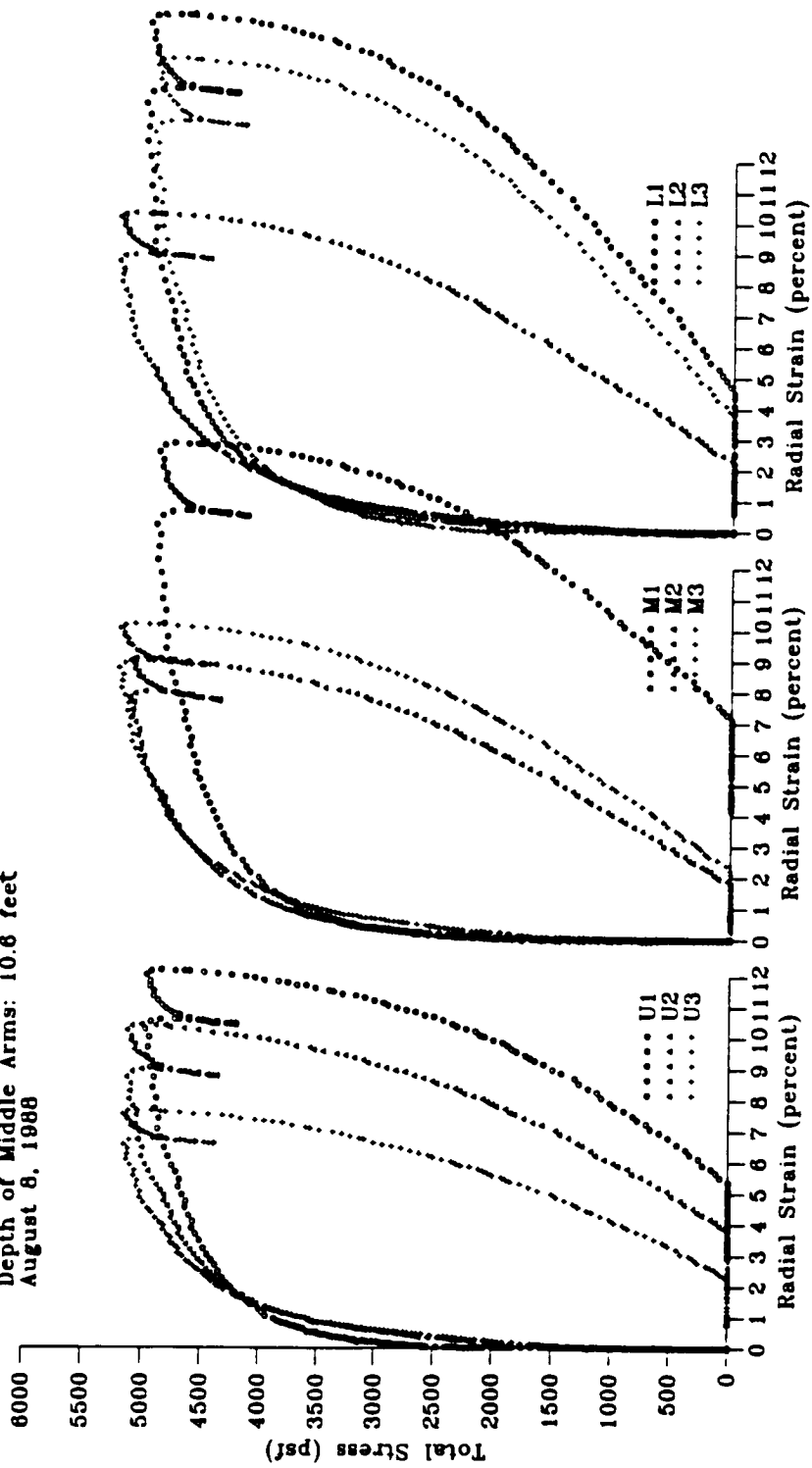
Test PMC 3.6II - Pease Air Force Base Site
Depth of Middle Arms: 21.1 feet
June 13, 1988



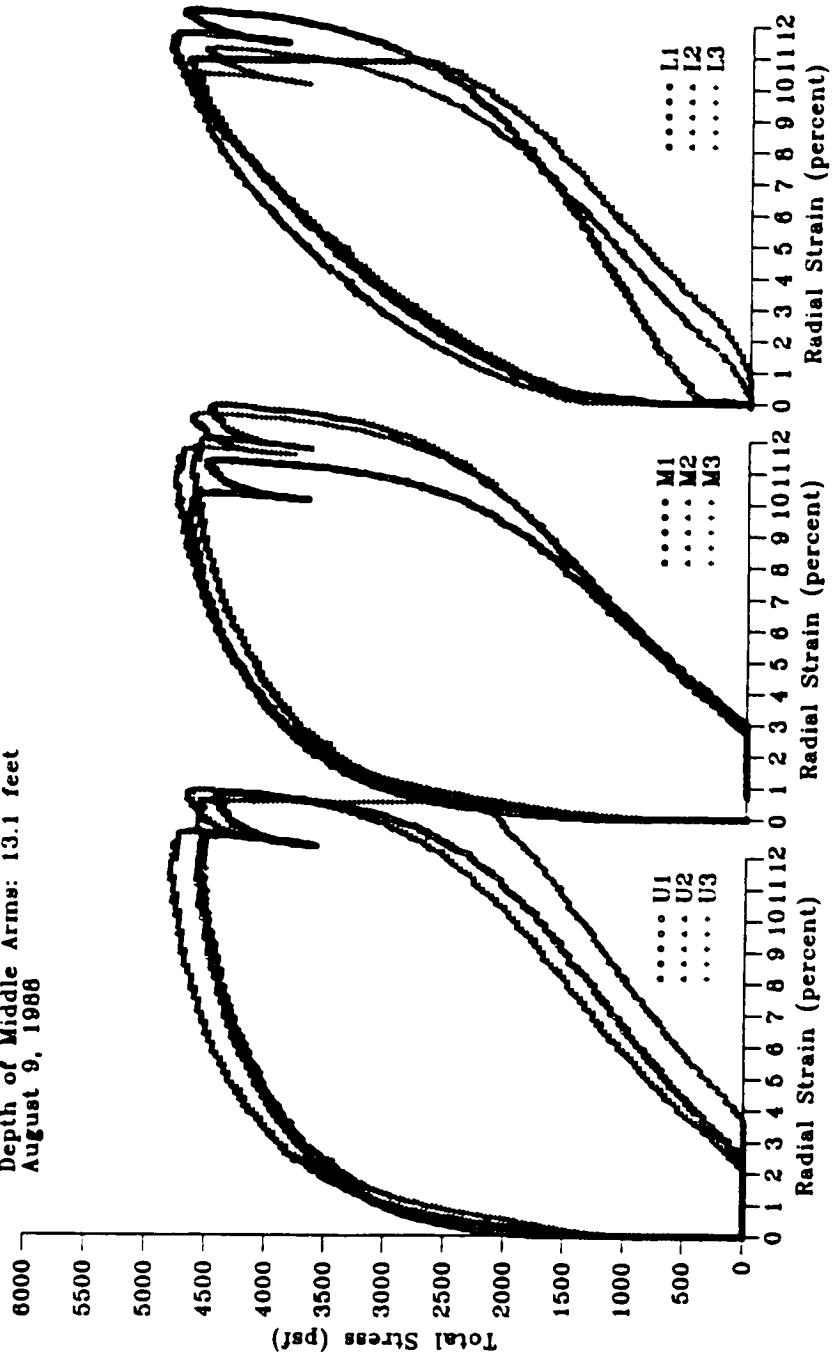
Test PMC 4.1 - Pease Air Force Base Site
 Depth of Middle Arms: 8.1 feet
 August 8, 1988



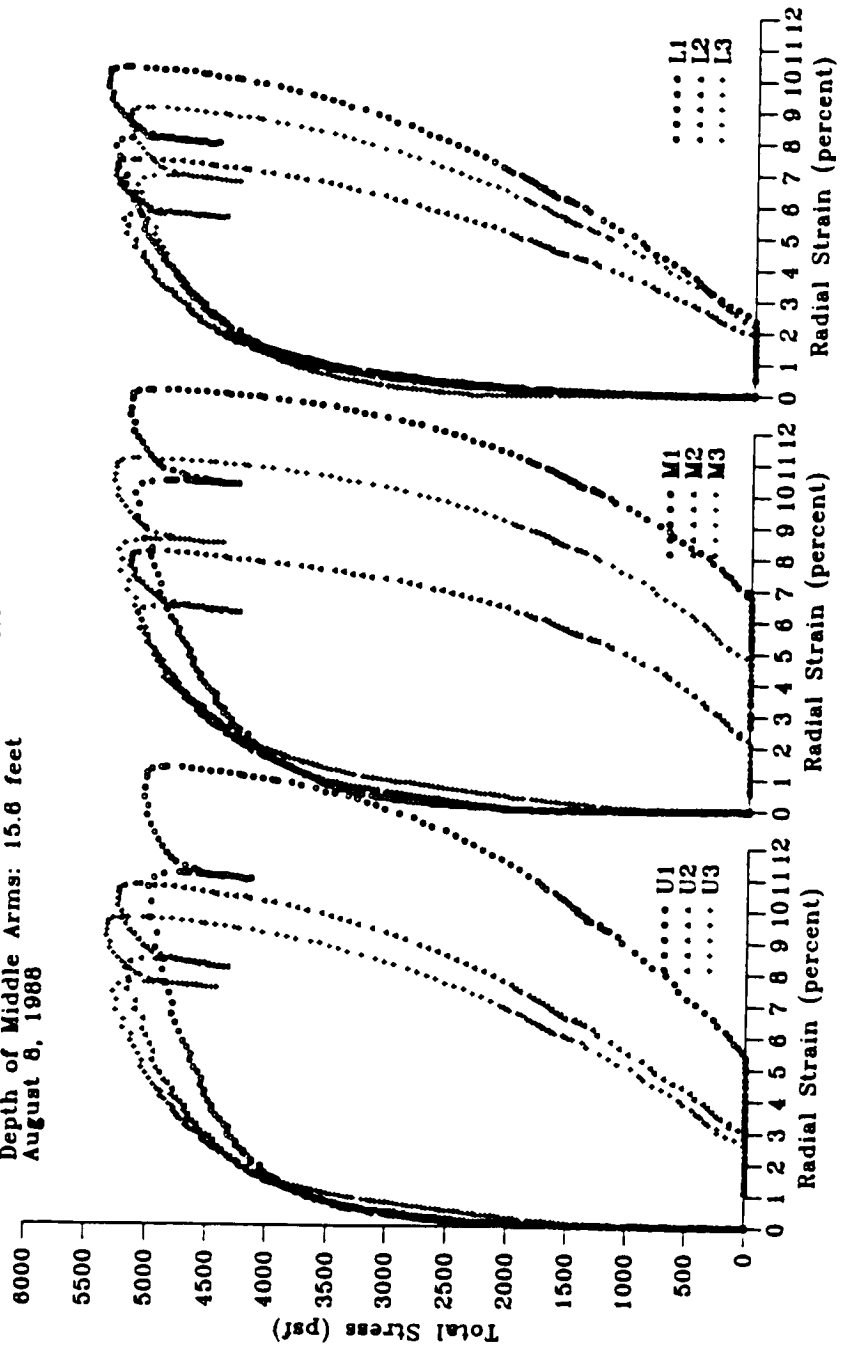
Test PMC 4.2 - Pease Air Force Base Site
 Depth of Middle Arms: 10.6 feet
 August 8, 1988



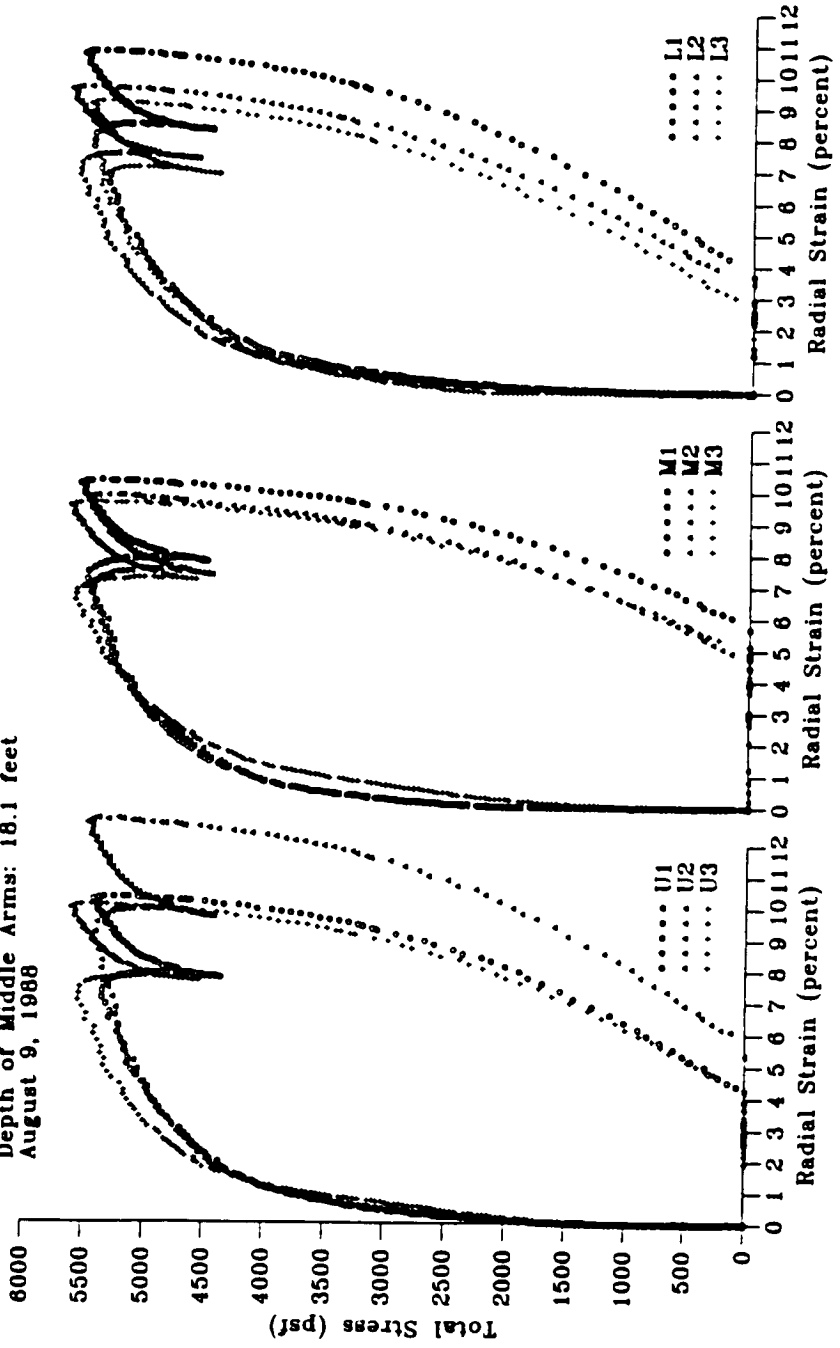
Test PMC 4.3 - Pease Air Force Base Site
 Depth of Middle Arms: 13.1 feet
 August 9, 1988



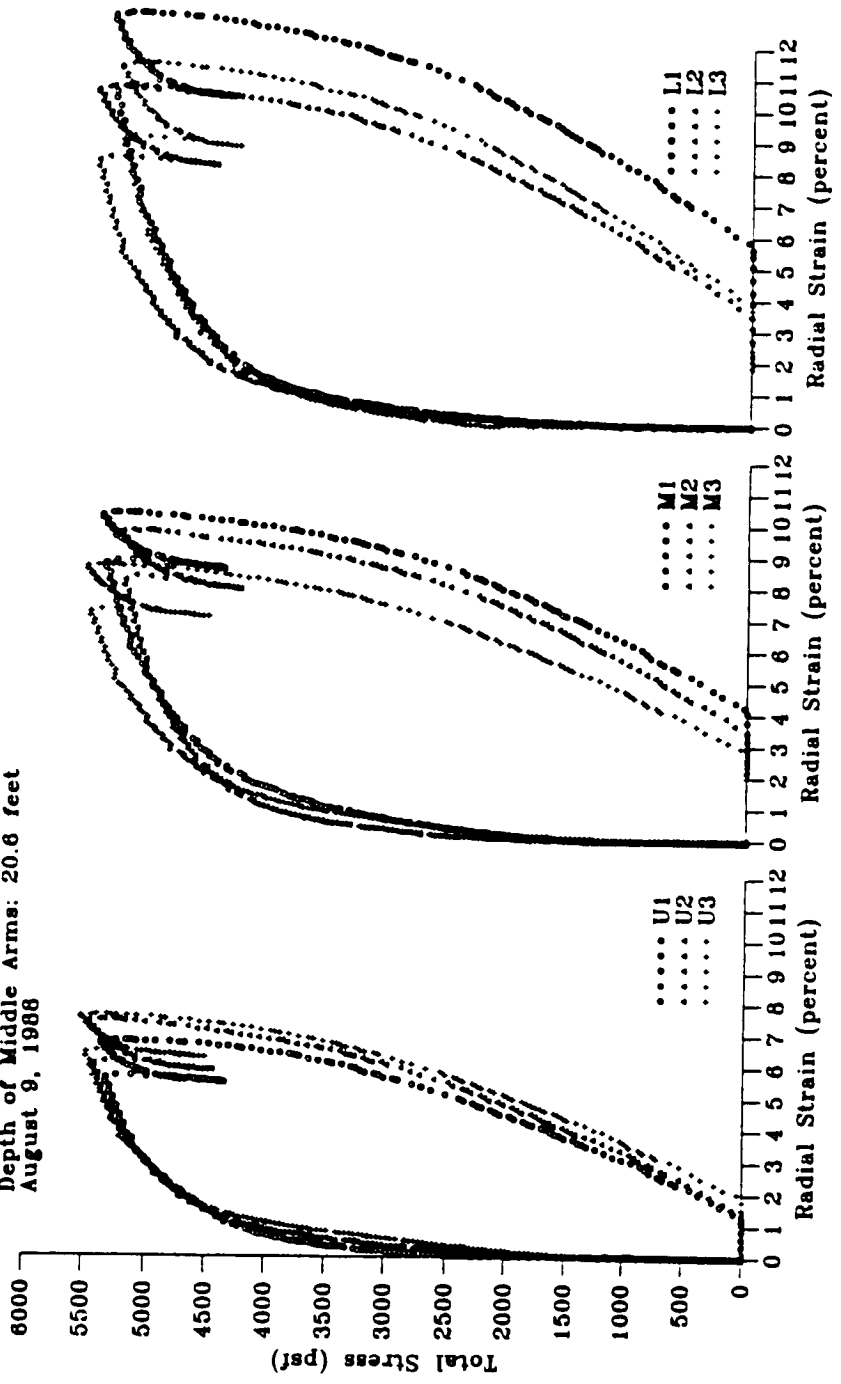
Test PMC 4.4 - Pease Air Force Base Site
 Depth of Middle Arms: 15.6 feet
 August 8, 1988



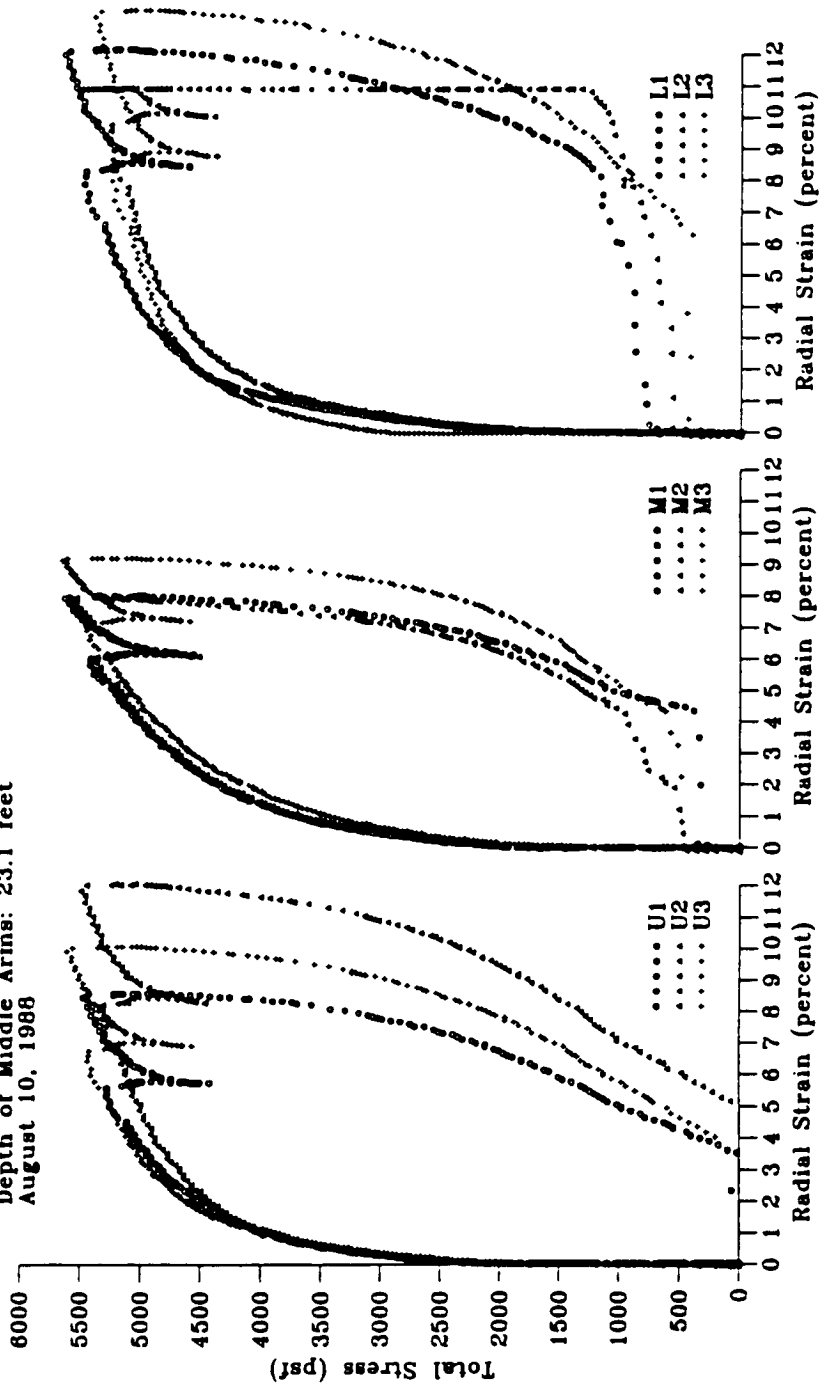
Test PMC 4.5 - Pease Air Force Base Site
 Depth of Middle Arms: 18.1 feet
 August 9, 1988



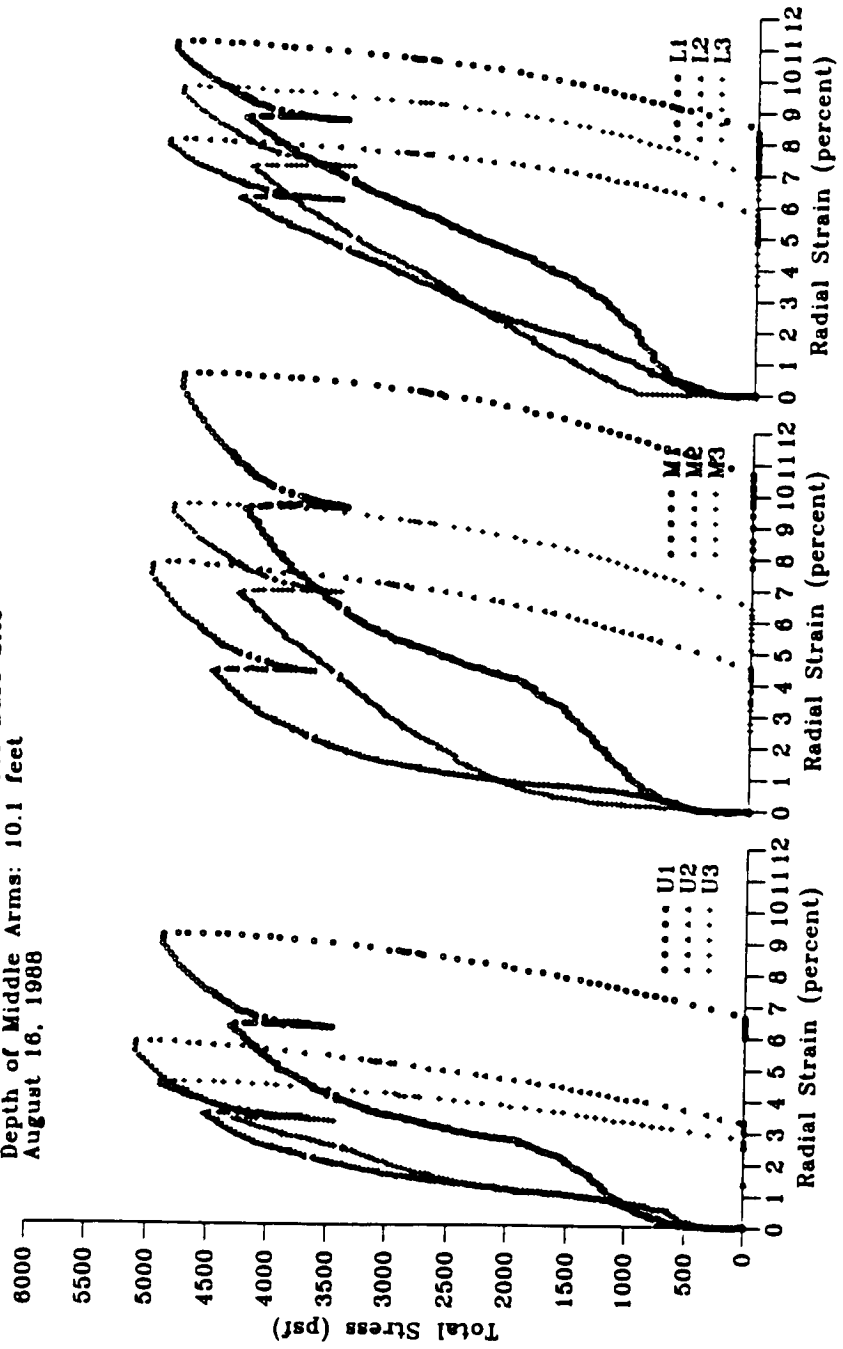
Test PMC 4.6 - Pease Air Force Base Site
 Depth of Middle Arms: 20.6 feet
 August 9, 1988



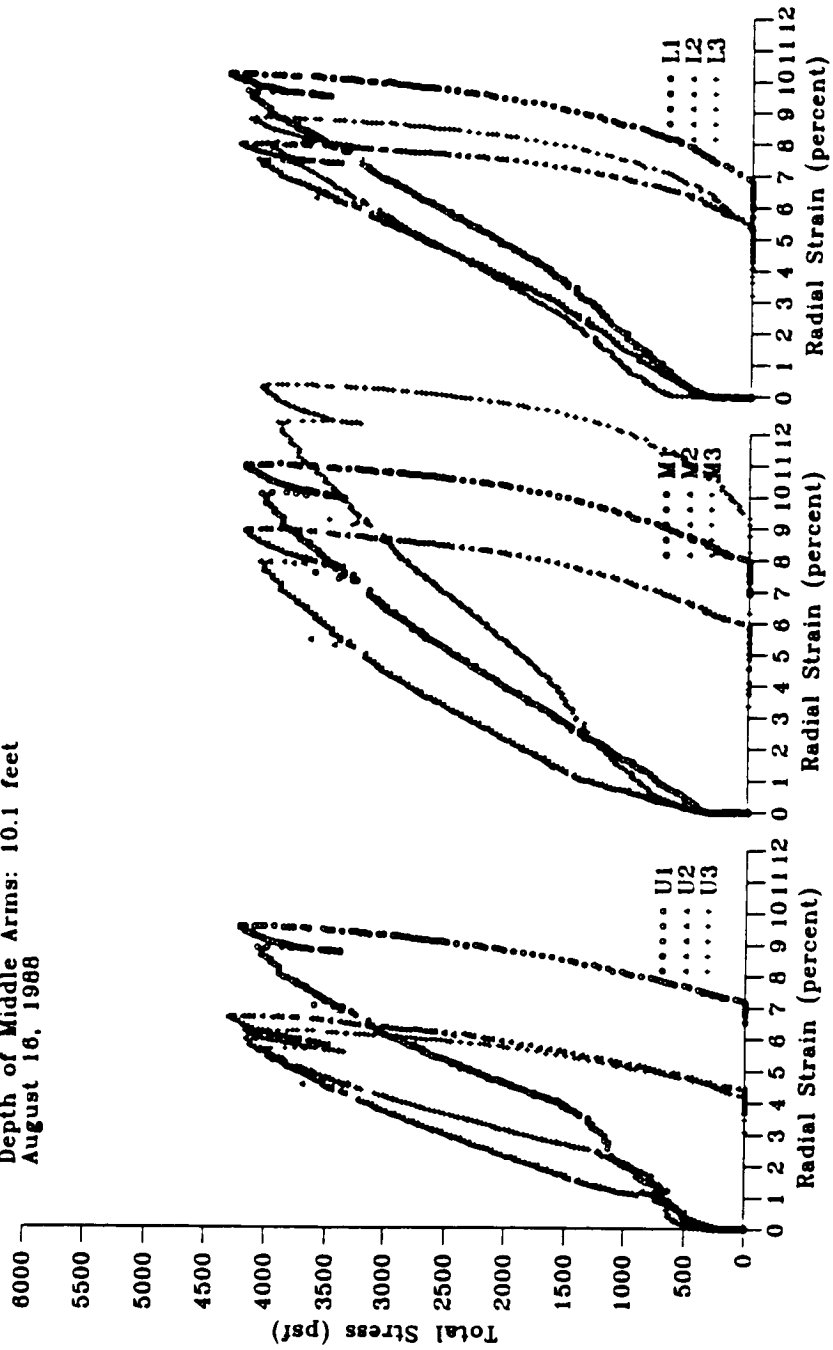
Test PMC 4.7 - Pease Air Force Base Site
 Depth of Middle Arms: 23.1 feet
 August 10, 1988



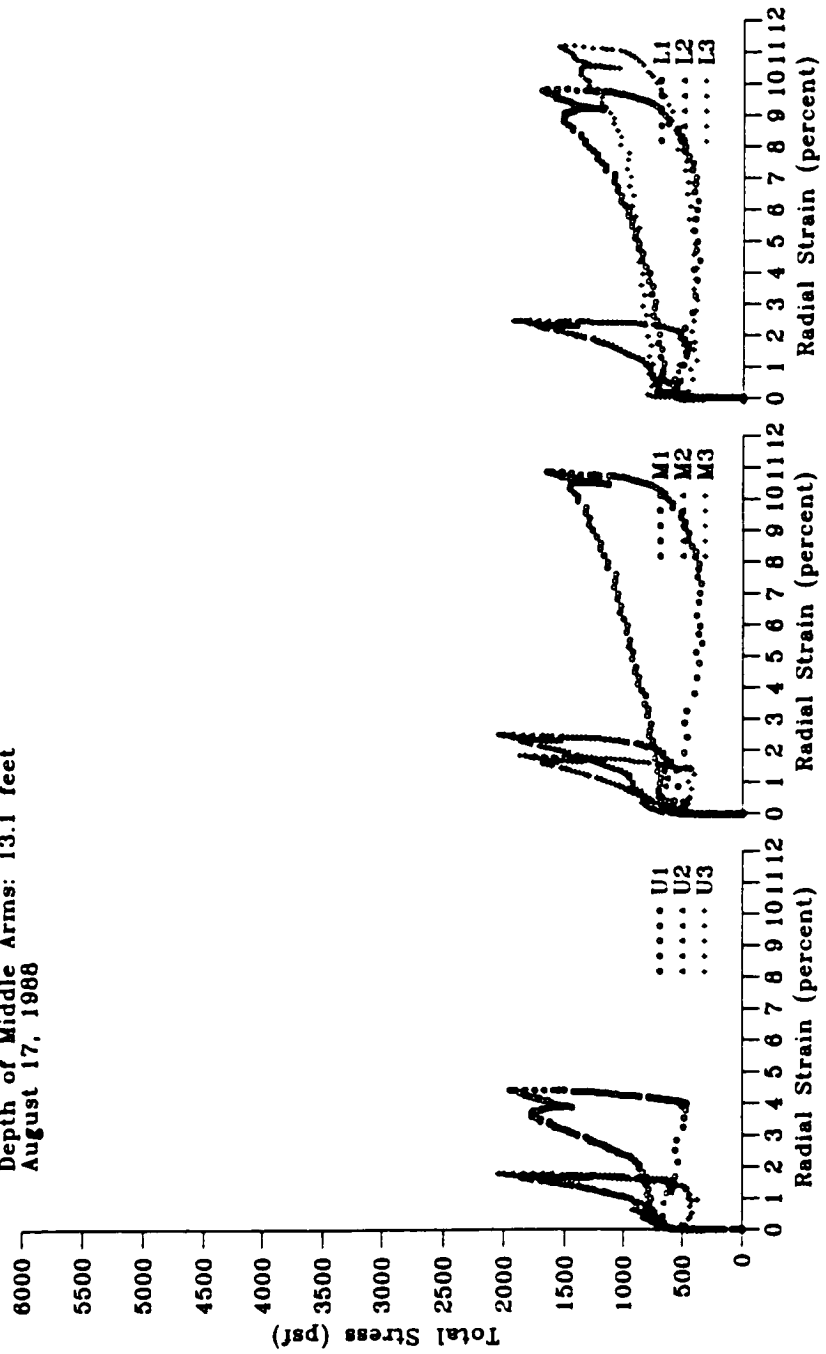
Test PMJ 3.2 - Pease Air Force Base Site
 Depth of Middle Arms: 10.1 feet
 August 16, 1988



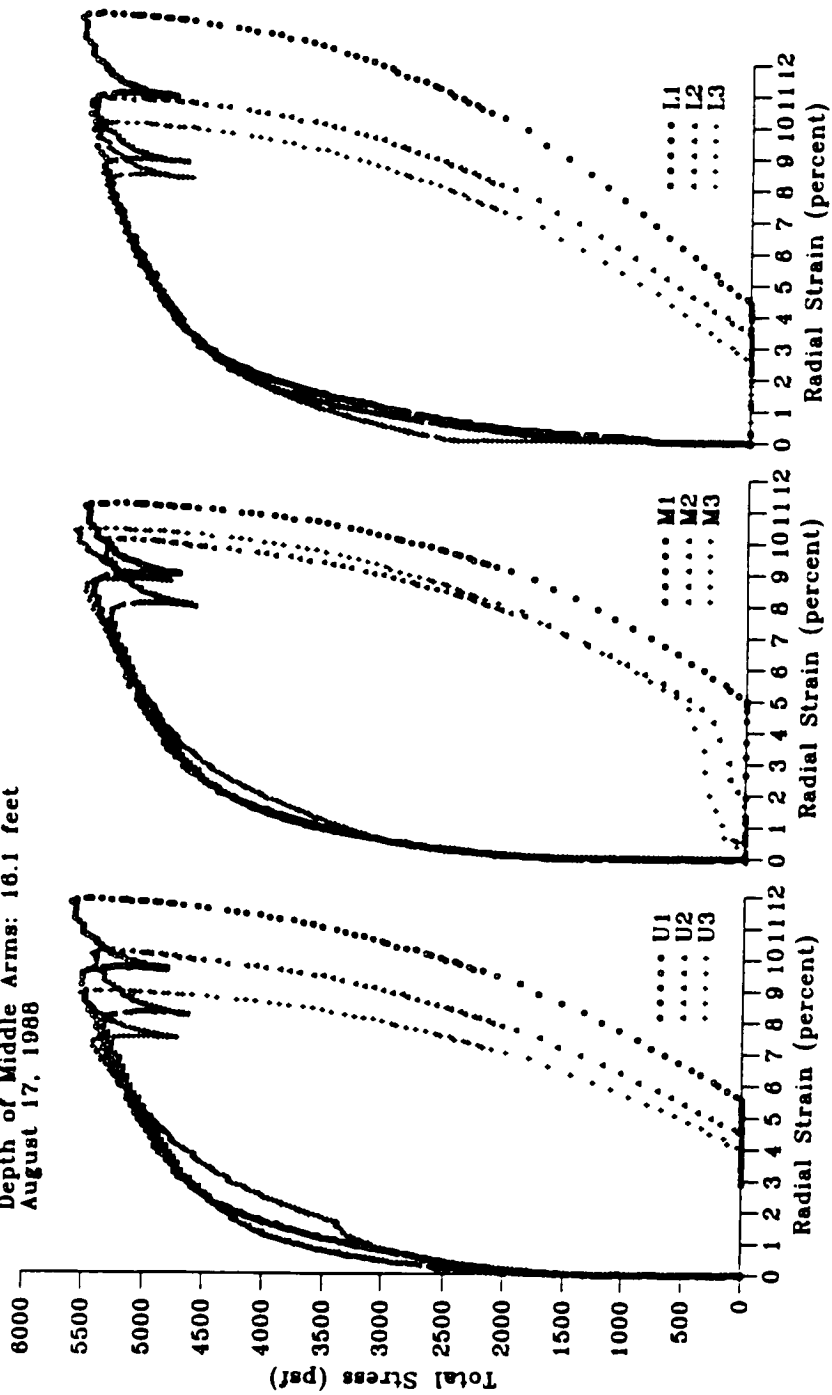
Test PMJ 3.2R - Pease Air Force Base Site
 Depth of Middle Arms: 10.1 feet
 August 16, 1968



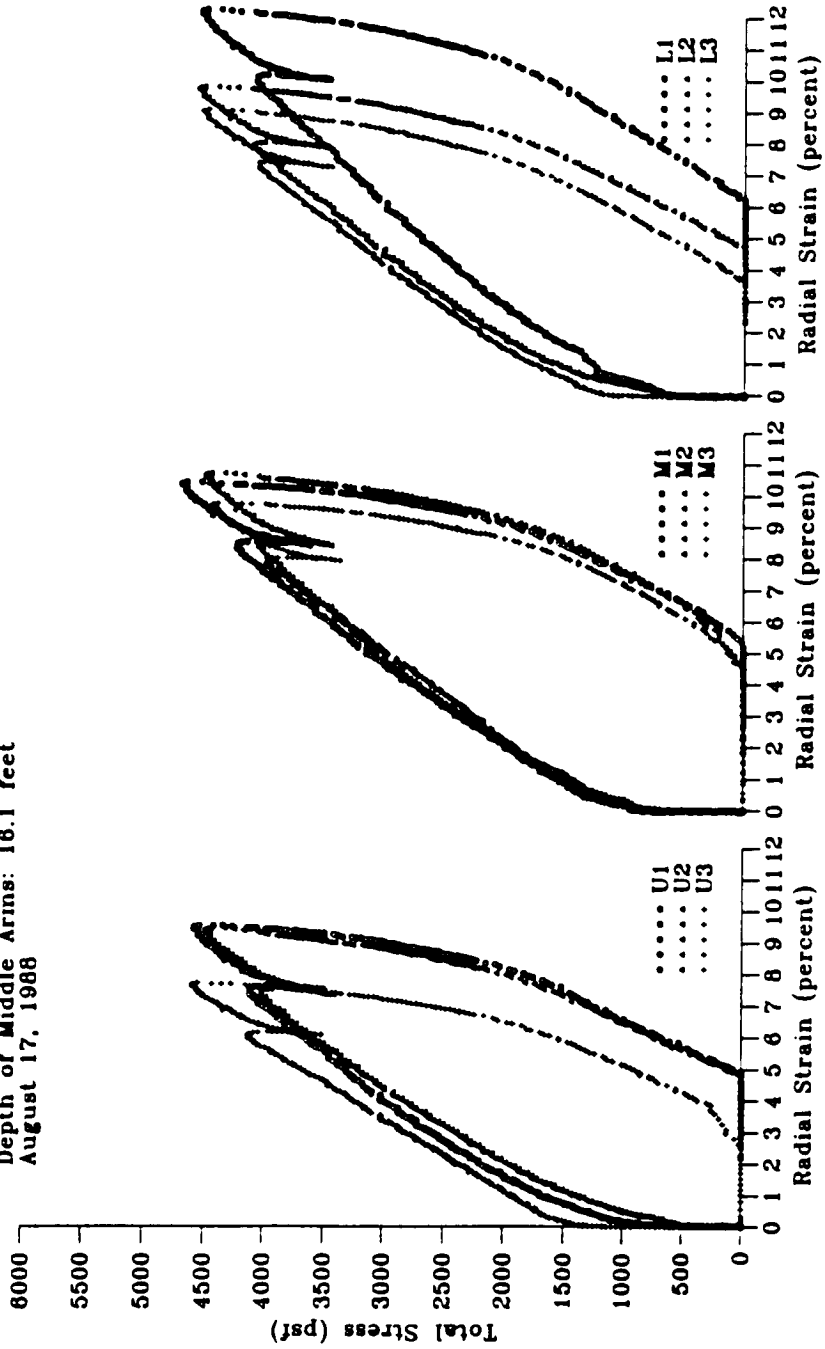
Test PMJ 3.3 - Pease Air Force Base Site
 Depth of Middle Arms: 13.1 feet
 August 17, 1968



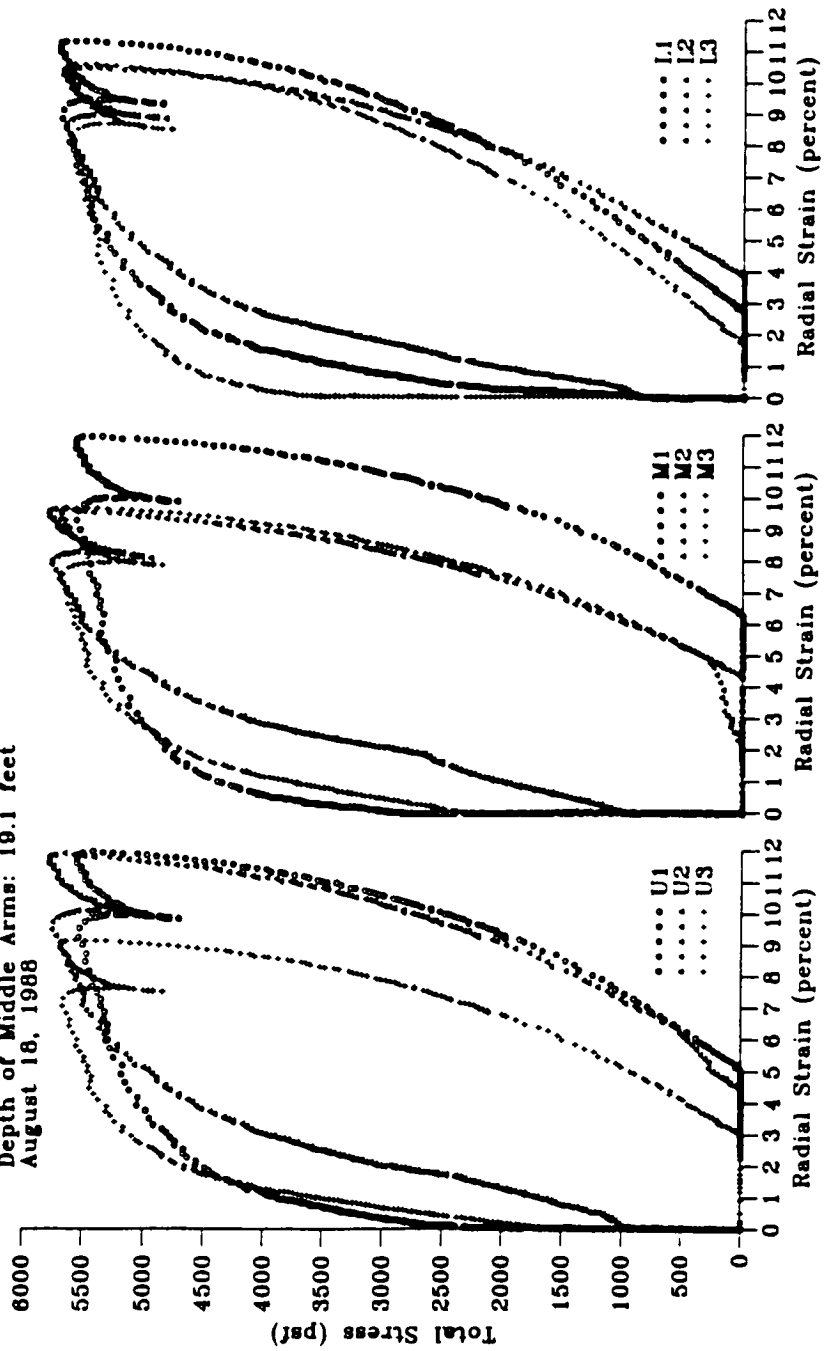
Test PMJ 3.4 - Pease Air Force Base Site
 Depth of Middle Arms: 16.1 feet
 August 17, 1988



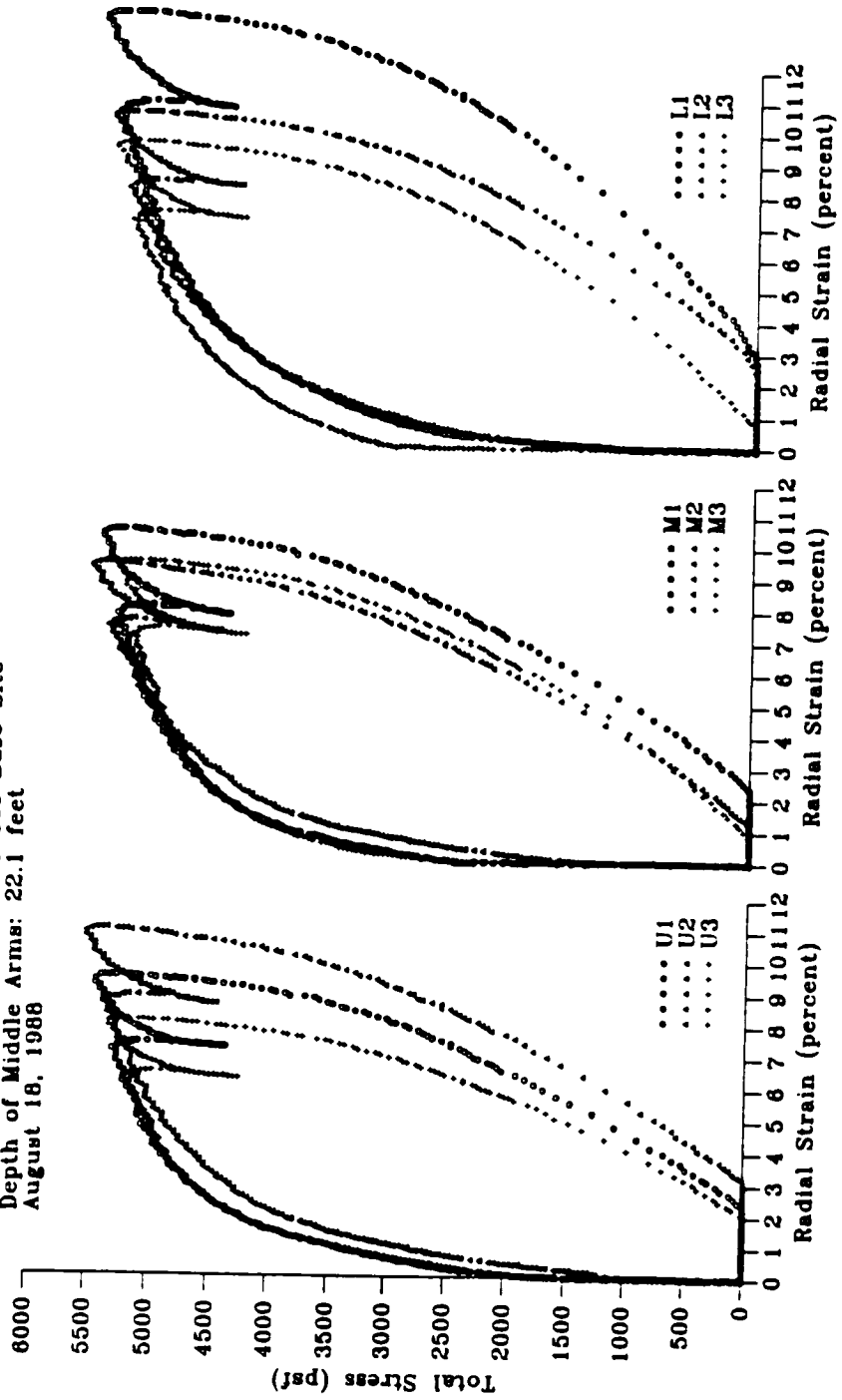
Test PMJ 3.4R - Pease Air Force Base Site
 Depth of Middle Arms: 16.1 feet
 August 17, 1988



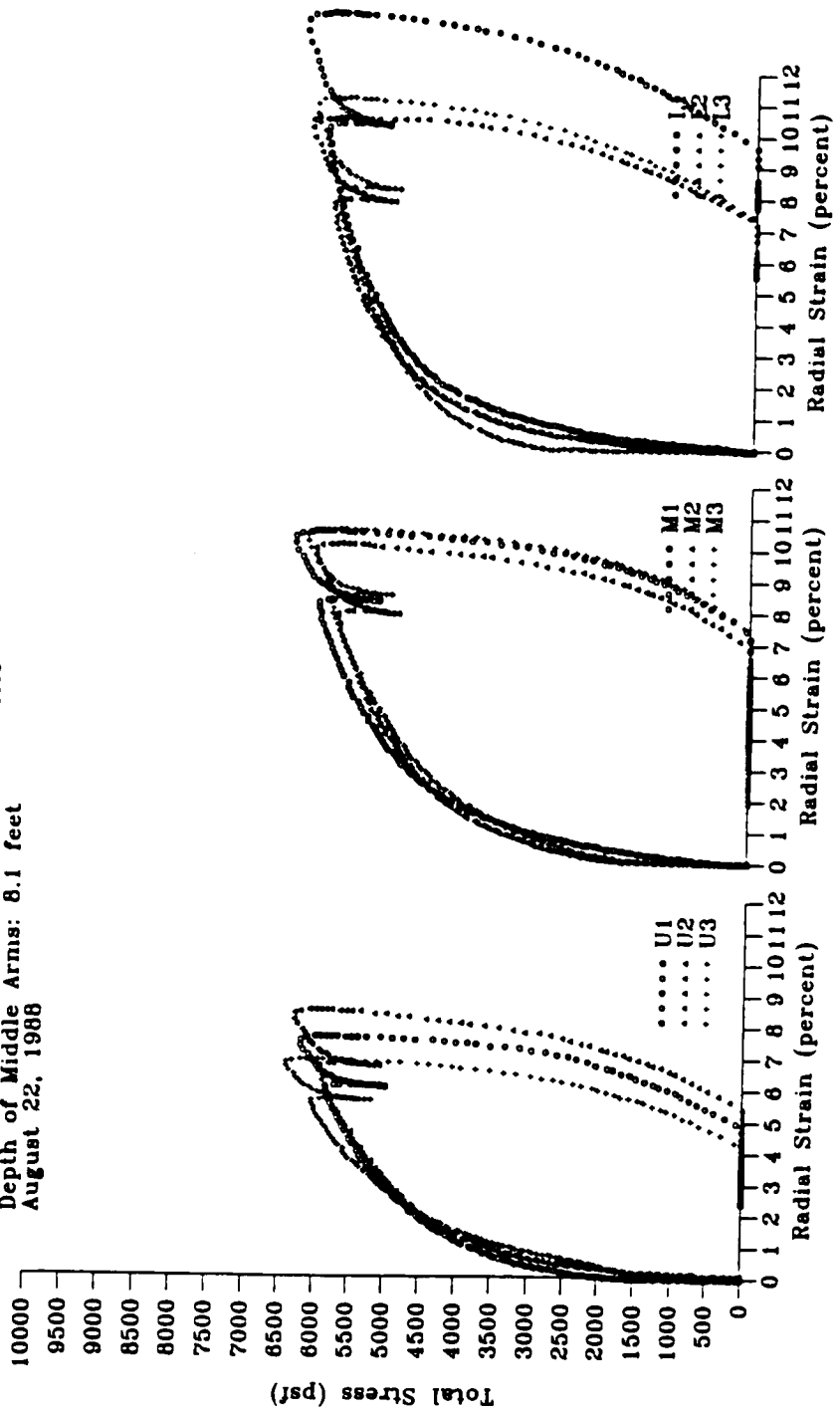
Test PMJ 3.5 - Pease Air Force Base Site
 Depth of Middle Arms: 19.1 feet
 August 18, 1988



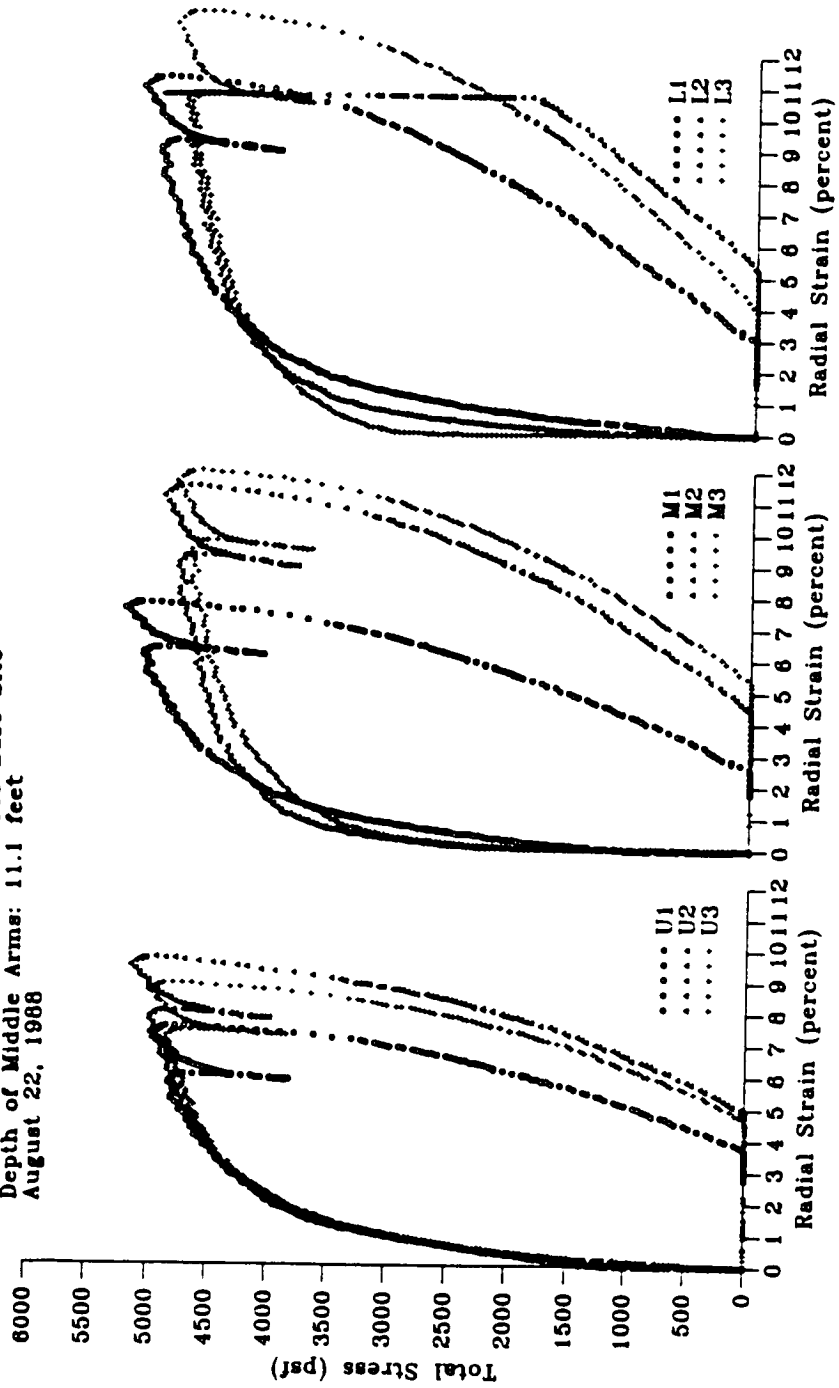
Test PMJ 3.6 - Pease Air Force Base Site
 Depth of Middle Arms: 22.1 feet
 August 18, 1988



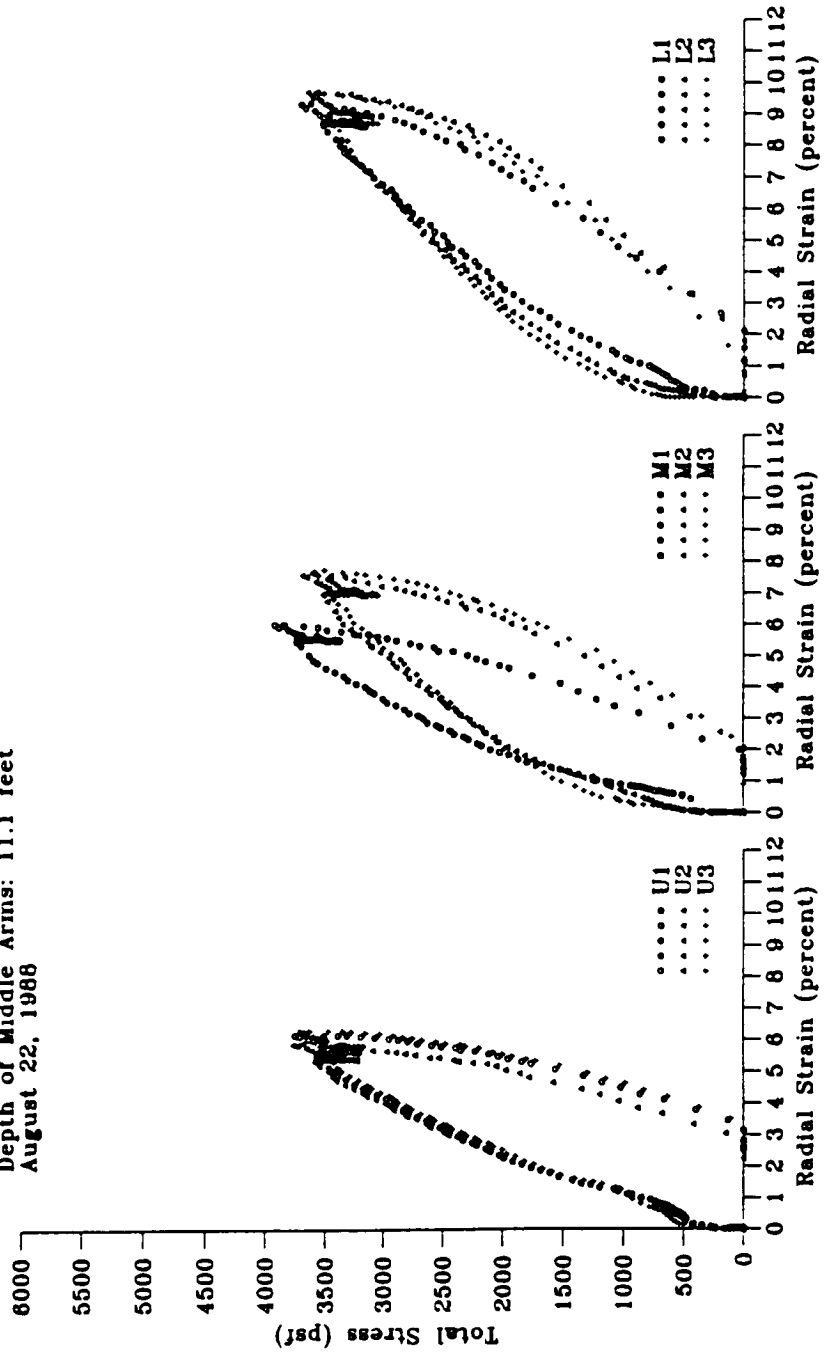
Test PMJ 4.1 - Pease Air Force Base Site
 Depth of Middle Arms: 8.1 feet
 August 22, 1988



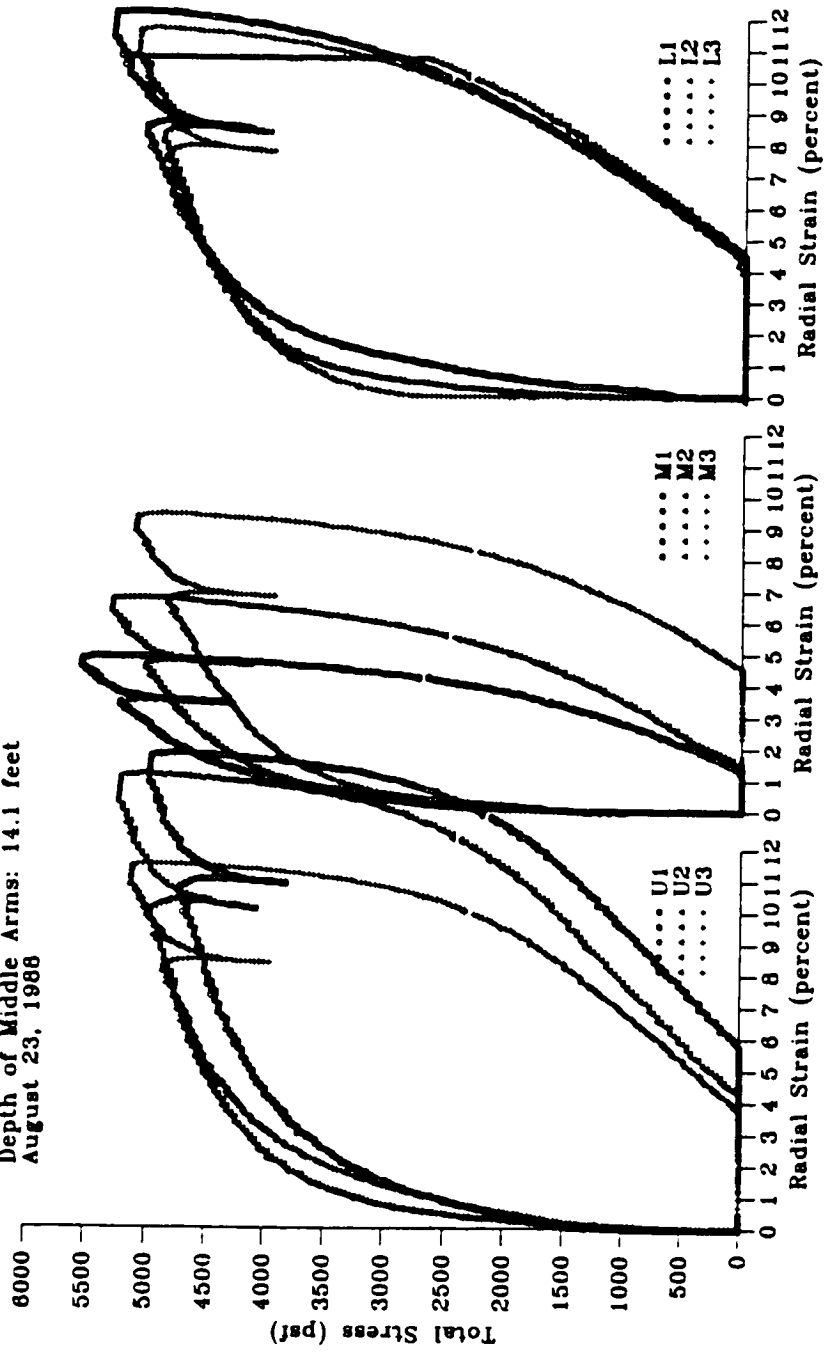
Test PMJ 4.2 - Pease Air Force Base Site
 Depth of Middle Arms: 11.1 feet
 August 22, 1988



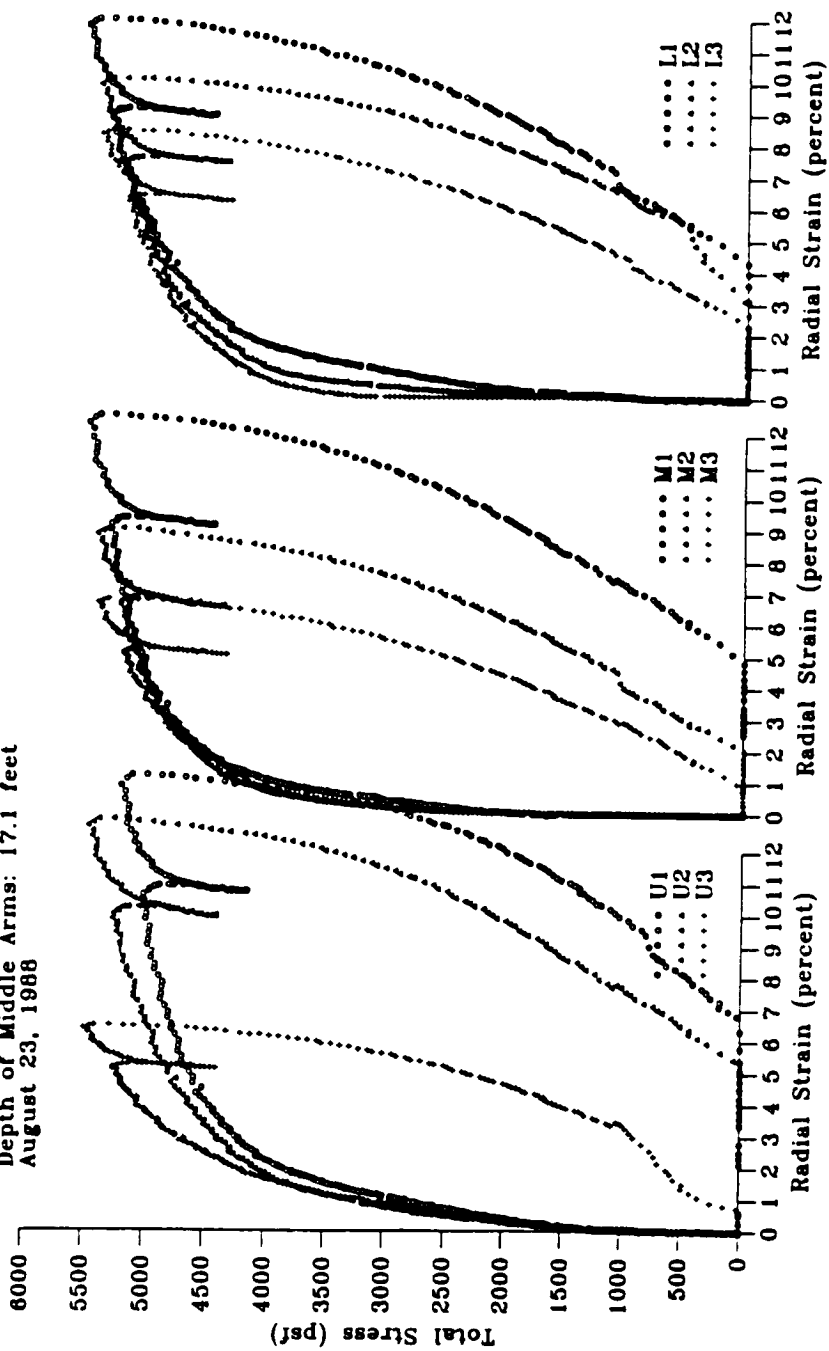
Test PMJ 4:2R - Pease Air Force Base Site
 Depth of Middle Arms: 11.1 feet
 August 22, 1988

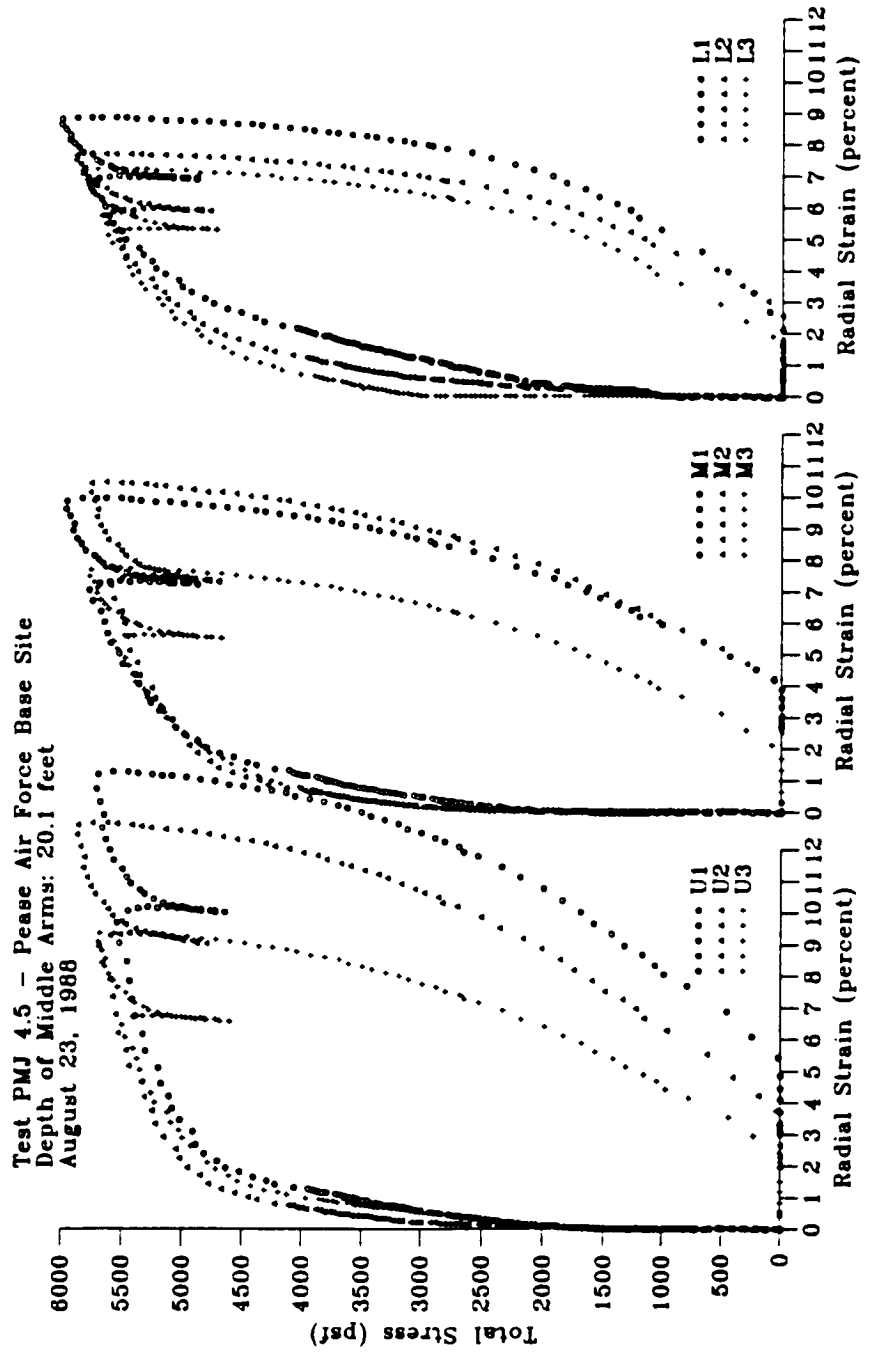


Test PMJ 4.3 - Pease Air Force Base Site
 Depth of Middle Arms: 14.1 feet
 August 23, 1988

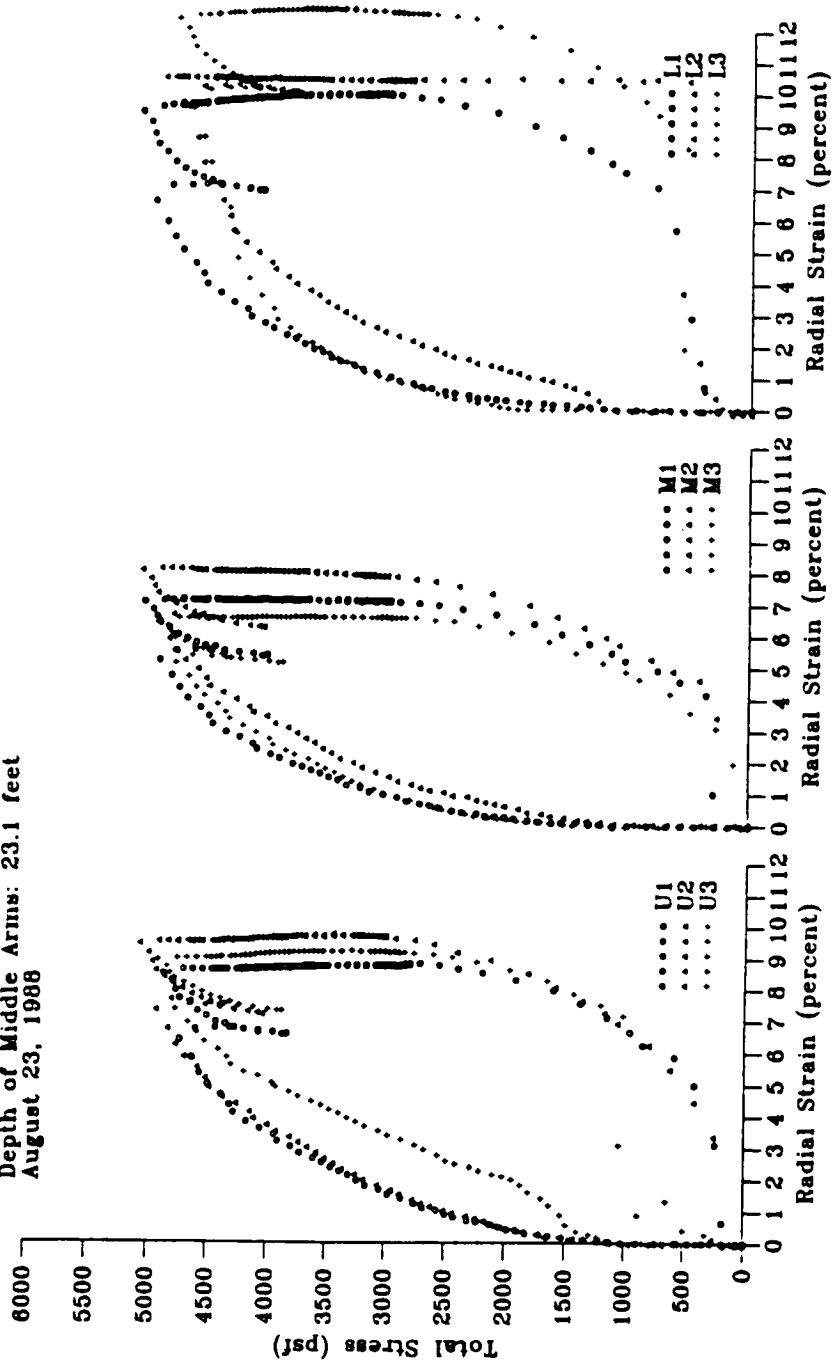


Test PMJ 4.4 - Pease Air Force Base Site
 Depth of Middle Arms: 17.1 feet
 August 23, 1988

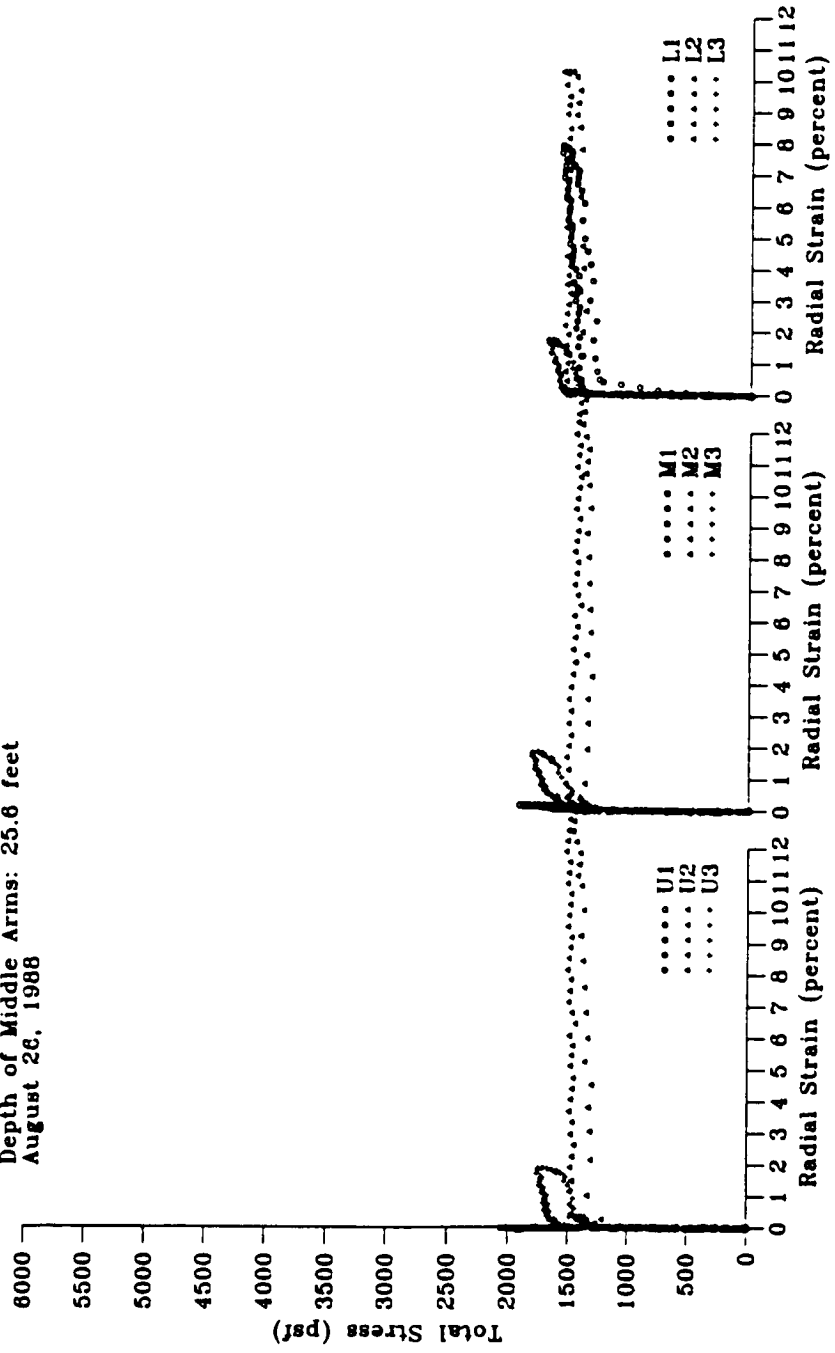




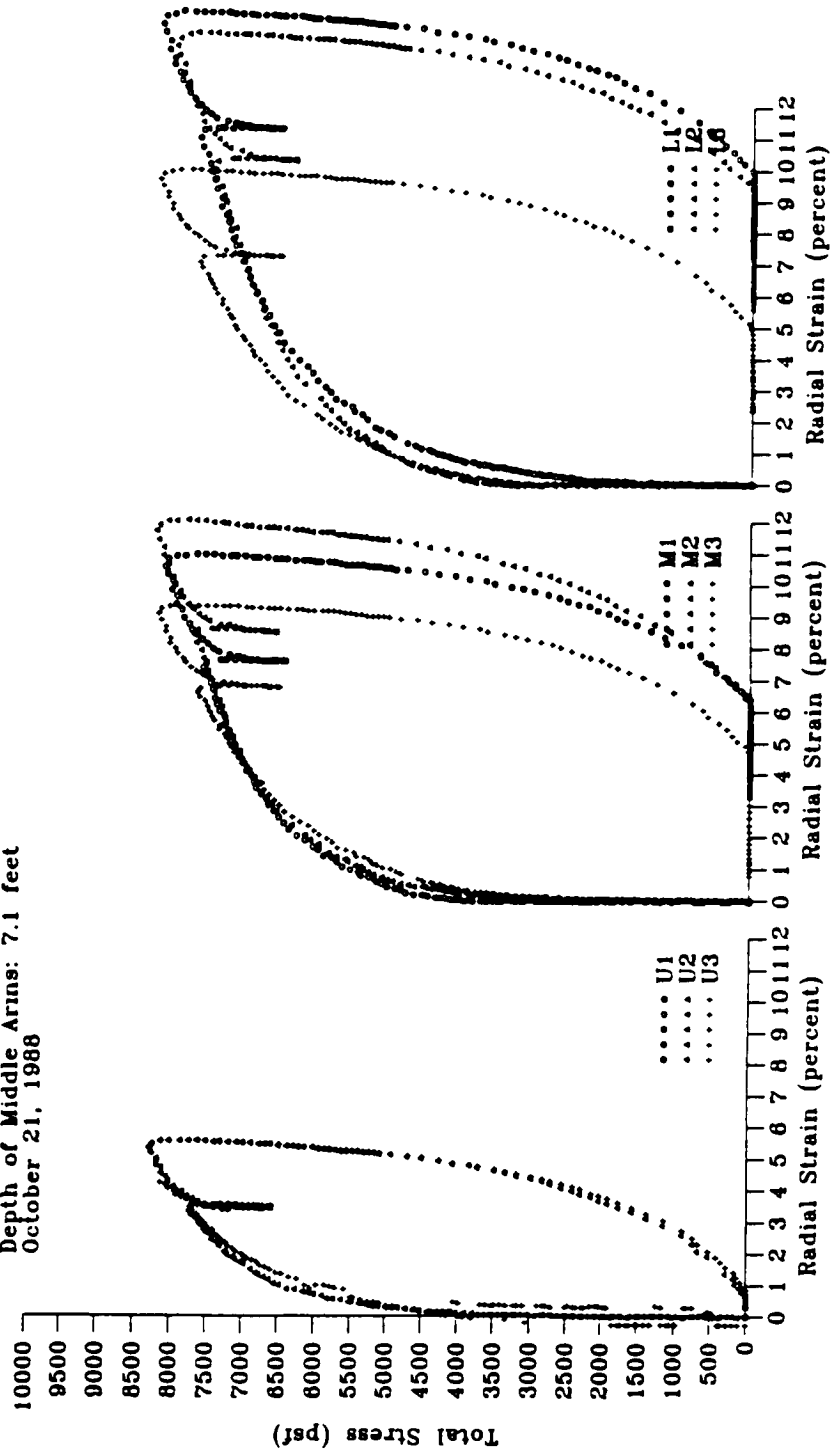
Test PMJ 4.6H - Pease Air Force Base Site
 Depth of Middle Arms: 23.1 feet
 August 23, 1968



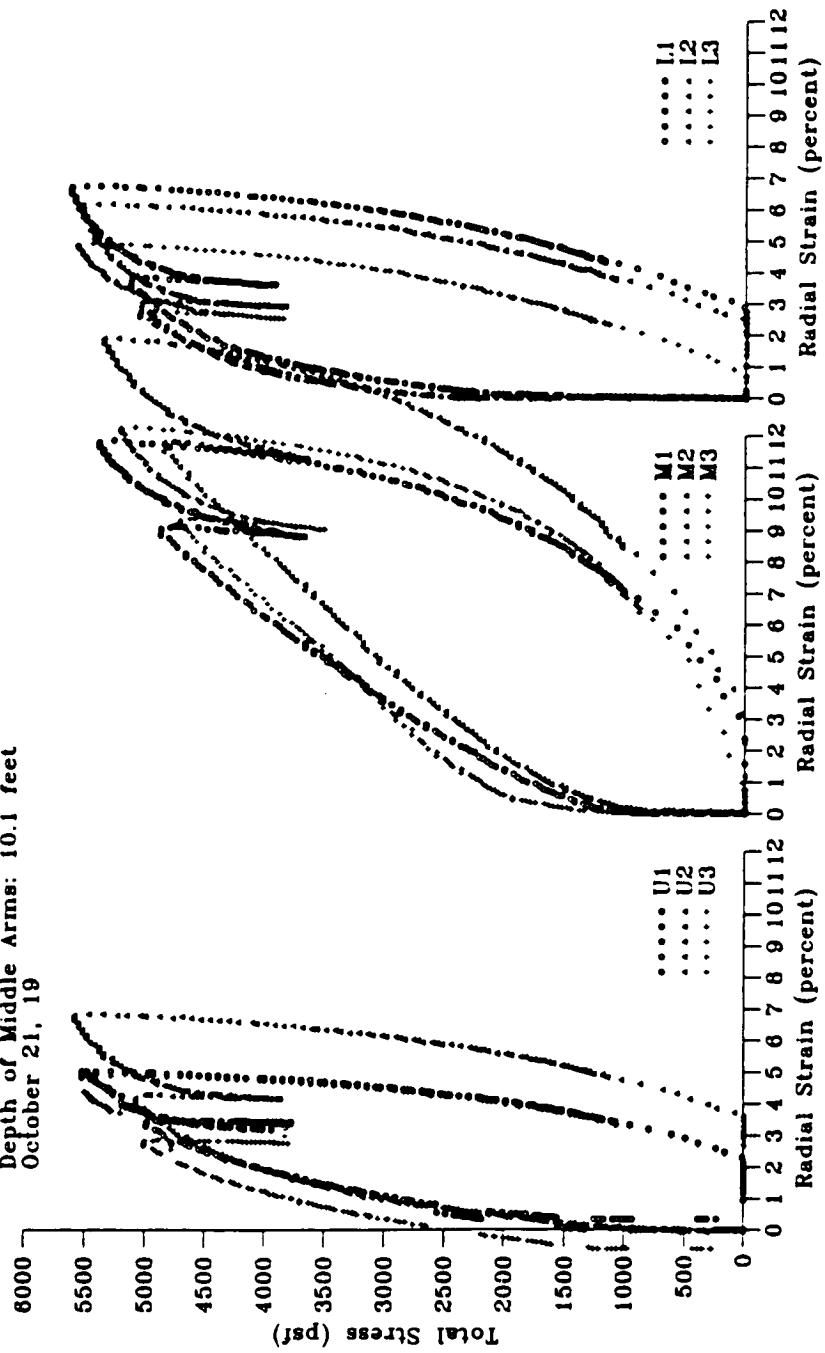
Test PMJ 4.7 - Pease Air Force Base Site
 Depth of Middle Arms: 25.6 feet
 August 26, 1988



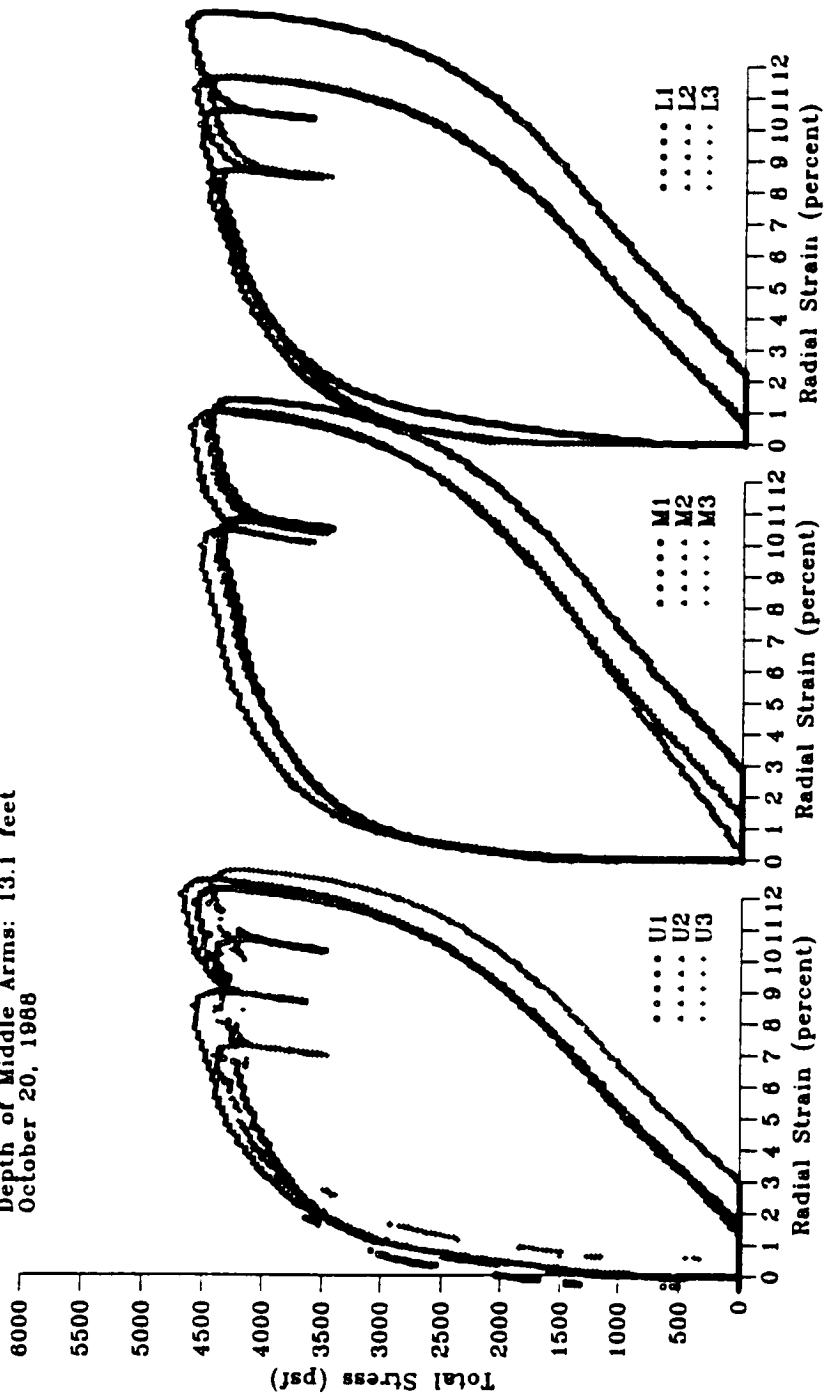
Test PMJ 5.1 - Pease Air Force Base Site
 Depth of Middle Arms: 7.1 feet
 October 21, 1988



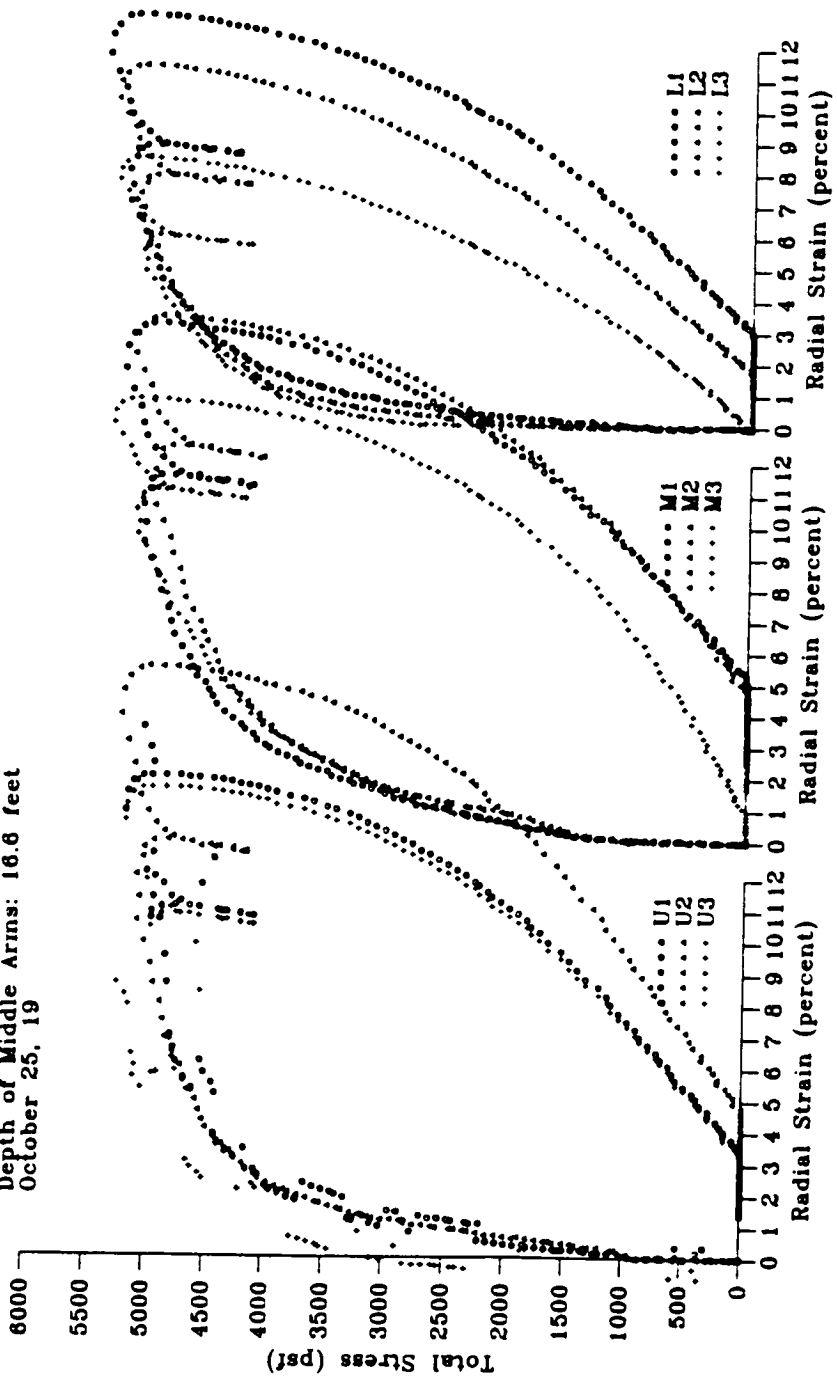
Test PMJ 5.2 - Pease Air Force Base Site
 Depth of Middle Arms: 10.1 feet
 October 21, 19



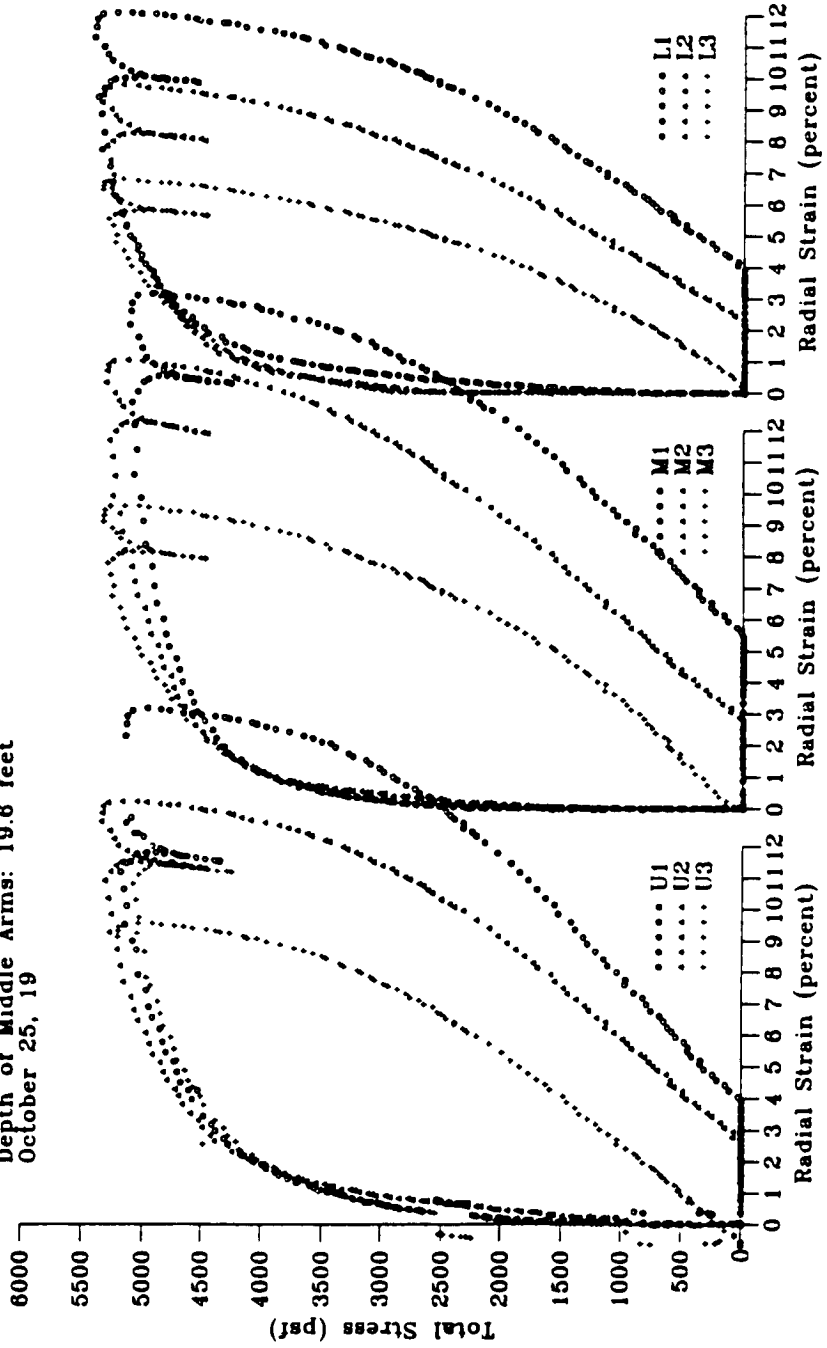
Test PMJ 5.3 - Pease Air Force Base Site
 Depth of Middle Arms: 13.1 feet
 October 20, 1988



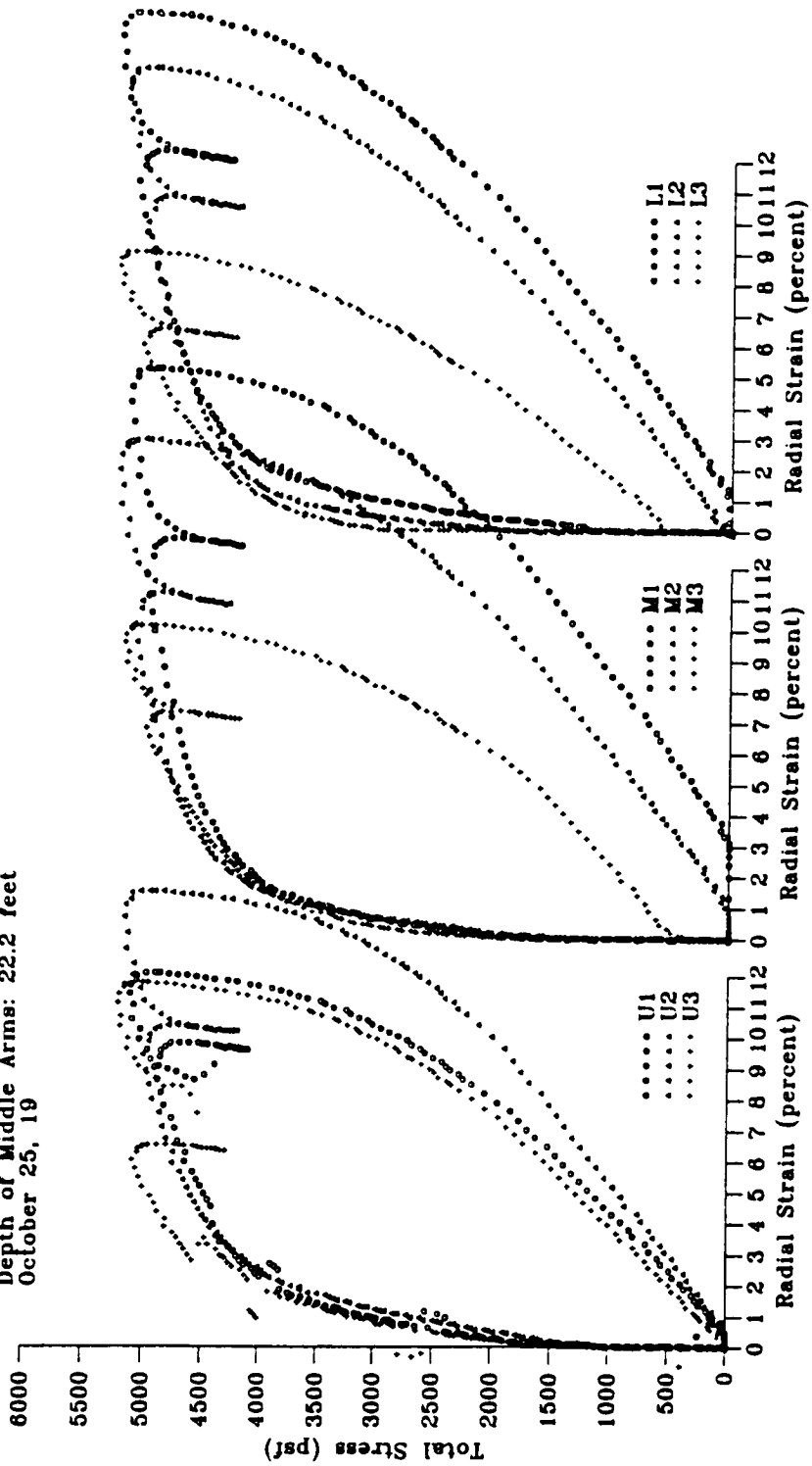
Test PMJ 5.4 - Pease Air Force Base Site
 Depth of Middle Arms: 16.6 feet
 October 25, 19



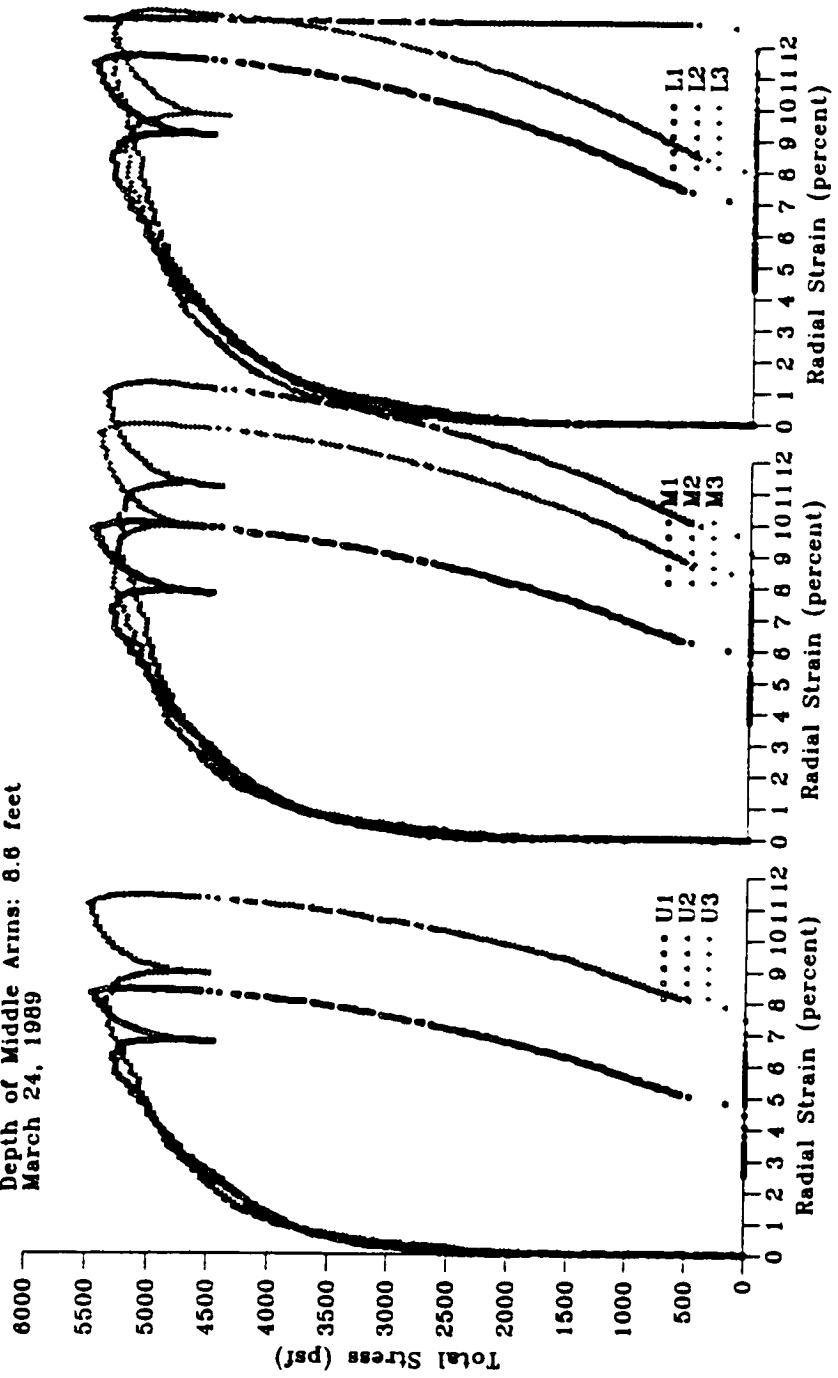
Test PMJ 5.5 - Pease Air Force Base Site
 Depth of Middle Arms: 19.6 feet
 October 25, 19



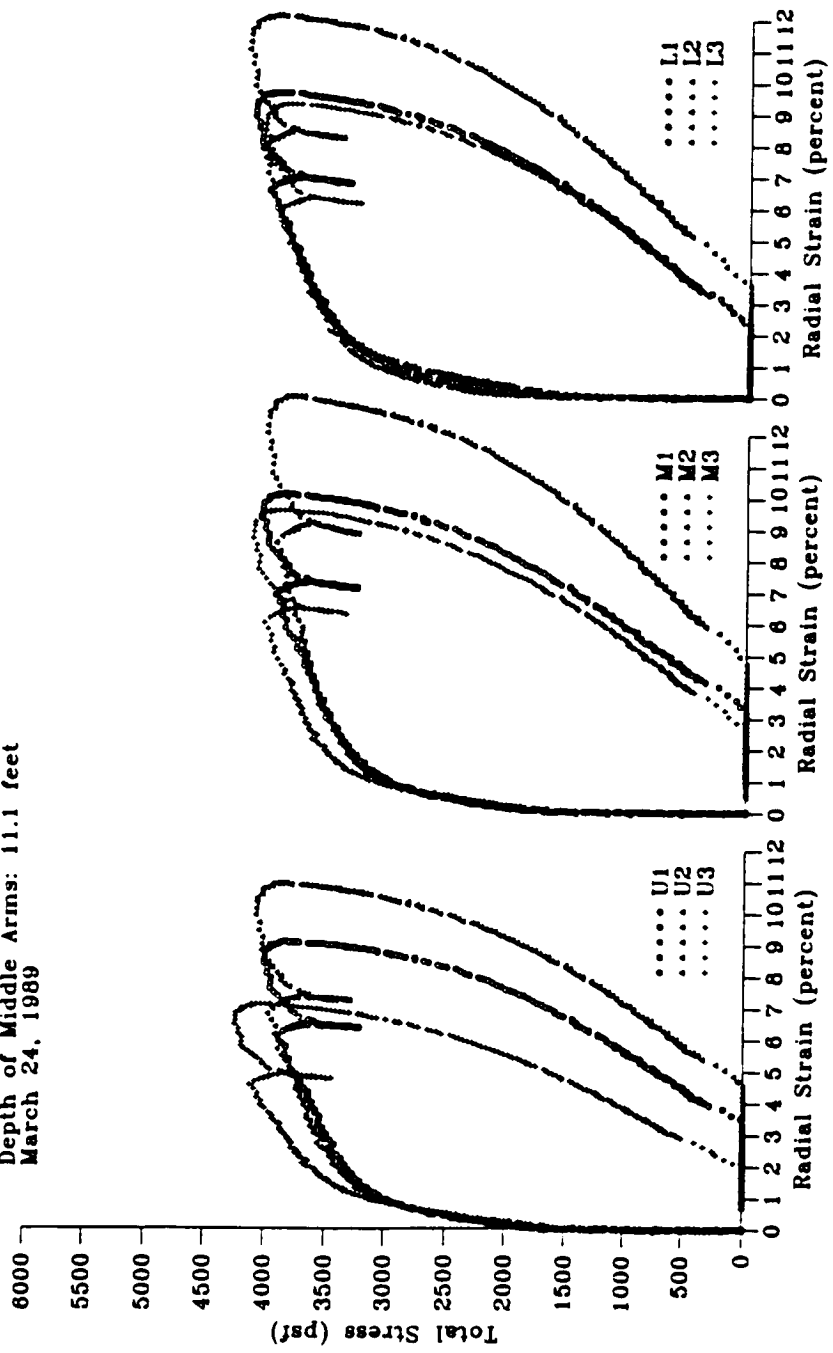
Test PMJ 5.6 - Pease Air Force Base Site
 Depth of Middle Arms: 22.2 feet
 October 25, 19



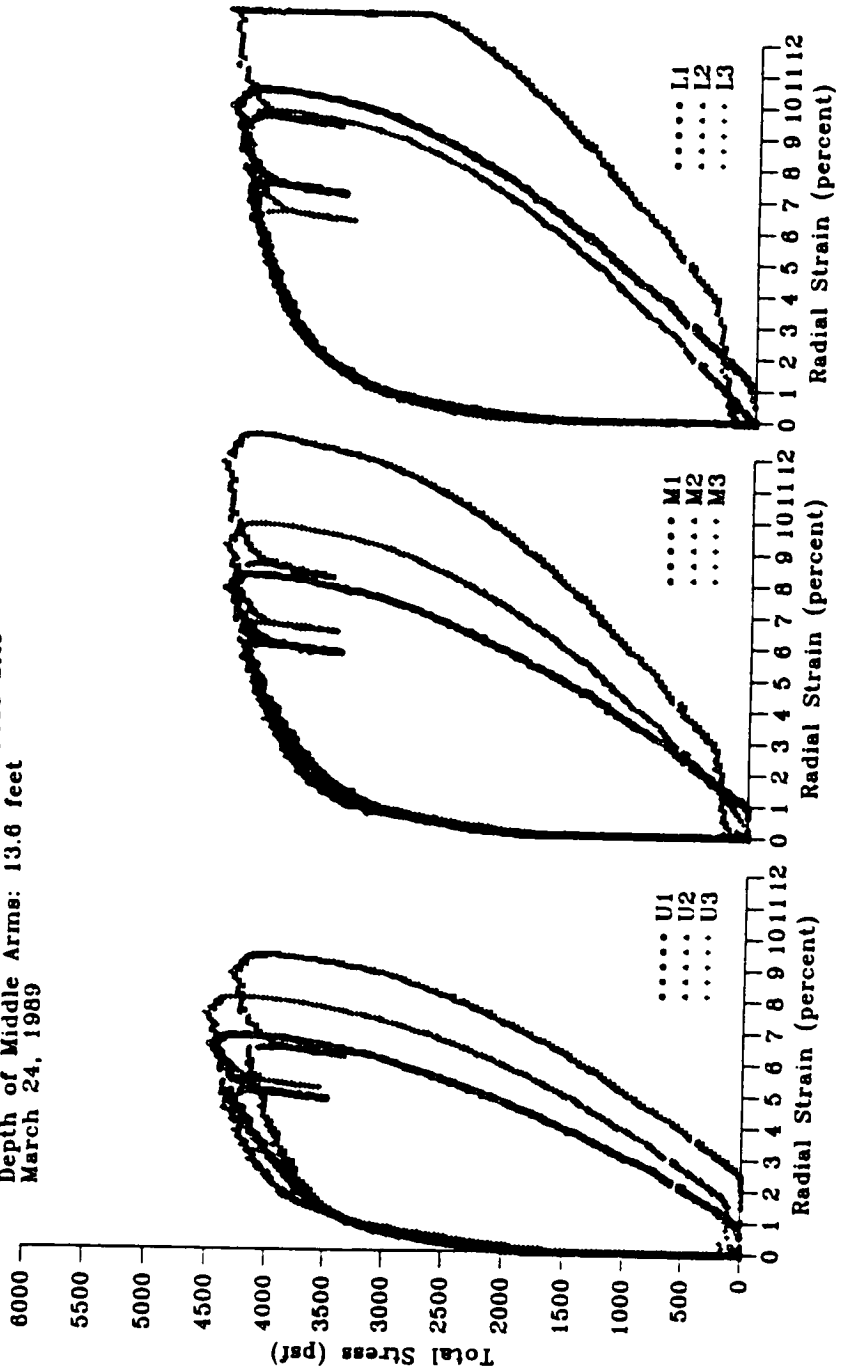
Test PMJ 6.1 - Pease Air Force Base Site
 Depth of Middle Arms: 8.6 feet
 March 24, 1989



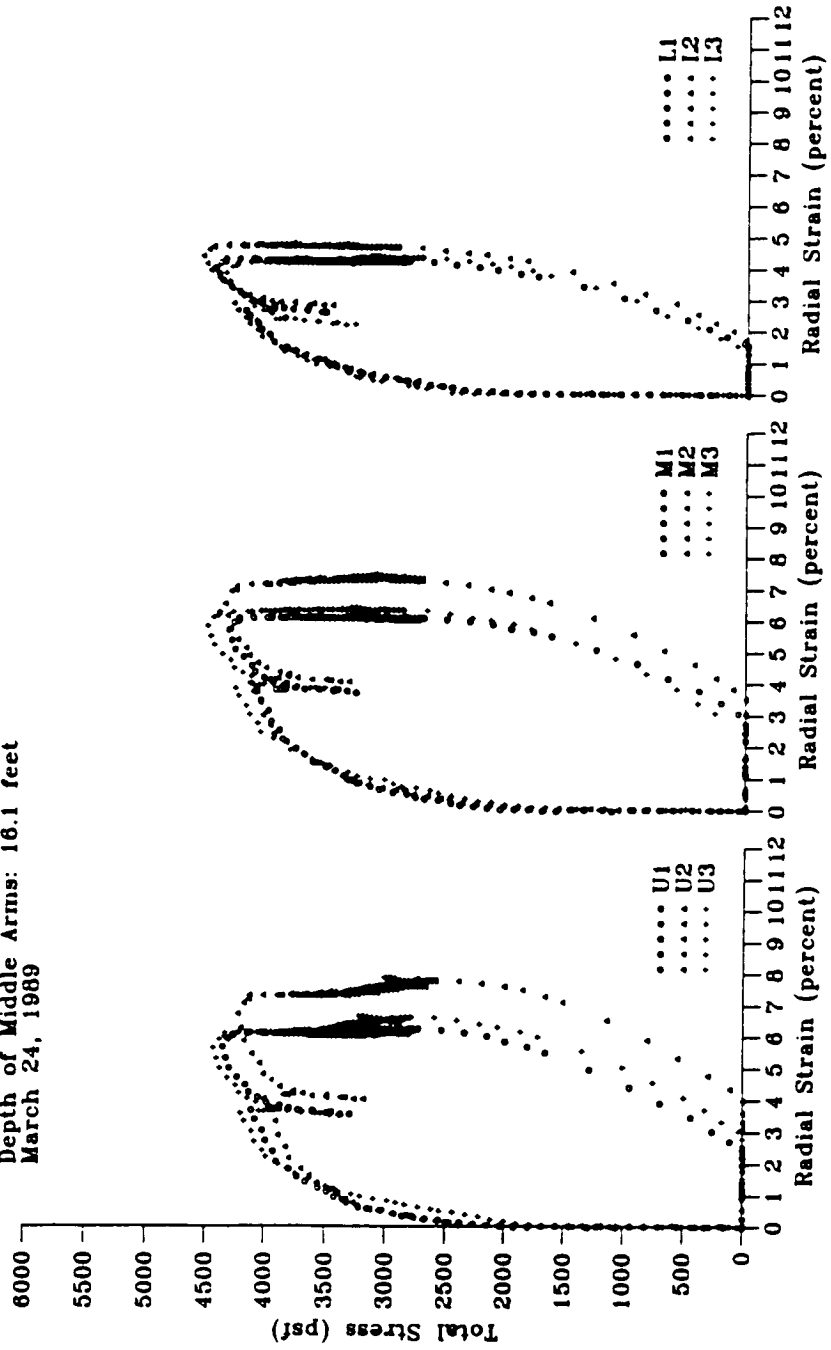
Test PMJ 6.2 - Pease Air Force Base Site
 Depth of Middle Arms: 11.1 feet
 March 24, 1989



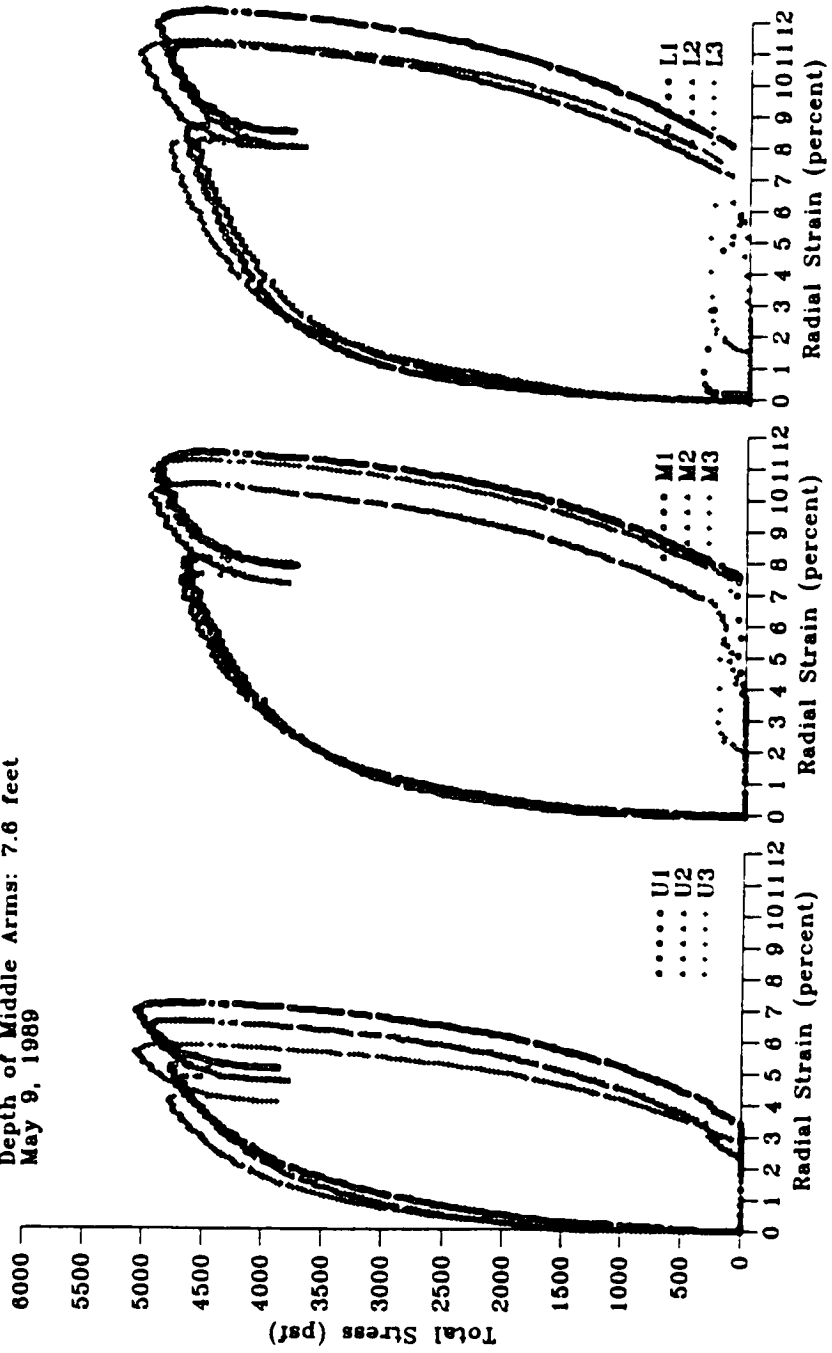
Test PMJ 6.3 - Pease Air Force Base Site
 Depth of Middle Arms: 13.6 feet
 March 24, 1989



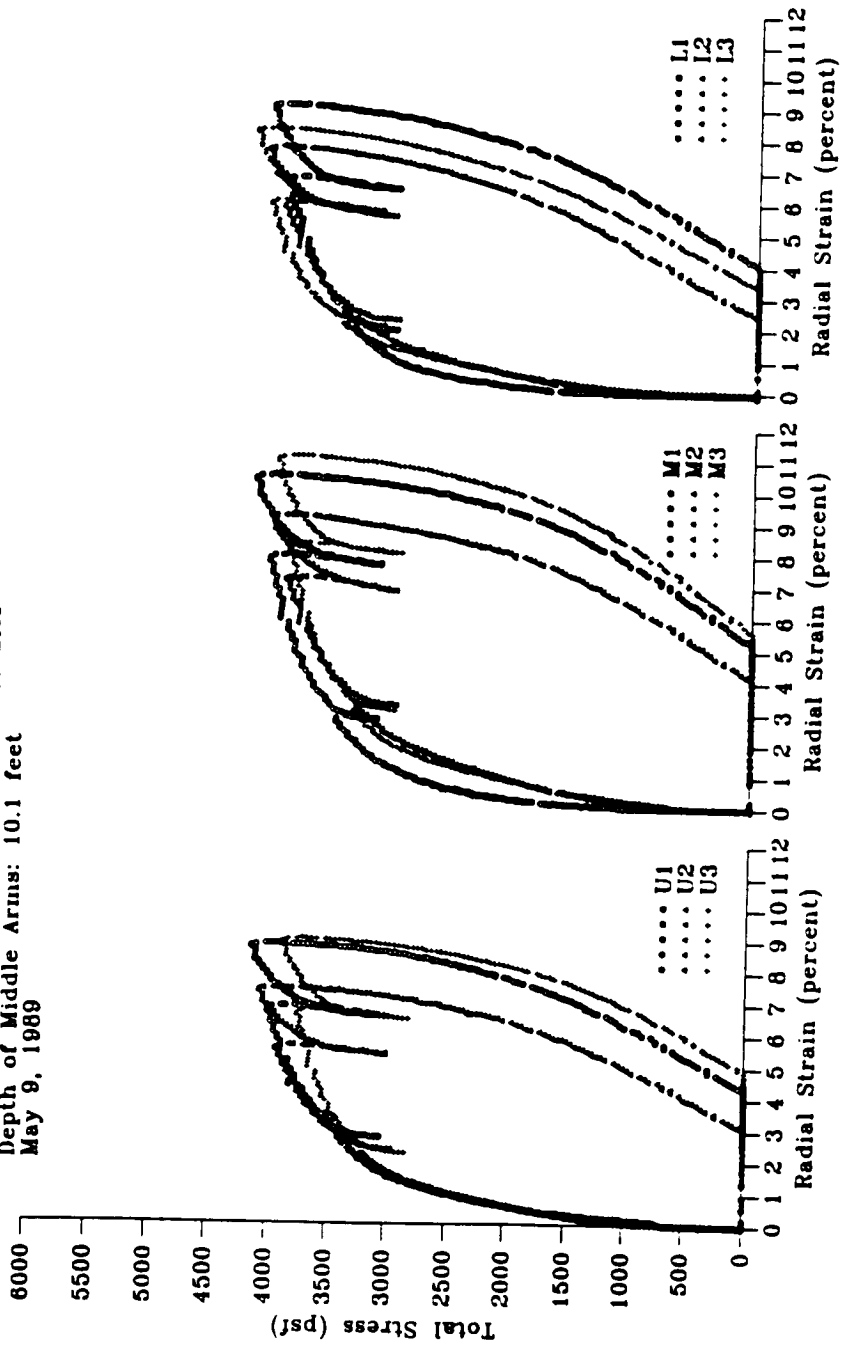
Test PMJ 6.4H - Pease Air Force Base Site
 Depth of Middle Arms: 16.1 feet
 March 24, 1989



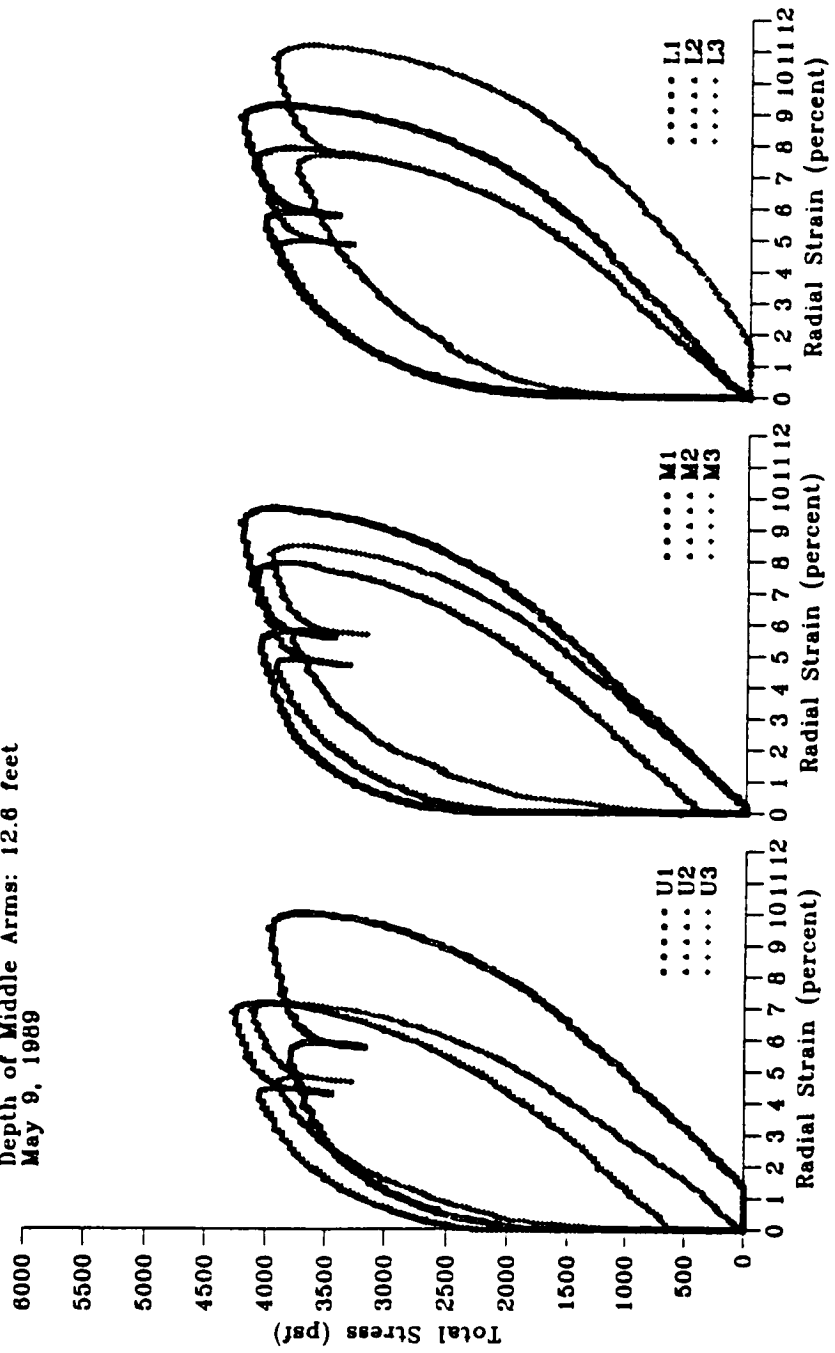
Test PMJ 7.1 - Pease Air Force Base Site
 Depth of Middle Arms: 7.6 feet
 May 9, 1989



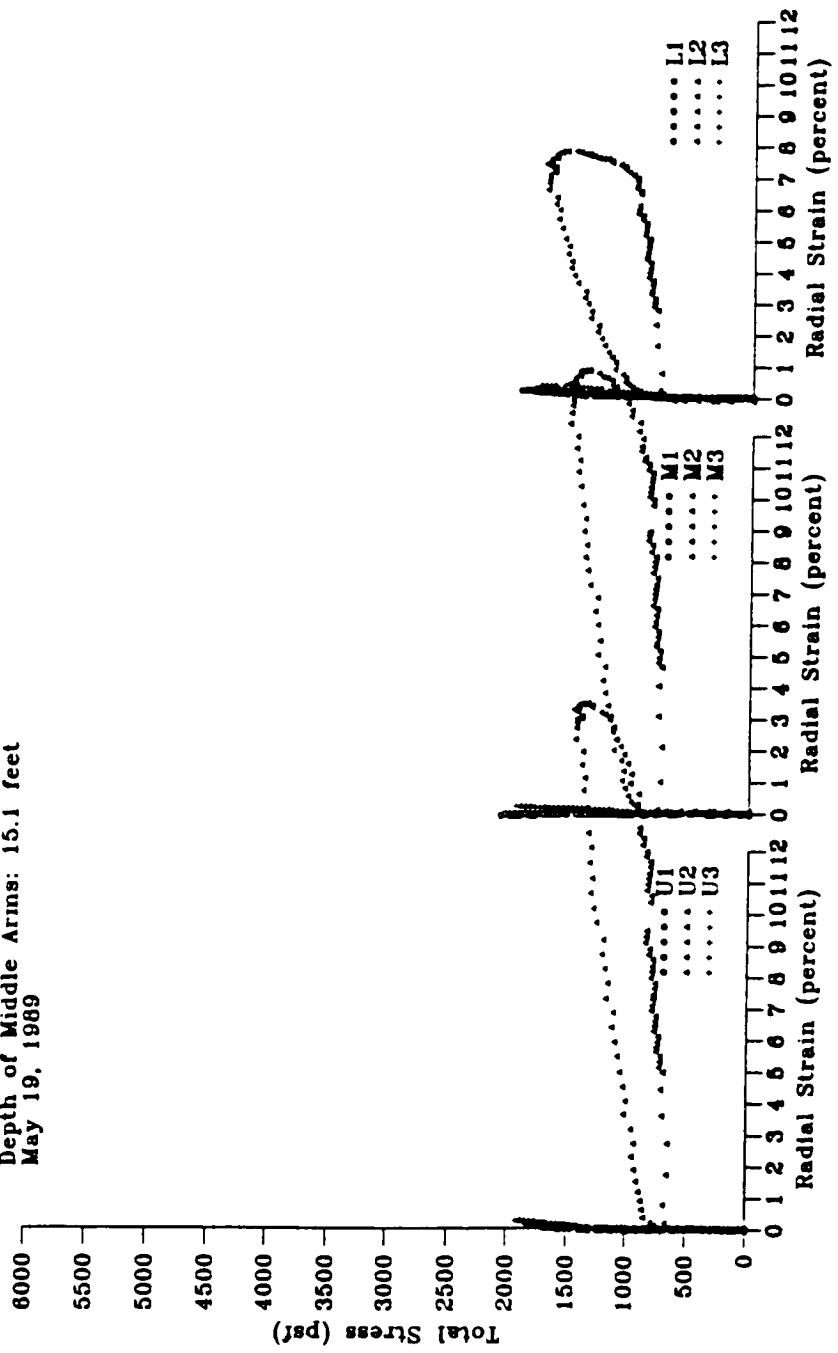
Test PMJ 7.2 - Pease Air Force Base Site
 Depth of Middle Arms: 10.1 feet
 May 9, 1989



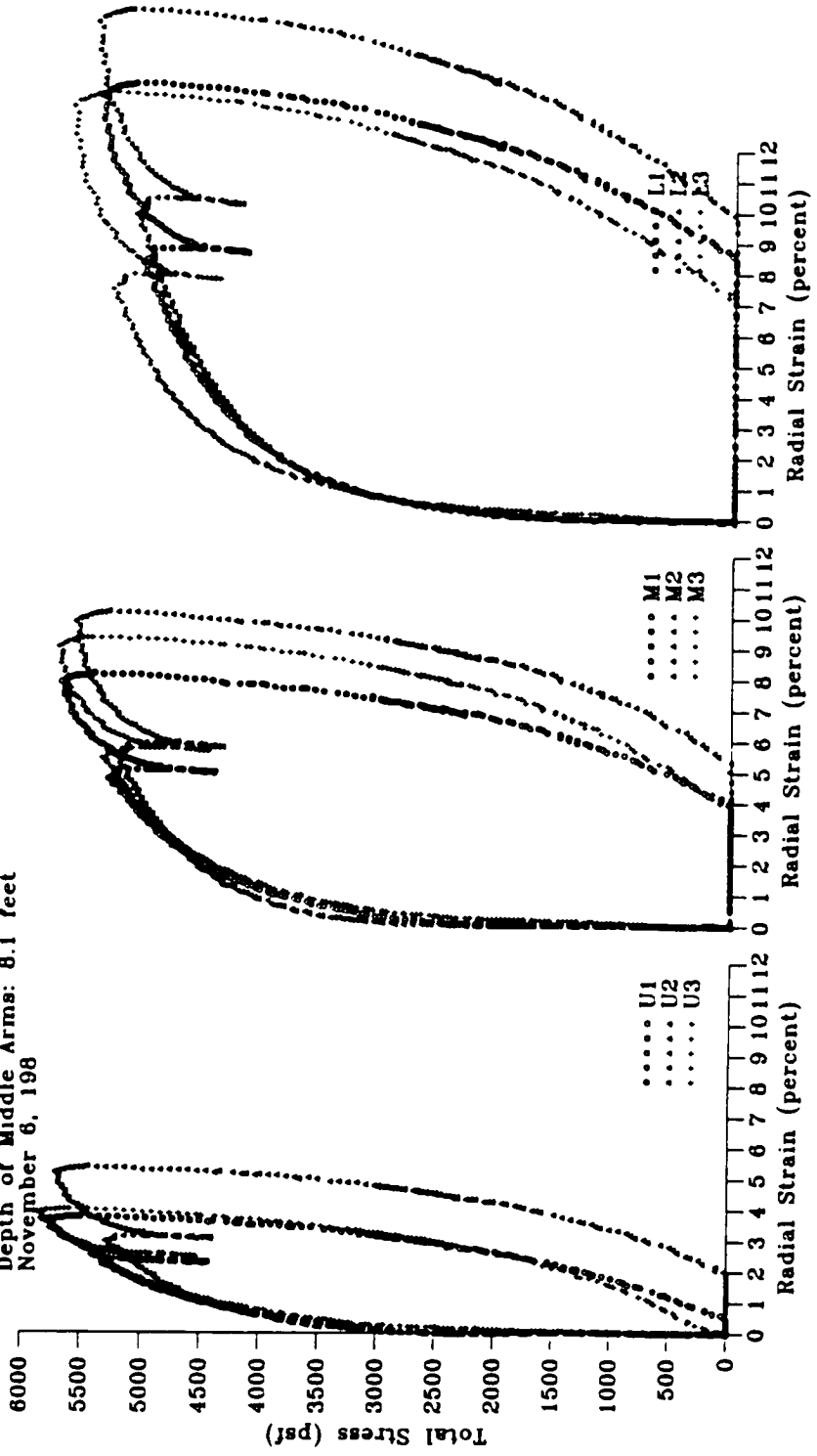
Test PMJ 7.3 - Pease Air Force Base Site
 Depth of Middle Arms: 12.6 feet
 May 9, 1989



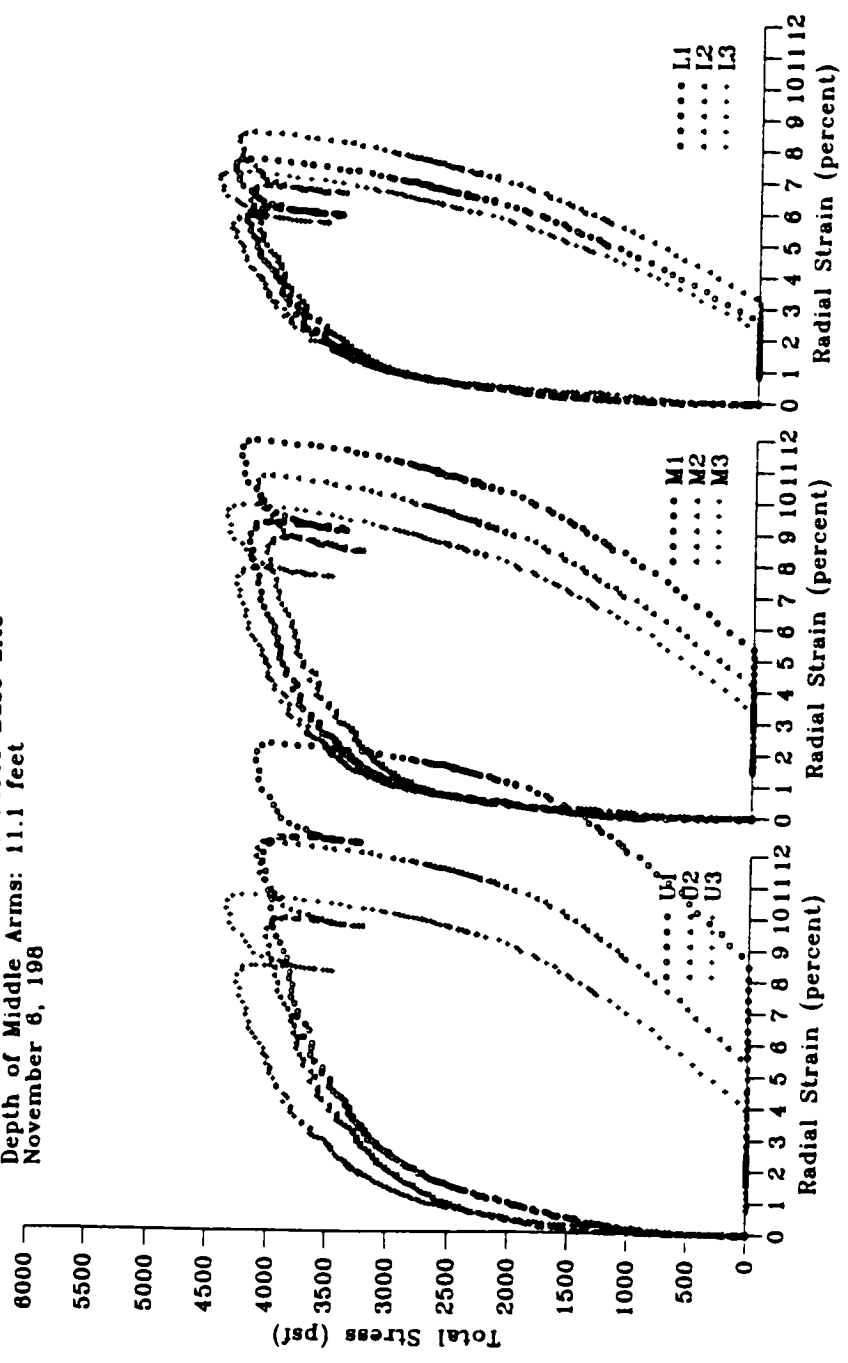
Test PMJ 7.4H - Pease Air Force Base Site
 Depth of Middle Arms: 15.1 feet
 May 19, 1989



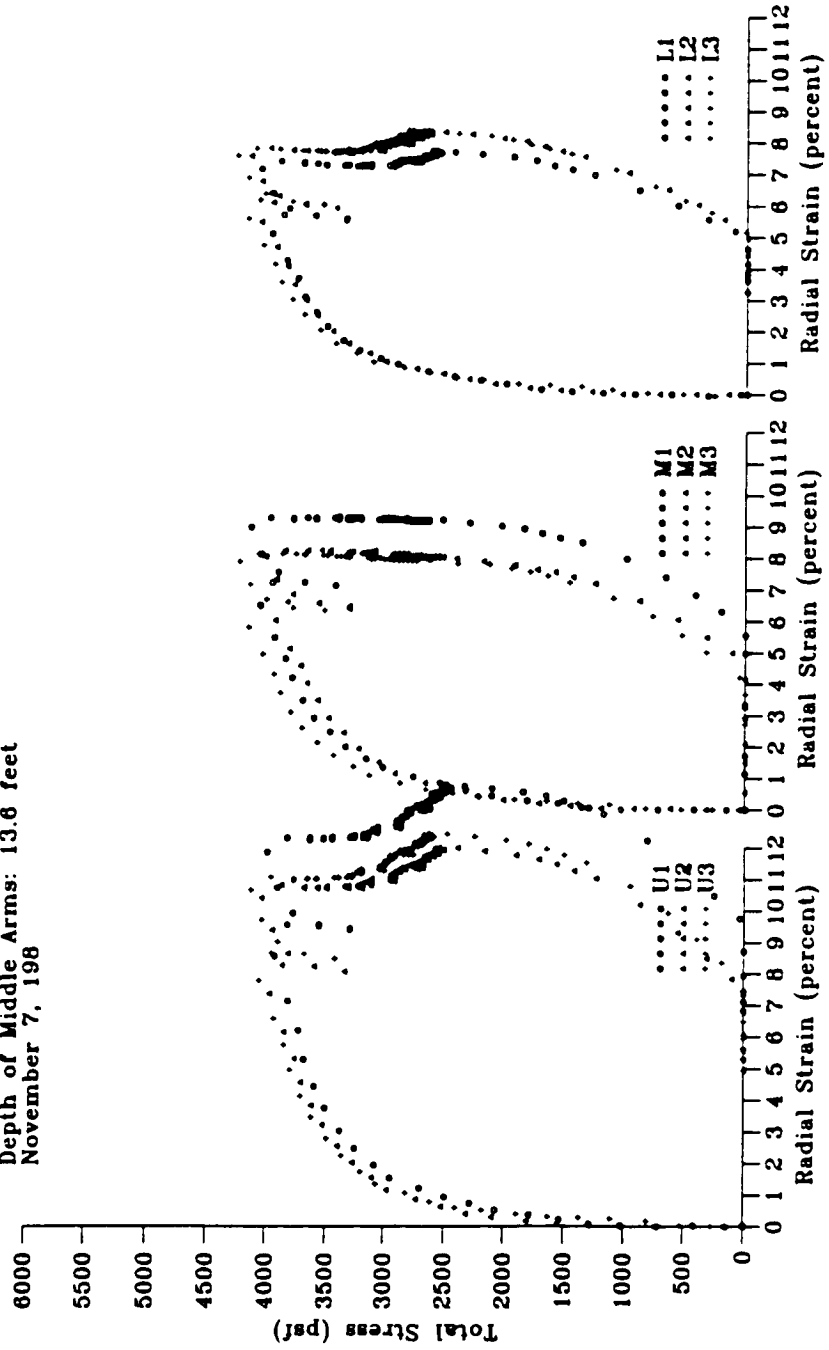
Test PMJ 8.1 - Pease Air Force Base Site
 Depth of Middle Arms: 8.1 feet
 November 6, 1988



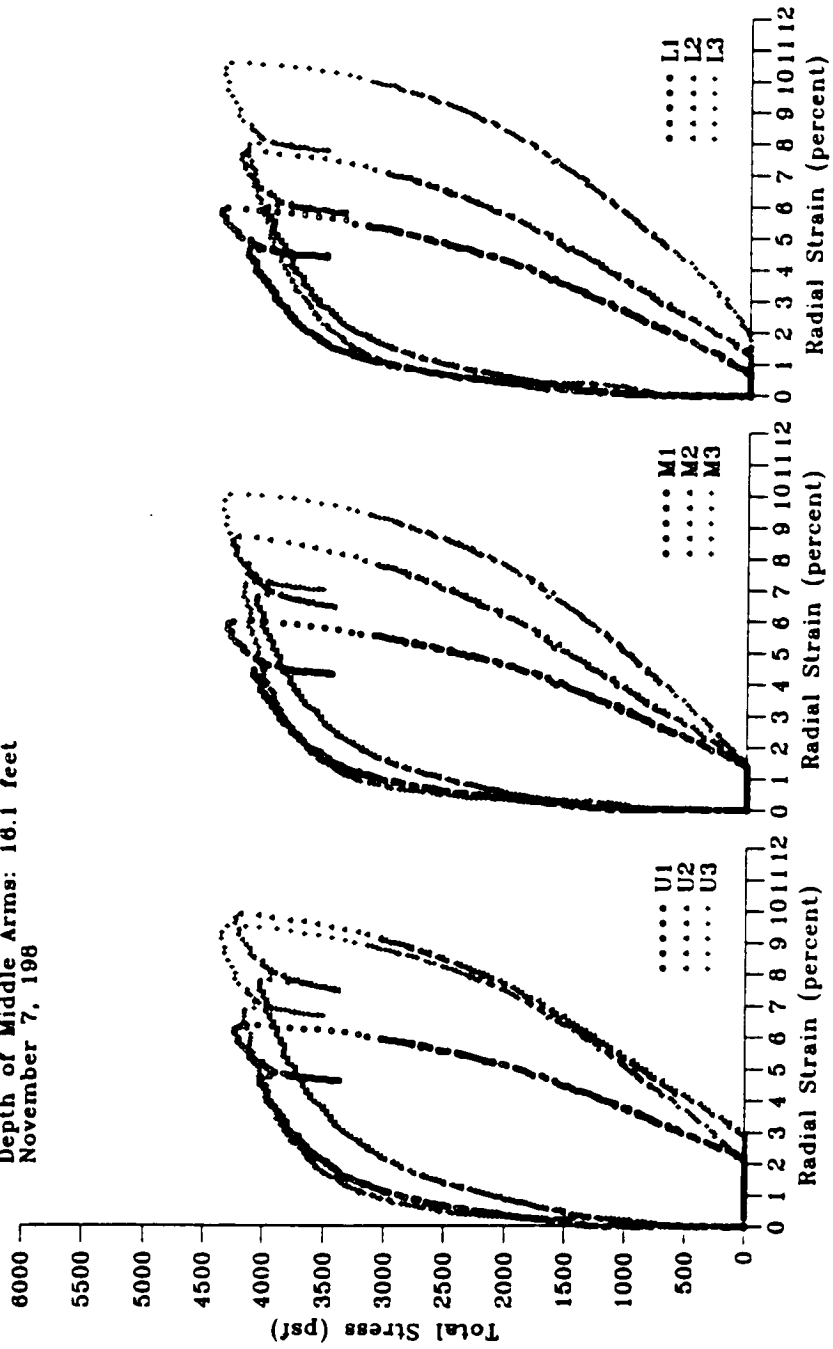
Test PMJ 8.2 - Pease Air Force Base Site
 Depth of Middle Arms: 11.1 feet
 November 6, 198



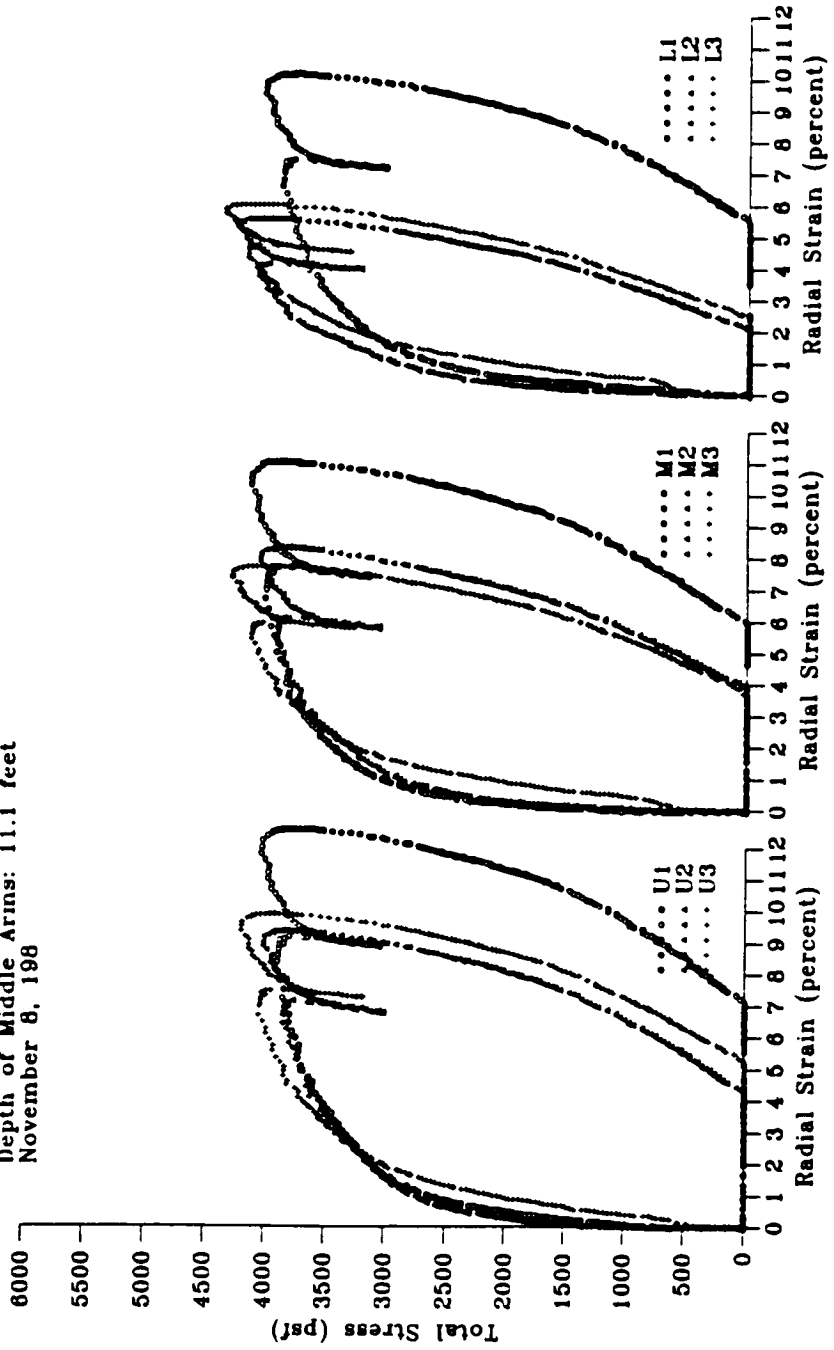
Test PMJ 8.3II - Pease Air Force Base Site
 Depth of Middle Arms: 13.6 feet
 November 7, 198



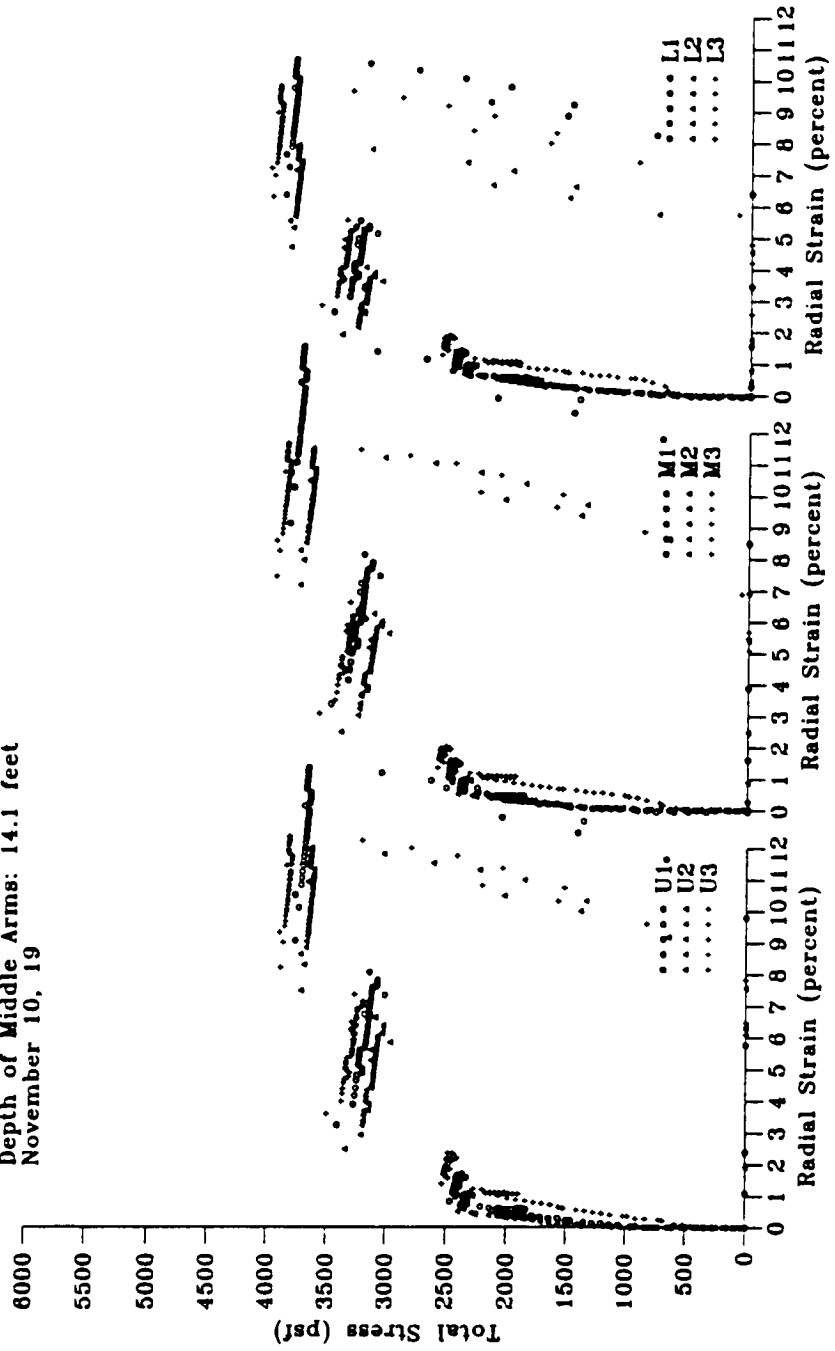
Test PMJ 8.4 - Pease Air Force Base Site
 Depth of Middle Arms: 16.1 feet
 November 7, 198



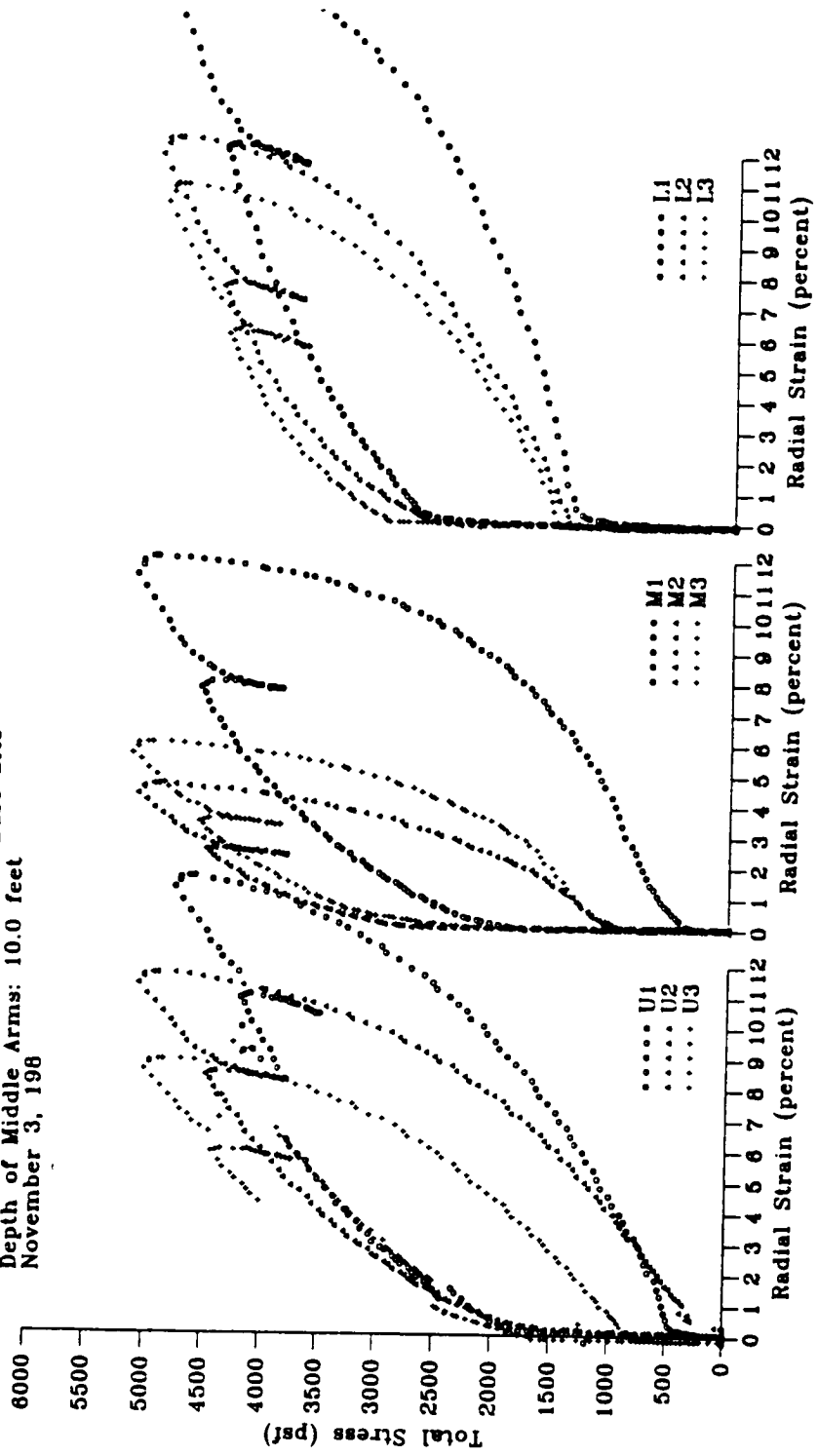
Test PMS 1.1 - Pease Air Force Base Site
 Depth of Middle Arms: 11.1 feet
 November 8, 1988



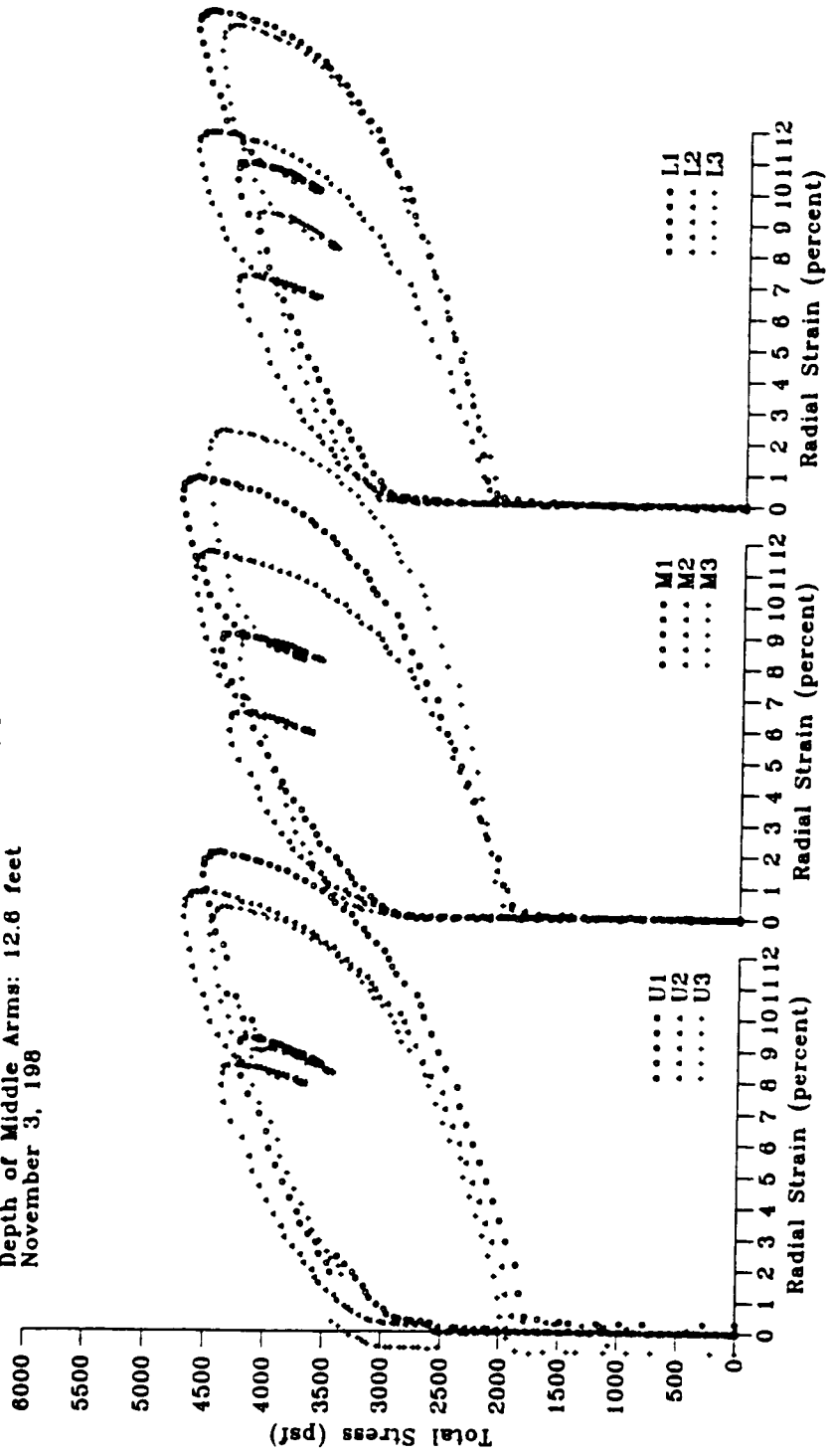
Test PMS 1.2 - Pease Air Force Base Site
 Depth of Middle Arms: 14.1 feet
 November 10, 19



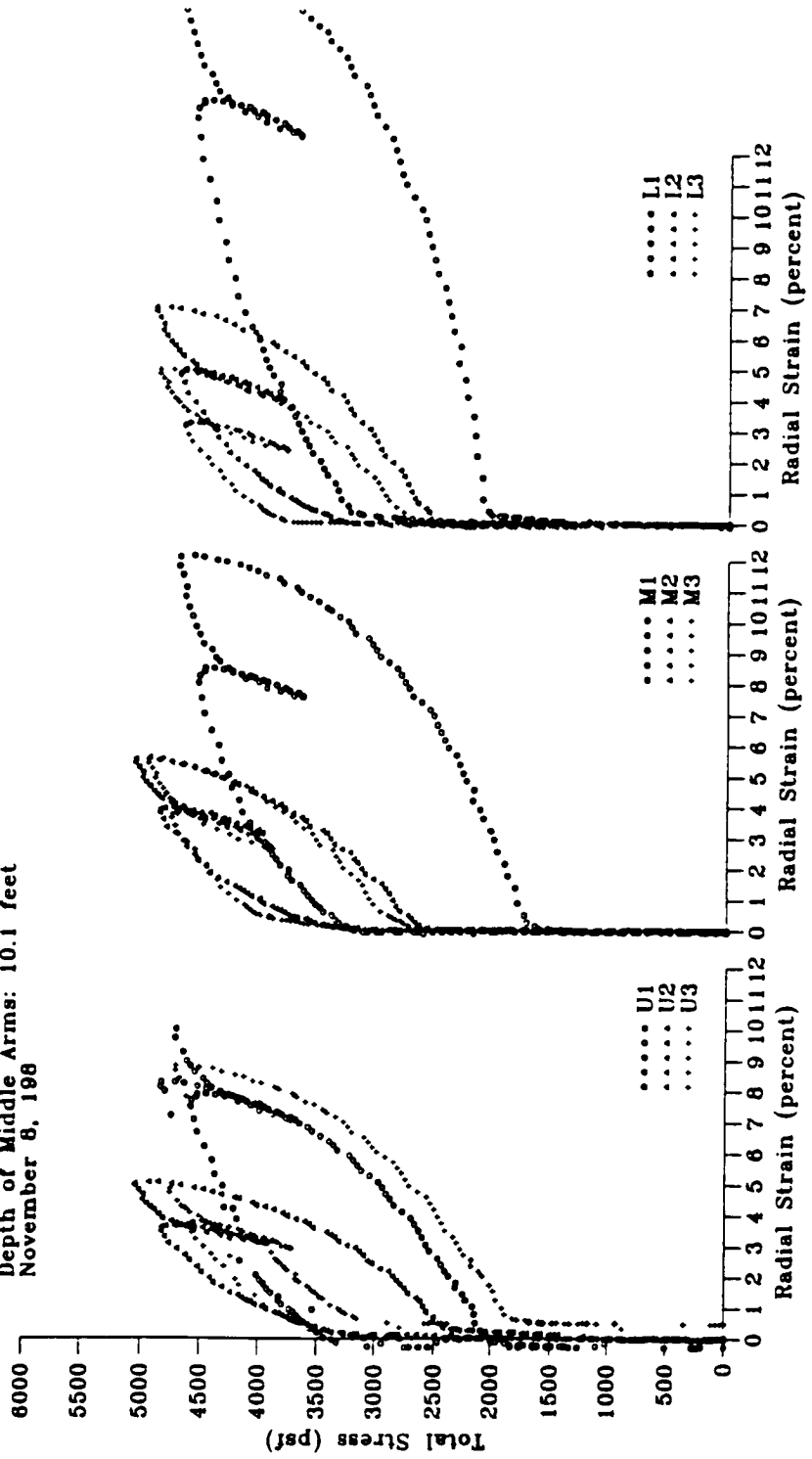
Test PMP 1.1 - Pease Air Force Base Site
 Depth of Middle Arms: 10.0 feet
 November 3, 198



Test PMP 1.2 - Pease Air Force Base Site
 Depth of Middle Arms: 12.6 feet
 November 3, 198



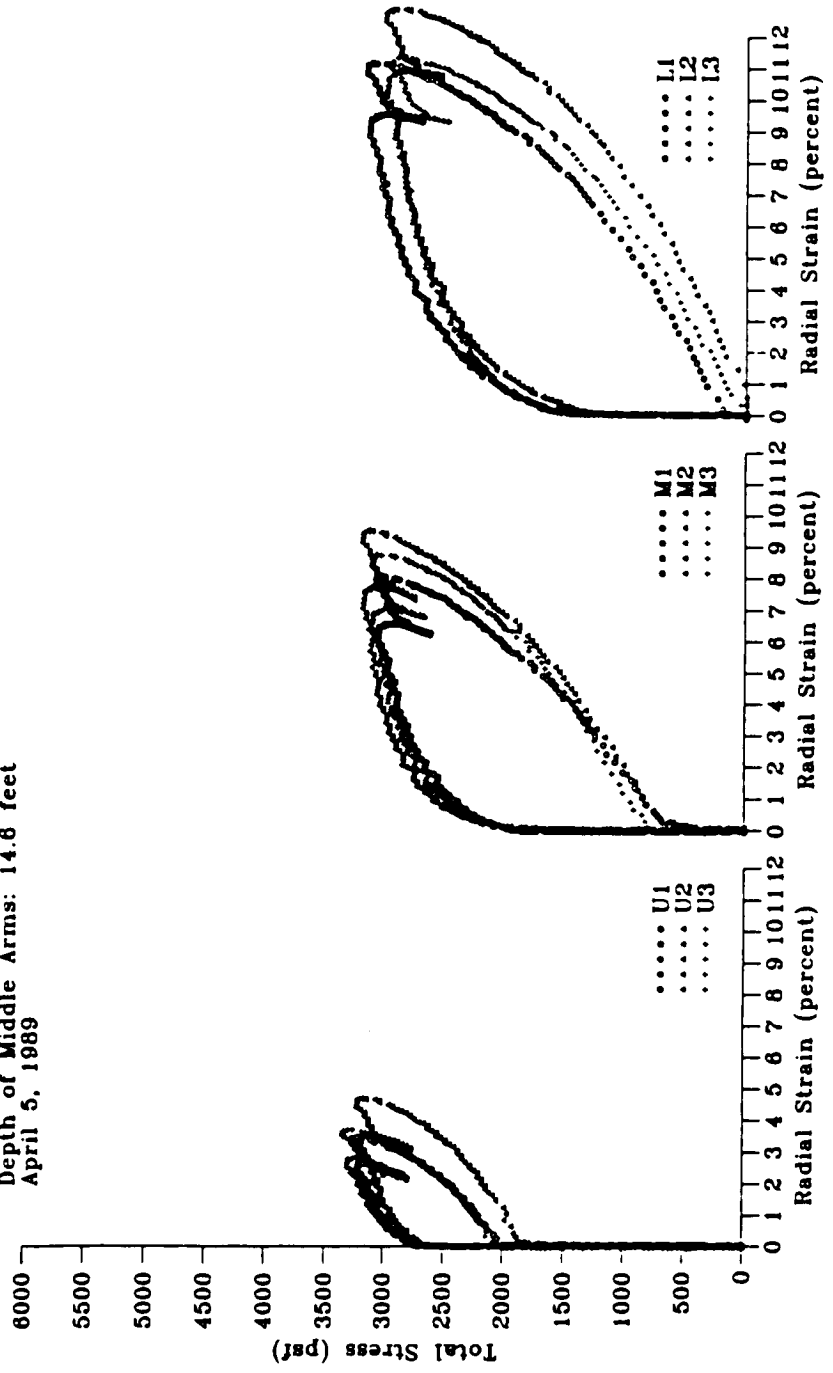
Test PMP 2.1 - Pease Air Force Base Site
 Depth of Middle Arms: 10.1 feet
 November 8, 1968



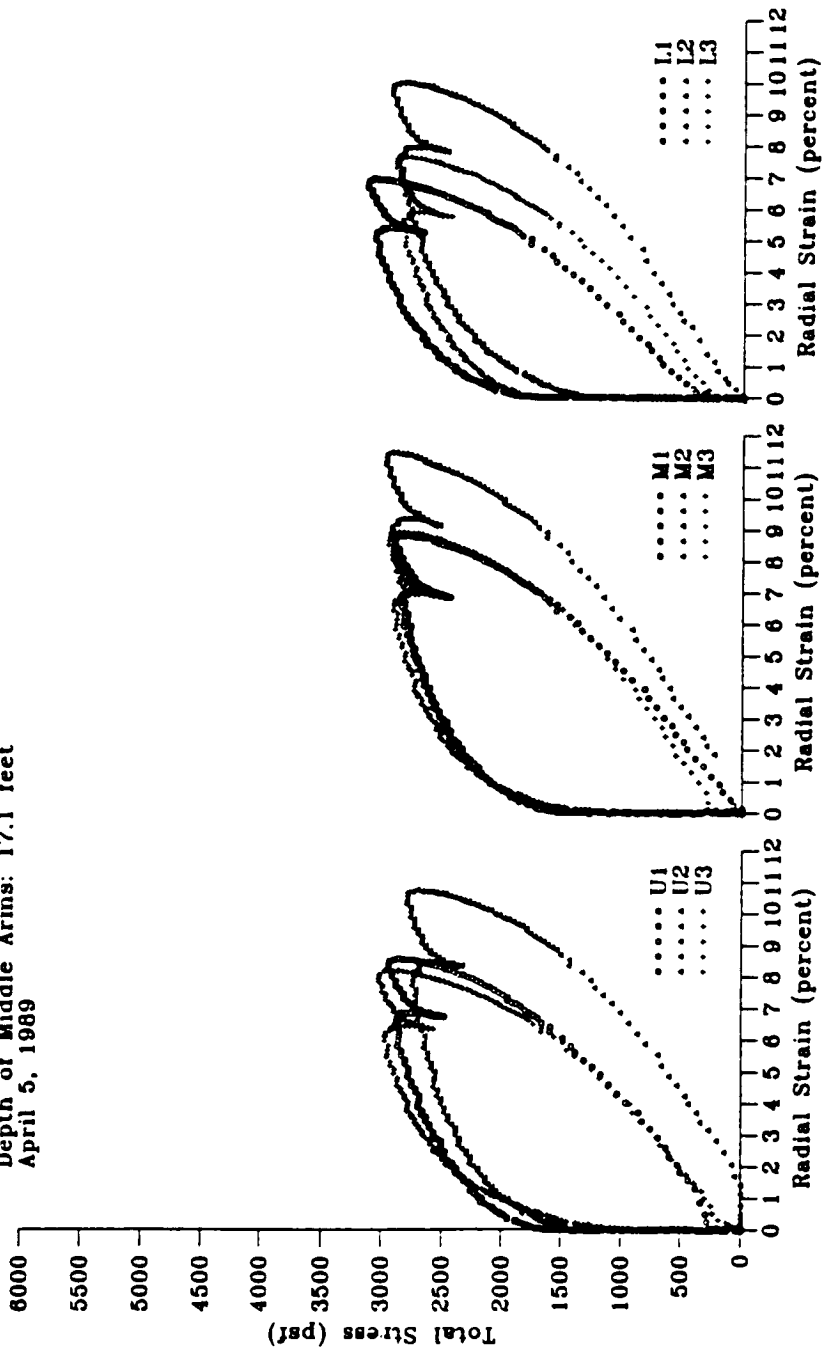
Test HAM 1.1 - Hamilton Air Force Base Site
 Depth of Middle Arms: 12.1 feet
 April 5, 1989



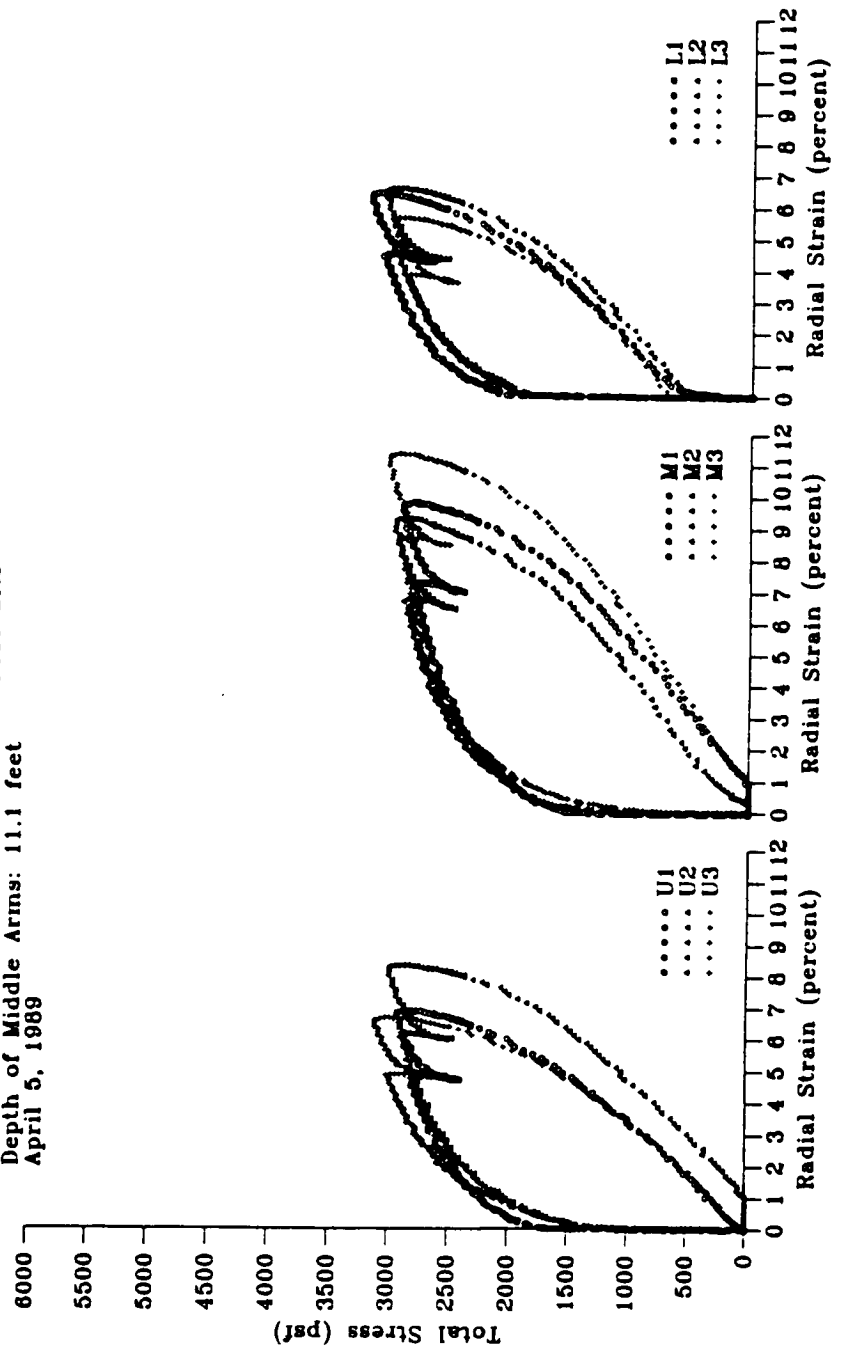
Test HAM 1.2 - Hamilton Air Force Base Site
 Depth of Middle Arms: 14.6 feet
 April 5, 1989



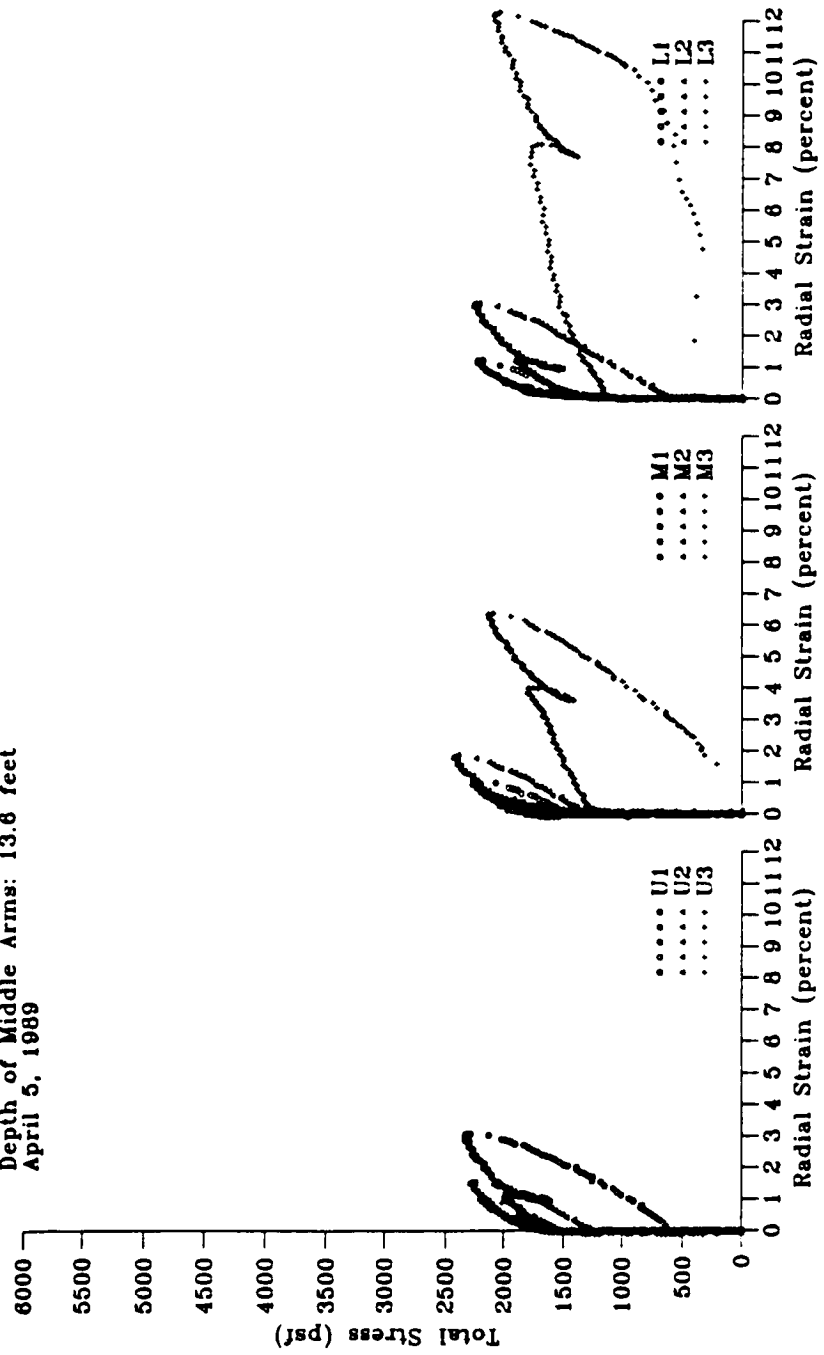
Test HAM 1.3 - Hamilton Air Force Base Site
 Depth of Middle Arms: 17.1 feet
 April 5, 1989



Test IAM 2.1 - Hamilton Air Force Base Site
 Depth of Middle Arms: 11.1 feet
 April 5, 1989



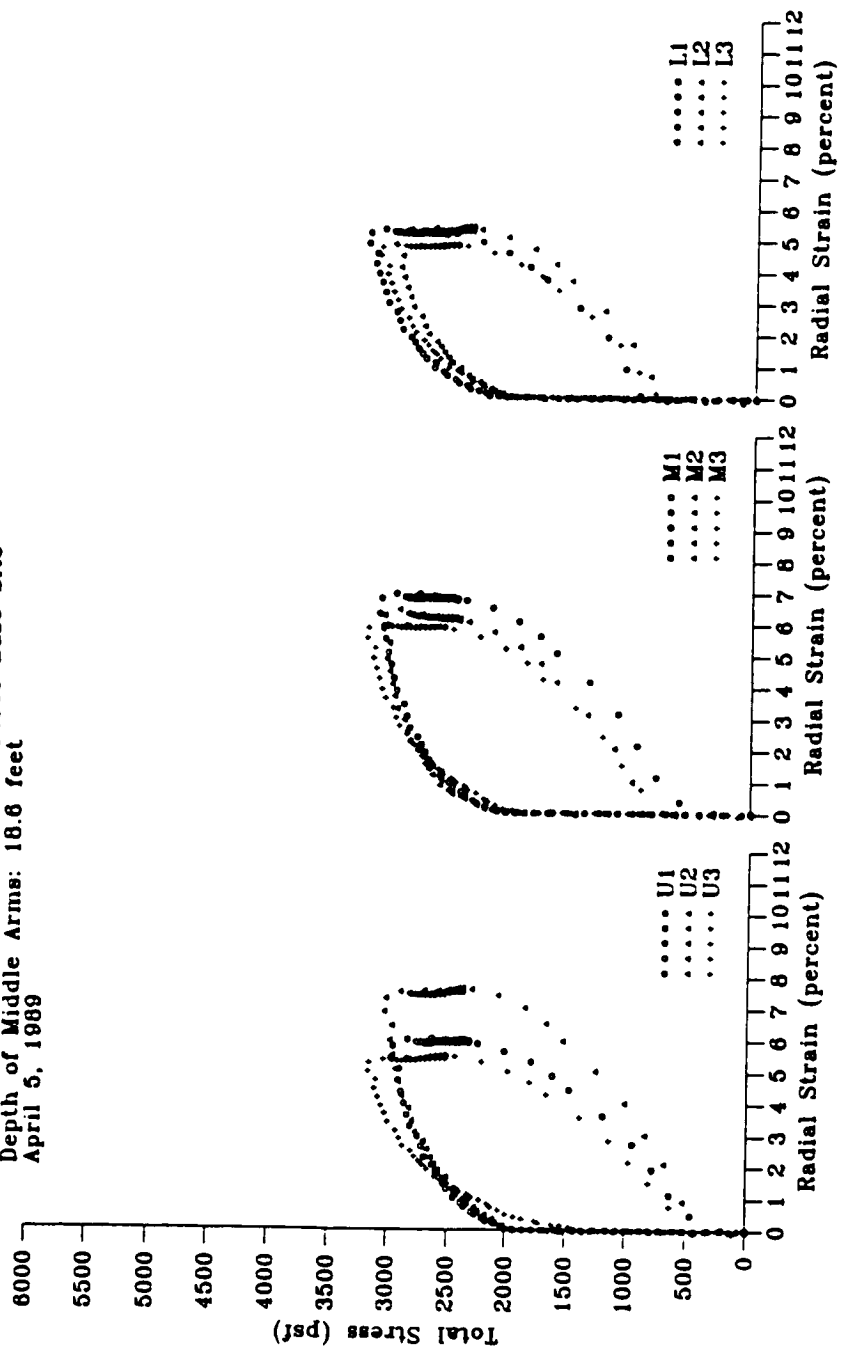
Test HAM 2.2 - Hamilton Air Force Base Site
 Depth of Middle Arms: 13.6 feet
 April 5, 1989



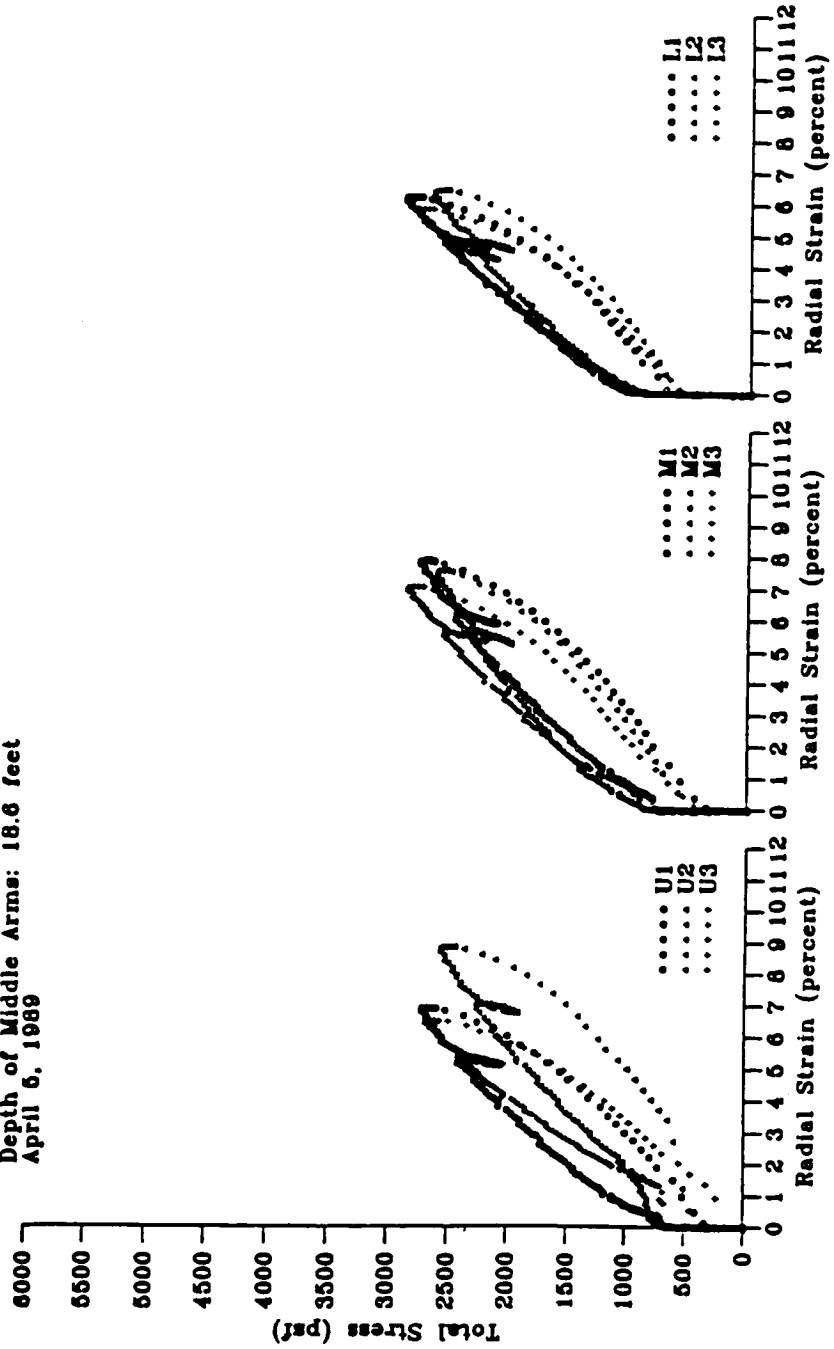
Test HAM 2.3 - Hamilton Air Force Base Site
 Depth of Middle Arms: 16.1 feet
 April 5, 1989



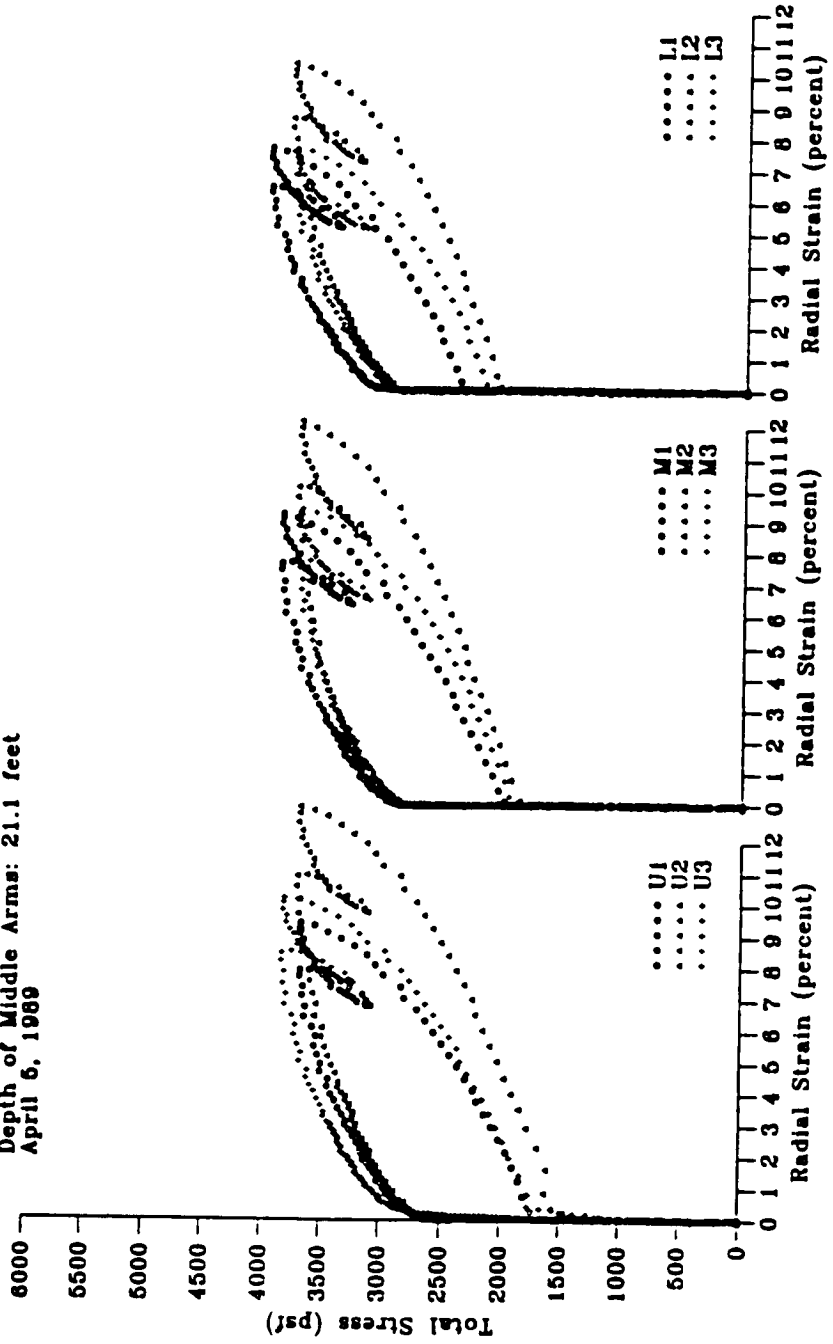
Test HAM 2.4H - Hamilton Air Force Base Site
 Depth of Middle Arms: 18.6 feet
 April 5, 1989



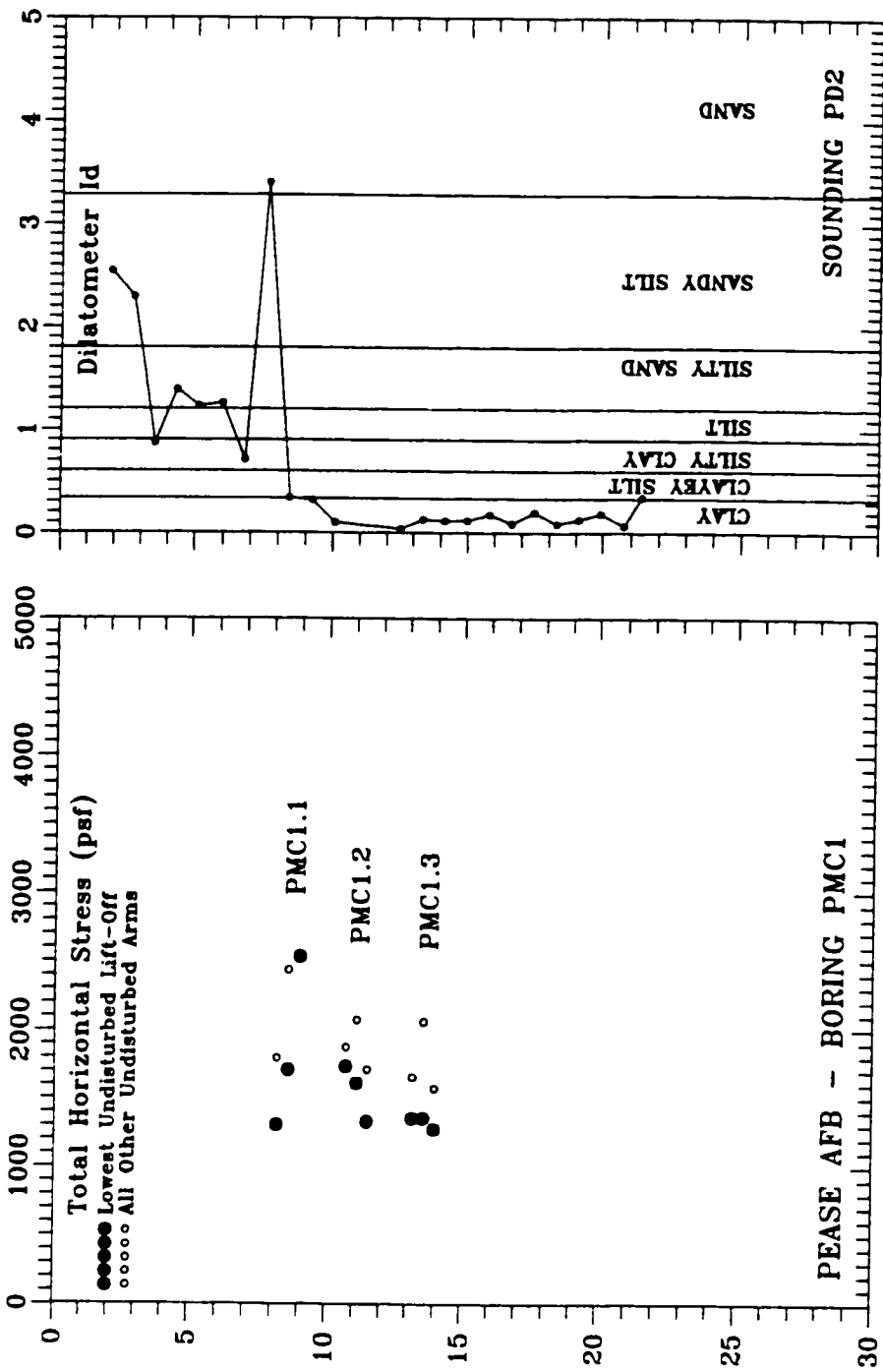
Test HAM 2.4R - Hamilton Air Force Base Site
 Depth of Middle Arms: 18.6 feet
 April 6, 1989

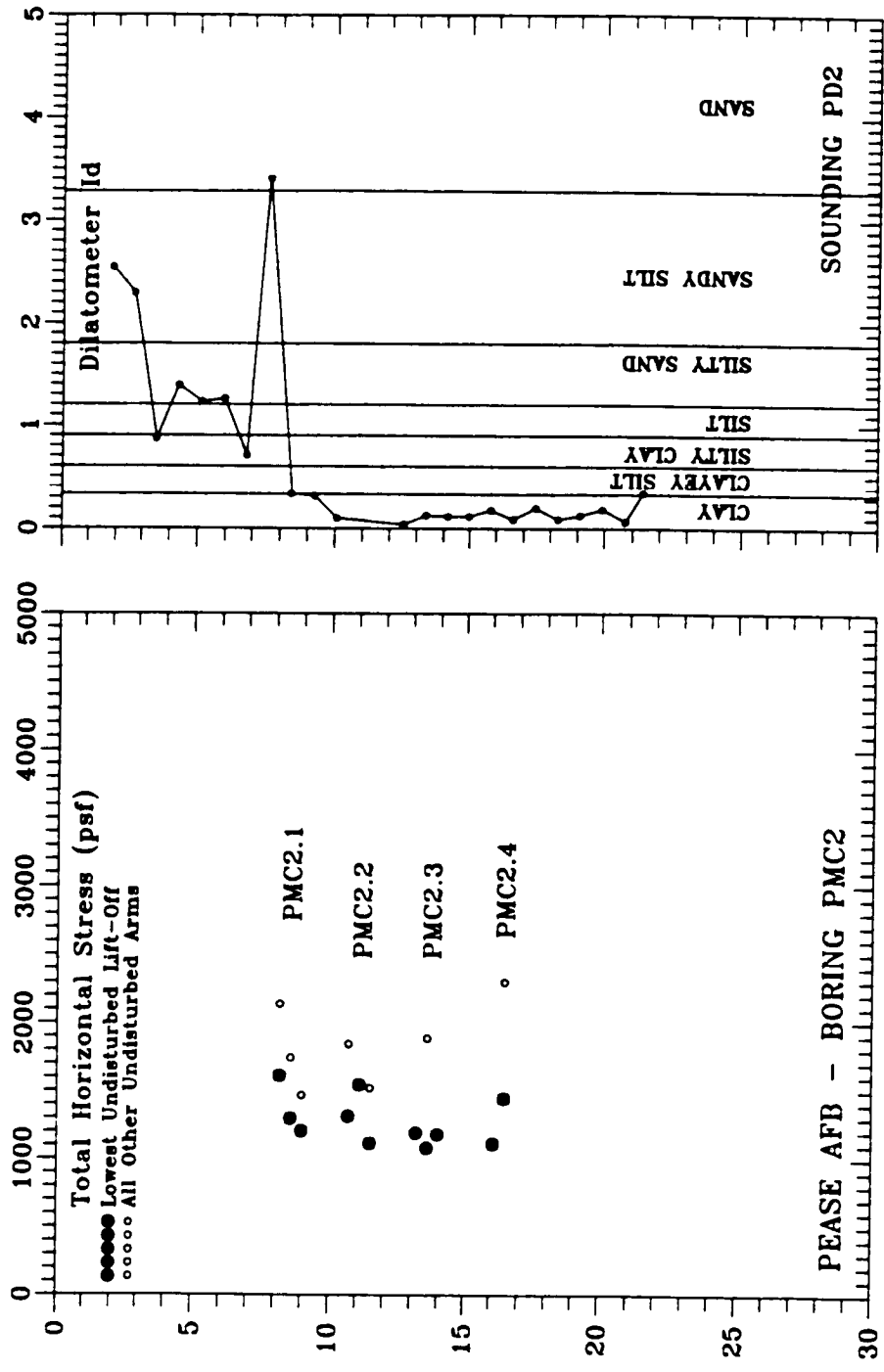


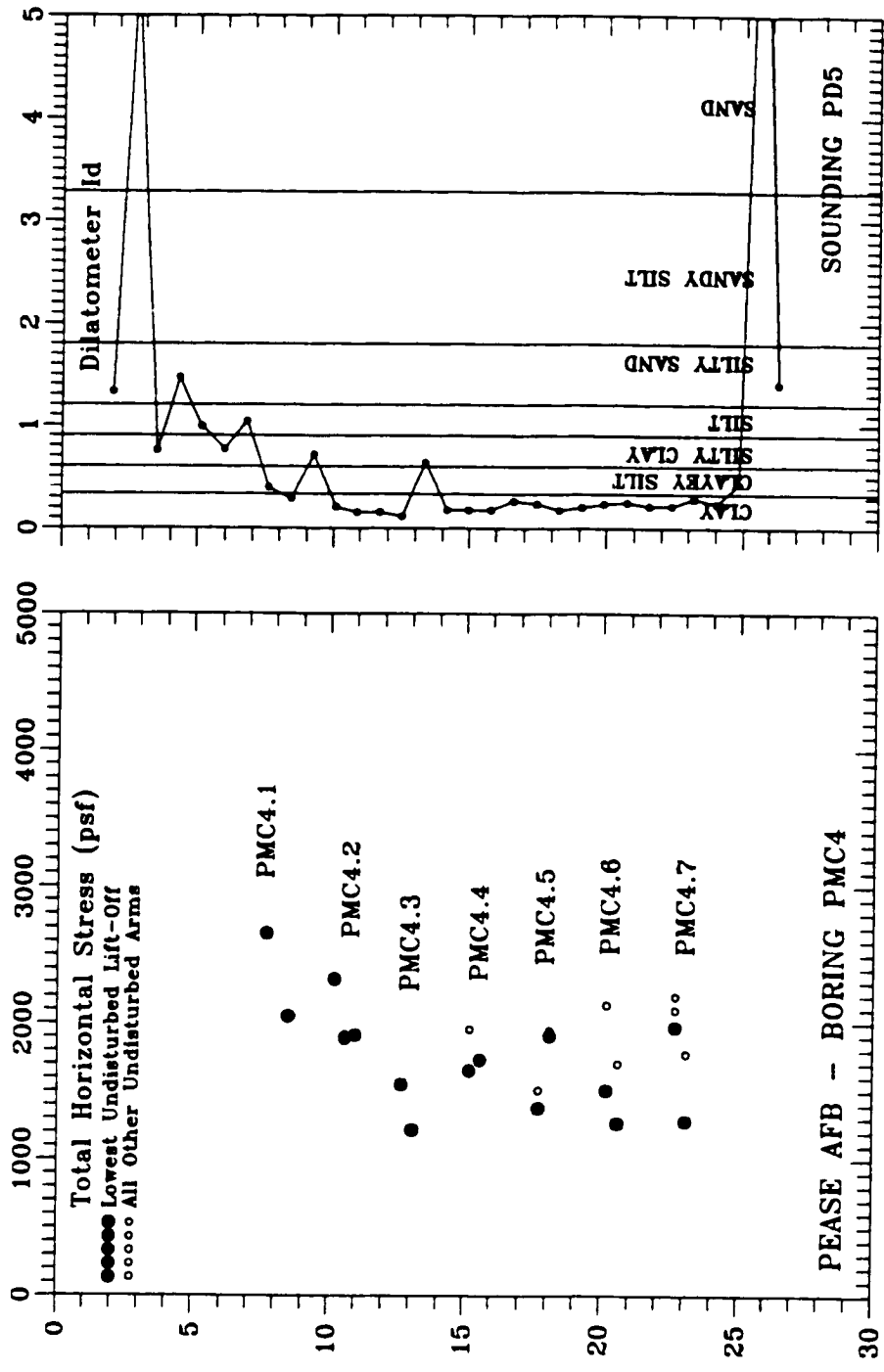
Test HAM 2.6P - Hamilton Air Force Base Site
 Depth of Middle Arms: 21.1 feet
 April 6, 1989

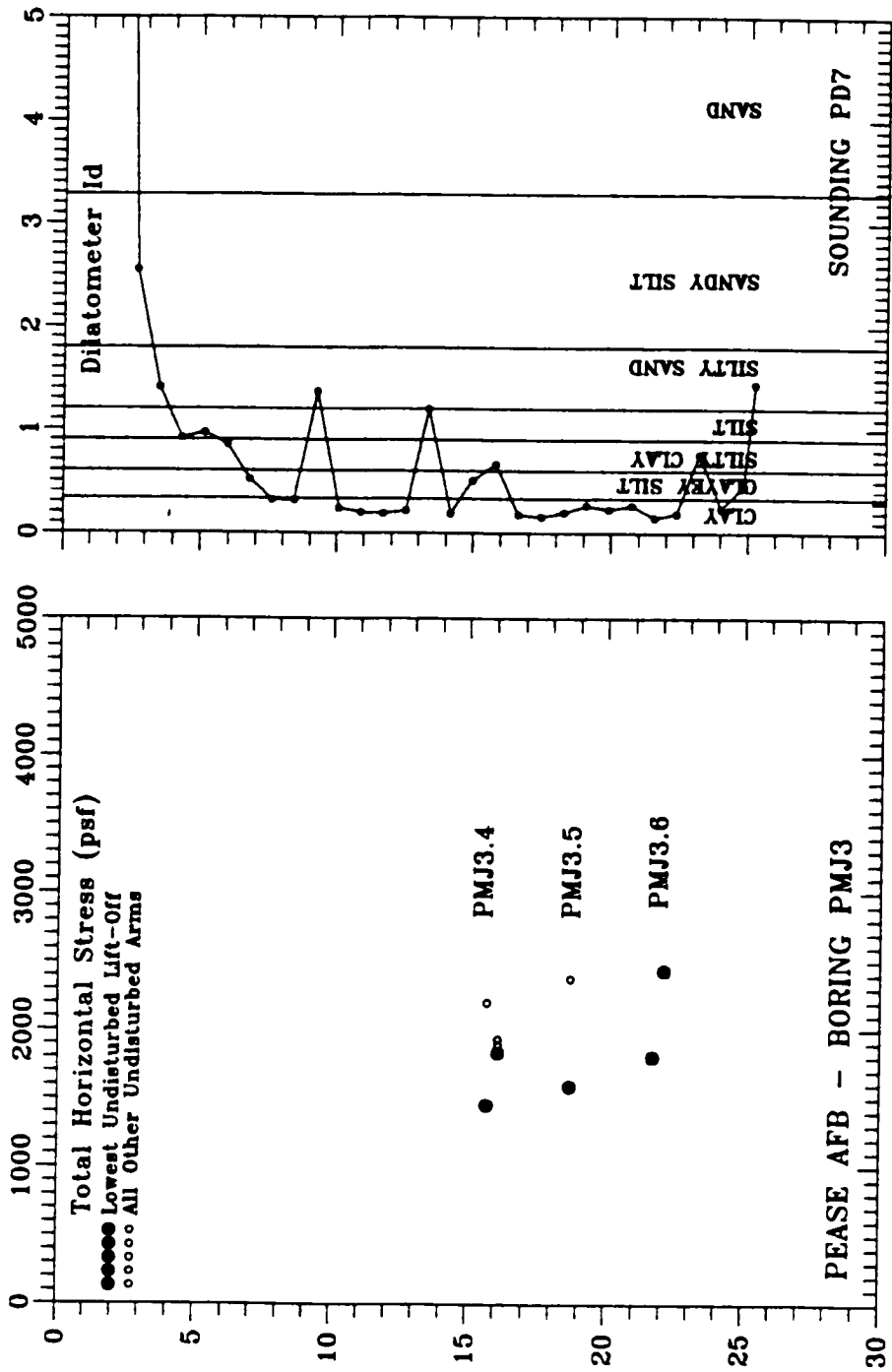


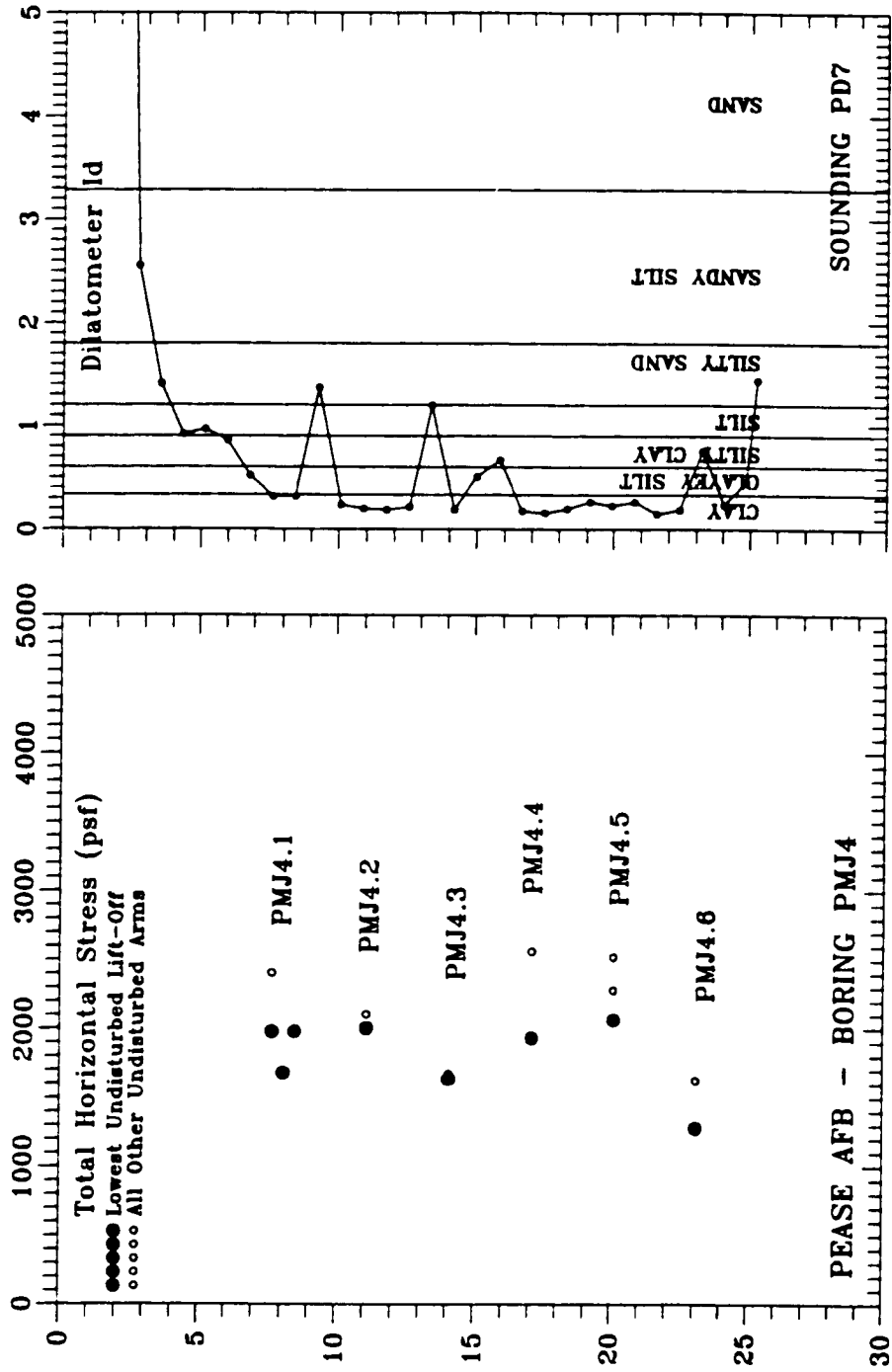
APPENDIX D
PROFILES OF SBPM HORIZONTAL STRESS
AND DILATOMETER ϵ_d VALUES

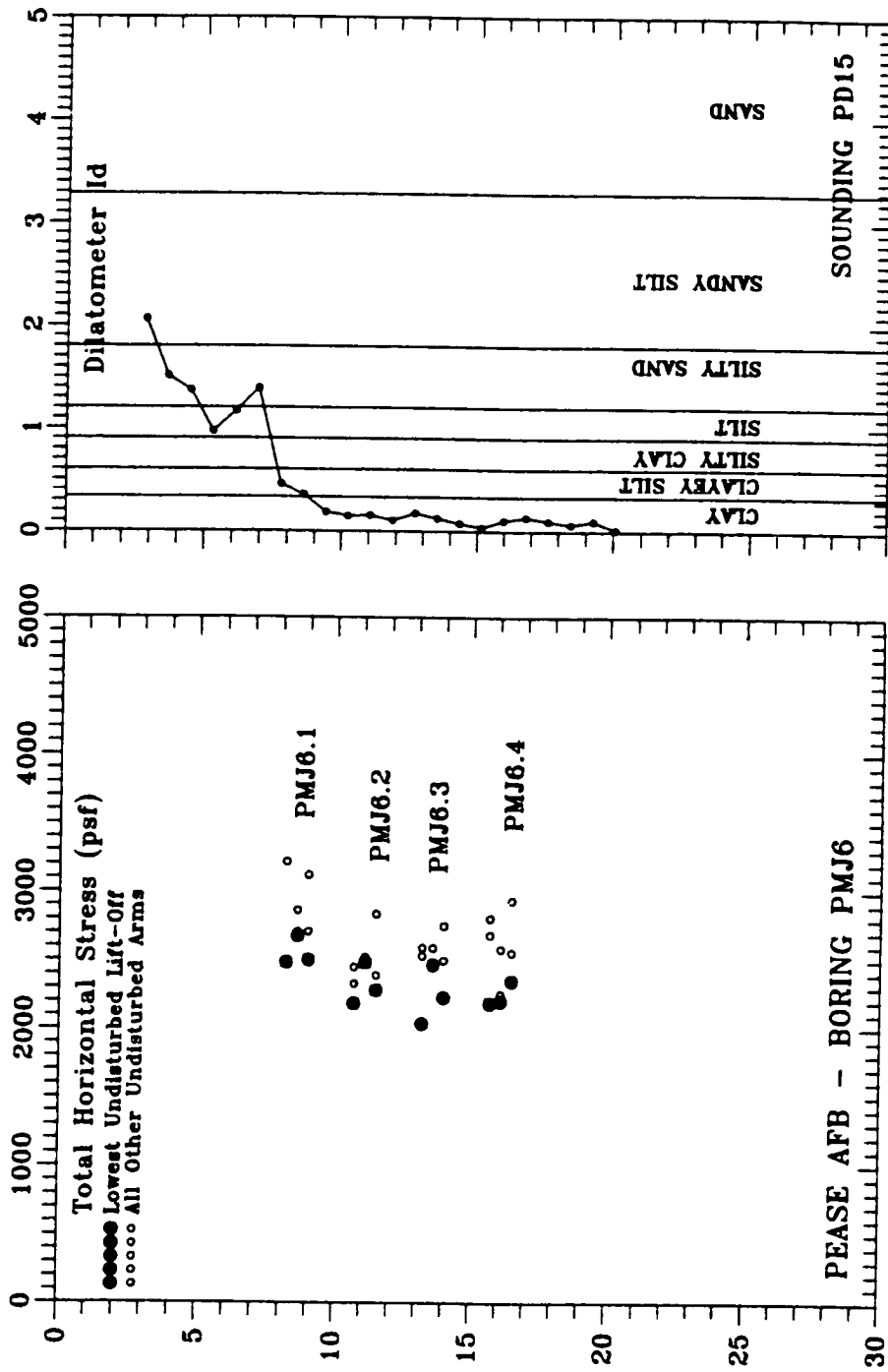


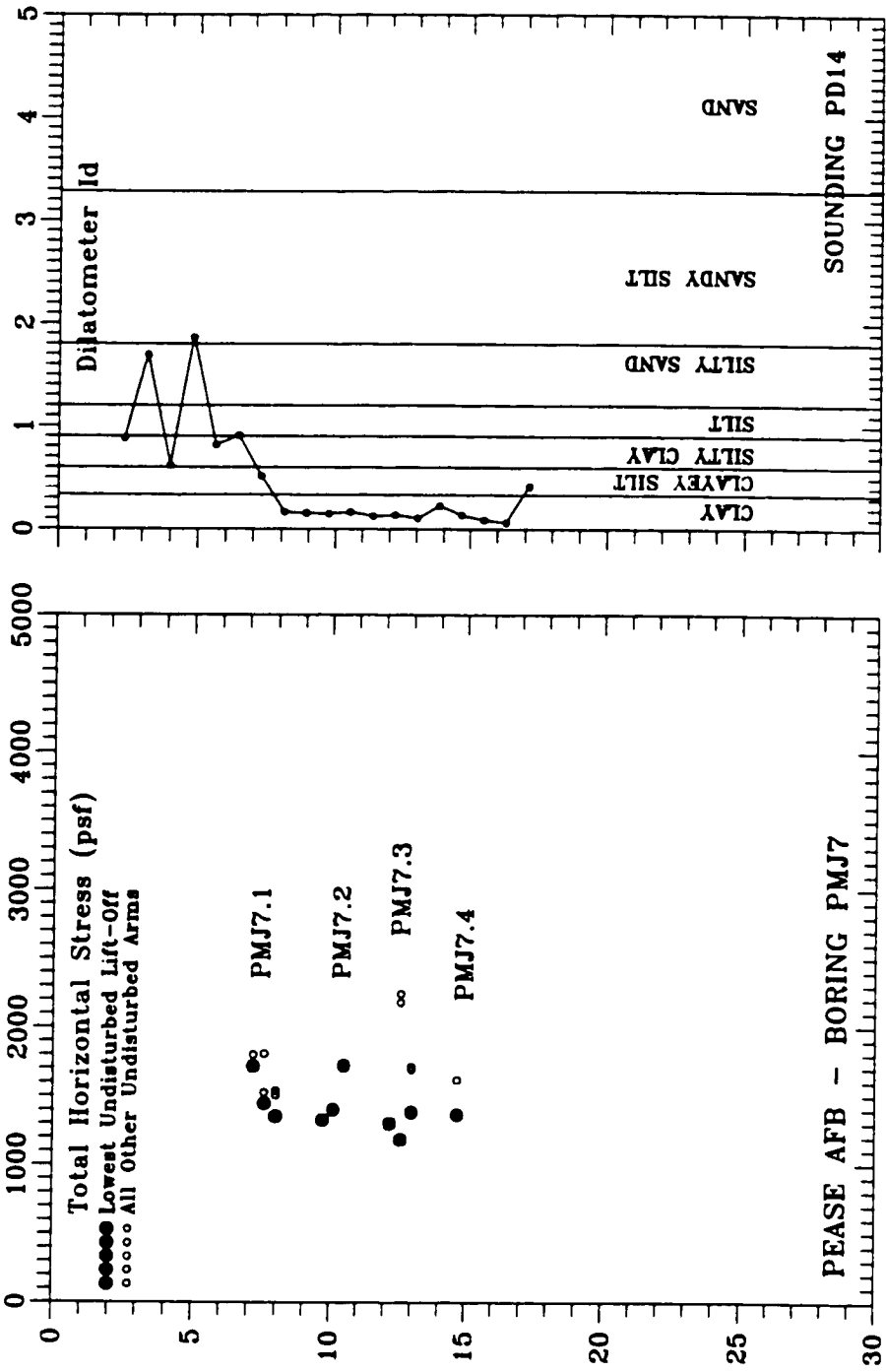












APPENDIX E
USERS GUIDE TO PROGRAM SOSAP

modules, is as follows:

- 1 **Read Data File:** A "raw" 13 column SBPM data file from a field test or a calibration expansion is read from disk and loaded into memory. The file is considered raw since it is the data file directly from field or calibration expansion data acquisition. This module is required as a prior step to modules 2 and 4. The 13 columns in the raw pressuremeter data file are as follows:

Column	Data
1	Displacement of Upper Arm 1 (volts)
2	" " " " Upper Arm 2 " "
3	" " " " Upper Arm 3 " "
4	" " " " Middle Arm 1 " "
5	" " " " Middle Arm 2 " "
6	" " " " Middle Arm 3 " "
7	" " " " Lower Arm 1 " "
8	" " " " Lower Arm 2 " "
9	" " " " Lower Arm 3 " "
10	Total Pressure Cell (TP) (volts)
11	Effective Stress Cell (PPA) (volts)
12	Effective Stress Cell (PPB) (volts)
13	Time (Minutes)

Upon entering module 1, the user is prompted to enter a file name of the raw pressuremeter data file, then is asked if the file is a standard SBPM file (answer yes). The data is loaded into memory and the user is returned to the main menu. The disk read will likely take some time since pressuremeter data files are generally large.

- 2 **Reduce SBPM Data:** After loading a data file into memory (module 1), module 2 can be used to convert the raw SBPM data from volts to values of strain (percent) and pressure (psf). Use of module 2 requires that 10 special conversion/calibration files are present in the same directory as the executable SOSAP program file. These special files include a file named SBPM.CAL, which is a file that contains data necessary to convert the raw data from volts to psf or strain, as appropriate, and 9 cubic-spline coefficient files, one for each strain arm, and named: U1.CAL, U2.CAL, U3.CAL, M1.CAL, M2.CAL, M3.CAL, L1.CAL, L2.CAL and L3.CAL. The SBPM.CAL file is assembled in a text editor and has the format indicated in Figure E-1. The *.CAL files are generated by spline fitting the curves resulting from the calibration expansion of the SBPM, prior to the field test. These files provide the data necessary to correct the field test data for membrane stiffness, and are generated by module 4 as subsequently described. Upon entering module 2, the user is prompted for the hydrostatic pressure at the test depth (psf) and then the excess pore pressure at lift-off due to insertion. This module does not write a disk file of the reduced data, and when processing is complete, leaves the user at the main menu. To save the reduced data to disk, Module 6 must be utilized.
- 3 **Analyze PM Data:** This module is used to determine SBPM undrained shear strength from SBPM field data reduced in module 2. Basically, three shear strength methods are available for use in two sub-modules. These methods include the Gibson and Anderson Method (1961) in one sub-module and both the sub-tangent method (Baguelin, et al., 1972), and the Denby and Clough Method (1980) in a separate sub-module. To determine shear strength, Reduced (not raw) SBPM data must be loaded into memory. This can be done by prior conversion of raw data to reduced data using module 2 or alternatively by reading a saved reduced data file into memory.

File sbpm.cal contains SBPM calibration factors and has the following format (within the quotes, eg, start of quotes is line 1):

```
"Strain Arm U1 = mm/volt
Strain Arm U2 = mm/volt
Strain Arm U3 = mm/volt
Strain Arm M1 = mm/volt
Strain Arm M2 = mm/volt
Strain Arm M3 = mm/volt
Strain Arm L1 = mm/volt
Strain Arm L2 = mm/volt
Strain Arm L3 = mm/volt
Total Press = psf/volt
Pore Press A = psf/volt
Pore Press B = psf/volt
Mem Stiff. U1 = volts
Mem Stiff. U2 = volts
Mem Stiff. U3 = volts
Mem Stiff. M1 = volts
Mem Stiff. M2 = volts
Mem Stiff. M3 = volts
Mem Stiff. L1 = volts
Mem Stiff. L2 = volts
Mem Stiff. L3 = volts
probe radius = mm
lift-off l1 = psf
lift-off l2 = psf
lift-off l3 = psf
lift-off m1 = psf
lift-off m2 = psf
lift-off m3 = psf
lift-off u1 = psf
lift-off u2 = psf
lift-off u3 = psf"
```

Note: to construct file, replace the units after the equal sign with a numerical value. The numerical value MUST be tabbed at least 25 spaces from the left margin. The text and equal sign preceding the numerical value, as above, must be within 24 spaces of the left margin. The text is optional and can be changed, if desired.

Figure E-1 - Configuration of SBPM.CAL File

After reading data into memory is done in module 3 using one of two sub-modules (one for the middle arms and one for the upper/lower arms) prior to selecting one of the shear strength sub-modules.

Gibson and Anderson (1961) - The Gibson and Anderson Method is the simpler of the shear strength modules to execute. After selecting module 3, the screen prompts the user with a choice between shear strength reduction or quit. Select shear strength and the screen prompts (module 3 menu):

```
Gibson & Anderson           =>1
Baguelin, et al.           =>2
Read Reduced Data-middle    =>3
Read Reduced Data-u&l arms  =>4
Return to previous menu     =>0
```

After selecting 1, the Gibson and Anderson method executes, and the user is prompted for a name to give the output file. Any file name permitted in DOS can be used. The user is then prompted for the arm tier for which shear strength data is to be determined. The computer executes and a disk file containing data for plot determination of the Gibson and Anderson Method is created. Column 1, 2 and 3 of the output file is radial strain ($\epsilon/100$), volumetric strain ($\Delta v/v$, %), and total pressure for arm 1 of the tier selected. Likewise, columns 4, 5 and 6 are the same values for arm 2, and columns 7, 8 and 9 for arm 3. Any standard graphing package can be used to plot this ASCII file.

The sub-tangent and Denby-Clough shear strength methods are executed by selecting sub-module 2, (Baguelin et al.). Execution of this sub-module involves curve fitting the reduced pressuremeter curves to allow the mathematical integration necessary for both the sub-tangent and Denby-Clough methods. After entering the sub-module, the user is prompted for a name to be given to the output file. Again, any legal DOS name is permitted. After entering the name, the user is prompted with the pressuremeter channel menu:

```
pressuremeter channels:  1 => upper strain arm 1
=====                2 => upper strain arm 2
                        3 => upper strain arm 3
                        4 => middle strain arm 1
                        5 => middle strain arm 2
                        6 => middle strain arm 3
                        7 => lower strain arm 1
                        8 => lower strain arm 2
                        9 => lower strain arm 3
                       10 => total pressure
                       11 => pore pressure cell
                       12 => pore pressure cell
                       13 => time (minutes)
```

The user is prompted to "select x-data column" which is the strain arm to be analyzed (generally a channel from 1 to 9) and then prompted "select y-data column", the total stress cell data (select channel 10). These are the sets of data that will be curve fitted by the cubic spline method. Next, the user is prompted as to how to average the data. If 1 is selected, all the data is used. If 3 is selected, every three values are averaged, and thus the amount of data that are spline fit is reduced to 1/3 the original amount. It is generally necessary to average data because the spline fitting routine requires monotonic data. Data irregularities causes the program to "crash", and the user will need to restart the program and re-read in the reduced SBPM data. Averaging of

every 5 values is common, and occasionally averaging up to 7 to 10 values is necessary in order to be able to spline fit a curve without crashing the program. After entering the number of data points to be averaged, the user is asked if the data should be displayed on the screen ("Do you wish to look at raw data?"). A response is given and the data is displayed or not, followed by a summary of minimum and maximum values. The user is next prompted for the number of "knots" he/she wishes to impose on the spline fitting. The section of curve to be spline fit will be divided into sections separated by the "knots" specified by the user. Each knot has a unique value of "X", or radial strain and the section of curve between the knots is fitted with a cubic equation that smoothly transitions into the adjacent portions of the curve on the other side of the knots. The user selects the number of knots that separate the more linear portions of the pressuremeter curve. Generally, it was found that 3 to 4 knots were sufficient to provide a good curve fit. After selecting the number of knots, the user is prompted for the X-axis location of each knot. Selection of knot locations is somewhat of an art form, and generally a lot of practice is required to become proficient without perpetual frustrating program crashes. Patience is required and it should be understood that crashes are more frequent than successful spline fits. As general guidance, the knots can be located along the pressuremeter curve at lift-off, at the location of highest curvature on the initial portion of the pressuremeter curve, and at a strain well after the anticipated maximum shear stress is expected (6 percent or more seems to generally be adequate). Reference to a graphic plot of the reduced pressuremeter curve is useful in selecting the knot locations. After all the x-axis locations of the knots are entered, execution of the spline fit begins. This is where the crash will occur if it is going to. If the screen fills with spline coefficient data, and no error code is indicated, the spline fitting was successful. If the program crashes, the user will find himself at the DOS prompt and must start over and try again. For re-trials after program crashes, the first thing to vary is the knot locations. Next the number of points averaged, and finally additional knots can be added. If the spline fit was successful, hit return to scroll through the spline coefficients until the next prompt appears. This prompt asks if the user desires the spline coefficients to be saved. The coefficients should be saved so that the "fit" of the spline generated curve with the actual data can be checked later on by generating spline curve x-y data for comparison to the actual reduced pressuremeter curve. The fit of the spline curve fit should be checked since the spline fit sometimes deviates from the reduced pressuremeter curve due to bad selection of knot locations. After being prompted to save the spline coefficients, the program writes a disk file of coefficients and then computes and writes a disk file of shear strength results. The shear strength output file consists of 7 columns, as follows:

Column	Data
1	Radial Strain, ϵ
2	Tangential Stress, σ_θ
3	Radial Stress σ_r
4	Radial Strain, in/in
5	Denby-Clough inverse pressuremeter curve slope
6	$p = (\sigma_1 + \sigma_3) / 2$
7	$q = (\sigma_1 - \sigma_3) / 2$

This data can be used to determine the sub-tangent and Denby-Clough SBPM shear strengths and plot p-q total stress path. Any standard graph package can be used to plot the ASCII output file. At the

completion of processing and writing the disk files, the user is returned to the module 3 menu.

- 4 **SBPM Calibration:** This module spline fits a SBPM calibration expansion curve for use in module 2 to correct for membrane stiffness. The procedure is the same (and equally as tedious due to spline crashes) as the Baguelin, et al. sub-module described above. This module is entered after first reading in the raw calibration expansion data using module 1. This data is left in terms of voltage, and is not first reduced using module 2. Also, the data in the data file must be "trimmed" so that only the load data after lift-off remains (in other words, remove the pre-lift-off and unload data). This is done with a text editor prior to running SOSAP. After entering the module, the user is prompted by the pressuremeter channel menu. This menu is presented previously in the description of the Baguelin et al. sub-module of module 3, and the reader is referred there (the previous section) for more detailed instructions. The sequence of key stroke entry is identical with that presented in the previous section, from the pressuremeter channel menu on. The difference is that a raw expansion curve is being spline curve fitted rather than a reduced pressuremeter curve. At the completion of processing, the user is prompted to save the spline coefficients to a file named as directed by the user, then the user is returned to the main menu.
- 5 **Generate Spline Data:** This module is entered if it is desired to generate x-y data from spline coefficients to check the goodness of fit with the actual test data. This can be done with spline coefficients generated for calibration expansion curves (from module 4) and reduced pressuremeter curves (from Baguelin et al., module 3). When the module is entered, the user is prompted for the data file containing the spline coefficients, followed by a prompt for the name of an output file for the x-y data generated from the spline coefficients. Next the user is prompted for the x range (minimum x and maximum x) for which y data is to be generated, and then is prompted for the number of points the user wants to generate between the minimum and maximum limits. After the prompts, processing occurs, and the data is saved to the output file (ASCII). The data is stored in two columns; the first column is x and the second column is y.
- 6 **Save Current Data:** This module saves reduced data from module 2. The user is prompted to either save all data or just x,f data. Reply to save all data, as the other module has been disabled. Next the user is prompted for a name to be given to the middle arm reduced data and then a name for the upper/lower arm data output file. These output files are in ASCII format and can be plotted using any graphing package. The structure of the output files is as shown on Figure E-2. After storing the output files, the user is returned to the main menu.
- 7 **QUIT:** This module terminates the program without saving any data. The user is returned to the DOS prompt.

Middle Arm Output File:	
Column	Data
1	M1 Radial Strain (in/in)
2	M1 Total Stress (psf)
3	M1 Effective Stress (psf)
4	M2 Radial Strain (in/in)
5	M2 Total Stress (psf)
6	M2 Effective Stress (psf)
7	M3 Radial Strain (in/in)
8	M3 Total Stress (psf)
9	M3 Effective Stress (psf)
10	PPA Excess Pore Pressure
11	PPB Excess Pore Pressure
12	Elapsed Time (minutes)
Upper/Lower Arm Output File:	
1	U1 Radial Strain (in/in)
2	U1 Total Stress (psf)
3	U2 Radial Strain (in/in)
4	U2 Total Stress (psf)
5	U3 Radial Strain (in/in)
6	U3 Total Stress (psf)
7	L1 Radial Strain (in/in)
8	L1 Total Stress (psf)
9	L2 Radial Strain (in/in)
10	L2 Total Stress (psf)
11	L3 Radial Strain (in/in)
12	L3 Total Stress (psf)
13	Elapsed Time (minutes)

Figure E-2 Structure of Reduced Data Output File